28th Annual Combustion Research Conference

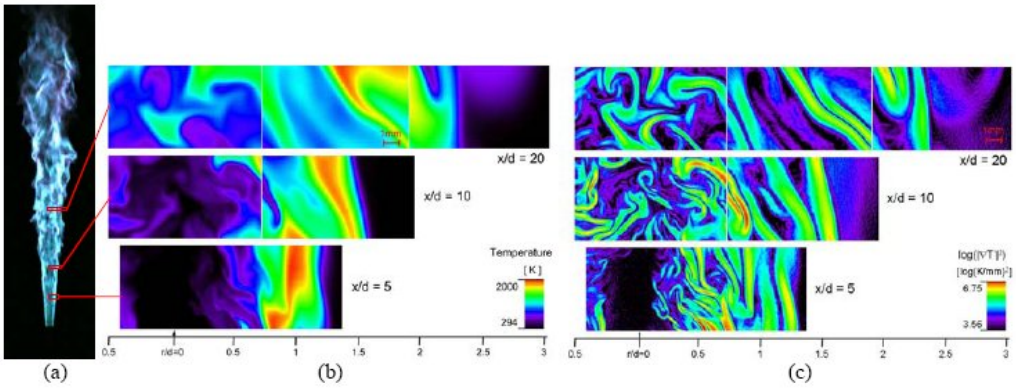

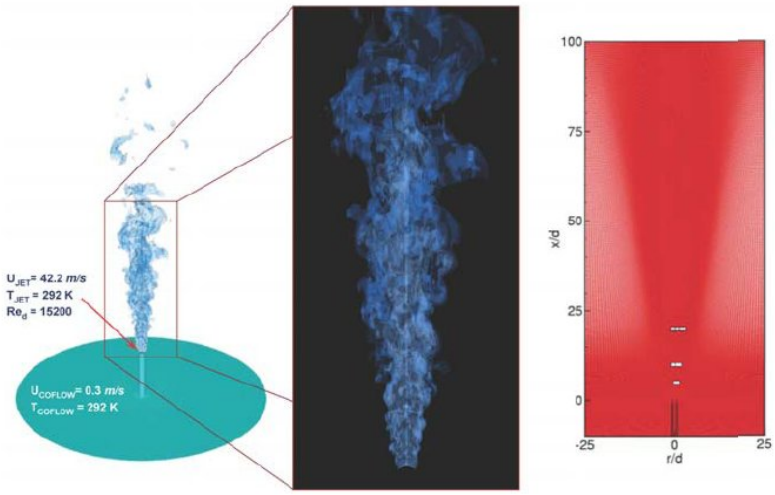

Airlie Conference Center
Warrenton, Virginia
May 29 – June 1, 2007

Office of Basic Energy Sciences

Chemical Sciences, Geosciences & Biosciences Division

Cover Images:
Top: (a) Measurement locations in a turbulent nonpremixed CH4/H2/N2 jet flame (DLR-A) , (b) Single-shot temperature measurements, (c) Single-shot measurements of the squared gradient of the temperature fluctuation reveals layers of high dissipation. "Quantitative Imaging Diagnostics for Reacting Flows", Jonathan H. Frank, pg. 65.
Bottom: Computational domain used for the same turbulent nonpremixed CH4/H2/N2 jet flame with close-up of the simulated flame and cross-section of the grid topology. White boxed regions on grid highlight field of view at x/d = 5, 10 and 20 where 2-D Rayleigh imaging was performed. "Large Eddy Simulation of Turbulence-Chemistry Interactions in Reacting Multiphase Flows", Joseph C. Oefelein, pg. 201.

FOREWORD

The achievement of National goals for energy security and environmental protection will rely on technology more advanced than we have at our disposal today. Combustion at present accounts for 85% of the energy generated and used in the U.S. and is likely to remain a dominant source of energy for the coming decades. Achieving energy conservation while minimizing unwanted emissions from combustion processes could be greatly accelerated if accurate and reliable means were at hand for quantitatively predicting process performance. Given current and future fuel content, cost, and climatic impact, a predictive, science-based approach to energy utilization is necessary.

The reports appearing in this volume present work in progress in basic research contributing to the development of a predictive capability for combustion processes. The work reported herein is supported by the Department of Energy's Office of Basic Energy Sciences (BES) and in large measure by the chemical physics program. The long-term objective of this effort is the provision of theories, data, and procedures to enable the development of reliable computational models of combustion processes, systems, and devices.

The development of reliable models for combustion requires the accurate knowledge of chemistry, turbulent flow, and the interaction between the two at temperatures and pressures characteristic of the combustion environment. In providing this knowledge, the research supported by BES addresses a wide range of continuing scientific issues of long standing.

- For even the simplest fuels, the chemistry of combustion consists of hundreds of reactions. Key reaction mechanisms, the means for developing and testing these mechanisms and the means for determining which of the constituent reaction rates are critical for accurate process characterization, are all required.
- For reactions known to be important, accurate rates over wide ranges of temperature, pressure and composition are required. To assess the accuracy of measured reaction rates or predict rates that would be too difficult to measure, theories of reaction rates and means for calculating their values are needed. Of particular importance are reactions involving open shell systems such as radicals and excited electronic states.
- To assess the accuracy of methods for predicting chemical reaction rates, the detailed, state-specific dynamics of prototypical reactions must be characterized.
- Methods for observing key reaction species in combustion environments, for interpreting these observations in terms of species concentrations, and for determining which species control the net reactive flux are all required
- Energy flow and accounting must be accurately characterized and predicted.
- Methods for reducing the mathematical complexity inherent in hundreds of reactions, without sacrificing accuracy and reliability are required. Methods for reducing the computational complexity of computer models that attempt to address turbulence, chemistry, and their interdependence and also needed.

Although the emphasis in this list is on the development of mathematical models for simulating the gas phase reactions characteristic of combustion, such models, from the

chemical dynamics of a single molecule to the performance of a combustion device, require validation by experiment. Hence, the DOE program represented by reports in this volume supports the development and application of new experimental tools in chemical dynamics, kinetics, and spectroscopy.

The success of this research effort will be measured by the quality of the research performed, the profundity of the knowledge gained, as well as the degree to which it contributes to goals of resource conservation and environmental stewardship. In fact, without research of the highest quality, the application of the knowledge gained to practical problems will not be possible.

The emphasis on modeling and simulation as a basis for defining the objectives of this basic research program has a secondary but important benefit. Computational models of physical processes provide the most efficient means for ensuring the usefulness and use of basic theories and data. The importance of modeling and simulation remains well recognized in the Department of Energy and is receiving support through the Scientific Discovery through Advanced Computing (SciDAC) program; some work-in-progress reports funded through SciDAC are included in this volume.

During the past year, this program has benefited greatly from the involvement of Dr. Richard Hilderbrandt, program manager for Chemical Physics and for Computational and Theoretical Chemistry, and Dr. Michael Casassa, team leader for the Fundamental Interactions programs. Finally, the efforts of Sophia Kitts and Lois Irwin of the Oak Ridge Institute for Science Education and Diane Marceau of the Division of Chemical Sciences, Geosciences, and Biosciences, Office of Basic Energy Sciences in the arrangements for the meeting are also much appreciated.

Frank P. Tully, SC-22.1
Division of Chemical Sciences, Geosciences, and Biosciences
Office of Basic Energy Sciences

May 29, 2007

28th Annual Combustion Research Conference
U.S. Department of Energy
Office of Basic Energy Sciences

Agenda

Tuesday, May 29, 2007

3:00 pm ***Registration***

7:00 pm ***Dinner***

Wednesday, May 30, 2007

7:00 am ***Breakfast***

Morning Session
Ronald K. Hanson, Chair

8:15 am *Welcome and Introduction,* Frank P. Tully

8:30 am **Plenary Speaker** *"A Few Words about Energy Transfer"***,**
Charles Parmenter, Indiana University

9:30 am **"***Flash Photolysis-Shock Tube Studies"*, Joe V. Michael 160

10:00 am **"***Laser Studies of Combustion Chemistry"*, John F. Hershberger 99

10:30 am ***Break***

10:45 am **"***Variational Transition State Theory"*, Donald G. Truhlar 273

11:15 am **"***Chemical Kinetics and Combustion Modeling"*, James A. Miller..... 168

11:45 am **"***Computer-Aided Construction of Chemical Kinetic Models"*,
William H. Green Jr.... 76

12:15 pm ***Lunch***

5:00 pm ***Dinner***

Wednesday, May 30, 2007

Evening Session

Laurie J. Butler, Chair

6:15 pm **"***Dynamics and Energetics of Elementary Combustion Reactions and Transient Species"*, Robert E. Continetti 29

6:45 pm **"***Bimolecular Dynamics of Combustion Reactions"*, H. Floyd Davis 41

7:15 pm **"***Production and Study of Ultra-cold Molecules Produced by Kinematic Cooling"*, David W. Chandler 21

7:45 pm ***Break***

8:00 pm **"***Turbulence-Chemistry Interactions in Reacting Flows"*, Robert S. Barlow 5

8:30 pm *"Terascale Direct Numerical Simulation and Modeling of Turbulent Combustion"*, Jacqueline H. Chen 25

Thursday, May 31, 2007

7:00 am ***Breakfast***

Morning Session

Stephen J. Klippenstein, Chair

8:15 am *"Theoretical Studies of Potential Energy Surfaces"*, Lawrence B. Harding..... 95

8:45 am *"Theoretical Studies of Combustion Dynamics"*, Joel M. Bowman 9

9:15 am *"Quantum Molecular Dynamic: Theoretical Studies in Spectroscopy and Chemical Dynamics*, Hua-Gen Yu 297

9:45 am ***Break***

10:15 am *"Reaction Dynamics in Polyatomic Molecular Systems"*, William H. Miller 176

10:45 am *"Multiphase Combustion Diagnostics Development"*, Hope A. Michelsen..... 164

11:15 am *"Scanning Tunneling Microscopy Studies of Chemical Reactions on Surfaces"*, George Flynn 61

12:00 pm ***Lunch***

Thursday, May 31, 2007
Afternoon and Evening Session
Marsha I. Lester, Chair

5:15 pm *"Gas Phase Molecular Dynamics: Spectroscopy and Dynamics of Transient Species,* Trevor J. Sears 241

5:45 pm *"Spectroscopy, Kinetics and Dynamics of Combustion Radicals,* David J. Nesbitt..... 192

6:15 pm ***Break***

6:30 pm *"Spectroscopic and Dynamical Studies of Highly Energized Small Polyatomic Molecules",* Robert W. Field 57

7:00 pm *"Fourier Transform Emission and Synchrotron Studies of Photofragmentation, Radical Reactions and Aerosol Chemistry,* Stephen R. Leone 134

7:30 pm ***Cash Bar***

8:00 pm ***Dinner***

Friday, June 1, 2007

7:00 am ***Breakfast***

Morning Session
Philip M. Johnson, Chair

8:15 am *"Elementary Reactions of PAH Formation",* Robert S. Tranter 269

8:45 am *"Studies of Flame Chemistry with Photoionization Mass Spectrometry"* Terrill A. Cool..... 33

9:15 am *"Elementary Reaction Kinetics of Combustion Species"*, Craig A. Taatjes..... 261

9:45 am ***Break***

10:00 am *"Active Thermochemical Tables – Progress Report",* Branko Ruscic..... 233

10:30 am *Closing Remarks*

11:00 am ***Lunch***

Table of Contents

Photoelectron Photoion Coincidence Studies: Heats of Formation of Ions, Molecules, and Free Radicals
Tomas Baer 1

Turbulence-Chemistry Interactions in Reacting Flows
Robert S. Barlow 5

Theoretical Studies of Combustion Dynamics
Joel M. Bowman 9

Combustion Chemistry
Nancy J. Brown 13

Probing Radical Intermediates of Bimolecular Combustion Reactions
Laurie J. Butler 17

Production and Study of Ultra-cold Molecules Produced by Kinematic Cooling
David W. Chandler 21

Terascale Direct Numerical Simulation and Modeling of Turbulent Combustion
Jacqueline H. Chen, Evatt R. Hawkes, Ramanan Sankaran, David Lignell, and Chun S. Yoo 25

Dynamics and Energetics of Elementary Combustion Reactions and Transient Species
Robert E. Continetti 29

Studies of Flame Chemistry with Photoionization Mass Spectrometry
Terrill A. Cool 33

State Controlled Photodissociation Of Vibrationally Excited Molecules And Hydrogen Bonded Dimers
F.F. Crim 37

Bimolecular Dynamics of Combustion Reactions
H. Floyd Davis 41

Multiple-Time–Scale Kinetics
Michael J. Davis 45

Comprehensive Mechanisms for Combustion Chemistry: Experiment, Modeling, And Sensitivity Analysis
Frederick L. Dryer 49

Hydrocarbon Radical Thermochemistry: Gas-Phase Ion Chemistry Techniques
Kent M. Ervin 53

Spectroscopic and Dynamical Studies of Highly Energized Small Polyatomic Molecules
Robert W. Field 57

Scanning Tunneling Microscopy Studies of Chemical Reactions on Surfaces
George Flynn 61

Quantitative Imaging Diagnostics for Reacting Flows
Jonathan H. Frank 65

Mechanism and Detailed Modeling of Soot Formation
Michael Frenklach 69

Chemical Dynamics in The Gas Phase: Quantum Mechanics Of Chemical Reactions
Stephen K. Gray 73

Computer-Aided Construction of Chemical Kinetic Models
William H. Green, Jr. 76

Wave Packet Based Statistical Model for Complex-Forming Reactions
Hua Guo 79

Gas Phase Molecular Dynamics: High-Resolution Spectroscopic Probes of Chemical Dynamics
Gregory E. Hall 83

Flame Chemistry and Diagnostics
Nils Hansen 87

Kinetics and Spectroscopy of Combustion Gases at High Temperatures
Ronald K. Hanson and Craig T. Bowman 91

Theoretical Studies of Potential Energy Surfaces
Lawrence B. Harding 95

Laser Studies of Combustion Chemistry
John F. Hershberger 99

Terascale High-Fidelity Simulations of Turbulent Combustion with Detailed Chemistry (TSTC)
Hong G. Im, Arnaud Trouvé, Christopher J. Rutland, Jacqueline Chen 103

Ionization Probes of Molecular Structure and Chemistry
Philip M. Johnson 107

Probing the Reaction Dynamics of Hydrogen-Deficient Hydrocarbon Molecules and Radical Intermediates via Crossed Molecular Beams
Ralf I. Kaiser 111

Dynamical Analysis of Highly Excited Molecular Spectra
Michael E. Kellman 115

Theory and Modeling of Small Scale Processes in Turbulent Flow
Alan R. Kerstein 119

Kinetics of Combustion-Related Processes at High Temperatures
J. H. Kiefer 123

Theoretical Chemical Kinetics
Stephen J. Klippenstein 126

Theoretical Modeling of Spin-Forbidden Channels in Combustion Reactions
Anna I. Krylov 130

Fourier Transform Emission and Synchrotron Studies of Photofragmentation, Radical Reactions and Aerosol Chemistry
Stephen R. Leone, Christopher Howle, Fabien Goulay, Leonid Belau, Jared Smith, Keving Wilson and Musahid Ahmed 134

Intermolecular Interactions of Hydroxyl Radicals on Reactive Potential Energy Surfaces
Marsha I. Lester 138

Theoretical Studies of Molecular Systems
William A. Lester, Jr. 142

Kinetics of Elementary Processes Relevant to Incipient Soot Formation
M. C. Lin 145

Advanced Nonlinear Optical Methods for Quantitative Measurements in Flames
Robert P. Lucht 149

Time-Resolved Infrared Absorption Studies of the Dynamics of Radical Reactions
R. Glen Macdonald 153

Quantum Chemical Studies of Chemical Reactions Related to the Formation of Polyaromatic Hydrocarbons and of Spectroscopic Properties of Their Key Intermediates
Alexander M. Mebel 156

Flash Photolysis-Shock Tube Studies
Joe V. Michael 160

Multiphase Combustion Diagnostics Development
Hope A. Michelsen 164

Chemical Kinetics and Combustion Modeling
James A. Miller 168

Detection and Characterization of Free Radicals Relevant to Combustion Processes
Terry A. Miller 172

Reaction Dynamics in Polyatomic Molecular Systems
William H. Miller 176

Gas-Phase Molecular Dynamics: Theoretical Studies of Combustion-Related Chemical Reactions and Molecular Spectra
James T. Muckerman 180

Dynamics of Activated Molecules
Amy S. Mullin 184

Reacting Flow Modeling with Detailed Chemical Kinetics
Habib N. Najm 188

Spectroscopy, Kinetics and Dynamics of Combustion Radicals
David J. Nesbitt 192

Determination of Accurate Energetic Database for Combustion Chemistry by High-Resolution Photoionization and Photoelectron Methods
C. Y. Ng 197

Large Eddy Simulation of Turbulence-Chemistry Interactions in Reacting Flows
Joseph C. Oefelein 201

Kinetics and Dynamics of Combustion Chemistry
David L. Osborn 205

Large Amplitude Motion and the Birth of Novel Modes of Vibration in Energized Molecules
David S. Perry 209

Chemical Kinetic Modeling of Combustion Chemistry
William J. Pitz and Charles K. Westbrook 213

Investigation of Non-Premixed Turbulent Combustion
Stephen B. Pope 217

Optical Probes of Atomic and Molecular Decay Processes
Stephen .T. Pratt 221

Photoinitiated Reactions of Radicals and Diradicals in Molecular Beams
Hanna Reisler 225

Accurate Calculations and Analyses of Electronic Structure, Molecular Bonding and Potential Energy Surfaces
Klaus Ruedenberg 229

Active Thermochemical Tables – Progress Report
Branko Ruscic 233

Theoretical Studies of Elementary Hydrocarbon Species and Their Reactions
Henry F. Schaefer III and Wesley D. Allen 237

Gas Phase Molecular Dynamics: Spectroscopy and Dynamics of Transient Species
Trevor J. Sears 241

Picosecond Optical Diagnostics
Thomas B. Settersten 245

Theoretical Studies of Potential Energy Surfaces and Computational Methods
Ron Shepard 249

Computational and Experimental Study of Laminar Flames
M. D. Smooke and M. B. Long 253

Universal and State-Resolved Imaging Studies of Chemical Dynamics
Arthur G. Suits 257

Elementary Reaction Kinetics of Combustion Species
Craig A. Taatjes 261

Theoretical Chemical Dynamics Studies of Elementary Combustion Reactions
Donald L. Thompson 265

Elementary Reactions of PAH Formation
Robert S. Tranter 269

Variational Transition State Theory
Donald G. Truhlar 273

Chemical Kinetic Database for Combustion Modeling
Wing Tsang 277

Time-Resolved Structural Probes of Molecular Dynamics
Peter M. Weber 281

Probing Flame Chemistry with MBMS, Theory, and Modeling
Phillip R. Westmoreland 285

Photoinitiated Processes in Small Hydrides
Curt Wittig 289

Theoretical Studies of the Reactions and Spectroscopy of Radical Species Relevant to Combustion Reactions and Diagnostics
David R. Yarkony 293

Gas-Phase Molecular Dynamics: Theoretical Studies in Spectroscopy and Chemical Dynamics
Hua-Gen Yu 297

Experimental Characterization of the Potential Energy Surfaces for Conformational Isomerization in Aromatic Fuels
Timothy S. Zwier 301

Author Index 305

Participants 307

Annual Progress report February 2007

Photoelectron Photoion Coincidence Studies: Heats of Formation of Ions, Molecules, and Free Radicals

Tomas Baer (baer@unc.edu)
Department of Chemistry
University of North Carolina
Chapel Hill, NC 27599-3290
DOE Grant DE-FG02-97ER14776

Program Scope

The threshold photoelectron photoion coincidence (TPEPICO) technique is utilized to investigate the dissociation dynamics and thermochemistry of energy selected medium to large organic molecular ions. The reactions include parallel and consecutive steps that are modeled with the statistical theory in order to extract dissociation onsets for multiple dissociation paths. These studies are carried out with the aid of molecular orbital calculations of both ions and the transition states connecting the ion structure to their products. The results of these investigations yield accurate heats of formation of ions, free radicals, and stable molecules. In addition, they provide information about the potential energy surface that governs the dissociation process. Isomerization reactions prior to dissociation are readily inferred from the TPEPICO data.

The PEPICO Experiment

The threshold photoelectron photoion coincidence (TPEPICO) experiment in Chapel Hill is carried out with a laboratory H_2 discharge light source. Threshold electrons are collected by velocity focusing them into a 1.5 mm hole on a mask located at the end of the 12 cm drift tube. Some hot electrons pass through a 2x5 mm opening located next to the central 1.5 mm hole. In this fashion, two TPEPICO spectra are simultaneously collected, one for threshold and one for hot electrons. Hot electron free data are obtained by subtracting a fraction of the hot from the threshold TPEPICO data. The ion TOF is either a linear version or a reflectron for studying H loss processes. The electrons provide the start signal for measuring the ion time of flight distribution. When ions dissociate in the microsecond time scale, their TOF distributions are asymmetric. The dissociation rate constant can be extracted by modeling the asymmetric TOF distribution. A high-resolution version of this experiment is currently being constructed in collaboration with Thomas Gerber at the Swiss Light Source (SLS), a synchrotron that will have a gas phase chemical dynamics beamline. Because of the high photon flux, we plan on developing the first multi-start multi-stop coincidence scheme using a master clock as the time base. When combined with coincidence ion detection, the results will permit the measurement of ion dissociation limits to within 1 meV or 0.1 kJ/mol.

Recent Results

Photoion Photoelectron Coincidence Spectroscopy of Primary Amines RCH_2NH_2 (R = H, CH_3, C_2H_5, C_3H_7, i-C_3H_7): Alkylamine and Alkyl Radical Heats of Formation by Isodesmic Reaction Networks

Alkylamines (RCH_2NH_2, R = H, CH_3, C_2H_5, C_3H_7, *i*-C_3H_7) have been investigated by dissociative photoionization by threshold photoelectron photoion coincidence spectroscopy (TPEPICO). The 0 K dissociation limits (9.754 ± 0.008, 9.721 ± 0.008, 9.702 ± 0.012 and 9.668

± 0.012 eV for R = CH_3, C_2H_5, C_3H_7, *i*-C_3H_7, respectively) have been determined by preparing energy selected ions and collecting the fractional abundances of parent and daughter ions. All alkylamine cations produce the methylenimmonium ion, $CH_2NH_2^+$, and the corresponding alkyl free radical. Two isodesmic reaction networks have also been constructed. The first one consists of the alkylamine parent molecules, and the other of the alkyl radical photofragments. Reaction heats within the isodesmic networks have been calculated at the CBS-APNO and W1U levels of theory. The two networks are connected by the TPEPICO dissociation energies. The heats of formation of the amines and the alkyl free radicals are then obtained by a modified least-squares fit to minimize the discrepancy between the TPEPICO and the *ab initio* values. The analysis of the fit reveals that the previous experimental heats of formation are largely accurate, but certain revisions are suggested. Thus, $\Delta_f H^o_{298K}[CH_3NH_2(g)] = -21.8 \pm 1.5$ kJ mol^{-1}, $\Delta_f H^o_{298K}[C_2H_5NH_2(g)] = -50.1 \pm 1.5$ kJ mol^{-1}, $\Delta_f H^o_{298K}[C_3H_7NH_2(g)] = -70.8 \pm 1.5$ kJ mol^{-1}, $\Delta_f H^o_{298K}[C_3H_7\cdot] = 101.3 \pm 1$ kJ mol^{-1}, and $\Delta_f H^o_{298K}[i\text{-}C_3H_7\cdot] = 88.5 \pm 1$ kJ mol^{-1}. The TPEPICO and the *ab initio* results for butylamine do not agree within 1 kJ mol^{-1}, therefore no new heat of formation is proposed for butylamine. It is nevertheless indicated that the previous experimental heats of formation of methylamine, propylamine, butylamine and isobutylamine may have been systematically underestimated. On the other hand, the error in the ethyl radical heat of formation is found to be overestimated, and can be decreased to ± 1 kJ mol^{-1}; thus, $\Delta_f H^o_{298K}[C_2H_5\cdot] = 120.7 \pm 1$ kJ mol^{-1}. Based on the data analysis, the heat of formation of the methylenimmonium ion is confirmed to be $\Delta_f H^o_{298K}[CH_2NH_2^+] = 750.3 \pm 1$ kJ mol^{-1}.

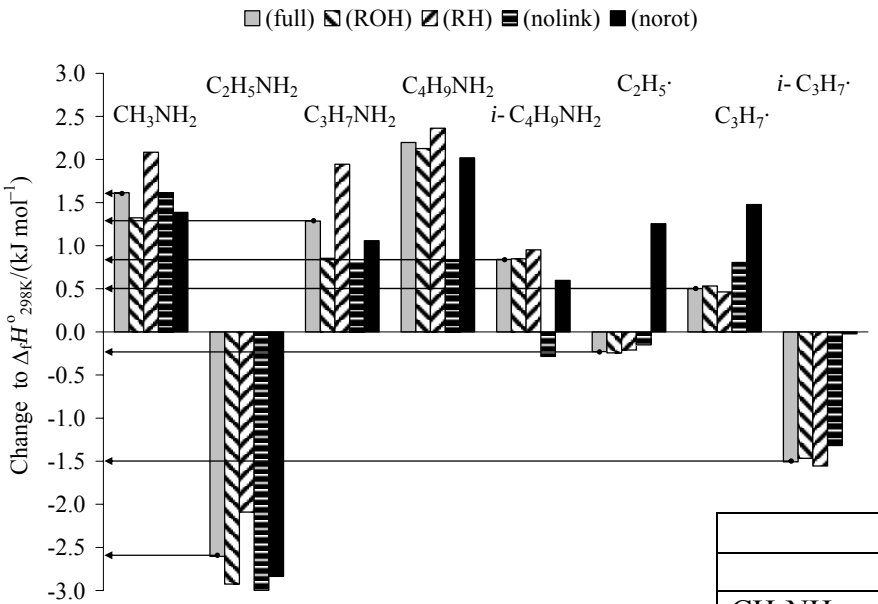

Figure 1: The plot shows the corrections to the literature values required to minimize the errors in our experimental and theoretical calculations. The $CH_3^\bullet$ heat of formatin was assumed accurate, as were the alcohols and the alkanes used in the isodesmic calculations.

	$\Delta_f H^o_{298K}$		$\Delta_f H^o_{0K}$
	/ (kJ mol^{-1})		
CH_3NH_2	–21.8	± 1.5	–7.0
$C_2H_5NH_2$	–50.1	± 1.5	–28.6
$C_3H_7NH_2$	–70.8	± 1.5	–43.3
$C_4H_9NH_2$	–89.6	± 2.0	–56.1
i-$C_4H_9NH_2$	–97.8	± 1.0	–64.9
$C_2H_5\cdot$	120.7	± 1.0	132.3
$C_3H_7\cdot$	101.3	± 1.0	119.1
i-$C_3H_7\cdot$	88.5	± 1.0	106.2
$NH_2CH_2^+$	750.3	± 1.0	763.9

An interesting finding in this study has been the effect of the hindered rotors. The TPEPICO dissociation energies and the isodesmic reaction heats are 0 K properties, to which the thermal enthalpy is explicitly added. On the other hand, other experimental results usually yield thermochemical data in which the thermal enthalpy is inherently included. The description of the hindered internal

rotation has been studied to account for its contribution to the 298 K dissociation energies and reaction heats. The internal rotation has little effect on the thermal enthalpies of the amines, but its contribution is about –1 kJ mol^{-1} for the alkyl radicals, in which a low barrier hindered internal rotor causes the harmonic approximation to introduce a considerable error. The agreement between the experimental heats of formation and our results is restored for the ethyl and propyl radicals when the hindered internal rotation is also considered. This effect is shown by the solid black bar in Figure 1, where the hindered rotors were removed.

Threshold Photoelectron-Photoion Coincidence Spectroscopy: Dissociation Dynamics and Thermochemistry of $Ge(CH_3)_4$, $Ge(CH_3)_3Cl$, and $Ge(CH_3)_3Br$

Threshold photoelectron-photoion coincidence spectroscopy (TPEPICO) has been used to investigate the gas-phase ionic dissociation energies and thermochemistry of Me_4Ge and Me_3GeX, (Me = methyl; X=Cl, Br) molecules. The 0 K dissociation onsets for these species have been measured from the breakdown diagram and the ion time-of-flight distributions, which were modeled with the statistical RRKM theory and DFT calculations. The measured 0 K dissociative photoionization onsets were: Me_3Ge^+ + Me (9.826 ± 0.010 eV); Me_3Ge^+ + Cl (10.796 ± 0.040 eV); Me_3Ge^+ + Br (10.250 ± 0.011 eV); Me_2GeCl^+ + Me (10.402 ± 0.010 eV); and Me_2GeBr^+ + Me (10.333 ± 0.020 eV). These onsets were used to obtain new values for $\Delta_f H^0_{298}$ (in kJ/mol) of the neutral molecules: Me_3GeCl (-239.8 ± 5.7) and Me_3GeBr (-196.5 ± 4.3); and also for the following ionic species: Me_3Ge^+ (682.3 ± 4.1), Me_2GeCl^+ (621.1 ± 5.8) and Me_2GeBr^+ (657.8 ± 4.7).

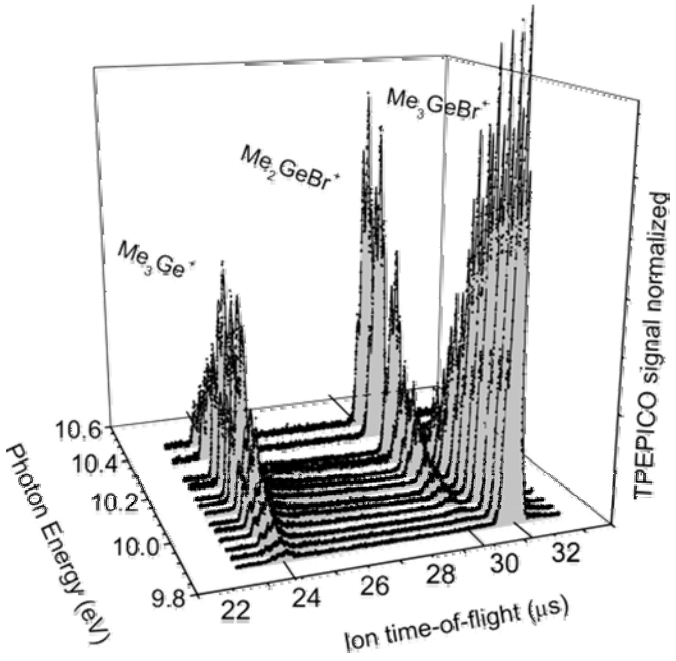

Publications from DOE supported work 2005 – 2007

A. Bodi, J. P. Kercher, T. Baer, and B. Sztáray On the Parallel Mechanism of the Dissociation of Energy-Selected $P(CH_3)_3^+$ Ions, *J. Phys. Chem. B* **109** 8393-8399 (2005).

A.F. Lago, J.P. Kercher, A. Bodi, B. Sztáray, B. Miller, D. Wurzelmann, and T. Baer, The heats of formation of the dihalomethanes, CH_2XY, (X,Y = Cl, Br, and I), by threshold photoelectron photoion coincidence, *J.Phys.Chem.A* **109** 1802-1809 (2005)

J.P. Kercher, E.A. Fogleman, H. Koizumi, B. Sztáray, and T. Baer, The Heats of Formation of the Propionyl ion and Radical and 2,3 Pentanedione by Threshold Photoelectron Photoion Coincidence Spectroscopy, *J. Phys. Chem*. A 109 939-946 (2005)

T. Baer, B. Sztáray, J. P. Kercher, A.F. Lago, A. Bödi, C. Skull, and D. Palathinkal, Threshold Photoelectron Photoion Coincidence Studies of Parallel and Sequential Dissociation Reactions, *Phys. Chem. Chem. Phys*. **7** 1507-1513 (2005)

J.Z. Davalos, A.F. Lago, and T. Baer, Thermochemical study of the liquid phase equilibrium reaction of dihalomethanes by NMR spectroscopy, *Chem. Phys. Lett*. **409** 230-234 (2005)

Z. Gengeliczki, B. Sztaray, T. Baer, C. Iceman, and P.B. Armentrout, Heats of Formation of $Co(CO)_2NOPR_3$, R = CH_3 and C_2H_5, and Its Ionic Fragments, *J. Am. Chem. Soc*. **127** 9393-9402, (2005)

A. Bodi, B. Sztaray, and T. Baer, Dissociative Photoionization of Mono-, Di- and Trimethylamine Studied by a Combined Threshold Photoelectron Photoion Coincidence Spectroscopy and Computational Approach, *Phys.Chem.Chem.Phys*. **8**, 613-623 (2006)

H. Koizumi, J. Davalos, and T. Baer, Heats of Formation of GeH_4, GeF_4 and $Ge(CH_3)_4$, *Chem. Phys*. **324** 385-392(2006)

A. Lago and T. Baer Dissociation dynamics and thermochemistry of chloroform and tetrachloroethane molecules studied by threshold photoelectron photoion coincidence, *Int. J. Mass Spectrom*. **252** 20-25 (2006)

James P. Kercher, Bálint Sztáray, and Tomas Baer, On the dissociation of 2-Pentanone ions by threshold photoelectron photoion coincidence spectroscopy, *Int. J. Mass Spectrom*. **249-250** 403-411 (2006)

Juan Z. Dávalos and Tomas Baer, Thermochemistry and Dissociative Photoionization of $Si(CH_3)_4$, $BrSi(CH_3)_3$, $ISi(CH_3)_3$, and $Si_2(CH_3)_6$ Studied by Threshold Photoelectron-Photoion Coincidence Spectroscopy, *J.Phys.Chem. A* **110** 8572-8579 (2006)

Juan Z. Dávalos, and Hideya Koizumi, and Tomas Baer, Threshold Photoelectron-Photoion Coincidence Spectroscopy: Dissociation Dynamics and Thermochemistry of $Ge(CH_3)_4$, $Ge(CH_3)_3Cl$, and $Ge(CH_3)_3Br$, *J. Phys. Chem. A* **110**, 5032-5037 (2006)

Agnes Revesz, Csaba I. Pongor, Andras Bodi, Balint Sztaray, and Tomas Baer, Manganese-Chalcarbonyl bond strengths from threshold photoelectron photoion coincidence spectroscopy, *Organometallics* **25,** 6061-6067 (2006)

Andras Bodi, Curtis Bond, Patcharica Meteesatien, James P. Kercher, Balint Sztaray, and Tomas Baer, Photoion Photoelectron Coincidence Spectroscopy of Primary Amines $RCH_2–NH_2$ (R = H, CH_3, C_2H_5, C_3H_7, *i*-C_3H_7): Alkylamine and Alkyl Radical Heats of Formation by the Means of Isodesmic Reaction Networks, *J. Phys.Chem. A* **110,** 13425-13433 (2006)

James P. Kercher, Zsolt Gengeliczki, Bálint Sztáray, and Tomas Baer, Dissociation dynamics of sequential ionic reactions: Heats of formation of tri−, di− and monoethyl phosphines, *J. Phys. Chem. A* **111**, 16-26 (2007)

James P. Kercher, Will Stevens, Zsolt Gengeliczki, and Tomas Baer, Modeling Ionic Unimolecular Dissociations from a Temperature Controlled TPEPCIO Study on *1*-C_4H_9I Ions, *Int. J. Mass Spectrom*. (2007) in press

Zsolt Gengeliczki, László Szepes, Bálint Sztáray, and Tomas Baer, Photoelectron spectroscopy and thermochemistry of tert-butylisocyanide substituted cobalt tricabonyl nitrosyl, *J. Phys. Chem. A* (2007) in press

Turbulence-Chemistry Interactions in Reacting Flows

Robert S. Barlow
Combustion Research Facility
Sandia National Laboratories, MS 9051
Livermore, California 94551
barlow@ca.sandia.gov

Program Scope

This program is directed toward achieving a more complete understanding of turbulence-chemistry interactions in flames. In the Turbulent Combustion Laboratory (TCL) at the CRF, simultaneous line imaging of spontaneous Raman scattering, Rayleigh scattering, and two-photon laser-induced fluorescence (LIF) of CO is applied to obtain spatially and temporally resolved measurements of temperature, the concentrations of all major species, and mixture fraction (ξ), as well as gradients in these quantities in hydrocarbon flames. The instantaneous three-dimensional orientation of the turbulent reaction zone is also measured by imaging of OH LIF in two crossed planes, which intersect along the laser axis for the multiscalar measurements. These combined data characterize both the thermo-chemical state and the instantaneous flame structure, such that the influence of turbulent mixing on flame chemistry may be quantified. Our experimental work is closely coupled with international collaborative efforts to develop and validate predictive models for turbulent combustion. This is accomplished through our visitor program and through the TNF Workshop series. Although the past emphasis has been on nonpremixed combustion, the workshop and this program are in the process of expanding their scope to address a broad range of combustion regimes, including premixed and stratified flames. Within the CRF we collaborate with Joe Oefelein to use highly-resolved large-eddy simulations (LES) of our experimental flames in order to gain greater fundamental understanding of dynamic, multi-scale, flow-chemistry interactions. We also collaborate with Tom Settersten and Jonathan Frank to refine our quantitative LIF methods and to apply complementary imaging diagnostics to selected turbulent flames.

Recent Progress

The past year has been active with regard to our visitor program. We have hosted two visiting researchers, Matthew Dunn of Sydney University and Bassam Dally of Adelaide University. Both brought burners designed to explore fundamental aspects of turbulent premixed flames. In addition, we have collaborated with Simone Hochgreb of Cambridge University to apply our multiscalar diagnostics to stratified V-flames. Data analysis is in progress on all these cases, so we only briefly describe the motivations for each experiment here.

Our internal work has continued to focus on the structure of reacting flows at the smallest scales of turbulence and on methods for accurate measurement of the mean mixture fraction dissipation in flames. This work on dissipation spectra in turbulent flames, combined with work by Jonathan Frank and Sebastian Kaiser (described in a separate abstract) constitutes a significant advance in fundamental knowledge of turbulent reacting flow. We have developed methods for measuring the local cutoff scale of the dissipation spectrum for temperature and for mixture fraction, and we have shown that these spectra are well represented by the model turbulence spectrum of Pope [*Turbulent Flows*, Cambridge University Press, 2000], even for upstream locations in jet flames, where there are significant fluctuations in fluid properties.

Results suggest that the same approach may be applicable in complex reacting flows where length scales are difficult to estimate.

We have also completed construction and installation of a new detection system for multi-scalar line imaging (Raman/Rayleigh/CO-LIF) that provides significant improvements in spatial resolution, collection efficiency, and rejection of interferences. This new system opens the opportunity for development of polarization separation Raman spectroscopy as a quantitative single-shot, diagnostic technique for investigation of turbulent flames of more complex fuels.

Piloted Premixed Jet Flames

A piloted premixed jet flame burner was developed at Sydney University in order to investigate highly turbulent premixed combustion regimes where the ratio of turbulent velocity fluctuation to laminar flame speed, u'/S_L, is comparable to that occurring in land-based gas turbine combustors. The piloted premixed jet is surrounded by a large (200-mm diameter) coflow of lean H_2/air combustion products at ~1500K. Several flames were measured with the equivalence ratio and velocity of the central jet being varied as parameters. The high turbulent shear in these flames can cause breaks in the reaction front, allowing mixing of products and reactants and introducing a more complex regime of combustion, which may be probed effectively using our multiscalar diagnostics. Experiments included crossed-planar OH imaging, along with the Raman/Rayleigh/CO-LIF measurements. Figure 1 shows example single-shot profiles of temperature and CO mass fraction from a laminar fuel-lean CH_4/air Bunsen flame. These profiles give an indication of the spatial resolution and measurement precision achieved in premixed flames by the line-imaging system, and they point to great potential for this research program to provide new physical insights and detailed model validation data for premixed flames and stratified flames. Analysis of the turbulent flame results is in progress.

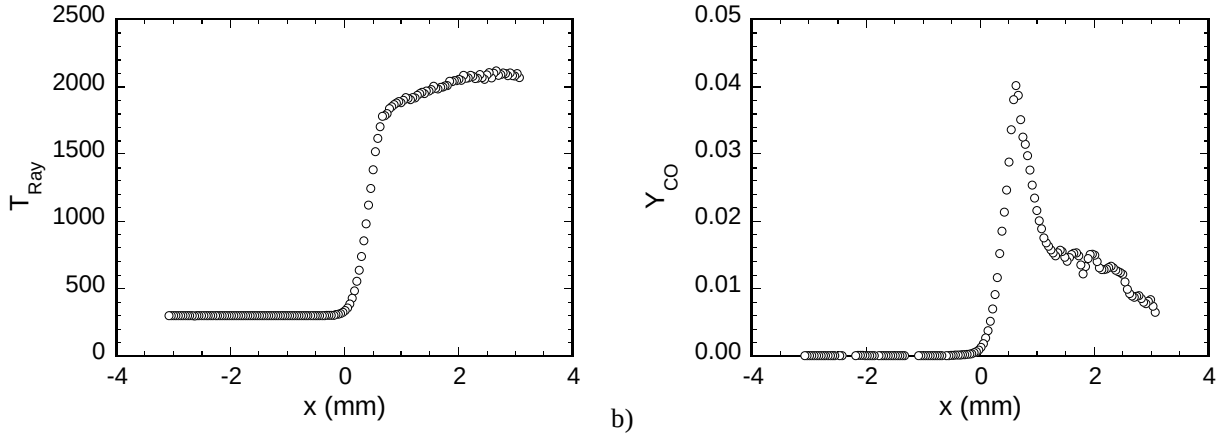

Figure 1. Single-shot realization of a) temperature (from Rayleigh scattering) and b) CO mass fraction (from 2-photon LIF) in a laminar fuel-lean CH_4/air Bunsen flame. The Rayleigh data spacing is 40 μm, while the CO line images have 100 μm spacing. CO-LIF signal profiles are interpolated onto the Rayleigh pixel locations for processing.

Turbulent Premixed Flames in Vitiated Coflow

This premixed burner, which was brought to Sandia by Bassam Dally (University of Adelaide, Australia) for his third visit to the CRF in 11 years, has interchangeable central nozzles for variation of the turbulence length scale. The central jet can also be heated up to ~800K, so that the effects of fuel preheat on flame structure may be investigated along with the influence of

turbulent length scale and u'/S_L. A special nozzle with small holes in the turbulence generating grid was added, after discussions with Jackie Chen, to allow experiments in a premixed combustion regime similar to that addressed in recent DNS work. Data analysis is in progress.

Stratified V-Flame Burner

In stratified combustion a turbulent flame propagates through a nonuniform mixture of fuel and oxidizer. This mode of combustion is common on practical systems but is not well understood and represents a significant challenge for combustion models. Stratified combustion is also challenging for laser diagnostics because high precision in the measurement of the local equivalence ratio is required and the thin reaction zones demand high spatial resolution. The multiscalar diagnostics that we have developed for measurement of scalar dissipation in nonpremixed flames define the state of the art, and we intend to pursue stratified combustion as a major research theme during the next few years. The stratified V-flame burner, developed at Cambridge University and shown in Fig. 2, is an excellent initial target because of its simple geometry and relatively low level of turbulence. We are currently evaluating the capabilities of the Raman/Rayleigh/CO-LIF technique to measure the internal structure of the thin reaction zones.

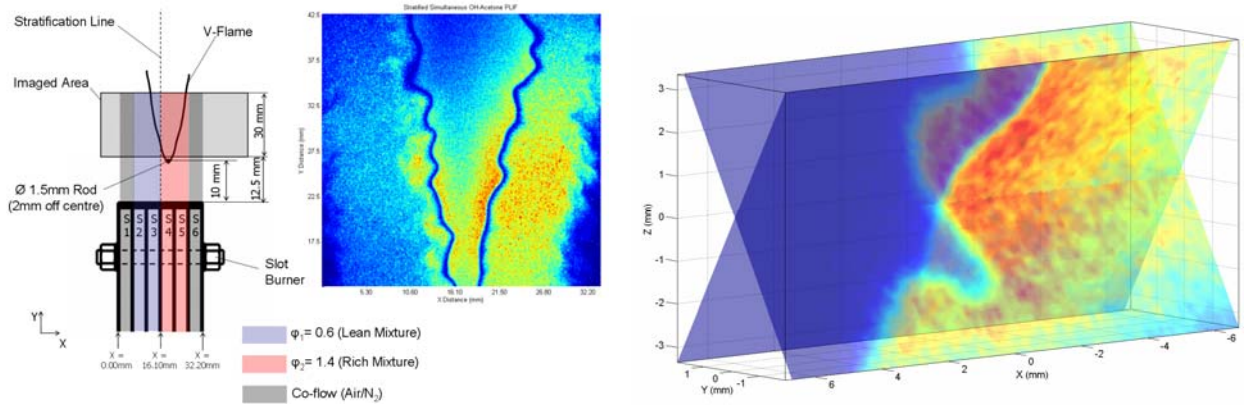

Figure 2. Cambridge stratified slot burner: Burner diagram (left), example of combined acetone and OH PLIF imaging performed at Cambridge (center), and example of crossed OH PILF from Sandia multiscalar experiments.

Future Plans

Our immediate focus will be to fully characterize the performance of the new detection system for line-imaged Raman/Raleigh/CO-LIF. The higher collection efficiency and imaging resolution that this system will provide to the Raman scattering measurements will further improve our ability to investigate stratified and premixed flames. Investigation of turbulent stratified combustion, in collaboration with Cambridge University and TU Darmstadt, will be a major thrust over the next 2-3 years. Another major thrust will be to develop polarization separation Raman spectroscopy as a single-shot method for investigation of turbulent flames of fuels more complex than previously addressed in this program. This method allows for measurement and subtraction of unpolarized interferences (fluorescence and chemiluminescence) from the polarized spontaneous Raman scattering signal. Exploratory experiments using a single detection system and separate measurements of two polarization components will be conducted on laminar flames of a range of fuels, including several alternative transportation fuels, in order to gauge the potential of the technique. Application of

the method to turbulent flames will require construction of a second Raman/Rayleigh detection system to mirror our newly developed multiscalar detection system.

In addition to these new research areas, we will continue our systematic investigation of nonpremixed turbulent flames by applying the full multiscalar diagnostic system to the Sydney bluff-body stabilized flames, which are currently prime targets for LES within the framework of the TNF Workshop. The primary objectives will be to determine local dissipation length scales in these flames and provide data on scalar dissipation for comparison with model predictions of these relatively complex, recirculating, reacting flow.

BES Supported Publications (2005 - present)

A.N. Karpetis and R.S. Barlow, "Measurements of Flame Orientation and Scalar Dissipation in Turbulent Partially Premixed Methane Flames," *Proc. Combust. Inst.* **30**, 665-672 (2005).

R.S. Barlow, A.N. Karpetis, "Scalar Length Scales and Spatial Averaging Effects in Turbulent Piloted Methane/Air Jet Flames," *Proc. Combust. Inst.* **30**, 673-680 (2005).

K. Kohse-Hoeinghaus, R. S. Barlow, M. Alden, J. Wolfrum, "Combustion at the Focus: Laser Diagnostics and Control," *Proc. Combust. Inst.* **30**, 89-123, (2005) (invited plenary paper).

R.S. Barlow, J.H. Frank, A.N. Karpetis, J.-Y. Chen, "Piloted Methane/Air Jet Flames: Transport Effects and Aspects of Scalar Structure," *Combust. Flame* **143**, 433-449 (2005).

R. Cabra, J.-Y. Chen, R.W. Dibble, A.N. Karpetis, R.S. Barlow, "Lifted Methane-Air Jet Flames in a Vitiated Coflow," *Combust. Flame* **143**, 491-506 (2005).

J.C. Oefelein, R.W. Schefer, R.S. Barlow, "Toward Validation of Large Eddy Simulation for Turbulent Combustion," *AIAA J.* **44**, 418-433 (2006).

G.-H. Wang, A.N. Karpetis, R.S. Barlow, "Dissipation Length Scales in Turbulent Nonpremixed Jet Flames" *Combust. Flame*, **148**, 62-75 (2007).

R.S. Barlow, "Laser Diagnostics and Their Interplay with Computations to Understand Turbulent Combustion," invited plenary paper, *Proc. Combust. Inst.* **31**, 49-75 (2007).

R.P. Lindstedt, H.C. Ozarovsky, R.S. Barlow, A.N. Karpetis, "Progression of Localised Extinction in High Reynolds Turbulent Jet Flames," *Proc. Combust. Inst.* **31**, 1551-1558 (2007).

D. Wang, C. Tong, R.S. Barlow, A.N. Karpetis, "Experimental Study of Scalar Filtered Mass Density Function in Turbulent Partially Premixed Flames," *Proc. Combust. Inst.* **31**, 1533-1541 (2007).

G.-H. Wang, R.S. Barlow, N.T. Clemens, "Quantification of Resolution and Noise Effects on Thermal Dissipation Measurements in Turbulent Non-premixed Jet Flames," *Proc. Combust. Inst.* **31**, 1525-1532 (2007).

A.R. Masri, P.A.M. Kalt, Y.M. Al-Abdeli, R.S. Barlow, "Turbulence-Chemistry Interactions in Non-Premixed Swirling Flames," *Combust. Theory Modelling*, in press.

G.-H. Wang, N.T. Clemens, R.S. Barlow, P.L. Varghese, "A System Model for Assessing Scalar Dissipation Measurement Accuracy in Turbulent Flows" *Meas. Sci. Technol*. in press.

Web-Based Information

http://www.ca.sandia.gov/CRF/staff/barlow.html http://www.ca.sandia.gov/TNF

Theoretical Studies of Combustion Dynamics
(DE-FG02-97ER14782)

Joel M. Bowman
Cherry L. Emerson Center for Scientific Computation and
Department of Chemistry, Emory University
Atlanta, GA 30322, jmbowma@emory.edu

Program Scope

This research program is a theoretical and computational one to develop and apply rigorous modeling techniques to chemical processes of importance in gas-phase combustion. These include quantum and quasiclassical calculations of bimolecular and unimolecular reactions using *ab initio*-based potentials that govern these processes. A recent focus is on developing new methods to obtain global potential energy surfaces that are fits to tens of thousands of *ab intio* energies using fitting bases that are manifestly invariant with respect to any permutation of like nuclei. Dynamics on these potentials, which may contain multiple minima and saddle points, can be done for long times and can reveal new pathways and mechanisms of chemical reactions. The choice of reaction system to study is always motivated by experiments that challenge and ultimately advance basic understanding of combustion reaction dynamics.

Recent Progress

H_2CO photodissociation

The photodissociation dynamics of formaldehyde has been of long-standing interest, both experimentally[1-4] and theoretically.[5-9] We have completed a series of papers on this reaction using a global, *ab initio*-based potential energy surface.[10] In collaboration with Arthur Suits' group a "roaming"-atom mechanism to form the molecular products, H_2+CO, has been elucidated.[11,P1] This channel can be described as a "self-reaction" of the nearly-formed radical products, H+HCO, where the nearly free H atom "roams" to portions of the potential surface that contains the cis and trans isomers HOCO and ultimately abstracts the H atom from HCO to form very highly vibrationally excited H_2 and rotationally cold CO. We also investigated the dynamics to form the H+HCO products on both the triplet and singlet potential energy surfaces in a joint experimental/theoretical paper with Scott Kable's group.[P2] Very recent work has focused on two aspects of H_2CO dissociation, namely the vector correlation (VC) of $\boldsymbol{j}_{CO}$ and the relative velocity vector $\boldsymbol{V}$ of the CO-H_2 products and the dependence of the radical branching on the total energy and angular momentum of H_2CO. We were stimulated to investigate the former property by a very recent paper reporting a possible "roaming" channel in CH_3CHO photodissociation by Houston and Kable (HK).[12] In that paper a striking difference in the VC as a function of j_{CO} was reported, i.e, no correlation for low j_{CO} and a high degree of correlation for high j_{CO}. This contradicted the results of a direct-dynamics study, which found a high degree of VC for the entire range of j_{CO}.[13] In those calculations trajectories were initiated at the molecular transition state, i.e., a well-defined potential saddle point. Based on that Houston and Kable argued that they were observing non-TS dynamics analogous to H_2CO. Our calculations of the VC of CO in H_2CO

dissociation were initiated at the global minimum and contain contributions from the roaming channel and are in good agreement with the HK experiments.[P3] We also investigated the effect of overall rotation, J, in H_2CO on the branching ratio for the radical products. At a fixed total energy we found that this ratio decreases as J increases.[P3] An application of Phase-Space Theory for the radical products and RRKM theory for the molecular products is underway and does appear to qualitatively to account for this result.

Reaction Dynamics of $C+C_2H_2 \rightarrow$ *linear, cyclic* C_3H+H, C_3+H_2

We have begun calculations of the reaction of $C(^3P)$ with C_2H_2. This reaction has been extensively studied in cross molecular beam experiments.[14,15] *Ab initio* calculations of the many stationary points of the potential have been reported,[16] and RRKM[17] and reduced dimensionality quantum calculations of the rate constant have also been reported.[18,19] This reaction forms *linear(l)*-C_3H and *cyclic(c)*-C_3H products and according to one experimental group, singlet C_3.[15] The singlet C_3 can only be formed in a spin changing process. We have developed a global potential energy surface, based on DFT calculations, for the triplet reaction and also portions of the potential for the singlet reaction and performed quasiclassical trajectory calculations on these surfaces. The first significant result of these calculations is a very different branching ratio for the C_3H isomers on these two potentials.[P4]

In response to a very recent experiment by Kaiser, Leone and co-workers at the Berkeley advanced light source we simulated the photoionization threshold behavior of *c*-C_3H and *l*-C_3H. The goal of this work is to develop a means to directly distinguish these two isomers experimentally. A preliminary account of this work indicates that it should be possible to do this.[P5,P6]

Future Plans

Our immediate future plans are to develop a global potential energy to describe the dissociation of CH_3CHO and to perform extensive quasiclassical trajectory calculations using the potential, analogous to the calculations we have done for H_2CO. The motivation for this research is the recent report by Houston and Kable,[12] mentioned above and interest in this system by other experimental research groups. This will be a major challenge for us as the CH_3CHO potential has many more isomers and reaction channels than H_2CO and of course more degrees of freedom (15 compared to six for H_2CO). The immediate goal is to investigate a possible "roaming" channel in this system analogous to the one found in H_2CO. Houston and Kable speculated that the radical products CH_3 + HCO somehow roam and self react to form the much lower energy molecular products CH_4 + CO.

We also plan to continue our studies of the $C+C_2H_2$ reaction to consider explicit spin-orbit coupling of the singlet and triplet potential energy surfaces.

References

1. For a review up to 1992, see, W. H. Green, C. B. Moore, and W. F. Polik, Ann. Rev. Phys. Chem. 1992, **43**, 591.

2. (a) T. J. Butenhoff, K. L. Carteton and C. B. Moore, J. Chem. Phys. **92**, 377 (1990); (b) W. F. Polik, D. R. Guyer and C. B. Moore, J. Chem. Phys. **92**, 3453 (1990); (c) R. D. Zee, M. F. Foltz, and C. B. Moore, J. Chem. Phys. **99**, 1664 (1993).
3. (a) A. C. Terentis, S. E. Waugh, G. F. Metha, and S. H. Kable, J. Chem. Phys. **108**, 3187 (1998); (b) H.-M. Yin, K. Nauta, and S. H. Kable, J. Chem. Phys. **122**, 194312 (2005).
4. L. R. Valachovic, M. F. Tuchler, M. Dulligan, Th., Droz-George, M., Zyrianov, A. Kolessov, H. Reisler, and C. J. Wittig, J. Chem. Phys. **112**, 2752 (2000).
5. Y. Chang, C. Minichino, and W. H. Miller, J. Chem. Phys. **96**, 4341 (1992).
6. Y. Yamaguchi , S. S. Wesolowski, T. J. Huis, H. F. Schaefer , J. Chem. Phys. **108**, 5281 (1998).
7. D. Feller, M. Dupuis, and B. C. Garrett, J. Chem. Phys. **113**, 218 (2000).
8. (a) X. Li, J. M. Millam and H. B. Schlegel , J. Chem. Phys. **113**, 10062 (2000); (b) W. Chen, W. L Hase. and H. B. Schlegel, Chem. Phys. Lett. **228**, 436 (1994).
9. T. Yonehara and S. J. Kato Chem. Phys. **117**, 11131 (2002).
10. X. Zhang, S.-L. Zou, L. B. Harding, and J. M. Bowman, J. Phys. Chem. A **108**, 8980 (2004).
11. D. Townsend, S. A. Lahankar, S. K. Lee, S. D. Chambreau, A. G. Suits, X. Zhang, J. L. Rheinecker, L. B. Harding, and J. M. Bowman, Science, **306**, 1158 (2004).
12. P. L. Houston and S. H. Kable, Proc. Natl. Acad. Sci. USA, **103**, 16079 (2006).
13. Y. Kurosaki and K. Yokoyama, J. Phys. Chem. A. **106**, 11416 (2002).
14. R. I. Kaiser, A. M. Mebel, and Y. T. Lee, J. Chem. Phys. **114**, 231 (2001).
15. L. Cartechini, A. Bergeat, G. Capozza, P. Casavecchia, G. G. Volpi, W. D. Geppert, C. Naulin, and M. Costes, J. Chem. Phys. **116**, 5603 (2002).
16. A. M. Mebel, W. M. Jackson, A. H. H. Chang, and S. H. Lin, J. Am. Chem. Soc. **120**, 5751 (1998).
17. R. Guadagnini, G. C. Schatz, and S. P. Walch, J. Phys. Chem. A 102, 5857 (1998).
18. E. Buonomo, and D. C. Clary, J. Phys. Chem. A, 105, 2694, (2001).
19. T. Takayanagi, J. Phys. Chem. A 110, 361 (2006).

PUBLICATIONS SUPPORTED BY THE DOE (2005-present)

1. Energy dependence of the roaming atom pathway in formaldehyde decomposition, S. A. Lahankar, S. D. Chambreau, X. Zhang J. M. Bowman, A. G. Suits, J. Chem. Phys. **126**, 044314 (2007).
2. Signatures of H_2CO photodissociation from two electronic states, H.M. Yin and S.H. Kable, X. Zhang and J.M. Bowman, Science, **311**, 1443 (2006).
3. Formaldehyde photodissociation: Dependence on total angular momentum and rotational alignment of the CO product, J. Farnum, X. Zhang and J.M. Bowman, J. Chem. Phys. in press.
4. Quasiclassical trajectory calculations of the reaction $C + C_2H_2 \rightarrow l\text{-}C_3H$, $c\text{-}C_3H + H$, $C_3 + H_2$ using full-dimensional triplet and singlet potential energy surfaces, W. K. Park, J. Park, S. C. Park, B. J. Braams, C. Chen, and J. M. Bowman, J. Chem. Phys. **125**, 081101 (2006).
5. Combined Experimental and Computational Study on the Ionization Energies of the

Cyclic and Linear C_3H Isomers. R. I. Kaiser, L. Belau, S. R. Leone, Musahid Ahmed, Y. Wang, B. J. Braams, and J. M. Bowman, ChemPhysChem 2007, 8 DOI: 10.1002/cphc.200700109

6. *Ab intio*-Based Potential Energy Surfaces and Franck-Condon Analysis of Ionization Thresholds of cyclic-C_3H and linear-C_3H,Yi. Wang, B. J. Braams, and J. M. Bowman, J. Phys. Chem. (Article); 2007; ASAP Article; DOI: 10.1021/jp0676787
7. New insights on reaction dynamics from formaldehyde photodissociation, J. M. Bowman and X. Zhang. Phys. Chem. Chem. Phys., invited review, **8** 313 (2006).
8. An *ab initio* potential surface describing abstraction and exchange for H+CH_4, X. Zhang, B. Braams, J. M. Bowman, J. Chem. Phys **124**, 021104 (2006).
9. Quasiclassical trajectory study of the reaction of fast H atoms with C-H stretch excited CHD_3, Z, Xie, J. M. Bowman, Chem. Phys. Lett. **429**, 355 (2006).
10. Quasiclassical trajectory study of the reaction H + $CH_4(\upsilon_3=0,1) \rightarrow CH_3 + H_2$ using a new *ab initio* potential energy surface, Z. Xie, J. M. Bowman, and X. Zhang, J. Chem. Phys. **125**, 133120 (2006).
11. Calculation of converged rovibrational energies and partition function for methane using vibrational–rotational configuration interaction, A. Chakraborty, D. G. Truhlar, J. M. Bowman, and S. Carter, J. Chem. Phys. **121**, 2071 (2004).
12. Construction of a global potential energy surface from novel *ab initio* molecular dynamics for the $O(^3P)$ + C_3H_3 reaction, S. C. Park, B. J. Braams, and J. M. Bowman, J. Theor. Comput. Chem. **4**, 163 (2005).
13. Quasiclassical trajectory studies of the dynamics of H_2CO on a global *ab initio*-based potential energy surface, J. L. Rheinecker, X. Zhang, and J. M. Bowman, Mol. Phys. **103**, 1067 (2005).
14. Quasiclassical trajectory study of formaldehyde: $H_2CO \rightarrow H_2$+CO, H+HCO, X. Zhang, J. L. Rheinecker, and J. M. Bowman, J. Chem. Phys. **122**, 114313 (2005).
15. Quantum and quasi-classical studies of the $O(^3P)$ + HCl → OH + $Cl(^2P)$ reaction using benchmark potential surfaces, T. Xie, J. M. Bowman, J. W. Duff and M. Braunstein, and B. Ramachandran, J. Chem. Phys. **122**, 014301 (2005).
16. Enhancement of tunneling due to resonances in pre-barrier wells in chemical reactions, J. M. Bowman, Chem. Phys. **308**, 255 (2005).
17. Termolecular kinetics for the Mu+CO+M recombination....J, J. Pan, D. J. Arseneau, M. Senba, D. M. Garner, D. G. Fleming, Ti. Xie and J. M. Bowman, J. Chem. Phys. **125**, 014307 (2006).

COMBUSTION CHEMISTRY

Principal Investigator: Nancy J. Brown
Environmental Energy Technologies Division
Lawrence Berkeley National Laboratory
Berkeley, California, 94720
510-486-4241
NJBrown@lbl.gov

PROJECT SCOPE

Combustion processes are governed by chemical kinetics, energy transfer, transport, fluid mechanics, and their complex interactions. Understanding the fundamental chemical processes offers the possibility of optimizing combustion processes. The objective of our research is to address fundamental issues of chemical reactivity and molecular transport in combustion systems. Our long-term research objective is to contribute to the development of reliable combustion models that can be used to understand and characterize the formation and destruction of combustion-generated pollutants. We emphasize studying chemistry at both the microscopic and macroscopic levels. To contribute to the achievement of this goal, our current activities are concerned with three tasks: Task 1) developing models for representing combustion chemistry at varying levels of complexity to use with models for laminar and turbulent flow fields to describe combustion processes; Task 2) developing tools to probe chemistry fluid interactions; and Task 3) modeling and analyzing combustion in multi-dimensional flow fields.

RECENT PROGRESS

Task 1: Developing models for representing combustion chemistry at varying levels of complexity to use with models for laminar and turbulent flow fields to describe combustion processes (**with Shaheen R. Tonse and Marcus Day)** Our objective in these studies [Tonse and Brown, 2003 and Tonse et al., 2007] is to develop reduced mechanisms for hydrocarbon fuels that are accurate and efficient because a substantial fraction of computing resources is frequently devoted to solving the chemical rate equations (ODEs) in reactive computational fluid dynamics (CFD) calculations. We recently completed our research on two approaches for mechanism reduction: an enhanced form of PRISM and DYSSA (Dynamic Steady State Approximation) for reducing chemical mechanisms dynamically. Our method of fast-slow time-scale separation and the framework of hypercube-shaped Chemical Composition Space (CCS) partitions are an essential part of each. PRISM and DYSSA apply their reduction techniques repeatedly and uniquely to each hypercube encountered, and this results in an optimal application of the techniques since species move from the slow category into the fast one as their time scales change during a simulation. The fast/slow species time separation is invariant in a hypercube, is different for each hypercube, and is accomplished dynamically during the simulation.

DYSSA and PRISM are evaluated for simulations of a counter-rotating pair of vortices interacting with a premixed CH_4/Air laminar flame. We use the adaptive low Mach number algorithm developed by Day and Bell [2000] and their Adaptive Mesh

Refinement (AMR) CFD code [Day, 2003]. We replaced their standard chemistry module in the AMR CFD code by either PRISM or DYSSA. DYSSA is shown to be sufficiently accurate for use in combustion simulations. DYSSA's speedup appears to be on the order of three or four for the most accurate simulations (relative error less than 1.0% for all species concentrations) and increases as accuracy requirements are decreased. PRISM does not perform as well as DYSSA with respect to accuracy and efficiency. We determined the computational burden imposed by the dynamic reduction is quite insignificant. We performed a sensitivity study of dynamic reduction to determine the factors that most contribute to its accuracy/efficiency and found that the partitioning of CCS into hypercubes, and how this is accomplished for individual species is very important. We determined that the partitioning of chemical composition space required by these two approaches affords an opportunity to investigate the chemistry/fluid interactions of a flame interacting with counter-rotating vortices of different strengths.

DYSSA, because it can be implemented in a straightforward fashion, offers the potential for more widespread use in the combustion community. We devised a new error determination scheme in DYSSA to assess the relative error in the reduction scheme. The accuracy of the reduced system is determined at the time of the initial call for each hypercube. This is accomplished by making a reduced call using the same non-FnL (non-fast and low) initial concentrations, temperature and timestep as were used for the full, unreduced system, and calculating the relative errors of the non-FnL species with respect to the unreduced system. A hypercube which does not meet the user-defined relative error requirement is noted, and the full unreduced ODE system is used on subsequent visits to the hypercube. The relative error determined in this manner correlates strongly with the relative error obtained by comparison with pure ODE simulations. A typical value for the user-specified relative error is less than 2%.

Hypercubes in DYSSA have smaller construction costs and lower computer memory requirements than those in PRISM since they do not require multiple ODE calls or the storage of $\sim N_s^2$ polynomial coefficients. In DYSSA, we tolerate lower hypercube reuse, store a larger number of hypercubes in memory, and use smaller hypercube edge sizes to provide better accuracy. In DYSSA, if a hypercube is no longer on the "most-recently used" list, we simply discard it and recalculate it if it is needed. PRISM constructs polynomial equations in each hypercube, and replaces the ODE system with simpler algebraic polynomials. Earlier versions of PRISM were applied to smaller chemical mechanisms and used *all* chemical species as independent variables in the polynomials. We enhanced PRISM by reducing the dimensionality of its polynomials based on differences in species time scales. In PRISM, we save hypercube data because of its high construction cost.

The Fast/low method performs well at separating species, and provides a useful means of applying dynamic chemical reduction on the fly when it is applied with the CCS hypercube partitioning concept. The amount of reduction varies considerably over the simulation. In contrast, static reduction, which attempts to maintain suitable accuracy, is limited to a dimensional reduction that is valid over all CCS encountered in a simulation, and it would use the part of CCS with the least reduction as being representative. The static dimensional reduction must be anticipated in advance, and an unexpected access to

some other portion of CCS resulting from changes in simulation initial conditions, boundary conditions, and model input would likely result in unanticipated inaccuracies.

A key target for efficiency is creating a reduced mechanism that has a computational burden equal to that of other processes in the reactive CFD simulation so that solving the chemical rate equations is no longer rate limiting. PRISM does not have sufficient accuracy and efficiency to be used in combustion modeling for larger mechanisms (30 species) of the sort treated here. PRISM works well for smaller mechanisms. If the Fast/low approach were applied to H_2/Air combustion with the Gosset designs, we envision that a factor of 15-20 gain in efficiency in the time required for the chemistry might be realized. PRISM might also be useful as part of a hybrid method for that part of CCS where quadratic polynomials are required as a surrogate for the ODE solution.

Task 2. A review of transport property formalisms and their underlying parameterizations is being prepared (Brown). It is important to properly describe the transport of species, momentum, and energy in flames. Transport coefficients required for the quantification of these processes are diffusion, viscosity, and thermal conductivity coefficients. Our recent sensitivity studies have demonstrated that transport property importance varies according to the dependent variable considered and the flame type. As an important step in improving the representation of transport in combustion modeling, we are inter-comparing calculated values of properties derived using different formalisms with experimentally determined values for conditions required for combustion modeling. We are focusing on properties required for modeling H_2 and CH_4 combustion.

Task 3 Research conducted to examine chemistry fluid mechanical interactions (Brown with Tonse and Day). We have examined vortex-flame interactions to determine how vortex strength affects chemical pathways. The metric used is the number of hypercubes that are constructed in CCS for a given simulation. The strain field and curvature of the flame surface induced by the impinging vortex leads to a shift in the chemical pathways of methane oxidation. The magnitude of these effects depends strongly on the length and time scales of the perturbing velocity field; the chemistry is not significantly affected if the vortex is weak or moves quickly through the flame zone. Important chemical processes are removed from the dominant methane oxidation pathways for moderate cases of vortex strength and velocity. This effect, observed experimentally [Nguyen and Paul, 1996] and theoretically by Bell et al. [2000], is reproduced in our current simulations. We observe that hypercube numbers increase with velocity to a point, and then decreases. The study also shows that different chemical pathways are emphasized as the velocity increases.

FUTURE PLANS

We will determine new strategies for improving DYSSA's efficiency while maintaining accuracy at acceptable levels for various combustion modeling applications. This will be achieved through devising a more sophisticated species separation algorithm, and through algorithmic improvements that result in larger hypercube sizes and greater reuse.

We will also extend the data set associated with the potential parameters that support the evaluation of transport properties for species important for H_2 and CH_4 combustion. We will improve the accuracy of transport properties important for supporting H_2 and CH_4combustion. We will work with Michael Frenklach as part of PrIMe

(hhtp://primekinetics.org), an international collaboration concerned with developing reaction models for combustion, which includes kinetics, thermochemistry, and transport. We will collaborate with Michael Frenklach on the homogeneous nucleation of carbon nanoparticles, and focus on collisions of aromatic-aliphatically-linked hydrocarbon compounds.

REFERENCES

M.S. Day, and J.B. Bell, Numerical Simulation of Laminar Reacting Flows with Complex Chemistry. Combust. Theory and Modeling, 4(4), pp 535-556 (2000). Also LBNL Report 44682.

M.S. Day, http://seesar.lbl.gov/CCSE/Software (2003).

J.B. Bell, N.J. Brown, M.S. Day, M. Frenklach, J.F. Grcar, and S.R. Tonse, "Effect of Stoichiometry on Vortex-Flame Interactions," Proceedings of the Combustion Institute 28, 1933-1939 (2000). Also Lawrence Berkeley National Laboratory Report No. LBNL-44730.

Q.V. Nguyen, and P.H. Paul, "The Time Evolution of a Vortex-Flame Interaction Observed in Planar Imaging of CH and OH, "26th Symp. (Intl.) on Combustion, The Combustion Inst., Pittsburgh, PA, 1996, pp 357-364.

PUBLICATIONS

Tonse, S.R., M.S. Day, and N.J. Brown. Dynamic Reduction of a CH4/Air Chemical Mechanism Appropriate for Investigating Vortex Flame Interactions. International Journal of Chemical Kinetics 39, pp 204-220, 2006. Also LBNL Report No. 59750

N.J. Brown and Revzan, K.L., "Comparative Sensitivity Analysis of Transport Properties and Reaction Rate Coefficients". International Journal Chemical Kinetics, 37, pp 538-553 (2005). Also LBNL Report No. 55671

S.R. Tonse and N.J. Brown, "Dimensionality Estimate of the Manifold in Chemical Composition Space for a Turbulent Premixed H_2+air Flame." International Journal of Chemical Kinetics 36, pp 326-336, 2004. Also LBNL Report No. 52058.

Probing Radical Intermediates of Bimolecular Combustion Reactions

Laurie J. Butler
The University of Chicago, The James Franck Institute
5640 South Ellis Avenue, Chicago, IL 60637
L-Butler@uchicago.edu

I. Program Scope

Polyatomic radical intermediates play an important role in a wide range of combustion processes. Our work for DOE in the past three years,[1-5] focuses on probing the radical intermediates of bimolecular reactions, including the reactions of O atoms and CH radicals with unsaturated hydrocarbons, that proceed through addition/insertion to form an energetically unstable radical intermediate along the reaction coordinate en route to products. Our experiments generate a particular isomeric form the key unstable radical intermediates along a bimolecular reaction coordinate and investigate the branching between the ensuing product channels of the energized radical as a function of its internal energy under collision-less conditions. The experiments allow us to probe the elementary reaction from the radical intermediate to the competing product channels and determine the energetic barriers in both the entrance and the product channels. The results develop insight on product channel branching in such reactions and provide a key benchmark for emerging electronic structure calculations on polyatomic reactions that proceed through unstable radical intermediates.

II. Recent Progress

Our work this year focused on investigating two bimolecular reactions that proceed through an addition/insertion mechanism: our second publication on the $CH_3O + CO \rightarrow CH_3OCO \rightarrow CH_3 + CO_2$ reaction and our first studies of a radical intermediate in the O + allyl reaction. Our work on the propargyl radical intermediate of the $CH + C_2H_2$ reaction described in publication 4, which was in final form in August, is not included below as the main results were described in our 2006 contractor's meeting abstract. Briefly, our data on that system evidenced the competing $H + C_3H_2$ and $H_2 + C_3H$ product channels of the reaction. Unlike most of the other systems we have investigated with this new methodology, the experimental results are not well-predicted by current high-level electronic structure calculations of the product channel energetics. Analysis of the photoionization detection of the c-C_2H_3 product in these experiments aids others who seek to interpret photoionization spectra of possible mixtures of the three C_3H_2 isomers.

The experiments described in Section A below outline our most recent results on the $CH_3O + CO \rightarrow CH_3 + CO_2$ reaction. Our work in 2005 on this system generated the CH_3OCO radical intermediate dispersed by internal energy and probed the branching between the CH_3O + CO and the $CH_3 + CO_2$ product channels. In the past year we continued investigating this system to both better characterize the photolytic precursor for the CH_3OCO radical, and, more importantly, develop an understanding from first principle quantum mechanics to understand why the barrier to the $CH_3 + CO_2$ channel from the cis conformer of the radical is 20 kcal/mol lower than that from the trans conformer. The results have important implications for the kinetic modeling of oxygenated fuels. They also suggest a paradigm for predicting the influence of stereoelectronic effects on the energetic barriers to fission of bonds beta to a radical center.

Section B describes our work in the past year on one of the key radical intermediates of the O + allyl reaction. This work includes velocity map imaging to characterize the internal energy distribution of the nascent H_2CCHCH_2O radical intermediates and extensive studies of the product channels formed from this radical intermediate. Most of the latter work was done on a molecular beam scattering apparatus with tunable VUV photoionization of the products at the National Synchrotron Radiation Research Center in Taiwan in collaboration with Prof. Jim Lin.

A. Electronic Interactions along the $CH_3OCO \rightarrow CH_3 + CO_2$ Reaction Coordinate

The methoxycarbonyl radical is key to the chemical kinetic modeling of the effects of oxygenated hydrocarbons on soot emissions from diesel engines (C. K. Westbrook, W. J. Pitz, H. J. Curran, J. Phys. Chem. A. 110, 6912-6922 (2006)). Our abstract last year described our prior work[3] on the CH_3OCO radical intermediate of the $CH_3O + CO \rightarrow CH_3 + CO_2$ reaction, in which we investigated the dynamics of this reaction by initiating the reaction from the CH_3OCO radical intermediate. The internal energies of the ground state radicals produced in our experiments allowed access to the low barrier $CH_3O + CO$ entrance channel of the bimolecular reaction and the exothermic $CH_3 + CO_2$ product channel of the bimolecular reaction, which was predicted to have a higher barrier in several early theoretical papers. An RRKM estimate of the product branching averaged over our ground state radical's internal energy distribution predicted a product branching of $CH_3O + CO$: $CH_3 + CO_2$ of 280:1 using the barrier energies predicted by B. Wang et al. (B. Wang, H. Hou, and Y. Gu, J. Phys. Chem. A 103, 8021-8029 (1999)). The $CH_3 + CO_2$ channel was also predicted to be the minor one using the early QCISD(T) predictions for the barrier energies and transition state frequencies of Francisco and coworkers. To test these theoretical predictions, our work probed the product channel branching from the ground electronic state CH_3OCO radicals (the photolytic precursor also forms some excited state radicals) using photoionization detection of the CH_3O and CO and the CH_3 and CO_2 products (the entrance and exit channels of the bimolecular reaction). Our measured product channel branching from the CO and CO_2 signal was 1.0 : 2.5 (+/-0.5), in dramatic disagreement with the theoretically predicted $CH_3O + CO$: $CH_3 + CO_2$ ratio of 280:1; the $CH_3 + CO_2$ products are the major products rather than the minor channel. Our CCSD(T) calculations resolved the discrepancy; they show that the reaction proceeds by isomerization of the trans- CH_3OCO radical to the cis- conformer, which can then dissociate via a much lower energy cis- transition state to produce the $CH_3 + CO_2$ products. Using the transition state calculated for this alternate path gives a theoretical prediction in good agreement with experiment. Our results are consistent with the recent work of Glaude et al. (Proc. Combust. Inst. 30, 1111 (2005)) which studied the chemical kinetics of dimethyl carbonate, a compound of interest as an oxygenate additive for diesel fuel, and with theoretical work of Good and Francisco (J. Phys. Chem. A 104, 1171 (2000)) reporting a lower transition state for the $CH_3OCO \rightarrow CH_3 + CO_2$ product channel than in the prior work from that group.

In our work this year[5] we sought to come to an understanding of the dramatic difference between the dissociation barriers for the trans- versus the cis-CH_3OCO conformers. Our experimental work in Publication 3 had definitively shown that the very large branching to the $CH_3 + CO_2$ channel was due to the fact that the cis- conformer can dissociate via a much lower energy transition state to produce the $CH_3 + CO_2$, about 20 kcal/mol lower than the trans-barrier. Yet the two conformers of the radical at equilibrium geometry only differ by 0.2 kcal/mol! What makes it easier to stretch the H_3C-O bond in one conformer but not the other? They both are heading toward identical products, it is only along the reaction

coordinate that the energetics is much lower for the cis-geometry transition state. Publication 5 below includes a natural bond orbital analysis along the $CH_3OCO \rightarrow CH_3 + CO_2$ reaction coordinate. Qualitatively, as the C-O bond stretches, the $\sigma^*(H_3C\text{-}O)$ orbital is lowered in energy, approaching the nonbonding carbon n(C) radical orbital energy. Then, in the cis conformer where the spatial overlap between the two is substantial (see figure below), these orbitals can constructively interfere and produce a lower energy linear combination orbital. Thus, the radical electron is in an orbital of substantially lower energy in the cis-conformer near the transition state, and the cis barrier is thus much lower than the trans barrier.

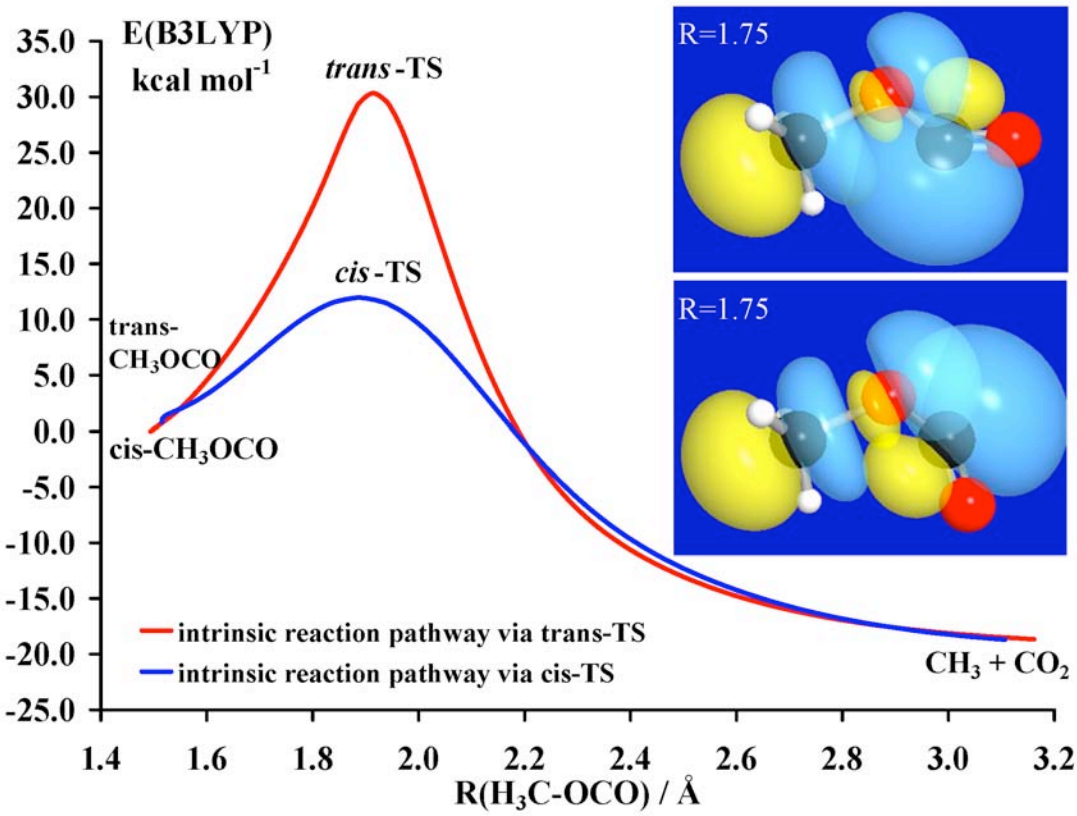

I expect this stereoelectronic preference along a bond fission reaction coordinate is quite general, leading to the lowering of the dissociation barrier for the cleavage of bonds beta to a radical center (or atom with a nonbonding pair) if the σ^* orbital of the breaking bond overlaps with the nonbonding orbital.

B. The H_2CCHCH_2O Radical Intermediate of the $O(^3P)$ + Allyl Reaction

Our new experiments on a key radical intermediate of the O + allyl reaction include 1) molecular beam scattering and velocity map imaging experiments to characterize the photofragmentation channels of the radical's photolytic precursor, epichlorohydrin, and the internal energy distribution of the nascent H_2CCHCH_2O radicals, and 2) molecular beam scattering measurements of the products formed from these radical intermediates, detecting them with tunable VUV ionization at the NSRRC beamline. The data on the photolytic precursor evidence two C-Cl bond fission channels of epichlorohydrin, one that produces nascent radical intermediates with internal energies ranging from about 25 to 50 kcal/mol (relative to the zero-point-level of the O-bridged intermediate (INT2) in the figure below)

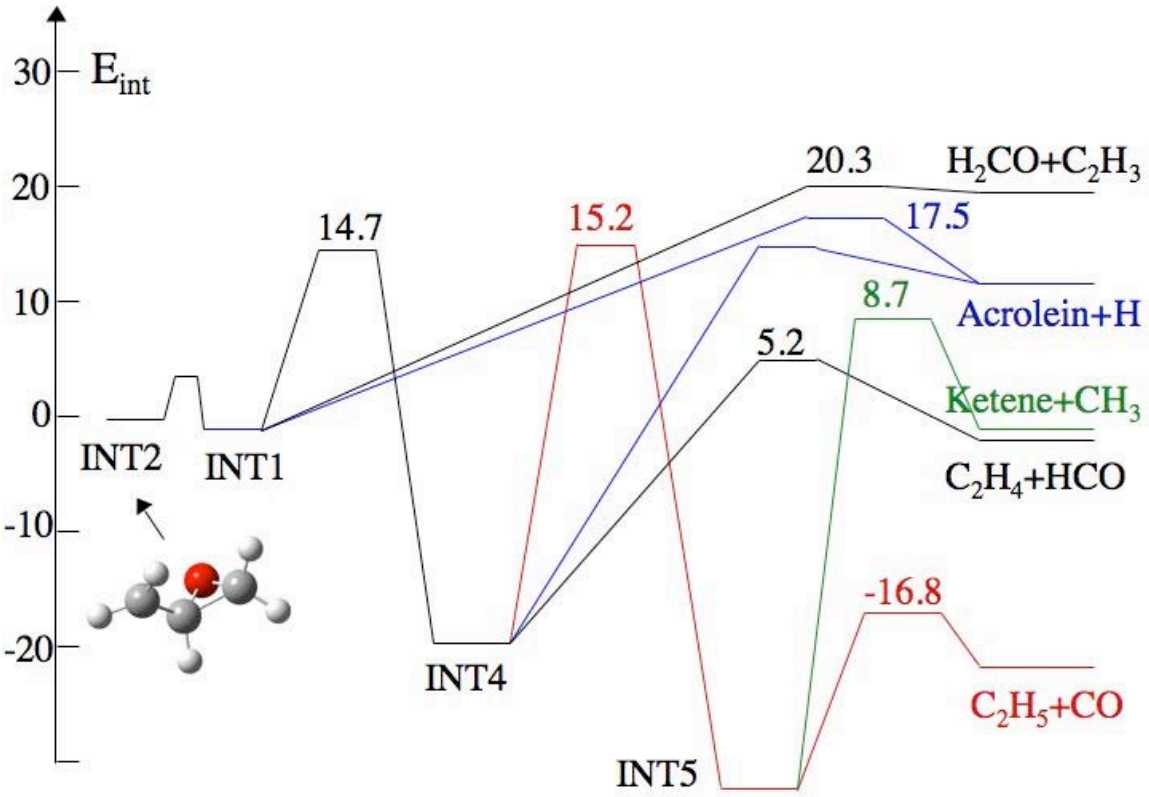

(The energetics shown are from the CBS-QB3 calculations of Park et al, J. Chem. Phys. 119, 8966 (2003)) and a second minor channel which produces electronically excited radicals. The product velocity distributions indicate that the ground state radicals give predominantly H + acrolein products, while the excited state radicals branch to $H_2CO + C_2H_3$, ketene + CH_3, and C_2H_4 + HCO, but not C_2H_5 + CO or H + acrolein. We are embroiled in the data analysis, which is complicated by daughter fragmentation even at the low photoionization energies used.

IV. Publications Acknowledging DE-FG02-92ER14305 (2005 or later)

1. Probing the barrier for $CH_2CHCO \rightarrow CH_2CH + CO$ by the velocity map imaging method, K. -C. Lau, Y. Liu and L. J. Butler, J. Chem. Phys. 123, 054322 (2005).
2. The photodissociation of propargyl chloride at 193 nm, L. R. McCunn, D. I. G. Bennett, L. J. Butler, H. Fan, F. Aguirre, and S. T. Pratt, J. Phys. Chem. A 110, 843-850 (2006).
3. Unimolecular dissociation of the CH_3OCO radical: An intermediate in the CH_3O + CO reaction, L. R. McCunn, K. –C. Lau, M. J. Krisch, L. J. Butler, J. – W. Tsung, and J. J. Lin, J. Phys. Chem. A 110, 1625-1634 (2006).
4. Unimolecular dissociation of the propargyl radical intermediate of the CH + C_2H_2 reaction, L. R. McCunn, B. L. FitzPatrick, M. J. Krisch, L. J. Butler, C. -W. Liang, and J. J. Lin, J. Chem. Phys. 125, 133306 (2006).
5. Characterization of the Methoxy Carbonyl Radical Formed via Photolysis of Methyl Chloroformate at 193.3 nm, M. J. Bell, K.-C. Lau, M. J. Krisch, D. I. G. Bennett, L. J. Butler and F. Weinhold, J. Phys. Chem. A, 111, 1762-1770 (2007).

Production and Study of Ultra-cold Molecules Produced by Kinematic Cooling

David W. Chandler
Combustion Research Facility
Sandia National Laboratory
Livermore, CA 94551-0969
Email:chand@sandia.gov

Program Scope

The goal of this program is to develop new tools for the study of gas phase chemical dynamics and to use them to study the dynamics of fundamental collisional processes. The processes we have studied in the past include inter- and intra- molecular energy transfer, photodissociation dynamics and reactive scattering. The primary tool we use to study these processes has been Ion Imaging. Ion Imaging is a technique for the measurement of the velocity (speed and direction) of a laser-produced ion. As such it extends and enhances the sensitivity of Resonant Enhanced Multi-Photon Ionization (REMPI) detection of molecules and atoms. We have been using Ion Imaging to study a new method for the production of ultra-cold molecules, kinematic cooling. We continue to develop the kinematic cooling technique for the production of samples of ultra-cold molecules and their use in the study of collisional processes. We also are studying half collisions that are sensitive to the long range part of the potential energy surface by the study of photodissociation of small molecules and clusters near threshold. In the future we are extending the kinematic cooling technique to the trapping and cooling molecules in a Magneto Optical Trap (MOT) for the purpose of collisional studies.

Background and Recent Progress

The cooling of atoms to ultra-cold temperatures (microKelvin to nanoKelvin) has resulted in spectacular discoveries such as the realization and study of new states of matter that include Bose Einstein Condensates, Bardeen-Cooper-Schrieffer (BCS) gasses and degenerate Fermi gasses. The production of ultra-cold atoms has enabled ultra-high resolution spectroscopy studies leading to more precise atomic clocks, the most accurate determination of the energy of the highest bound vibrational levels in diatomic wells, along with such things as the development of gravity gradient detectors and the production of matter-wave lasers. All of these areas of research have molecular analogues that can be explored when methods for achieving molecules at ultra-cold temperatures are developed. Furthermore, the added complexity of molecules including, permanent dipoles and quadrupole moments, complex rotational and vibrational structure and chemistry, offer rich areas of unexplored scientific investigation and possible new sorts of measurements (i.e. dipole moment of the electron and studies of quantum entanglement) and devices (i.e. quantum computers) in the future. All of these areas have remained unexplored due to the inability to routinely make ultra-cold samples of molecules. The cooling and trapping of molecules has proven more difficult than cooling and trapping of atoms because the electronic structure of even the simplest molecules renders laser cooling ineffectual. We have demonstrated a unique technique for formation of milli-Kelvin temperature molecules based on our own fundamental research in molecular collision dynamics.

My research focuses on the field of chemical dynamics of gas phase molecular species. Our interest is to study collisions at very low collision energies in an effort to learn about the long range potential between the atoms and molecules. At low energies the deBroglie wavelengths of the particles grow to be much larger than their hard-sphere collision

diameter and understanding the coupling between collision partners at long range is what we hope to uncover. These collisions are important for many practical reasons, for instance collisions that change the quantum state of a molecule, by a reorienting collision, can take a trapped molecule and allow it to escape a magnetic or electrostatic trap. Collisions that exchange translational energy but do not change internal quantum state of the molecules will contribute to the thermalization of a sample of molecules in a trap. Our immediate goal is to trap some of the cold molecules. We have demonstrated we are capable of producing and measuring their lifetime in a trap as a function of density and well depth of the trap. Here we report on the progress we have made toward this goal.

Our collisional cooling method[1,2] does not rely on any specific physical property of either colliding species except their masses, because production of a zero velocity sample is a consequence of the experimentally selectable energy and momenta of the collision pair. Moreover, this technique can be used to prepare a single, selectable ro-vibronic quantum state for trapping. We first demonstrated this technique using inelastic collisions between NO molecules in one beam and Ar in the other, specifically $NO(^2\Pi_{1/2},j=0.5) + Ar \rightarrow NO(^2\Pi_{1/2},j'=7.5) + Ar$. Using the Ion Imaging technique for measuring the velocity distribution, we measured scattered $NO(^2\Pi_{1/2},j'=7.5)$ with a velocity distribution that is centred about zero, with an upper limit root-mean-square (rms) velocity of 15 m s^{-1}.

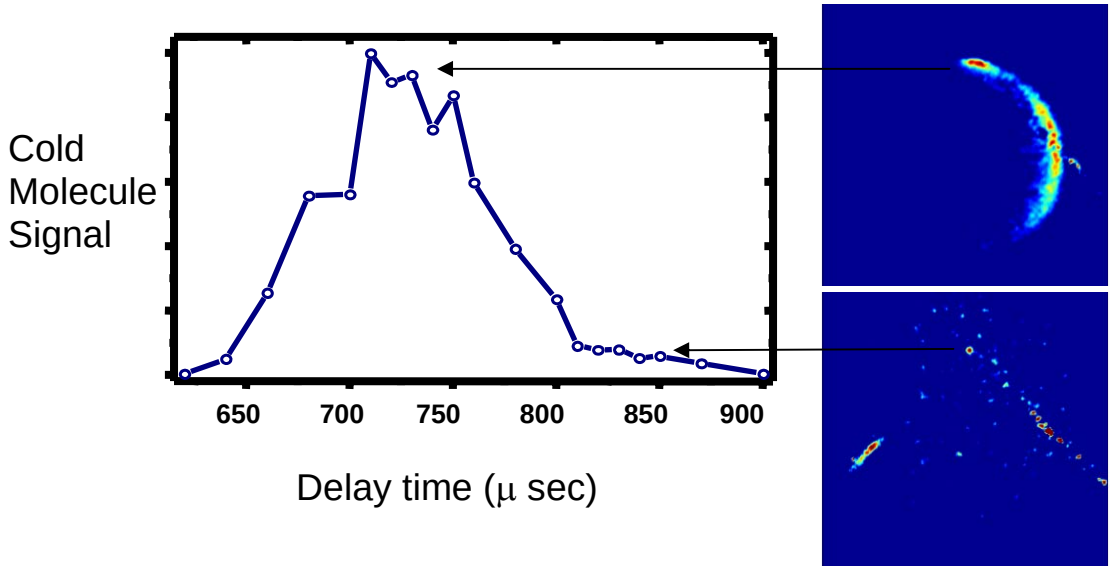

The largest hurdle to trapping molecules produced by this collisional cooling technique is that the molecules that are slowed are stopped (upper image Fig. 1) at the intersection of the two molecular beams. These slow molecules are then collided with and removed by the effusive molecular beam that follows the supersonic beam. We have worked hard to develop experimental condition such that the cold molecules are left in the wake of the atomic and molecular beams. In Figure 1 is shown a plot of the time evolution of the cold molecules as the 120 μsec long molecular beam collides with the atomic beam. We have now been able to have cold molecules live for longer than 100 microsecond after the beams have been turned off (lower image of Fig. 1). It should be now possible to trap these molecules. From measuring the "fly out" time of the ultra-cold molecules from the laser beams we estimate the mean velocity of the NO to be about 4.5 m/s corresponding to a temperature of roughly 40 milli-Kelvin.

In a separate group of experiments we are studying the near threshold dissociation of the NO-Ar complex. The NO-Ar cluster forms a T-shaped cluster with a well depth of about 88 cm^{-1}, which will dissociate when excited by light at slightly higher energy than the NO (A-X) transitions at 226 nm. The dissociation products are NO (A) and an Ar atom. In the past we[3], and others, have studied the rotational distribution obtained when this cluster is dissociated at several energies above the threshold for dissociation (44290 cm^{-1}). In 1993 the group of Tsuji, Shibuya and Obi[4] published a paper where they state-selectively monitored the A state NO dissociation products by using resonant ionization through the E state of NO. As the NO (A) state has a lifetime of about 80 nanoseconds it is possible to monitor the nascent distribution of NO formed in the dissociation by this resonant ionisation scheme. They reported observing broad resonances near threshold when monitoring the NO (A, J=0,1,2,3) states. A spectrum we recorded of these resonances is shown in Figure 2. These resonances were assigned to tunnelling resonances of the NO (A) state and a barrier to dissociation of approximately 25 cm^{-1} was postulated for the cluster at the NO (A) state asymptote. The problem is that if one does a simplified calculation of the tunnelling probability of an NO molecule through a 25 cm^{-1} high barrier 1 angstrom wide one finds the probability to be on the order of 10^{-14}, corresponding to a lifetime of seconds, yet dissociation must take place on a nanosecond time scale for the products to be observed in the experiment. The nature of these resonances is what we wish to explore. We have measured action spectra, the recoil energy of the products, the alignment of the NO products, and the time evolution of the products. In figure 2 are two images taken using resonant ionization to select a particular state of the NO (A) product. They were taken with a 10 nanosecond time delay between the excitation laser and the probe (ionisation) laser.

Spectrum and Images of NO (A) recoil
after NO-Ar dissociation at 44316.5 cm^{-1}

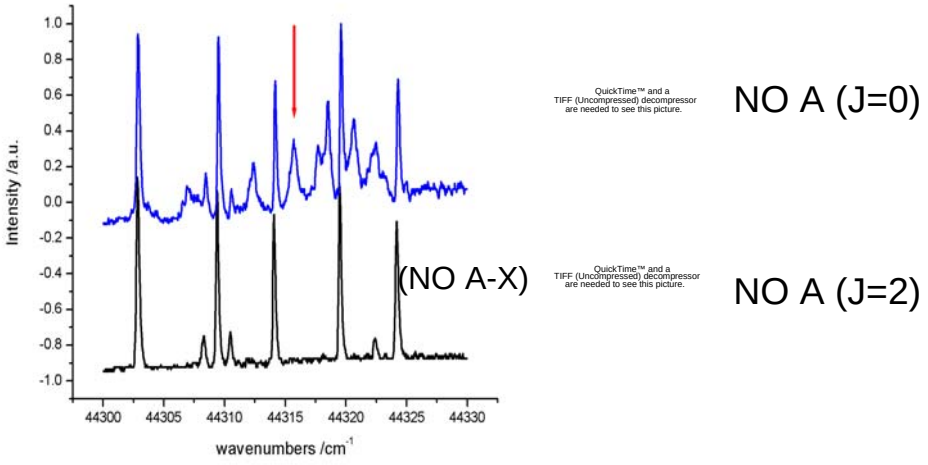

Future studies

The kinematic cooling in a MOT technique involves the formation of ultra-cold atoms by the well-established techniques of laser cooling and trapping in a magnetic field. Once a cloud of cold atoms is formed then the cloud will be exposed to molecules of the same (or nearly identical) mass. Some of the collisions between the atoms and the molecule will lead to a displacement of the atom from the cloud and the deposition of the molecule in its place. These molecules will then be trapped by external electric and magnetic fields. In

order for this process to work the mass difference between the atom and molecule must be small, reactive collisions between the atoms and molecules must be minimized, a suitable trap for the cooled molecule must be built and the ultra-cold molecules sensitively detected. This idea is unique and will require significant development to be successful. Items such as design of a molecular trap, determination of parameters for production of a dense ultra-cold atomic cloud, and sensitive and selective detection of ultra-cold molecules must be optimized. The objective is to build this first-of-a-kind apparatus and demonstrate the ability to produce samples of microKelvin temperature molecules and utilize them for study of collision dynamics at these low energies.

The field of ultra-cold-molecule physical chemistry is in its infancy. To be able to utilize cold molecules for collisional studies as proposed here as well as the study of stereochemistry, photochemistry, high resolution spectroscopy, molecular optics, entangled states, tunneling barriers, Feschbach resonances and a host of other possible research areas a robust and reliable manner to produce ultra-cold molecules must be developed. To imagine the potential impact of such a development one needs only to think of the impact of other technologies for cooling molecules and controlling the velocity of molecules: supersonic molecular beams, liquid helium droplet production, or the impact ultra-cold atom production has had on the Atomic Physics community. This is the science what we are interested in pursuing. As the first step along this path one must learn to reliably produce samples of ultra-cold molecules and accurately characterize those sources.

References:

1) *Subkelvin Cooling NO Molecules via "Billiard-Like" Collisions with Argon*. Elioff, MS; Valentini, JJ; Chandler, DW. Science; vol.302, no.5652, p.1940-3, (2003).

2) *Formation of NO(j '=7.5) Molecules with Sub-Kelvin Translational Energy via Molecular Beam Collisions with Argon Using the Technique of Molecular Cooling by Inelastic Collisional Energy-Transfer*. Elioff MS, Valentini JJ, Chandler DW, Euro. Phys. J. D, 31 (2): 385-393 (2004).

3) *Photodissociation Dynamics of ArNO Clusters*. Parsons BF, Chandler DW, Sklute EC, Li SL, Wade EA, J. Phys. Chem A. 108 (45): 9742-9749 (2004).

4) *Bound-Bound A-x transitions of NO-Ar van der Waals Complexes*, Tsuji K, Shibuya K and Obi K, J. Chem. Phys., 100(8):5443-5447 (1994).

Publications For: 2005 and 2006

1) *Probing Spin-Orbit Quenching in Cl(2P)+H2 via Crossed Molecular Beam Scattering*. Parsons B, Strecker K, Chandler DW, European Physical Journal D, 38(1): 2985-2989 (2006).

2) *Differential Cross Sections for Collisions of Hexapole State-Selected NO with He.* Gijsbertsen A, Linnartz H, Rus G, Wiskerke AE, Stolte S, Chandler DW, Klos J J. Chem. Phys. 123 (22): Art. No. 224305 (2005).

3) *Simultaneous Time- and Wavelength-Resolved Fluorescence Microscopy of Single Molecules.* Luong AK, Gradinaru GC, Chandler DW, Hayden CC, J. Phys. Chem. B. 109 (33): 15691-15698 (2005).

4) *An Investigation of Nonadiabatic Interactions in Cl(P-2(j))+D-2 via Crossed-Molecular-Beam Scattering*, Parsons BF, Chandler DW, J. Chem.. Phys. 122 (17): Art. No. 174306 (2005).

5) *Modification of the velocity distribution of H-2 molecules in a supersonic beam by intense pulsed optical gradients*, Ramirez-Serrano J, Strecker KE, Chandler DW Phys. Chem. Chem. Phys. 8 (25): 2985-2989 JUL 7 2006

6) *Inelastic Energy Transfer: The NO-Rare-Gas System*, D. W. Chandler and S. Stolte, Chapter in Chemical Dynamics, Research Signpost, India. (2007).

Terascale Direct Numerical Simulation and Modeling of Turbulent Combustion

Jacqueline H. Chen (PI**)**, Evatt R. Hawkes[1], Ramanan Sankaran[2], David Lignell, and Chun Sang Yoo
Sandia National Laboratories, Livermore, California 94551-0969
Email: **jhchen@sandia.gov**

Program Scope

In this research program we have developed and applied massively parallel three-dimensional direct numerical simulation **(**DNS) of building-block, laboratory scale flows that reveal fundamental turbulence-chemistry interactions in combustion. The simulation benchmarks are designed to expose and emphasize the role of particular physical subprocesses in turbulent combustion. The simulations address fundamental science issues associated with chemistry-turbulence interactions that underlie all practical combustion devices: extinction and reignition, flame propagation and structure, flame stabilization in autoignitive flows, autoignition under homogeneous charge compression ignition (HCCI) environments, and differential transport of soot in turbulent jet flames. In addition to the new understanding provided by these simulations, the resultant data are being used to develop and validate predictive models required in engineering simulations.

Recent Progress

In the past year, significant computer allocations from a 2007 DOE Innovative and Novel Computational Impact on Theory and Experiment (INCITE) grant and from a 2006 Leadership Computing Facility grant have enabled us to perform terascale three-dimensional direct numerical simulations of turbulent flames with detailed chemistry. These studies focused on understanding: 1) extinction and reignition in turbulent CO/H_2 jet flames; 2) the influence of intense turbulence on the structure of lean premixed methane-air turbulent flames; 3) the preferential diffusion of soot in a turbulent sooting ethylene-air jet flame; and 4) transient ignition of hydrogen/air in an axisymmetric heated counterflow. DNS data are also being used to evaluate and improve combustion models. For example, mixing models required by the transported PDF approach for treating HCCI combustion were evaluated against DNS data with different initial temperature variance. Highlights of our accomplishments in the past year are summarized below, followed by a summary of future research directions.

Extinction and reignition in DNS of CO/H_2 temporal plane jet flames[1]

Massively parallel, three-dimensional direct numerical simulations of temporally evolving turbulent CO/H_2 plane jet flames with up to 500 million grids and Reynolds numbers of 9500 employing a skeletal chemical mechanism were analyzed to shed light on the phenomena of extinction and reignition [1]. A total "extinguished" surface area, defined according to a threshold value of a reacting scalar such as a product or radical species on an iso-mixture fraction surface, was introduced as a marker of the total amount of extinction. Use of this marker led naturally to the consideration of the motion of the flame-edges that separate areas above and below the threshold. Analysis of the behavior of the joint pdf of the edge flame speed and scalar dissipation rate showed a transition in character that has not previously been observed. At early times, during extinction, the edge flame speed revealed a strong negative correlation with scalar dissipation rate, as previously found [2], but during reignition the speed becomes positively correlated with scalar dissipation at low and intermediate scalar dissipation rates, and becomes negatively correlated only at extreme dissipation rates. The result is that the peak reignition rate occurs at a moderately high dissipation rate. We use evidence of the alignment of the normal vectors to the mixture-fraction and reacting scalar isosurfaces to show that these high reignition rates tend to occur where heat and radicals are being supplied normal to the flame surface, as turbulent straining brings burning and non-burning sections of the flame surface into close proximity. We also find that simultaneous reignition can occur by propagation of edge flames along the stoichiometric surface in regions of low scalar dissipation rate. However the propagation rates of these structures are significantly lower and we find the scenario of reignition by "turbulent folding" to be dominant. Work is in progress to assess the effect of our assumptions on the results – namely, the choice of mixture fraction isosurfaces, the choice of reacting

[1] Present address: U. New South Wales, Sydney, AU, evatthawkes@gmail.com
[2] Present address: NCCS/ORNL, sankaranr@ornl.gov

scalar and its threshold value. We are also investigating the influence of Reynolds number and differential diffusion on the findings.

DNS of stationary lean premixed methane-air flames under intense turbulence[3]

There is strong interest in achieving lean premixed combustion in practical applications due to high thermal efficiencies and low NO_x emissions. Because lean flames are thicker and propagate more slowly, these devices operate in the thin reaction zones regime, where intense turbulence can penetrate the broader preheat zone of the flame, but presumably not the reaction zone. There have been contradictory experimental results in this regime, with some reporting thinner flames and others reporting thicker flames. To understand the influence of turbulence on the structure of the preheat and reaction zones, we performed direct numerical simulation of a three-dimensional turbulent slot Bunsen flame at different turbulence intensities. The simulations were performed using a reduced methane-air chemical mechanism which was specifically tailored for the lean premixed conditions simulated here [3]. The turbulence characteristics at the jet inflow were selected such that combustion occurs in the thin reaction zones (TRZ) regime. The simulations span the TRZ between the corrugated flamelet and the broken reaction zones regimes. The data were analyzed to understand the effect of turbulent stirring on the flame structure and thickness. Using statistical measures, it was found that turbulence thickens the preheat layer of the flame. However beyond a certain level, further increase in turbulence intensity does not alter the mean thickness of the flame. A higher probability of flame interaction and annihilation at the higher turbulence intensities is a possible reason for the observed saturation in thickness as the turbulence intensity is increased beyond a certain level. The structure of the preheat and reaction zones were analyzed by obtaining mean reaction rates (fuel consumption, heat release, OH reaction rates) and progress variable conditional on a distance function defined such that at every point in the computational domain it is the shortest normal distance from the flame surface. The results show that although the preheat layer is thickened on average by as much as 30%, there is no influence of small scale mixing on the reaction zones and they remain unperturbed for all of the cases considered. This is attributed to the attenuation of the small scale turbulence through the preheat zone due to heat release.

DNS of transient ignition of diluted hydrogen versus heated air in axisymmetric counterflow[4]

In a previous study [5], the transient characteristics of ignition of hydrogen diluted by nitrogen versus heated air in axisymmetric counterflow were studied both experimentally and numerically. From the experiments, a high degree of OH overshoot was observed during ignition. However, 1–D computational results did not capture the degree of OH overshoot measured in the experiments, and it was hypothesized that multi-dimensional effects on edge flames may account for the discrepancy between the computation and experiment. The sensitivity of super-equilibrium OH to the initial width and amplitude of the O-atom deposition has been investigated using DNS in a two-dimensional axisymmetric counterflow configuration. The simulations show that the spatial distribution and the magnitude of the OH overshoot are indeed governed by multi-dimensional effects. The degree of OH overshoot increases as the diameter of the initial O-atom deposition region decreases. This result is attributed to preferential diffusion of hydrogen in the highly curved flame leading to enhanced reaction rates. The curvature effects originate not only from the leading portion of the edge flame, but also from the radial extent of the initial ignition kernel. As expected, the ignition delay decreases as the amplitude of the initial O-atom deposition increases. However, the degree of OH overshoot decreases with increasing amplitude due to initial transients in establishing a steady edge flame. For the present highly diluted hydrogen mixture, it is found that the structure of the resulting diffusion flame corresponds to Liñán's 'premixed flame regime' and thus, the flame resides towards the heated oxidizer stream. The curved topology of the edge flame structure resulting from thermal runaway in the nonpremixed counterflow configuration is attributed to the preference of the ignition front for high temperature regions.

DNS of soot formation and transport in non-premixed turbulent ethylene flames[6]

We have performed direct numerical simulations of two- and three-dimensional turbulent non-premixed ethylene flames with soot formation. A 15 step, 19 species reduced mechanism was used for gas chemistry, with a two-moment, four-step soot model [6]. This represents the first extension of fully

resolved DNS with detailed chemistry and transport to unsteady sooting flames. The purpose of this work has been to examine soot-flame interactions in a multi-dimensional, unsteady configuration. We have shown that the location of soot relative to a flame, as measured by the mixture fraction, has a strong impact on the local concentrations of soot, the rates of soot reaction, and the soot temperatures. Flame curvature is shown to result in flames that move, relative to the fluid, either towards, or away from rich soot formation regions, resulting in soot being essentially convected into or away from the flame and transported in the mixture fraction coordinate. In regions where the flame motion relative to convection is towards the fuel stream, soot is located nearer the flame at higher temperatures, hence having higher reaction rates and radiative heat fluxes. Fluid convection and flame displacement velocity relative to fluid convection are of similar magnitudes while the thermophoretic velocity is five to ten times lower. These results emphasize the importance of both unsteady and multidimensional effects on soot formation and transport in turbulent flames.

Future Plans

Extinction and Reignition in Hydrocarbon Turbulent Jet Flames

As a logical progression of the CO/H_2 jet flame INCITE project, we propose to perform three-dimensional DNS of an ethylene/air temporal jet flame to study the effect of Reynolds number and fuel kinetics on local extinction and re-ignition. These fuels have a narrower reaction layer, higher activation energy, consistent with most hydrocarbon fuels, and therefore, are more likely to exhibit bi-modal PDF behavior and complete local extinction. As in the INCITE simulation, we adopt the temporal jet configuration to facilitate reignition occurring by either autoignition via chemical chain-branching or by flame propagation (either normal or tangential to the stoichiometric surface of the extinguished flame). The goals of this proposed study are to provide new understanding of the dynamics of extinction and reignition in comparison with the CO/H_2 flame, and to provide a numerical benchmark for model development.

Due to the inherent unsteadiness associated with extinction and reignition phenomena we propose to perform in-situ particle and flame element tracking. The Lagrangian statistics thus obtained will provide cumulative time histories encountered by the burning and extinguished fluid parcels, and enable a study of the transient response of the flame to intermittency. We also plan to study the dynamics underlying the evolution of the passive and reactive scalar dissipation rate in relation to the local kinematics of the velocity field.

Soot Formation and Transport in Turbulent Nonpremixed Ethylene Jet Flames

Future directions for DNS of sooting flames center around: (1) simulations of three-dimensional jet flame configurations, (2) increasing the sophistication of the soot models, and (3) evaluating modeling approaches (such as CMC and unsteady flamelets) for sooting flames for LES/RANS implementations that can be applied to practical combustion configurations. We have implemented more complex soot models with three transported moments, closed with an assumed lognormal distribution, as well as a four moment model closed using quadrature schemes. Future plans include implementing detailed HACA-based soot mechanisms in DNS. The DNS evolution of the mixture fraction and soot mass fraction will be used to assess the importance of various terms in a conditional-moment closure (CMC) equation for the evolution of a large-Lewis number scalar, soot. Of particular interest are terms involving differential diffusion and its correlation with the soot mass fraction. In collaboration with Alan Kerstein, a new spatially-evolving formulation of One-Dimensional Turbulence (ODT) will be evaluated using the DNS data, especially in light of incorporating multi-dimensional effects.

Stabilization of Lifted Turbulent Hydrogen/Air Jet Flames in an Ignitive Coflow

In many modern combustion systems such as diesel engines and gas turbines, fuel is injected into an environment of hot gases, and a flame may be stabilized through the recirculation of hot air and combustion products. Under such conditions, this leads to a turbulent lifted flame, and the hot environment admits the possibility of autoignition as a mechanism of stabilization of the flame base. In addition to autoignition, edge flame propagation has been considered as a competing mechanism for stabilization. The first three-dimensional DNS of a lifted nonpremixed turbulent hydrogen/air jet flame

issuing into a vitiated coflow of heated air have been performed at a Reynolds number of 12000. A parametric study will be performed, varying the temperature of the coflow. The DNS data will be analyzed to evaluate competing theories for flame stabilization.

Transient Extinction/Reignition with NO Addition in Axisymmetric Counterflow

We propose to perform the companion simulations to a recent experiment by Jonathan Frank and coworkers of a hydrogen flame-vortex interaction in an axisymmetric counterflow. This configuration enables the study of transient re-ignition mechanisms following local quenching induced by an impulsively driven vortex pair into a hydrogen nonpremixed flame supported by heated air. This is a repeatable, canonical configuration that provides detailed information on the dynamics of re-ignition observed in a more complex, turbulent jet flame undergoing extinction and reignition. We propose to perform DNS in the same configuration to understand the detailed coupling between ignition and flame kinetics and transport during the extinction and reignition processes. The computations will be used to determine parametric dependencies affecting the boundaries of an experimentally determined regime diagram for reignition. The diagram delineates the regimes between autoignition versus edge flame propagation as competing mechanisms for reignition as a function of oxidizer temperature, fuel stream composition, and strain rate. Furthermore, to enhance the autoignition mechanism, a small amount of NO was introduced into the oxidizer stream, since NO_x is known to have a catalytic effect on ignition. In the future, other additives will also be considered. The computations will also be used to understand the coupling of transport and key reactions associated with fuel additives, e.g. the NO catalytic effect, during extinction and reignition.

References:

1. E. R. Hawkes, R. Sankaran, and J. H. Chen, "Extinction and reignition in DNS of CO/H_2 temporal plane jet flames," 5th US Combustion Joint Sections Meeting, 2007, Paper B05.
2. C. Pantano, J. Fluid Mech. 514: 231-70 (2004).
3. R. Sankaran, E. Hawkes, C. Yoo, J. Chen, T. Lu and C. Law, "DNS of stationary lean premixed methane-air flames under intense turbulence," 5th US Combustion Joint Sections Meeting, 2007, Paper B09.
4. C. S. Yoo, J. H. Chen, and J. H. Frank, "DNS of transient ignition of diluted hydrogen versus heated air in axisymmetric counterflow," 5th US Combustion Joint Sections Meeting, 2007, Paper A01.
5. R. Seiser, J. H. Frank, S. Liu, J. H. Chen, R. J. Sigurdsson, K. Seshadri, *Proc. Combust. Inst.* 30 (2005) 423
6. D. Lignell, J. H. Chen, P. J. Smith, T. Lu and C. K. Law, "The effect of flame structure on soot formation and transport in turbulent nonpremixed flames using DNS," submitted to *Combust. Flame* (2006).

BES Publications (2005-2007)

1. E. R. Hawkes and J. H. Chen, "Comparison of Direct Numerical Simulations of Lean Premixed Methane-Air Flames with Strained Laminar Flame Calculations," *Combust. Flame*, **144**: 112-125. (2005).
2. J. C. Sutherland, P. J. Smith, and J. H. Chen, "Quantification of Differential Diffusion in Nonpremixed Systems," *Combust. Theory and Modelling*, **9:2,** pp. 365-383. (2005).
3. J. H. Chen, E. R. Hawkes, R. Sankaran, S. D. Mason, and H. G. Im, "DNS of Ignition Front Propagation in a Constant Volume With Temperature Inhomogeneities, Part I: Fundamental Analysis and Diagnostics,"*Combust. Flame*, **145**: 128-144. (2006).
4. E. R. Hawkes, R. Sankaran, P. Pebay, and J. H. Chen, "DNS of Ignition Front Propagation in a Constant Volume With Temperature Inhomogeneities, Part II: Parametric Study", *Combust. Flame*, **145**: 145. (2006).
5. S. Liu, J. C. Hewson, and J. H. Chen, "Nonpremixed *n*-heptane autoignition in unsteady counterflow, " *Combust. Flame*, **145**: 730-739, (2006).
6. R. Sankaran, E. R. Hawkes, J. H. Chen, T. Lu, and C. K. Law, "Structure of a Spatially-Developing Lean Methane-Air Turbulent Bunsen Flame," *Proceedings of the Combustion Institute*, **31**:1291-1298, (2007).
7. E. Hawkes, R. Sankaran, J. Sutherland, and J. H. Chen, "Scalar Mixing in DNS of Temporally-Evolving Plane Jet Flames with Detailed CO/H2 Kinetics," *Proc. of the Combustion Institute*, **31**:1633-1640, (2007).
8. D. J. Cook, H. Pitsch, J. H. Chen, and E. R. Hawkes, "Flamelet-Based Modeling of Autoignition with Thermal Inhomogeneities for Application to HCCI Engines," *Proceedings of the Combustion Institute*, **31**: 2903-2911, (2007).
9. J. C. Sutherland, P. J. Smith, and J. H. Chen, "A quantitative method for apriori evaluation of combustion reaction models," *Combust. Theory and Modelling*, **11**, 287-303, (2007).
10. D. Lignell, J. H. Chen, P. J. Smith, T. Lu and C. K. Law, "The effect of flame structure on soot formation and transport in turbulent nonpremixed flames using DNS," submitted to *Combust. Flame* (2006).

Dynamics and Energetics of Elementary Combustion Reactions and Transient Species
Grant DE-FG03-98ER14879

Robert E. Continetti
Department of Chemistry and Biochemistry
University of California San Diego
9500 Gilman Drive
La Jolla, CA 92093-0340
rcontinetti@ucsd.edu

April 6, 2007

Program Scope

This research program focuses on preparing transient neutral species and collision complexes relevant to combustion phenomena, with a focus on intermediates important in hydroxyl radical reactions and oxygenated organic compounds. Information on the energetics and reaction dynamics of these species is critical to evaluating the roles they may play in combustion and the validation of theoretical approaches to predicting the dynamics of combustion reactions. The approach taken to these studies uses photodetachment of precursor anions. The technique of photoelectron-photofragment coincidence (PPC) spectroscopy on a mass-selected negative ion beam allows the preparation of mass- and energy-selected neutral species. The dissociation pathways of unstable neutral products can then be measured using translational spectroscopy. In addition, the employment of large-solid-angle imaging techniques enables measurement of the angular distributions for both the photoelectrons and photofragments, providing further insights into the dissociative photodetachment (DPD) dynamics.

In the past year, three major experimental efforts have been the focus. We extended previous work at a number of wavelengths on studies of the OH + CO → HOCO → H + CO_2 potential by photodetachment of $HOCO^-$, including examination of the DOCO system and threshold photodetachment phenomena. We have also completed a new series of experiments on the OH + F → O + HF reaction by photodetachment of OHF^- at a higher photon energy (5.42 eV, 229 nm), allowing access to the higher energy OH + F product channel. Finally, we have studied the photodetachment of the propanoate anion $CH_3CH_2CO_2^-$ at 258 nm. This anion is found to undergo complete dissociative photodetachment – no stable propanoyloxyl radical $CH_3CH_2CO_2$ was observed. These results are now discussed in more detail.

Recent Progress

1. Probing the OH + CO → HOCO → H + CO_2 reaction by photodetachment of $HOCO^-$

An experimental study of the dissociative photodetachment (DPD) dynamics of $HOCO^-$ and $DOCO^-$ at a photon energy of 3.21 eV was carried out to probe the potential energy surface of the HOCO free radical and the dynamics of the OH + CO → H + CO_2 reaction. These experiments extend our earlier work on this system at a photon energy of 4.80 eV.[1] These photoelectron-photofragment coincidence experiments allow the identification of photodetachment processes leading to the production of stable HOCO free radicals and both the H + CO_2 and OH + CO dissociation channels on the neutral surface, in coincidence with the detached electron. At all wavelengths studied to date, it is found that the H + CO_2 + e^- channel is open below the calculated dissociation barrier,[2] indicating that quantum mechanical tunneling is important for this channel even near the bottom of the HOCO well. These new measurements at

lower photon energies also show that the OH + CO product channel is also observed at and below the calculated energetic limit. In this case, tunneling is not possible and the most likely explanation are hot bands in the $HOCO^-$ anion, assuming the quantum chemical calculations on the energetics of this system are accurate. Isotopic substitution by deuterium in the parent ion is observed to reduce the product branching ratio for the D + CO_2 channel, consistent with tunneling playing a role in this dissociation pathway. These results can be compared with recent six-dimensional quantum dynamics simulations of the DPD of $HOCO^-$ by Gray, Goldfield and co-workers.[3] There is good qualitative agreement with the theory, with the exception of the absence of a significant tunneling in the HOCO → H + CO_2 pathway on the LTSH potential energy surface[4] used in the calculations. Given that this surface was optimized for reproducing kinetic data, and thus has a relatively poor description of the HOCO well and the barrier between the well and the H + CO_2 product channel, this may not be a major surprise. A refined potential energy surface for both the neutral and the parent anion are required for more accurate quantum dynamics predictions. Experimentally, better characterization of the parent anion vibrational temperature is an outstanding question.

Experiments were also carried out near the threshold for photodetachment of $HOCO^-$ at a photon energy of 1.60 eV. Resolved structure corresponding to either bending vibrations or the cis- and trans-$HOCO^-$ isomers was observed. A striking two-photon process was also observed, yielding a very anisotropic photoelectron angular distribution (PAD) consistent with a strong molecular alignment in absorption of the first photon. A quantitative analysis of the PAD reveals this is associated with a temporary anion formed by a *p*-wave shape resonance and the PAD in the two-photon signal is a result of interfering *s*- and *d*-partial waves within the atomic approximation. The extracted intensity and phase shift of the partial waves were found to be consistent with the Wigner threshold law for photodetachment. Use of a continuum resonance for alignment has, to the best of our knowledge, not been observed before. In the case of the two-photon photodetachment of $HOCO^-$, this phenomenon may even provide a route to manipulation of the product channels, since the one- and two-photon photoelectron spectra at 386 and 772 nm, respectively, both encode a photoelectron kinetic energy-dependent product branching ratio.

Finally, the dynamics of the dissociative photodetachment of $HOCO^-$ and $DOCO^-$ were also explored by photoelectron-photofragment angular correlations. Anisotropic photofragment angular distributions were observed in the $HOCO^-/DOCO^-$ + hν → OH/OD + CO + e^- channel. The anisotropy parameters were obtained for the laboratory frame (LF) angular distributions of photoelectrons of all three DPD channels and photofragments OH + CO. Using the photoelectron-photofragment coincident measurement, the photoelectron angular distributions (PAD) were also studied within the photofragment recoil frame (RF). The comparison of LF- and RF-PAD in the OH + CO + e^- channel shows the latter one is more isotropic, indicating that the lifetime of the neutral HOCO free radicals that dissociate into OH + CO is commensurate with the molecular rotational period. The analysis of these angular distributions and the isotope effects observed is ongoing at this time.

2. Photodetachment of OHF^- and the dynamics of the O + HF → OH + F reaction

The O + HF → OH + F system represents a fundamental reaction of the hydroxyl radical that is complicated by the presence of a number of low-lying electronic states, and has become a benchmark for comparison of detailed experiments, *ab initio* calculations and quantum dynamics. The photoelectron spectroscopy measurements of OHF- by Neumark and co-workers[5,6] have prompted extensive theoretical calculations of both the potential energy surfaces and dynamics by Roncero and co-workers,[7,8,9] focusing on non-adiabatic effects on the reaction dynamics on the neutral potential energy surface. Previously, we have carried out photoelectron-photofragment coincidence studies of this system at a photon energy of 4.8 eV (258 nm), (DOE

publication 1 below). In this earlier work, evidence for both vibrationally adiabatic and non-adiabatic processes were seen in the O + HF(v = 1) channel. The calculations of Roncero and co-workers support the presence of non-adiabatic channels and suggest that these are mediated by conical intersections between the $^3\Sigma^-$ and $^3\Pi$ states along the reaction coordinate near the linear configuration.

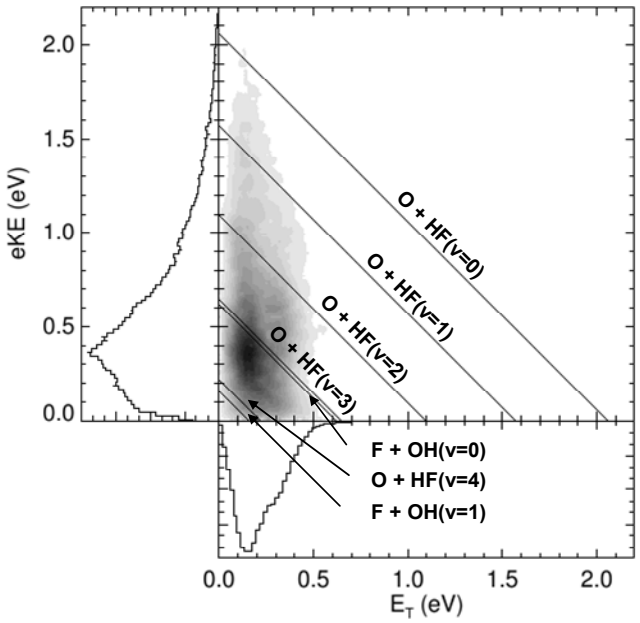

Fig. 1 Photoelectron-photofragment coincidence spectrum of OHF^- at 5.42 eV

In the present experiments, the OHF^- anion was studied at 229 nm (5.42 eV) generated by frequency doubling the output of a kHz 1.8 ps Ti:Sapphire/OPA laser system. With this higher energy photon, the OH + F dissociation channel can be accessed as well, thus accessing total energies on the neutral surface in the vicinity of the transition state for the bimolecular reaction. The coincidence spectrum of OHF^- at 5.42 eV is plotted in Fig. 1. The eKE curve shown here has only a broad structure, but if examined at higher resolution by considering only photoelectrons with small velocity components perpendicular to the detector face, exhibits six identifiable features in agreement with earlier work at 213 nm.[5] The E_T spectrum peaks at ~0.15 eV with a higher energy shoulder at ~0.33 eV. The diagonal lines in the coincidence spectrum represent the onset of the energetically allowed O(^{3}P) + HF(v = 0-4) and, right above the O + HF(v = 3) limit, the OH(v = 0) + F channel. There are two vertical bands representing the two features in the E_T spectrum, consistent with our earlier work at 258 nm. The lower energy band has significant intensity extending to each of the energetic limits, while the higher energy band begins well away from the O + HF(v = 1) limit. This is clear evidence for the role of at least two electronic states channeling distinct repulsive energies into product translation. In addition, the correlation spectrum shows that a significant feature is observed immediately above the opening of the OH + F product channel. Comparison of these results to the predictions of ongoing calculations by Roncero and co-workers should be useful.

3. Stability of oxygenated reactive intermediates: the propanoyloxyl radical $CH_3CH_2CO_2$

Photodetachment studies of the propanoate anion at a photon energy of 4.8 eV have been carried out. The photoelectron spectra are consistent with an electron affinity for the propanoyloxyl radical $CH_3CH_2CO_2$ of approximately 3.4 eV. There is no evidence, however, for the production of the stable radical on the several μs time-scale of these experiments. The smaller acetyloxyl radical CH_3CO_2 was previously found to branch between rapid dissociation and a stable component, so it was unexpected to find this larger radical to be completely dissociative. The radical is found to dissociate to ethyl radical (C_2H_5) + CO_2 products, with a relatively large kinetic energy release peaking at ~ 0.6 eV. The observation that the $CH_3CH_2CO_2$ radical is unstable is of interest, given that propionic acid, $CH_3CH_2CO_2H$ is observed as a product in propane flames.[10] Extension of these studies to larger carboxylate species should allow examination of the stability of a number of oxygenated radicals.

Future plans

In the coming months we are first going to examine further carboxylate anions and their corresponding neutral oxygenated radicals. Extending the precursors beyond the alkyl carboxylic acids to substituted and aromatic acids will allow examination of a range of neutral species that may play a role in combustion phenomena. Extension of our studies of the HOCO system this year will involve examining one- and two-photon interference experiments to see if interference phenomena can be used to affect the overall photoelectron spectrum and product branching ratios in a type of quantum control experiment. The transition state dynamics of hydroxyl radical reactions will continue to be pursued, with efforts to study the OH + H_2 and OH + Cl reactions planned, as well as studying hydroxyl radical reactions with organic species by forming precursor cluster anions such as hydroxide – acetone (OH^-)(CH_3COCH_3) and others. The possible role played by vibrationally excited anions in the $HOCO^-$ experiments indicate that it is essential to consider new approaches to cooling the anions used in these experiments, possibly in a cryogenically cooled ion trap.

DOE Publications: 2005 – Present

1. H.J. Deyerl and R.E. Continetti, "Photoelectron-photofragment coincidence study of OHF^-: transition state dynamics of the reaction OH + F $\rightarrow$ O + HF.", Phys. Chem. / Chem. Phys. **7**, 855-860 (2005).
2. Z. Lu, Q. Hu, J.E. Oakman and R.E. Continetti, "Dynamics on the HOCO potential energy surface studied by dissociative photodetachment of $HOCO^-$ and $DOCO^-$.", J. Chem. Phys. (in press, 2007).
3. Z. Lu and R.E. Continetti, "Alignment of a molecular anion via a shape resonance in near-threshold photodetachment.", Phys. Rev. Lett. (submitted, 2007).

References Cited

1. T.G. Clements, R.E. Continetti and J.S. Francisco, J. Chem. Phys. **117**, 6478 (2002).
2. H.-G. Yu, J.T. Muckerman and T. Sears, Chem. Phys. Lett. **349**, 547 (2001).
3. S. Zhang, D. M. Medvedev, E. M. Goldfield, and S. K. Gray, J. Chem. Phys. **125**, 164312 (2006).
4. M. J. Lakin, D. Troya, G. C. Schatz, and L. B. Harding, J. Chem. Phys. **119**, 5848 (2003).
5. S.E. Bradforth, D.W. Arnold, R.B. Metz, A. Weaver and D.M. Neumark, J. Phys. Chem. **95**, 8066 (1991).
6. D.M. Neumark, Phys. Chem. Chem. Phys. **7**, 433 (2005).
7. L. González-Sánchez, S. Gómez-Carrasco, A. Aguado, M. Paniagua, M. L. Hernández, J. M. Alvariño and O. Roncero, J. Chem. Phys. **121**, 309 (2004). ; S. Gómez-Carrasco, L. González-Sánchez, A. Aguado, O. Roncero, J. M. Alvariño, M. L. Hernández and M. Paniagua, J. Chem. Phys. **121**, 4605 (2004).
8. L González-Sánchez, S Gomez-Carrasco, A. Aguado, M. Paniagua, M. Luz Hernandez, J. M. Alvarino and O. Roncero, J. Chem. Phys. **121**, 9865 (2004).
9. S. Gómez-Carrasco, A. Aguado, M. Paniagua and O. Roncero, J. Chem. Phys. **125**, 164321 (2006).
10. E. Zervas, Environmental Engineering Science **22**, 651 (2005).

Studies of Flame Chemistry with Photoionization Mass Spectrometry

Terrill A. Cool
School of Applied and Engineering Physics
Cornell University, Ithaca, New York 14853
tac13@cornell.edu

Project Scope

Principal themes of our current research are: (1) develop further understanding of the chemical mechanisms that are precursors to the formation of PAH (polycyclic aromatic hydrocarbons) and soot, and (2) study the flame chemistry of oxygenated fuels or fuel additives (dimethyl ether, ethanol, alkyl esters) proposed as clean burning alternatives to conventional liquid hydrocarbon fuels derived from petroleum.

Kinetic model development in all of these reaction systems requires direct measurements of the absolute concentrations of combustion intermediates in laboratory flames chosen to reveal underlying reaction mechanisms. Photoionization mass spectrometry (PIMS) using monochromated synchrotron radiation, applied to the selective detection of flame species, is uniquely suited for the development and testing of kinetic models of combustion chemistry. A flame-sampling PIMS instrument, developed at the Advanced Light Source (ALS) of the Lawrence Berkeley National Laboratory is leading to major advances in the detection of reaction intermediates in laboratory flames and the measurement of their concentrations. These advances yield improved kinetic models for the combustion of the major classes of modern fuels and fuel blends, including biofuels. They also enable measurements of fundamental properties (photoionization cross sections and ionization energies) of selected reaction intermediates. This instrument is the first to use easily tunable vacuum ultraviolet synchrotron radiation for PIMS studies of flame species.

The experiments at the ALS are conducted in a collaborative effort between investigators at the Sandia Combustion Research Facility, Cornell University, Bielefeld University and the University of Massachusetts (Amherst). Kinetic modeling is carried out by Fred Dryer (Princeton University), Charles Westbrook and William Pitz (The Lawrence Livermore National Laboratory), and Phillip Westmoreland (University of Massachusetts).

Recent Progress

Interest is growing in the use of biofuels to reduce the current dependence on conventional fuels derived from petroleum, and to alleviate the harmful effects of global climate change by controlling aerosol formation and decreasing net CO_2 emissions. However, the combustion chemistry of bio-derived fuels is not nearly as well documented as that of hydrocarbon fuels. Accurate information on the fuel decomposition and oxidation mechanisms of several classes of oxygenated fuels including alcohols, ethers and esters are urgently needed to characterize their potential vehicle emission characteristics, which are of paramount significance in the control of airborne toxics.

The influences of fuel-specific destruction pathways on flame chemistry were determined for two isomeric ester fuels, methyl acetate, $CH_3(CO)OCH_3$, and ethyl formate, $H(CO)OC_2H_5$, used as model representatives for biodiesel compounds; their potential for forming air pollutants was also addressed. Measurements of major and intermediate species mole fractions in premixed, laminar flat flames were performed using molecular-beam sampling and isomer-selective VUV-photoionization mass spectrometry. The observed intermediate species concentrations depend crucially on decomposition of the different radicals formed initially from the fuels. The methyl acetate structure leads to preferential formation of formaldehyde, while the ethyl formate isomer favors the production of acetaldehyde. Ethyl formate also yields higher concentrations of the C_2 species (C_2H_2 and C_2H_4) and C_4 species (C_4H_2 and C_4H_4). Benzene concentrations, while larger for ethyl formate, are at least an order of magnitude smaller for both flames than seen for simple hydrocarbon fuels (ethylene, ethane, propene, propane).

Substantial reductions in emissions of PAH and particulates are possible when dimethyl ether is used as a partial or complete replacement for petroleum diesel. Similar reductions result when ethanol is introduced as an additive to conventional gasoline. We have completed experimental studies of the chemistry of (1): stoichiometric and fuel-rich DME/oxygen and ethanol/oxygen flames and (2): fuel mixtures in which the isomeric fuels DME and ethanol are introduced as additives in DME/propene and ethanol/propene flames. These studies were undertaken to provide a mechanistic characterization of the roles of the oxygenate function and fuel structure in reducing the formation of PAH and soot. DME/propene and ethanol/propene mixtures with molar ratios of zero (pure propene), 0.25, 0.50, 0.75 and 1.00 (pure DME or ethanol) were used in a series of fuel-rich flame studies conducted under similar conditions of flame temperature and pressure.

Kinetic modeling and reaction path analyses were completed for a series of the DME/oxygen flames for equivalence ratios ranging from 1.0 to 2.0. The measurements agree well with these flame modeling predictions, using a recently revised high-temperature DME kinetic mechanism. The measurements reveal the presence of ethyl methyl ether, a molecule previously unobserved in flames and not included in present flame models.

Experimental measurements of species mole fraction profiles were also recently completed and analyzed for other fuel-rich flames:

1. The isomeric C_6H_{12} fuels cyclohexane and 1-hexene were studied to examine the influences of their respective fuel structures on flame chemistry.
2. Experimental mole fraction profiles for a fuel-rich cyclopentene flame were obtained for 49 important combustion intermediates with masses ranging from m/z=2 (H_2) to 106 (C_8H_{10}), providing a broad data base for flame modeling studies. The isomeric compositions were resolved for most intermediates, and a new model for cyclopentene flames has been developed based in part on our new data.
3. Quantitative analyses of mole fraction profiles for stoichiometric and fuel-rich toluene flames reveal a large and complex assortment of 46 stable and radical reaction intermediates with m/z values ranging from 15 to 168.

Future Plans

Several papers are in preparation for publication. These include studies of flames of cyclohexane, 1-hexene, propene/ethanol, DME, DME/ethanol, and cyclopentene. A paper reporting absolute photoionization cross sections for 15 key combustion intermediates and a paper reporting measurements and calculations of ionization energies for several higher $C_{2n}H_2$ polyacetylenes and other related polyynes.will soon be submitted for publication.

Much more work is planned on biodiesel fuel surrogates. We have recently completed experimental measurements of species mole fraction profiles for flames of methyl formate and ethyl acetate. Preliminary kinetic modeling is nearing completion on our measurements for the methyl and ethyl formate and methyl and ethyl acetate flames. Preliminary experimental measurements for flames of ethyl and methyl propanoate and ethyl and methyl butanoate are also in progress.

Finally, we will continue our measurements of photoionization cross sections to fill in gaps in our Collaboratory for Multiscale Chemical Systems (CMCS) data repository. Knowledge of absolute photoionization cross sections is required for quantitative measurements of flame species mole fractions. These data are critically needed not just for quantitative analyses, but also because ion fragments of a given mass-to-charge (*m/z*) ratio may interfere with the detection of parent ions with the same *m/z* value. Hence partial photoionization cross sections for many dissociative ionization channels are required for successful strategies for quantitative measurements of flame species composition. In general, as we consider heavier species, the number of isomers becomes larger and the ability to identify species by their ionization thresholds through photoionization efficiency (PIE) measurements becomes critical. A recent example is the successful identification of the 1-butene, 2-butene, and methyl ketene isomers at m/z=56 in a fuel-rich cyclopentene flame.

DOE Publications for 2005-2007

1. C. A. Taatjes, N. Hansen, A. McIlroy, J. A. Miller, J. P. Senosiain, S. J. Klippenstein, F. Qi, L. Sheng, Y. Zhang, T. A. Cool, J. Wang, P. R. Westmoreland, M. E. Law, T. Kasper, K. Kohse-Höinghaus, "Enols are common intermediates in hydrocarbon oxidation", *Science* **309**, 1887-1889, published online May 12, 2005 [DOI: 10.1126/science.1112532] (2005).

2. T. A. Cool, A. McIlroy, F. Qi, P. R. Westmoreland, L. Poisson, D. S. Peterka and M. Ahmed, "A photoionization mass spectrometer for studies of flame chemistry with a synchrotron light source", *Rev. Sci. Instrum.* (2005) **76,** 094102.

3. T. A. Cool, Juan Wang, K. Nakajima, C. A. Taatjes, and A. McIlroy, "Photoionization cross sections for reaction intermediates in hydrocarbon combustion", *Intl J. Mass Spectrom.*, **247** (2005) 18-27.

4. C. A. Taatjes, S. J. Klippenstein, N. Hansen, J. A. Miller, T. A. Cool, J. Wang, M. E. Law, and P. R. Westmoreland, “Synchrotron photoionization measurements of combustion intermediates: photoionization efficiency of C_3H_2 Isomers", *Phys. Chem. Chem. Phys.* **6**, 1-9 (2005).

5. T. A. Cool, K. Nakajima, C. A. Taatjes, A. McIlroy, P. R. Westmoreland, M. E. Law and A. Morel, "Studies of a fuel-rich propane flame with photoionization mass spectrometry" *Proc. Combust. Inst.,* **30**, 1681 (2005).

6. M.E. Law, T. Carriere, P.R. Westmoreland. "Allene addition to a fuel-lean ethylene flat flame," *Proc. Combust. Inst,* **30***,* 1353-1361 (2005).

7. C.A. Taatjes, N. Hansen, J.A. Miller, T.A. Cool, J. Wang, P.R. Westmoreland, M.E. Law, Tina Kasper and K. Kohse-Höinghaus, "Combustion chemistry of enols: possible ethenol precursors in flames", *J. Phys. Chem. A,* **110**, 3254-3260 (2006).

8. P. R. Westmoreland, M.E. Law, T.A. Cool, J. Wang, C.A. Taatjes, N. Hansen, T. Kasper. "Analysis of Flame Structure by Molecular-Beam Mass Spectrometry Using Electron-Impact and Synchrotron-Photon Ionization."
In Russian: *Fizika Goreniya i Vzryva,* **42**(6), 58–63 (November/December 2006).
In English: *Combustion, Explosion and Shock Waves,* **42**(6), 672-677 (2006).

9. N. Hansen, S. J. Klippenstein, C. A. Taatjes, J. A. Miller, J. Wang, Terrill A. Cool, B. Yang, R. Yang, L. Wei, C. Huang, J. Wang, F. Qi, M. E. Law, P. R. Westmoreland, "Identification and Chemistry of C_4H_3 and C_4H_5 Isomers in Fuel-Rich Flames", *J. Phys. Chem. A*, **110** 3670-3678 (2006).

10. N. Hansen, S.J. Klippenstein, J.A. Miller, J. Wang, T.A.Cool, M.E.Law, P.R.Westmoreland, T. Kasper, and K. Kohse-Höinghaus, "Identification of C_5H_x Isomers in fuel-rich flames by photoionization mass spectrometry and electronic structure calculations", *J. Phys. Chem. A*, **110**, 4376-4388 (2006).

11. M. E. Law, P. R. Westmoreland, T. A. Cool, J. Wang, Nils Hansen, Craig A. Taatjes, Tina Kasper and K. Kohse-Höinghaus, "Benzene precursors and formation routes in a stoichiometric cyclohexane flame", *Proc. Combust. Inst.* **31**, 565-573 (2007).

12. K. Kohse-Höinghaus, P. Oßwald, U. Struckmeyer, T. Kasper, N. Hansen, C. A. Taatjes, J. Wang, T. A. Cool, S. Gon, P. R. Westmoreland, "The influence of ethanol addition on a premixed fuel-rich propene-oxygen flame", *Proc. Combust. Inst.* **31**, 1119-1127 (2007).

13. N. Hansen, J. A. Miller, C.A. Taatjes, J. Wang, T. A. Cool, M.E. Law, P.R. Westmoreland, T. Kasper, and K. Kohse-Höinghaus, "Photoionization mass spectrometric studies and modeling of fuel-rich allene and propyne flames", *Proc. Combust. Inst.* **31**, 1157-1164 (2007).

14. T. A. Cool, J. Wang, N. Hansen, P. R. Westmoreland, F. L. Dryer, Z. Zhao, A. Kazakov, T. Kasper and K. K.-Höinghaus, "Photoionization mass spectrometry and modeling studies of the chemistry of fuel-rich dimethyl ether flames", *Proc. Combust. Inst.* **31**, 285-293 (2007).

15. N. Hansen, T. Kasper, S. J. Klippenstein, P. A. Westmoreland, M. E. Law, C. A. Taatjes, K. Kohse-Höinghaus, J. Wang, T. A. Cool, "Initial steps of aromatic ring formation in a laminar premixed fuel-rich cyclopentene flame", *J. Phys. Chem. A,* accepted for publication in the James A. Miller Festschrift, May 17, 2007.

16. P. Oßwald, U. Struckmeier, T. Kasper, K. Kohse-Höinghaus, J. Wang, T. A. Cool, N. Hansen, P. R. Westmoreland, "Isomer-specific fuel destruction pathways in rich flames of methyl acetate and ethyl formate and consequences for the combustion chemistry of esters", *J. Phys. Chem. A,* accepted for publication in the James A. Miller Festschrift, May 17, 2007.

STATE CONTROLLED PHOTODISSOCIATION OF VIBRATIONALLY EXCITED MOLECULES AND HYDROGEN BONDED DIMERS

F.F. Crim
Department of Chemistry
University of Wisconsin–Madison
Madison, Wisconsin 53706
fcrim@chem.wisc.edu

Our research investigates the chemistry of vibrationally excited molecules. The properties and reactivity of vibrationally energized molecules are central to processes occurring in environments as diverse as combustion, atmospheric reactions, and plasmas and are at the heart of many chemical reactions. The goal of our work is to unravel the behavior of vibrationally excited molecules and to exploit the resulting understanding to determine molecular properties and to control chemical processes. A unifying theme is the preparation of a molecule in a specific vibrational state using one of several excitation techniques and the subsequent photodissociation of that prepared molecule. Because the initial vibrational excitation often alters the photodissociation process, we refer to our double resonance photodissociation scheme as *vibrationally mediated photodissociation.* In the first step, fundamental or overtone excitation prepares a vibrationally excited molecule, and then a second photon, the photolysis photon, excites the molecule to an electronically excited state from which it dissociates. Vibrationally mediated photodissociation provides new vibrational spectroscopy, measures bond strengths with high accuracy, alters dissociation dynamics, and reveals the properties of and couplings among electronically excited states.

Several recent measurements illustrate the scope of the approach and point to new directions. We have used our new ion imaging capabilities to follow the adiabatic and nonadiabatic dissociation pathways in ammonia and to make new measurements on the vibrationally mediated photodissociation of the hydrogen bonded dimer of formic acid. In each case, the goals are understanding and exploiting vibrations in the ground electronic state, studying the vibrational structure of the electronically excited molecule, and probing and controlling the dissociation dynamics of the excited state.

Ammonia

Ammonia is a famously well-studied molecule that holds interesting opportunities for vibrationally mediated photodissociation experiments because it has both a nonadiabatic dissociation to yield ground state NH_2 + H and an adiabatic dissociation to form excited state NH_2* + H. Our previous studies, in which we observed excited state vibrations and monitored reaction products, provided new insights into the nonadiabatic dynamics that set the stage for our recent ion imaging experiments. The most interesting observation in our previous study is for initially excited stretching vibrations in the electronically excited state. Dissociation from the state containing one quantum of symmetric stretch (ν_1) produces a distribution with both fast and slow components that are similar to that for the origin. Dissociation from the antisymmetric N-H stretch state (ν_3), however, produces dramatically different results. It forms *only* slow hydrogen atoms, likely reflecting preferential decomposition to make solely the excited state product. Calculations by D. Yarkony (J. Chem. Phys. **121**, 628 (2004)) seem consistent with molecules that have excited asymmetric N-H stretching vibrations preferentially remaining on the excited state surface, apparently avoiding

one conical intersection by moving toward another intersection for which the crossing probability is smaller. It seems that the coupled electronic surfaces of ammonia provide a challenging target for theory (Nangia and Truhlar, J. Chem. Phys. **124**, 124309 (2006)) and that careful experiments provide a useful point of comparison.

Ion imaging is allowing us to explore the dissociation dynamics even more incisively. The quantum state populations of the NH_2 fragment that we obtain by ion imaging of the H-atom product of the one-photon dissociation of ammonia agree with earlier measurements using Rydberg tagged H-atom detection. Even though the signal is much smaller in the vibrationally mediated photodissociation experiments, we are able to observe the products of the decomposition from molecules with excited umbrella and excited bending vibrations. The distribution of energy among the NH_2 product states is again consistent with the recoil energy distributions we measured earlier. The NH_2 product from dissociation through the *symmetric* stretching state is similar to that for one-photon photolysis. By contrast, images for the dissociation through the *antisymmetric* stretching state show that there is much less energy in translation, in agreement with our previously measured H-atom Doppler profiles.

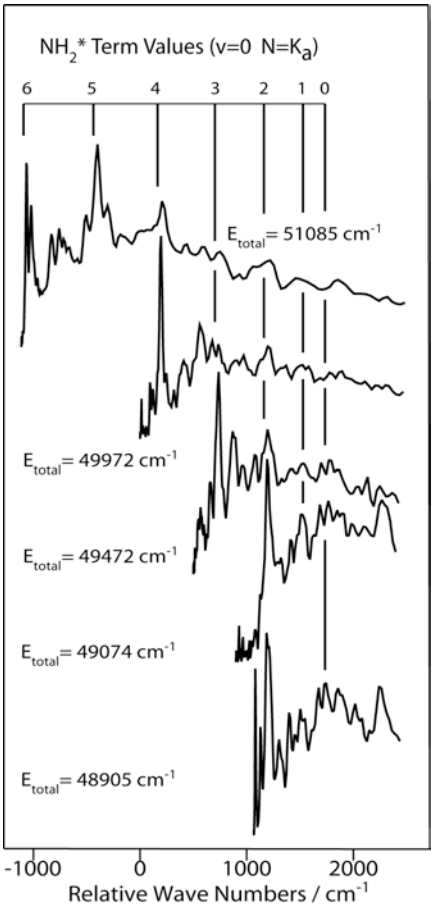

Now we have tested our inference that antisymmetric stretching excitation causes ammonia to decompose adiabatically by using velocity map ion imaging of the H atoms to identify the rotational states of the NH_2 product. The figure shows the total kinetic energy distribution of the products from dissociation of electronically excited NH_3 molecules having an excited N-H antisymmetric stretch. By measuring the distribution for different total excitation energies, E_{total}, we are able to track the rotational state populations of the NH_2 fragment, which is born with near the maximum amount of energy available in rotation. Most important, the state structure clearly matches that of the electronically product, NH_2*, demonstrating that it is indeed the primary product from vibrationally mediated photodissociation through the antisymmetric stretching state and that the vibrational excitation preferentially drives the system along the adiabatic dissociation path.

Formic Acid and Formic Acid Dimers

Another primary goal of our work is understanding the dissociation dynamics in vibrationally excited dimers, and we have applied our newly developed capabilities to studying formic acid and its hydrogen bonded dimer,

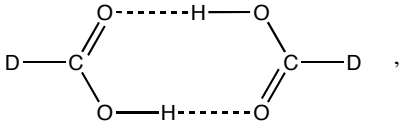

,

shown here for partially deuterated formic acid. We have developed schemes for distinguishing the monomer from the dimer in both one-photon dissociation and vibrationally mediated photodissociation.

Exciting either the O–H or C–H stretch while observing the H-atom product from the undeuterated dimer gives vibrational action spectra that agree with the absorption spectrum in a supersonic expansion. Using the partially deuterated molecule and exciting the C-D stretch while detecting the D atom product gives the first vibrational spectrum of the cold partially deuterated dimer. Cooling reveals the structure shown in the figure below.

The spectrum in the region of the C-D stretch shows three features arising from the interaction of the anti-symmetric C-D stretch with two different combinations of the C-O stretch and the DCO bend, each having the proper symmetry to interact with the infrared active b_u-symmetry C-D stretch. The combination states gain transition probability from their interaction with the C-D stretching vibration. A simple analysis of the spectrum shows that the interaction matrix element for this Fermi resonance is about 20 cm^{-1} and produces roughly equal mixing of the states.

We are studying the vibrational excitation and energy dependence of the yield of H atoms (from the hydrogen bonds) compared to that of D atoms upon excitation of either the C–D or the O–H stretch. The usual advantage of being able to obtain spectra of cold molecules and explore their dissociation dynamics with vibrationally mediated photodissociation opens many possibilities for studying these strongly bound dimers.

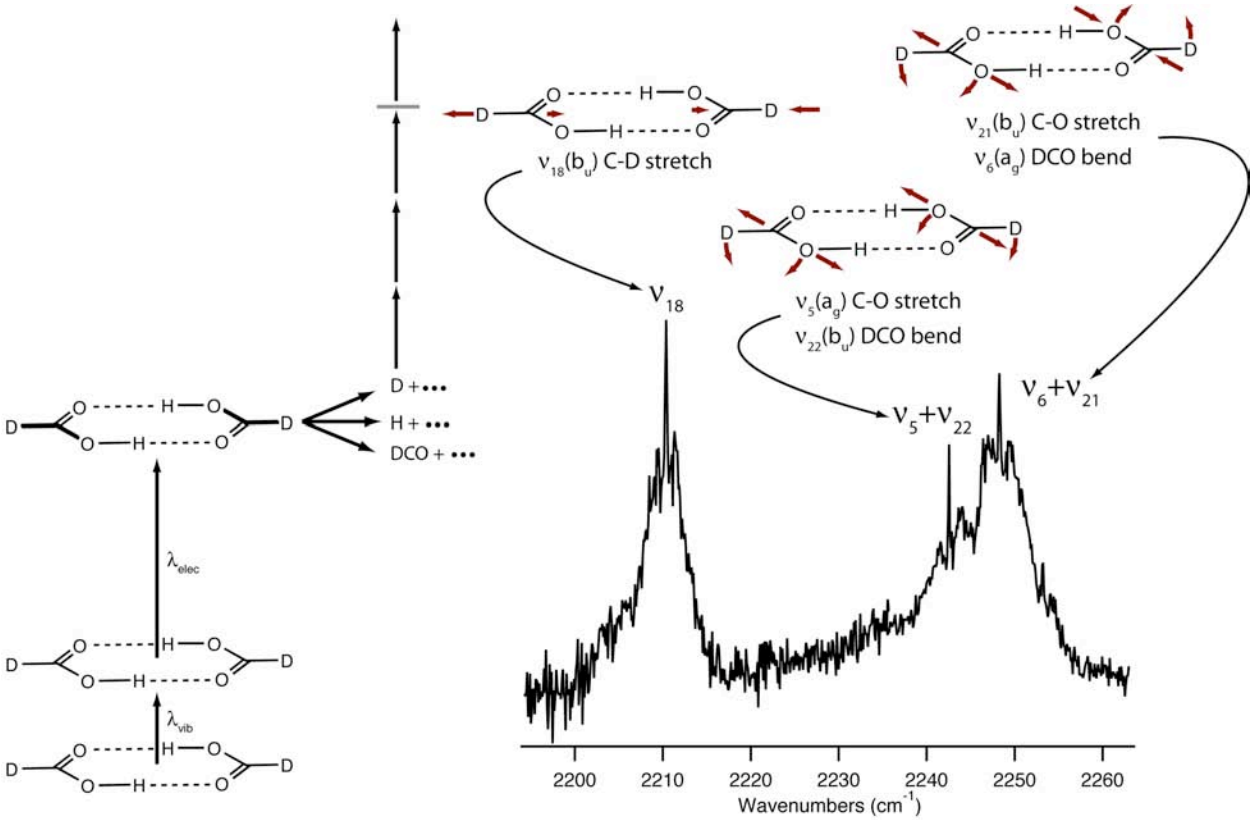

FUTURE DIRECTIONS

The influence of vibrational excitation on the behavior of ammonia at a conical intersection should be more general. There are theoretical predictions of similar behavior in other molecules, such as phenol (Domcke and coworkers, J. Chem. Phys. **122**, 224315 (2005)), and we have recently observed vibrationally mediated photodissociation of phenol in our ion imaging apparatus. The ability to detect the products with the velocity resolution of ion imaging is crucial for distinguishing one-photon and multiphoton processes. We are now setting out on a systematic study of phenol and other molecules where vibrational excitation can influence the competition between adiabatic and nonadiabatic decomposition.

Now that we can perform vibrationally mediated photodissociation of strongly bound dimers, our primary goal is to refine the study of formic acid and extend our measurements and analysis to other carboxylic acid dimers. We can capitalize on the investment in the development of these new experimental capabilities. We intend to obtain both spectra that reveal couplings in the dimers and to learn about their excited state decomposition dynamics for different initial vibrational states.

PUBLICATIONS SINCE 2005 ACKNOWLEDGING DOE SUPPORT

Vibrationally Mediated Photodissociation of Ammonia: The Influence of N-H Stretching Vibrations on Passage through Conical Intersections, Michael L. Hause, Y. Heidi Yoon, and F. Fleming Crim, J. Chem. Phys. **125**, 174309 (2006).

Bimolecular Dynamics of Combustion Reactions

H. Floyd Davis
Department of Chemistry and Chemical Biology
Baker Laboratory, Cornell University, Ithaca NY 14853-1301
hfd1@Cornell.edu

I. Program Scope:

The aim of this project is to better understand the mechanisms and product energy disposal in elementary bimolecular reactions fundamental to combustion chemistry. Using the crossed molecular beam method, a molecular beam containing highly reactive free radicals is crossed at right angles with a second molecular beam. The angular and velocity distributions of the products from single reactive collisions are measured, primarily using Rydberg tagging methods.

II. Recent Progress:

i. Reactive Quenching of OH ($A^2\Sigma^+$) + D_2 Studied by Crossed Beams

It has been known for many years that electronically excited hydroxyl radicals are rapidly quenched by collisions with small molecules. The OH ($A\ ^2\Sigma^+$) quenching rate constants for many different atomic and molecular partners have been measured as a function of temperature. In most studies, the quenching was monitored through the disappearance of OH ($A^2\Sigma^+$); the products resulting from the quenching events were not identified. For quenching of OH ($A\ ^2\Sigma^+$) by molecules containing hydrogen (RH), both physical quenching forming OH ($X^2\Pi$) + RH, as well as bimolecular reaction forming H_2O + R, are possible.[1] The OH ($A\ ^2\Sigma^+$) + H_2 (D_2) reaction has become a benchmark system for examining nonadiabatic quenching processes. The crossing regions between the ground state and excited state potential energy surfaces for OH ($A\ ^2\Sigma^+$) + H_2 (D_2) lead to conical intersections.

We have studied the quenching reaction using crossed molecular beams, employing the Rydberg time-of-flight method. The product flux contour map is shown in Fig. 1. The D atom products are preferentially forward-scattered relative to the incident D_2 molecules. This implies that the dominant reaction mechanism is direct, occurring on timescales shorter than that for rotation of the OH-D_2 pair, *i.e.,* on subpicosecond timescales. The preferential forward- scattering is a signature of a mechanism in which the incoming OH ($A\ ^2\Sigma^+$) reactant picks up a D atom from D_2 at relatively large impact parameters, with the newly-formed HOD continuing in nearly the same direction as the

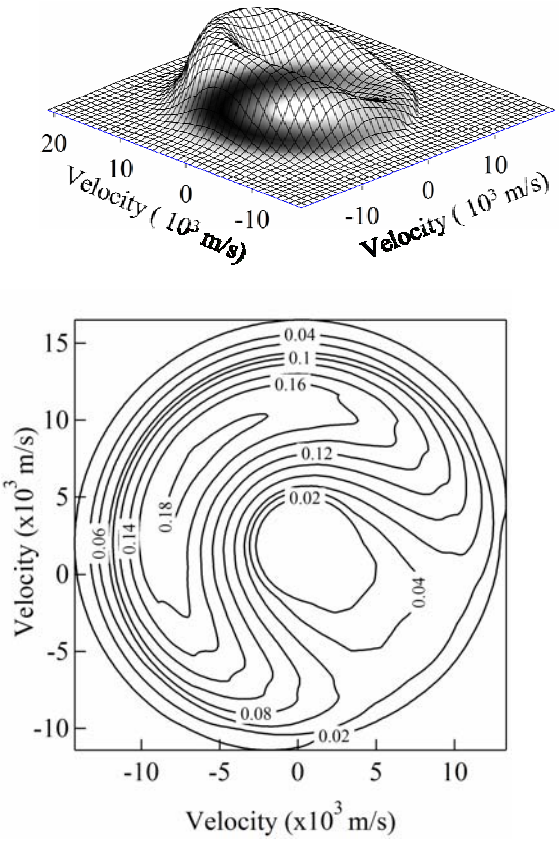

Fig. 1: D atom product flux contour map for OH(A) + D_2→ HOD + D quenching reaction.

incident OH (A). This behavior is exactly the opposite to that for the ground state reaction, which involves small-impact parameter collisions with the D atoms backward-scattered relative to the incident D_2 molecules (*i.e.,* HOD is backward-scattered relative to OH). The OH ($A\ ^2\Sigma^+$, v = 0) + $D_2 \rightarrow$ HOD + D is exoergic by 451 kJ/mol. The translational energy distribution peaks at ~ 55 kJ/mol, but includes contributions up to ~ 340 kJ/mol. Thus, the most probable internal energy of the HOD product is ~ 410 kJ/mol, which at the collision energy of this experiment corresponds to ~ 88% of the total available energy.

ii. VUV Photodissociation of OH Radicals

Although the photodissociation of OH has been extensively studied, most investigations have been restricted to wavelengths around 300 nm, where the $A^2\Sigma^+$ state undergoes predissociation. Relatively little is known about the VUV photodissociation of OH and OD. In 1974, Douglas concluded that the OH Rydberg D $^2\Sigma^-$ state is responsible for the strong ($\sim 1 \times 10^{-17}$ cm^2) absorption near 120 nm. Energetically, the following channels are available for the OH photodissociation at 121nm:

$$\begin{aligned} OH + 121\ nm &\rightarrow O(^3P_{1,2,3}) + H(^2S) \\ &\rightarrow O(^1D_2) + H(^2S) \\ &\rightarrow O(^1S_0) + H(^2S) \end{aligned}$$

We have observed all three channels following photolysis of OH using H atom Rydberg tagging TOF spectroscopy. The determination of accurate branching ratios requires measurement of the anisotropy parameters (β) for each channel. These experiments, as well as studies of OD photodissociation, are underway.

iii. Production and Characterization of Simple Hydrocarbon Free Radicals

As a first step in our upcoming studies of bimolecular reactions of hydrocarbon radicals with small molecules such as O_2, we have been evaluating the performance of several different approaches for the preparation of intense pulsed hydrocarbon radical beams. So far, we have found that UV photolysis of stable precursors, either an alkyl halide or a carbonyl, in a 1mm ID quartz tube attached to a supersonic pulsed molecular nozzle, produces the most intense radical beams. The beams were characterized using both electron impact ionization with quadrupole mass spectrometry, as well as 118 nm photoionization TOF spectroscopy. Several different hydrocarbon radicals have been prepared, including methyl, ethyl, and vinyl.

By addition of O_2 to the carrier gas, we have found that electron impact mass spectrometry (as well as photoionization TOF spectroscopy), can be used to detect CH_3O_2 at m/e = 47, corresponding to the parent ion, $CH_3O_2^+$. In agreement with several recent studies, however, we find that $C_2H_5O_2$ fragments strongly, both upon VUV as well as electron impact ionization.[2,3]

III. Future Plans:

i. H + $O_2 \rightarrow$ OH ($^2\Pi$) + O (^3P_J).

We developed the ORTOF method largely with the intention of studying H + $O_2 \rightarrow$ OH ($^2\Pi$) + O (^3P_J). The reaction is endoergic by more than 0.6 eV, with the OH preferentially formed in high-N levels. A number of experimental and theoretical studies of this system have suggested that the reaction cross section increases substantially with collision energy above threshold, reaching a maximum at collision energies near 2.0 eV. Several years ago, we first attempted to study this reaction in crossed beams using fast photolytic H atoms produced by

photodissociation of HI at 248 nm, but we were unsuccessful in observing signal. This is largely due to the small cross section for reaction. We have subsequently improved the sensitivity of our apparatus for studying reactions with small cross sections by decreasing the distances between each of the nozzle sources and interaction region by approximately a factor of two. We have also improved the source and main chamber pumping regions, and have improved the VUV generation through the construction of a new VUV cell with improved vacuum system. In addition, we have added the capability of separating the VUV from the UV using a dispersing prism, thereby decreasing background resulting from photoinduced processes involving the relatively intense UV beams. Experiments are presently underway using this improved setup in order to investigate this reaction using ORTOF.

ii. Studies of $OH + D_2 (v = 1) \rightarrow HOD + D$

The $OH + D_2$ reaction is important in combustion, and is the simplest member of the family of abstraction reactions involving OH. It involves a substantial potential energy barrier, leading to a small reaction cross section even at relatively high collision energies. The OH moiety acts much like a spectator, and is not appreciably excited in the product HOD. On the other hand, the D-D bond in D_2 is broken during the course of the reaction; vibrational excitation of this reactant is thus expected to strongly enhance reactivity.[4]

The most challenging aspect of this experiment is vibrational excitation of an appreciable fraction of D_2 molecules. We have constructed and optimized performance of a home-made narrow band optical parametric oscillator (OPO) for NSF-supported studies of reactions involving vibrationally-excited hydrocarbons with transition metal atoms in crossed beams. The OPO[5] is based on the use of KTP (potassium titanyl phosphate), and facilitates production of high energy pulsed light in the 700 – 900 nm range, as well as at 1.4 – 4.0 μm. Following the approach of Lucht and coworkers,[6] we have been able to obtain near transform-limited pulses through injection seeding with a narrow bandwith distributed feedback (DFB) diode laser. We plan to use the tunable narrowband near IR radiation from this device for SRP of D_2. By seeding at the idler wavelength using a DFB laser operating at 1.55 μm, the 532 nm pumped nonresonant oscillator produces several mJ of near-transform-limited 807 nm radiation as the signal. This 807 nm light will be amplified to produce ≈ 50 mJ/pulse of near-transform-limited radiation. The SRP process in D_2 to be used will employ this beam and the residual narrowband 1064 nm fundamental from the Nd:YAG pump laser.

iii. Crossed beam studies of reactions of hydrocarbon radicals with O_2

The reaction of simple hydrocarbon radicals (e.g., CH_3, C_2H_5, C_2H_3, etc.) with O_2 is initiated by addition, forming alkylperoxy radicals which subsequently undergo unimolecular decomposition:

$$C_2H_5 + O_2 \rightarrow C_2H_5O_2 \quad \rightarrow C_2H_4 + HO_2$$
$$\rightarrow C_2H_4O + OH$$

We plan to study this family of reactions in crossed molecular beams. While electron impact ionization of products is less sensitive than photoionization or Rydberg tagging, it has the advantage that all competing processes can be studied, and it is possible to calibrate the detection sensitivity for competing channels directly. Once can therefore determine product branching ratios as a function of collision energy.

Miller's group has been carrying out a systematic study of the $A^2A' \leftarrow X^2A''$ near infrared transitions in simple hydrocarbon peroxy radicals.[7] Unlike the UV absorptions that are broad and structureless, the absorption features in the near IR differ considerably for different alkyl moieties. The absorption spectra of CH_3O_2 and $C_2H_5O_2$ around 8000-9000 cm^{-1} are highly structured, indicating that these species do not undergo fast unimolecular decomposition following electronic excitation. However, Ellison and coworkers have pointed out that organic peroxy radicals in their low-lying A^2A' states are likely to undergo 1,4 cyclization, leading to unimolecular decomposition. In the case of CH_3O_2, the decomposition would lead to formation of $CH_2O + OH$. For the heavier analogues, multiple reaction pathways are possible; $C_2H_5O_2$ could undergo decomposition via two competing pathways:

$$C_2H_5O_2 + h\nu \rightarrow C_2H_5O_2\ A^2A' \quad \rightarrow C_2H_4 + HO_2$$
$$\rightarrow C_2H_4O + OH$$

These products are the same as those expected for the bimolecular reaction of $C_2H_5 + O_2$. We are planning to search for evidence for unimolecular decomposition of peroxy radicals following electronic excitation to the A′ states in the near IR.

IV. Publications since 2005:

1. Photodissociation Dynamics of N_2O at 130 nm: The $N_2(A\ ^3\Sigma_u^+, B\ ^3\Pi_g) + O(^3P_{J=2,1,0})$ Channels, Mark F. Witinski, Mariví Ortiz-Suárez, and H. Floyd Davis, *J. Chem. Phys.* **122**, 174303 (2005).
2. Reaction Dynamics of $CN + O_2 \rightarrow NCO + O(^3P_2)$, Mark F. Witinski, Mariví Ortiz-Suárez, and H. Floyd Davis, *J. Chem. Phys.*, **124**, 094307 (2006).
3. Reactive Quenching of OH $(A\ ^2\Sigma^+)$ + D_2 Studied by Crossed Molecular Beams, Mariví Ortiz-Suárez, Mark F. Witinski, and H. Floyd Davis, *J. Chem. Phys.* **124**, 201106 (2006).

V. References:

1. D. T. Anderson, M. W. Todd, and M. I. Lester, *J. Chem. Phys.* **110**, 11117 (1999).
2. H. B. Fu, Y.J. Hu, and E.R. Bernstein, *J. Chem. Phys.* **125**, 014310 (2006).
3. G. Meloni, P. Zou, S. J. Klippenstein, M. Ahmed, S.R. Leone, C.A. Taatjes, and D. L. Osborne, *J. Am. Chem. Soc.* **128**, 13559 (2006).
4. M. J. Lakin, D. Troya, G. Lendvay, M. Gonzalez and G.C. Schatz, *J. Chem. Phys.* **115**, 5160 (2001).
5. W.R. Bosenberg and D. Guyer, *J. Opt. Soc. Am. B.* **10**, 1716 (1993).
6. W.D. Kulatilaka, T.N. Anderson, T.L. Bougher, and R.P. Lucht, *Appl. Phys. B*. **80**, 669 (2005).
7. M. B. Pushkarsky, S.J. Zalyubovsky, and T.A. Miller, *J. Chem. Phys.* **112**, 10695 (2000).

Multiple–time–scale kinetics

Michael J. Davis

Chemistry Division
Argonne National Laboratory
Argonne, IL 60439
Email: davis@tcg.anl.gov

Research in this program focuses on three interconnected areas. The first involves the study of intramolecular dynamics, particularly of highly excited systems. The second area involves the use of nonlinear dynamics as a tool for the study of molecular dynamics and complex kinetics. The third area is the study of the classical/quantum correspondence for highly excited systems, particularly systems exhibiting classical chaos.

Recent Progress

Over the last several years, progress has been made on the dynamics of partial differential equations related to combustion. Steady state conditions and transient conditions have been studied. The main focus has been the study of the types of model reduction that could be made for these systems, as well as the relative role of chemical reaction vs. transport processes in the reduction, particularly diffusion. These projects have been divided into three groups labeled as "species reduction", "dimension reduction", and "steady conditions". In species reduction, the number of species that need to be followed is reduced, but the problem still involves the solution of partial differential equations. In the case of dimension reduction, the number of species and the number of spatial grid points are both reduced and two papers were published in this area. The third group of projects involves the study of the dynamics of steady systems in the spatial domain and has been the main focus of recent progress.

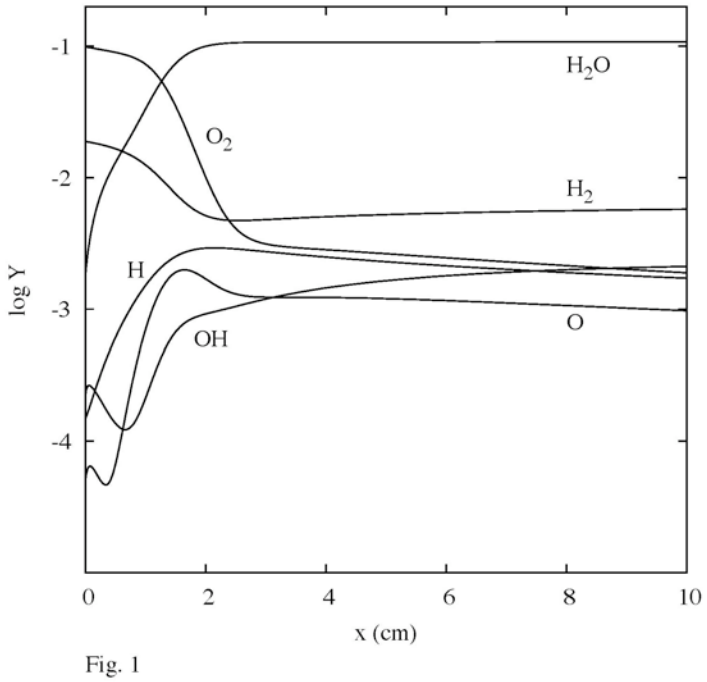

Fig. 1

The progress on steady systems has occurred in three areas. The first is the development of dynamical systems approaches to the spatial dynamics of simple reaction-diffusion systems. This includes a detailed analysis of the structure of phase space and the nature

of nonlinear invariants for these systems. The second area is the development of numerical methods in these systems that can be applied to premixed, steady one-dimensional flames. The third area is the study of the spatial dynamics of the flames. In this type of problem the reduction of the chemical kinetics occurs along the spatial domain. Our approach to reduction is geometric and depends on the resolution of low-dimensional manifolds. The work described here includes collaborations with Tomlin (Leeds) on premixed flames and Tomlin, Zagaris and Kaper (Boston University) on fundamental aspects.

We have studied burner stabilized H_2/O_2 flames as generated in the Chemkin program premix. An example is shown in Fig. 1 above. We have studied these flames within a dynamical systems framework, based on the approach of Hirschfelder and Curtiss[1] and Dixon-Lewis.[2] The dynamics of a flame is described by a set of first order ordinary differential equations. The flames are studied in a phase space consisting of the mole fractions and the mass flux fractions as outlined in Refs. 1 and 2, but for purposes of comparison with the pure chemical-kinetics problem we often plot the mass fractions. The top panel of Fig. 2 on the right shows the flame of Fig. 1 projected onto three of the mass fractions. This approach replaces the usual boundary value problem for steady flames with an initial value problem. The two approaches coincide as the boundary is taken to larger values. The coordinates used in the present approach are similar to those in Ref. 3, which also studied manifolds for steady flames in phase space.

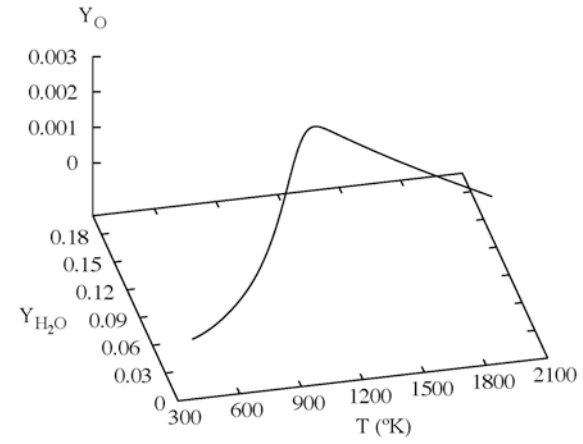

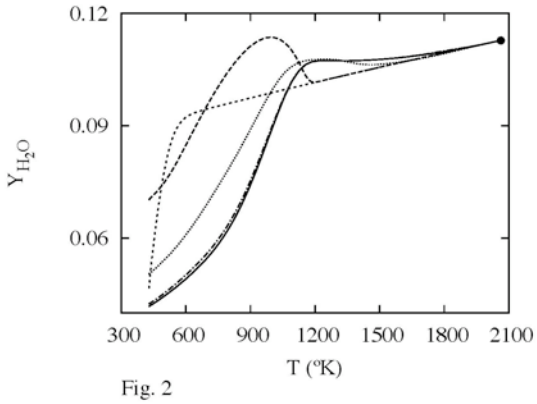

Fig. 2

It is well known that these systems are unstable,[4] and it is not possible to directly integrate the differential equations. However, all steady flames lie on the stable manifold of a saddle point lying at infinite spatial extent. This saddlepoint is an equilibrium point of the pure chemical-kinetics problem at the asymptotic enthalpy of the flame and possesses the same constants of motion. The dimension of the stable manifold of the flame saddlepoint is the same as the full dimension of the chemical-kinetic problem.

Because the system is unstable and it is not possible to integrate trajectories directly on the stable manifold, orbits of the system are generated by a Newton-Raphson procedure. The Newton iterations give a series of guesses that converge, as demonstrated in the bottom panel of Fig. 2 above. The dark black line is the final result of the iteration. Although the initial guess [the dashed line starting at (430.0, 0.05)] is not very accurate, convergence is complete after only about 10 iterations.

By generating many trajectories for the flame system it becomes apparent that within the stable manifold of the saddle fixed point there are sub-manifolds of lower dimension, so-called “low-dimensional manifolds. This is demonstrated in Fig. 3 on the

right. Several trajectories are generated in the manner described above and plotted in a 2-D projection on the top panel and a 3-D projection on the bottom panel. These plots suggest that there are low-dimensional manifolds in this system, with a 1-D manifold most apparent at temperatures above 1200 K and a two-dimensional manifold over a much larger temperature range in the bottom panel.

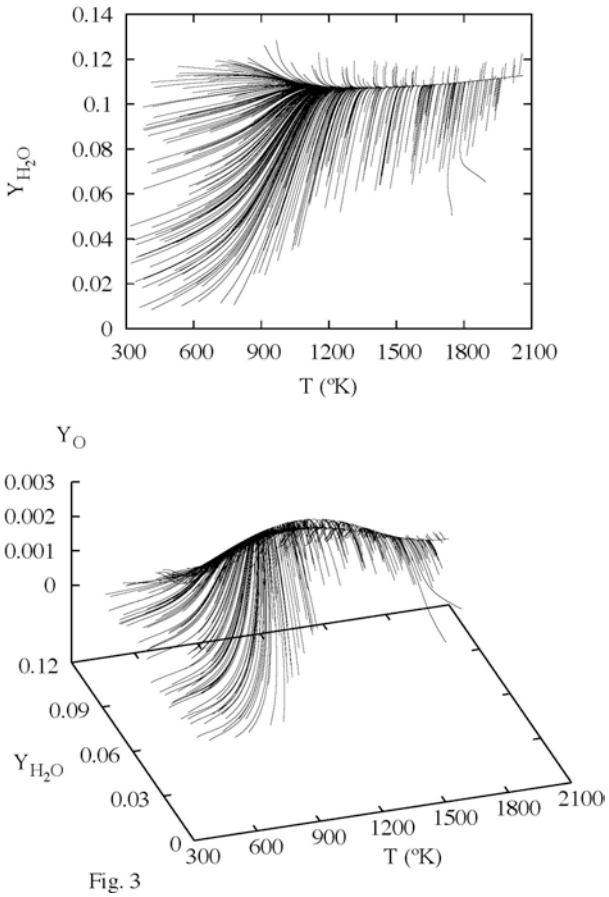

Fig. 3

It is possible to generate these manifolds, although the often used method of Maas and Pope[5] is not very accurate for the 2-D manifolds in the flame problem, and a method due to Fraser[6,7] is used instead. The nature of the 1-D and 2-D manifolds are demonstrated in Fig. 4 where the original flame trajectory of Fig. 1 is plotted along with a 1-D manifold in the top panel and a 2-D manifold in the bottom panel. Figure 4 shows that the flame trajectory is first attracted to the two-dimensional manifold, then a one-dimensional manifold at longer spatial scales.

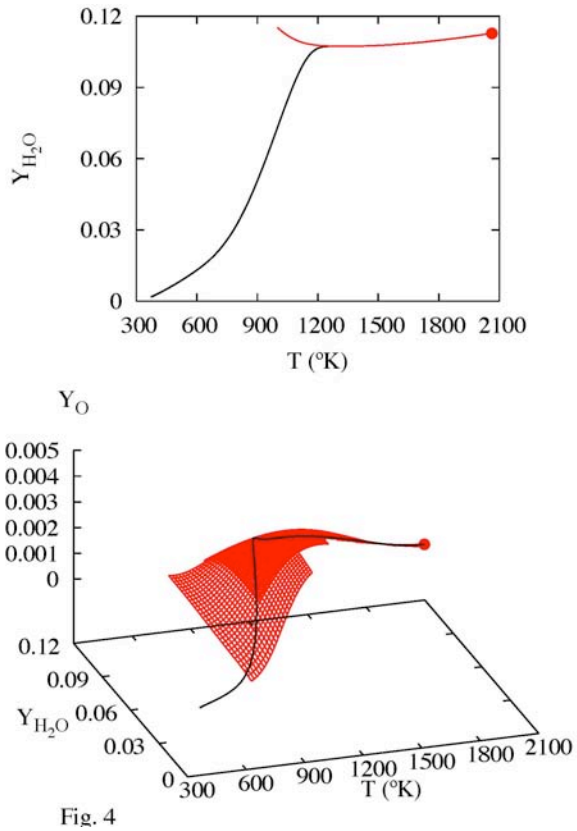

Fig. 4

The manifold for the flame is compared to a composite set of manifolds for the pure chemical kinetics problem in Fig. 5. The top panel shows a thick line representing the 1-D manifold for the flame. The dots are a composite from a set of 1-D manifolds for the chemical-kinetics problem. This set of manifolds arises from variations in the constants of motion, including the enthalpy of the mixture. A set of dotted lines on the top panel of Fig. 5 shows a series of 1-D manifolds for the kinetic problem that differ only in the enthalpy. It is a series of manifolds like these that define the composite shown as a set of dots in the panel. Although composite manifolds are accurate for the one-dimensional manifolds in the top panel of Fig. 5, there can be a breakdown for this system in the two-dimensional manifolds. The bottom panel compares the two-dimensional manifold

of the flame system with composites for the kinetics problem in the lower temperature regime (see Fig. 4). The curves in the panel are temperature isoclines of the 2-D manifold for the two cases. The solid lines show isoclines for the flame system and the dashed lines show isoclines for the composites of the kinetics systems. The isoclines vary in temperature from 768 K for the bottom curve in the panel to 1182 K for the top curve. It is evident from the plot that the manifold of the flame differs from the composites for the kinetics system and that this difference is greatest at the lowest temperatures.

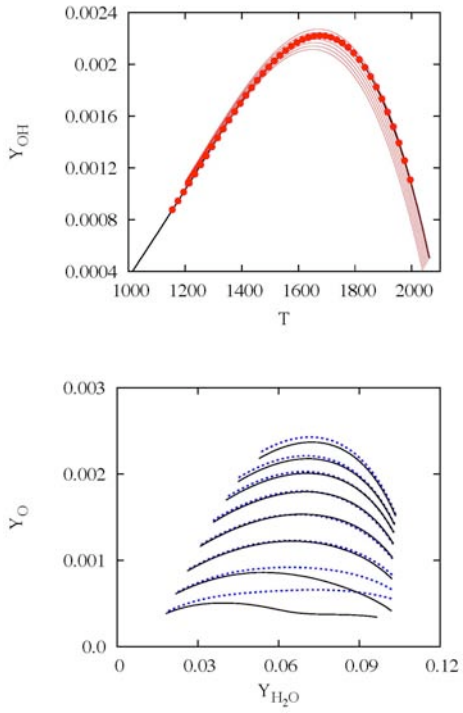

Fig. 5

Future Plans

In the near term, it is expected that reduction methods for steady problems will be improved and be made more efficient so that they can be more readily applied to hydrocarbon combustion, including methane oxidation. This will lead to a study of methane flames. It is also expected that the study of species reduction will be undertaken. In particular, that work will include manifolds in function space and species reduction methods in extended spaces that include species and moments.

References

[1] For example, J. O. Hirschfelder and C. F. Curtiss, Adv. Chem. Phys. **3**, 59 (1961).

[2] For example, G. Dixon-Lewis, Proc. Roy. Soc. **A307**, 111 (1968).

[3] H. Bongers, J.A. Van Oijen, and L.P.H. De Goey, *Proc. Combust. Inst.* **29**, 1371 (2002).

[4] M. D. Smooke, J. Comp. Phys. **48**, 72 (1982).

[5] U. Maas and S. B. Pope, Combust. Flame **88**, 239 (1992).

[6] S. J. Fraser, J. Chem. Phys. **88**, 4732 (1988).

[7] M. J. Davis and R. T. Skodje J. Chem. Phys. **111**, 859 (1999).

Publications

M. J. Davis, "Low-dimensional manifolds in reaction-diffusion equations. 1. Fundamental aspects", J. Phys. Chem. A **110,** 5235 (2006).

M. J. Davis, "Low-dimensional manifolds in reaction-diffusion equations. 2. Numerical analysis and method development", J. Phys. Chem. A **110,** 5257 (2006).

M. J. Davis and A. S. Tomlin, "Spatial dynamics of steady systems with reaction and transport. One-dimensional premixed flames", preprint.

COMPREHENSIVE MECHANISMS FOR COMBUSTION CHEMISTRY: EXPERIMENT, MODELING, AND SENSITIVITY ANALYSIS

Frederick L. Dryer
Department of Mechanical and Aerospace Engineering
Princeton University, Princeton, New Jersey 08544 5263
fldryer@princeton.edu

Grant No. DE FG02 86ER 13503

Program Scope

Experiments conducted in a Variable Pressure Flow Reactor (VPFR) at pressures from 0.3 to 20 atm and temperatures from 500 K to 1200 K, with observed reaction times from 0.5×10^{-2} to 2 seconds, and laminar flame speed measurements are combined with literature data and numerical studies to develop and validate chemical kinetic reaction mechanisms and to improve determinations of important elementary rates. Continuing efforts are: (1) utilizing the perturbations of the H_2/O_2 and CO/H_2O/Oxidant reaction systems by the addition of small amounts of other species to further clarify elementary reaction properties; (2) further elucidating the reaction mechanisms for the pyrolysis and oxidation of hydrocarbons (alkanes, olefins) and oxygenates (aldehydes, alcohols, and ethers).

Recent Progress

In the work summarized below, we provide further insights into the kinetics of the H_2/CO system and discuss recently reported discrepancies between kinetic model predictions and experimentally measured ignition delays of hydrogen/carbon monoxide (syngas) - air mixtures. We also report on new experimental and modeling results using our recently developed DME and ethanol kinetic models.

Oxidation of H_2/CO mixtures

Our comprehensive kinetic model for the oxidation of H_2, CO, CH_2O, and CH_3OH [1] has been used by many authors to model ignition delays, laminar flame speed measurements of H_2/CO/air systems [2-4], and temporally evolving systems, e.g. [5]. These investigations, especially [2-4] have been driven by interest in syngas or hydrogen use in Integrated Gasification Combined Cycle (IGCC) systems. References 2-4 as well as [6-11] have indicated the importance of the $CO+HO_2$ reaction at high pressures, and new theoretical studies [9-11] support a lower rate constant correlation than that we have employed in [1]. We have shown that this reaction is more significant for high reactant density cases [6] as opposed to those involving highly dilute mixtures [8]. Using a modified Computational Singular Perturbation (CSP) technique [12], we have shown that the $CO+HO_2$ reaction is principally important only during chemical induction and is of little relevance to predicting heat release rate and subsequent reaction observables. The C_1 mechanism [1], modified with a new rate correlation for the $CO+HO_2$ reaction [e.g., 6] reasonably predicts all of the recently published ignition delay measurements for mixtures of CO, hydrogen, and diluents [6, 7]. For highly dilute systems, further studies of the HO_2+OH reaction should lead to refinements of kinetic predictions at high pressures. In other work [4], we have shown that recent high pressure measurements of syngas laminar flame speeds [9] are subject to corrections due to flow field perturbations ahead of the flame, and that the present C_1 mechanism [1] predicts the corrected, as well as new laminar high pressure flame speeds [4] accurately.

Ignition delay is an important parameter in the design of fuel/air mixing systems to produce lean premixed combustion, a technique used to control NO_x emissions in gas turbine applications. Several research groups have been investigating ignition of syngas/ and hydrogen/air mixtures at gas turbine design conditions (~20 atm and ~900 K [2, 3, 13]. These studies present new data showing that at temperatures below ~1100 K, there is considerable disagreement (several orders of magnitude) between observed ignition delays determined in shock tubes, flow reactors, and rapid compression machines and zero-dimensional homogenous gas phase kinetic predictions (Fig. 1). We have shown [14] that similar discrepancies have been observed in shock tubes (since as early as the 1960's) and in Princeton flow reactors (as early as 1985 [15]) previously. The ignition delay times for hydrogen/air as well as syngas/air at these conditions (between the extended second and third explosion limits of the H_2/O_2 system) are strongly perturbed by the production of radicals through the formation and reaction of hydrogen peroxide and subsequent heat release. As a result, the chemical induction process is very sensitive to local temperature fluctuations, mixing conditions, and catalytic surface reactions [14]. Once ignition occurs, chain branching processes are sufficiently fast that these phenomena no longer affect chemical reaction rate [14]. The reaction time shifting approach that we utilize in comparing predictions with post induction experimental observations in flow reactors eliminates the need to consider induction chemistry effects [15, 16]. Measurements influenced by chemical

induction kinetics at these lower temperature conditions should not be utilized in refining gas phase kinetic mechanisms for hydrogen and syngas oxidation without considering mixing, temperature fluctuation, and catalytic coupling effects.

Dimethyl Ether

Last year we reported an updated high-temperature model for DME pyrolysis and oxidation which includes revised sub-models and thermochemistry for hydrogen as well as C_1-C_2 reactions developed in recent experimental and modeling studies of ethanol pyrolysis and oxidation (discussed below). The mechanism was validated originally against high-temperature flow reactor, jet-stirred reactor, shock-tube ignition, burner-stabilized flames, and laminar premixed flame speed experimental data. Recently, mechanism predictions have been compared successfully with low pressure flame data obtained via molecular-beam-sampling photoionization mass spectrometery (PIMS) [17]. Furthermore the model has also been shown to reproduce not only measurements of pure DME flame speeds but also those of DME-doped CH_4/air premixed flames at atmospheric pressure [18]. Further developments of the DME kinetic model have focused on low-temperature oxidation pathways. The model has been extended by including molecular oxygen addition to the methoxymethyl radical (CH_3OCH_2) formed by H-abstraction from DME and its associated isomerization reactions. The low temperature reaction subset was adopted from [19] with additional modifications to improve agreement with experimental ignition data (see Fig. 2). More specifically, the rate of HO_2 addition to DME was increased as well as the rate for the decomposition of hydroperoxymethyl formate (HO_2CH_2OCHO). The latter revisions significantly reduce predicted intermediate concentration of HO_2CH_2OCHO in comparison to those found using previous models [19, 20], and improve predictive performance for a wide range of experimental validation targets. New DME pyrolysis data have been collected in the VPFR at pressure and temperature conditions not previously reported. Figure 3 shows the experimentally measured pyrolysis profiles compared against the present model predictions as well as those using the model in [19]. Results show that our theoretical treatment of the DME decomposition reaction (which results in a higher degree of fall-off than used in [19, 20]) properly describes the fuel decay at high pressure conditions (Fig. 3). This work is presently in press [21].

Ethanol

A detailed mechanism for ethanol combustion has been developed, previously under this program, in a hierarchical manner, which combines our H_2/O_2 and C_1 mechanism [1] and C_2H_X/O_2 (X = 1 – 6), CH_3CHO/O_2, and C_2H_5OH/O_2 subsets, in order of increasing complexity. At each level, the newly added portions of the mechanism were tested and validated by thorough comparison between numerically predicted and experimentally observed results found in laminar premixed flames, shock tubes, and flow reactors. In conjunction with sensitivity and reaction flux analyses, important updates/modifications were made to reflect recent updates of thermodynamic data, rate coefficients, and branching ratios. The ethanol mechanism so derived predicts reasonably well the major species profiles for both pyrolysis and oxidation experiments in the VPFR, as well as shock tube ignition data and laminar burning velocities [22]. As shown in [22], the present mechanism significantly improves VPFR predictions over those obtained using the model of Marinov [23] as well as those using the San Diego mechanism [24]. Recently, new data have appeared [24] that present an opportunity to further test model predictions under partially premixed and diffusive conditions. *A priori* comparisons of the present model predictions of these experimental data (Fig 4.) are very reasonable. Additional comparisons against other data are underway and will appear in archival publication in the near future. The present model, thus, continues to perform favorably for a wide range of pressure and temperature conditions as well as for different experimental configurations.

Plans

Reaction systems of presently under investigation and of continuuing interest over the coming year, include the pyrolyses and oxidations of acetaldehyde, acetone, and toluene, all over a range of pressures and temperatures similar to our previous work.

References (items in *italics* show present publications)

1. *J. Li, Z. Zhao, A. Kazakov, M. Chaos, F.L. Dryer, and J.J. Scire, "A Comprehensive Kinetic Mechanism for CO, CH_2O, CH_3OH Combustion," International Journal of Chemical Kinetics, 39 (2007) 109-136.*
2. E.L. Petersen, D.M. Kalitan, A.B. Barrett, SC. Reehal, J.D. Mertens, D.J. Beerer, R.L. Hack, and V.G. McDonell, "New Syngas/Air Ignition Data at Lower Temperature and Elevated Pressure and Comparison to Current Kinetics Models," Combustion and Flame, 149 (2007) 244-247.
3. S.C. Reehal, D.M. Kalitan, T. Hair, A. Barrett, and E.L. Petersen, "Ignition Delay Time Measurements of Synthesis Gas Mixtures at Engine Pressures," Paper C24, 5th US Combustion Meeting, San Diego, CA, March 25-28, 2007.
4. *M.P. Burke, X. Qin, Y. Ju, and F.L. Dryer, "Measurements of Hydrogen Syngas Flame Speeds at Elevated Pressures," Paper A16, 5th US Combustion Meeting, San Diego, CA, March 25-28, 2007.*

5. E. R. Hawkes R. Sankaran, J. C. Sutherland, and J.H. Chen, "Scalar Mixing in Direct Numerical Simulations of temporally Evolving Plane Jet Flames with Skeletal CO/H_2 Kinetics," Proceedings of the Combustion Institute 31 (2007) 1633–1640.
6. G. Mittal, C.-J. Sung, and R.A. Yetter, "Autoignition of H_2/CO at Elevated Pressures in a Rapid Compression Machine," International Journal of Chemical Kinetics, 38 (2006) 516-529.
7. G. Mittal, C.J. Sung, M. Fairweather, A.S. Tomlin, J.F. Griffiths, and K.J. Hughes, "Significance of the HO_2 + CO Reaction During the Combustion of CO + H_2 Mixtures at High Pressures," Proceedings of the Combustion Institute, 31 (2007) 419-428.
8. R. Sivaramakrishnan, A. Comandini, R.S. Tranter, K. Brezinsky, S.G. Davis, and H. Wang, "Combustion of CO/H_2 Mixtures at Elevated Pressures," Proceedings of the Combustion Institute, 31 (2007) 429-438.
9. H. Sun, S.I. Yang, G. Jomaas, and C.K. Law, "High-Pressure Laminar Flame Speeds and Kinetic Modeling of Carbon Monoxide/Hydrogen Combustion," Proceedings of the Combustion Institute, 31 (2007) 439-446.
10. X. You, H. Wang, E. Goos, C.-J. Sung, and S. J. Klippenstein, "Reaction Kinetics of CO+HO_2→Products: Ab Initio Transition State Theory Study with Master Equation Modeling," Paper C36, 5th US Combustion Meeting, San Diego, CA, March 25-28, 2007.
11. J.W. Bozzelli, R. Asatryan, C.J. Montgomery, and C. Sheng, "Pressure Dependent Mechanism for H/O/C(1) Chemistry," Poster P22, 5th US Combustion Meeting, San Diego, CA, March 25-28, 2007.
12. A. Kazakov, M. Chaos, Z. Zhao, and F.L. Dryer, "Computational Singular Perturbation Analysis of Two-Stage Ignition of Large Hydrocarbons," Journal of Physical Chemistry A, 110 (2006) 7003-7009.
13. S.M. Walton, X. He, B.T. Zigler, and M.S. Wooldridge, "An Experimental Investigation of the Ignition Properties of Hydrogen and Carbon Monoxide Mixtures for Syngas Turbine Applications," Proceedings of the Combustion Institute, 31 (2007) 3147-3154.
14. *F.L. Dryer and M. Chaos, "Ignition of Hydrogen/Air and Syngas/Air Mixtures: Experimental Data Interpretation and Kinetic Modeling Implications," Workshop on Hydrogen Combustion in Gas Turbines, EPRI Washington, March 22, 2007.*
15. R.A. Yetter, F.L. Dryer, and H. Rabitz, "Flow Reactor Studies of Carbon Monoxide/Hydrogen/Oxygen Kinetics," Combustion Science and Technology, 79 (1991) 129-140.
16. J. Li, A. Kazakov, F.L. Dryer, "Ethanol Pyrolysis Experiments in a Variable Pressure Flow Reactor," International Journal of Chemical Kinetics, 33 (2001) 859-867.
17. *T.A. Cool, J. Wang, N. Hansen, P.R. Westmoreland, F.L. Dryer, Z. Zhao, A. Kazakov, T. Kasper, and K. Kohse-Höinghaus, "Photoionization Mass Spectrometry and Modeling Studies of the Chemistry of Fuel-Rich Dimethyl Ether Flames," Proceedings of the Combustion Institute, 31 (2007) 285-294.*
18. *Z. Chen, X. Qin, Y. Ju, Z. Zhao, M. Chaos, and F.L. Dryer, "High Temperature Ignition and Combustion Enhancement by Dimethyl Ether Addition to Methane-Air Flames," Proceedings of the Combustion Institute, 31 (2007) 1215-1222.*
19. S.L. Fischer, F.L. Dryer, H.J. Curran, "The Reaction Kinetics of Dimethyl Ether. I: High-Temperature Pyrolysis and Oxidation in Flow Reactors," International Journal of Chemical Kinetics, 32 (2000) 713-740.
20. X.L. Zheng, T.F. Lu, C.K. Law, C.K. Westbrook, H.J. Curran, "Experimental and Computational Study of Nonpremixed Ignition of Dimethyl Ether in Counterflow," Proceedings of the Combustion Institute, 30 (2006) 1101-1109.
21. *Z. Zhao, M. Chaos, A. Kazakov, and F.L. Dryer, "Thermal Decomposition Reaction and a Comprehensive Kinetic Model of Dimethyl Ether," International Journal of Chemical Kinetics, in press.*
22. *J. Li, A. Kazakov, M. Chaos, and F.L. Dryer, "Chemical Kinetics of Ethanol Oxidation," Paper C26, 5th US Combustion Meeting, San Diego, CA, March 25-28, 2007.*
23. N.M. Marinov, "A Detailed Chemical Kinetic Model For High Temperature Ethanol Oxidation," International Journal of Chemical Kinetics, 31 (1999) 183-220.
24. P. Saxena, F.A. Williams, "Numerical and Experimental Studies of Ethanol Flames," Proceedings of the Combustion Institute, 31 (2007) 1149-1156.

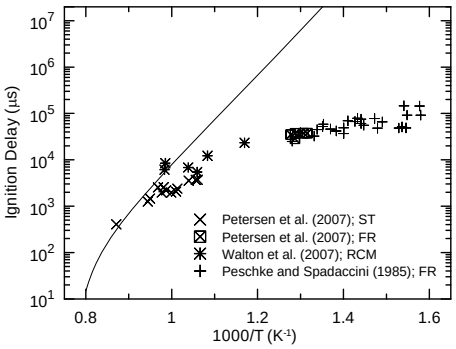

Fig. 1. Ignition of syngas/air mixtures reported from a number of experiments (as reviewed in Ref. 2) compared to predictions using the model of Li et al. [1].

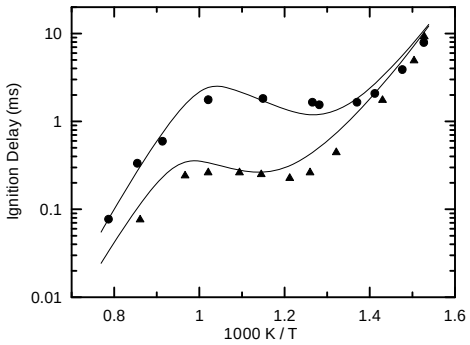

Fig. 2. Stoichiometric DME/air ignition delay measurements against model predictions. Circles and triangles denote measurements at 13 bar and 40 bar, respectively.

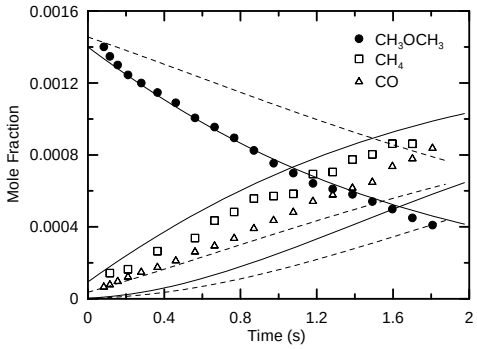

Fig. 3. Measured species profiles in a flow reactor under pyrolysis conditions (P = 10 atm, T = 980 K, 1500 ppm DME in balance N_2). Solid lines are predictions using the present model, dashed lines are calculated profiles using the model of Fischer et. al. [19].

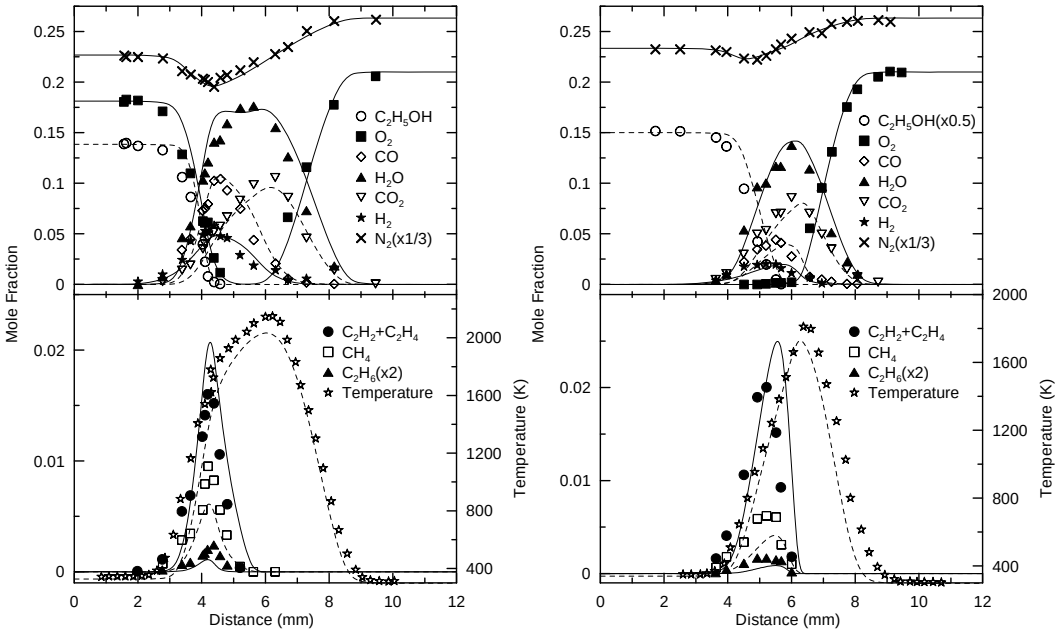

Fig. 4. Species and temperature profiles of ethanol partially premixed (left) and diffusion (right) counterflow flames. Symbols are measurements of Saxena and Williams [24], lines are present model predictions. Dashed lines correspond to open symbols.

Hydrocarbon Radical Thermochemistry: Gas-Phase Ion Chemistry Techniques

Kent M. Ervin
Department of Chemistry/216
University of Nevada, Reno
Reno, Nevada 89557
E-mail: ervin @ unr.edu

Project Scope

Gas-phase ion chemistry methods are employed to determine enthalpies of formation of hydrocarbon radicals that are important in combustion processes and to investigate the dynamics of ion–molecule reactions. Guided ion beam tandem mass spectrometry is used to measure the activation of endoergic ion-molecule reactions as a function of kinetic energy. Modeling the measured reaction cross sections using statistical rate theory or empirical reaction models allows extraction of reaction threshold energies. These threshold energies yield relative gas-phase acidities, proton affinities, or hydrogen-atom affinities, which may then be used to derive neutral R–H bond dissociation enthalpies using thermochemical cycles involving established electron affinities or ionization energies. The reactive systems employed in these studies include endoergic bimolecular proton transfer reactions, hydrogen-atom transfer reactions, and collision-induced dissociation of heterodimer complex anions and cations. Electronic structure calculations are used to evaluate the possibility of potential energy barriers or dynamical constrictions along the reaction path, and as input for RRKM and phase space theory calculations.

Recent Progress

O-H bond dissociation energy of phenol

The phenoxy radical and therefore the OH bond dissociation energy of phenol is important in combustion processes, especially involving oxygenated fuels. Recent literature determinations of the phenoxy radical thermochemistry are not in good agreement.[1-6] Following up on previous work,[7] we have recently published a new study using competitive threshold collision-induced dissociation (TCID) techniques to determine the bond dissociation energy of phenol, $D(C_6H_5O-H)$.[8] This work extended our study of the gas-phase acidity of phenol, from which the bond dissociation energy is derived, by using multiple reference acids including HCN, H_2S, and HOO. We also included several cresols in a local thermochemical network of relative acidities for a more precise determination. The fits to the TCID cross sections of proton-bound dimer anions of these acid/base pairs employ RRKM theory to model the product branching fractions as a function of available energy. To construct the local thermochemical network, 48 independent measurements of 16 different complexes were undertaken. Our new bond

dissociation energy is $D_{298}(C_6H_5O-H)$ = 361 ± 4 kJ/mol, i.e., very close to the value of 359 ± 8 kJ/mol we obtained previously based upon TCID of just the single $[C_6H_5O..H..CN]^-$ complex. Our value agrees with the lower prediction of Mulder and coworkers,[3,4] which is based upon both theory and photoacoustic calorimetry measurements in solution corrected to the gas phase, but does not agree well with the higher value advocated by Canuto and coworkers,[5,6] which is based upon complete-basis-set extrapolated coupled-cluster calculations and supported by a 1998 literature evaluation by Santos and Simões.[9] The still-higher experimental values of 381 ± 4 kJ/mol by Anderson and co-workers[2] and ≤377 ± 13 kJ/mol in early work in our lab,[1] both based on threshold energies for bimolecular proton transfer reactions, can be definitely excluded.

Threshold collision-induced dissociation of proton-bound carboxylate heterodimer anions

A new project in progress is a study of proton-bound dimers of carboxylate anions with a reference acid or another carboxylic acid molecule. Our motivation for this work is to extend the TCID method to the determination of gas-phase acidities of molecules with carboxylic acid groups. The TCID cross sections for several proton-bound dimers are shown in the figure below with fits from RRKM modeling of the branching ratios as a function of the available energy.

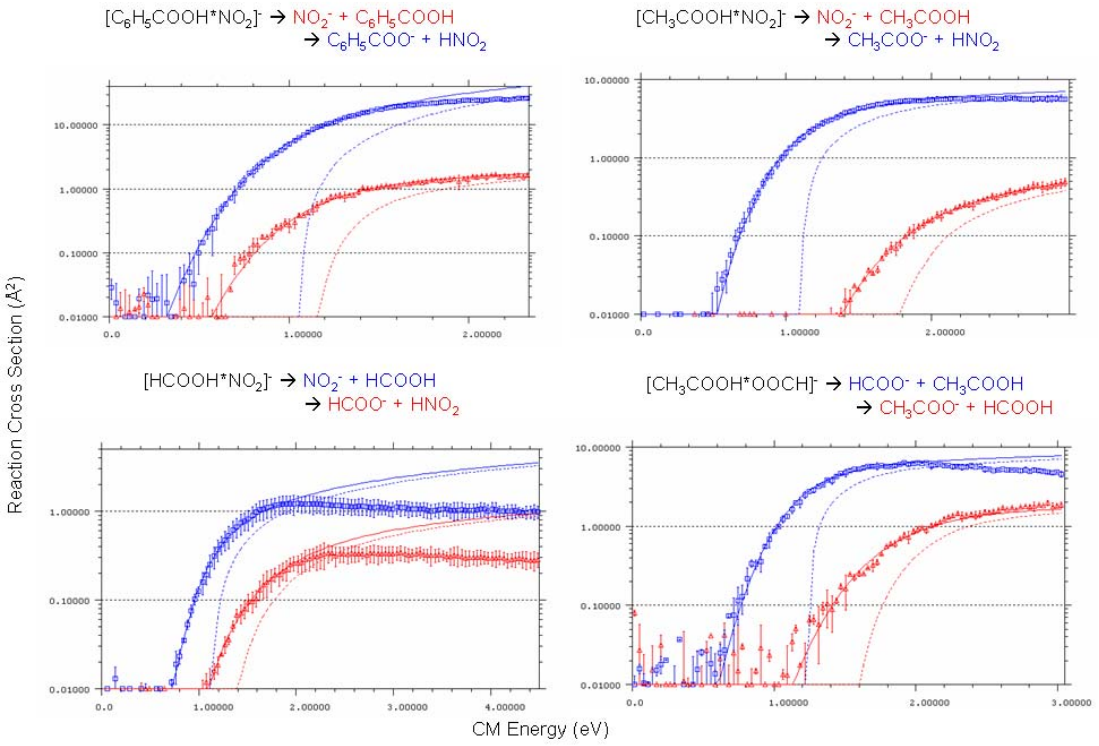

The results show interesting effects due to multiple hydrogen bonding interactions between the two electronegative oxygen atoms in the anions and the second acid. These interactions can stabilize conformations of the acids in the complex heterodimer anions that are *not* the ground state conformations of the isolated molecules. In turn, that can give rise to measured dissociation energies that do not correspond to ground state products. To elucidate these effects, a significant theoretical effort has gone into characterizing the conformations and

the isomerization transition states. As an example, a preliminary energy level diagram for various isomers and dissociation products of $[CH_3COO\text{-}HCOOH]^-$ complexes is shown below. A publication describing this work is in preparation.[10]

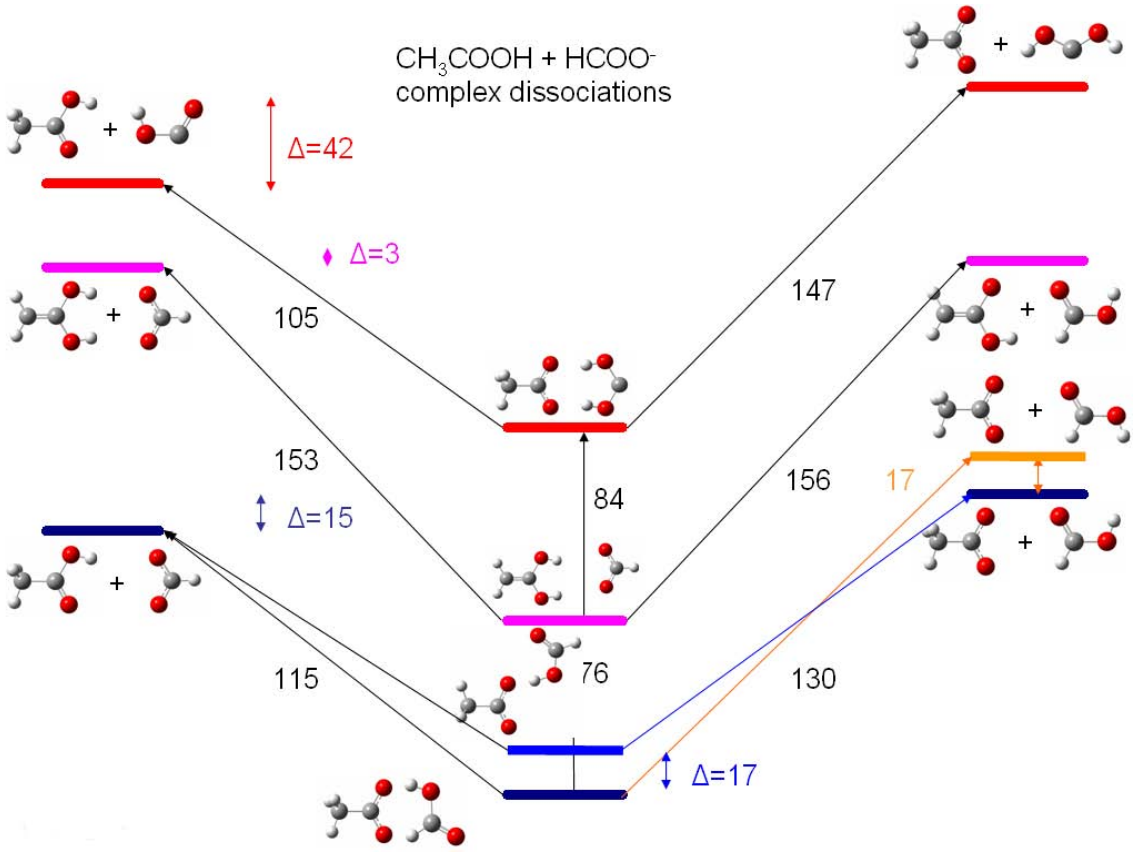

Instrumentation project

In an instrumental modification project, we are converting our guided ion beam tandem mass spectrometers to allow study of positive ions as well as negative ions. This will open up the possibility of using TCID methods to measure proton affinities of hydrocarbon radicals, including the phenoxy radical which will give an independent thermochemical handle on the bond dissociation energy of phenol. This modification is straightforward in principle, but the age of the current electronics and data acquisition computer and the large number of ion lens elements means that it is quite involved. At this stage, the custom ion lens voltage control units have been fabricated and installed and we are progressing on the compter control and data acquisition.

Future Directions

Because of the importance of oxygen-containing species in combustion, especially with oxygenated fuels, we will target the O–H bond dissociation enthalpies of unsaturated alcohols, carboxylic acids, and peroxides. We will examine additional ions for their suitability as proton transfer and hydrogen atom transfer reagents. For proton affinity measurements, the

experimental apparatus is being modified to allow the positive ion reactions as well as negative ions. The first target experiment with the new positive-ion capability of the instrument is collision-induced dissociation of phenoxy-ammonium complexes, which will allow an independent measurement of the bond dissociation energy of phenol via the proton affinity thermochemical cycle.

References

(1) DeTuri, V. F.; Ervin, K. M. *Int. J. Mass Spectrom.* **1998**, *175*, 123.

(2) Kim, H.-T.; Green, R. J.; Qian, J.; Anderson, S. L. *J. Chem. Phys.* **2000**, *112*, 5717.

(3) Mulder, P.; Korth, H.-G.; Pratt, D. A.; Dilabio, G. A.; Valgimigli, L.; Pdulli, G. F.; Ingold, K. U. *J. Phys. Chem. A* **2005**, *109*, 2647.

(4) DiLabio, G. A.; Mulder, P. *Chem. Phys. Lett.* **2006**, *417*, 566.

(5) Costa Cabral, B. J.; Canuta, S. *Chem. Phys. Lett.* **2005**, *406*, 300.

(6) Costa Cabral, B. J.; Canuto, S. *Chem. Phys. Lett.* **2006**, *417*, 570.

(7) Angel, L. A.; Ervin, K. M. *J. Phys. Chem. A* **2004**, *108*, 8345.

(8) Angel, L. A.; Ervin, K. M. *J. Phys. Chem. A* **2006**, *110*, 10392.

(9) Borges dos Santos, R. M.; Martinho Simoes, J. A. *J. Phys. Chem. Ref. Data* **1998**, *27*, 707.

(10) Jia, B.; Angel, L. A.; Ervin, K. M. **2007**, ((to be submitted)).

Publications, 2005–present

"Gas-phase acidities and O-H bond dissociation enthalpies of phenol, 3-methylphenol, 2,4,6-trimethylphenol, and ethanoic acid", L. A. Angel and Kent M. Ervin, *J. Phys. Chem. A.*,**110**, 10392-10403 (2006).

"Collision-induced dissociation of $HS^-(HCN)$: unsymmetrical hydrogen bonding in a proton-bound dimer anion", F. Ahu Akin and Kent M. Ervin, *J. Phys. Chem. A*, **110**, 1342 -1349 (2006).

"Threshold collision-induced dissociation of diatomic molecules: A case study of the energetics and dynamics of O_2^- collisions with Ar and Xe", F. A. Akin, J. Ree, K. M. Ervin and H. K. Shin, *J. Chem. Phys.* **123**, 064308:1-12 (2005).

"Photoelectron spectroscopy of phosphorus hydride anions", K. M. Ervin and W. C. Lineberger, J. Chem. Phys. **122**, 194303:1-11 (2005).

PESCAL, Fortran program for Franck-Condon analysis of photoelectron spectra, K. M. Ervin, (revised 2007).

CRUNCH, Fortran program for analysis of reaction cross sections with RRKM and PST models, K. M. Ervin and P. B. Armentrout, version 5.10 (revised 2007).

Spectroscopic and Dynamical Studies of Highly Energized Small Polyatomic Molecules

Robert W. Field
Massachusetts Institute of Technology
Cambridge, MA 02139
rwfield@mit.edu

Program Definition

The fundamental goal of this program is to develop the experimental techniques, diagnostics, interpretive concepts, and pattern-recognition schemes needed to reveal and understand how large-amplitude motions are encoded in the vibration-rotation energy level structure of small, gas-phase, combustion-relevant polyatomic molecules. We are focusing our efforts on unimolecular isomerization in several prototypical systems, including the HNC ↔ HCN, the HCCH ↔ CCHH, and the CNCN ↔ NCCN isomerization systems. We are also developing methods to use millimeter-wave pure rotational spectroscopy as a probe for absolute species- and vibrational level-populations of combustion-relevant molecules formed in nonequilibrium sources, such as a discharge jets, pyrolysis jets, and photolysis jets.

Recent Progress

HNC ↔ HCN Isomerization

The S_0 HNC-HCN potential energy surface is a prototype for high-barrier, bond-breaking isomerization. One of the primary goals of this research program is to observe and identify barrier-proximal states, i.e. the states that are energetically located near the isomerization barrier and have amplitude localized along the minimum energy isomerization path. The large amplitude motion embodied in the barrier-proximal states provides the basis for their detectability. When a large amplitude motion alters the molecular geometry, the electronic structure of the molecule inevitably changes as well. Thus, electronic properties, such as the Stark effect or hyperfine structure, can serve as markers to distinguish the rare barrier proximal states from the vastly more numerous "ergodic" states in which excitation is divided among many modes. In the HNC ↔ HCN system, the magnitude of the dipole moment is a sensitive diagnostic because the barrier-proximal states have significantly reduced dipole moments (~1 D) due to cancellation from the two oppositely signed dipole moments in the HCN(~ + 3 D) and HNC(~ – 3 D) configurations. Hyperfine structure, which arises from the interaction of the nuclear quadrupole moment of the nitrogen nucleus with the gradient of the field due to the electronic wavefunction, is another nuclear dynamics-sensitive electronic property. For HCN in the ground vibrational state, the quadrupole coupling constant is large and negative, $(eQq)_N = -4.7$ MHz, whereas for HNC in the ground vibrational state, it is small and positive $(eQq)_N =$ 0.26 MHz. Electronic structure calculations in our group have demonstrated that the quadrupole coupling constant is strongly dependent on the bond angle and therefore on the extent of bend excitation. These changes in quadrupole coupling constant have recently been experimentally verified in our laboratory. We plan to use both the quadrupole-coupling constant and the dipole moment as sensitive diagnostics for the onset of isomerization.

Before we can probe electronic properties of barrier proximal states, however, we must populate these highly excited vibrational levels. Based on calculations of the HNC excited state geometry, we believe that these bending levels are better accessed through stimulated emission pumping (SEP) experiments originating on the HNC side of the potential surface rather than on the HCN side. The first excited electronic state of HNC, however, has not previously been observed, in part because HNC is an unstable molecule and the excited state is predicted to be predissociated. We have successfully produced HNC in a discharge jet and have undertaken a systematic search for the excited state of HNC using laser induced fluorescence (LIF) and photofragment fluorescence excitation (PHOFEX) of the CN fragments. Figure 1 shows LIF and PHOFEX spectra between 193 and 197 nm. Although the region is rich with spectral features, none of them can be attributed to HNC. Indeed, all the LIF features and most of the PHOFEX features can be assigned as HCN hot bands. The spectral interference of the HCN hot bands and other molecules produced in the discharge jet limit our sensitivity and hamper our search efforts. Thus, we are exploring alternative methods for HNC production.

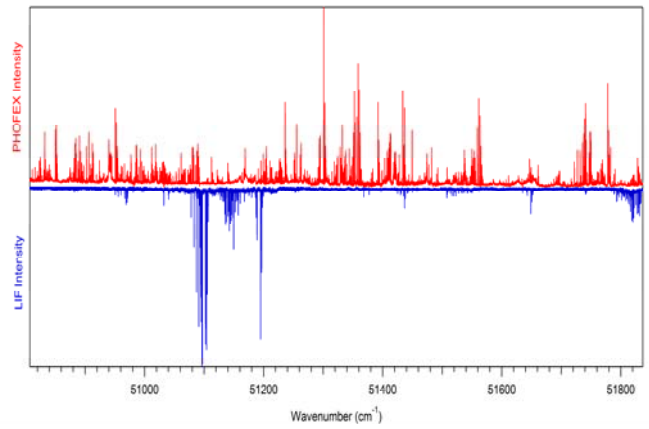

Figure 1. High resolution (0.1 cm^{-1}) LIF and PHOFEX spectra between 193 and 197 nm obtained in a discharge jet. All LIF transitions and most PHOFEX transitions can be attributed to HCN $\tilde{A} - \tilde{X}$ hot bands.

Acetylene ↔ Vinylidene Isomerization

As in the HNC ↔ HCN system, the goal of our studies on the acetylene ↔ vinylidene system is to observe barrier-proximal states. Large-amplitude motion on the acetylene S_0 surface, however, is considerably more complicated than in HCN, due both to the increased number of vibrational modes and to the inversion symmetry of the molecule. Many studies have demonstrated that the vibrational eigenstates of acetylene and similar molecules undergo a normal-to-local transition in which the normal modes appropriate to describe small deviations from the equilibrium geometry evolve into local modes in which the excitation is isolated in a single C-H bond stretch or CCH bend. The evolution of vibrational character is of particular interest in the acetylene bending system because the local bending vibration bears a strong resemblance to the reaction coordinate for isomerization from acetylene to vinylidene with one hydrogen moving a large distance off of the C-C bond axis, while the other hydrogen remains relatively stationary.

In order to observe these local-bender states, we must first locate special eigenstates on the S_1 surface that have the unique capability of serving as "local-bender plucks." In collaboration with Anthony Merer (University of British Columbia) and Nami Yamakita (Japan Women's University), we have recorded two types of high resolution spectra with the aim of locating and identifying these levels: one-photon laser-induced fluorescence spectra of jet-cooled acetylene have given the positions (see Figure 2) of many low-lying gerade levels and infrared-ultraviolet double resonance spectra via the $\tilde{X}$, ν_3 and $\tilde{X}$, $\nu_3+\nu_4$ vibrational levels as intermediates have identified large numbers of ungerade vibrational levels. Almost every vibrational level of the $\tilde{A}$ state expected below 3400 cm^{-1} has now been identified, including over 40 previously unassigned bending vibrational levels involving the two lowest frequency vibrations, the torsion (ν_4) and the in-plane bend (ν_6). The normal mode frequencies of these two vibrations are nearly degenerate and form polyads, which we label as B^n. Moreover, the strong a-axis Coriolis coupling massively distorts the K-structures of the individual vibrational levels. Our results show that the ν_4 and ν_6 modes are coupled through a strong 2:2 Darling-Dennison resonance. A good fit to the structure of the pure bending polyads has been obtained, fully characterizing the Darling-Dennison resonance and Coriolis coupling between modes 4 and 6.

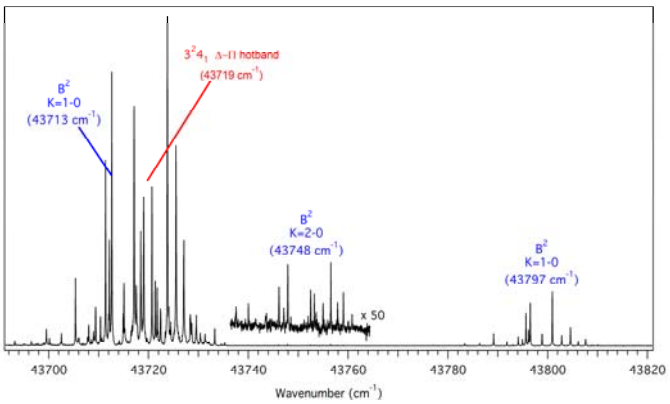

Figure 2. High resolution (0.1 cm^{-1}) one-photon LIF spectrum of B^2 (6^2, 6^14^1, or 4^2) polyad members in $\tilde{A}\,^1A_u$ C_2H_2. Transitions into the B^2 polyad are approximately 1000 times weaker than transitions into nearby 3^n trans-bend Franck-Condon active levels.

Isocyanogen (CNCN) ↔ Cyanogen (NCCN) Isomerization

The isomerization dynamics of acetylene and HNC are expected to be heavily influenced by the quantum-mechanical tunneling of the H-atom through the isomerization barrier. However, bond-breaking isomerization may manifest itself in the vibrational energy level structure in a qualitatively different way for systems where the bonds broken and formed are between heavy (non-H) atoms. For example, large-amplitude motions of heavy atoms along the isomerization coordinate probably do not decouple from the bath of orthogonal vibrational motions, thereby behaving ergodically as required by statistical rate theories. In order to elucidate the relationship between the vibrational spectrum and isomerization dynamics in all-heavy atom systems, highly vibrationally excited levels of the ground state of isocyanogen will be accessed through SEP from selected vibrational levels of the highly bent first electronically excited state. We have recently observed the first electronic spectrum of the less stable isomer of cyanogen using PHOFEX of the CN radicals produced by the dissociation of excited isocyanogen. Experiments have been performed both in a static cell and in a supersonic expansion in order to reduce the spectral congestion and to aid in vibrational assignment. It appears that predissociation of the CNCN S_1 state is too rapid to permit the use of SEP to interrogate the isomerization region of the S_0 potential surface.

Mm-wave Rotational Spectroscopy

In collaboration with Liam Duffy (University of North Carolina, Greensboro), we have developed a new technique called Beam Action Spectroscopy via Inelastic Scattering (BASIS). The BASIS method uses the rotational distribution of molecules in the beam as a "virtual" bolometer for detecting energetic processes that occur within the molecular beam. Analogous to the optothermal detection technique, absorption of radiation or fragmentation of molecules and/or clusters is indirectly detected by their resonant contribution to inelastic scattering within the beam and by the resultant changes in the rotational distribution of a "reporting" molecule within the beam. Specifically, action spectra are obtained by monitoring changes in pure rotational line intensities of the reporting spectator molecule. The technique relies on the fact that the probed rotational transitions of the reporting molecule are very sensitive ($\propto T^{-2}$) to the rotational temperature in the beam. Because of this sensitivity, when a parent molecule seeded in the molecular beam absorbs radiation and undergoes fragmentation, subsequent collisions with a spectator reporting molecule can result in a measurable change in the reporting molecule's rotational temperature. Furthermore, a gain effect is observed whereby the rotational line intensity changes are significantly larger than those predicted in traditional "hole burning" experiments (i.e., greater than the product of laser fluence and absorption cross sections) because a single parent absorption event can lead to a cascade of collisions with multiple reporting molecules. We have demonstrated the use of the BASIS technique in two very different experiments: 1) to reveal previously unreported vibrational structure in the UV spectrum of OClO between 30,000 and 36,000 cm^{-1}, and 2) to record the mid-IR vibrational spectrum of acetylene (see Figure 3). With the dynamic range afforded by mm/submm-wave techniques, the BASIS technique should be sufficiently sensitive to reveal rotational temperature shifts of a reporting molecule as small as 200 μK, making the technique highly sensitive to any energetic process that results in inelastic scattering within the molecular beam. We suggest that the technique may find particular utility in experiments with dark states, i.e. states that cannot be observed by conventional spectroscopic techniques.

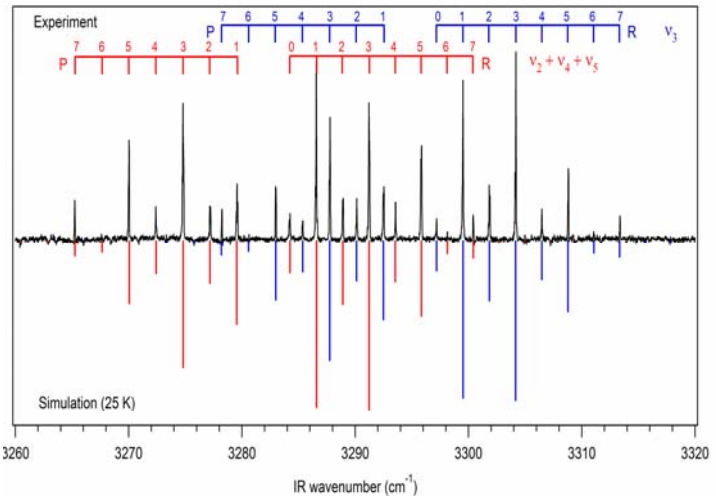

Figure 3. Vibration-rotation spectrum of acetylene observed with the BASIS technique. The spectrum was recorded by monitoring the change in intensity of a pure rotational transition of OCS (J=7←6) seeded in the molecular beam with acetylene. The laser excitation and subsequent thermalization occurred in the high density region near the nozzle, and the mm-wave absorption intensity change was monitored in the period immediately following the IR laser pulse.

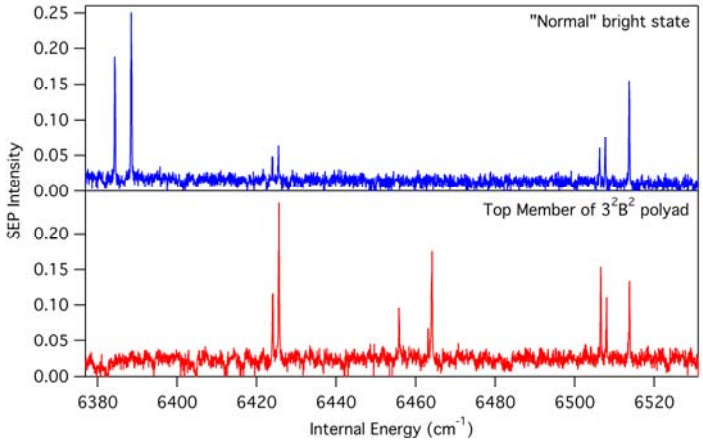

Figure 4. C_2H_2 SEP spectra obtained with the PUMP beam locked on the Q(1) line of a normal bright state (3^2) and from a potential "local bender pluck" (3^2B^2). These different PUMP transitions ultimately give access to different classes of vibrational levels on the ground potential surface.

Future Plans

In the near future, we plan to concentrate on the acetylene ↔ vinylidene system to locate and identify barrier-proximal states. Our extensive analysis of the anharmonic and Coriolis couplings on the S_1 surface of acetylene has identified several candidates for "local-bender plucks." Indeed, we have performed preliminary SEP experiments that indicate that these special S_1 states provide access to a different class of pure-bending levels on the S_0 surface (see Figure 4). We plan to record more SEP spectra in a higher energy region where vibrational levels at the local bending limit are expected to be present. The large amplitude motion associated with the local bending vibrations lead to changes in the electronic properties of acetylene, which result in a transition dipole between rotational levels of the two near-degenerate g/u vibrational eigenstates. This g/u degeneracy is a signature of local-mode behavior. This transition dipole moment gives rise to a Stark effect and the ability to observe "pure rotational" transitions in acetylene. We have recently utilized a one-dimensional reaction path-like Hamiltonian to put predictions of these dipole moments on a quantitative basis. Calculations performed at the CCSD(T) level of theory with a cc-pVQZ basis predict an approximately linear dependence of the dipole moment on the number of quanta in the local bending excitation. Thus, Stark effect measurements will be able to identify (and to provide a quantitative measure of progress along) the interesting extreme local-bend excited barrier-proximal states, which coexist with the vastly more numerous SEP-populated uninteresting ergodic vibrational levels of the electronic ground state.

Recent DOE-supported Publications (since 2005)

1. A. H. Steeves, H. A. Bechtel, S. L. Coy, and R. W. Field, "Millimeter-wave detected, millimeter-wave optical polarization spectroscopy (mmOPS)," *J. Chem. Phys.* **123**, 141102 (2005).
2. B. M. Wong, R. L. Thom, R. W. Field, "Accurate inertias for large-amplitude motions: Improvements on prevailing approximations," *J. Phys. Chem. A* **110**, 7406 (2006).
3. Z. Duan, N. Yamakita, S. Tsuchiya, and R. W. Field, "Differential temperature laser induced fluorescence spectroscopy," *Chem. Phys.*, **324**, 709 (2006).
4. H. A. Bechtel, A. H. Steeves, and R. W. Field, "Laboratory measurements of the hyperfine structure of $H^{14}N^{12}C$ and $D^{14}N^{12}C$," *Astrophys. J.* **649**, L53-L56 (2006).
5. B. M. Wong, A. H. Steeves, and Robert W. Field, "Electronic signatures of large amplitude motions: Dipole moments of vibrationally excited local-bend and local-stretch states of S_0 acetylene," *J. Phys. Chem. B*, **110**, 18912-18920 (2006).
6. B. H. Layne, L. M. Duffy, H. A. Bechtel, A. H. Steeves, and R. W. Field, "Beam Action Spectroscopy via Inelastic Scattering, *J. Phys. Chem. A*, submitted (2007).
7. W. B. Lynch, H. A. Bechtel, A. H. Steeves, J. J. Curley, and R. W. Field, "Observation of the $\tilde{A}\,^1A''$ State of Isocyanogen," *J. Chem. Phys.* submitted (2007).

Scanning Tunneling Microscopy Studies of Chemical Reactions on Surfaces

George Flynn, Department of Chemistry, Columbia University
Mail Stop 3109, 3000 Broadway, New York, New York 10027
gwf1@columbia.edu

Introduction and Overview

Our Department of Energy sponsored work is now focused on fundamental chemical events taking place on graphite, modified graphite, and metal surfaces with the intent of shedding light on the role of these surfaces in mediating the formation of polycyclic aromatic hydrocarbons (PAHs) and the growth of soot particles. Interest in soot is ultimately driven by the environmental and health implications arising from its formation in combustion reactions [1]. Soot growth can be divided into four consecutive stages [2-4]: formation of molecular precursors, heavy polycyclic aromatic hydrocarbons (PAHs), through homogeneous reactions of small aliphatics; nucleation of particles from these heavy PAHs followed by further coagulation; continued growth of particles through surface reactions; and finally, particle agglomeration. Polyacetylene [5] and ionic species [6] are among the proposed, key gaseous species in the formation and continuous growth of PAHs, and acetylene is thought to play a major role in the growth process via the hydrogen-abstraction-C_2H_2-addition (HACA) mechanism [7]. The application of this mechanism to the surface reaction stage of soot formation is based on the assumption that reactions occurring at the soot surface are similar to gaseous reactions taking place at the edges of PAH molecules. Experimental support for this mechanism is derived from the observation that surface growth rates for soot particle formation are proportional to the concentration of C_2H_2 in both laminar premixed [8,9] and diffusion [10] flames.

Since its invention some 25 years ago, scanning tunneling microscopy (STM) has become a powerful tool for interfacial studies mainly because of its ability to investigate surface structure and dynamics with molecular or even atomic resolution. For example, the same region of a surface can be investigated before and after exposure to reactive species using STM tip engagement techniques[11], thereby extracting information about reaction mechanisms localized at single atomic surface sites. In terms of chemical reactivity, the edges of large PAHs and the surfaces of soot particles in the third stage of growth are analogous to the edges of pits, defect sites and step edges on the highly oriented pyrolytic graphite (HOPG) samples used in the present study. Exposure of these relatively well characterized, defected HOPG sample surfaces to hydrocarbon fuels (e.g. C_2H_2) in a controlled manner under ultra-high vacuum (UHV) conditions, thus, provides an opportunity to investigate the fundamental chemical steps involved in soot formation. Scanning Tunneling Microscopy can be used to identify surface defects and step edges, as well as to resolve and probe individual molecules on surfaces. The convenience and importance of being able to probe single molecules and/or single sites on surfaces probably cannot be overemphasized. Graphite itself is largely inert and reactive events are likely to occur when individual molecules

are at or near dangling surface bonds typically found only at defect sites or step edges.

In the present study deliberately defected HOPG samples were prepared by standard etching procedures and placed in an ultra-high vacuum scanning tunneling microscope. After high temperature annealing of the sample, STM images were taken of selected defect sites on the surface before and after exposure to acetylene. Surface temperatures during exposure were typically 625 K. Both amorphous and ordered growth of carbonaceous material was observed at several defect sites as a result of reaction with C_2H_2.

Results: Chemistry and Imaging of Acetylene at Graphite Defects

C_2H_2 dosing experiments were carried out in a UHV chamber with a base pressure of 2×10^{-10} torr. The preparation chamber is equipped with standard UHV surface science analytical instruments. A variable temperature STM (VT STM, Omicron GmbH) capable of scanning at temperatures ranging from 25 K to 1400 K is attached to the preparation chamber. Nanometer sized defects were etched in ZYB grade HOPG, which was then inserted into the UHV chamber.

After intensive annealing treatment in vacuum at 1050 K, the sample was inserted into the STM scanning stage where the temperature was raised to 625 K before the Pt-Ir scanning tip was engaged in tunneling. An area of the surface with characteristic markers was chosen for study, and the pits in this area were imaged first. The tip was then moved away from this focused, characterized area by 300 nm, but kept engaged during this process. Following this initial imaging procedure, 1×10^{-8} torr of C_2H_2 gas was leaked into the chamber for 100 seconds (1 L) and allowed to react with the surface for 10 min. The tip was then moved back to the original imaging area, and STM topographs of the same pits before and after exposure to C_2H_2 were compared. (The tip is moved before acetylene exposure to avoid any surface "shadow effect" [12,13], which could affect the reaction rate for areas of the surface under the tip. Continual engagement, on the other hand, guarantees that the same areas can be reliably imaged both before and after exposure to reactive gas.)

The images of four pits were recorded and compared before and after C_2H_2 dosing. Two of them showed clear changes. New features were observed to grow in at the lower part of pit # 2 and covered about 60% of the pit area. A honeycomb superstructure [14], which is adjacent to the pit edge, can be seen by zooming in on the growth area. Line profiles show that the honeycomb superstructure possesses the same periodicity (0.219 nm) as the hexagonal symmetric carbon (0001) periodicity (0.211 nm) on the graphite surface. In addition to the honeycomb superstructure, two clumps of carbonaceous material with sizes of ~1 nm long and ~1 nm wide can be identified. They do not show the normal carbon (0001) hexagonal periodicity or any of the superstructure periodicity mentioned above.

A number of observations can be made about the reactivity of solid carbon substrates with the simple hydrocarbon fuel acetylene based on the results of the present study. First, not surprisingly, there is no evidence of reactivity at surface sites other than defects or step edges, at least for the modest temperatures (625 K) used here. Presumably the stability of the delocalized π-bonded graphite sheet structure creates such a significant barrier to attack by stable gas phase reagents, that most of the graphite surface structure is left un-reacted.

Second, defect sites are clearly more reactive as demonstrated in the present study where 2 of 4 investigated defects exhibited carbonaceous growth using even mild temperature reaction conditions and modest C_2H_2 exposure times. The low reactivity of graphite compared to soot is well documented, and the present results suggest that at least one reason for this is the paucity of reactive surface sites on typical graphite samples. Indeed, the ability of STM methods to probe a single "interesting" (i.e. reactive) site in the midst of a plethora of un-reactive sites is one of the great advantages of the technique. Nevertheless, to the extent that the electronic structure around graphite defect sites mimics the electronic structure of traditional soot material, graphite reactivity can serve as an excellent model system for unraveling the mechanisms of soot growth.

Third, there is clear evidence for the growth of both amorphous and graphitic material at defect sites due to reaction with acetylene. An interesting question for further study will be whether graphite can be cleanly "healed" to remove defects by using some combination of different hydrocarbon fuels or reaction conditions. From a standpoint of soot formation mechanisms, it will be important to see if both amorphous and ordered graphitic structures can be observed at higher temperatures and with different fuel mixes.

Present and Future Experimental Program

These STM images have provided convincing evidence for chemical reactions of acetylene at defect sites on graphite surfaces. Of particular interest for the future will be Scanning Tunneling Spectroscopy studies of the defect edges after growth of carbonaceous material has occurred. Such studies should provide clear information about the electronic states and structure of the newly formed material. In addition it will be particularly interesting to see if other small molecule fuels, dosed on a defect site, also produce growth and if the growth rate has a strong temperature dependence.

References

(1) Neilson, A. H.; Editor *The Handbook of Environmental Chemistry, Volume 3: Anthropogenic Compounds, Part J: PAHs and Related Compounds: Biology*, 1997.

(2) Harris, S. J.; Weiner, A. M. *Annual Review of Physical Chemistry* **1985**, *36*, 31.

(3) Richter, H.; Howard, J. B. *Progress in Energy and Combustion Science* **2000**, *26*, 565.

(4) Frenklach, M. *Physical Chemistry Chemical Physics* **2002**, *4*, 2028.
(5) Homann, K. H.; Wagner, H. G. *Symposium (International) on Combustion, [Proceedings]* **1967**, *11*, 371.
(6) Calcote, H. F. *Combustion and Flame* **1981**, *42*, 215.
(7) Frenklach, M.; Wang, H. *Symposium (International) on Combustion, [Proceedings]* **1991**, *23rd*, 1559.
(8) Harris, S. J.; Weiner, A. M. *Combustion Science and Technology* **1983**, *32*, 267.
(9) Xu, F.; Sunderland, P. B.; Faeth, G. M. *Combustion and Flame* **1997**, *108*, 471.
(10) Xu, F.; Faeth, G. M. *Combustion and Flame* **2001**, *125*, 804.
(11) Rim, K. T.; Mueller, T.; Fitts, J. P.; Adib, K.; Camillone, N., III; Osgood, R. M.; Batista, E. R.; Friesner, R. A.; Joyce, S. A.; Flynn, G. W. *Journal of Physical Chemistry B* **2004**, *108*, 16753.
(12) Stipe, B. C.; Rezaei, M. A.; Ho, W. *Journal of Chemical Physics* **1997**, *107*, 6443.
(13) Dobrin, S.; Harikumar, K. R.; Jones, R. V.; McNab, I. R.; Polanyi, J. C.; Waqar, Z.; Yang, J. *Journal of Chemical Physics* **2006**, *125*, 133407/1.
(14) Niimi, Y.; Matsui, T.; Kambara, H.; Tagami, K.; Tsukada, M.; Fukuyama, H. *Physical Review B* **2006**, *73*.

DOE Publications: (2004-2007)

1. Markus Lackinger, Thomas Müller, T.G. Gopakumar, Falk Müller, Michael Hietschold and George W. Flynn, "Tunneling Voltage Polarity Dependent Submolecular Contrast of Naphthalocyanine on Graphite – a STM Study of Close Packed Monolayers under Ultra-high Vacuum Conditions", J. Phys. Chem. 108, 2279-2284 (2004)
2. Gina M. Florio, Tova L. Werblowsky, Thomas Mueller, Bruce J. Berne, and George W. Flynn, "The Self-Assembly of Small Polycyclic Aromatic Hydrocarbons on Graphite: A Combined STM and Theoretical Approach", J. Phys. Chem. B, 109, 4520-4532 (2005)
3. K. Rim, S. Xiao, M. Myers, L. Liu, C. Su, M. Steigerwald, M. S. Hybertsen, C. Nuckolls, and G. W. Flynn, "Marrying Polycyclic Aromatic Hydrocarbons to Transition Metal Surfaces", submitted.
4. Li Liu, Kwang Taeg Rim, Daejin Eom, and George W. Flynn, "Acetylene Induced Growth of Graphitic Layers at Defect Sites on Highly Ordered Pyrolytic Graphite Studied by Scanning Tunneling Microscopy", in preparation.

Quantitative Imaging Diagnostics for Reacting Flows

Jonathan H. Frank
Combustion Research Facility
Sandia National Laboratories
P.O. Box 969, MS 9051
Livermore, CA 94551-0969
email: jhfrank@sandia.gov

Program Scope

The primary objective of this project is the development and application of laser-based imaging diagnostics for studying the interactions of fluid dynamics and chemical reactions in reacting flows. Imaging diagnostics provide temporally and spatially resolved measurements of species, temperature, and velocity distributions over a wide range of length scales. Multi-dimensional measurements are necessary to determine spatial correlations, scalar and velocity gradients, flame orientation, curvature, and connectivity. Current efforts in the Advanced Imaging Laboratory focus on planar laser-induced fluorescence (PLIF) and Rayleigh scattering techniques for probing the detailed structure of both isolated flow-flame interactions and turbulent flames. The investigation of flow-flame interactions is of fundamental importance in understanding the coupling between transport and chemistry in turbulent flames. These studies require the development of new imaging diagnostic techniques to measure key species in the hydrocarbon-chemistry mechanism as well as to image rates of reaction and dissipation.

Recent Progress

Recent research has continued to emphasize imaging diagnostics for probing the detailed structure of reaction zones during flow-flame interactions. Research activities have included: i) Highly resolved dissipation measurements in turbulent jet flames, ii) Studies of flame extinction and re-ignition dynamics, iii) Exploration of applications of laser-induced fluorescence imaging in microscopy.

Resolving Length Scales and Morphology of Dissipative Structures in Turbulent Flames

We have made significant advances in resolving the fine-scale dissipation structures in turbulent non-premixed flames using high-resolution 2-D Rayleigh imaging to measure thermal dissipation rates. The thermal dissipation is closely correlated with the mixture fraction dissipation, which is a fundamental quantity governing the rate of molecular mixing in turbulent non-premixed combustion. Highly spatially resolved dissipation measurements reveal layered structures at the smallest scales of turbulence, as is illustrated in Fig. 1.

Noise reduction is critical for accurate dissipation measurements. We have developed a noise suppression method using adaptive smoothing that enables detection of the dissipation layers without significantly attenuating the dissipation. We have measured distributions of dissipation layer widths and orientations in non-premixed $CH_4/H_2/N_2$ jet flames that are target flames in the TNF Workshop. The results provide unique insight into the length scales and morphology of dissipative structures. We combined spectral and spatial analyses of the dissipation field to determine the relationship between the dissipation layer widths, λ_D, and the Batchelor scale, λ_B. On the jet centerline, we measured $\lambda_D = 7.4\lambda_B$. In regions off the jet centerline, the ratio of λ_D to λ_B was larger than 7.4. These results are distinctly different from

previous studies in non-reacting flows, which measured smaller ratios of λ_D to λ_B. This discrepancy highlights the need for understanding scaling relationships in turbulent reacting flows rather than adopting scaling laws from non-reacting flows when modeling turbulent flames. Our dissipation studies provide a fundamental understanding of turbulent flow-flame interactions, and results will be used in developing turbulent combustion models.

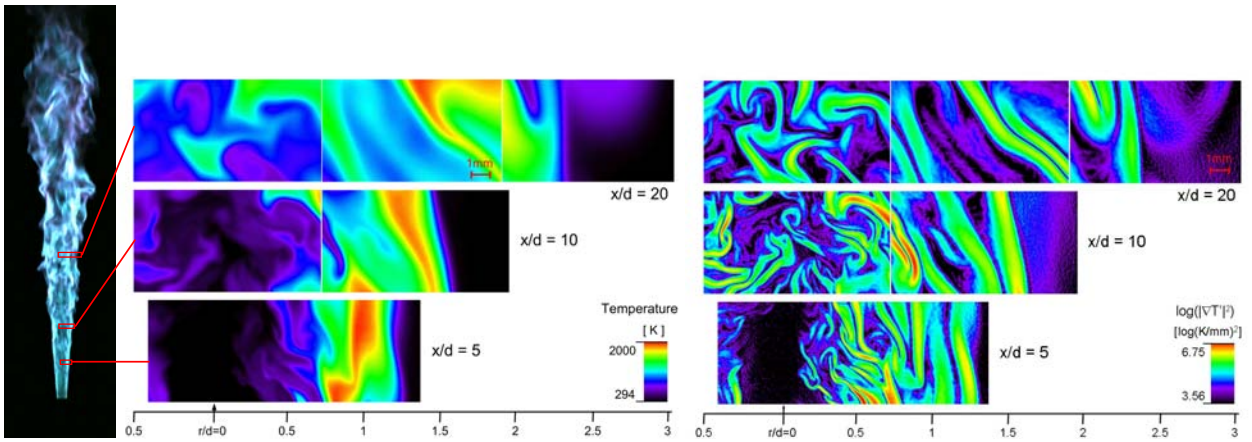

Fig. 1: (a) Measurement locations in DLR-A jet flame, (b) Single-shot temperature measurements, (c) Single-shot measurements of the squared gradient of the temperature fluctuation $|\nabla T'|^2$ reveals layers of high dissipation.

Dynamics of Extinction and Ignition

We are conducting an extensive series of experimental and computational studies on the response of ignition and extinction processes to transient flows and chemical perturbations. The experiments are closely coupled with direct numerical simulations by Jackie Chen. The goal of this effort is to provide a detailed understanding of the interactions between ignition chemistry and unsteady transport, including effects of diluents and trace species. We recently built a counterflow burner with a heated air flow and a pulsed vortex generator to investigate a broad range of ignition and extinction conditions in pulsed flows. This burner enables us to study ignition, extinction, and edge-flame propagation in highly repeatable flow-flame interactions.

As an illustration of the ignition and extinction phenomena that we are studying, Fig. 2 shows measurements of the effects of NO on the extinction and re-ignition of H_2 counterflow diffusion flames. This sequence of OH LIF images shows the perturbation of a counterflow flame by a toroidal vortex impinging from the fuel (bottom) side of the flame. When NO is

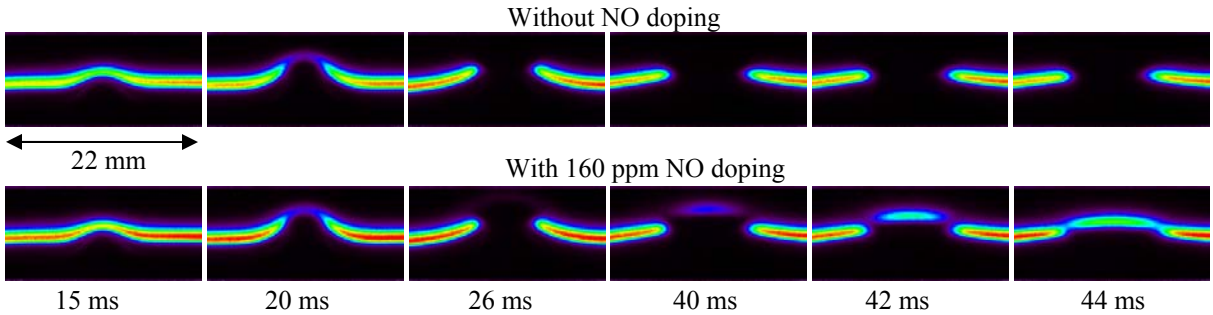

Fig. 2: Temporal sequence of OH LIF measurements shows the effects of NO doping on the response of a H_2 counter-flow diffusion flame to perturbation by a toroidal vortex. The vortex composition is the same as the fuel (12.5%H_2 in N_2 at 294K), and the oxidizer flow from the top is air heated to 938 K.

added to the heated oxidizer (top), the re-ignition process is significantly accelerated by the creation of an ignition kernel within the extinguished region. The mechanism for the catalytic effects of NO on hydrogen and hydrocarbon ignition is well established. In H_2-air mixtures, NO transforms the chain-terminating reaction of HO_2 formation, $H+O_2+M=HO_2+M$, into chain-propagation by OH production via reactions $NO+HO_2=NO_2+OH$ and $NO_2+H=NO+OH$. The doping of the reactants with NO provides a means to alter a specific set of reactions in the ignition chemistry and study the effects on flow-flame interactions. This approach enables us to understand the impact of unsteady transport on these chemical pathways and to map out different regimes of extinction/ignition processes. We are investigating the effects of NO as well as other dopents that are important in practical combustion devices. We expect that these studies will provide insight into the interplay between ignition chemistry and transient flows and will be valuable in developing models of extinction, ignition, and flame stabilization in turbulent flames.

Laser-induced Fluorescence Techniques for Microscopy

As an invited visiting scientist at Cambridge University, I have explored applications of laser diagnostics in wide-field and confocal microscopes. This effort focuses on developing a suite of fluorescence measurement techniques that enable quantitative non-intrusive probing of microfluidic and biological systems. The exploration of laser diagnostics in microscopy can provide new opportunities for studying reacting flows, and diagnostic developments in microscopy can potentially impact our development of combustion diagnostics. The interpretation of LIF signals in microscopy presents many of the same challenges that exist in fluorescence measurements of gas-phase reacting flows. For example, the LIF signals depend not only on the fluorophore concentration but also on interactions with the local environment. These interactions present opportunities for sensitive detection of local properties, such as pH, viscosity, or the presence of quenchers, as well as processes, such as binding events or conformational changes in macromolecules.

We have demonstrated quantitative measurements of sub-ns fluorescence lifetimes in a wide-field microscope using frequency-domain fluorescence lifetime imaging with a 40-MHz modulated LED for fluorescence excitation and an image intensifier for detection. We have used this fluorescence lifetime imaging system for quantitative analysis of molecular diffusion of iodide ions across a microchannel and measurements of polymer conformational dynamics.

Confocal fluorescence microscopy is one of the most powerful techniques in the biological sciences. Advances in microscope instrumentation are required to implement multiplexed fluorophore measurements and to provide a more complete characterization of the interactions of fluorophores with their local environment. We recently developed a confocal microscope system with continuously tunable fluorescence excitation and detection wavelengths and bandwidths throughout the visible spectrum. For fluorescence excitation, a fiber-laser pumped photonic crystal fiber is used to generate supercontinuum radiation. We demonstrated that this microscope system provides optimal excitation and detection of a wide range of fluorophores and provides a new capability for multi-parameter fluorescence measurements.

Future Plans

The high-resolution 2-D thermal dissipation measurements described above will be applied to several TNF target flames and will be combined with measurements of reactive scalars to better understand the relationship between dissipation structures and local extinction. Our experimental results will be coupled with large-eddy simulations (LES) by Joe Oefelein

(Sandia), providing a unique comparison of measured and simulated flame structures.

During the past year, we have constructed a distributed feedback dye laser to provide tunable 100-ps laser pulses for improved PLIF imaging in the Advanced Imaging Laboratory. This effort builds upon our demonstration of interference-free two-photon O-atom LIF imaging with a ps pulsed laser for excitation. We will investigate two-photon H-atom LIF excitation with ps lasers ($\lambda_{excitation}$=205 nm, $3d\ ^2\mathrm{D} \leftarrow\leftarrow 1s\ ^2\mathrm{S}$) as a potential method for eliminating photolytic interference from H-atom LIF imaging ($\lambda_{detection}$=656 nm $3d\ ^2\mathrm{D} \rightarrow 2p\ ^2\mathrm{P}$). These studies will be conducted in collaboration with Tom Settersten (Sandia).

We plan to develop the capability for high repetition-rate imaging of turbulent flames. The measurement of temporal sequences can provide unique insight into the behavior of turbulent flames. It is important to understand time history effects in the interactions between turbulent flows and flames. This information is not available from ensemble statistics of instantaneous snapshot measurements because the measurements are temporally uncorrelated. The ability to measure time sequences, or movies, will allow us, and users of this facility from the combustion community, to study the temporal development of turbulent structures. It will be particularly useful in determining the events that lead up to and follow extinction and re-ignition.

DOE Supported Publications (2005–2007)

J. H. Frank, S. A. Kaiser, M. B. Long, "Multiscalar Imaging in Partially Premixed Jet Flames with Argon Dilution," *Combust. Flame,* 143:507-523 (2005) (invited).

S. A. Kaiser, J. H. Frank, M. B. Long, "Use of Rayleigh Imaging and Ray Tracing to Correct for Beam-Steering Effects in Turbulent Flames," *Appl. Opt.,* 44:6557-6564 (2005) (invited).

R. S. Barlow, J. H. Frank, A. N. Karpetis, J.-Y. Chen, "Piloted Methane/Air Jet Flames: Transport Effects and Aspects of Scalar Structure," *Combust. Flame* 143:433-449 (2005).

B.O. Ayoola, R.Balachandran, J.H. Frank, E.Mastorakos, C.F. Kaminski, "Spatially resolved heat release rate measurements in turbulent premixed flames," *Combust. Flame* 144:1 (2006).

A. D. Elder, S. M. Matthews, J. Swartling, K. Yunus, J. H. Frank, C. M. Brennan, A. C. Fisher, C. F. Kaminski, "The application of frequency-domain fluorescence lifetime imaging microscopy as a quantitative analytical tool for microfluidic devices," *Opt. Exp.* 14:5456 (2006).

C.M. Vagelopoulos, J.H. Frank, "Transient Response of Premixed CH_4 Flames," *Combust. Flame* 146:572 (2006).

G. Amantini, J. H. Frank, M. D. Smooke, A. Gomez, "Computational and experimental study of standing CH_4 edge flames in the two-dimensional axisymmetric counterflow geometry", *Combust. Flame* 147:133 (2006).

A.D. Elder, J.H. Frank, J. Swartling, C.F. Kaminski, "Calibration of a wide-field frequency-domain fluorescence lifetime microscopy system using LEDs as light sources", *J. Microscopy* 224:166 (2006).

G. Amantini, J. H. Frank, M. D. Smooke, A. Gomez, "Computational and experimental study of steady axisymmetric non-premixed CH_4 counterflow flames," *Combust. Theory and Modeling* 11:47 (2007).

J.H. Frank, S.A. Kaiser, "Imaging of dissipative structures in the near field of a turbulent non-premixed jet flame," *Proc. Combust. Inst.* 31:1515 (2007).

MECHANISM AND DETAILED MODELING OF SOOT FORMATION

Principal Investigator: Michael Frenklach
Department of Mechanical Engineering
The University of California
Berkeley, CA 94720-1740
Phone: (510) 643-1676; E-mail: myf@me.berkeley.edu

Project Scope: Soot formation is one of the key environmental problems associated with operation of practical combustion devices. Mechanistic understanding of the phenomenon has advanced significantly in recent years, shifting the focus of discussion from conceptual possibilities to specifics of reaction kinetics. However, along with the success of initial models comes the realization of their shortcomings. This project focuses on fundamental aspects of physical and chemical phenomena critical to the development of predictive models of soot formation in the combustion of hydrocarbon fuels, as well as on computational techniques for the development of predictive reaction models and their economical application to CFD simulations. The work includes theoretical and numerical studies of gas-phase chemistry of gaseous soot particle precursors, soot particle surface processes, particle aggregation into fractal objects, and development of economical numerical approaches to reaction kinetics.

Recent Progress:

Graphene Layer Growth Chemistry: Five-Six-Flip Reaction (with R. Whitesides, D. Domin, W. A. Lester, Jr.)

Soot production as a by-product of hydrocarbon combustion remains an important engineering problem. Surface growth of soot particles is a critical part of modeling soot producing systems, as most of the soot mass is acquired via gas-surface reactions. Our goal is to gain fundamental understanding of evolution of soot particles, including their atomistic structures and surfaces. In recent studies, a new phenomenon was discovered—migration of five-membered rings along the zigzag edge of the evolving graphene layer. This phenomenon of migration alters significantly the framework for surface chemistry of graphene layer, and introduces a large number of possible elementary reaction steps that could take place on an evolving surface. One such example is the "collision" of migrating rings examined in our prior study, which results in the following transformation

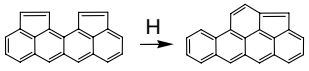

Reaction rates of this pathway were found to be comparable to those of the migration reaction, and the latter was reported to be one of the fastest reaction steps in zigzag-edge graphene chemistry.

In considering the fate of the product of the above reaction, we identified a new reaction pathway, re-orientation, or "flipping", of the surface complex

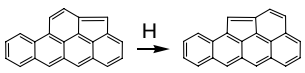

The potential energy surface, computed at the B3LYP/6-311G(d,p) level of quantum theory, is shown in the figure below. The upper, higher-energy, pathway is initiated by hydrogen atom

abstraction, and the lower-energy pathway is initiated by hydrogen atom addition. The numbering scheme for the species is consistent with the previously published collision pathway. The split radical dot shown on species **20** indicates that the species has a single delocalized unpaired electron.

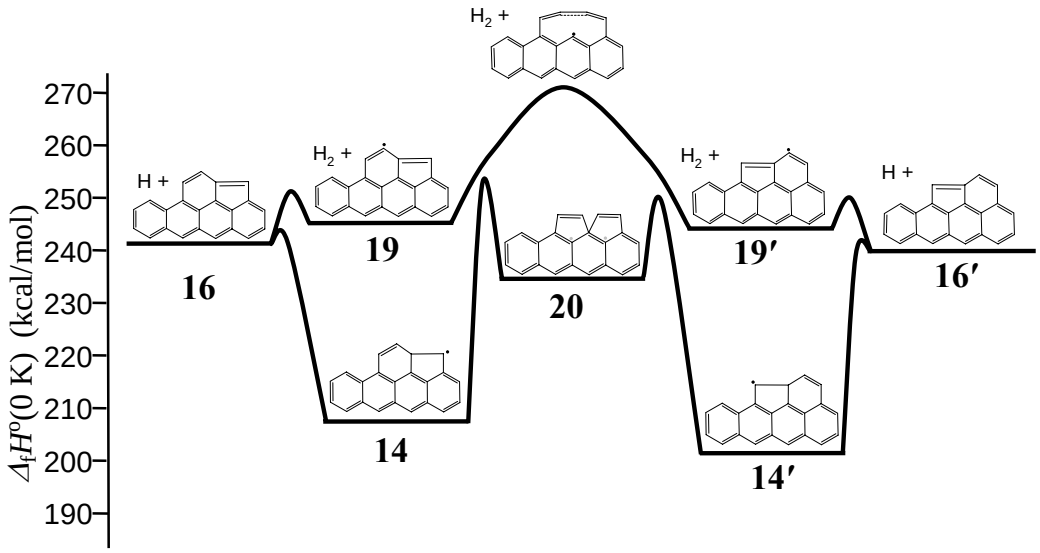

The total rate for the flip transformation is displayed in the figure on the right, and compared with the previously reported rates of graphene-edge ring migration and collision reactions. Inspection of these results indicates that the rate of the combined flip reaction is on the same order of magnitude and faster than those for the collision and migration reactions. Comparison among the two channels of the flip transformation indicated that the abstraction channel is more than 100 times faster than the addition channel.

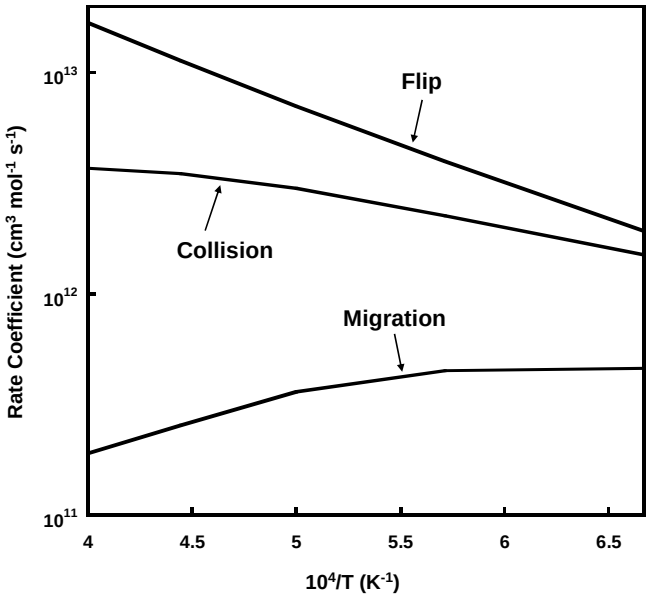

The analysis of the proposed flip reaction thus indicates that it occurs with rates comparable to and exceeding those of migration and collision reactions, while the latter was suggested to play an important role in graphene zigzag edge chemistry in flame environments. The new reaction adds a possibly important step in graphene layer growth, thus suggesting an even more complex network of elementary reaction steps than suspected earlier.

Molecular Dynamics Simulations of PAH Dimerization (with D. Wong and A. C. Schuetz)

In pursuit of mechanistic understanding of soot nucleation, we continued the study of collisions between aromatic molecules using molecular dynamics simulations with on-the-fly quantum forces. Simulations were conducted at a temperature of 1600 K investigating the formation of dimers for a series of aromatic hydrocarbons. Our previous study emphasized the development of rotations by starting the simulations with rotationally cold molecules. The present study extended the simulations to rotationally equilibrated colliders, and no significant effect on the investigated phenomenon was observed: dimer formation results from the transfer upon collision of the intermolecular kinetic energy into the internal rotational and/or vibrational modes of each molecule, and this transfer is highly dependent on collision geometry.

The principal finding is that observed dimer lifetimes increase with dimer mass, as shown in the table below for a series of peri-condensed aromatic hydrocarbons (PCAH)

Dimer	Mass (amu)	Number of runs	% runs with lifetime > 2 ps	Longest lifetime (ps)
$(\text{naphthalene})_2$	256	45	2	2.5
$(\text{anthracene})_2$	356	67	21	6.2
$(\text{phenanthrene})_2$	356	44	38	11.6
$(\text{pyrene})_2$	404	339	20	10.5
pyrene–coronene	502	112	40	15.6
$(\text{coronene})_2$	600	120	38	20.0

We extended our study to collision of aromatic-aliphatic-linked hydrocarbons (AALH), which was motivated by the fact that AALH molecules have a larger number of internal rotors than PCAH ones. In the initial set of simulations, out of 70 biphenyl-biphenyl runs, 11 % produced dimers with lifetimes greater than 2 ps, with the longest lived biphenyl-biphenyl dimer having a lifetime of 8.25 ps. Contrasting these results with those of comparable-size two-ring peri-condensed aromatics, we note that collisions of naphthalene molecules essentially did not produce dimers, and the lifetimes of biphenyl dimers are comparable to those of anthracene and pyrene, whose longest lifetimes were 6.25 and 10.5 ps, respectively. While these preliminary results indicate an increased stickiness of AALH as compared to PCAH, the effect, perhaps surprisingly, is not as dramatic as one would expect.

Future Plans

Graphene Layer Growth Chemistry: We will continue exploration of reactions on zigzag edges of a graphene sheet. This work will be performed in collaboration with William Lester's group, performing DFT analysis of the reaction systems and then QMC analysis on most critical reaction steps identified in the prior DFT studies. For every reaction system, a complete set of rate coefficients will be established in master-equation solutions.

Homogeneous Nucleation of Carbon Nanoparticles: We will continue exploration of clustering of aromatic species through molecular dynamics simulations with on-the-fly quantum forces. Our objective is to complete the comparison of the AALH and PCAH collision dynamics.

Developing Models for Representing Combustion Chemistry at Varying Levels of Complexity to Use with Models for Laminar and Turbulent Flow Fields to Describe Combustion Processes: The collaboration with the Sandia group of Habib Najm will continue on the combination of the

CSP-slow-manifold projection method and PRISM to construct an adaptive reduced-order model for stiff dynamical systems.

DOE-BES Supported Publications (2005-2007)

1. "Detailed Kinetic Modeling of Soot Aggregate Formation in Laminar Premixed Flames," M. Balthasar and M. Frenklach, *Combust. Flame* **140**, 130–145 (2005).
2. "Migration Mechanism of Aromatic-edge Growth," M. Frenklach, C. A. Schuetz, and J. Ping, *Proc. Combust. Inst.* **30**, 1389–1396 (2005).
3. "Monte-Carlo Simulation of Soot Particle Coagulation and Aggregation: The Effect of a Realistic Size Distribution," M. Balthasar and M. Frenklach, *Proc. Combust. Inst.* **30**, 1467–1475 (2005).
4. "Kinetic Monte Carlo Simulations of Soot Particle Aggregation," M. Balthasar, M. Kraft, and M. Frenklach, *Prepr. Pap.-Am. Chem. Soc., Div. Fuel Chem.* **50**(1), 2005, pp. 135–136.
5. "On Chain Branching and Its Role in Homogeneous Ignition and Premixed Flame Propagation," J. C. Lee, H. N. Najm, S. Lefantzi, J. Ray, M. Frenklach, M. Valorani, and D. Goussis, in *Computational Fluid and Solid Mechanics* 2005, K. J. Bathe, Ed., Elsevier, New York, 2005, pp. 717–720.
6. "Quantum Monte Carlo Study of Heats of Formation and Bond Dissociation Energies of Small Hydrocarbons," A. C. Kollias, D. Domin, G. Hill, M. Frenklach, D. M. Golden, and W. A. Lester, Jr., *Int. J. Chem. Kinet.* **37**, 583–592 (2005).
7. "The Role of Explosive Modes in Homogeneous Ignition and Premixed Flames," J. C. Lee, H. N. Najm, S. Lefantzi, J. Ray, M. Frenklach, M. Valorani, and D. A. Goussis, Proceedings of the *20th International Colloquium on the Dynamics of Explosions and Reactive Systems*, Montreal, 2005.
8. "An Adaptive Reduced-Order Chemical Model," J. C. Lee, H. N. Najm, S. Lefantzi, J. Ray, M. Frenklach, M. Valorani, and D. A. Goussis, Proceedings of the *20th International Colloquium on the Dynamics of Explosions and Reactive Systems*, Montreal, 2005.
9. "Graphene Layer Growth: Collision of Migrating 5-Member Rings," R. Whitesides, A. C. Kollias, D. Domin, W. A. Lester, Jr., and M. Frenklach, Fall Meeting of the Western States Section of the Combustion Institute, Stanford, CA, October 17-18, 2005, paper 05F-62.
10. "Quantum Monte Carlo Study of Small Hydrocarbon Atomization Energies," A. C. Kollias, D. Domin, G. Hill, M. Frenklach, W. A. Lester, Jr., *Mol. Phys.* **104**, 467 (2006).
11. "Graphene Layer Growth: Collision of Migrating Five-Membered Rings," R. Whitesides, A. C. Kollias, D. Domin, W. A. Lester, Jr., and M. Frenklach, *Prepr. Pap.-Am. Chem. Soc., Div. Fuel Chem.* **51**, 174 (2006).
12. "A CSP and Tabulation Based Adaptive Chemistry Model," J. C. Lee, H. N. Najm, S. Lefantzi, J. Ray, M. Frenklach, M. Valorani, and D. A. Goussis, *Combust. Theory Model.* **11**, 73 (2007).
13. "Transforming Data into Knowledge—Process Informatics for Combustion Chemistry," M. Frenklach, *Proc. Combust. Inst.* **31**, 125 (2007)**,** Invited Topical Review.
14. "Graphene layer growth: Collision of migrating five-member rings," R. Whitesides, A. C. Kollias, D. Domin, W.A. Letser, Jr., and M. Frenklach, *Proc. Combust. Inst.* **31**, 539 (2007).
15. "Numerical Simulations of Soot Aggregation in Premixed Laminar Flames," N. Morgan, M. Kraft, D. Wong, M. Frenklach, P. Mitchell, *Proc. Combust. Inst.* **31**, 693 (2007).
16. "Efficient Slow Manifold Identification for Tabulation Based Adaptive Chemistry," *Proceedings of the 5th U.S. National Combustion Meeting*, San Diego, CA, March 25-28, 2007, Paper No. C31.
17. "Graphene Layer Growth Chemistry: Five-Six-Ring Flip Reaction," R. Whitesides, D. Domin, W. A. Lester, Jr., and M. Frenklach, *Proceedings of the 5th U.S. National Combustion Meeting*, San Diego, CA, March 25-28, 2007, Paper No. D31.
18. "Molecular Dynamics Simulations of PAH Dimerization," D. Wong, C. A. Schuetz, and M. Frenklach, *Proceedings of the 5th U.S. National Combustion Meeting*, San Diego, CA, March 25-28, 2007, Paper No. F21.
19. "Efficient Slow Manifold Identification for Tabulation Based Adaptive Chemistry," J. Ortega, H. Najm, M. Valorani, D. Goussis, and M. Frenklach, 21st International Colloquium on the Dynamics of Explosions and Reactive Systems, Poitiers, France, July 22-27, 2007, accepted.
20. "Enthalpies of formation for the C_4H_3 and C_4H_5 isomers using diffusion Monte Carlo," D. Domin, W. A. Lester, Jr., R. Whitesides, and M. Frenklach, *J. Chem Phys.*, submitted.

CHEMICAL DYNAMICS IN THE GAS PHASE: QUANTUM MECHANICS OF CHEMICAL REACTIONS

Stephen K. Gray

Chemistry Division
Argonne National Laboratory
Argonne, IL 60439

Email: gray@tcg.anl.gov

PROGRAM SCOPE

This program focuses on theoretical chemical reaction dynamics, with an emphasis on the development and application of rigorous quantum dynamics approaches. In particular, time-dependent quantum methods (wave packets) and iterative time-independent quantum methods are often used to study the spectroscopy and dynamics of combustion relevant problems. The results obtained allow one to gauge the quality of potential energy surfaces, and to infer the validity of more approximate theoretical methods such as quasiclassical trajectories and statistical theories. The results also yield important mechanistic insights into the dynamics.

RECENT PROGRESS

Motivated by the experimental work of Continetti and coworkers [1], a six-dimensional quantum dynamics study of the neutral HOCO system that results after electron photodetachment from HOCO anions was completed in collaboration with Goldfield [2]. The potential energy surface developed by Schatz, Harding and coworkers was employed [3], and the four-atom real wave packet methodology [4] was used for the quantum dynamics. The previously developed parallel four-atom code [5] was essential to the successful completion of the project. Figure 1(a) depicts the relevant energetics. In addition to fragmentation products H + CO_2 and OH + CO, stable and long-lived HOCO complexes can also form because the departing electron's kinetic energy can take up a significant fraction of the energy made available by the photon. Indeed, in agreement with experimental estimates, 80% of the anions are converted to very long-lived HOCO complexes. Regarding the fragmentation products, Figure 1(b) shows very good agreement between the theoretical and experimental electron kinetic energy distributions associated with the OH + CO product channel. (Electron kinetic energies are inferred from energy conservation considerations.) There were some discrepancies between theory and experiment regarding the H + CO_2 electron kinetic distributions which are still under investigation.

Building on our previous total angular momentum J = 0 work on the CH + $H_2 \rightarrow CH_2$ + H reaction [6], a variety of J > 0 wave packet calculations were undertaken. Work is currently in progress, using a capture model/phase space theory approached, motivated by the work of Chen and Guo [7], to construct the first quantum dynamics based estimates of the rate constant for this reaction and to compare with experimental results [8].

We also continued work on selected triatomic systems using the real wave packet methodology, including a detailed study of the $O^+ + H_2$ system in collaboration with Gonzalez and coworkers [7] and an analysis of differential cross sections for $H + H_2$ in collaboration with Balint-Kurti and coworkers [8].

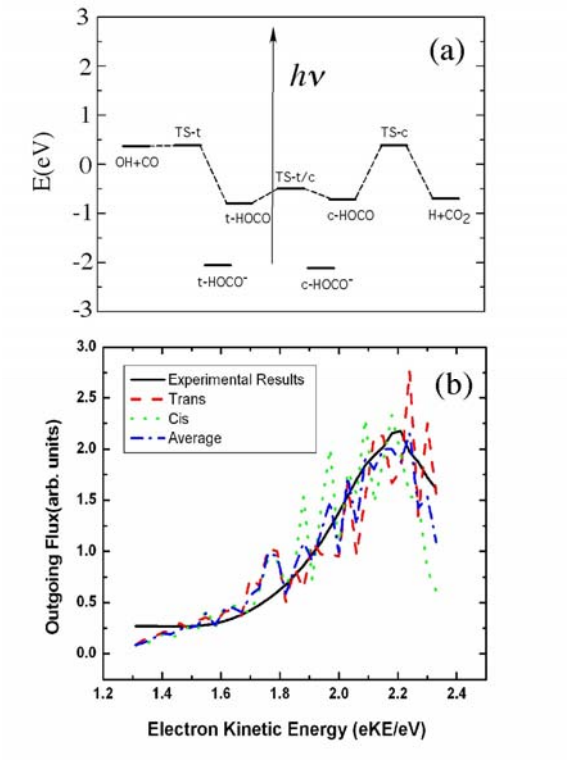

Figure 1. (a) The energetics of the $HOCO^- + h\nu \rightarrow e^- +$ neutral products process. (b) Comparison of experimental [1] and theoretical [2] electron kinetic energy distributions associated with the OH + CO product channel.

FUTURE PLANS

In addition to completing work on a quantum dynamics based estimate of the rate constant for $CH + H_2$, work will be initiated on the OO bond dissociation dynamics in hydrogen peroxide, HOOH [11,12]. Zero-point energy violation issues have been noted by Guo and Thompson in classical trajectory work on HOOH [12]. Our quantum dynamics work should lead to results more comparable to previous experimental [11] results, and new insights into the dissociation dynamics.

REFERENCES

[1] T. G. Clements, R. E. Continetti, and J. S. Francisco, J. Chem. Phys. **117**, 6478 (2002).
[2] S. Zhang, D. M. Medvedev, E. M. Goldfield, and S. K. Gray, J. Chem. Phys. **125**, 164312 (2006).
[3] M. J. Lakin, D. Troya, G. C. Schatz, and L. B. Harding, J. Chem. Phys. **119**, 5848 (2003).
[4] E. M. Goldfield and S. K. Gray, J. Chem. Phys. **117**, 1604 (2002).
[5] D. M. Medvedev, E. M. Goldfield, and S. K. Gray, Comp. Phys. Comm. **166**, 94 (2005).
[6] J. Mayneris, A. Saracibar, E. M. Goldfield, M. Gonzalez, E. Garcia, and S. K. Gray, J. Phys. Chem. A, **110**, 5542 (2006).
[7] S. Y. Lin and H. Guo, J. Chem. Phys. **120**, 9907 (2004).
[8] R. A. Brownsword, A. Canosa, B. R. Rowe, I. R. Sims, I. W. M. Smith, D. W. A. Stewart, A. C. Symonds and D. Travers, J. Chem. Phys. **106**, 7662 (1997).
[9] R. Martinez, J. D. Sierra, S. K. Gray, and M. Gonzalez, J. Chem. Phys. **125**, 164305 (2006).
[10] M. Hankel, S. C. Smith, R. J. Allan, S. K. Gray, and G. G. Balint-Kurti, J. Chem. Phys. **125**, 164393 (2006).
[11] B. Kuhn and T. R. Rizzo, J. Chem. Phys. **112**, 7461 (2000).
[12] Y. Guo and D. L. Thompson, Chem. Phys. Lett. **382**, 654 (2003).

DOE COMBUSTION PROGRAM SUPPORTED PUBLICATIONS (2005-2007)

1. D. M. Medvedev, E. M. Goldfield, and S. K. Gray, An OpenMP/MPI approach to the parallelization of iterative four-atom quantum mechanics, Comp. Phys. Comm. **166**, 94-108 (2005).
2. D. M. Medvedev, L. B. Harding, and S. K. Gray Methyl radical: ab initio global potential energy surface, vibrational levels, and partition function, Mol. Phys. **104**, 73-82 (2006).
3. J. Mayneris, A. Saracibar, E. M. Goldfield, M. Gonzalez, E. Garcia, and S. K. Gray, Theoretical study of the complex-forming $CH + H_2 \rightarrow CH_2 + H$ reaction, J. Phys. Chem. A, **110**, 5542-5548 (2006).
4. S. Zhang, D. M. Medvedev, E. M. Goldfield, and S. K. Gray, Quantum dynamics study of the dissociative phototodetachment of $HOCO^-$, J. Chem. Phys. **125**, 164312 (2006) (8 pages).
5. R. Martinez, J. D. Sierra, S. K. Gray, and M. Gonzalez, Time-dependent quantum dynamics study of the $O^+ + H_2(v=0,j=0) \rightarrow OH^+ + H$ ion-molecule reaction and isotopic variants (D_2, HD), J. Chem. Phys. **125**, 164305 (2006) (7 pages).
6. M. Hankel, S. C. Smith, R. J. Allan, S. K. Gray, and G. G. Balint-Kurti, State-to-state reactive differential cross sections for the $H + H_2 \rightarrow H_2 + H$ reaction on five different potential energy surfaces: DiffRealWave, J. Chem. Phys. **125**, 164393 (2006) (12 pages).
7. E. M. Goldfield and S. K. Gray, An accurate approach to quantum reaction dynamics, Adv. Chem. Phys., *in press* (2007).

This work was supported by the Office of Basic Energy Sciences, Division of Chemical Sciences, Geosciences, and Biosciences, U.S. Department of Energy under Contract No. DE-AC02-06CH11357

Computer-Aided Construction of Chemical Kinetic Models

William H. Green, MIT Department of Chemical Engineering,
77 Massachusetts Ave., Cambridge, MA 02139. email: whgreen@mit.edu

Project Scope

The combustion chemistry of even simple fuels can be extremely complex, involving hundreds or thousands of kinetically significant species. The most reasonable way to deal with this complexity is to use a computer not only to numerically solve the kinetic model, but also to construct the kinetic model in the first place. Our research spans a wide range from quantum chemical calculations on individual molecules and elementary-step reactions, through the development of improved rate/thermo estimation procedures, the creation of algorithms and software for constructing and solving the simulations, the invention of methods for model-reduction while maintaining error control, through comparisons with experiment. We are developing methods needed to make computer-construction of accurate combustion models practical, as well as tools to make it feasible to handle and solve the resulting large kinetic models, even in multidimensional reacting flows. Many of the parameters in the models are derived from quantum chemistry, and the models are compared with experimental data measured in collaboration with other researchers.

Recent Progress

The main focus of our research continues to be the development of methodology for constructing and solving combustion simulations, supplemented by experimental measurements. We have recently released our extensible mechanism-construction software and, with funding from NSF, we are currently integrating this software with the PrIMe database. During 2006-2007 we made significant progress in numerical methods for solving reacting flow simulations involving complex chemistry, and in numerical methods for checking whether kinetic simulations are consistent with experimental data. We also constructed a new laser flash photolysis apparatus, and used it to measure the rates of several reactions of the vinyl radical.

Notable accomplishments during this grant period include:

1) Distribution of version 2.0 of our open-source easily-extensible automated reaction-mechanism generation software: http://sourceforge.net/projects/rmg
2) Use of the above software to construct models for the hexane pyrolysis data measured in Marin's lab [8], for the neo-pentane oxidation experiments conducted in Taatjes's lab [14], and for molecular weight growth chemistry measured by Fahr and by McEnally & Pfefferle. In each case the detailed kinetic models revealed features that were difficult or impossible to infer from the experimental data alone.
3) Development of the first rigorous method for controlling the error associated with use of reduced chemistry models in CFD reacting-flow simulations.[4,11,12]
4) Development of the first automated method for constructing a reduced kinetic model guaranteed to be accurate to any user-specified error tolerance over any user-specified range of reaction conditions [12].

5) Demonstration of new global optimization algorithms useful in combustion modeling and kinetics, e.g. [3,9,11,12], including the first algorithm guaranteed to find the global best-fit to the nonlinear least-squares problems that arise when interpreting kinetic decays [9]. This allows one to draw firmer conclusions about whether or not these data are consistent with model predictions.

Future Plans

We are developing an improved automated method for estimating pressure-dependent rate constants for incorporation into the publicly-distributed reaction mechanism generator. We will soon begin to add nitrogen chemistry to the mechanism-generation software (currently it is restricted to C,H,O chemistry). With separate funding, we have developed predictive kinetic models for complicated gas-phase chemical systems including Fe, P, Ti, and Cl atoms, and we plan to incorporate this chemistry into the open-source software as well. With NSF funding, all of this modeling software will be integrated with the PrIMe experimental data.

Our existing automated error-controlled mechanism-reduction methods work by eliminating reactions. We are now developing methods for simultaneous elimination of species while maintaining control of the error these reductions introduce in reacting flow simulations. Most of our focus has been on steady-state laminar flame simulations, where we can guarantee error control, but we have also recently developed a new species-reduction method for time-dependent simulations.

We have measured the rates of several reactions of vinyl radical and allyl radical using the new flexible flash photolysis facility at MIT at several pressures, up to 750 K:

CH_2=CH● + CH_2=CH_2 → CH_2=$CHCH_2CH_2$●

CH_2=CH●+ CH_3CH=CH_2 → products

CH_2=CH● + CH_3CH_2CH=CH_2 → products

CH_2=CH● + CH_3CH=$CHCH_3$ → products

CH_2=CH● + $(CH_3)_2$C=CH2 → products

CH_2=CH● → products

2 CH_2=$CHCH_2$● → products

We are currently analyzing and writing up this data, and comparing the results with quantum chemistry and master equation calculations. Initial indications are that below 1000 K vinyl radical adds to C-C double bonds much faster than it abstracts H atoms, with E_a for addition ~5 kcal/mole.

Acknowledgements

Most of our recent flash photolysis experiments have been done in collaboration with Craig Taatjes, and these experiments were made possible by Bob Field lending us lasers and other equipment. The probe laser system was paid for in part by an NSF equipment grant to the Harrison Spectroscopy Laboratory. The HCCI engine experiments at MIT were made possible through funding by Ford and BP, and technical collaboration with Wai Cheng. Our work on numerical methods has benefited significantly from ongoing interactions with Paul Barton.

Publications Resulting from DOE Sponsorship (Since 2005)

1. H. Richter, S. Granata, W.H. Green, & J.B. Howard, "Detailed Modeling of PAH and Soot Formation in a Laminar Premixed Benzene/Oxygen/Argon Low-Pressure Flame", *Proc. Combust. Inst.* **30**(1), 1397-1405 (2005).
2. H. Ismail, J. Park, B.M. Wong, W.H. Green, & M.C. Lin, "A Theoretical and Experimental Kinetic Study of Phenyl Radical Addition to Butadiene", *Proc. Combust. Inst.* **30**(1), 1049-1056 (2005).
3. B. Bhattacharjee, P. Lemonidis, W.H. Green and P.I. Barton "Global Solution of Semi-infinite Programs", *Math. Programming (Series A)* **103**(2), 283-307 (2005).
4. O.O. Oluwole and W.H. Green, "Rigorous Error Control in Reacting Flow Simulations Using Reduced Chemistry Models", in *Computational Fluid and Solid Mechanics 2005*, ed. by K.J. Bathe (Elsevier, 2005).
5. B.M. Wong & W.H. Green, "Effects of Large-Amplitude Torsions on Partition Functions: Beyond the Conventional Separability Assumption", *Mol. Phys.* **103**, 1027-1034 (2005).
6. K. Schuchardt, O. Oluwole, W. Pitz, L.A. Rahn, W.H. Green, D. Leahy, C. Pancerella, M. Sjoberg, and J. Dec, "Development of the RIOT Web Service and Information Technologies to Enable Mechanism Reduction for HCCI Simulations", *Journal of Physics: Conference Series* **16**, 107-112 (2005).
7. J.L. Chesa Rocafort, M. Andreae, W.H. Green, W.K. Cheng, & J.S. Cowart, "A Modeling Investigation into the Optimal Intake and Exhaust Valve Event Duration and Timing for a Homogeneous Charge Compression Ignition Engine", *SAE* 2005-01-3746 (2005).
8. K.Van Geem, M.F. Reyniers, G. Marin, J. Song, D.M. Matheu, and W.H. Green, "Automatic Reaction Network Generation using RMG for Steam Cracking of n-Hexane", *A.I.Ch.E. Journal* **52**(2), 718-730 (2006).
9. A.B. Singer, J.W. Taylor, P.I. Barton, and W.H. Green, "Global Dynamic Optimization for Parameter Estimation in Chemical Kinetics", *Journal of Physical Chemistry A* **110**(3), 971-976 (2006).
10. J. Yu, R. Sumathi, and W.H. Green, "Accurate and Efficient Estimation Method for Predicting the Thermochemistry of Furans and *ortho*-Arynes -- Expansion of the Bond-Centered Group Additivity Method", *J. Phys. Chem. A* **110**(21), 6971(2006).
11. O.O. Oluwole, B. Bhattacharjee, J.E. Tolsma, P.I. Barton, and W.H. Green, "Rigorous Valid Ranges for Optimally-Reduced Kinetic Models", *Combustion and Flame* **146**, 348-365 (2006).
12. O.O. Oluwole, P.I. Barton, & W.H. Green, "Obtaining Accurate Solutions using Reduced Chemical Kinetic Models: A new Model Reduction method for models rigorously validated over ranges", *Combust. Theory Model.* **11**(1), 127-146 (2007).
13. W.H. Green, "Predictive Kinetics: A New Approach for the 21st Century", *Advances in Chemical Engineering* (2007, in press).
14. S.V. Petway, H. Ismail, W.H. Green, E.G. Estupiñán, L.E. Jusinski, and C.A. Taatjes, "Measurements and Automated Mechanism Generation Modeling of OH Production in Photolytically-Initiated Oxidation of the Neopentyl Radical", *Journal of Physical Chemistry A* (2007, in press).

Wave packet based quantum statistical model for complex-forming reactions

Hua Guo

Department of Chemistry, University of New Mexico

ABSTRACT

Complex-forming reactions are prevalent in combustion, in atmospheres and in interstellar media. Such reactions proceed on potential energy surfaces (PESs) dominated by deep wells. Because of the large number of quantum states supported by the potential wells and their often long lifetimes, quantum mechanical characterization of such reactions is quite challenging. However, much progress has been made in the last few years, due partly to the ever increasing computer power and partly to efforts of several theoretical groups including us. Here, we summarize some recent progress in our group.

We have applied the wave packet-based statistical model[1] to study several complex-forming reactions, including the O + O_2 isotope exchange reaction[2,3] and the H + O_2 → HO + O reaction.[4] The recent crossed molecular beam study on the former reaction[3] strongly suggested a non-statistical component, which might be related to the non-statistical behavior of the mass-independent isotope effects in ozone formation.[5] The wave packet based statistical model recognizes the quantum capture dynamics in both the entrance and exit channels and provides a limiting case to gauge the statistical nature of the reaction. Interestingly, our statistical model yielded product distributions that are in reasonable agreement with experimental time-of-flight profiles at a number of scattering angles, as shown in Fig. 1. This is quite interesting because the statistical model significantly underestimates the rate constant and is incapable of describing the forward-backward asymmetry in the differential cross section.[2] One possible explanation is that the statistical model underestimates the non-reactive flux that might be long lived. Further investigations are underway.

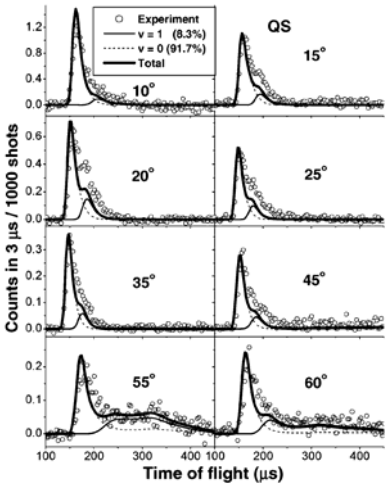

Fig. 1 Comparison of experimental time-of-flight signals with quantum statistical (QS) model results for the ^{18}O + $^{32}O_2$ exchange reaction.[3]

The second reaction we investigated, namely $H + O_2 \rightarrow HO + O$, is considered as the single most important reaction in combustion because of its role in chain initiation.[6] Its statistical nature has been questioned.[7] We have found using the statistical model that the rate constant of the reverse reaction can be accurately obtained, at least in low temperatures. Based on these, we further computed the rate constant of the forward reaction using the experimentally determined temperature dependent equilibrium constant.[4] The result is in quite good agreement with the available experimental data, see Fig. 2. These results seem to suggest that the reaction in the reverse direction is capture dominated and quite statistical, at lease at low energies. However, the rate constant is a highly averaged quantity and may not be necessarily the best yardstick for gauging the statistical nature of the reaction.

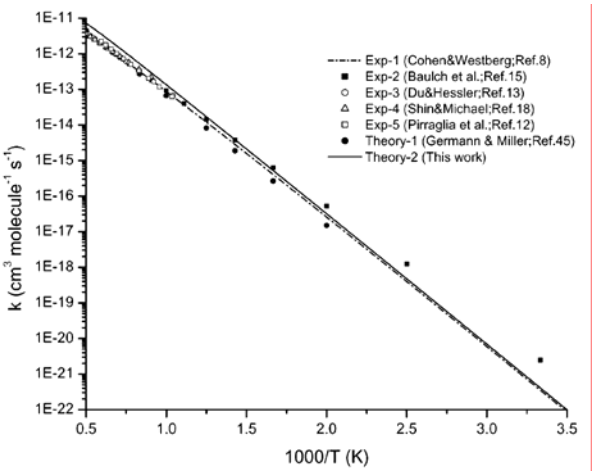

Fig. 2 Comparison between experimental rate constant for the $H + O_2$ reaction and that obtained from our statistical model.[4]

To investigate unambiguously the statistical nature of these important complex-forming reactions, it is vital to have exact quantum scattering results, to which the approximate models can be compared. To this end, we have mounted a major effort to develop an efficient and accurate method to compute S-matrix elements for reactive scattering.[8] Our method is based on the efficient and accurate Chebyshev propagation and thus scales well with the dimensionality of the system. In addition, it yields energy dependence from a single wave packet propagation and thus is ideal for computing the energy dependence of cross sections as well as rate constants. This method was first applied to the $H + H_2$ reaction and the agreement with the well-established time-independent quantum method was shown to be excellent.[8] It has then used to compute the differential and integral cross sections of an insertion reaction, namely $N + H_2 \rightarrow NH + H$, which is dominated by a deep potential well.[8,9] Figure 3 displays the calculated differential cross section as a function of the collision energy, which shows significant oscillations. We believe that such oscillations might be due to quantum bottleneck states formed near the entrance channel barrier, and are currently seeking experimental verification with Prof. Xueming Yang at Dalian Institute of Chemical Physics. Very recently, we have applied our exact method to the $H + O_2$ reaction, which yielded the same results as those obtained with a time-independent quantum method by Prof. Pascal Honvault at Universite de Frenche-Comte.[10]

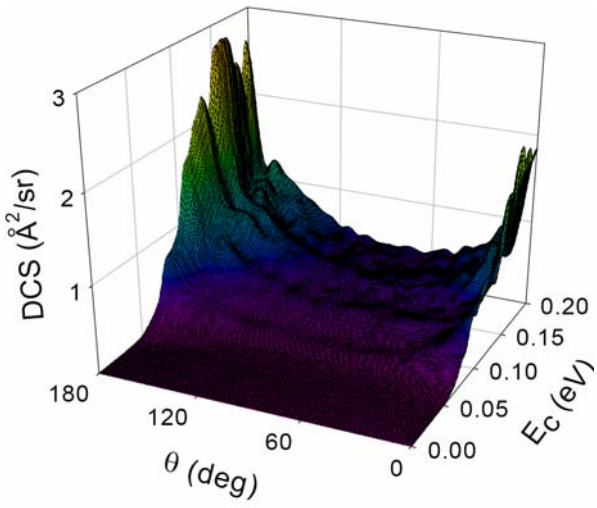

Fig. 3 Exact quantum mechanical differential cross section for the N + H_2 reaction.[9]

The advances in exact quantum scattering calculations expose many inaccuracies in PESs. For example, the widely used semi-empirical DMBE IV PES[11] is known to underestimate the vibrational frequencies of HO_2. In collaboration with Prof. Daiqian Xie of Nanjing University, we have developed a global and accurate PES for HO_2 based on spline fit of ~15000 ab initio points at the icMRCI+Q/aug-cc-pVQZ level of theory.[12] The J=0 vibrational spectrum and reaction probability on the new ab initio PES are very different from those on the DMBE IV PES. Specifically, the highly excited vibrational levels of HO_2 were found to have significant regularity,[13] as evidenced by highly excited O-O stretching overtones shown in Fig. 4. This is in sharp contrast to the earlier conclusion based on the DMBE IV PES that the vibration is completely irregular.[14] The root of the problem stems apparently from the overestimation of the density of states by the semi-empirical PES due to the underestimation of the fundamental frequencies. Also, the ab initio PES challenged the existence of a direct channel suggested on the DMBE IV PES,[15] and demonstrated that the reaction is completely resonance mediated.[10] This is shown in Fig. 4 where the reaction probabilities from the two PESs are compared.

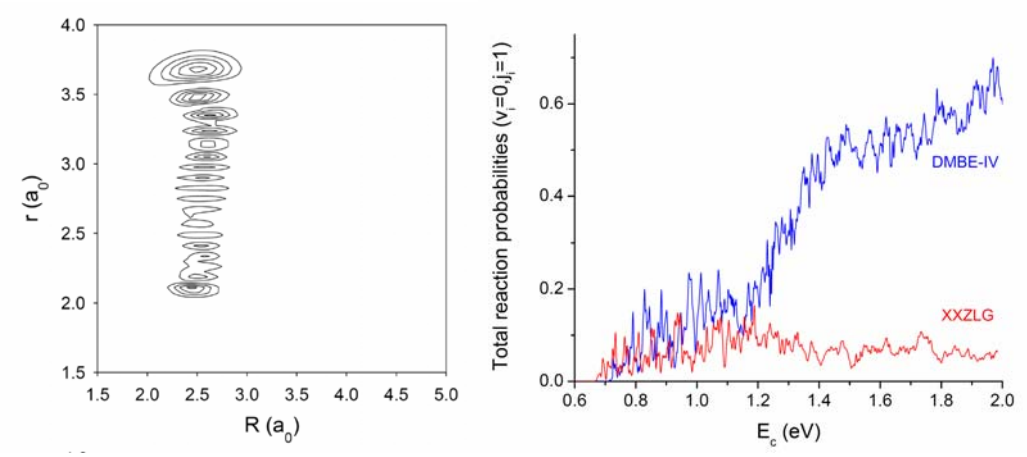

Fig. 4 Highly excited O-O stretching overtone of HO_2 on the ab initio PES (left panel)[13] and comparison of J=0 reaction probabilities on two PESs (right panel).[10]

The spline PES of HO_2 is still inefficient for quasi-classical trajectory calculations. To address this problem, we have, in collaboration with Tak-San Ho and Hersch Rabitz at Princeton University, constructed an analytical fit of the ab initio points.[16] We plan to use this new potential to examine scattering attributes of the H + O_2 reaction in the near future, in collaboration with Prof. György Lendvay at Hungarian Academy of Sciences.

In the next funding year, we will concentrate on the complete elucidation of the H + O_2 reaction and its reverse reaction using quantum and classical methods. The issues that we plan to address include, but not limited to, the statistical nature of the forward and reverse reactions, the differential and integral cross sections of the reaction, the temperature dependent rate constants, and the unimolecular decay rates. Furthermore, we are also engaged in improving the PES of the HO_2 system, particularly in the HO + O channel which is dominated by long-range interactions. We hope these results will stimulate experimental interests for this prototypical complex-forming reaction, which will eventually lead to a better understanding of this most important combustion reaction.

References:

1 S. Y. Lin and H. Guo, J. Chem. Phys. **120**, 9907 (2004).
2 S. Y. Lin and H. Guo, J. Phys. Chem. **A110**, 5305 (2006).
3 A. L. Van Wyngarden, K. A. Mar, K. A. Boering, J. J. Lin, Y. T. Lee, S.-Y. Lin, H. Guo, and G. Lendvay, J. Am. Chem. Soc. **129**, 2866 (2007).
4 S. Y. Lin, E. J. Rackham, and H. Guo, J. Phys. Chem. **110**, 1534 (2006).
5 R. Schinke, S. Y. Grebenshchikov, M. V. Ivanov, and P. Fleurat-Lessard, Annu. Rev. Phys. Chem. **57**, 625 (2006).
6 J. A. Miller, R. J. Kee, and C. K. Westbrook, Annu. Rev. Phys. Chem. **41**, 345 (1990).
7 J. A. Miller and B. C. Garrett, Int. J. Chem. Kinet. **29**, 275 (1997).
8 S. Y. Lin and H. Guo, Phys. Rev. A **74**, 022703 (2006).
9 S. Y. Lin, H. Guo, and L. Banares, J. Phys. Chem. A (2007).
10 S. Y. Lin, H. Guo, P. Honvault, and D. Xie, J. Phys. Chem. B **110**, 23641 (2006).
11 M. R. Pastrana, L. A. M. Quintales, J. Brandao, and A. J. C. Varandas, J. Phys. Chem. **94**, 8073 (1990).
12 C. Xu, D. Xie, D. H. Zhang, S. Y. Lin, and H. Guo, J. Chem. Phys. **122**, 244305 (2005).
13 S. Y. Lin, D. Xie, and H. Guo, J. Chem. Phys. **125**, 091103 (2006).
14 A. Dobbyn, M. Stumpf, H.-M. Keller, and R. Schinke, J. Chem. Phys. **103**, 9947 (1995).
15 A. J. H. M. Meijer and E. M. Goldfield, J. Chem. Phys. **108**, 5404 (1998).
16 D. Xie, C. Xu, T.-S. Ho, H. Rabitz, G. Lendvay, S. Y. Lin, and H. Guo, J. Chem. Phys. **126**, 074315 (2007).

GAS PHASE MOLECULAR DYNAMICS: HIGH-RESOLUTION SPECTROSCOPIC PROBES OF CHEMICAL DYNAMICS

Gregory E. Hall (gehall@bnl.gov)
Chemistry Department, Brookhaven National Laboratory, Upton, NY 11973-5000

PROGRAM SCOPE

This research is carried out as part of the Gas Phase Molecular Dynamics group program in the Chemistry Department at Brookhaven National Laboratory. High-resolution spectroscopic tools are developed and applied to problems in chemical dynamics. Recent topics have included the state-resolved studies of collision-induced electronic energy transfer, coherent effects in multiple surface reactions, dynamics of barrierless unimolecular reactions, and the kinetics and spectroscopy of transient species.

RECENT PROGRESS

Double-resonance energy transfer studies in CH_2

Because of the close connection between collision-induced intersystem crossing and rotational energy transfer in the sparse mixed-state limit, we have been performing a double resonance study of collisional energy transfer in CH_2. In these experiments, individual CH_2 rotational levels are bleached by a tunable ns dye laser or OPO, while monitoring the populations of the same or nearby rotational levels with near-infrared transient FM spectroscopy. Saturation recovery experiments have characterized the rotational energy transfer rates as the rotational population hole is filled in by collisions of CH_2 with rare gases and ketene.

Compared to the behavior of rotational energy transfer among "normal" singlet CH_2 states, the saturation transfer behavior of singlet-triplet mixed states is revealing. The mixed states come in pairs, sharing the line strength of the zero-order singlet. The pairs are typically observed as a strong line, perturbed from its predicted frequency, and a weaker extra line, arising from a near-degenerate triplet state level, made bright by mixing with the zero-order singlet level. The two components of mixed state pairs are typically separated by several cm^{-1} and can be independently depleted in a saturation transfer experiment. We find extremely rapid collisional sharing of the population depletion between the two components of a mixed state pair, followed by a slower diffusion of the hole among other detected states.

Reversible kinetics of intersystem crossing in CH_2

Time resolved FM absorption permits high dynamic range measurement of singlet methylene decay kinetics, revealing double exponential decays. The relative amplitudes of fast and slow decay components are observed to vary with the nuclear spin state of CH_2 in the vibrationless singlet state, confirming distinct, uncoupled decay pathways in the two nuclear spin modifications. The pattern of singlet-triplet mixed gateway levels differs for these nuclear spin manifolds, and the vibrational energies of the zero-order triplet states responsible for the mixing is the key variable responsible for the differences in reversibility. These results are being extended with measurements on vibrationally excited singlet CH_2 and temperature dependent kinetics

Coherent and incoherent polarization observables in molecular photodissociation

Recoil angle-dependent rotational polarization of molecular photofragments provides an experimental probe of phase differences between paths on multiple potential energy surfaces leading to the same products. Our work on CN photofragments arising from ICN photodissociation has been extended to include circularly polarized photolysis and Doppler-resolved circular dichroism. The Doppler resolution provides clear distinction between the coincident I ($^2P_{3/2}$) and I* ($^2P_{1/2}$) channels for each CN rotational state, as well as resolving for the first time the dependence of diatomic photofragment orientation on the

recoil angle. The functional form of the vector correlations is the same as has been developed and tested in the case of electronic polarization of atomic photofragments from diatomic precursors, but the interpretation of the polarization parameters is more challenging in the case of triatomic molecules, where the additional bending coordinate and broken degeneracy of Ω states introduces new issues. Additional polarization symmetries, previously unobserved in atomic photofragments are predicted for coherent excitation of A" and A' transitions. Preliminary observations of asymmetric Doppler lineshapes measured with circularly polarized probe light are consistent with an extended semiclassical treatment of coherent excitation.

CH_2 *c* $^1A_1$ state double resonance measurements.

Double resonance spectra have been measured to confirm several tentative theoretical assignments of rovibrational states belonging to the previously uncharacterized *c* $^1A_1$ electronic state of CH_2. Direct excitation from the singlet *a* $^1A_1$ state is very weak, nominally a two-electron excitation. In a two-step excitation via the *b* $^1B_1$ state, a sequence of fully allowed transitions permit detection by transient FM spectroscopy of the *c*-*b* lines following a pulsed laser preparation of selected *b* state levels by *b*-*a* transitions. In addition to this obvious ladder-climbing, excited state absorption double resonance scheme, we have implemented an inverted "probe-pump" sequence involving the same levels. In this scheme, the *c*-*b* transition is saturated by a scanning pulsed laser, while observing a transient AC Stark perturbation on a fixed *b*-*a* transition with FM spectroscopy. Similar sensitivities are achieved with the two schemes. The AC Stark method has the strong practical advantage of scanning an OPO instead of a high resolution ring laser for survey spectra.

FUTURE WORK

Decoherence of mixed state pairs in collision-induced intersystem crossing

Two distinct collisional mechanisms appear to contribute to collision-induced intersystem crossing in cases like CH_2 , where isolated pairs of zero-order singlet and triplet rovibrational states are mixed by weak spin-orbit coupling. One mechanism, described by Curl *et al*[1] and by Gelbart and Freed[2] involves rotationally inelastic collisions that transfer population from into and out of the mixed state pairs with collisions that are sudden compared to the inverse frequency separation of the mixed states. The spin change occurs in the isolated molecule after the collision, driven by the weak spin-orbit coupling, with a periodically evolving, nonstationary spin in the coherently generated mixed state pair. The next collision at a random subsequent time samples the oscillating spin character and provides a path to the initially unpopulated spin state by means of two collisions, neither of which involve spin-orbit coupling. This mechanism predicts a rate that varies with collision partner in a way similar to rotational energy transfer, and depends on the number of mixed states, their mixing coefficients, and their steady-state Boltzmann populations.[3] The temperature dependences, *ortho/para* dependences in CH_2, and collision partner dependences are all inconsistent with these predictions.

An additional mechanism, not previously considered in problems of this type, appears to be important, based on double resonance saturation transfer experiments and state-resolved kinetics studies. A highly efficient collisional process converts population from one member of the mixed state pairs to its partner, through a process we envision as a decoherence, characterized by a rephasing of the zero-order spin components of the molecular eigenstates during weakly interacting collisions. The effects of such an additional step in the intersystem crossing mechanism would be to include a dependence on the attractive potentials between the collision partner and CH_2, decrease the relative importance of the mixing coefficients in the overall rate of intersystem crossing, and modify the temperature dependence of the

intersystem crossing rate, all of which were issues of quantitative disagreement with the simpler mechanism that excludes this decoherence step.

We will test and extend these notions with more systematic studies of bimolecular kinetics and double resonance saturation transfer in CH_2 mixed states driven by different collision partners. Collaborative work with Hua Gen Yu seeks to explore the inelastic scattering of singlet and triplet CH_2 with He, looking for connections between rigorous quantum dynamics of the weakly coupled surfaces and the phenomenology of mixed states.

Polarization effects in saturation transfer and saturation recovery

Our initial double resonance measurements on CH_2 found strong and saturated bleaching amplitudes with no Doppler selectivity, which encouraged a simplified identification of the fractional depletion approaching 50% as a true population measurement. Recent studies comparing different rotational branches used for bleaching and probing, and varying the relative polarization of bleach and probe lasers reveal this to be an oversimplification. Substantial alignment persists at the bleaching intensities used for these studies, giving us access to polarization transfer rates in addition to population transfer. Few previous studies have addressed the propensities for M-changing collisions in polyatomic molecules, particularly in radicals. Preliminary measurements suggest that even these challenging experiments will be possible with equipment and methods at hand.

Reversible kinetics and reactions of CH_2

Insights gained into the reversible singlet-triplet interconversion in CH_2 may have consequences in the interpretation of several previous studies of CH_2 kinetics, where high concentrations of rare gas were assumed to irreversibly quench singlet to triplet methylene and eliminate the singlet channel from consideration. In particular, reactions with O_2, H_2 and C_2H_2 will be investigated. We will reconsider the interpretation of recent experiments investigating ketene dissociation at 193 nm, assessing the relation between the assumed kinetic models and the inferences regarding relative yields of singlet and triplet methylene. We have claimed that a significant part of the CH_2 kinetics occurs under conditions of rotational disequilibrium and is not accurately described by simple rate equations. We will attempt to find compelling examples for this claim. In the case of O_2 reaction with singlet methylene, an intersystem crossing mechanism not requiring accidentally mixed states is evidently operative, and its signature in the state-resolved and reversible kinetics should be illuminating. Recent independent work in the Pilling and Hancock labs argues from product kinetic studies that singlet CH_2 undergoes no significant reaction with O_2 other than intersystem crossing.

Cited References

[1] R. F. J. Curl, J. V. V. Kasper, and K. S. Pitzer, J. Chem. Phys. **46**, 3220 (1967).
[2] W. M. Gelbart and K. F. Freed, Chem. Phys. Lett. **18**, 470 (1973).
[3] U. Bley and F. Temps, J. Chem. Phys. **98**, 1058 (1993).

DOE SPONSORED PUBLICATIONS SINCE 2005

Coherent and incoherent orientation and alignment of ICN photoproducts
M. L. Costen and G. E. Hall
Phys.Chem.Chem.Phys. **9**, 272-287 (2007)

Observation of the $c\ ^1A_1$ (0,10,0) state of CH_2 by optical-optical double resonance
Y. Kim, G.E. Hall and T. J. Sears
J. Mol. Spectr. **240**, 269-71 (2006)

State-resolved thermalization of singlet and mixed singlet-triplet states of CH_2

A. V. Komissarov, A. Lin, T. J. Sears and G. E. Hall

J Chem. Phys. **125**, 084308 (2006)

Anisotropy of photofragment recoil as a function of dissociation lifetime, excitation frequency, rotational level and rotational constant

Hahkjoon Kim, Kristin S. Dooley, S. W. North, G. E. Hall and P. L. Houston

J Chem. Phys. **125** 133316 (2006)

AC Stark detection of optical-optical double resonance in CH_2

Y. Kim, G. E. Hall and T. J. Sears

Phys. Chem. Chem. Phys, **8,** 2823-2825 (2006)

The spectrum of CH_2 near 1.36 and 0.92 microns: Re-evaluation of rotational level structure and perturbations in *a* (010)

K. Kobayashi, G. E. Hall and T. J. Sears

J. Chem. Phys. **124**, 184320 (2006)

Correlated product distributions from ketene dissociation measured by DC sliced ion imaging

A. V. Komissarov, M. P. Minitti, A. G. Suits, and G. E. Hall

J. Chem. Phys. **124**, 014303 (2006)

Rotationally resolved spectrum of the *A* (060) – *X* (000) band of HCBr

G. E. Hall, T. J. Sears and H-G. Yu

J. Mol. Spectr. **235** , 125-131 (2006)

Reflectron velocity map ion imaging

B. D. Leskiw, M. H. Kim, G. E. Hall and A. G. Suits

Reviews of Scientific Instruments, **76**, 104101; Erratum 129901 (2005)

Observation of the $c\ ^1A_1$ state of methylene by optical-optical double resonance

Y. Kim, A. Komissarov, G. E. Hall and T. J. Sears

J. Chem. Phys. **123**, 024306 (2005)

Hyperfine quantum beats from photolytic orientation and alignment

M. L. Costen and G. E. Hall

Phys. Chem. Chem. Phys., **7** 1408-13 (2005)

Flame Chemistry and Diagnostics

Nils Hansen
Combustion Research Facility, Sandia National Laboratories, Livermore, CA 94551-0969
Email: nhansen@sandia.gov

SCOPE OF THE PROGRAM

The goal of this program is to provide a rigorous basis for the elucidation of chemical mechanisms of combustion, combining experimental measurements employing state of the art combustion diagnostics with detailed kinetic modeling. The experimental program concentrates on the development and application of combustion diagnostics for measurements of key chemical species concentrations. These measurements are carried out in low-pressure, one-dimensional laminar flames and are designed to serve as benchmarks for the validation of combustion chemistry models. Comparison of experimental data to models employing detailed chemical kinetics is critical to determining important chemical pathways in combustion and in pollutant formation in combustion systems. As turbulent combustion models become increasingly sophisticated, accurate chemical mechanisms will play a larger role in computations of realistic combustion systems. Verification of detailed chemistry models against a range of precise measurements under thoroughly characterized, steady conditions is necessary before such flame models can be applied with confidence in turbulent combustion calculations.

PROGRESS REPORT

Molecular Beam Mass Spectrometry at the Advanced Light Source

In collaboration with T. A. Cool of Cornell University and P. R. Westmoreland of the University of Massachusetts, great progress has been made measuring low pressure flames using molecular beam mass spectrometry with synchrotron photoionization at the Advanced Light Source at Lawrence Berkeley National Laboratory. In the past year, different flames over a wide range of stoichiometry using the following fuels have been characterized, and the data is currently being reduced for comparison to detailed models: allene, butane, cyclohexane, cyclopentene, dimethylether, ethylformate, ethylacetate, 1-hexene, isobutane, methane, methylacetate, methylformate, propene, propyne, and toluene. In addition, the influence of ethanol and dimethylether addition to a fuel-rich propene flame has been studied.

Combustion Chemistry in Fuel-Rich Hydrocarbon Flames

Fuel-consumption and initial steps of aromatic ring formation were studied in fuel-rich flames of allene, propyne, cyclopentene, cyclohexane, and 1-hexene. These experimental studies provide a broad database for flame modeling.

Allene and Propyne Flames: The comparison between the experimental results and the current flame model from J. A. Miller (Sandia National Laboratories) revealed the following results: The fuel is mainly consumed by reacting with hydrogen atoms: $C_3H_4(A, P) + H \rightleftarrows C_3H_3 + H_2$. Furthermore, hydrogen atoms catalyze the isomerization of propyne and allene via $C_3H_4(P) + H \rightleftarrows C_3H_4(A) + H$. Because of the higher thermodynamic stability of propyne over allene (~1 kcal/mol), there is more propyne formed in the allene flame than allene formed in the propyne flame. As a consequence, the $C_3H_4(P) + H \rightleftarrows CH_3 + C_2H_2$ reaction is expected to occur more readily in the propyne flame, thus resulting in a somewhat smaller C_3H_3 concentration. Benzene formation in both flames is dominated by C_3H_3 recombination. In the allene flame, a small contribution towards benzene originates from $C_3H_5 + C_3H_3$, where the C_3H_5 is formed by H adding to allene. For those reasons, the observed C_6H_6 mole fraction is slightly larger in the allene flame.

Cyclopentene Flame: The comparison between the experimental results and the preliminary model by P. R. Westmoreland implies that fuel consumption is dominated by elimination of H_2 to form cyclopentadiene, *cyclo*-$C_5H_8 \rightleftarrows$ *cyclo*-$C_5H_6 + H_2$, and subsequent H-atom abstraction to form the resonantly stabilized cyclopentadienyl: c*yclo*-$C_5H_6 + R \rightleftarrows$ *cyclo*-$C_5H_5 + RH$. The following thermal decomposition reaction of *cyclo*-C_5H_5 starts with a fast ring opening process to form the linear $CHCCHCHCH_2$ isomer, which dissociates into acetylene and propargyl radicals. Thus, propargyl is a major decomposition product of the fuel and, indeed, our current model indicates that propargyl self-combination dominates benzene formation. Nevertheless, assuming $C_3H_3 + C_3H_3$ to be the only formation pathway of benzene leads to an underprediction of the benzene mole fraction and consequently, the $CH_3 + C_5H_5$ reaction sequence is also found to be of importance.

1-Hexene and Cyclohexane: Mole fraction profiles were determined for benzene and known precursors in flames fueled by cyclohexane and 1-hexene. While the peak mole fractions of C_3H_3 and C_3H_5 are identical or even higher for the 1-hexene flame, the observed benzene mole fraction is a factor of 2.5 higher in the cyclohexane flame. Most likely this is the result of a major benzene formation pathway through the dehydrogenation of cyclohexane.

Species-Identification: A New Potential Molecular-Weight Growth Mechanism

In collaboration with S. J. Klippenstein (Argonne National Laboratory) we revealed the presence of -CHCHCHCHC(C=CH_2)- and/or -CH_2CHCHCHC(C≡CH)- in a fuel-rich cyclopentene flame. The identification is accomplished by comparing experimental photoionization efficiency spectrum with theoretical simulations based on calculated ionization energies and Franck-Condon factors. In the

environment of a fuel-rich cyclopentene flame, C_7H_6 isomers are likely formed by the $C_5H_5 + C_2H_2 \rightleftarrows C_7H_6 + H$ reaction. The presence of $C_5H_5CCH/C_5H_4CCH_2$ suggests a new potential molecular-weight growth mechanism that is characterized by C_5-C_7 ring enlargement reactions. C_7H_6 might react with acetylene to ultimately form indene, or H-atom addition might open a new route to a five-membered ring C_7H_7 radical species which undergoes isomerization to form the resonantly stabilized cycloheptatrienyl or benzyl radicals. Both radical species are good precursor candidates for forming multi-ring structures including indene and naphthalene.

Rydberg-Fingerprint Spectroscopy

In collaboration with P. M. Weber (Brown University) the applicability of Rydberg spectroscopy as a method to fingerprint molecular structures of combustion intermediates was demonstrated. Rydberg states are highly excited electronic levels and their energies are sensitive to the geometrical structure of the molecular ion core. Using the isomers 1,3-pentadiene and cyclopentene, 1,3- and 1,4-cyclohexadiene, toluene and cycloheptatriene, and 1- and 2-methylnaphthalene, we demonstrated that known combustion intermediates can be distinguished using this type of photoelectron spectroscopy.

FUTURE DIRECTIONS

In collaboration with S. J. Klippenstein we will explore the identity and possible formation pathways of several polyynes and polyeneynes in a variety of different fuel-rich flames. Those species are known to play key roles in many physical-chemical processes, including formation of polycyclic aromatic hydrocarbons and soot in combustion environments.

One key immediate task is the analysis of the large body of ALS data accumulated in the past year, which may compel further or confirmatory measurements during subsequent beam cycles. We will continue to explore isomer specific pathways of fuel-consumption and aromatic ring formation in flames fueled by C_6H_{12} isomers. Future work on the cyclopentene flame will be concerned with a more detailed modeling and with characterizing the growth of aromatic species beyond the first ring; that is, for example, the formation of indene and naphthalene.

Studies of oxygenated fuel chemistry will continue with investigations of flames fueled by esters which are of considerable interest because they are constituents of biodiesel. Direct studies of typical biodiesels, usually methyl or ethyl esters of fatty acids, are currently beyond our capabilities, thus, we will use model compounds such as methyl butanoate or ethyl propanoate.

We will incorporate the ALS flame data into the web based “Collaboratory for Multi-Scale Chemical Science – CMCS” (http://cmcs.org). This will make the data widely available for the interested scientific community – especially theorists will be able to compare their flame models with the data.

The Rydberg-fingerprint spectroscopy experiments were performed using molecular beams of pure substances and mixtures of isomers, thus the practicality of this technique for actual flame experiments needs to be proven.

PUBLICATIONS ACKNOWLEDGING BES SUPPORT 2005-PRESENT

1. C. A. Taatjes, S. J. Klippenstein, N. Hansen, J. A. Miller, T. A. Cool, J. Wang, M. E. Law, and P. R. Westmoreland, **"**Synchrotron Photoionization Measurements of Combustion Intermediates: Photoionization Efficiency of C_3H_2 Isomers", *Phys. Chem. Chem. Phys.* **7,** 806-813 (2005).
2. C. A. Taatjes, N. Hansen, A. McIlroy, J. A. Miller, J. P. Senosiain, S. J. Klippenstein, F. Qi, L. Sheng, Y. Zhang, T. A. Cool, J. Wang, P. R. Westmoreland, M. E. Law, T. Kasper, and K. Kohse-Höinghaus, "Enols are Common Intermediates in Hydrocarbon Oxidation", *Science* **308,** 1887-1889 (2005).
3. A. McIlroy and F. Qi, "Identifying Combustion Intermediates via Tunable Vacuum Ultraviolet Photoionization Mass Spectrometry", *Combust. Sci. Technol.* **177,** 2021-2037 (2005).
4. N. Hansen, A. M. Wodtke, J. C. Robinson, N. E. Sveum, S. J. Goncher, D. M. Neumark, "Photofragment Translational Spectroscopy of ClN_3: Determination of the primary and secondary Dissociation Pathways", *J. Chem. Phys.* **123,** 104305-1-104305-11 (2005).
5. P. C. Samartzis, N. Hansen, A. M. Wodtke, „Imaging ClN_3 Photodissociation from 234 to 280 nm", *Phys. Chem. Chem. Phys,* **8,** 2958-2963 (2006).
6. C. A. Taatjes, N. Hansen, J. A. Miller, T. A. Cool, J. Wang, P. R. Westmoreland, M. E. Law, T. Kasper, K. Kohse-Höinghaus, "Combustion Chemistry of Enols: Possible Ethenol Precursors in Flames", *J. Phys. Chem. A,* **110,** 3254-3260 (2006).
7. N, Hansen, S. J. Klippenstein, C. A. Taatjes, J. A. Miller, J. Wang, T. A. Cool, B. Yang, R. Yang, L. Wei, C. Huang, J. Wang, F. Qi, M. E. Law, P. R. Westmoreland, "Identification and Chemistry of C_4H_3 and C_4H_5 Isomers in Fuel-Rich Flames", *J. Phys. Chem. A,* **110,** 3670-3678 (2006).
8. N. Hansen, S. J. Klippenstein, J. A. Miller, J. Wang, T. A. Cool, M. E. Law, P. R. Westmoreland, T. Kasper, K. Kohse-Höinghaus, "Identification of C_5H_x Isomers in Fuel-Rich Flames by Photoionization Mass Spectrometry and Electronic Structure Calculations", *J. Phys. Chem A,* **110,** 4376-4388 (2006).
9. P. R. Westmoreland, M. E. Law, T. A. Cool, J. Wang, A. McIlroy, C. A. Taatjes, N. Hansen, "Analysis of Flame Structure by Molecular-Beam Mass Spectrometry Using Electron Impact and Synchrotron-Photon Ionization", *Combust. Expl. Shock Waves,* **42,** 672-677 (2006).
10. T. A. Cool, J. Wang, N. Hansen, P. R. Westmoreland, F. L. Dryer, Z. Zhao, A. Kazakov, T. Kasper, K. Kohse-Höinghaus, „Photoionization Mass Spectrometry and Modeling Studies of the Chemistry of fuel-rich Dimethyl Ether Flames", *Proc. Combust. Inst.,* **31,** 285-293 (2007).
11. M. E. Law, P. R. Westmoreland, T. A. Cool, J. Wang, N. Hansen, C. A. Taatjes, T. Kasper, "Benzene Precursors and Formation Routes in a Stoichiometric Cyclohexane Flame", *Proc. Combust. Inst.,* **31,** 565-573 (2007).
12. K. Kohse-Höinghaus, P. Oßwald, U. Struckmeier, T. Kasper, N. Hansen, C. A. Taatjes, J. Wang, T. A. Cool, S. Gon, P. R. Westmoreland, „The Influence of Ethanol Addition on a premixed fuel-rich Propene-Oxygen-Argon Flame", *Proc. Combust. Inst.,* **31,** 1119-1127 (2007).
13. N. Hansen, J. A. Miller, C. A. Taatjes, J. Wang, T. A. Cool, M. E. Law, P. R. Westmoreland, "Photoionization Mass Spectrometric Studies and Modeling of Fuel-Rich Allene and Propyne Flames", *Proc. Combust. Inst.,* **31,** 1157-1164 (2007).
14. N. Hansen, T. Kasper, S. J. Klippenstein, P. R. Westmoreland, M. E. Law, C. A. Taatjes, K. Kohse-Höinghaus, J. Wang, T. A. Cool, „Initial Steps of Aromatic Ring Formation in a Laminar Premixed Fuel-Rich Cyclopentene Flame", *J. Phys. Chem. A,* in press
15. P. Oßwald, U. Struckmeier, T. Kasper, K. Kohse-Höinghaus, J. Wang, T. A. Cool, N. Hansen, P. R. Westmoreland, „Isomer-Specific Fuel Destruction Pathways in Rich Flames of Methyl Acetate and Ethyl Formate and Consequences for the Combustion Chemistry of Esters", *J. Phys. Chem. A,* in press.

KINETICS AND SPECTROSCOPY OF COMBUSTION GASES AT HIGH TEMPERATURES

Ronald K. Hanson and Craig T. Bowman
Department of Mechanical Engineering
Stanford University, Stanford, CA 94305-3032
rkhanson@stanford.edu, ctbowman@.stanford.edu

Program Scope:

This program involves two complementary activities: (1) shock tube measurements of rate coefficients of elementary chemical reactions relevant to combustion; and (2) development of cw, narrow-linewidth laser absorption diagnostics for sensitive and quantitative detection of species concentrations in shock tube kinetics experiments. Reactions studied include CH_3 decomposition: $CH_3 + Ar \rightarrow CH + H_2 + Ar$ and $CH_3 + Ar \rightarrow CH_2 + H + Ar$; CH and N_2: $CH + N_2 \rightarrow H + NCN$ and $CH + N_2 \rightarrow N + HCN$; and aromatic reactions: toluene + Ar, + O_2, + H, and + OH. Research on laser absorption spectroscopy is driven by the need for quantitative, sensitive diagnostics of relevant species. Diagnostics being developed include: visible laser absorption of CH at 431 nm; UV laser absorption of benzyl ($C_6H_5CH_2$) at 266 nm; and near-UV laser absorption of NCN at 329 nm.

Recent Progress: Shock Tube Chemical Kinetics

Methyl Decomposition: We have studied the two-channel thermal decomposition of methyl radicals in argon, (1a) $CH_3 + Ar \rightarrow CH + H_2 + Ar$ and (1b) $CH_3 + Ar \rightarrow CH_2 + H + Ar$, in shock tube experiments over the 2253-3527 K temperature range, at pressures between 0.7 and 4.2 atm. CH was monitored by cw, narrow-linewidth laser absorption at 431.1311 nm. The rate coefficient of reaction (1a) was measured by monitoring CH radicals generated upon shock-heating highly dilute mixtures of ethane, C_2H_6, or methyl iodide, CH_3I, in an argon bath. A detailed chemical kinetic mechanism was used to model the measured CH time-histories. Measurements of k_{1a} between 0.7 and 1.1 bar are presented in Figure 1a. The k_{1a} data are in good agreement with Dean and Hanson (1992) and with a recent evaluation by Baulch et al. (2005). The current high temperature data are also consistent with the lower temperature results of Rohrig et al. (1997). The effect of pressure on the bimolecular rate constant is shown in Figure 1b. Within experimental uncertainty and scatter, a pressure dependence could not be discerned for k_{1a} in the 0.7-4 atm pressure range. A least-squares, two-parameter fit of the current measurements, valid over the 2706-3527 K temperature range, is given by the following expression,

$$k_{1a} = 3.09 \times 10^{15} \exp(-40700/T\,[K]),\ cm^3\ mol^{-1}\ s^{-1}$$

The rate coefficient of reaction (1b) was determined by shock-heating dilute mixtures of C_2H_6 or CH_3I and excess O_2 in argon. During the course of reaction, OH radicals were monitored using the well-characterized $R_1(5)$ line of the OH A-X (0,0) band at 306.6871 nm (32606.52 cm^{-1}). H-atoms generated via reaction (1b) rapidly react with O_2, which is present in excess, forming OH. The OH traces are primarily sensitive to reaction (1b), reaction (2): $H + O_2 \rightarrow OH + O$, and reaction (3): $CH_3 + O_2 \rightarrow$ Products, where the rate coefficients of reactions (2) and (3) are well-established. A two-parameter, least-squares fit of the current data, valid over the 2253-2975 K temperature range, yields the following rate expression:

$$k_{1b} = 2.24 \times 10^{15} \exp(-41600/T\,[K]),\ cm^3\ mol^{-1}\ s^{-1}$$

Figure 2a summarizes the current measurements of k_{1b} and previous work reported for this reaction. The k_{1b} data agree very well with the H-atom ARAS measurements of Eng et al. (2001) at high temperatures and of Lim and Michael (1994) at low temperatures and are in excellent agreement

with the Baulch et al. (2005) evaluation. As shown in Fig. 2b, no pressure dependence could be discerned for reaction (1b) between 1.1 and 3.9 atm. Theoretical calculations carried out using a master equation-RRKM analysis fit the measurements reasonably well.

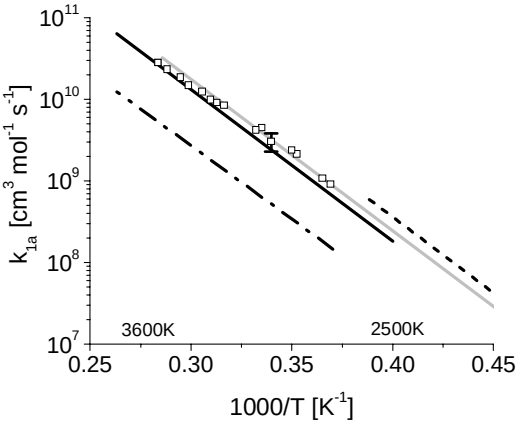

Figure 1 (a) Comparison of current measurements of k_{1a} with previous work: open squares, this work (± 25% error bars), 0.7-1.1 bar; solid black line, Dean and Hanson (1992), 0.5-1.3 bar; dashed black line, Rohrig et al. (1997), 1.2 bar; dash-dotted line, Markus et al. (1992), 1.1-1.8 bar; solid gray line, Baulch et al. (2005).

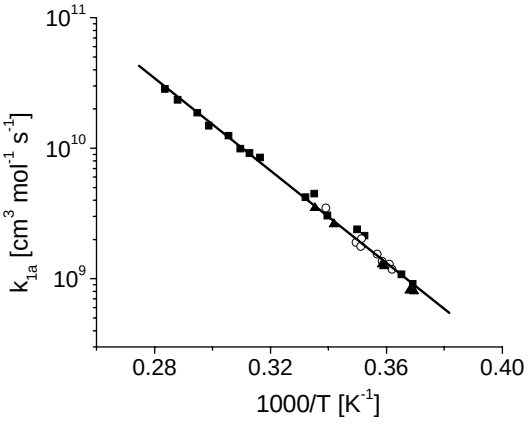

Figure 1 (b) Pressure dependence of k_{1a}: solid squares, 0.7-1.1 atm data; open circles, 1.8-2.9 atm data; solid triangles, 3.6-4.2 atm data; solid black line, least-squares fit to data.

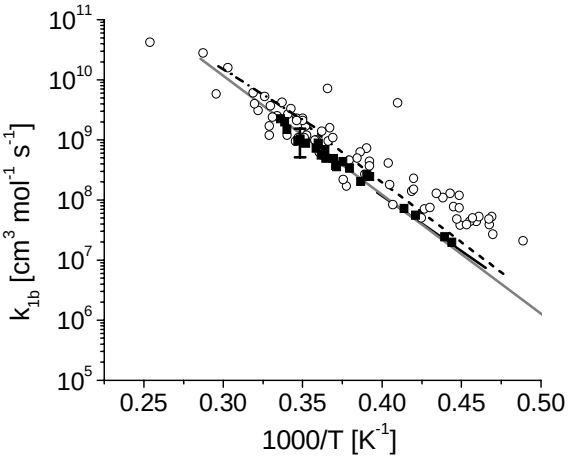

Figure 2 (a) Comparison of current measurements of k_{1b} with previous work: solid squares, this work (± 50% error bars); open circles, Eng et al. (2001); dash-dotted line, Kiefer and Kumaran (1993); dashed line, Markus et al. (1992); solid black line, Lim and Michael (1994); solid gray line, Baulch et al. (2005) .

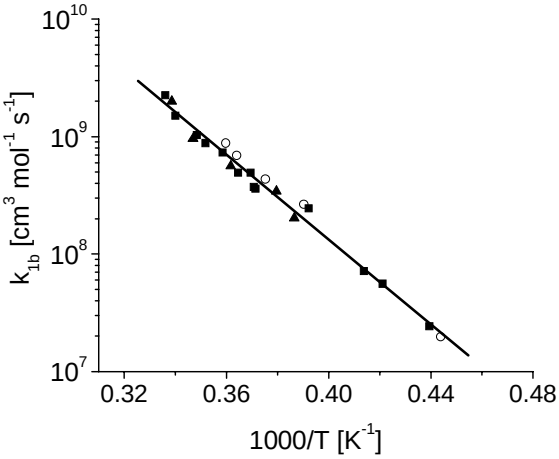

Figure 2 (b) Pressure dependence of k_{1b}: solid squares, 1.09-1.41 atm data; open circles, 1.42-1.75 atm data; solid triangles, 2.99-3.89 atm data; solid black line, least-squares fit to data .

Prompt-NO Initiation: We have begun studying the prompt-NO initiation reactions, (4a) CH + N_2 → NCN + H and (4b) CH + N_2 → HCN + N. Measurements of the overall rate ($k_4 = k_{4a} + k_{4b}$) have been made behind reflected shock waves over a broad temperature range using a perturbation approach. Ethane and acetic anhydride were used as CH precursors at high (2600-3600 K) and low (1900–2300 K) temperatures, respectively. A sample perturbation experiment is shown in Figure 3.

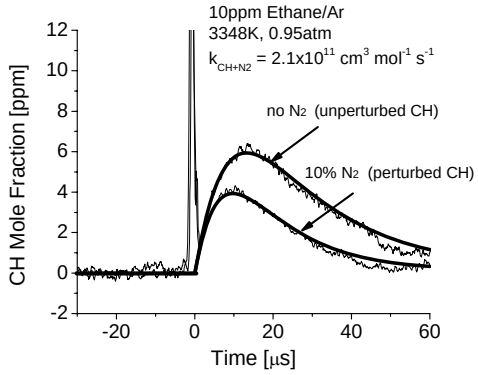

Figure 3 Example high-temperature CH perturbation experiment.

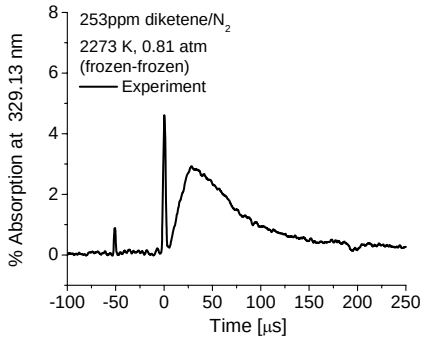

Figure 4 First laser absorption measurement of NCN.

The perturbation in the CH trace upon the addition of N_2 is primarily due to the CH+N_2 reaction. The rate coefficient of reaction (4) was adjusted to match the perturbation observed in the experiment. The current measurements agree with Dean and Hanson (1991) at high temperatures and extend the temperature range over which this reaction has been studied. A two-parameter, least-squares fit of the current data, valid over the 1943-3543 K temperature range, yields the following rate expression:

$$k_4 = 6.03 \times 10^{12} \exp(-11147/T\,[K]),\ cm^3\ mol^{-1}\ s^{-1}$$

We have also confirmed that NCN is a key product of the CH + N_2 reaction; NCN was generated by shock heating mixtures of diketene in a nitrogen bath. Diketene rapidly decomposes to form ketene which yields CH. The CH reacts with N_2 to form NCN, which was monitored via laser absorption at 329.13 nm. A sample NCN absorption time-history is shown in Figure 4. Work is in progress to establish the rate k_{4a}.

Aromatic Reactions: The overall decomposition rate and branching ratio of the decomposition of toluene to $C_6H_5CH_2$ + H and C_6H_5 + CH_3 was measured using laser absorption of benzyl radicals at 266 nm. The overall rate measurement is in good agreement with recent reviews. The measured rate of the C_6H_5 + CH_3 channel is faster than older measurements, but is in agreement with more recent studies by Luther et al. (1990). See Oehlschlaeger et al. (2007) for details.

We have also measured the primary initiation reaction in the oxidation of toluene: toluene + O_2 = benzyl + HO_2. The use of laser absorption of benzyl radicals to directly measure the reaction rate permitted the use of low reactant concentrations (1000 ppm toluene) and resulted in concentration time-histories with high signal-to-noise ratios that are well-suited for use as kinetic modeling targets in the refinement of large aromatic reaction mechanisms. The current rate measurements are in agreement with the previous work of Eng et al. (1998), but with substantially smaller uncertainty. See Oehlschlaeger et al. (2006) for details.

Recent Progress: Spectroscopy

CH Spectroscopy: The collision-broadening coefficient for CH in argon, $2\gamma_{CH\text{-}Ar}$, was measured via repeated single-frequency experiments in the ethane pyrolysis system behind reflected shock waves. The initial mixture was 20-21 ppm ethane in argon. The experimental line shape was simulated using LIFBASE with the broadening coefficient as the only free parameter. The measured $2\gamma_{CH\text{-}Ar}$ value and updated spectroscopic and molecular parameters were used to calculate the CH absorption coefficient at 431.1311 nm, which was then used to convert raw traces of fractional transmission to quantitative CH concentration time-histories in the methyl decomposition and CH + N_2 experiments.

NCN Spectroscopy: Current work is focused on developing a cw laser absorption system for the NCN radical. A detailed survey of NCN spectroscopy has identified the $X^3\Sigma$ - $A^3\Pi$ transition near 329 nm as well-suited for monitoring the NCN radical at shock tube conditions. Light at 329 nm is generated by doubling 658 nm radiation generated in a ring dye laser cavity with an external-cavity frequency doubler with a BBO crystal. To the best of our knowledge, a quantitative absorption analysis of this transition has not been carried out previously. The relative absorption spectrum for this transition is being mapped out using repeated shock tube kinetic experiments. An extensive literature survey was performed to identify strategies to quantitatively calibrate the NCN laser absorption diagnostic.

Future Plans:

1) Continue development of external-cavity frequency-doubling methods for the generation of laser radiation in the deep ultraviolet. Apply these frequency-doubling methods to wavelengths of interest including the detection of NCN at 329 nm, HCO at 230 and 258 nm, HO_2 at 230 nm, and propargyl radicals at 335 nm. 2) Continue measurement of the overall rate and product branching ratio of the reaction $CH+N_2 \rightarrow NCN+H$ using CH and NCN laser absorption.

Recent Publications of DOE Sponsored Research: 2005-2007

V. Vasudevan, R.K. Hanson, D.M. Golden, C.T. Bowman, D.F. Davidson, "High-Temperature Shock Tube Measurements of Methyl Radical Decomposition," *Journal of Physical Chemistry A*, in press.

M. A. Oehlschlaeger, D. F. Davidson and R. K. Hanson, "Experimental Investigation of Toluene + H → Benzyl + H_2 at High Temperatures," *Journal of Physical Chemistry A* 110, 9867-9873 (2006).

M. A. Oehlschlaeger, D. F. Davidson and R. K. Hanson, "Investigation of the Reaction of Toluene with Molecular Oxygen in Shock-heated Gases," *Combustion and Flame* 147, 195-208 (2006).

M. A. Oehlschlaeger, D. F. Davidson and R. K. Hanson, "High Temperature Thermal Decomposition of Benzyl Radicals," *Journal of Physical Chemistry A* 110, 6649-6653 (2006).

M. A. Oehlschlaeger, D. F. Davidson and R. K. Hanson, "Thermal Decomposition of Toluene: Overall Rate and Branching Ratio," *Proceedings of the Combustion Institute* 31, 211-219 (2007); and presented as Paper 05F-59, Fall Meeting of the Western States Section of the Combustion Institute, Stanford CA, October (2005).

M. A. Oehlschlaeger, D. F. Davidson and J. B. Jeffries, "Temperature Measurements Using Ultraviolet Laser Absorption of Carbon Dioxide behind Shock Waves," *Applied Optics* 44, 6599-6605 (2005).

V. Vasudevan, D.F. Davidson, R.K. Hanson, "High Temperature Measurement of the Reactions of OH with Toluene and Acetone," *Journal of Physical Chemistry A* 109**,** 3352-3359 (2005); also presented at the *25th International Symposium on Shock Waves*, Bangalore, India (2005); and at the Joint Meeting of the US Sections of the Combustion Institute Philadelphia PA, March (2005).

M. A. Oehlschlaeger, D. F. Davidson and R. K. Hanson, "High Temperature UV Absorption of Methyl Radicals behind Shock Waves," *Journal of Quantitative Spectroscopy and Radiative Transfer* 92, 393-402 (2005).

J.T. Herbon, R.K. Hanson, C.T. Bowman, and D.M. Golden, "The Reaction of CH_3+O_2: Rate Coefficients for the Product Channels at High Temperatures," *Proceedings of the Combustion Institute* 30, 955-963 (2005).

M. A. Oehlschlaeger, D. F. Davidson, and R. K. Hanson, "High-Temperature Ethane and Propane Decomposition," *Proceedings of the Combustion Institute* 30, 1119-1127 (2005).

M. A. Oehlschlaeger, D. F. Davidson, J. B. Jeffries, and R. K. Hanson, "Carbon Dioxide Thermal Decomposition: Observation of Incubation," *Zeitschrift für Physikalische Chemie* 219, 555-567 (2005).

Theoretical Studies of Potential Energy Surfaces*

Lawrence B. Harding
Chemistry Division
Argonne National Laboratory
Argonne, IL 60439
harding@anl.gov

Program Scope

The goal of this program is to calculate accurate potential energy surfaces for both reactive and non-reactive systems. Our approach is to use state-of-the-art electronic structure methods (CASPT2, MR-CI, CCSD(T), etc.) to characterize multi-dimensional potential energy surfaces. Depending on the nature of the problem, the calculations may focus on local regions of a potential surface (for example, the vicinity of a minimum or transition state), or may cover the surface globally. A second aspect of this program is the development of techniques to fit multi-dimensional potential surfaces to convenient, global, analytic functions that can then be used in dynamics calculations. Finally a third part of this program involves the use of direct dynamics for high dimensional problems to by-pass the need for surface fitting.

Recent Results

Radical-Radical Abstraction Reactions: This year, in collaboration with Stephen Klippenstein, we completed a study of the abstraction reaction,

$$H+CH_2CHCH_2 \rightarrow H_2 + CH_2CCH_2$$

This reaction is involves large changes in both geometry and electronic structure and as a result has a fairly large barrier (8.2 kcal/mol) in spite of being 43 kcal/mol exothermic. A TST calculation of the rate of reaction gave a result of $4x10^{-12}$ cm^3/molecule sec at 1500K, in excellent agreement with a recent measurement by Davidson et al[1] ($5x10^{-12}$ cm^3/molecule sec). Previous estimates assumed a much higher, temperature independent rate characteristic of a barrierless reaction.

Radical-Radical Association Reactions: In a continuation of a long-term collaborative effort with Stephen Klippenstein, we completed a study of a series of hydrogen atom plus resonance stabilized hydrocarbon radical (RSR) association reactions. Treating the RSR's required two modifications of the method we have used previously on non-resonance stabilized radicals. Our approach involves doing the vast majority of the CASPT2 electronic structure calculations using a very small cc-pVDZ basis set and then correcting these small basis set energies with a one dimensional, orientation independent correction that depends only on the distance of the approaching hydrogen atom from the radical center. For non-resonance stabilized radicals we found that a correction based on $H+CH_3 \rightarrow CH_4$ worked well for all H+R reactions. For RSR's we find it necessary to develop correction potentials specific to each individual reaction. The reaction specific correction is calculated by taking the difference between MEP energies calculated with cc-pVDZ and aug-cc-pVDZ basis sets. To this we add a small, non-reaction specific correction determined by taking the difference between aug-cc-pVDZ and aug-cc-pVTZ MEP's for $H+CH_3 \rightarrow CH_4$. This approach was tested for $H+{}^3HCCCH$, $H+CH_2CCH$ and $H+CH_2CHCH_2$ and shown to accurately reproduce three dimensional potentials calculated entirely with the aug-cc-pVTZ basis set. The second modification necessary for the RSR's is the

use of larger active spaces in the CASPT2 calculations. To obtain sufficiently accurate H+RSR interaction potentials we find it necessary to include in the active space, π and π* orbitals for each π bond.

Using this approach we have calculated rates for the following H+RSR association reactions:

H+^{3}CHCCH→ CH_2CCH	H+CH_3CHCCH→ CH_3CHCCH_2
H+CH_2CCH→ CH_3CCH	H+CH_3CHCCH→ CH_3CH_2CCH
H+CH_2CCH→ CH_2CCH_2	H+CH_3CCCH_2→ CH_3CCCH_3
H+CH_2CHCH_2→ CH_3CHCH_2	H+ CH_2CCCCH → CH_3CCCCH
H+CH_2CCCH→ CH_2CCCH_2	H+ CH_2CCCCH → CH_3CCCCH
H+CH_2CCCH→ CH_2CHCCH	H+ CH_2CCCCH → CH_3CCCCH
H+CH_2CHCCH_2→ CH_3CHCCH_2	H+CHCCHCCH→ $CH_2CCHCCH$
H+CH_2CHCCH_2→ $CH_2CHCHCH_2$	H+CHCCHCCH→ $CHCCH_2CCH$
H+cyclo-C_4H_5→ cyclo-C_4H_6	H+cyclo-C_7H_7→ Toluene
H+cyclo-C_5H_5 ($^2A_2$)→ cyclo-C_5H_6	H+cyclo-C_7H_7→ p-isotoluene
H+cyclo-C_5H_5 ($^2B_1$)→ cyclo-C_5H_6	H+cyclo-C_7H_7→ o-isotoluene

The high-pressure limit rates for these reactions are shown in Figure 1 (for those reactions where more than one product is possible we show only the total rate of reaction). For those reactions where experimental results are available (propargyl, allyl, cyclopentadienyl and benzyl) the theoretical rates are in good agreement with the observed rates.

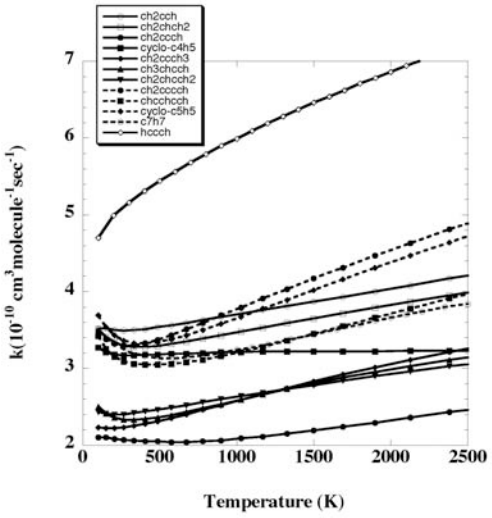

Figure 1.

Some of the general conclusions from this study include:

(1) Triplet RSR's such as propargylene are significantly more reactive than doublet RSR's.

(2) RSR's having more than two reactive sites are no more reactive than those having only two reactive sites.

(3) RSR's having out-of-plane radical orbitals (CH_2CCH and CH_2CCCCH) are more reactive than RSR's having in-plane radical orbitals (CH_2CCCH).

(4) As for alkyl radicals, unsubstituted RSR's (such as CH_2CCH) are more reactive than substituted RSR's (such as CMeHCCH and CH_2CCMe).

Future Work:

We plan to initiate a CASPT2 study of mechanisms for hydrocarbon decompositions. Preliminary results for cyclohexane show two distinct mechanisms: (1) the generally accepted biradical mechanism[2] in which cyclohexane ring opens to a 1,6 biradical which then undergoes a 1,5 intramolecular hydrogen abstraction to form 1-hexene and (2) a direct path to 1-hexene which does not go through the biradical intermediate.

Acknowledgement: This work was performed under the auspices of the Office of Basic Energy Sciences, Division of Chemical Sciences, Geosciences and Biosciences, U.S. Department of Energy, under Contract W-31-109-Eng-38.

References:

(1) D. F. Davidson, M. A. Oehlshlaeger and R. K. Hanson, *Proc. Combust. Inst.* **31**, 321 (2007)

(2) B. Sirjean, P. A. Glaude, M. F. Ruiz-Lopez and R. Fournet, *J. Phys. Chem. A*, **110,** 12693 (2006)

PUBLICATIONS (2005 - Present):

Reaction of Oxygen Atoms with Hydrocarbon Radicals: A Priori Kinetic Predictions for the CH_3+O, C_2H_5+O and C_2H_3+O Reactions
L.B. Harding, S.J. Klippenstein and Y. Georgievskii
Proc. Combust. Inst. **30**, 985-993 (2005)

Rate Constants for the D+C_2H_4 → C_2H_3D+H at High Temperature: Implications to the High Pressure Rate Constant for H+C_2H_4 → C_2H_5
J.V. Michael, M.-C. Su, J.W. Sutherland, L.B. Harding and A.F. Wagner
Proc. Combust. Inst. **30**, 965-973 (2005)

Predictive Theory for Hydrogen Atom – Hydrocarbon Radical Association Kinetics
L. B. Harding, Y. Georgievskii and S. J. Klippenstein
J. Phys. Chem. A **109**,4646-4656(2005)

The Determination of molecular properties from MULTIMODE with an application to the calculation of Franck-Condon factors for photoionization of CF_3 to CF_3^+
J. M. Bowman, X. Huang, L.B. Harding and S. Carter
Mol. Phys. **104**, 33-45(2006)

Methyl Radical: Ab Initio Global Potential Surface, Vibrational Levels, and Partition Function
D. M. Medvedev, L.B. Harding and S. K. Gray
Mol. Phys. **104**, 73-81(2006)

Predictive Theory for the Association Kinetics of Two Alkyl Radicals
S.J. Klippenstein, Y. Georgievskii, L.B. Harding
Phys. Chem. Chem. Phys. **8**,1133-1147 (2006)

Pyrolysis of Acetaldehyde, Rates for Dissociation and Following Chain Decomposition
K.S. Gupte, J.H. Kiefer, R.S. Tranter, S.J. Klippenstein and L.B. Harding
Proc. Combust. Inst. **31**,167-174(2007)

On the Formation and Decomposition of C_7H_8
S.J. Klippenstein. L.B. Harding and Y. Georgievskii
Proc. Combust. Inst. **31**,221-229(2007)

Initiation in CH_4/O_2: High Temperature Rate Constants for $CH_4+O_2 \rightarrow CH_3+HO_2$
N.K. Srinivasan, J.V. Michael, L.B. Harding and S.J. Klippenstein
Comb. and Flame **149**, 104-111 (2007)

Direct Measurement and Theoretical Calculation of the Rate Coefficient for $Cl+CH_3$ from T=202-298 K
J. K. Parker, W. A. Payne, R. J. Cody, F.L. Nesbitt, L.J. Stief, S.J. Klippenstein, and L.B. Harding
J. Phys. Chem. A **111**, 1015-1023 (2007)

On the Combination Reactions of Hydrogen Atoms with Resonance Stabilized Hydrocarbon Radicals
L.B. Harding, S.J. Klippenstein and Y. Georgievskii
J. Phys. Chem. A (in press)

Kinetics of Methyl Radical-Hydroxyl Radical collisions and Methanol Decomposition
A. W. Jasper, S. J. Klippenstein, L. B. Harding, and B. Ruscic
J. Phys. Chem. A (in press)

Dissociative Ionization of Hot C_3H_5 Radicals
H. Fan, L. B. Harding, and S. T. Pratt
Mol. Phys. (in press)

Reflected Shock Tube Studies of High-Temperature Rate Constants for $OH+CF_3H \leftrightarrow CF_3+H_2O$ and $CF_3+OH \rightarrow$ Products
N. K. Srinivasan, M.-C. Su, J. V. Michael, S. J. Klippenstein and L. B. Harding
J. Phys. Chem. A (in press)

Laser Studies of Combustion Chemistry

John F. Hershberger

Department of Chemistry
North Dakota State University
Fargo, ND 58105
john.hershberger@ndsu.edu

Time-resolved infrared absorption and laser-induced fluorescence spectroscopy are used in our laboratory to study the kinetics and product channel dynamics of chemical reactions of importance in the gas-phase combustion chemistry of nitrogen-containing radicals. This program is aimed at improving the kinetic database of reactions crucial to the modeling of NO_X control strategies such as Thermal de-NO_X, RAPRENO$_X$, and NO-reburning. The data obtained is also useful in the modeling of propellant chemistry. The emphasis in our study is the quantitative measurement of both total rate constants and product branching ratios.

HCNO Kinetics

Previous to the studies reported here, there have been virtually no literature data available on the kinetics of HCNO, the fulminic acid molecule. Recent modeling studies have suggested the importance of this molecule in NO-reburning mechanisms.[1] In combustion, HCNO is primarily formed via acetylene oxidation:

$$O + C_2H_2 \rightarrow HCCO + H \quad (1a)$$
$$\rightarrow CH_2 + CO \quad (1b)$$
$$HCCO + NO \rightarrow HCNO + CO \quad (2a)$$
$$\rightarrow CO_2 + HCN \quad (2b)$$

Recent experimental and computational work in several laboratories, including ours, has identified (2a) as a major product channel.[2-5]

One reason for the paucity of experimental data on HCNO kinetics is the difficulty of synthesizing this reagent, and it's limited stability. After recent work in our laboratory to reliably synthesize pure HCNO to calibrate IR absorption signals in our HCCO+NO studies,[2] we are in a position to examine the kinetics of this species. The HCNO synthesis is slow and inefficient, but our reaction cell geometry is ideally suited to dealing with reagents that are only available in small quantities.

A preliminary part to these studies was to use static infrared detection of HCNO to verify that this molecule is sufficiently stable to survive the duration of our experiment, which requires approximately 5 minutes of reagent

mixing/data collection. We have shown that by minimizing contact with metal surfaces, only very slight decomposition is observed over this timescale at room temperature. Above about 100 ^{0}C, the decomposition is sufficiently rapid to prevent reliable data.

A. OH+HCNO Reaction.

The following product channels are possible:

OH + HCNO	$\rightarrow H_2O + (NCO)$	ΔH^0_{298} = -364.0 kJ/mol	(3a)
	$\rightarrow NH_2 + CO_2$	ΔH^0_{298} = -413.4 kJ/mol	(3b)
	$\rightarrow HNO + HCO$	ΔH^0_{298} = - 67.1 kJ/mol	(3c)
	$\rightarrow HCN + HO_2$	ΔH^0_{298} = - 73.0 kJ/mol	(3d)
	$\rightarrow CH_2O + NO$	ΔH^0_{298} = -235.8 kJ/mol	(3e)
	$\rightarrow CO + H_2NO$	ΔH^0_{298} = -247.6 kJ/mol	(3f)
	$\rightarrow CO + H_2 + NO$	ΔH^0_{298} = -230.4 kJ/mol	(3g)

Initially, we produced OH using 193 nm photolysis of N_2O to produce $O(^1D)$, followed by reaction with H_2O. We have verified that the small amount of H_2O does not significantly increase the rate of HCNO decomposition in our cell. More recently, we have used 248 nm photolysis of H_2O_2 to directly form OH. This approach is preferable because the UV absorption of HCNO is much smaller at 248 nm than at 193 nm. Secondary reactions involving HCNO photofragments are therefore less prevalent when using 248 nm photolysis. Our measured total rate constants are the same using either method, but only the 248 nm photolysis is suitable for product detection.

For total rate constant measurements, OH was detected by laser-induced fluorescence at 307.966 nm. We obtain a rate constant of:

$$k(T) = (2.69\pm0.41)\times10^{-12} \exp[(750.2\pm49.8)/T] \text{ cm}^3 \text{ molecule}^{-1} \text{ s}^{-1}$$

over the temperature range 298-386 K. At 296 K, the rate constant is $k=(3.39\pm0.3)\times10^{-11}$ cm^3 molecule^{-1} s^{-1}.

This is the first experimental measurement reported on this reaction, and the 296 K rate constant is in excellent agreement with an estimate of 3.32×10^{-11} cm^3 molecule^{-1} s^{-1} used in a modeling study.[1]

Infrared diode absorption spectroscopy was used to detect products. After consideration of possible secondary chemistry and background signals due to HCNO photolysis, we conclude that channel (3f) and (3c) predominate, with branching fractions of 0.61±0.06 and 0.35±0.06, respectively. Channel (3e) also

appears as a minor contribution, with φ=0.04±0.02. Surprisingly, channel (3a) appears to not be significant, although a large background from HCNO photolysis may mask a small yield of this channel.

B. CN + HCNO Reaction.

CN + HCNO	→ CO + HCNN	(4a)	ΔH_f^{298} = -256.9 kJ/mol
	→ C_2N_2 + OH	(4b)	ΔH_f^{298} = -258.1 kJ/mol
	→ NO + HCCN	(4c)	ΔH_f^{298} = -32.4 kJ/mol
	→ (NCO) + HCN	(4d)	ΔH_f^{298} = -343.5 kJ/mol
	→ HCCO + N_2	(4e)	ΔH_f^{298} = -428.9 kJ/mol
	→ HCO + NCN	(4f)	ΔH_f^{298} = -89.6 kJ/mol
	→ NH + NCCO	(4g)	ΔH_f^{298} = -19.4 kJ/mol
	→ N_2 + H + CCO	(4h)	ΔH_f^{298} = -7.2 kJ/mol
	→ H + CO + NCN	(4i)	ΔH_f^{298} = -122.5 kJ/mol
	→ N_2 + CO + CH	(4j)	ΔH_f^{298} = -122.5 kJ/mol
	→ HCN + CO + N	(4k)	ΔH_f^{298} = -108.6 kJ/mol

CN is produced by photolysis of ICN or C_2N_2, and detected by LIF at ~388 nm. We have obtained the following rate constants:

$k = (3.95\pm0.53)\times10^{-11} \exp[(287\pm45)/T]$ cm^3 $molecule^{-1}$ s^{-1} (T=298-388 K)

k (296 K) $= (1.03\pm0.04)\times10^{-10}$ cm^3 $molecule^{-1}$ s^{-1}

Using infrared detection of many products, we have eliminated most of the possible product channels, and concluded that NO+HCCN (channel 4c) is the only major channel. We have detected evidence of substantial NCO formation, but isotopic labeling experiments show that most of this NCO is produced not by channel (4d), but via secondary chemistry such as HCCN+NO.

C. NCO+HCNO

NCO + HCNO	→ NO + CO + HCN	(5a)	ΔH_f^{298} = -183.7 kJ/mol
	→ CO_2 + HCNN	(5b)	ΔH_f^{298} = -232.3 kJ/mol

$\rightarrow CO + HCO + N_2$ (5c) $\Delta H_f^{298} = -365.6$ kJ/mol

$\rightarrow N_2O + HCCO$ (5d) $\Delta H_f^{298} = -38.0$ kJ/mol

NCO is produced by ICN photolysis followed by the $CN+O_2$ reaction, and detected by infrared absorption spectroscopy. The total rate constant is $(1.58\pm0.2)\times10^{-11}$ cm^3 $molecule^{-1}$ s^{-1} at 298 K, somewhat slower than the OH and CN reactions. Unfortunately, signal/noise limitations prevented measurements at elevated temperatures. After detected of products, and consideration of secondary chemistry, we conclude that NO + CO + HCN is the dominant product channel, with a minor contribution from CO_2 + HCNN.

Ongoing and Future Work: We are using a relative rate technique to measure the rate of O+HCNO. Preliminary data suggest a rather slow rate constant of $\sim4.0\times10^{-12}$ cm^3 $molecule^{-1}$ s^{-1} at 298 K. Future work will extend this to the H+HCNO reaction.

References

1. J.A. Miller, S.J. Kilppenstein, and P. Glarborg, Comb. Flame **135**, 357 (2003).
2. J.P. Meyer and J.F. Hershberger, J. Phys. Chem B **109**, 8363 (2005).
3. I.V. Tokmakov, L.V. Moskaleva, D.V. Paschenko, and M.C. Lin, J. Phys. Chem. A **107**, 1066 (2003).
4. L. Vereecken, R. Sumathy, S.A. Carl, and J. Peeters, Chem. Phys. Lett. **344**, 400 (2001).
5. U. Eickhoff and T. Temps, Phys. Chem. Chem. Phys. **1**, 243 (1999).

Publications acknowledging DOE support (2005-present)

1. "Product Channels of the HCCO+NO Reaction", J.P. Meyer and J. F. Hershberger, J. Phys. Chem. B **109**, 8363 (2005).
2. "Kinetics of the $HCCO+NO_2$ Reaction", J.P. Meyer and J.F. Hershberger, J. Phys. Chem. A **109**, 4772 (2005).
3. "Ab Initio Study of the $HCCO+NO_2$ Reaction", J.P. Meyer and J.F. Hershberger, Chem. Phys. **325**, 545 (2006).
4. "Kinetics of the OH+HCNO Reaction", W. Feng, J.P. Meyer, and J.F. Hershberger, J. Phys. Chem. A **110**, 4458 (2006).
5. "Kinetics of the CN+HCNO Reaction", W. Feng and J.F. Hershberger, J. Phys. Chem. A **110**, 12184 (2006).
6. "Kinetics of the NCO+HCNO Reaction", W. Feng and J.F. Hershberger, J. Phys. Chem. A, accepted for publication.

Terascale High-Fidelity Simulations of Turbulent Combustion with Detailed Chemistry (TSTC) http://purl.org/net/tstc

SciDAC: Computational Chemistry
(DOE Office of Science, BES: Chemical Sciences, Program Manager: R. Hilderbrandt)
Work-in-Progress Report – *Period from 04/01/06 to 03/31/07*

Principal Investigators

• Hong G. Im (University of Michigan, UMI, *hgim@umich.edu*)
• Arnaud Trouvé (University of Maryland, UMD, *atrouve@eng.umd.edu*)
• Christopher J. Rutland (University of Wisconsin, UWI, *rutland@engr.wisc.edu*)
• Jacqueline Chen (Sandia National Laboratories, SNL, *jhchen@ca.sandia.gov*)

Project Summary

The TSTC project is a multi-university collaborative effort to develop a high-fidelity turbulent reacting flow simulation capability utilizing terascale, massively parallel computer technology. The main paradigm of our approach is direct numerical simulation (DNS) featuring highest temporal and spatial accuracy, allowing quantitative observations of the fine-scale physics found in turbulent reacting flows as well as providing a useful vehicle towards description of sub-models needed in device-level simulations. The new S3D software is enhanced with new numerical algorithms and physical models to provide predictive capabilities for spray dynamics, combustion, and pollutant formation processes in turbulent combustion.

Program Scope

The primary goal of the SciDAC TSTC project for FY04-07 is to extend the S3D code with enhanced physical and algorithmic modules, and undertake several large-scale simulations to investigate important scientific issues. The specific objectives of this project include:

- To enhance the computational architecture and numerical algorithms in order to allow more robust, accurate, and efficient simulations of multi-dimensional turbulent combustion in the presence of strong turbulence and chemical stiffness. The efforts include new algorithms for characteristic boundary condition treatment and improved code architecture for various hardware platforms.
- To expand and upgrade the physical submodels to describe the underlying mechanisms in greater detail. The existing modules of radiation, soot, and spray evaporation models are being further enhanced to reproduce realistic combustion processes. In particular, advanced soot formation model to account for detailed soot precursors and improved spray model to incorporate droplet distortion effects are being developed.
- The TSTC team has been awarded the INCITE 2007 project entitled "Direct Numerical Simulation of Turbulent Flame Quenching by Fine Water Droplets," which will serve as a showcase of the modeling capabilities developed under this program. The targeted science issue to be addressed is fundamental characteristics of flame suppression by the complex interaction between turbulence, chemistry, radiation, and water spray. The high quality simulation data with full consideration of multi-physics processes will allow fundamental understanding of the key physical and chemical mechanisms in the flame quenching behavior.

Recent Progress

We present here a summary of progress made during the past 12 months work period of this project extending from *04/01/06 to 03/31/07*.

Computational developments:

- A new turbulence injection procedure have been developed, which allows time evolving turbulence from an ancillary cold non-reacting DNS to be fed in at the inflow of the main reacting DNS. This procedure was used in the DNS of a spatially developing flame-wall interaction problem where a realistic wall-bounded turbulence inflow was necessary for accuracy (SNL).

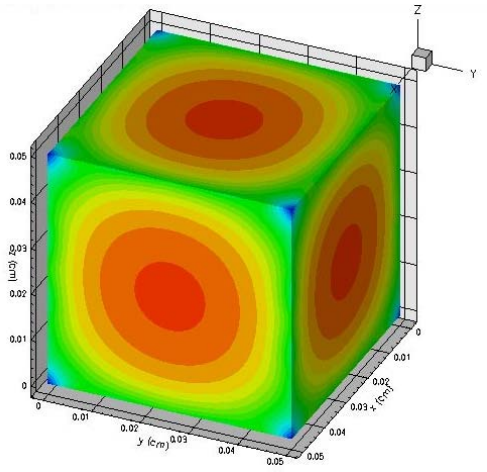

Figure 1: 3D test simulation of ignition kernel growth: temperature profiles show that the improved NSCBC accurately captures the ignition fronts passing across the computational boundaries.

- The characteristic boundary conditions have been further extended to account for multi-dimensional, viscous, and reaction effects in nonreflecting and solid surface boundaries. The new development shows great promise in successful simulations of many challenging problems such as turbulent counterflow flames, spray combustion, and wall-bounded combustion problems (UMI/UMD).
- As an effort toward the INCITE 2007 project, the S3D code has been extensively validated in a series of 3D test simulations with the new boundary conditions, turbulence injections, and physical submodels (Figure 1). The code will soon be deployed for preliminary production runs to study 3D turbulent counterflow flames.

Physical model developments:

- Two alternative radiative heat transfer models, discrete ordinate method (DOM) and discrete transfer method (DTM) have been validated and tested for their performance metrics in multi-dimensional DNS (UMI/UMD). The spray module has also been tested for its effectiveness in conjunction with the improved outflow characteristic boundary conditions (UWI/UMI).

New combustion science:

- Using the developed radiation and soot models, characteristics of soot formation in turbulent nonpremixed flames have been studied, in which the effects of turbulent transport on the transient soot dynamics and their impact on the overall soot production have been examined in detail (Figure 2). The study revealed the importance of detailed information of the local

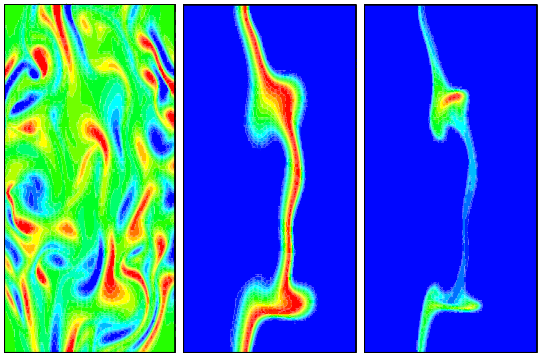

Figure 2: Simulations of turbulent nonpremixed ethylene-air flames, showing from left to right the vorticity, temperature, and soot volume fraction.

and transient flow-chemistry interaction in accurate prediction of the soot formation characteristics (UMI).

- 2D simulations have been performed on the basic interaction of a turbulent ethylene-air jet diffusion flame with cold solid wall boundaries. The simulations feature sooting flames (using a semi-empirical soot formation model) and thermal radiation transport (using the gray gas assumption and DTM) and provide fundamental insight into flame extinction events, soot blockage mechanisms, and turbulence-radiation interactions. The structure of the simulated wall flames is studied in terms of a classical fuel-air-based mixture fraction and an excess enthalpy variable. The excess enthalpy concept provides a convenient description of the deviations from adiabatic behavior, due to both convective and radiative cooling. Flame extinction is explained in terms of an extended scalar dissipation rate criterion; the extended criterion accounts for flame weakening due to convective/radiative thermal losses (UMD).

- 2D simulations of a fuel spray jet were performed to investigate the ignition and propagation of the flame front. Figure 3 shows the heat release contours in an evolving fuel spray jet, where the white line denotes the stoichiometric line. The ignition kernels propagated upstream as well as downstream along the stoichiometric lines. In the upstream direction stabilized lifted flames were formed and in the downstream direction flamelet regions developed. The improved characteristic boundary conditions and enhance code efficiency with a large number of droplets have enabled successful demonstration of accurate and robust realization of fuel spray combustion (UWI).

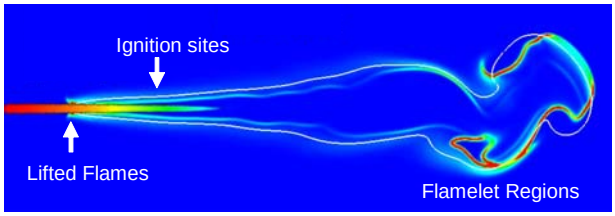

Figure 3: Heat release contours of combustion in the evolving fuel spray jet. The liquid jet is shown at the left by droplets colored by their temperature.

Future Plans

- In conjunction with the INCITE 2007 project, large scale 3D simulations will be conducted for turbulent nonpremixed flames in the presence of mean flow strain and fine water droplets. Some large scale simulations on NERSC and PSC machines are to be conducted and the effects of water spray on turbulent flame extinction characteristics will be investigated. (UMI/UMD/UWI/SNL).

- 3D simulations will be conducted on two-stage ignition behavior in a three-dimensional jet flow with fuel spray. In the simulation, some 20 million computational meshes will be used and half million liquid droplets will be included (UWI). Current investigations are focusing on the lift-off trends for different spray settings as observed in the experimental investigations. In particular the effect of injection pressure, orifice diameter, spray cone angle and ambient temperature on the lift-off length is being studied. The studies will emphasize near diesel like operating conditions that is expected to assist in new combustion technologies.

Publications

***Journals* (2005-2007)**

1. Wang, Y. and Rutland, C.J. (2007), "Direct numerical simulation of ignition in turbulent n-heptane liquid fuel spray jets", *Comb. and Flame*, accepted.
2. Yoo, C. S. and Im, H. G. (2007), "Characteristic boundary conditions for simulations of compressible reacting flows with multi-dimensional, viscous, and reaction effects," *Combust. Theory Modelling*, **11**:259-286.
3. Cook, D. J., Pitsch, H., Chen, J. H., and Hawkes, E. R. (2007), "Flamelet-based modeling of H2/Air Auto-ignition with thermal inhomogeneities," *Proc. Combust. Inst.*, **31**, 2903-2911.
4. Hawkes, E. R., Sankaran, R., Sutherland, J., and Chen, J. H. (2007), "Scalar mixing in direct numerical simulations of temporally-evolving plane jet flames with detailed CO/H2 kinetics," *Proc. Combust. Inst.*, **31**, 1633-1640.
5. Sankaran, R., Hawkes, E. R., Chen, J. H., Lu, T., and Law, C. K. (2007), "Structure of a spatially-developing lean methane-air turbulent bunsen flame," *Proc. Combust. Inst.*, **31**, 1291-1298.
6. Yoo, C. S. and Im, H. G. (2007), "Transient soot dynamics in turbulent nonpremixed ethylene-air counterflow flames," *Proc. Combust. Inst.*, **31**, 701-708.
7. Chen, J. H., Hawkes, E. Sankaran, R., Mason, S. D., and Im, H. G. (2006), "Direct numerical simulation of ignition front propagation in a constant volume with temperature inhomogeneities, Part I: Fundamental analysis and diagnostics," *Combustion and Flame*, **145**:128-144.
8. Hawkes, E., Sankaran, R., Pébay, P. P., and Chen, J. H. (2006), "Direct numerical simulation of ignition front propagation in a constant volume with temperature inhomogeneities, Part II: Parametric Study," *Combustion and Flame*, **145**:145-159.
9. Wang, Y. and Trouvé A. (2006), "Direct numerical simulation of non-premixed flame-wall interactions", *Combustion and Flame*, *Combust. Flame*, **144**:461-475.
10. Yoo, C. S., Wang, Y., Trouvé A. and Im, H. G. (2005), "Characteristic boundary conditions for direct simulations of turbulent counterflow flames", *Combust. Theory Modelling*, **9**:617-646.

***Selected Recent Communications* (2006-2007)**

1. Narayanan, P. and Trouvé, A. (2007) "Direct numerical simulation of turbulent, non-premixed, non-adiabatic, boundary layer combustion", *5th U.S. Combustion Meeting*, San Diego, CA, March 26-28, 2007
2. Srinivasan, S., Rutland, C.J., and Wang, Y., (2006) "Fundamental Simulations of Mixing and Combustion of Turbulent Liquid Sprays," IEA Combustion Agreement, 2007 Conference, Detroit, MI, April 14, 2007.
3. Rutland, C.J., and Wang, Y., (2006) "Turbulent Liquid Spray Mixing and Combustion – Fundamental Simulations," SciDAC 2006 Conference, Denver, CO, June 25-29, 2006.
4. Sankaran, R., Hawkes, E. R., and Chen, J. H., "Direct Numerical Simulations of Turbulent Lean Premixed Combustion." SciDAC 2006 Conference, Denver, CO, June 25-29, 2006.
5. Cook, D. J., Pitsch, H., Chen, J. H., and Hawkes, E. R. (2006), "Flamelet-based modeling of H2/Air Auto-ignition with thermal inhomogeneities," *31st International Symposium on Combustion*, August 6-11, Heidelberg, Germany.
6. Hawkes, E. R., Sankaran, R., Sutherland, J., and Chen, J. H. (2006), "Scalar mixing in direct numerical simulations of temporally-evolving plane jet flames with detailed CO/H2 kinetics," *31st International Symposium on Combustion*, August 6-11, Heidelberg, Germany.
7. Sankaran, R., Hawkes, E. R., Chen, J. H., Lu, T., and Law, C. K. (2006), "Structure of a spatially-developing lean methane-air turbulent bunsen flame," *31st International Symposium on Combustion*, August 6-11, Heidelberg, Germany.
8. Yoo, C. S. and Im, H. G. (2006), "Transient soot dynamics in turbulent nonpremixed ethylene-air counterflow flames," *31st International Symposium on Combustion*, August 6-11, Heidelberg, Germany.
9. Chen, J. H., Hawkes, E. R., and Sankaran, R. (2006), "Terascale direct numerical simulations of turbulent combustion," *Eleventh SIAM International Conference on Numerical Combustion*, April 23-26, Granada, Spain.
10. Hawkes, E. R., Sankaran, R., Sutherland, J. C., and Chen, J. H. (2006), "Terascale direct numerical simulations of turbulent nonpremixed CO/H2 plane jet flames," *Eleventh SIAM International Conference on Numerical Combustion*, April 23-26, Granada, Spain.
11. Yoo, C. S. and Im, H. G. (2006), "Effects of turbulence on soot formation in strained nonpremixed flames," *Eleventh SIAM International Conference on Numerical Combustion*, April 23-26, Granada, Spain.

IONIZATION PROBES OF MOLECULAR STRUCTURE AND CHEMISTRY

Philip M. Johnson
Department of Chemistry
Stony Brook University, Stony Brook, NY 11794
Philip.Johnson@sunysb.edu

PROGRAM SCOPE

Photoionization processes provide very sensitive probes for the detection and understanding of molecules and chemical pathways relevant to combustion processes. Laser based ionization processes can be species-selective by using resonances in the excitation of the neutral molecule under study or by exploiting different sets of ionization potentials of different molecules. Therefore the structure and dynamics of individual molecules can be studied, or species monitored, even in a mixed sample. We are continuing to develop methods for the selective spectroscopic detection of molecules by ionization, to use these spectra for the greater understanding of molecular structure, and to use these methods for the study of some molecules of interest to combustion science.

RECENT PROGRESS

The introduction of a high resolution CW pulse-amplified dye laser into our laboratory has given us the capability of studying the spectroscopy and photophysics of larger, less symmetric molecules with rotational resolution. To exploit this capability, recently we have been looking at various interesting properties of the molecules benzonitrile and phenylacetylene. These molecules have both singlet-singlet and photoinduced Rydberg ionization (PIRI) transitions in the wavelength range of the high resolution CW pulse-amplified dye laser, enabling a more controlled examination of the spectroscopy and energy dynamics of both the neutral and cationic species. Phenylacetylene, in particular, plays an important role in soot formation in combustion, and in the chemistry of the atmosphere of Saturn's moon Titan. Our recent discovery that phenylacetylene can store electronic energy practically indefinitely (on a molecular time scale) could have some implications in its reactivity in those situations.

Long-lived excited states of large molecules

In radiationless transition theory, it is assumed that the wavefunction of an isolated excited singlet state of a large molecule can mix with the high density of isoenergetic triplet and ground singlet states. This mixing can be experimentally followed in time by ionizing the molecule at various times after its excitation, since when the system evolves into the high vibrational levels of the ground state, the Franck-Condon factors prevent ionization and the signal disappears. In this way, one can measure the lifetimes of the triplet states isoenergetic with the pumped singlet state. These are typically on the order of hundreds of nanoseconds to a few microseconds in substituted benzenes.

While measuring the pump-probe decays of benzonitrile and phenylacetylene, in addition to the excited triplet decays we saw very long lived decays (longer than we can measure accurately—we are limited to about 150 μs by the size of our apparatus). This was not unexpected since we have seen similar things in other molecules, where we attributed it to the dissociation of clusters removing energy from the molecules. The dissociation allows them to drop down to the lower vibrational levels of the lowest triplet state where the excited state lifetimes are quite long. This time, however, we were exciting with a pulse-amplified CW laser system and able to scan over the rotational structure of the transition. The action spectrum of the long-lived component shows that the active molecules are strictly monomers, thus eliminating the cluster mechanism from possibility.

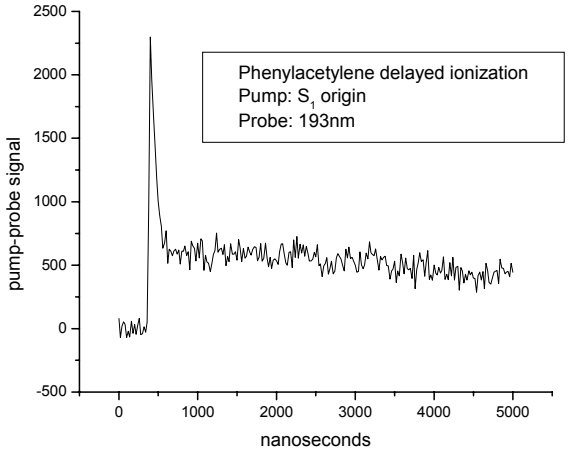

One reasonable mechanism for producing a long-lived state is that the molecules are crossing into the triplet manifold and losing energy by radiation. Emission lifetimes for excited vibrational states are too long for their IR emission to play a part in molecular decay in the triplet manifold. However, there is nothing to prevent an electronic transition from playing a role if there is an excited triplet state just below the excited singlet. We have done calculations to show that there is an excited triplet state in the vicinity of the singlet, with sufficient oscillator strength. Therefore we searched for evidence of a triplet-triplet emission in the vicinity of one micron wavelength using a variety of near-IR photomultipliers. No signals were seen whatsoever, with a sensitivity level several orders of magnitude higher than that able to detect UV fluorescence from phenylacetylene under the same conditions.

To establish whether the long-lived state is a cold or hot triplet, or perhaps even some isomer, we have extensively explored the photoelectron spectrum (PES) with respect to delay times. It is seen that, using 193 nm photons, the spectrum evolves from having prominent singlet state transitions (terminating in both the X and the A state of the ion, the two peaks to higher energy in the spectra) to one dominated by low energy electrons. The remarkable thing is that the

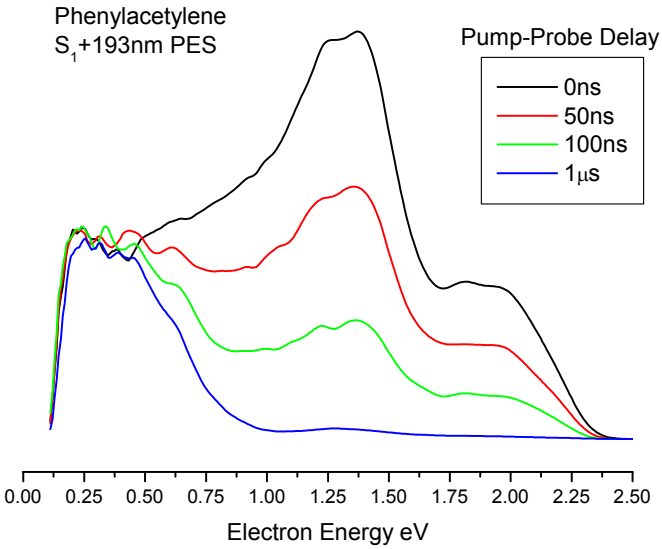

long-lived component is present immediately, and does not grow during the singlet lifetime. Before or after the singlet decays, the low-energy PES stays unchanged for as long as 90 μs and is a continuously rising signal from a little below 1 eV to about 0.1 eV, below which there is no information because the electron collection efficiency becomes negligible.

The conclusion one can make from this is that there are two species created during the laser pulse, or perhaps one species or superposition state that collapses rapidly into two populations. One, the singlet, decays by fluorescence (J= 75ns), and possibly other pathways, but it does not convert into the other. The long-lived component is spectrally consistent with a hot triplet state, but could be anything with an IP of around 5.5 eV.

There are a large number of isomers of phenylacetylene, some of which require minimal bond rearrangement, and we have considered whether the long-lived state is one of them. It is unlikely that the molecule has undergone a permanent isomerization since that would raise the ionization potential of the molecule enough that 193 nm photons would not have enough energy to produce electrons. However, there could be some dynamic situation where the molecule is floating above a variety of potential wells in the triplet manifold and the Franck-Condon factors are so low in much of the phase space that there is no substantial coupling to the singlet ground state. If this were the case, there could be some probability of returning to the singlet state. We have searched for this in the PES to no avail, but it is probable that the singlet population would be too small to be detectable.

We are left with the puzzle that there are two populations created in the laser pulse. One fluoresces and the other lives indefinitely, but they do not detectably interconvert. They have different ionization potentials, but have the same rotational excitation signature. One would expect a hot triplet to continue to receive population for the lifetime of the singlet., casting doubt on that candidate unless somehow there are two different types of singlet states excited. A careful examination of the PES spectra with respect to the quantum levels excited in S_1 will be necessary to determine if different levels have differing couplings to the long-lived states. For signal-strength reasons, present PES studies have excited a band-head, with a variety of rotational levels present.

As far as we are aware, no-one has ever studied whether the "triplet" component in pump-probe ionization studies is formed instantly, or continuously during the lifetime of the singlet, for any large molecule. This has to be done my some technique like PES that can distinguish the singlet and triplet, and little excited state PES has been done. Since a kinetic model for intersystem crossing in which IC competes with fluorescence is a general concept in molecular photophysics, it is important to know that answer.

FUTURE PLANS

We would like to see if long-lived species are present in other molecules similar to phenylacetylene, such as styrene, diethynylbenzene, ethynylpyridine, etc. We are also going to examine the radiationless transition properties of some classic systems like pyrazine with the high resolution pulsed laser. We can do rotationally dependent PES, and directly compare the triplet signal with the absorption and fluorescence intensities. Gathering all this information in the same experiment has never been accomplished, and should provide more insight into the basics of radiationless transitions.

Another project involves a puzzling enormous broadening of the line width of molecular transitions when a high resolution laser pulse is modulated in time. Comparing molecular

photophysics using transform limited pulses versus CW excitation or modulated pulses will give insights into how the excited state wavefunctions are affected by the light characteristics.

DOE PUBLICATIONS

Andrew. B. Burrill, You K. Chung, Heather. A. Mann, and Philip M. Johnson, "The Jahn-Teller effect in the lower electronic states of benzene cation: Part III The ground state vibrations of $C_6H_6^+$ and $C_6D_6^+$," J. Chem. Phys. **120**, 8587-8599 (2004).

Haifeng Xu, Trevor Sears, and Philip Johnson, "Photoinduced Rydberg Ionization spectroscopy of Phenylacetylene: Vibrational assignments of the $\tilde{C}$ state of the cation," J. Phys. Chem. A, 110, 7822-7825 (2006).

Philip Johnson, Haifeng Xu, and Trevor Sears, "The calculation of vibrational intensities in forbidden electronic transitions," J. Chem. Phys. **125**, 164330 (2006).

Haifeng Xu, Philip Johnson, and Trevor Sears, "Photoinduced Rydberg ionization spectroscopy of the $\tilde{B}$ state of benzonitrile cation," J. Chem. Phys. **125**, 164331 (2006).

Probing the Reaction Dynamics of Hydrogen-Deficient Hydrocarbon Molecules and Radical Intermediates via Crossed Molecular Beams

Ralf I. Kaiser
Department of Chemistry
University of Hawai'i at Manoa
Honolulu, HI 96822
ralfk@hawaii.edu

1. Program Scope

The major goals of this project are to explore experimentally in crossed molecular beams experiments the reaction dynamics and potential energy surfaces (PESs) of hydrocarbon molecules and their corresponding radical species which are relevant to combustion processes. The reactions are initiated under single collision conditions by crossing two supersonic reactant beams containing radicals and/or closed shell species under a well-defined collision energy and intersection angle. By recording angular resolved time of flight (TOF) spectra, we obtain information on the reaction products, intermediates involved, on branching ratios for competing reaction channels, on the energetics of the reaction(s), and on the underlying reaction mechanisms. These data are of crucial importance to understand the formation of carbonaceous nanostructures as well as of polycyclic aromatic hydrocarbons and their hydrogen deficient precursors in combustion flames.

Chemical reaction networks modeling the formation of polycyclic aromatic hydrocarbons (PAHs) in combustion flames imply that the phenyl radical, C_6H_5, presents one of the most important transient species involved in the formation of PAHs. The crucial steps of these reaction models are believed to be hydrogen abstraction – unsaturated hydrocarbon addition sequences. All chemical networks concur that reactions of the phenyl radical with acetylene, for instance, initiates the PAH synthesis via an addition of phenyl to the carbon-carbon triple bond. Due to the central role of the phenyl – unsaturated hydrocarbon reactions, the kinetics of these systems have been well-established up to temperatures of a couple of thousand Kelvin. Theoretical studies of these benchmark systems predicted the initial formation of adducts which either decomposed back to the reactants or fragmented to the reactant molecules such as phenylacetylene and styrene, for instance. Nevertheless, despite the central role of the phenyl – unsaturated hydrocarbon reactions as the trigger to PAH formation, the theoretical investigations have never been verified experimentally under single collision conditions and, consequently, the nature of the true reaction products of these elementary reactions have remained elusive so far. Therefore, we initiated a systematic research program to investigate the reaction dynamics of phenyl radicals with unsaturated hydrocarbons.

2. Recent Progress

2.1. Supersonic Phenyl Radical Source

We built, calibrated, and optimized a supersonic phenyl radical source. Briefly, the supersonic phenyl radical beam was generated via flash pyrolysis of helium-seeded nitroso benzene (C_6H_5NO, Aldrich) at seeding fractions of less than 0.1 %. 4 atm of helium were introduced into a reservoir which holds the nitroso benzene sample at a temperature of 283 K. This mixture was expanded at a stagnation pressure of about 900 torr through a resistively heated silicon carbide tube at temperatures of 1200 – 1500 K. The pulsed valve was operated at 200 Hz with pulses of 80 - 150 μs wide. Under these conditions, the decomposition of the nitroso benzene precursor was *quantitative*. Number densities of $4–6 \times 10^{12}$ radicals cm^{-3} in the interaction region of the scattering chamber were obtained.

2.2. Scattering Experiments

We utilized the phenyl radical source to complete the crossed beams reactions of phenyl radicals with acetylene, ethylene, methylacetylene, and allene together with their (partially) deuterated counterparts; for each system, two collision energies have been investigated. So far, the data analysis and fits of the phenyl – acetylene and phenyl – ethylene systems have been completed (see below). The data analysis of the reactions of phenyl with methylacetylene and allene is ongoing.

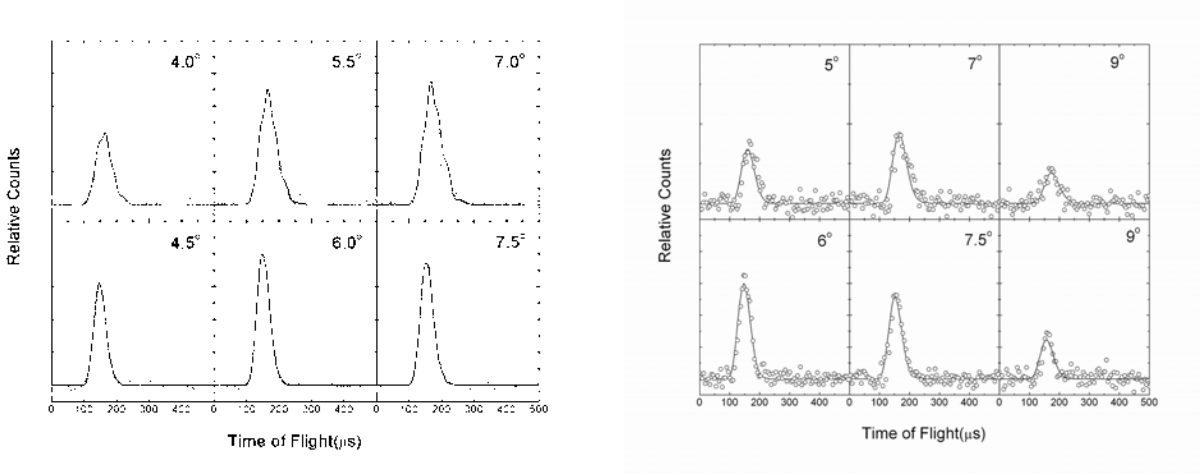

Figure 1: Left: Selected time-of-flight data recorded at a mass-to-charge (m/z) ratio of 102 ($C_8H_6^+$) at collision energies of 71.5 (top) and 99.0 kJmol^{-1} for the phenyl – acetylene reaction. Right: Selected time-of-flight data recorded at a mass-to-charge (m/z) ratio of 104 ($C_8H_8^+$) at collision energies of 83.6 (top) and 105.3 kJmol^{-1} for the phenyl – ethylene reaction. The circles indicate the experimental data, the solid lines the calculated fits. TOF spectra have been accumulated over 8 – 15 × 10^6 scans.

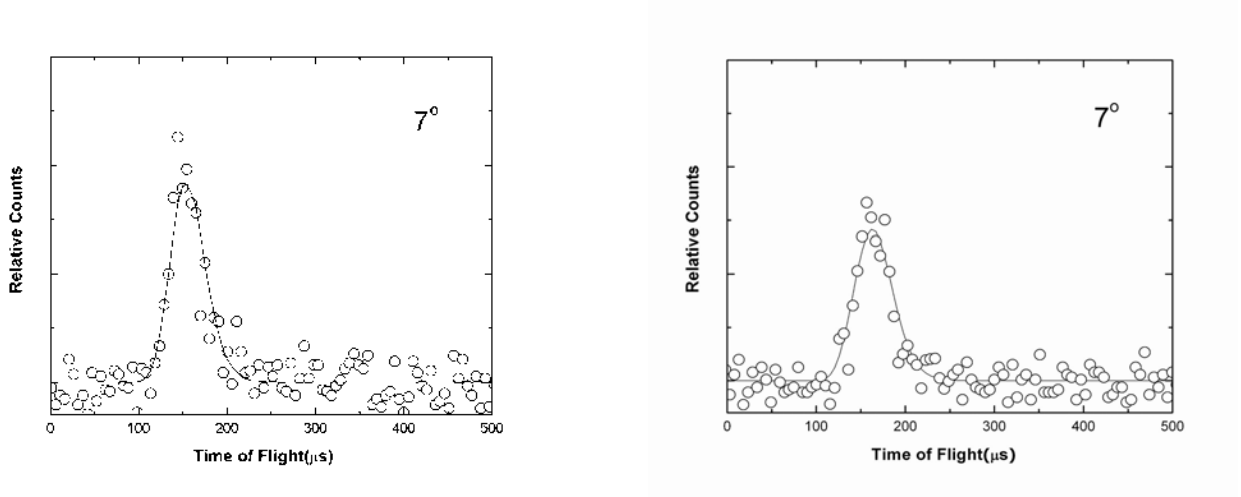

Figure 2: Left: Time of flight spectrum recorded at mass-to-charge (m/z) of 103 ($C_8H_5D^+$) (phenyl – d2-acetylene reaction). Right: Time of flight spectrum recorded at mass-to-charge (m/z) of 107 ($C_8H_5D_3^+$) (phenyl – d4-ethylene reaction). These data, the fragmentation pattern, and absent signal at m/z = 104 ($C_8H_4D_2^+$) (phenyl – d2-acetylene reaction) and m/z = 108 ($C_8H_4D_4^+$) (phenyl – d4-ethylene reaction) show that the phenyl group is conserved in both reactions and that only the phenyl versus atomic deuterium pathways are open.

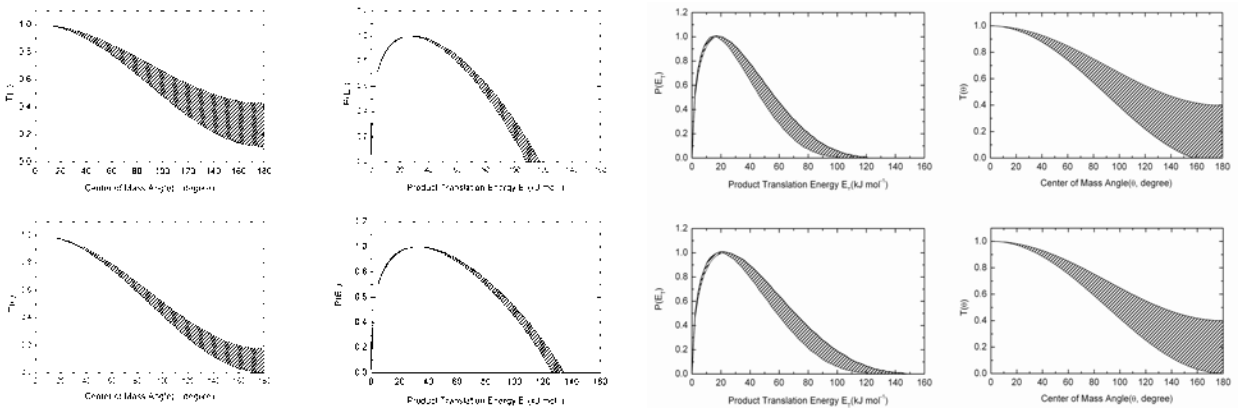

Figure 3: Left Block: Center of mass translational energy (right section) and angular distributions (left section) for the reaction of phenyl plus acetylene to form C_8H_6 plus atomic hydrogen for two collision energies of 71.5 (upper) and 99.0 kJmol^{-1} (lower). Right Block: Center of mass translational energy (left section) and angular distributions (right section) for the reaction of phenyl plus ethylene to form C_8H_8 plus atomic hydrogen for two collision energies of 83.6 (upper) and 105.3 kJmol^{-1} (lower). The data indicate the formation of phenylacetylene (acetylene reaction) and of phenylethylene (ethylene reaction) ($C_6H_5C_2H_3$) via indirect scattering dynamics through short-lived reaction intermediates which decompose via a tight exit transition states to the final products.

3. Future Plans

After the crossed beams data of the phenyl radical reactions with acetylene, ethylene, methylacetylene, and allene have been analyzed and the data submitted for publication, we intent to continue the studies of phenyl radical reactions. In the following year, our plan is to investigate the dynamics of phenyl radicals with propylene, benzene, and molecular oxygen.

4. Acknowledgements

This work was supported by US Department of Energy (Basic Energy Sciences; DE-FG02-03ER15411).

5. Publications Acknowledging DE-FG02-03ER15411 (2005-2007)

1. X. Gu, Y. Guo, E. Kawamura, R.I. Kaiser, *Design of a convection-cooled, cluster-based voltage divider chain for photomultiplier tubes*, Rev. Sci. Instr. 76 083115-1-6 (2005).

2. X. Gu, Y. Guo, H. Chan, E. Kawamura, R.I. Kaiser, *Design and Characteristics of a High Precision Chopper Wheel Motor Driver.* Rev. Sci. Instr. 76, 116103-1-3 (2005).

3. Y. Guo, X. Gu, E. Kawamura, R.I. Kaiser, *Design of a modular and versatile interlock system for ultra high vacuum machines: A crossed molecular beams setup as a case study.* Rev. Sci. Instr. 77, 034701-9 (2006).

4. X. Gu, Y. Guo, E. Kawamura, R.I. Kaiser, *Characteristics and Diagnostics of a ultrahigh vacuum Compatible Laser Ablation Source for Crossed Molecular Beams Experiments*. J. Vac. Science & Technology A, 24, 505-511 (2006).

5. X. Gu, Y.Guo, R.I. Kaiser, *Mass Spectrum of the Butadiynyl Radical (C_4H; $X^2\hat{a}^+$).* Int. J. Mass Spectr. 246, 29-34 (2005).

6. Y. Guo, X. Gu, R.I. Kaiser, *Mass Spectrum of the 1-Buten-3-yne-2-yl Radical (i-C_4H_3; X^2A').* Int. J. Mass Spectrometry 249-250, 420-425 (2006).

7. X. Gu, Y. Guo, R.I. Kaiser, *Mass Spectra of the 2,4-Pentadiynylidyne (C_5H; X^2P) and the 2,4-Pentadiynyl-1 Radicals (n-C_5H_3; X^2B_1).* Int. J. Mass Spectrometry 261, 100-107 (2007).

8. A.M. Mebel, V. V. Kislov, R. I. Kaiser, *Potential Energy Surface and Product Branching Ratios for the Reaction of Dicarbon, $C_2(X^1S_g^+)$, with Methylacetylene, $CH_3CCH(X^1A_1)$: An Ab Initio/RRKM Study,* JPCA 110, 2421-2433 (2006).

9. A.M. Mebel, V. V. Kislov, R. I. Kaiser, *Ab Initio/RRKM Study of the Singlet C_4H_4 Potential Energy Surface and of the Reactions of $C_2(X^1S_g^+)$ with $C_2H_4(X^1A_{1g})$ and $C(^1D)$ with C_3H_4 (Allene and Methylacetylene),* J. Chem. Phys. 125, 133113-1/15(2006).

10. A.M. Mebel, G.S. Kim, V.V. Kislov, R.I. Kaiser, *The Reaction of Tricarbon with Acetylene: An Ab Initio/RRKM Study of the Potential Energy Surface and Product Branching Ratios*, JPCA (in press 2007).

11. A.M. Mebel, V. V. Kislov, R. I. Kaiser, *Theoretical Studies of Potential Energy Surfaces and Product Branching Ratios for the Reactions of C_2 with Small Unsaturated Hydrocarbons (Acetylene, Ethylene, Methylacetylene, and Allene)*, in: Recent Trends in Reaction Dynamics, World Scientific, Singapore, K.C. Lin, editor (in press 2007).

12. Y. Guo, X. Gu, N. Balucani, R.I. Kaiser, *Formation of the 2,4-pentadiynyl-1 radical ($H_2CCCCCH$, X^2B_1) in the Crossed Beams Reaction of Dicarbon Molecules with Methylacetylene*. JPCA 110, 6245-6249 (2006).

13. X. Gu, Y. Guo, A.M. Mebel, R.I. Kaiser, *Chemical Dynamics of the Formation of the 1,3-Butadiynyl Radical ($C_4H(X^2S^+)$) and its Isotopomers*. JPCA, 110, 11265-11278 (2006).

14. Y. Guo, X. Gu, F. Zhang, A.M. Mebel, R.I. Kaiser, *Unimolecular Decomposition of Chemically Activated Pentatetraene ($H_2CCCCCH_2$) Intermediates – A Crossed Beams Study of Dicarbon Molecule Reactions with Allene*. JPCA 110, 10699-10707 (2006).

15. X. Gu, Y. Guo, F. Zhang, A. M. Mebel, R.I. Kaiser, *A Crossed Molecular Beams Study of the Reaction of Dicarbon Molecules with Benzene*, Chem. Phys. Lett 436, 7-14 (2007).

16. X. Gu, Y. Guo, F. Zhang, A.M. Mebel, R.I. Kaiser, *A Crossed Molecular Beams Study on the Formation and Energetics of the Resonantly Stabilized i-C_4H_3 radical, $H_2CCCH(X^2A')$, together with its Isotopomers*. Chemical Physics (in press 2007).

17. Y. Guo, X. Gu, F. Zhang, A.M. Mebel, R.I. Kaiser, *A Crossed Molecular Beams Study on the Formation of Hexenediynyl Radicals ($H_2CCCCCCH$; C_6H_3 (X^2A')) via Reactions of Tricarbon Molecules, $C_3(X^1S_g^+)$, with Allene (H_2CCCH_2; X^1A_1) and Methylacetylene (CH_3CCH; X^1A_1).* PCCP (in press 2007).

18. X. Gu, Y. Guo, A.M. Mebel, R.I. Kaiser, *A Crossed Beams Investigation of the Reactions of Tricarbon Molecules, $C_3(X^1S_g^+)$, with Acetylene, $C_2H_2(X^1S_g^+)$, Ethylene, $C_2H_4(X^1A_g)$, and Benzene $C_6H_6(X^1A_{1g})$.* PCCP (submitted 2007).

DYNAMICAL ANALYSIS OF HIGHLY EXCITED MOLECULAR SPECTRA

Michael E. Kellman
Department of Chemistry, University of Oregon, Eugene, OR 97403

kellman@uoregon.edu

PROGRAM SCOPE:

The goal of our program is to develop theoretical tools to understand spectra and dynamics of highly excited species of importance in combustion, including intramolecular energy transfer and isomerization reactions. It is now clear that anharmonic effects lead to profound changes in the vibrational dynamics of molecules when nonlinearities can no longer be treated as perturbative effects, and the standard picture of anharmonic normal modes breaks down. References to numerous examples can be found in a recent detailed study of acetylene bends spectra [2] and a recent review [3]. We have emphasized particularly the role of bifurcations and the "birth of new modes in bifurcations from the low energy normal modes". For these purposes we use bifurcation analysis of semiclassical versions of the effective Hamiltonians used by spectroscopists to fit complex experimental spectra. Observable phenomena associated with bifurcations such as changes in spectral patterns have been predicted and observed.

RECENT PROGRESS:

Bifurcation analysis: Branchings of the normal modes into new anharmonic modes. The acetylene/vinylidene system is of great importance in combustion, acetylene as an intermediate, and the vinylidene isomer as precursor of the radical pool formed by reaction with O_2. We have completed [2] an effort to gain a systematic understanding of the bending dynamics of the acetylene system with vibrational angular momentum $\mathbf{l} = 0$.

Higher $\mathbf{l}$-vibrational angular momentum states of acetylene. The bifurcation analysis of the pure bends system described above is for spectra with vibrational angular momentum $\mathbf{l} = 0$ in the fitting Hamiltonian. Obviously, it is of great interest to extend the analysis to systems with $\mathbf{l} > 0$. We have performed the bifurcation analysis for $\mathbf{l}$ up to 20 in work to be submitted [5]. We find that there are four new modes born in bifurcations, as for the $\mathbf{l} = 0$ case. However, these new modes are precessing orbits, due to the $\mathbf{l}$ excitation. The figure (below left) shows one of these, the precessing Orthogonal mode.

Catastrophe map analysis of acetylene bends system. The bifurcation behavior observed in Ref. [2] has certain key resemblances to that obtained with a simplified integrable model of two bend modes coupled by a single resonance. However, the real acetylene bends system is a four-mode system with three resonances, nonintegrability and chaotic dynamics. The system is not separable in any sense. We have undertaken to

understand the evident regularities observed in Ref. [2] , while keeping sight of the full complexity of the system.

We approach this problem using a catastrophe map analysis, developed for single resonance molecular systems in our group in 1990. The catastrophe map is a kind of "phase diagram" of the dynamics of the effective fitting Hamiltonian. We have performed the catastrophe map analysis for the four-mode acetylene bends Hamiltonian [6] . We find that a very satisfactory account can be given of the similarities to the simple two-mode models, as well as the essential differences and greater complexity. The key insight to understanding this comes from analysis of the symmetry of the catastrophe map, in the figure (below right).

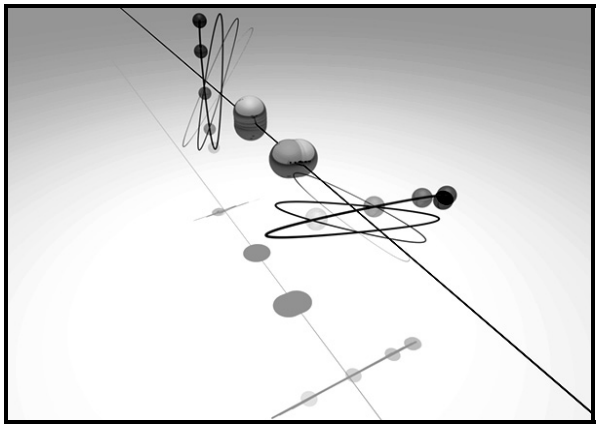

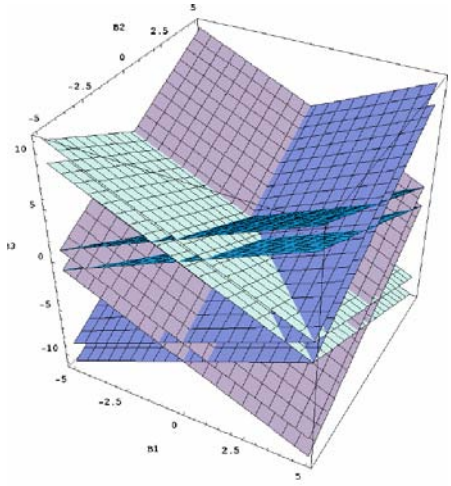

Spectral anomalies, experimental signature of bifurcation, moment of inertia backbending. While bifurcation effects in purely vibrational dynamics and spectra are starting to be well-understood, the interplay of bifurcations and angular momentum remains mostly a mystery. In a recently submitted paper [4], we are focusing on the most elementary possible systems involving bifurcations and angular momentum. We consider pure vibrational angular momentum $J = \mathbf{l}$ excitations of acetylene. From the effective fitting Hamiltonian we predict clearly anomalous spectral behavior. In order to understand this, we invoke a moment of inertia "backbending" effect as the molecule undergoes a sequence of bifurcations. Essentially, the molecule undergoes a change in vibrational "shape" due to the bifurcations, while retaining its linear equilibrium symmetry. This spectral pattern represents both a departure from and extension of the standard rotational dynamics paradigm of a linear symmetric top molecule, as treated, for example, by Herzberg.

Rotation-vibration spectra and dynamics: The analysis above starts with bending dynamics with $\mathbf{l} = 0$, then progressed to include vibrational angular momentum, with $\mathbf{l} > 0$. The next step is to go beyond pure vibrational angular momentum, to include full rotation-vibrations dynamics. This includes new, rotation-vibration couplings due to Coriolis effects. We have succeeded in performing the bifurcation analysis for full

rotation-vibration dynamics of triatomics and are currently preparing this work for publication.

FUTURE PLANS:

In the future, our goals are (1) completion of a major effort to understand the full range of bending dynamics for high values both of the total bend quantum number N_b and vibrational angular momentum $\mathbf{l} > 0$; (2) extension to full stretch-bend dynamics; (3) continued progress on bifurcation analysis for rotation-vibration dynamics; (4) effective Hamiltonians for spectra in which the total or polyad number is broken on the route to isomerization; (5) along these lines, incorporation of multiple potentials and above-barrier dynamics, with the goal of extending our methods to encompass isomerization phenomena; (6) establishment of contact with recent new developments in the theory of the classical transition state.

Spectral patterns for general bend excitations: variable total quantum number N_b and $\mathbf{l} > 0$ excitation. Above we have described our work on moment of inertial backbending with sequences of high $\mathbf{l}$ excitations in acetylene. These sequences are only the beginning of spectral patterns in these systems. We are investigating a "tetracritical point" in the "phase diagram" of the spectrum, with a very rich set of spectral patterns associated with the bifurcation behavior.

The challenge of higher dimensions: Analytically scalable bifurcation analysis. As the dimensionality of the problem becomes larger, one of the challenges is whether our analysis can be performed, in a way that is still understandable and useful. The key to making tractable larger systems such as the full stretch-bend degrees of freedom is use of the polyad quantum number, which is an integral part of the standard spectroscopic fitting Hamiltonian. The polyad Hamiltonian makes possible determination of the mode bifurcation structure by *analytic* means, i.e. by solution of simple algebraic equations related to the Hamiltonian function, rather than numerical solution of the equations of motion. In our approach we seek the critical points or "flat spots" of the polyad Hamiltonian. It is not necessary to perform numerical integration of Hamilton's equations and analysis of surfaces of section. We are working on full stretch-bend analysis of acetylene in this approach.

Full rotation-vibration spectra dynamics of acetylene including bends, stretches, and rotations: As described above, a major achievement has been the performance of the bifurcation analysis for full rotation-vibration dynamics of triatomics. We are extending this analysis for acetylene. The Coriolis couplings in acetylene necessarily couple the bending to the stretching modes.

Spectroscopic Hamiltonians for polyad breaking spectra. All spectroscopic Hamiltonians to date invoke the "polyad approximation" of a conserved total vibrational quantum number. We are investigating highly excited model systems in which the

polyad approximation breaks down, and the development of an effective spectroscopic Hamiltonian to encompass this.

Spectroscopic Hamiltonians for multiple wells and above barrier spectroscopy. Isomerization dynamics are of extreme interest in combustion. The challenge in performing bifurcation analysis related to "isomerization spectra" is to build an effective spectroscopic Hamiltonian. There are two challenges. The first is to define separate zero-order quantum numbers for each of the well regions and for the above-barrier region. The second is to define coupling operators that couple the zero-order states. Most challenging is to devise cross-barrier couplings that act above and below the barrier, and between wells.

Bimolecular reaction dynamics and internal molecular motions. There have recently been profound new mathematical developments in classical transition state theory. We would like to relate our work on new anharmonic modes to this. How do these modes "connect up" with the transition state? Consider the reaction $H + O_2 \rightarrow HO + O$ which has been called "the most important reaction in combustion". What is the role of the vibrations of the highly excited metastable intermediate HO_2? Recent computational work of Hua Guo has shown, contrary to earlier expectations, that there is pronounced non-RRKM behavior in this system. We want to investigate (1) the nature of the highly excited vibrations of the radical HO_2 and (2) the relation of these to the reaction $H + O_2 \rightarrow HO + O$.

Recent publications (in print, in press 2005-2007) related to DOE supported research:

1. S. Yang and M.E. Kellman, "Semiclassical Wave Function From a Quantizing Cantorus", Chem. Phys., 322, 30 (2006).

2. V. Tyng and M.E. Kellman, "Bending Dynamics of Acetylene: New Modes Born in Bifurcations of Normal Modes", J. Phys. Chem. B, 110, 18859 (2006)

3. M.E. Kellman and V. Tyng, "Dances with Molecules", in press, Accounts of Chemical Research.

Other references:

4. V. Tyng and M.E. Kellman, "Spectral Anomaly, Moment of Inertia Backbending, and Bifurcations", submitted to Phys. Rev. Lett.

5. V. Tyng and M.E. Kellman, "Critical Points Bifurcation Analysis of High- **l** Bending Dynamics in Acetylene", manuscript in preparation.

6. V. Tyng and M.E. Kellman, "Catastrophe Map Analysis of C_2H_2 Bending Dynamics", manuscript in preparation.

Theory and Modeling of Small Scale Processes in Turbulent Flow

Alan R. Kerstein
Combustion Research Facility
Sandia National Laboratories
Livermore, CA 94551-0969
Email: arkerst@sandia.gov

PROJECT SCOPE

Predictive simulation of combustion processes in turbulent flow environments of practical (as well as scientific) interest generally requires physically motivated simplifications of the governing equations that drastically reduce computational cost. The most common and effective cost-reduction strategy is to under-resolve small-scale processes, representing them instead by models that evolve the statistics of the local thermochemical state without explicit representation of associated physical-space processes such as gradient-driven diffusive transport. As the application of this strategy is extended to increasingly challenging combustion environments, its limitations are becoming more apparent, indicating that turbulence interactions with diffusive transport and related small-scale processes require more explicit, detailed treatment. This project explores various strategies for filling this need.

The strategy that has been the longstanding focus of this project is map-based representation of advection. Advection (fluid motion) is continuous in time, but its representation as a sequence of instantaneous events (maps) at instants in time reduces the computational cost of turbulence simulations, while in many cases providing enough fidelity for accurate treatment of advective coupling to small-scale processes. In particular, it enables useful simulations in one spatial dimension using the Linear Eddy Model (LEM) and its subsequent generalization, One-Dimensional Turbulence (ODT), as demonstrated by numerous applications during this effort. Ongoing pursuits include investigation of fire phenomenology and development of strategies for 3D simulation involving LEM or ODT small-scale representations. Recent work has shown that a 3D map-based flow representation is advantageous for certain multiphase regimes relevant to cloud dynamics, motivating future fundamental studies and geophysical applications.

Another strategy that is being pursued is explicit evaluation of averages over the complete ensemble of flow histories using quantum-field-theory methods, supplemented by rigorous mathematical analysis, heuristic reasoning, and computational validation studies. The challenge of this approach is to develop formulations that are both tractable and physically relevant. This new effort has yielded detailed understanding of the weak-turbulence regime of premixed combustion and has significant implications for strongly turbulent flames, which are the focus of ongoing and planned continuations of this effort.

RECENT PROGRESS

Owing to its novelty within this project, a recent field-theoretic analysis of advected propagating fronts (idealizing turbulent premixed combustion) is highlighted in this progress report. Consider advection (random or deterministic) characterized by a root-mean-square velocity fluctuation u' and front propagation at speed u_0 (laminar flame speed). For weak advection ($u' << u_0$), Clavin and Williams [A] derived the relation $u_T/u_0 - 1 \sim (u'/u_0)^2$, where the turbulent burning velocity u_T is defined as the volume flux through the front per unit projected lateral surface area. This relation is demonstrably valid for periodic flow. Kerstein and Ashurst [B] argued heuristically

that a different relation, $u_T/u_0 - 1 \sim (u'/u_0)^{4/3}$, holds for random weak advection, and reported simulations of propagation in idealized random flows that support this result. Subsequently [C] they showed that the weak advection regime is equivalent to propagation through a fixed (in time) medium with spatially varying u_0, where u' now represents the spatial variability of u_0.

From this starting point, the recent effort addressed two questions: (1) Can the 4/3 exponent be derived rigorously? (2) Writing the flame speed relation as $u_T/u_0 - 1 = c(u'/u_0)^{4/3}$, can the dependence of c on the spatial structure of the medium be obtained by analysis? The investigation yielded the answers: (1) Yes. (2) Yes, to a good approximation, for isotropic media in which the flame speed pdf $f(u)$, with mean u_0, and the spatial autocorrelation $A(\mathbf{r}) = < [u(\mathbf{x}) - u_0][u(\mathbf{x}+\mathbf{r}) - u_0]> / u_0^2$ are arbitrary (but exclude certain pathologies).

The 4/3 exponent was derived rigorously by starting from the ray-equation formulation of propagation in a fixed random medium and noting that, for the regime of interest, space and time can be rescaled so that ray perturbations correspond to a white noise whose properties depend on $A(\mathbf{r})$. This rescaling generalizes a procedure [D] previously used in geometrical optics but not, in its original form, applicable to the first-arrival problem. The rescaling yields the asymptotically exact relation $u_T/u_0 - 1 = c(u'/u_0)^{4/3}$, where c is a property of propagation in a white-noise medium that depends, in a way not yet determined at this stage of the analysis, on $A(\mathbf{r})$, but does not depend on u'/u_0. A recent rigorous result [E] guarantees, under weak assumptions, that the white-noise process determining c is well behaved, completing the exact derivation of the 4/3 exponent.

An approximate closed-form dependence of c on $A(\mathbf{r})$ is derived as follows. The derivation of the 4/3 exponent shows that, to leading order in u'/u_0, the travel time $t(P)$ along a path P through the medium is equivalent to the classical action for the randomly forced inviscid Burgers equation that governs flow of a notional pressure-free fluid. It is useful to consider nonzero viscosity $\nu/2$ initially, later allowing it to vanish. For small ν, the integral of $\exp[-t(P)/\nu]$ over paths P is dominated by the term $\exp[-t(P^*)/\nu]$, where P^* is the path for which t is smallest. Setting $\exp[-t(P^*)/\nu]$ equal to the path integral of $\exp[-t(P)/\nu]$, the relation $t(P^*) = -\nu \ln I$, valid for vanishing ν, is obtained, where I denotes the path integral. This relation expresses the shortest travel time as a functional of the travel times for all possible paths in a given realization of the medium. Now this relation is averaged over all possible realizations, denoted by angle brackets. After the rescaling that extracts the dependence on u'/u_0, this gives $c = K<\ln Z>$, where K is a known quantity and the mathematical expression for Z corresponds to the partition function for a directed polymer at temperature ν in a random potential given by the rescaled form of $A(\mathbf{r})$. This equivalence of randomly forced Burgers dynamics and polymer thermodynamics is well known, as is the formal methodology that exploits this equivalence [F]. The technical key is that evaluation of $<Z^n>$ is tractable, but evaluation of $<\ln Z>$ is not, so $<\ln Z>$ is expressed formally as the $n \to 0$ limit of $(<Z^n>-1)/n$. For positive integer n, evaluation of $<Z^n>$ involves evaluation of the ground state energy E of a particular non-relativistic n-particle quantum-mechanical system. A variational method is used to bound E, and the result is analytically continued in order to bound $<Z^n>$ in the $n \to 0$ limit. Although the extrapolation to vanishing n is a well known strategy [G], the mathematical treatment of the low-temperature limit is novel and yields a closed form bound on the dependence of c on $A(\mathbf{r})$.

Simulations for representative choices of $A(\mathbf{r})$ verify that the bound is usefully sharp. Simulations are affordable in 2D but not in 3D, so the analytical result is the only available information in 3D. (There are no pertinent experimental data.) The bound indicates that the dependence of c on $A(\mathbf{r})$ is quantitatively significant in 3D, and hence that the turbulent burning velocity depends on details of the spatial structure of the advection process, as well as on the overall amplitude of

velocity fluctuations. This sensitivity is inferred from weak turbulence behavior, but implies comparable or greater sensitivity in the strong turbulence regime (considered in the next section).

FUTURE WORK

An important implication of the derived upper bound on the coefficient c of the weak-advection scaling is a constraint that is directly applicable to advected propagating fronts for arbitrary values of u'/u_0 (assuming flame propagation at constant speed u_0 with no flame-to-flow feedback). The constraint arises because reduction of u_0 can only reduce u_T, so an upper bound on u_T that is established for any value of u'/u_0 must also apply to the given flow for any smaller value of u_0, in particular for arbitrarily small u_0 and commensurately large u'/u_0.

One possibility that is ruled out by this constraint is a dependence of the form $u_T = f(\mathrm{Re})\, u'$ where f monotonically increases with Reynolds number Re and is unbounded as Re diverges. (This behavior is ruled out because the analysis yields the important result that the derived upper bound on c remains finite as Re diverges.) In particular, this rules out $u_T = c\, \mathrm{Re}^p\, u'$ for positive p. An analysis by Fedotov [H] implies that this dependence, with $p = ¼$, is an upper bound on the true parameter dependence of u_T for a solvable case, the 'rapid-change' flow model [I]. It is now clear that this bound is not sharp; p cannot be positive for this or any other non-pathological flow.

Exact mathematical analysis of the rapid-change model shows that certain flow properties that are ostensibly tied to the scaling of u_T scale as $\mathrm{Re}^{1/4}$, yet the new bound assures no such dependence of u_T. It is anticipated that further analysis of this case will provide more insight into the connections between flow statistics and u_T scaling.

The significance of these results is that they offer a new perspective on the fundamental question of whether Damköhler's relation $u_T \sim u'$ is a sufficient canonical (i.e., omitting real-flame effects) parameterization of the turbulent burning velocity [J]. The results obtained thus far establish that u_T/u' cannot diverge as a function of any diverging flow parameter, notably Re.

It remains to be determined whether the possibility that u_T/u' vanishes as a function of any diverging flow parameter can be ruled out for physically realistic flows. There have, in fact, been several proposals that u_T/u' vanishes as u'/u_0 diverges [K,L,M]. This issue will be investigated.

The methods used in this study cannot address real-flame effects such as thermal expansion. Engineering models of premixed turbulent combustion are often based on analyses that neglect these effects, supplemented by empirical corrections intended to capture them [J]. In this approach, it is important to start from a physically sound analysis of the idealized case so that the resulting engineering model transitions correctly to known limiting behaviors.

Diverse approaches to, and applications of, the map-based advection representation for turbulence simulation are being pursued through ongoing collaborative efforts, for example:

- Turbulent jet diffusion flames studied at the Sandia Combustion Research Facility (CRF) were previously simulated using ODT [N]. The comparisons will be revisited and extended after the physical model and numerical implementation are improved in several ways. Planned improvements include simulation of streamwise flame development using spatial flow advancement rather than a temporal analog, incorporation of cylindrical geometry, improved treatment of variable-density effects [1], and radiative coupling. Radiative coupling is achieved as follows. An ODT realization is run using an assumed background radiation field. Based on local emission and absorption during that realization, a new background radiation field is computed. This procedure is iterated, but

with each subsequent background radiation field computed as a weighted average of the newest result and previous results, yielding convergence after roughly ten iteration cycles. The radiation coupling will enable future studies of radiating flames, notably fires, which are buoyancy-driven flames that generate gaseous fuel (and subsequently soot) by heating solid or liquid fuel sources.

- LEM simulations of turbulent counterflow flames will be used to develop chemistry look-up tables for subgrid closure of large eddy simulations (LES) of turbulent nonpremixed combustion. The LES with this closure will be used to predict extinction-reignition phenomena observed in the CRF turbulent jet flames, and it will then be applied to other thermochemically challenging environments.
- Multiphase extensions of LEM and ODT are under development in order to study (1) breakup of a liquid jet (e.g., injected fuel) induced by internal turbulence and/or surface shear, (2) particle-gas kinetic-energy and momentum exchange in, e.g., a fluidized-bed combustor, and (3) effects of inertia-induced droplet clustering [4] on coalescence leading to rain formation in clouds.

REFERENCES

A. P. Clavin and F. A. Williams*, J. Fluid Mech.* **90**, 589 (1979).
B. A. R. Kerstein and Wm. T. Ashurst, *Phys. Rev. Lett.* **68**, 934 (1992).
C. A. R. Kerstein and Wm. T. Ashurst, *Phys. Rev.* E **50**, 1100 (1994).
D. B. S. White, *SIAM J. Appl. Math.* **44**, 127 (1984).
E. R. Iturriaga and K. Khanin, *Commun. Math. Phys.* **232**, 377 (2003).
F. J. P. Bouchaud, M. Mézard, and G. Parisi, *Phys. Rev.* E **52**, 3656 (1995).
G. M. Mézard, G. Parisi, and M. A. Virasoro, Spin Glass Theory and Beyond (World Scientific, Singapore, 1987).
H. S. Fedotov, *Phys. Rev.* E **55**, 2750 (1997).
I. R. H. Kraichnan, *J. Fluid Mech.* **64**, 737 (1974).
J. N. Peters, Turbulent Combustion (Cambridge U. Press, Cambridge, 2000).
K. V. Yakhot, *Combust. Sci. Tech.* **60**, 191 (1988).
L. A. R. Kerstein, *Combust. Sci. Tech.* **60**, 163 (1988).
M. M. Chertkov and V. Yakhot, *Phys. Rev. Lett.* **80**, 2837 (1998).
N. T. Echekki, A. R. Kerstein, J.-Y. Chen, and T. D. Dreeben, *Combust. Flame* **125**, 1083 (2001).

PUBLICATIONS SINCE 2005

1. Wm. T. Ashurst and A. R. Kerstein, "One-Dimensional Turbulence: Variable-Density Formulation and Application to Mixing Layers," *Phys. Fluids* **17**, 025107 (2005).
2. S. Wunsch and A. R. Kerstein, "A Stochastic Model for High Rayleigh Number Convection," *J. Fluid Mech.* **528**, 173 (2005).
3. R. J. McDermott, A. R. Kerstein, R. C. Schmidt, and P. J. Smith, "The Ensemble Mean Limit of the One-Dimensional Turbulence Model and Application to Residual Stress Closure in Finite Volume Large-Eddy Simulation," *J. Turbul.* **6**, 1 (2005).
4. A. R. Kerstein and S. K. Krueger, "Clustering of Randomly Advected Low-Inertia Particles: A Solvable Model," *Phys. Rev.* E **73**, 025302 (2006).
5. J. Cuxart, A. A. M. Holtslag, A. R. Kerstein, S. Wunsch, *et al*., "Single-Column Model Intercomparison for a Stably Stratified Atmospheric Boundary Layer," *Bound. Layer Meteorol.* **118**, 273 (2006).
6. A. R. Kerstein and S. Wunsch, "Simulation of a Stably Stratified Atmospheric Boundary Layer Using One-Dimensional Turbulence," *Bound. Layer Meteorol.* **118**, 325 (2006).

KINETICS OF COMBUSTION-RELATED PROCESSES AT HIGH TEMPERATURES

J. H. Kiefer

Department of Chemical Engineering

University of Illinois at Chicago
Chicago, IL 60607
(kiefer@uic.edu)

Program Scope

As before, this program involves the use of the shock tube with laser-schlieren (LS) and time-of-flight mass spectrometry (TOF), as diagnostics for the exploration of reaction rates and energy relaxation processes over an extremely wide range of temperatures and pressures. We are interested in both energy transfer and the kinetics of reactions at combustion temperatures and above. Our efforts usually emphasize the phenomena of unimolecular reaction including incubation and falloff for whose observation LS provides a unique capability. As noted, this work is now supplemented by product profiles from TOF experiments conducted at Argonne by Robert Tranter and Binod Giri.

Relaxation in the fluoroethanes and vinyl fluoride

. New experiments on relaxation in all the many other possible fluoroethanes have now been completed, and this material is being readied for publication. Unfortunately, in some of the more heavily fluoridated species, like C_2F_5H and the two $C_2F_4H_2$, relaxation is simply too fast to resolve, and only a rough estimate of the relaxation time can be made. There is no sign of the double relaxation seen in the 1,1,1-trifluoroethane in any of these, but since relaxation is very rapid in all, any such relaxation may simply be unresolved. In the particular case of 1,1-difluoroethane, where we have also measured dissociation rates, relaxation is sufficiently rapid to preclude any significant incubation delay.

Dissociation in 1,1-difluoroethane

In a continuing effort to understand our observation of non-RRKM dissociation in 1,1,1-trifluoroethane [1], we have carried out a study of dissociation in the closely related 1,1-difluoroethane. This work is now complete and our combined LS, TOF study of HF elimination from 1,1-difluoroethane has been submitted for publication to PCCP. Here the modeling is slightly dependent on the rate of decomposition of the product vinyl fluoride and we have also determined rates for this that cover the range of the 1,1-difluoroethane experiments (see below). Dissociation in the difluoroethane is quite unremarkable. The data show falloff easily modeled with the usual RRKM with a G3B3 derived set of TS parameters, and the high pressure rates are in full agreement with the single-pulse data of Tschiukow-Roux, et al. [2]. There certainly is no sign of non-RRKM behavior in any of the rate measurements.

Dissociation in vinyl fluoride

This dissociation is complicated by the presence of two channels with the same products, a 1,1-HF elimination to vinylidene and then to acetylene, and a 1,2-elimination leading directly to acetylene.

1,1-elimination) $C_2H_3F \rightarrow CH_2C: + HF$

$CH_2C: \rightarrow C_2H_2$

1,2-elimination) $C_2H_3F \rightarrow C_2H_2 + HF$

These two paths have very similar barriers, according to augmented G3B3 calculations (the 1,1- is 74..2 kcal/mol and 1,2-, 71.8 kcal/mol), so there should be little effect of falloff on the branching ratio. We find the calculated k_∞ (TST) is below the Tschuikow-Roux group's single pulse data [3] for their low-T, high-P conditions, and in this our data actually seem to be in agreement with their results. In fact, with the theoretical k_∞, a fit to all the data clearly requires an anomalously large $<\Delta E>_{down}$ at low T. The data are, however, quite consistent with a larger k_∞, as shown in the figure, when the barrier for the 1,1-elimination has been reduced by 3 kcal/mol. Why this is necessary is not yet clear. Nonetheless, this work has now been submitted for publication to PCCP.

New and planned work

We have started an examination of the dissociation of the six-member, saturated oxygen heterocycles, in a collaboration with the TOF group at Argonne. Here we include cyclohexane as the "zero oxygen" member. So far we have data on cyclohexane, 1,3-dioxane and 1,4-dioxane. We plan to also treat tetrahydropyran (one oxygen) shortly.

We have just begun experiments on the relaxation and dissociation of s-triazine, the symmetric aromatic three-nitrogen heterocycle. The molecule evidently simply dissociates to three HCN, and, interestingly, these cannot initially include any of the HNC isomer. The *effective* endothermicity of this dissociation is small (~12kcal/mol including the effect of increase in mole number), less than that of the HCN isomerization. Can we observe this isomerization? It seems possible.

References

1) J. H. Kiefer, C. Katapodis, S. Santhanan, N. K.Srinivasan, R.S. Tranter, J. Phys. Chem. A **108** 2443 (2004)
1) J. M. Simmie, W. J. Quiring and E. Tschuikow-Roux, J. Phys. Chem. **74**, 992 (1970)
2) E. Tschuikow-Roux, W. J. Quiring, and J, M, Simmie, J. Phys. Chem. **74**, 2449 (1970).

Publications

1) "Dissociation, Relaxation, and Incubation in the High-Temperature Pyrolysis of Ethane, and a Successful RRKM Modeling", J. H. Kiefer, S. Santhanam, N. K. Srinivasan, R.S. Tranter, and S. J. Klippenstein, Proc. Combust. Inst. **30**, 1129 (2005)

2) "Decomposition of Acetaldehyde: Experiment and Theory", K. S. Gupte, J. H. Kiefer, R.S. Tranter, S. J. Klippenstein, and L,B. Harding, Proc. Combust. Inst. 31, 167 (2007)
3) "Relaxation, Incubation, and Dissociation in CO_2", S. Saxena, J. H. Kiefer, and R.S. Tranter, accepted for J. Phys. Chem.

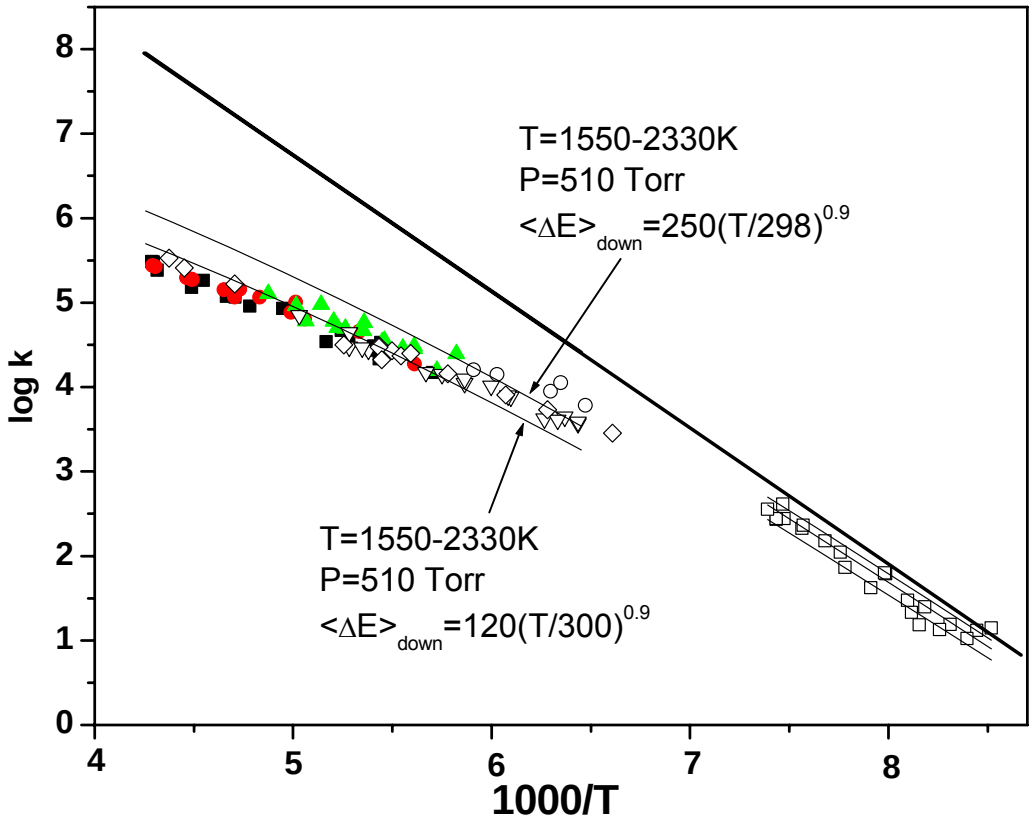

Results from the LS and TOF experiments for vinyl fluoride dissociation with a comparison with the literature data [2] and RRKM calculations using a barrier of 70kcal/mol. LS experiments: 10% $CHF=CH_2$/Kr [■] 75-140 torr, [●] 206-300 torr, [▲] 311-482 torr. In 4% $CHF=CH_2$/Kr [□] 459 to 652 torr. TOF experiments: [◊] 4% VF, 516 - 633 torr, [○]1210 - 1373 torr. The lines illustrate RRKM calculations (100, 250, 400, 550 and 1250 Torr)using the parameters of Table 1. Here the collision efficiency, $\langle\Delta E\rangle_{down} = 9775(T/298)^{-1}$ cm^{-1}, was chosen to produce a best fit. The heavy, steep line at the top shows the sum of k_∞ for reactions (**2**) and (**3**) taken from the TST calculations. RRKM calculations are thin black lines. The rates obtained in the single-pulse experiments of Simmie, et al.[37], are shown as [□] for their 2800-3600 torr range.

THEORETICAL CHEMICAL KINETICS

Stephen J. Klippenstein
Chemistry Division
Argonne National Laboratory
Argonne, IL, 60439
sjk@anl.gov

Program Scope

The focus of this program is the theoretical estimation of the kinetics of elementary reactions of importance in combustion chemistry. The research involves a combination of *ab initio* quantum chemistry, variational transition state theory, direct dynamics, and master equation simulations. The emphasis of our current applications is on (i) reactions of importance in soot formation, (ii) radical oxidation reactions, and (iii) NO_x chemistry. We are also interested in a detailed understanding of the limits of validity of and, where feasible, improvements in the accuracy of specific implementations of transition state theory. Detailed comparisons with experiments, and with other theoretical methods are used to explore and improve the predictive properties of the transition state theory models. Direct dynamics simulations are being performed as a means for testing the statistical assumptions, for exploring reaction mechanisms, and for generating theoretical estimates where statistical predictions are clearly inadequate. Master equation simulations are used to study the pressure dependence of the kinetics and to obtain phenomenological rate coefficients for use in kinetic modeling.

Recent Progress

Hydrocarbon Oxidation

In collaboration with Ahren Jasper, Larry Harding, Joe Michael, and Branko Ruscic we have completed a detailed analysis of the elementary kinetics of key reactions in the CH_3OH system employing ab initio transition state theory based master equation simulations. This analysis included the generalization of our direct CASPT2 variable reaction coordinate transition state theory (VRC-TST) approach to the treatment of OH radicals. As part of this analysis the direct CASPT2 VRC-TST approach was applied to the CH_3 + OH, CH_3O + H, CH_2OH + H, $^3CH_2$ + OH, $^3CH_2$ + $^3CH_2$, and $^3CH_2$ + CH_3 reactions. Other channels were studied with variational transition state theory employing rigid rotor harmonic oscillator energy estimates with parameters obtained from high level electronic structure calculations. For the $^1CH_2$ + H_2O channel, it was important to consider both a long range barrierless transition state and a short range tight transition state. The resulting kinetic model provided a remarkable reproduction of the OH time traces observed in Michael's shock tube studies. The combination of theory and experiment provided a consistent picture for the rate constants and product branching in the CH_3OH system for a wide range of temperatures and pressures.

In other collaborations with Joe Michael and Larry Harding we have studied the reaction of CF_3H with OH, the reaction of CF_3 with OH, and the decomposition of CF_3 radicals. These reactions are of importance in understanding the flame retardant properties of Halons. Good agreement between theory and experiment was observed in each case.

In collaboration with Hai Wang we have examined the kinetics of the CO + HO_2 reaction. A number of recent high pressure oxidation studies have suggested that this rate constant needs to be lower than assumed in prior models. Ab initio transition state theory predictions agree with these suggestions.

In collaboration with Craig Taatjes and Carlo Cavallotti we have studied the oxidation of cyclohexyl radical, which is a prototypical cyclic alkyl radical. The phenomenological rate model arising from ab initio transition state theory based master equation simulations was incorporated in a kinetic model for the OH and HO_2 time traces observed in photoloysis initiated experiments of cyclohexyl oxidation. Modest adjustments of a few key saddle point energies yielded good agreement between the model predictions and the experimental observations.

Soot Formation

In collaboration with Larry Harding and Yuri Georgievskii we have predicted the kinetics for the addition of H atoms to a wide range of resonantly stabilized radicals. More detail on this aspect is provided in Larry Harding's abstract. In collaboration with Yuri Georgievskii and Jim Miller we have predicted the addition kinetics for the C_3H_3 + C_3H_3; C_3H_3 + C_3H_5; and C_3H_5 + C_3H_5 reactions. Each of these studies employed our direct CASPT2 VRC-TST approach. For the latter reactions, it was important to also optimize the geometry of the fragments along the reaction path and as a function of the orientations.

Radical Identification (in collaboration with ALS Flame Team)

Our radical identification efforts continued with an analysis of the initial steps of aromatic formation in a laminar premixed fuel-rich cyclopentene flame cyclopentene flame. One interesting aspect of this study was the apparent observation of cycloheptatriene.

Future Directions

We will continue our studies of hydrocarbon oxidation, aromatic ring formation, and NO_x chemistry. Our oxidation studies will consider the reaction of alkyl radicals with HO_2, and the decompositions of ethanol and butanol. We will consider the reaction of CH_2 with various alkenes. We will also consider the reaction of CH + N_2, for which recent studies of Hanson are in disagreement with the predictions of Lin.

DOE Supported Publications, 2005-Present

1. **Synchrotron Photoionization Measurements of Combustion Intermediates: Photoionization Efficiency of C_3H_2 Isomers,** Craig A. Taatjes, Stephen J. Klippenstein, Nils Hansen, James A. Miller, Terrill A. Cool, Juan Wang, Matthew E. Law, and Phillip R. Westmoreland, *Phys. Chem. Chem. Phys.,* **7**, 806-813, (2005).
2. **Measurements and Modeling of HO_2 Formation in the Reactions of n-C_3H_7 and i-C_3H_7 Radicals with O_2,** Edgar G. Estupinan, Stephen J. Klippenstein, and Craig A. Taatjes, *J. Phys. Chem. B*, **109**, 8374-8387 (2005).

3. **Transition State Theory for Long-Range Potentials,** Yuri Georgievskii and Stephen J. Klippenstein, *J. Chem. Phys.,* **122,** 194103;1-17 (2005).
4. **The Addition of Hydrogren Atoms to Diacetylene and the Heats of Formation of i-C_4H_3 and n-C_4H_3,** Stephen J. Klippenstein and James A. Miller, *J. Phys. Chem. A*, **109**, 4285-4295 (2005).
5. **Predictive Theory for Hydrogen Atom-Hydrocarbon Radical Association Kinetics,** Lawrence B. Harding, Yuri Georgievskii, and Stephen J. Klippenstein, *J. Phys. Chem. A,* feature article, **109**, 4646-4656 (2005).
6. **Channel Specific Rate Constants Relevant to Thermal Decomposition of Disilane,** Keiji Matsumoto, Stephen J. Klippenstein, Kenichi Tonokura, and Mitsuo Koshi, *J. Phys. Chem. A,* **109**, 4911-4920 (2005).
7. **The Vinyl + NO Reaction: Determining the Products with Time-Resolved Fourier Transform Spectroscopy,** Peng Zou, Stephen J. Klippenstein, and David L. Osborn, *J. Phys. Chem. A,* **109**, 4921-4929, (2005).
8. **Enols are Common Intermediates in Hydrocarbon Oxidation,** Craig A. Taatjes, Nils Hansen, Fei Qi, Andrew McIlroy, James A. Miller, Juan P. Senosiain, Stephen J. Klippenstein, Terrill A. Cool, Juan Wang, Phillip R. Westmoreland, Matthew E. Law, Tina Kasper, and Katharina Kohse-Hoinghaus, *Science,* **308,** 1887-1889 (2005).
9. **A Two Transition State Model for Barrierless Radical-Molecule Reactions: A Case Study of the Addition of OH to C_2H_4,** Erin E. Greenwald, Simon W. North, Yuri Georgievskii, and Stephen J. Klippenstein, *J. Phys. Chem. A*, **109,** 6031-6044 (2005).
10. **The Reaction of Acetylene with Hydroxyl Radicals,** Juan P. Senosiain, Stephen J. Klippenstein and James A. Miller, *J. Phys. Chem. A,* **109,** 6045-6055 (2005).
11. **Predictive Theory for the Association Kinetics of Two Alkyl Radicals,** Stephen J. Klippenstein, Yuri Georgievskii, and Larry B. Harding, *Phys. Chem. Chem. Phys*., invited article, **8**, 1133-1147 (2006).
12. **Identification and Chemistry of C_4H_3 and C_4H_5 Isomers in Fuel Rich Flames,** Nils Hansen, Stephen J. Klippenstein, Craig A. Taatjes, James A. Miller, Juan Wang, Terrill A. Cool, Bin Yang, Rui Yang, Lixia Wei, Chaoqun Huang, Jing Wang, Fei Qi, Matthew E. Law, and Phillip R. Westmoreland, *J. Phys. Chem. A*, **110**, 3670-3678, (2006).
13. **Identification of C_5H_x Isomers in Fuel-Rich Flames by Photoionization Mass Spectrometry and Electronic Structure Calculations,** Nils Hansen, Stephen J. Klippenstein, James A. Miller, Juan Wang, Terrill A. Cool, Matthew E. Law, Phillip R. Westmoreland, Tina Kasper, and Katharina Kohse-Hoinghaus,, *J. Phys. Chem. A,* **110**, 4376-4388 (2006).
14. **Pathways and Rate Coefficients for the Decomposition of Vinoxy and Acetyl Radicals ,** Juan P. Senosiain, Stephen J. Klippenstein, and James A. Miller, *J. Phys. Chem. A,* **110,** 5772-5781 (2006).
15. **Reaction of Ethylene with Hydroxyl Radicals: A Theoretical Study,** Juan P. Senosiain, Stephen J. Klippenstein, and James A. Miller, *J. Phys. Chem. A*, **110**, 6960-6970 (2006).
16. **Master Equation Methods in Gas Phase Chemical Kinetics,** James A. Miller and Stephen J. Klippenstein, *J. Phys. Chem. A*, feature article, **110**, 10528-10544 (2006).
17. **Energy-Resolved Photoionization of Alkyl Peroxy Radicals and the Stability of their Cations,** Giovanni Meloni, Peng Zou, Stephen J. Klippenstein, Musahid Ahmed, Stephen R. Leone, Craig A. Taatjes, and David L. Osborn, *J. Am. Chem. Soc.,* **128,** 13559-13567 (2006).

18. **Bimolecular Reactions,** Antonio Fernandez Ramos, James A. Miller, Stephen J. Klippenstein, and Donald G. Truhlar, *Chem. Rev.,* **106,** 4518-4584 (2006).
19. **Decomposition of Acetaldehyde: Experiment and Detailed Theory,** K. S. Gupte, J. H. Kiefer, R. S. Tranter, S. J. Klippenstein, and L. B. Harding, *Proc. Comb. Inst.,* **31,** 167-174 (2007).
20. **Oxidation Pathways in the Reaction of Diacetylene with OH Radicals,** Juan P. Senosiain, Stephen J. Klippenstein, and James A. Miller, *Proc. Comb. Inst.,* **31**, 185-192 (2007).
21. **On the Formation and Decomposition of C_7H_8,** Stephen J. Klippenstein, Lawrence B. Harding, and Yuri Georgievskii, *Proc. Comb. Inst.,* **31,** 221-229 (2007).
22. **Experimental and Theoretical Rate Constants for $CH_4 + O_2 \rightarrow CH_3 + HO_2$**, N. K. Srinivasan, J. V. Michael, L. B. Harding, and S. J. Klippenstein, *Comb. Flame*, **149,** 104-111 (2007).
23. **Direct Measurement and Theoretical Calculation of the Rate Coefficient for $Cl + CH_3$ from T = 202 – 298 K,** James K. Parker, Walter A. Payne, Regina J. Cody, Fred L. Nesbitt, Louis J. Stief, Stephen J. Klippenstein, and Lawrence B. Harding, *J. Phys. Chem. A,* **111**, 1015-1023 (2007).
24. **On the Combination Reactions of Hydrogren Atoms with Resonance Stabilized Hydrocarbon Radicals,** Lawrence B. Harding, Stephen J. Klippenstein, and Yuri Georgievskii, *J. Phys. Chem. A*, ASAP (2007). [Miller Festschrift issue]
25. **Measurements and Modeling of DO_2 Formation in the Reactions of C_2D_5 and C_3D_7 Radicals with O_2,** Edgar G. Estupinan, Jared D. Smith, Atsumu Tezaki, Stephen J. Klippenstein, and Craig A. Taatjes, *J. Phys. Chem. A, in press* (2007). [Miller Festschrift issue]
26. **Kinetics of the Reaction of Methyl Radical with Hydroxyl Radical and Methanol Decomposition,** Ahren W. Jasper, Stephen J. Klippenstein, Lawrence B. Harding, and Branko Ruscic, *J. Phys. Chem. A,* ASAP (2007). [Miller Festschrift issue]
27. **Reaction Kinetics of $CO + HO_2 \rightarrow$ Products: Ab Initio Transition State Theory Study with Master Equation Modeling,** Xiaoqing You, Hai Wang, Elke Goos, C.-J. Sung, Stephen J. Klippenstein, *J. Phys. Chem. A,* ASAP (2007). [Miller Festschrift issue]
28. **Strange Kinetics of the $CN + C_2H_6$ Reaction Explained**, Yuri Georgievskii and Stephen J. Klippenstein, *J. Phys. Chem. A,* ASAP (2007). [Miller Festschrift issue]
29. **Initial Steps of Aromatic Formation in a Laminar Premixed Fuel-Rich Cyclopentene Flame,** N. Hansen, T. Kasper, S. J. Klippenstein, P. R. Westmoreland, M. E. Law, C. A. Taatjes, K. Kohse-Hoinghaus, J. Wang, and T. A. Cool, *J. Phys. Chem. A,* ASAP (2007). [Miller Festschrift issue]
30. **Reflected Shock Tube and Theoretical Studies of High-Temperature Rate Constants for $OH + CF_3H \leftrightarrows CF_3 + H_2O$ and $CF_3 + OH \rightarrow$ Products,** N. K. Srinivasan, M.-C. Su, J. V. Michael, S. J. Klippenstein, and L. B. Harding, *J. Phys. Chem. A*, ASAP (2007). [Lin Festschrift issue]
31. **A Two Transition State Model for Radical-Molecule Reactions: Applications to Isomeric Branching in the OH-Isoprene Reaction,** Erin E. Greenwald, Simon W. North, Yuri Georgievskii, and Stephen J. Klippenstein, *J. Phys. Chem. A*, accepted (2007).
32. **Association Rate Constants for Reactions between Resonance Stabilized Radicals: $C_3H_3 + C_3H_3$, $C_3H_3 + C_3H_5$, and $C_3H_5 + C_3H_5$,** Yuri Georgievskii, Stephen J. Klippenstein, and James A. Miller, *Phys. Chem. Chem. Phys.,* accepted (2007). [Theory/Experiment Synergy Special Issue]

Theoretical modeling of spin-forbidden channels in combustion reactions

Anna I. Krylov
Department of Chemistry, University of Southern California,
Los Angeles, CA 90089-0482
krylov@usc.edu

April 12, 2007

1 Scope of the project

The goal of our research is to develop predictive theoretical methods, which can provide crucial quantitative data (e.g., rate constants, branching ratios, heats of formation), identify new channels and refine reaction mechanisms. Specifically, we are developing tools for computational studies of spin-forbidden and non-adiabatic pathways of reactions relevant to combustion, and applying these tools to study electronic structure and reactions of open-shell and electronically excited species involved in these processes.

2 Summary of recent major accomplishments

During the past year, we conducted several computational studies of open-shell and electronically excited species. The common theme in these studies is interactions between states of different character and intersections between the corresponding potential energy surfaces (PESs). Continuing our research on electronic structure of open-shell hydrocarbon species[1], we characterized the electronic structure of the 1,2,3 tridehydrobenzene triradical[2]. We also investigated complicated Jahn-Teller intersections in cyclic N_3 and N_3^+[3, 4] and predicted that a similar pattern would occur in other species with doubly degenerate HOMO and LUMO, e.g., benzene. In collaboration with Prof. Hanna Reisler, we characterized electronically excited states of the diazomethane[5].

We have been also developing methodology for modeling spin-forbidden and non-adiabatic reaction pathways, e.g., we implemented an algorithm for characterizing intersections between PESs of the same and different multiplicity within the equation-of-motion family of methods (manuscript in preparation) and are currently employing this new tool for characterization of singlet-triplet crossings in formaldehyde (in collaboration with Prof. Joel Bowman). We also conducted extensive benchmarking of different energy additivity schemes within the spin-flip family of methods for accurate calculation of energy differences[2] and

bond-breaking (manuscript in preparation, in collaboration with Stephen Klippenstein and Larry Harding). Some of the recent results are highlighted below.

2.1 Theoretical and experimental investigations of electronic Rydberg states of diazomethane

In collaboration with Prof. Hanna Reisler, we characterized the electronic structure of diazomethane, a precursor for producing triplet and singlet methylene. Despite its importance in synthetic organic chemistry (as well as in chemistry of planetary atmospheres rich in N_2), electronically excited states of diazomethane have not been fully assigned. We conducted detailed coupled-cluster and equation-of-motion calculations of the ground, electronically excited, and ionized states of diazomethane, which facilitated the assignment of the electronic states observed in REMPI and photoelectron imaging experiments of Prof. Reisler. Moreover, our combined data allowed us to untangle vibronic interactions between the states, e.g., $3p_x$ and $3p_y$ Rydberg states are coupled by the CNN in-plane bending mode.

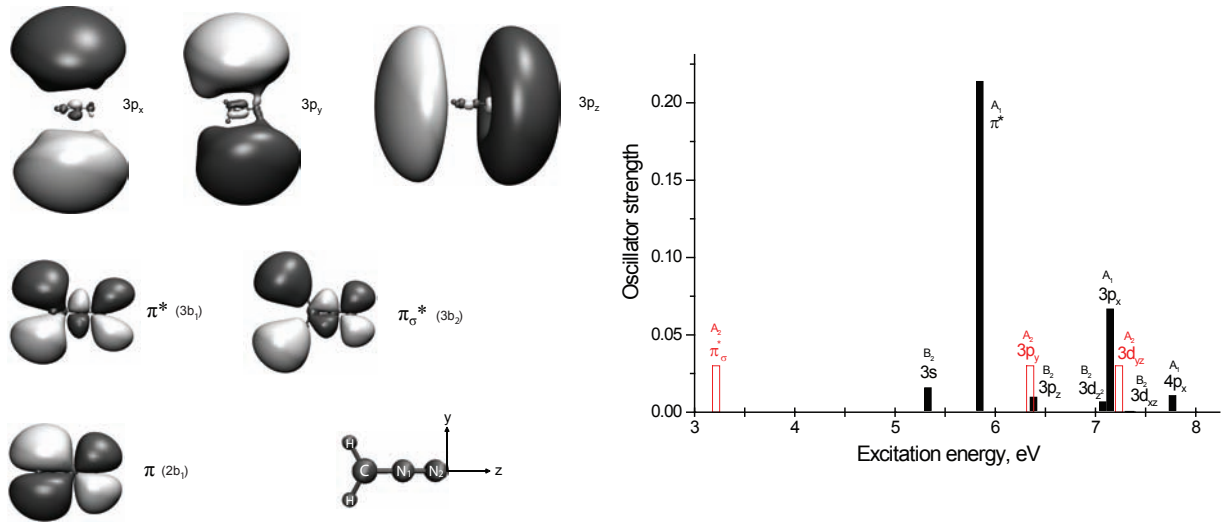

Figure 1: Relevant Hartree-Fock molecular orbitals and vertical stick spectrum. Low-lying excited states of diazomethane are derived from excitations from the π orbital (HOMO).

An interesting story emerged from investigating Rydberg-valence interactions and perturbation of the Rydberg states by the molecular core. We found that the out-of-plane Rydberg p state is strongly perturbed by a $\pi \rightarrow \pi^*$ state located almost 1 eV below. The valence state lends its intensity to the Rydberg state, and distorts the geometry of the core (relative to the equilibrium structure of the cation). This yields a broad progression in the REMPI spectra. The two other Rydberg p states are retain their Rydberg character, and their equilibrium structures are very similar to those of the cation. The vibrational frequencies of the three Rydberg states also reflect this difference.

One counter-intuitive finding is that the frequency of out-of-plane CH_2 vibration *increases* upon $3p \leftarrow \pi$ excitation (or ionization). By performing the Natural Bond Orbital analysis of correlated wave functions, we explained this result in terms of the competition of two

resonance structures of diazomethane in the ground electronic state. The paper on excited electronic states and their interactions is already accepted for publication[5], and the second manuscript, which focuses on the vibronic spectra, is underway.

2.2 Characterization of the ground electronic state of the 1,2,3-tridehydrobenzene triradical

While the electronic structures of the phenyl radical and the three benzyne isomers, which are formally derived from benzene by removal of two hydrogen atoms, have been the subject of many investigations, tridehydrobenzenes, the next step in the systematic decomposition of benzene, are characterized less extensively. By conducting a series of high-level calculations[2] we were able to identify the character of the electronic ground state of 1,2,3-tridehydrobenzene. The two lowest electronic states of the triradical, $^2B_2$ and $^2A_1$, are characterized by different interactions of the unpaired electrons. Vertically, the two states are well separated in energy — by 4.9 and 1.4 eV, respectively. However, due to different bonding patterns, their equilibrium structures are very different and adiabatically the two states are nearly degenerate. The adiabatic energy gap between the states is estimated to be 0.7-2.1 kcal/mol, in favor of the $^2A_1$ state. Comparison with the three experimentally observed IR transitions supports the assignment of the $^2A_1$ ground state for the triradical with a weakly bonding distance of $1.67 - 1.69$ Å between the meta radical centers. The extremely small energy gap between the states suggests that the character of the ground state can be easily manipulated by introduction of appropriate substituents. In view of the different bonding patterns, the two electronic states of are expected to differ considerably in their properties and reactivity

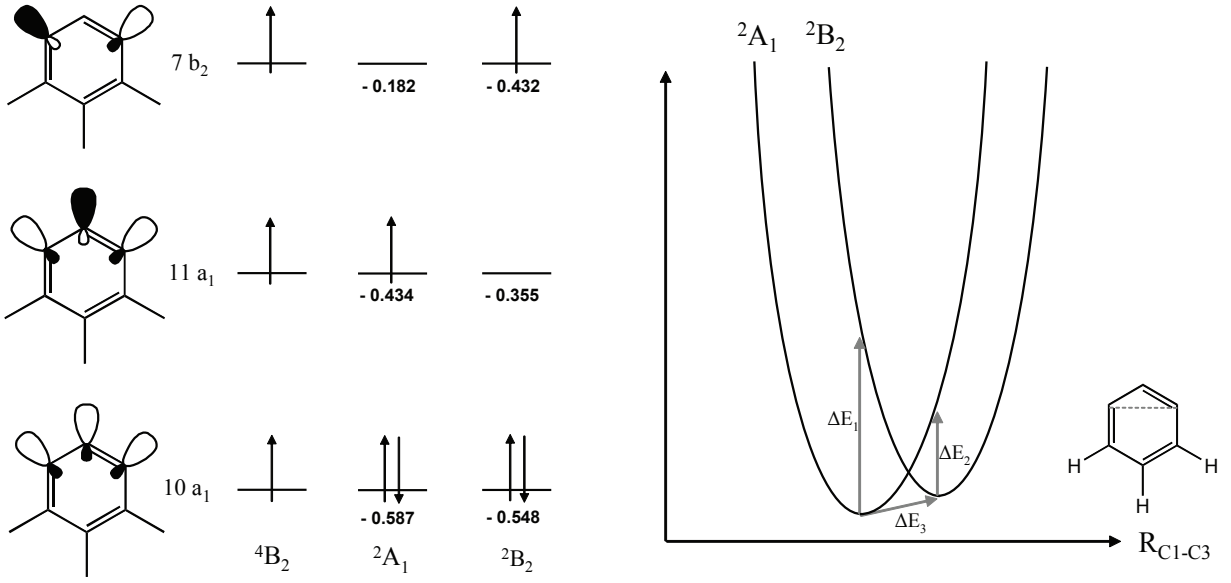

Figure 2: Leading electronic configurations of the quartert and the two doublet states of 1,2,3 tridehydrobenzene and energy diagram. The two states, which are well separated in energy vertically, become nearly degenerate adiabatically, and very high level of theory was required to elucidate their relative ordering.

3 Current developments and future plans

In collaboration with Prof. Joel Bowman, we are characterizing singlet-triplet crossings in formaldehyde by using our implementation of intersection minimization algorithm within the EOM family of methods. Once the intersections are located, we plan to evaluate spin-orbit couplings, in order to estimate the rate of spin-forbidden transitions. We are also developing PESs for H_2CO and its important isomer, HCOH, and the respective ionized species, in order to facilitate modeling of isomerization dynamics and photoelectron spectra. Methodological developments include the implementation of non-adiabatic couplings for EOM wave functions.

References

[1] L. Koziol, S.V. Levchenko, and A.I. Krylov, Beyond vinyl: Electronic structure of unsaturated propen-1-yl, propen-2-yl, 1-buten-2-yl, and trans-2-buten-2-yl hydrocarbon radicals, J. Phys. Chem. A **110**, 2746 (2006).

[2] L. Koziol, M. Winkler, K.N. Houk, S. Venkataramani, W. Sander, and A.I. Krylov, The 1,2,3-tridehydrobenzene triradical: ^{2}B or not ^{2}B? The answer is ^{2}A!, J. Phys. Chem. A (2007), in press.

[3] V.A. Mozhayskiy, D. Babikov, and A.I. Krylov, Conical and glancing Jahn-Teller intersections in the cyclic trinitrogen cation, J. Chem. Phys. **124**, 224309 (2006).

[4] D. Babikov, V.A. Mozhayskiy, and A.I. Krylov, Photoelectron spectrum of elusive cyclic-N_3 and characterization of potential energy surface and vibrational states of the ion, J. Chem. Phys. **125**, 084306 (2006).

[5] I. Fedorov, L. Koziol, G. Li, J.A. Parr, A.I. Krylov, and H. Reisler, Theoretical and experimental investigations of electronic Rydberg states of diazomethane: Assignments and state interactions, J. Phys. Chem. A (2007), in press.

FOURIER TRANSFORM EMISSION AND SYNCHROTRON STUDIES OF PHOTOFRAGMENTATION, RADICAL REACTIONS AND AEROSOL CHEMISTRY

Stephen R. Leone, Christopher Howle, Fabien Goulay, Leonid Belau,
Jared Smith, Kevin Wilson, and Musahid Ahmed
Departments of Chemistry and Physics and Lawrence Berkeley National Laboratory
University of California
Berkeley, California 94720
(510) 643-5467 srl@berkeley.edu

Scope of the Project

Combustion is a complex process involving short-lived radical species, highly excited states, kinetics, transport processes, heterogeneous chemistry on aerosols such as soot, fluid dynamics, and energy transfer. Detailed measurements of microscopic reaction pathways, rate coefficients, vibrational and rotational product state distributions, and thermochemistry result in considerable information to aid in the understanding of combustion processes. Infrared and visible emissions, as well as vacuum ultraviolet (VUV) light, are used here to probe combustion processes and intermediates. Chemiluminescence or emission and a Fourier transform spectrometer are used to explore laser-initiated radical reactions and/or VUV-initiated photofragmentation processes. Vibrationally and low-lying visible electronically excited species generated in chemical processes are investigated, specifically for C_2H reactions and CH_3CN dissociation. VUV light from the Chemical Dynamics Beamline of the Advanced Light Source (ALS) provides a powerful tool to selectively detect reaction products of carbon-based species (e.g. C_2H, CH) with unsaturated hydrocarbons and to measure the energetics and photoionization spectroscopy of important combustion species. For example, the photoionization of carbon cluster species (work performed by Mike Duncan) is studied using a laser ablation apparatus to produce C_1 through C_{15}. Furthermore, products from key combustion reactions are detected and branching ratios estimated in collaboration with Craig Taatjes and David Osborn (Combustion Research Facility, Sandia). A new theme is being initiated to study aerosol formation, light scattering, and heterogeneous chemistry. This endeavor will explore aerosol species, their roles and production in combustion, and the resulting soot species.

Photodissociation Processes - CH_3CN

Nitrile species, such as CH_3CN (acetonitrile), are involved in chemical mechanisms of relevance to combustion processes as reaction byproducts and flame additives. Indeed, CH_3CN has recently been detected as a constituent of vehicle exhaust fumes. To investigate the photodissociation dynamics and pathways of CH_3CN, Fourier transform visible (FTVIS) emission spectroscopy, in conjunction with VUV photons produced at the ALS, is employed. Rotationally-resolved emission is observed from both the $CN(B^2\Sigma^+ - X^2\Sigma^+)$ and $CH(A^2\Delta - X^2\Pi)$ transitions; only the former is observed in spectra recorded at 10.2 and 11.5 eV photon energies, whereas both are observed in the 16 eV dissociation. Surprisal analyses indicate clear bimodal rotational distributions for $CN(B^2\Sigma^+)$, suggesting this excited fragment is formed via both linear and bent transition states, depending on the extent of rotational excitation. From thermodynamic calculations, it is evident that $CH(A^2\Delta)$ is produced along with ground state $CN(X^2\Sigma^+)$ + H_2. These products can be formed by a two step mechanism (via excited CH_3* and $CN(X^2\Sigma^+)$) or a process similar to the "roaming" atom mechanism; the data obtained here are insufficient to definitively conclude whether either pathway occurs. A comparison of the $CH(A^2\Delta)$ and $CN(B^2\Sigma^+)$ rovibrational distributions from the 16 eV dissociation, obtained from spectral simulations, allows the branching ratio between the two fragments at this energy to be determined. The derived $CH(A^2\Delta)$:$CN(B^2\Sigma^+)$ ratio is (1.2 ± 0.1):1.

Photoionization Measurements – carbon clusters C_n and carbon rich radicals C_3H

At the ALS, a laser vaporization source has been developed to produce carbon cluster species for photoionization spectral studies. Such investigations provide basic thermodynamic and structural information for these ubiquitous species. The cluster source is used to produce C_n species (n = 1–15) by

vaporization of a graphite rod, and the ionization potentials are measured. The experimental values for clusters from n = 4–10 are compared to calculated data. The comparison of computed and measured ionization potentials makes it possible to investigate the isomeric structures of the neutral clusters produced in this experiment. The measurements are inconclusive for the n = 4–6 species because of unquenched excited electronic states. However, the data provide evidence for the prominence of linear structures for the n = 7, 9, 11, etc. species and the presence of cyclic C_{10}. This work is performed in collaboration with Henry Schaefer and Michael Duncan (both from the University of Georgia). A detailed study was also performed on C_4 in collaboration with theoretical work of Majdi Hochlaf.

Both the cyclic and linear isomers of C_3H are implicated in a number of chemical processes leading to the formation of large carbon molecules and soot particles in combustion flames. We combine experimental and theoretical studies on the adiabatic ionization energies to study these carbon rich radicals. By reaction of atomic C with acetylene, a supersonic beam containing C_3H radicals is obtained. Subjecting the neutral molecules of this beam to VUV photoionization, the mass spectra of the ionized molecules are recorded at various photon energies. This study suggests the formation of both the cyclic and the linear C_3H radicals in the supersonic beam. By recording photoionization efficiency curves and simulating the experimental spectrum with computed Frank-Condon factors, we reproduce the general pattern of the photoionization efficiency curve of C_3H isomers. This work was performed in collaboration with Ralph Kaiser (University of Hawai'i) and Joel Bowman (Emory University).

C_2H and CH Radical-Molecule Reaction Mechanism Studies

In combustion processes, the formation of polycyclic aromatic hydrocarbons (PAHs) is initiated by reaction of carbon radicals with unsaturated hydrocarbons, such as ethynyl radical with benzene or phenyl radical with ethylene. In order to accurately model the flame chemistry it is important to understand the reaction kinetics of these key reactions by directly measuring the rate coefficients. Using a chemiluminescence technique, we have measured the rate coefficient for the benzene reaction with the ethynyl radical at room temperature and lower temperature. The rate coefficient is found to be five times larger than the value used in combustion models. The temperature dependence of the rate coefficient provides a new insight into the reaction mechanism.

An important reaction of the ethynyl radical in hydrocarbon flames is $C_2H + O_2$. The room temperature rate constant of the $CH(A^2\Delta) + CO_2$ producing channel of this reaction is $1/500^{th}$ that of the $C_2H + O(^3P) \rightarrow CH(A^2\Delta) + CO$ reaction, making its detection using FTVIS spectroscopy considerably more challenging under the low pressure experimental conditions required to obtain a nascent product distribution. This reaction was studied in our lab by observing the rotationally-resolved electronic emission spectrum of the $CH(A^2\Delta)$ product at ~430 nm. C_2H is produced by 193 nm photolysis of acetylene. Extraction of the rotational and vibrational populations reveals rotationally and vibrationally excited $CH(A^2\Delta)$ products, with a rotational temperature of ~1150 K and a vibrational temperature of ~1600 K. The mechanism of this reaction is complex, involving multiple intermediates and an electronic surface crossing. The results suggest that the final step of this reaction involves dissociation from a bent intermediate state to form the $CH(A^2\Delta)$ and CO_2 products.

Although polyacetylenes are identified in carbon rich flames, the reactions leading to their formation are still unknown. In a recent work, we used the kinetics apparatus developed at the ALS to measure the product branching ratio for the reaction of the ethynyl radical with propyne and allene at room temperature. The tunability of the synchrotron radiation allows selective ionization of the reaction products, with subsequent detection by mass spectrometry. Each product can be identified by its mass and ionization energy. Polyacetylenes and other C_5 species produced by these two reactions are identified in the experiments. By using estimated photoionization cross sections for the different species, we determine the reaction product branching ratios. These results are in agreement with previous theoretical calculations and unravel an addition-elimination mechanism for both reactions. An ongoing project aims to probe the products of CH radical reactions with unsaturated hydrocarbons. Allene has been detected as the main product of the CH reaction with acetylene, propyne being produced in a lower amount. Very recently propargylene has been identified as the main product of the CH radical reaction with acetylene.

Aerosol Chemistry – dynamics of aerosol droplet reactions and OH and O_3 initiated aerosol chemistry

New experiments are being developed to investigate the oxidation of biodiesel nanodroplet surfaces using FTIR spectroscopy. Nanoparticles of combustion-related organic molecules are formed using a nebulizer and size selected using a scanning mobility particle sizer (SMPS). Oxidation reaction dynamics will be studied by detecting infrared emission resulting from excited products. As a preliminary investigation, we are studying the interaction of $O(^3P)$ with alkyl iodide molecules by monitoring emission of the O-H stretch in the HOI product. Further investigations will look at the excited products formed by reaction on droplets of a suitable biodiesel proxy, such as long chain methyl ethers, with a variety of radical species.

Ambient aerosols are known to play a significant role in a variety of atmospheric processes such as direct and indirect effects on radiative forcing. Chemical composition can be an important factor in determining the magnitude of these effects (optical density, hygroscopicity, etc.). However, a major fraction (80 – 90%) of organic aerosols cannot be resolved on a molecular level. Recent identification of high mass oligomeric species as a major component in laboratory and ambient organic aerosols has received much attention due to the possibility that these species may account for much of the unknown organic mass in ambient aerosols. Although, a few mechanisms have been proposed, the origin and formation processes of these compounds remain largely unknown. Using VUV photoionization aerosol mass spectrometry we provide strong evidence for a previously unidentified mechanism of rapid condensed phase oligomer formation, via OH radical initiated oxidation of organic aerosols. This process appears capable of converting a sizable fraction of an organic particle to higher mass oligomers within only a few hours of exposure to OH radicals at typical atmospheric concentrations. Rapid volatilization, followed by oligomerization, is also important for specific reaction systems (i.e. n-alkane particles), and can lead to the loss of a large fraction (> 60%) of a particle within 15 minutes of exposure to atmospheric OH. Such rapid processing (oligomerization and volatilization) is possible due to radical chain reactions that propagate throughout the particle when initiated by the surface OH reaction.

The OH radicals also lead to efficient generation of secondary organic aerosols (SOA). Currently, there is much interest in the formation rates and mechanisms of SOA from ozone reactions with both biogenic and anthropogenic precursors. However, with the exception of isoprene, little work has been done to understand SOA formation from OH radical reactions with other volatile organic compounds. Using a coated flow tube reactor, rapid SOA formation is observed when an organic film (such as stearic acid) is exposed to OH radicals. In addition to films, we have also observed that OH oxidation of submicron organic particles also leads to similar SOA formation. These results suggest an entirely new, and very efficient, formation mechanism of SOA via OH radical oxidation of organic surfaces. Analysis of these SOA particles, via VUV photoionization mass spectrometry, suggests that they are chemically complex and perhaps oligomeric in nature.

In other experiments, we have investigated the chemistry of particle surfaces coated by PAHs. The reaction between gas phase ozone and solid anthracene deposited at the surface of sodium chloride particles is studied by measuring both the particle size and chemical composition using a SMPS and a VUV aerosol mass spectrometer. Experiments varying ozone concentration and anthracene coating thickness have been recorded to better understand the surface chemistry of semi-volatile PAHs.

Future Plans

New studies will explore radical-molecule and radical-radical reactions using both the Fourier transform spectrometer and VUV-ionization. Reactions such as NCO + hydrocarbon species, C_2H + NO, CH_3 + N and NCO + O will be studied using FTIR spectroscopy by looking at the excited products. Using the kinetics machine developed in conjunction with Sandia National Laboratory, we will investigate the coupled carbon-nitrogen chemistry by studying the products of CN radical reactions with unsaturated hydrocarbons, especially aromatic molecules. Important experiments will be performed concerning the reaction of radicals on biodiesel-related nanodroplets using the time-resolved FTIR method to examine

heterogeneous processes. Major studies will exploit the aerosol generation and detection instrumentation described above.

Recent Publications Citing DOE Support (2006-2007)

C. R. Howle, A. N. Arrowsmith, V. Chikan and S. R. Leone "State-resolved dynamics of the CN($B^2\Sigma^+$) and CH($A^2\Delta$) excited products resulting from the VUV photodissociation of CH_3CN," *J. Phys. Chem. A*, (in press).

R. I. Kaiser, L.Belau, S. R. Leone, M. Ahmed, Y. Wang, B. J. Braams, and J. M. Bowman, "A combined experimental and computational study on the ionization energies of the cyclic and linear C_3H Isomers," *ChemPhysChem* (in press).

F. Goulay, D. L. Osborn, C. A. Taatjes, P. Zou, G. Meloni, and S. R. Leone, "Direct detection of polyynes formation from the reaction of ethynyl radical (C_2H) with propyne (CH_3-CCH) and allene (CH_2=C=CH_2)," *Phys. Chem. Chem. Phys.* (DOI: 10.1039/b614502g) (in press).

L. Belau, K. R. Wilson, S. R. Leone, and M. Ahmed, "Vacuum-Ultraviolet photoionization studies of the micro-hydration of DNA bases (Guanine, Cytosine, Adenine and Thymine)," *J. Phys. Chem. A*. (In press).

C. Nicolas, J. Shu, D. S. Peterka, M. Hochlaf, L. Poisson, S. R. Leone, and M. Ahmed, "Vacuum ultraviolet photoionization of C_3," *J. Am. Chem. Soc.* **128**, 220 (2006).

F. Goulay and S. R. Leone "Low temperature rate coefficients for the reaction of ethynyl radical (C_2H) with benzene," *J. Phys. Chem. A*, **110**, 1875 (2006).

A. N. Arrowsmith, V. Chikan, and S. R. Leone, "Dynamics of the CH($A^2\Delta$) product from the reaction of C_2H with O_2 studied by Fourier transform visible spectroscopy," *J. Phys. Chem. A*, **110**, 7521 (2006).

E. Gloaguen, E. R. Mysak, S. R. Leone, M. Ahmed, and K. R. Wilson "Investigating the chemical composition of mixed organic-inorganic particles by "soft" VUV photoionization: the reaction of ozone with anthracene on sodium chloride particles," *Int. J. Mass Spectrom.* **258**, 74 (2006).

G. Meloni, P. Zou. S.J. Klippenstein, M. Ahmed, S. R. Leone, C. A. Taatjes, and D. L. Osborn, "Energy-resolved photoionization of alkyl peroxy radicals and the stability of their cations, " *J. Am. Chem. Soc.* **128,** 13559 (2006).

J. Shu, K. R. Wilson, M. Ahmed, and S. R. Leone, "Coupling a versatile aerosol apparatus to a synchrotron: vacuum ultraviolet light scattering, photoelectron imaging, and fragment free mass spectrometry," *Rev. Sci. Instrum.* **77**, 043106 (2006).

J. Shu, K. R. Wilson, M. Ahmed, S. R. Leone, C. E. Graf, and E. Ruhl, "Elastic light scattering from nanoparticles by monochromatic vacuum-ultraviolet radiation," *J. Chem. Phys*. **124**, 034707 (2006).

J. Plenge, C. Nicolas, A. G. Caster, M. Ahmed, and S. R. Leone, "Two-Color Visible/Vacuum Ultraviolet Photoelectron Imaging Dynamics of Br_2," *J. Chem. Phys.* **125**, 133315 (2006).

K. R. Wilson, M. Jimenez-Cruz, C. Nicolas, L. Belau, S. R. Leone, and M. Ahmed, "Thermal Vaporization of Biological Nanoparticles: Fragment-Free VUV Photoionization Mass Spectra of Tryptophan, Phenylalanine-Glycine-Glycine and β-carotene**,"** *J. Phys. Chem. A* **110**, 2106 (2006).

K. R. Wilson, D. S. Peterka, M. Jimenez-Cruz, S.R. Leone, and M. Ahmed. "VUV Photoelectron Imaging of Biological Nanoparticles – Ionization energy determination of nano-phase glycine and phenylalanine-glycine-glycine". *Phys. Chem. Chem. Phys.* **8**, 1884 (2006).

K. R. Wilson, L. Belau, C. Nicolas, M. Jimenez-Cruz, S. R. Leone, and M. Ahmed, "Direct determination of the ionization energy of histidine with VUV synchrotron radiation" *Int. J. Mass Spectrom*. **249-250**, 155, (2006).

R. B. Metz, C. Nicolas, M. Ahmed, and S. R. Leone, "Direct determination of the ionization energies of FeO and CuO with VUV radiation," *J. Chem. Phys*. **123,** 114313 (2005).

J. Shu, K. R. Wilson, A. N. Arrowsmith, M. Ahmed, and S. R. Leone, "Light scattering of ultrafine silica particles by VUV synchrotron radiation*," Nano Lett.* **6,** 1009 (2005).

V. Chikan and S. R. Leone, "Vibrational distributions of the CO(v) products of the C_2H_2 + O(^{3}P) and HCCO + O(^{3}P) reactions studied by FTIR emission," *J. Phys. Chem. A* **109**, 2525 (2005).

V. Chikan, S. R. Leone, "Vibrational and rotational distributions of the CH($A^2\Delta$) product of the C_2H + O(^{3}P) reaction studied by Fourier transform visible (FTVIS) emission spectroscopy," *J. Phys. Chem. A* **109**, 10646 (2005).

V. Chikan, B. Nizamov, and S. R. Leone, "State-resolved dynamics of the CH($A^2\Delta$) channels from single and multiple photon dissociation of bromoform in the 10–20 eV energy range," *J. Phys. Chem. A* **110**, 2850 (2006).

INTERMOLECULAR INTERACTIONS OF HYDROXYL RADICALS ON REACTIVE POTENTIAL ENERGY SURFACES

Marsha I. Lester
Department of Chemistry
University of Pennsylvania
Philadelphia, PA 19104-6323
milester@sas.upenn.edu

PROGRAM SCOPE

The primary objective of the DOE-sponsored research in this laboratory is to characterize the interactions of hydroxyl radicals with reactive partners of combustion relevance (e.g. H_2/D_2, CH_4, CO, and C_2H_2). In the current grant period, we are examining the origin of quenching of electronically excited OH $A\ ^2\Sigma^+$ radicals by molecular partners, e.g. water, a process known to be efficient in gaseous and condensed phase environments. As a first step toward understanding such processes, we have extended our investigation of collisional quenching of OH $A\ ^2\Sigma^+$ by molecular hydrogen,[1-3] which has emerged as a benchmark system for investigation of the nonadiabatic processes that lead to quenching. In addition, we are focusing our efforts on the solvation of hydroxyl radicals as a prototype for interactions of radicals in aqueous environments. In particular, we are examining the binary interaction of an open-shell OH $X\ ^2\Pi$ radical with a water molecule as well as the characteristics of an OH radical embedded in small water clusters. Our goal is to understand the solvation structures, energetics, dynamics, and reactions of OH radicals in aqueous systems.

RECENT PROGRESS

The hydroxyl radical plays a major role in combustion and atmospheric environments, where it is often detected by laser-induced fluorescence (LIF) using the $A\ ^2\Sigma^+ - X\ ^2\Pi$ band system.[4] Collision partners (M) that efficiently quench electronically excited OH $A\ ^2\Sigma^+$ radicals are ubiquitous in these environments. Thus, great effort has been made to quantify the rates and/or cross sections for collisional quenching, so that its effects on LIF signals may be taken into account, thereby allowing for an accurate determination of OH concentrations.[5-8] Studies have shown that quenching cross sections for OH generally increase with decreasing temperature and decrease with initial rotational excitation.[4,7-10] The negative temperature dependence suggests that long-range attractive forces govern the quenching dynamics. The rotational dependence has been attributed to the anisotropy of the OH $A\ ^2\Sigma^+$ + M potential energy surfaces, suggesting that certain orientations of the collision partners preferentially lead to quenching. Rotational excitation of OH $A\ ^2\Sigma^+$ will increasingly average over orientations of the collision partners, thereby decreasing the influence of the specific configurations that preferentially lead to quenching.[5] Despite the experimental determination of the magnitude of overall quenching rates, the mechanism by which OH $A\ ^2\Sigma^+$ is quenched by H_2 or other molecular partners has remained elusive, and only recently have experimental studies begun to examine the outcome of OH $A\ ^2\Sigma^+$ electronic quenching events. The experimental work carried out under DOE funding in this laboratory is aimed at understanding the fundamental chemical dynamics governing quenching

of OH $A\ ^2\Sigma^+$ by H_2 and other partners, with the ultimate goal of developing a model that may be used to predict the rate and outcome of quenching events.

Quenching of OH $A\ ^2\Sigma^+$ by H_2 or D_2 has been the subject of several theoretical and experimental studies, and has emerged as a benchmark system for examining the nonadiabatic processes that lead to quenching.[1-3,6,11-14] Quenching collisions with molecular hydrogen can lead to OH radicals in their ground $X\ ^2\Pi$ electronic state

$$\text{OH } A\ ^2\Sigma^+ + H_2 \rightarrow \text{OH } X\ ^2\Pi + H_2, \qquad \Delta E = -4.02 \text{ eV} \qquad \text{(R1)}$$

or reaction[15]

$$\text{OH } A\ ^2\Sigma^+ + H_2 \rightarrow H_2O + H, \qquad \Delta E = -4.66 \text{ eV} \qquad \text{(R2)}$$

The generation of OH $X\ ^2\Pi$ products (R1) is denoted as nonreactive quenching and the production of H_2O and H products (R2) is referred to as reactive quenching.

Kinetic studies have shown that OH $A\ ^2\Sigma^+$ ($v'=0$) is efficiently quenched by H_2/D_2, with a cross section of ~10 Å^2 at room temperature.[7-9] *Ab initio* calculations of the interaction energy between H_2 and OH in its ground $X\ ^2\Pi$ and excited $A\ ^2\Sigma^+$ electronic states have identified specific orientations that lead to *conical intersection*(s) between the ground and excited state surfaces.[6,12,13] A symmetry-allowed C_{2v} conical intersection is predicted between the ground and excited state surfaces ~1.4 eV below the OH $A\ ^2\Sigma^+ + H_2$ asymptote. For this *T*-shaped HO–H_2 geometry, the electronic quenching process is calculated to be barrierless.[6] Furthermore, strong nonadiabatic coupling has been predicted to occur in C_{2v}, $C_{\infty v}$ and C_s configurations, leading to both reactive and nonreactive quenching channels.[12,13]

The reactive quenching of OH $A\ ^2\Sigma^+ + H_2/D_2$ was the first channel to be investigated experimentally.[1,2,14] Doppler profiles of H/D atoms produced from reactive quenching, measured previously by this group,[1,2] exhibited a bimodal velocity distribution, which was attributed to direct abstraction and indirect (statistical) dynamical pathways through the conical intersection region(s). In both cases, a significant fraction of the OH $A\ ^2\Sigma^+$ electronic energy was channeled into internal excitation of the water products. In addition, H-atom products were observed from reactive quenching of OH $A\ ^2\Sigma^+$ by D_2 with a broad velocity distribution, suggesting that an insertion-like mechanism produces D_2O. More recently, Ortiz-Suarez *et al*. have reexamined the reactive quenching of OH $A\ ^2\Sigma^+$ by D_2 using crossed molecular beams to characterize in more detail the broad translational energy release and determine the angular distribution of the D-atom products.[14]

Very recently, we began to probe the outcome of OH $A\ ^2\Sigma^+$ ($v'=0$, $N'=0$) + H_2 quenching events that lead to OH $X\ ^2\Pi + H_2$ products (nonreactive quenching). Initially, we measured the OH $X\ ^2\Pi$ product state distribution in $v''=1$ (and in the lowest rotational levels of $v''=2$).[3] We found that the OH products were generated with significant rotational excitation. We attribute this signature to the forces at play as the OH–H_2 system passes through the conical intersection region(s) that couple the ground and excited state potential energy surfaces. The time delay between the quenching event and probe laser detection of the OH $X\ ^2\Pi$ products, however, allowed for the possibility of relaxation of the nascent OH $X\ ^2\Pi$ product state distribution by secondary collisions.

Over the past year, the OH $X\ ^2\Pi$ products from nonreactive quenching of OH $A\ ^2\Sigma^+$ by H_2 have been reexamined under *single-collision conditions*. This study encompasses a broader range of quantum states than had been reported previously,[3] including OH $X\ ^2\Pi$ (v″=1, 2), and fine-structure (spin-orbit and Λ-doublet) propensities.[16] The OH products are produced with an exceedingly high degree of rotational excitation, with the populations in each vibrational level peaking around N''=15. There is also a clear Λ-doublet propensity, as the OH products of quenching are preferentially produced in the Π(A') Λ-doublet, with the pπ orbital containing the unpaired electron lying in the plane of rotation of the OH radical. By contrast, the F_1 and F_2 spin-orbit manifolds are equally (statistically) populated. In addition, very recent studies of OH $X\ ^2\Pi$ (v″=0, N'') products – extremely challenging because of the similar pump, probe, and detection wavelengths – have shown that the OH radicals are generated with minimal vibrational excitation, with most of the population in $X\ ^2\Pi$ (v″=0) and sequentially less in v″=1 and v″=2, as shown in Fig. 1. The latter results are currently being written up for publication.[17]

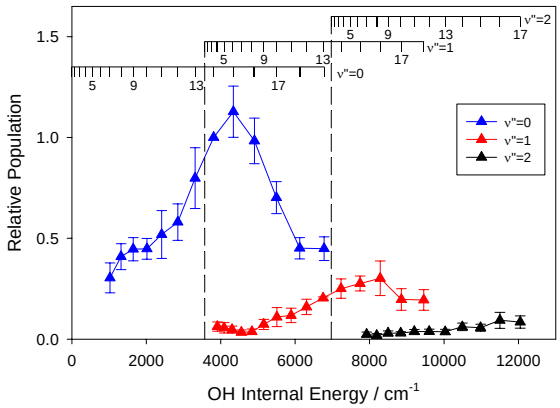

Fig. 1 Nascent OH $X\ ^2\Pi$ (v″, N″) state distribution following collisional quenching of OH $A\ ^2\Sigma^+$ by H_2. Only the Π(A') Λ-doublet component is shown.

To better understand these results, the measurements have been complemented by an extensive theoretical study of the OH-H_2 interaction potential in the conical intersection region by Kłos and Alexander.[16] Calculations exploring the potential energy surface (PES) show a steep angular gradient into and away from the conical intersection whenever the O-end of the OH radical, $|\theta_{OH}| \leq 90°$, approaches the H_2 molecule (see Fig. 2). This causes a substantial torque to be placed on the OH radical as it passes through the conical intersection, resulting in the pronounced rotational excitation observed experimentally. The recent calculations did not examine the OH vibrational dependence. The earlier theoretical work of Hoffman and Yarkony[13] indicated little change in OH bond length as the system evolves through the conical intersection region, suggesting minimal vibrational excitation of OH products as now observed experimentally. The experimental observations of highly rotationally excited products OH $X\ ^2\Pi$ products in low vibrational levels are a dynamical signature of the forces impacting the OH–H_2 system as it evolves through the conical intersection region(s).

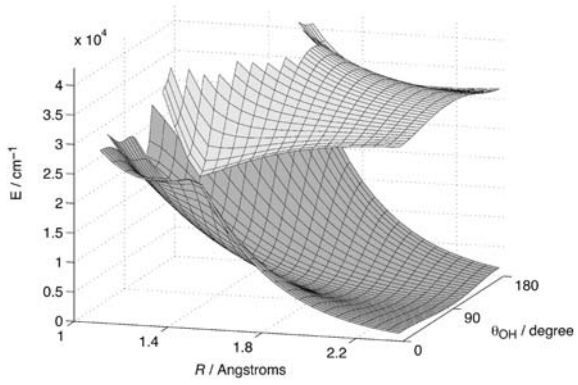

Fig. 2 1A' and 2A' coplanar potential energy surfaces correlating with OH $X\ ^2\Pi + H_2$ and OH $A\ ^2\Sigma^+ + H_2$, respectively, displayed as a function of the distance R between the centers-of-mass of the OH and H_2 moieties and the OH angle θ_{OH}. Only the region from $0° \leq \theta_{OH} \leq 180°$ is shown to provide a clear depiction of the conical intersection region.

FUTURE PLANS

Experiments are underway to examine the nonreactive quenching of OH $A\ ^2\Sigma^+$ by D_2 and compare its outcome with that from H_2. Initial results indicate that the OH $X\ ^2\Pi$ products are even more highly rotationally excited with D_2 than H_2, but that far less of the outcome (3-fold) is due to nonreactive quenching. We are currently determining the change in the branching ratio between nonreactive (R1) and reactive (R2) quenching upon deuteration as well as the fraction of molecules that decay by each route. Experiments on OH-water interactions are gearing up and should be online very soon. These experiments will build on our predictions for the rotational band structure of infrared transitions of the OH-water complex, which are expected to be quite complicated and very different from analogous closed-shell systems.[18]

REFERENCES

1 D. T. Anderson, M. W. Todd, and M. I. Lester, J. Chem. Phys. **110**, 11117 (1999).
2 M. W. Todd, D. T. Anderson, and M. I. Lester, J. Phys. Chem. A **105**, 10031 (2001).
3 I. B. Pollack, Y. X. Lei, T. A. Stephenson, and M. I. Lester, Chem. Phys. Lett. **421**, 324 (2006).
4 D. R. Crosley, Laser fluorescence detection of atmospheric hydroxyl radicals, in *Progress and Problems in Atmospheric Chemistry*, edited by J. R. Barker (World Scientific Publishing Company, Singapore, 1995), Vol. 3, pp. 256.
5 D. R. Crosley, J. Phys. Chem. **93**, 6273 (1989).
6 M. I. Lester, R. A. Loomis, R. L. Schwartz, and S. P. Walch, J. Phys. Chem. A **101**, 9195 (1997).
7 B. L. Hemming, D. R. Crosley, J. E. Harrington, and V. Sick, J. Chem. Phys. **115**, 3099 (2001).
8 B. L. Hemming and D. R. Crosley, J. Phys. Chem. A **106**, 8992 (2002).
9 D. E. Heard and D. A. Henderson, Phys. Chem. Chem. Phys. **2**, 67 (2000).
10 D. J. Creasey, D. E. Heard, M. J. Pilling, B. J. Whitaker, M. Berzins, and R. Fairlie, Appl. Phys. B: Lasers Opt. **65**, 375 (1997).
11 D. R. Yarkony, J. Phys. Chem. **100**, 18612 (1996).
12 D. R. Yarkony, J. Chem. Phys. **111**, 6661 (1999).
13 B. C. Hoffman and D. R. Yarkony, J. Chem. Phys. **113**, 10091 (2000).
14 M. Ortiz-Suarez, M. F. Witinski, and H. F. Davis, J. Chem. Phys. **124**, 201106 (2006).
15 M. Alagia, N. Balucani, P. Casavecchia, D. Stranges, G. G. Volpi, D. C. Clary, A. Kliesch, and H. J. Werner, Chem. Phys. **207**, 389 (1996).
16 P. A. Cleary, L. P. Dempsey, C. Murray, M. I. Lester, J. Klos, and M. H. Alexander, J. Chem. Phys., in press (2007).
17 L. P. Dempsey, P. A. Cleary, C. Murray, and M. I. Lester, manuscript in preparation (2007).
18 M. D. Marshall and M. I. Lester, J. Phys. Chem. B **109**, 8400 (2005).

DOE SUPPORTED PUBLICATIONS
2005-2007

1. M. D. Marshall and M. I. Lester, "Spectroscopic Implications of Partially Quenched Orbital Angular Momentum in the OH-Water Complex", *J. Phys. Chem. B* **109**, 8400-8406 (2005).
2. I. B. Pollack, Y. Lei, T. A. Stephenson, and M. I. Lester, "Electronic Quenching of OH $A\ ^2\Sigma^+$ Radicals in Collisions with Molecular Hydrogen", *Chem. Phys. Lett.* **421**, 324-328 (2006).
3. P. A. Cleary, L. P. Dempsey, C. Murray, M. I. Lester, J. Kłos and M. H. Alexander, "Electronic Quenching of OH $A\ ^2\Sigma^+$ Radicals in Single Collision Events with Molecular Hydrogen: Quantum State Distribution of the OH $X\ ^2\Pi$ Products", *J. Chem. Phys.*, in press (2007).

Theoretical Studies of Molecular Systems

William A. Lester, Jr.
Chemical Sciences Division,
Ernest Orlando Lawrence Berkeley National Laboratory and
Kenneth S. Pitzer Center for Theoretical Chemistry
Department of Chemistry, University of California, Berkeley
Berkeley, California 94720-1460
walester@lbl.gov

Program Scope

This research program is directed at extending fundamental knowledge of atoms and molecules. The approach combines the use of ab initio basis set methods and the quantum Monte Carlo (QMC) method to describe the electronic structure and energetics of systems of primarily combustion interest.

Recent Progress

QMC Study of Electrophilic Aminiation (with C. Amador, R. Salomon-Ferrer, W. A Lester Jr., J. A. Vazquez-Martinez, and A. Aspuru-Guzik). QMC calculations have been performed of several amines in order to study their reactivity in the amination reaction. The resulting electronic densities have been analyzed in terms of electron (pair) localization functions previously proposed by other researchers as well as modifications thereof. These functions have been variously projected and integrated in order to obtain quantitative descriptors of the nature of the electron pair. It is possible to make predictions in terms of a new Electron Pair Localization Function Density, but a much clearer picture emerges when these results are combined with those of the Electron Localization Function.

Graphene Layer Growth: Collision of Five-Membered Rings (with R. Whitesides, D. Domin, and M. Frenklach). Research of the past couple of years has led to identification of a new reaction pathway for the five-member ring migration along a graphene edge. The migration sequence is initiated by H-atom addition to an adsorbed cyclopenta group. Earlier simulation results showed that the evolving surface morphology and ensuing growth rate are determined by competition between the migration of five-member rings and other gas-surface and surface processes such as "nucleation" of six-member rings at surface corners and their desorption. The elementary steps of the migration pathway were analyzed by DFT. These calculations were performed on substrates modeled by the zigzag edges of tetracene and pentacene. Rate constants for the process were obtained by the solution of an energy master equation utilizing the DFT energies, frequencies, and geometries. The results indicate that this reaction pathway is competitive with other pathways important to the edge evolution of aromatic species in high temperature environments.

Small Combustion Molecules and Radicals (with D. Domin)

Selected systems from the recently completed diffusion Monte Carlo (DMC) benchmark studies of atomization energies of small hydrocarbons carried out in this laboratory were studied further owing to their importance for combustion mechanisms. The benchmark study was limited to the use of single-determinant trial functions, which are not always adequate for establishment of combustion mechanisms. Key systems for further study included C_2H, C_2H_2, C_4H_3, C_4H_5. The two leading systems in this list are pertinent to experiments at the ALS (Advanced Light Source) and their study continues using trial functions of various types beyond the single-determinant form. These include valence bond functions that are being pursued owing to their compactness. A manuscript describing the latter two systems is in press.

Future Plans

QMC studies of trial function construction will continue. This is an area of critical importance for the development of the DMC method where the emphasis remains on achieving compact descriptions. As mentioned, valence bond functions are being investigated along with molecular-orbital based approaches. Small combustion molecules and radicals remain the test bed for the various approaches.

The collaborative effort with M. Frenklach on the growth of carbonaceous systems will continue. The plan is to explore this and other related reactions using quantum chemical methods (ab initio, DFT, and QMC), and, as previously indicated, determine reaction rates from the solution of master equations.

Efforts will continue in the pursuit of approaches for the accurate calculation of forces in DMC in collaboration with Roland Assaraf, CNRS (Paris). Although methods for the evaluation of forces have been pursued in this and other laboratories for a number of years, there is still no approach that can be routinely applied that yields accuracy of predictive merit.

DoE Supported Publications (2005-2007)

1. A. C. Kollias, D. Domin, G. Hill, M. Frenklach, D. M. Golden, and W. A. Lester, Jr., "Quantum Monte Carlo Study of Heats of Formation and Bond Dissociation Energies of Small Hydrocarbons," Int. J. Chem. Kinetics **37**, 583 (2005).
2. A. Aspuri-Guzik, R. Salomon-Ferrer, and W. A. Lester, Jr., "A Sparse Algorithm for the Evaluation of the Local Energy in Quantum Monte Carlo," J. Comput. Chem. **26**, 708 (2005).
3. A. Aspuru-Guzik and W. A. Lester, Jr., "Quantum Monte Carlo: Theory and Application to Molecular Systems," Adv. Quant. Chem. **49**, 209 (2005).
4. A. C. Kollias, D. Domin, G. Hill, M. Frenklach, and W. A. Lester, Jr., "Quantum Monte Carlo Study of Small Hydrocarbon Atomization Energies," Mol. Phys. **104**, 467 (2006).
5. A. Aspuri-Guzik, R. Salomon-Ferrer, B. Austin, R. Perusquia-Flores, M. A. Griffin, R. A. Oliva, D. Skinner, D. Domin, and W. A. Lester, Jr., "Zori 1.0: A Parallel Quantum Monte Carlo Electronic Structure Package," J. Comp. Chem. **26**, 856 (2005).

6. R. Whitesides, A.C. Kollias, D. Domin, W.A. Lester, Jr., and M. Frenklach, "Graphene Layer Growth: Collision of Migrating 5-Member Rings," Fall Meeting of the Western States Section of the Combustion Institute, Stanford, CA, October 17-18, 2005, paper 05F-62.
7. R. Whitesides, A. Kollias, D. Domin, W. A. Lester, Jr., and M. Frenklach, "Graphene layer growth: Collision of migrating five-membered rings," Symposium on *Nanoparticles in Energy Processes: Friend and Foe: Combustion Synthesis: From Pollutants to Advanced Materials*, 231st National Meeting of the American Chemical Society, Atlanta, GA, March 26-30, 2006.
8. R. Whitesides, A. Kollias, D. Domin, W. A. Lester, Jr., and M. Frenklach, "Graphene Layer Growth: Collision of Migrating Five-Membered Rings", *Prepr. Pap.-Am. Chem. Soc., Div. Fuel Chem.* **51**(1), 2006, pp. 174-175.
9. W. A. Lester, Jr. and R. Salomon-Ferrer, "Some Developments in Quantum Monte Carlo for Electronic Structure: Methods and Application to a Bio System," THEOCHEM 771, 51 (2006).
10. R. Whitesides, A. C. Kollias, D. Domin, W. A. Lester, Jr., and M. Frenklach, "Graphene Layer Growth: Collision of Migrating Five-Member Rings," Proc. Comb. Inst. **31,** 539 (2007).
11. R. Prasad, N. Umezawa, D. Domin, R. Solomon-Ferrer, and W. A. Lester Jr. "Quantum Monte Carlo study of first-row atoms using transcorrelated variational trial functions," accepted by J. Chem. Phys.
12. C. Amador-Bedolla, R. Salomon-Ferrer, W. A Lester Jr., J. A. Vazquez-Martinez, and A. Aspuru-Guzik, "Reagents for electrophilic amination: A quantum Monte Carlo study." accepted by J. Chem. Phys.

Kinetics of Elementary Processes Relevant to Incipient Soot Formation

PI : M. C. Lin
Co-PI : M. C. Heaven
Department of Chemistry
Emory University, Atlanta, GA 30322
chemmcl@emory.edu, heaven@euch4e.chem.emory.edu

I. Program Scope

Soot formation and abatement processes are some of the most important and challenging problems in hydrocarbon combustion. The key reactions involved in the formation of polycyclic aromatic hydrocarbons (PAH's), the precursors to soot, remain elusive. Small aromatic species such as C_5H_5, C_6H_6 and their derivatives are believed to play a pivotal role in incipient soot formation.

The goal of this project is to establish a kinetic database for elementary reactions relevant to soot formation in its incipient stages. In the past year, our major focus has been placed on the experimental studies of the reactions C_6H_5 with $C_6H_5C_2H_x$ (x=1,3), CH_3OH and C_2H_5OH; their mechanisms have been elucidated computationally by quantum-chemical calculations. The photodissociation dynamics of nitrosobenzene and o-nitrotolune have been studied experimentally and computationally, and the OH + CH_3OH/C_2H_5OH and NCN+O reactions have been investigated by *ab initio* molecular orbital calculation. In addition, a new pulsed slit molecular beam system has been constructed for spectroscopic studies of aromatic radicals and their derivatives by the cavity ringdown technique (CRDS).

II. Recent Progress

1. C_6H_5 + $C_6H_5C_2H_x$ (x=1, 3) → products (ref. #1)

Studies on the reactions of C_6H_5 with phenylacetylene ($C_6H_5C_2H$) and styrene ($C_6H_5C_2H_3$) have been completed using CRDS at 3.6 Torr in the temperature range 297 - 410 K. The weighted least squares analysis for each reaction gave rise to the following rate constant expressions in units of cm^3 mol^{-1} s^{-1}:

$$k(C_6H_5 + C_6H_5C_2H) = 10^{13.0 \pm 0.1} \exp [-(1224 \pm 76)/T] \quad \text{(R1)}$$

$$k(C_6H_5 + C_6H_5C_2H_3) = 10^{13.3 \pm 0.1} \exp [-(1294 \pm 91)/T]. \quad \text{(R2)}$$

Additional DFT and MP2 calculations have been carried out to assist our interpretation of the measured kinetic data and predict product distributions of the title reactions at combustion temperatures. Reactions R1 and R2 predominantly produce β-adducts, stabilized by π–conjugation. Such resonantly stabilized radicals (RSRs) have a relatively long lifetime in combustions regimes and may be involved in the mechanism of PAH formation. The calculated 0 K barriers fall in the range from 0.5 to 2.5 kcal/mol for reaction R1, and from -1.4 to 1.3 kcal/mol for reaction R2. The rate constants calculated by conventional TST exhibit substantial deviations from the experimental values, which we attribute in part to the errors in theoretical barriers and in part to the limited accuracy of the harmonic oscillator treatment of several low frequency vibrational modes. Our experimental k_{R2} is in good agreement with the room-T rate constant of Scaiano et al.,[2] measured in a Freon solution.

A comparison of the k_{R1}-k_{R2} rate constants with those for the C_6H_5-addition to ethylene and acetylene shows that C_6H_5-substitution increases the reactivity of unsaturated CC bonds. The following reactivity scale can be suggested based on the trapping efficiency of phenyl radical by selected HC at room-T:

$$C_2H_2 : C_2H_4 : C_6H_5C_2H : C_6H_5C_2H_3 \approx 1 : 1.8 : 240 : 380.$$

2. C_6H_5 + CH_3OH/C_2H_5OH → C_6H_6 + other products (ref. #3)

The kinetics of the C_6H_5 reactions with CH_3OH and C_2H_5OH, which are important alternate fuels, have been measured by pulsed-laser photolysis/mass-spectrometry (PLP/MS) employing acetophenone as the radical source. Kinetic modeling of the benzene formed in the reactions over the temperature range 483 -771 K allows us to reliably determine the total rate constants for H-abstraction reactions. In order to extend our temperature range down to 304 K we have also applied the cavity ring-down spectrometric technique using nitrosobenzene as the radical source. Additionally we also performed PLP/MS experiment using nitrosobenzene as the radial source. Three sets of data agree closely. A weighted least-squares analysis of the

three complementary sets of data for the two reactions gave the total rate constants $k(CH_3OH) = (7.82 \pm 0.44) \times 10^{11}$ exp [-(853 ± 30)/T] and $k(C_2H_5OH) = (5.73 \pm 0.58) \times 10^{11}$ exp [-(1103 ± 44)/T] $cm^3\ mol^{-1}\ s^{-1}$ for the temperature range studied. Theoretically, four possible product channels of the $C_6H_5 + CH_3OH$ reaction producing $C_6H_6 + CH_3O$, $C_6H_6 + CH_2OH$, $C_6H_5OH + CH_3$ and $C_6H_5COCH_3 + H$ and five possible product channels of the $C_6H_5 + C_2H_5OH$ reaction producing $C_6H_6 + C_2H_5O$, $C_6H_6 + CH_2CH_2OH$, $C_6H_6 + CH_3CHOH$, $C_6H_5OH + CH_3CH_2$ and $C_6H_5OCH_3 + H$ have been computed at the G2M//B3LYP/6-311+G(d, p) level of theory.

The hydrogen abstraction channels were predicted to have lower energy barriers and their rate constants were calculated by the microcanonical variational transition state theory. The predicted rate constants are in good agreement with the experimental values and their total rate constants and its branching rate constants can be expressed in units of $cm^3mol^{-1}s^{-1}$ in the temperature range 200 – 3000 K as following: $k(CH_3OH) = 4.82 \times 10^1\ T^{3.29}$ exp(597.1/T), $k\ (C_6H_6 + CH_3O) = 4.88 \times 10^3\ T^{2.55}$ exp(470.2/T), $k\ (C_6H_6 + CH_2OH) = 5.13 \times 10^2\ T^{3.00}$ exp(-483/T), $k(C_2H_5OH) = 1.52 \times 10^3\ T^{2.85}$ exp(-97.8/T), $k\ (C_6H_6 + C_2H_5O) = 4.41 \times 10^4\ T^{2.18}$ exp(-177.7/T), $k\ (C_6H_6 + CH_2CH_2OH) = 3.57 \times 10^4\ T^{2.35}$ exp(-378.1/T), $k\ (C_6H_6 + CH_3CHOH) = 13.8\ T^{3.41}$ exp(-1287.5/T).

3. Photodissociation dynamics of nitrobenzene and o-nitrotoluene (ref. # 4)

Nitrobenzene and nitrotoluene are prototypical molecules employed in studies of the combustion and decomposition of energetic materials. Early studies of nitrobenzene using discharge lamp photolysis and flash lamp photolysis found that photodissociation of nitrobenzene generates several different products, including nitrogen dioxide, nitrosobenzene, cyclopentadiene. Resonance enhanced multiphoton ionization study of nitrobenzene detected NO and a number of C_nH_m (n = l-6, m = 0-5) fragments. In a recent study, Galloway et al. employed vacuum ultraviolet (VUV) photoionization mass spectrometry to detect dissociation products in the photolysis of nitrobenzene at wavelengths between 220 and 280 mn.[5] The observed products can be attributed to the following three major channels:

$$C_6H_5NO_2 + hv \rightarrow C_6H_5 + NO_2 \quad (1)$$

$$C_6H_5NO_2 + hv \rightarrow C_6H_5NO + O \quad (2)$$

$$C_6H_5NO_2 + hv \rightarrow C_6H_5O + NO\ (\text{or } C_5H_5 + CO + NO) \quad (3)$$

The dissociation mechanism was proposed to start from the internal conversion to the ground electronic state, followed by the isomerization to phenyl nitrite C_6H_5ONO, and subsequently breaking the C-ONO bond to release NO_2; or the O-NO bond to produce NO, or the ON-O bond to form O. Dissociation of the nitrotoluene also has been studied. Femtosecond laser multiphoton ionization mass spectroscopic experiment at 375 nm showed that $C_7H_7^+$ and $C_7H_7O^+$, corresponding to NO_2 and NO loss channels, were observed for all three nitrotoluene isomers. Ions of C_7H_7NO, corresponding to the loss of O fragments, were observed from p-nitrotoluene. The theoretical calculations for the geometries and energies of nitrobenzene in the ground electronic state, singlet and triplet excited states have been computed by the CASSCF method. Recently, theoretical studies on the kinetics and mechanisms for the thermal unimolecular decomposition of nitrobenzene and o-nitrotoluene have been carried out respectively by our laboratory.

In collaboration with C. K. Ni, Y. T. Lee et al., the photodissociation of nitrobenzene (NB) at 193, 248, and 266 nm and o-nitrotoluene (o-NT) at 193 and 248 nm was investigated separately using multimass ion imaging techniques. Fragments corresponding to NO and NO_2 elimination from both nitrobenzene and o-nitrotoluene were observed. The translational energy distributions for the NO elimination channel show bimodal distributions, indicating two dissociation mechanisms involved in the dissociation process. The branching ratios between NO and NO_2 elimination channels were determined to be $NO/NO_2 = 0.32 \pm 0.12$ (193 nm), 0.26±0.12 (248 nm), and 0.4±0.12 (266 nm) for nitrobenzene and 0.42±0.12 (193 nm), 0.3±0.12 (248 nm) for o-nitrotoluene, respectively. Additional dissociation channels, O atom elimination from nitrobenzene and OH elimination from o-nitrotoluene, were observed. New dissociation mechanisms were proposed and the results are compared with potential energy surfaces obtained from ab initio calculations.[6] Observed absorption bands of photodissociation are assigned by the assistance of the ab initio calculations for the relative energies of the triplet excited states and the vertical excitation energies of the singlet and triplet excited states of nitrobenzene and o-nitrotoluene. Finally, the dissociation rates and lifetimes of photodissociation of nitrobenzene and o-nitrotoluene were predicted and compared to experimental results.

4. OH + $CH_3OH/C_2H_5OH \rightarrow H_2O$ + other products (ref. # 7)

Kinetics and mechanisms for reactions of OH with methanol and ethanol have been investigated at the CCSD(T)/6-311+G(*3df*, *2p*) // MP2/6-311+G(*3df*, *2p*) level of theory. The two reactions may take place potentially by the following product channels:

$$OH + CH_3OH \rightarrow H_2O + CH_2OH \quad (1a)$$
$$\rightarrow H_2O + CH_3O \quad (1b)$$
$$OH + C_2H_5OH \rightarrow H_2O + CH_3CHOH \quad (2a)$$
$$\rightarrow H_2O + CH_2CH_2OH \quad (2b)$$
$$\rightarrow H_2O + CH_3CH_2O \quad (2c)$$

The total and individual rate constants, and product branching ratios for the reactions have been computed in the temperature range 200-3000 K with variational transition state theory by including the effects of multiple reflections above the wells of their pre-reaction complexes, quantum-mechanical tunneling and hindered internal rotations. The predicted results can be represented by the expressions $k_1 = 4.65\times10^{-20}\times T^{2.68}$ exp (414/*T*) and $k_2 = 9.11\times10^{-20}\ T^{2.58}$ exp (748/*T*) cm^3 $molecule^{-1}$ s^{-1} for the CH_3OH and C_2H_5OH reactions, respectively. The former reaction produces 96-89% of the $H_2O + CH_2OH$ products, whereas the latter process produces 98-70% of $H_2O + CH_3CHOH$ and 2-21% of the $H_2O + CH_2CH_2OH$ products in the temperature range computed (200 – 3000 K). The predicted overall and individual rate constants for the primary channels of the reactions of $OH + CH_3OH$ in whole temperature range and $OH + C_2H_5OH$ in low temperature range are in reasonable agreements with the previous experimental data. But the predicted rate constants for $OH + C_2H_5OH$ in the high temperature range are significantly higher than the existing data. Our predicted total and individual rate constants, and product branching ratios for the two reactions may be employed for high temperature kinetic modeling.

5. NCN + $^3O \rightarrow$ products (ref. #8):

The fast and highly exothermic oxidation reaction, NCN + ^3O, has been investigated. The reaction of NCN with O is relevant to the formation of prompt NO according to the new mechanism, $CH + N_2 \rightarrow$ cyclic-C(H)NN- $\rightarrow$ HNCN $\rightarrow$ H + NCN. The reaction has been investigated by *ab initio* molecular orbital calculation for a detailed potential energy surface and transition state theory calculations for rate constants prediction. The mechanisms for formation of possible product channels involved in the singlet and triplet potential energy surfaces have been predicted at the highest level of the modified GAUSSIAN-2 (G2M) method, G2M (CC1). The barrierless association/dissociation processes on the singlet surface were also examined with the third order Rayleigh-Schrödinger perturbation (CASPT3) and the multireference configuration interaction methods including Davidson's correction for higher excitations (MRCI+Q) at the CASPT3(6,6)/6-311+G(3df)//UB3LYP/6-311G(d) and MRCI+Q(6,6)/6-311+G(3df)//UB3LYP/6-311G(d) levels. The rate constants for the low-energy channels producing $CO + N_2$, CN + NO and $N(^4S)$ + NCO have been calculated in the temperature range of 200 - 3000 K. The results show that the formation of CN + NO is dominant and its branching ratio is over 99% in the whole temperature range; no pressure dependence was noted at pressures below 100 atm. The predicted individual values via the singlet surface can be presented in units of cm^3 $molecule^{-1}$ s^{-1} by: k_1 (CO +N_2) = $4.03 \times 10^{-22}\ T^{2.32}$ exp(571/T) and k_2 (CN + NO) = $8.09 \times 10^{-12}\ T^{0.18}$ exp(23/T), and the values obtained via the triplet surface can be represented as: k_3 (CN + NO) = $3.44 \times 10^{-11}\ T^{0.15}$ exp(15/T) and k_4 [^{4}N + NCO] = $3.67 \times 10^{-15}\ T^{0.42}$ exp(79/T). The total rate constant can be effectively represented by the expression: $k_t = 4.23 \times 10^{-11}\ T^{0.15}$ exp(17/T) in the temperature range of 200 – 3000 K.

III. Future work

We shall devote our effort to kinetic studies of phenylvinyl and naphthyl radical reactions with combustion species by CRDS and PLP/MS techniques. Spectroscopic studies of these and other small aromatic radicals by CRDS in a molecular beam will be initiated. Construction of the apparatus for these experiments has been completed, and evaluation experiments are in progress. The results of the spectroscopic studies are expected to improve the diagnostics of the radicals such as the naphthyls. Once the instrument testing and development work has been completed, the first objective will be studies of the phenyl radical. All experimental studies

will be complemented by quantum chemical calculations to help elucidate the reaction mechanisms and spectroscopic data obtained.

III. References (DOE publications denoted by *)

1. G. Nam, I. V. Tokmakov, J. Park and M. C. Lin, Proceedings of the Combustion Institute 31 (2007) 249-256.*
2. J. C. Scaiano, L. C. Stewart, J. Am. Chem. Soc. 1983, 105, 3609.
3. J. Park, Z. F. Xu, K. Xu and M. C. Lin, J. Phys. Chem. A submitted.*
4. Ming-Fu Lin, Yuan T. Lee, Chi-Kung Ni, Shucheng Xu and M.C. Lin, J. Chem. Phys., 126, 064310 (2007).*
5. D. B. Galloway, J. A. Bartz, L. G. Huey, and F. F. Crim, J. Chem. Phys. **98**, 2107 (1993).
6. S. C. Chen, S. C. Xu, E. Diau, and M. C. Lin, *J. Phys. Chem. A* 2006**,** *110,* 10130-10134.*
7. Shucheng Xu and M.C. Lin, Proceedings of the Combustion Institute 31 (2007) 159-166.*
8. R. S. Zhu and M. C. Lin, J. Phys. Chem. A, in press.*

Other DOE Publications (2004-current) not mentioned above:

1. J. Park, Liming Wang and M. C. Lin, Int. J. Chem. Kinet., 36, 49-56 (2004).
2. I. V. Tokmakov, L. V. Moskaleva, and M. C. Lin, Int. J. Chem. Kinet., 36, 139-51 (2004).
3. Y. M. Choi and M. C. Lin, ChemPhysChem., 5, 225-32 (2004).
4. Z. F. Xu and M. C. Lin, Int. J. Chem. Kinet., 36, 205-15 (2004).
5. Y. M. Choi and M. C. Lin, ChemPhysChem., 5, 661-68 (2004).
6. Z. F. Xu, J. Park and M. C. Lin, J. Chem. Phys., 120, 6593 – 99 (2004).
7. R. S. Zhu, Z. F. Xu and M. C. Lin, J. Chem. Phys., 120, 6566 – 73 (2004).
8. I. V. Tokmakov and M. C. Lin, J. Phys. Chem., A, 108, 9697-714 (2004).
9. Y. M. Choi, J. Park, Liming Wang, and M. C. Lin, ChemPhysChem, 5, 1231-34 (2004).
10. Cheng-Ming Tzeng, Y. M. Choi, Cheng-Liang Huang,Chi-Kung Ni, Yuan T. Lee, and M. C. Lin, J. Phys. Chem., A, 108, 7928-35, (2004).
11. Chih-Wei Lu and Yu-Jong Wu, Yuan-Pern Lee, R. S. Zhu and M. C. Lin, J. Chem. Phys., 121, 8271-78 (2004).
12. Huzeifa Ismail, Joonbum Park, Bryan M. Wong, W. H. Green, Jr. and M. C. Lin, Proc. Combust. Inst., 30, 1049 - 56 (2005).
13. Y. M. Choi and M. C. Lin, Int. J. Chem. Kinet., 37, 261-74 (2005).
14. Chih-Liang Huang, Shiang Yang Tseng, Tzu Yi Wang, N. S. Wang, , Z. F. Xu and M. C. Lin, J. Chem. Phys., 122, 184321/1-184321/9 (2005).
15. Shucheng Xu and M. C. Lin, J. Phys. Chem., B, 109, 8367-8373 (2005).
16. R. S. Zhu and M. C. Lin, Int. J. Chem. Kinet., 37, 593-98 (2005).
17. J. Park, I. V. Tokmakov and M. C. Lin, ChemPhysChem, 6, 2075-85 (2005).
18. Chih-Wei Lu and Shen-Long Chou,Yuan-Pern Lee, Shucheng Xu, Z. F. Xu and M. C. Lin, J. Chem. Phys., 122, 244314/1-244314/11 (2005).
19. R. S. Zhu, J. Park and M. C. Lin, Chem. Phys. Lett., 408, 25-30 (2005).
20. Z. F. Xu, H.-C. Hsu and M. C. Lin, J. Chem. Phys., 122, 234308/1-234308/11 (2005).
21. I.V. Tokmakov, G.-S. Kim, V. V. Kislov, A. M. Mebel and M. C. Lin, J. Phys. Chem. A, 109, 6114-27 (2005).
22. Z. F. Xu and M. C. Lin, J. Phys. Chem., A, 109, 9054-60 (2005).
23. Z. F. Xu and M. C. Lin, J. Phys. Chem., A, 110, 1672-77 (2006).
24. Shucheng Xu, R. S. Zhu, and M. C. Lin, Int. J. Chem. Kinet, 38, 322-6 (2006).
25. Kun Xu, Z. F. Xu and M. C. Lin, J. Phys. Chem., A, *110*, 6718-23 (2006).
26. C. W. Lu, W. J. Wu, Yuan-Pern Lee, R. S. Zhu and M. C. Lin, J. Chem. Phys., 125, 164329/1-10 (2006).
27. G. J. Nam, J. Park, I. V. Tokmakov, and M. C. Lin, J. Phys. Chem., A, 110, 8729-35 (2006).
28. J. Park, I. V. Tokmakov, and M. C. Lin, J. Phys. Chem. A, in press.

ADVANCED NONLINEAR OPTICAL METHODS FOR QUANTITATIVE MEASUREMENTS IN FLAMES

Principal Investigator: Robert P. Lucht
School of Mechanical Engineering, Purdue University, West Lafayette, IN 47907-2088
(Lucht@purdue.edu)

I. PROGRAM SCOPE

Nonlinear optical techniques such as laser-induced polarization spectroscopy (PS) and resonant wave mixing (RWM) are techniques that show great promise for sensitive measurements of transient gas-phase species, and diagnostic applications of these techniques are being pursued actively at laboratories throughout the world. Over the last few years we have also begun to explore the use of three-laser electronic-resonance-enhanced (ERE) coherent anti-Stokes Raman scattering (CARS) as a minor species detection method with enhanced selectivity. We have also initiated both theoretical and experimental efforts to investigate the potential of femtosecond (fs) laser systems for sensitive and accurate measurements in gas-phase media. Our initial efforts have focused on fs CARS.

The objective of this research program is to develop and test strategies for quantitative concentration measurements using nonlinear optical techniques in flames and plasmas. We are investigating the physics of these processes by direct numerical integration (DNI) of the time-dependent density matrix equations for the resonant interaction. Significantly fewer restrictive assumptions are required using this DNI approach compared with the assumptions required to obtain analytical solutions. Inclusion of the Zeeman state structure of degenerate levels has enabled us to investigate the physics of PS and of polarization effects in DFWM and ERE CARS. We have incorporated the effects of hyperfine structure in our numerical calculations of H-atom PS and 6WM. We are concentrating on the accurate simulation of two-photon processes, including Raman transitions, where numerous intermediate electronic levels contribute to the two-photon transition strength. The DNI numerical methods can be extended to the calculation of the interaction of laser pulses as short as 50 fs simply by decreasing the integration time step (for pulses shorter than this the rotating wave approximation will no longer be valid and the density matrix equations will need to include terms that are negligible for longer pulses).

During the last year we continued our studies of two-photon, two-color PS and 6WM of atomic hydrogen. We are still trying to resolve some differences between our experimental results for H-atom PS and our theoretical predictions. In collaboration with Tom Settersten and Joe Oefelein at Sandia, we modified the H-atom PS/6WM code for parallel processing and are running it on Joe Oefelein's computational cluster. We have also started to build up a cluster computing facility (Densitymatrix) at Purdue University; at present we have sixteen processors on our cluster. We have performed numerical simulations of our high-resolution two-photon-induced laser-induced fluorescence (LIF) measurements of nitric oxide (NO). We have incorporated an effective intermediate electronic level in our calculations to account for the effects of the numerous intermediate electronic levels for the $A^2\Sigma^+$-$X^2\Pi$ two-photon resonances. We also continued a detailed investigation of ERE CARS spectroscopy of nitric oxide, and have demonstrated the capability of measuring accurate NO profiles in counterflow diffusion flames without the need for corrections for collisional effects. Finally, we have performed a detailed analysis of the fs CARS process for gas-phase N_2; this study was aided greatly by the use of the Densitymatrix cluster machine in our laboratory. The fs CARS signal for N_2 is very strong because of the efficient pumping of the Raman coherences by Fourier-transform-limited pump and Stokes pulses, and temperatures can be extracted from the fs CARS signal without any effect of collisions.

II. RECENT PROGRESS

A. Two-Photon, Two-Color Polarization Spectroscopy and Six-Wave Mixing of Atomic Hydrogen

In collaboration with Thomas Settersten at the Combustion Research Facility at Sandia National Laboratories, we have continued our theoretical and experimental investigation of atomic hydrogen [P4]. The dependence of the PS, 6WM, and LIF signals from atomic hydrogen on the polarization state of the 243-nm two-photon pump beam was investigated in our initial experiments. It was also found that the 6WM signal is at least two orders of magnitude stronger than the PS signal. We have developed a detailed numerical model for resonant interaction of pulsed laser radiation with atomic hydrogen, and have used this code to model the PS, 6WM, and LIF processes. Modeling the 6WM process requires spatial integration along the signal beam path and the inclusion of Doppler broadening, and parallel processing is needed to make the calculations feasible. Some initial 6WM results are shown in Fig. 1.

B. High-Resolution Two-Photon-Induced Fluorescence Spectroscopy of Nitric Oxide

As an initial demonstration of the use of our optical parametric generator (OPG)/optical parametric amplifier (OPA) system, we performed two-photon-excited fluorescence of the NO molecule for both a single-beam configuration and a two-beam counterpropagating configuration. Following two-photon excitation of transitions within the (0,0) band of the $A^2\Sigma^+$ -$X^2\Pi$ electronic transition, ultraviolet fluorescence was monitored from this same band. The measurements were performed in a room-temperature gas cell at pressures of 0.8-3.0 kPa for a mixture of 3000 ppm NO in N_2 buffer gas. For the counter-propagating configuration, the two-photon absorption process is Doppler-free when a single-photon is absorbed from each of the pump beams, and the transitions were resolved to approximately 200 MHz. Saturation and Stark shifting of the transitions starts to become apparent when the pulse energy is increased to 2 mJ for a beam diameter of approximately 3 mm.

We developed a computer code for numerical simulation of this process and have investigated the saturation and Stark shifting of the two-photon line shape in detail. We have included Doppler broadening in our calculations in recent months; these calculations can be completed in a reasonable amount of time on the Densitymatrix cluster. A comparison of theory and experiment for a two-photon NO LIF spectrum for the counterpropagating geometry is shown in Fig. 2.

C. Electronic-Resonance-Enhanced CARS Spectroscopy of Nitric Oxide

We have investigated the physics and explored the diagnostic potential of ERE CARS for measurements of NO [P2,P3,P5,P6,P10]. The motivation for the work is to determine whether ERE CARS can be used to measure NO in high-pressure environments, where LIF measurements are very difficult because of interfering LIF signals from species such as O_2, H_2O, and CO_2. ERE CARS is inherently more selective because of the requirement for both electronic and Raman resonance for signal generation. During the last year we completed a detailed series of ERE CARS measurements of NO in counterflow diffusion flames with diluted hydrogen as the fuel. The NO profiles measured in flames with pure hydrogen as the fuel and a 75% H_2/25% N_2 fuel mixture are shown in Fig. 3. Surprisingly we obtained excellent agreement between calculated and experimental NO number density profiles without correcting for either collisional line broadening or collisional quenching. The estimated detection limit for NO in these diluted flames was approximately 10 ppm.

D. Femtosecond CARS Calculations

We used our DNI computational methods to perform a detailed investigation of the physics of fs CARS for gas-phase transitions [P9]. For Fourier-transform-limited pump and Stokes pulses, the Raman coherence can be excited to close its maximum value of 0.5 ρ_{gg}^0, as shown in Fig. 4, for pump and Stokes irradiances above 10^{17} W/m^2, which corresponds to a 25 μj, 100-fs pulse focused to a diameter of 50 μm.

Irradiance levels greater than 10^{17} W/m^2 can be achieved easily with current commercial fs laser systems. For Fourier-transform-limited laser pulses, the phase of the Raman coherence is the same for Q(J) transitions, regardless of J, right after the impulsive pump-Stokes excitation. Consequently, they all contribute to the creation of a giant Raman coherence that decays with time because the Q(J) transitions oscillate with different frequencies.

III. FUTURE WORK

Our investigation of the physics of two-photon, two-color PS and 6WM for H-atom measurements will continue in collaboration with Tom Settersten at Sandia. We will continue to explore the physics of these processes using our DNI code.

We are currently modifying our injection-seeded optical parametric systems by using pulsed dye amplifiers (PDAs) rather than OPAs with multiple BBO crystals. We plan to use diode lasers in the wavelength range from 760 nm to 1000 nm as injection seeding lasers for our OPG. The signal radiation from the OPG can then be amplified using pulsed dye amplifiers with Rhodamine or DCM dyes. We anticipate that the use of PDAs will simplify the alignment of the system and allow us to optimize the beam quality of the amplified beams. This OP source technology will enhance greatly the potential for quantitative application of nonlinear techniques such as PS, 6WM, dual-pump CARS, and ERE CARS spectroscopy. We plan to compare PS and 6WM for measurements of atomic oxygen.

We plan to pursue further theoretical and experimental investigations of the ERE CARS process for NO, CH, and C_2H_2, especially at higher pressures where collisional narrowing may result in significant improvement in the detection limits. The DNI code for ERE CARS has been developed and will be used to explore the physics of the ERE CARS process. The different effects of saturation of the Raman transition and saturation of the ultraviolet probe transition will be investigated.

Further theoretical investigations of the interaction of fs laser radiation with gas-phase resonances will be performed. The pumping of two-photon absorption resonances with fs laser radiation is of particular interest; this process is expected to be quite efficient for the same reasons that the pumping of Raman coherences with fs laser radiation is so efficient.

IV. BES-SUPPORTED PUBLICATIONS 2005-2007

1. W. D. Kulatilaka, T. N. Anderson, T. L. Bougher, and R. P. Lucht "Development of an Injection-Seeded, Pulsed Optical Parametric Generator for High-Resolution Spectroscopy," *Appl. Phys. B* **80**, 669-680 (2005).
2. S. Roy, W. D. Kulatilaka, N. Chai, S. V. Naik, N. M. Laurendeau, R. P. Lucht, J. P. Kuehner, and J. R. Gord, "Effect of Quenching on Electronic-Resonance-Enhanced CARS of Nitric Oxide," *Appl. Phys. Lett.* **89**, 104105 (2006).
3. W. D. Kulatilaka, N. Chai, S. V. Naik, N. M. Laurendeau, R. P. Lucht, J. P. Kuehner, S. Roy, and J. R. Gord, "Measurement of Nitric Oxide Concentrations in Flames Using Electronic-Resonance-Enhanced Coherent Anti-Stokes Raman Scattering," *Opt. Lett.* **31**, 3357-3359 (2006).
4. W. D. Kulatilaka, R. P. Lucht, S. Roy, J. R. Gord, and T. B. Settersten, "Detection of Atomic Hydrogen in Flames Using Two-Color Two-Photon-Resonant Six-Wave-Mixing Spectroscopy," *Appl. Opt.*, accepted for publication (2007).
5. N. Chai, W. D. Kulatilaka, S. V. Naik, N. M. Laurendeau, R. P. Lucht, J. P. Kuehner, S. Roy, and J. R. Gord, "Nitric Oxide Concentration Measurements in Atmospheric Pressure Flames using Electronic-Resonance-Enhanced Coherent Anti-Stokes Raman Scattering" *Appl. Phys. B*, accepted for publication (2007).
6. W. D. Kulatilaka, N. Chai, S. V. Naik, S. Roy, N. M. Laurendeau, R. P. Lucht, J. P. Kuehner, and J. R. Gord, "Effects of Pressure Variations on Electronic-Resonance-Enhanced Coherent Anti-Stokes Raman Scattering of Nitric Oxide," *Opt. Commun.*, accepted for publication (2007).

7. N. Chai, W. D. Kulatilaka, S. V. Naik, N. M. Laurendeau, R. P. Lucht, S. Roy, and J. R. Gord, "Detection of Acetylene by Electronic-Resonance-Enhanced Coherent Anti-Stokes Raman Scattering" *Appl. Phys. B*, accepted for publication (2007).
8. R. P. Lucht, P. J. Kinnius, S. Roy, and J. R. Gord, "Theory of Femtosecond Coherent Anti-Stokes Raman Scattering for Gas-Phase Transitions," *J. Chem. Phys.*, submitted for publication (2007).
9. S. V. Naik, J. Hwang, R. P. Lucht, and N. M. Laurendeau, "Optical-Heterodyne Raman-Induced Polarization Spectroscopy of Molecular Nitrogen: Experiments and Theory," *J. Raman Spectrosc.*, submitted for publication (2007).
10. S. V. Naik, N. Chai, W. D. Kulatilaka, N. M. Laurendeau, R. P. Lucht, S. Roy, and J. R. Gord, "ERE-CARS Measurements of Nitric Oxide and Kinetic Analysis in Diluted Hydrogen Counter-flow Flames at Atmospheric Pressure," *Combust. Flame*, submitted for publication (2007).

Graduate Student Supported at Present Time: Daniel R. Richardson (PhD student at Purdue University)

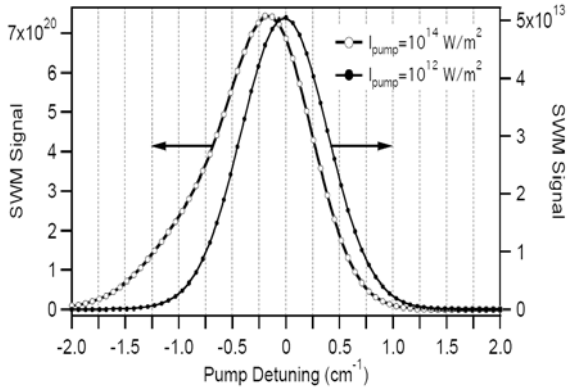

Fig. 1. Calculated H-atom 6WM signals for 243-nm pump irradiances of 10^{12} and 10^{14} W/m^2. Stark shifting and saturation are evident for $I_{pump} = 10^{14}$ W/m^2.

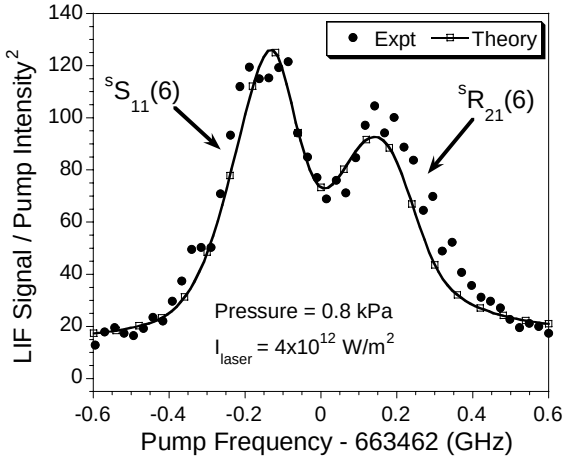

Fig. 2. Comparison of high-resolution data and DNI calculations of the two-photon LIF spectrum of NO. The counterpropagating pump beam geometry was used.

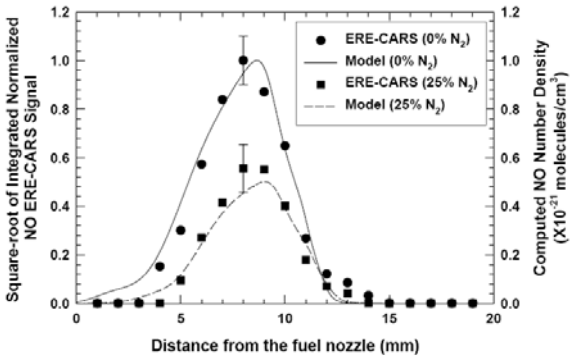

Fig. 3. Measured and calculated NO number density profiles in laminar counterflow diffusion flames with H_2/N_2 fuel mixtures. ERE CARS was used to measure the NO profile.

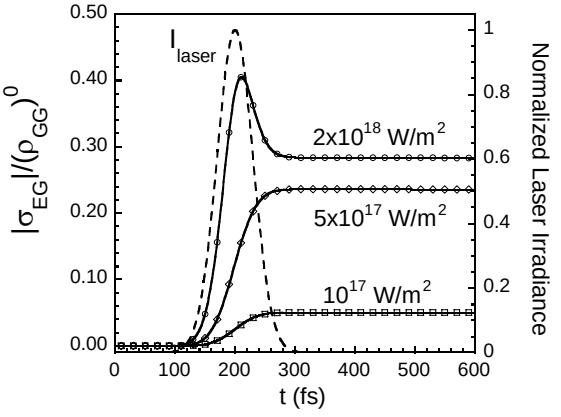

Fig. 4. Calculated temporal dependence of the Raman coherence for a Q-branch transition of gas-phase N_2 at room temperature and pressure. The peak pump and Stokes laser irradiances are both equal to the indicated values.

Time-Resolved Infrared Absorption Studies of the Dynamics of Radical Reactions

R. G. Macdonald
Chemistry Division
Argonne National Laboratory
Argonne, IL 60439
Email: rgmacdonald@anl.gov

Background

There is very little information available about the dynamics of radical-radical reactions. These processes are important in combustion being chain termination steps as well as processes leading to new molecular species. For almost all radical-radical reactions, multiple product channels are possible, and the determination of product channels will be a central focus of this experimental effort. Two approaches will be taken to study radical-radical reactions. In the first, one of the species of interest will be produced in a microwave discharge flow system with a constant known concentration and the second by pulsed-laser photolysis of a suitable photolyte. The rate constant will be determined under pseudo-first order conditions. In the second approach, both transient species will be produced by the same photolysis laser pulse, and both followed simultaneously using two different continuous-wave laser sources. This approach allows for the direct determination of the second-order rate constant under any concentration conditions if the appropriate absorption cross sections have been measured. In both approaches, the time dependence of individual ro-vibrational states of the reactants and/or products will be followed by frequency- and time-resolved absorption spectroscopy. In order to determine branching ratios and second-order rate constants, it is necessary to measure state-specific absorption coefficients and transition moments of radicals and these measurements will play an important role in this experimental study.

Recent Results

(a) $OH(^2\Pi) + OH(^2\Pi)$. The rate constant for the reaction, $OH + OH \rightarrow O(^3P) + H_2O$, k_{OH+OH} has been measured *via* direct concentration measurements of the OH radical using high-resolution diode laser absorption spectroscopy on Λ-doublet resolved rotational transitions of the first OH(2,0) overtone. The OH radical was created by pulsed-laser photolysis of N_2O to create $O(^1D)$ atoms, which reacted with H_2O to create the OH radical. The measurements were conducted in two carrier gases, Ne and Ar, to provide different conditions for removal of OH by diffusion and electronic quenching of $O(^1D)$, with no difference in the determination of k_{OH+OH}. The results were independent of carrier gas and pressure. The OH temporal concentration profiles were recorded with high signal-to-noise, greater than 200 for OH concentrations of 1.0×10^{13} molecules cm^{-3}. With this high signal-to-noise ratio, the value of k_{OH+OH} could be determined to within an uncertainty of about 10% (at the $\pm 1\sigma$ level), neglecting systematic errors, even though k_{OH+OH} only accounted for between 30 and 40% removal of the OH radicals. Several potential sources of error were explored but shown to be negligible.

Separate experiments were carried out with H_2 at low and high concentrations to further verify the experimental method (Figure 1). At low H_2 concentrations, the

measured values of k_{OH+OH} were in agreement with the different carrier gas results. At high concentrations of H_2, the experiments enabled the OH + H_2 rate constant, k_{OH+H2} to be measured. Good agreement was found with recent determinations.

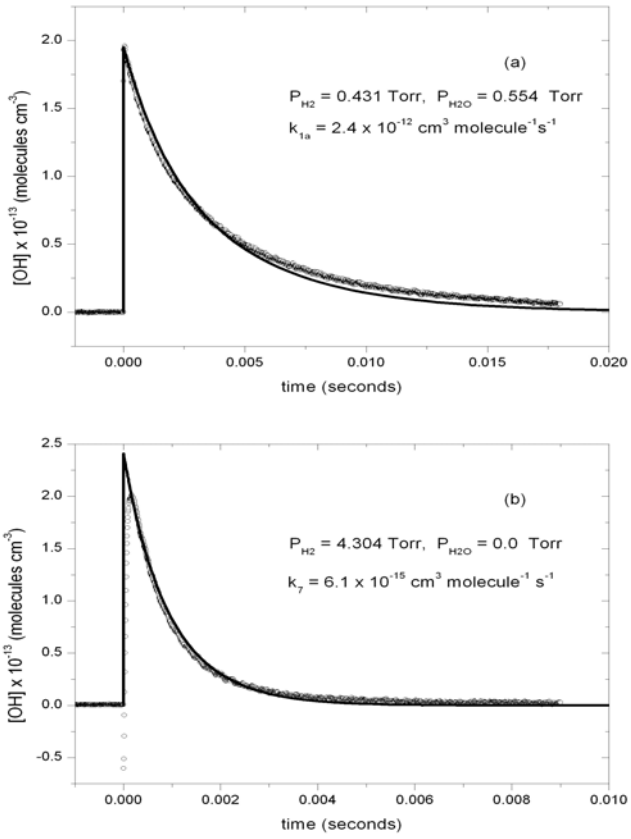

Figure 1(a) An OH (2←0) $P_{1f}(4.5)$ absorption profile used to determine the OH + OH →O + H_2O rate constant in dilute $Ar/H_2O/N_2O/H_2$ mixtures, P_{H2}=0.43 Torr. The open circles (○) are the experimental data points and the solid line the OH profile generated with the optimum value of k_{OH+OH}.. The OH + H_2 reaction dominates over diffusion for removal of OH at long times. (b) The determination of the k_{OH+H2} at high P_{H2} = 4.30 Torr under the same conditions as in (a). The open circles (○) are the experimental data points, and the solid line the OH profile generated with the optimum value $k_{OH + H2}$.

The OH + OH rate constant was measured at three temperatures to be: $(2.7 \pm 0.9) \times 10^{-12}$ at 293 ± 2 K; $(2.0 \pm 0.7) \times 10^{-12}$ at 347 ± 4 K; $(2.2 \pm 0.7) \times 10^{-12}$ cm^3 molecule^{-1} s^{-1} at 373 ± 3 K, where the uncertainty includes an estimate of both random and systematic errors at the 95% confidence limit. The observed-negative temperature dependence of the rate constant is in agreement with recent experimental measurements (H. Sun and Z. Li, Chem. Phys. Lett. **399**, 33 (2004)), but is in disagreement with another experimental work. These results confirm that the rate constant has a slight negative temperature dependence near 300 K. The measurements at 293 K are in good agreement with early work using the ESR technique to measure the OH radical concentration, but differ by almost a factor of two from other results and the IUPAC recommendation. Although within the 95% confidence limit of random and systematic errors, the results of this work and the IUPAC evaluation for k_{OH+OH} just overlap, but this is an unsatisfactory situation. Various sources of error were examined and evaluated but cannot account for this disagreement. It is noted that the more direct methods of determining the OH concentration, time-resolved absorption spectroscopy and ESR appear to give similar results.

(b) $NH_2(X^2B_1)$+ $NH_2(X^2B_1)$. The rate constant for the $NH_2 + NH_2 \rightarrow N_2H_2 + H_2$ disproportionation reaction is under current investigation. The NH_2 radical is created

from the 193 nm photolysis of NH_3 dilute in CF_4. Temporal concentration profiles of both NH_3 and NH_2 were monitored simultaneously following the photolysis laser pulse. The NH_2 radical was monitored using rotational lines of the (070) ← (000) vibrational band of the $NH_2(A^2A_1) \leftarrow (X^2B_1)$ electronic transition near 675 nm. The NH_3 molecule concentration was monitored using the $^rR(6)_{s/a}$ rotational transition of the $\nu_1 + \nu_3$ combination band. The absorption coefficient for the NH_2 transition was determined from the initial depletion of NH_3 after determining the NH_3 feature absorption coefficient in static experiments. Monitoring the temporal concentration of NH_3 also sheds some light on the chemistry that can occurs in this system and establishes the removal rate constant by diffusion and flow. Preliminary measurements indicate that $k_{NH2+NH2}$ is substantially larger than a recent room temperature measurement (N. Stothard, R. Humpfer, and H.-H. Grotheer, Chem. Phys. Lett. **240**, 474 (1995)) but secondary chemistry could be influencing our measurements and further work is needed to understand the chemistry in the system.

Future Work

Work will continue on the study of the both the OH + OH and $NH_2 + NH_2$ reactions. These studies will be extended to higher pressure so that the recombination channel can be investigated.

Publications 2005-present.

Determination of the rate constants for the $NCO(X^2\Pi) + Cl(^2P)$ and $Cl(^2P) + ClNCO(X\ ^2A')$ reactions at 293 and 345 K.
-Y. Gao and R. G. Macdonald
J. Phys. Chem. 109A, 5388-5397 (2005).

Determination of the rate constant for the $NCO(X^2\Pi) + CH_3(X^2A_2'')$ reaction at 293 K and an estimate of possible product channels.
-Y. Gao and R. G. Macdonald
J. Phys. Chem. 110A , 977-989 (2006).

Determination of the rate constant for the $OH(X^2\Pi) + OH(X^2\Pi) \rightarrow O(^3P) + H_2O$ reaction over the temperature range 293-373 K.
-Mi-Kyung Bahng and R. G. Macdonald
J. Phys. Chem. 111A, (2007) web release Jan. 25 2007.

Determination of the rate constant and product channels for the radical-radical reaction $NCO(X^2\Pi) + C_2H_5(X^2A_2'')$ at 293 K.
-R. G. Macdonald
Phys. Chem. Chem. Phys. accepted for publication (2007).

Quantum chemical studies of chemical reactions related to the formation of polyaromatic hydrocarbons and of spectroscopic properties of their key intermediates

Alexander M. Mebel
Department of Chemistry and Biochemistry, Florida International University
Miami, Florida 33199. E-mail: mebela@fiu.edu

Program Scope. The goal of this project is to theoretically investigate the mechanism of formation of polyaromatic hydrocarbons (PAHs) from smaller ring and chain hydrocarbons, of the key reactions of PAH oxidation, and the reactions of dicarbon and tricarbon molecules with simplest unsaturated hydrocarbons leading to hydrogen-deficient resonance-stabilized radicals relevant to the PAH growth. We use chemically accurate ab initio calculations to predict reaction potential energy surfaces and statistical theories to compute absolute reaction rate constants and product branching ratios. In addition, we calculate molecular properties of most important reaction intermediates and products in order to facilitate their experimental spectroscopic identification and monitoring.

Recent Progress

Ab initio G3-type / statistical theory studies of the formation of indene in combustion flames: the pathways involving benzene and phenyl radical. We have performed calculations of potential energy surfaces (PES) for the formation reactions of the smallest cyclopentafused polycyclic aromatic hydrocarbon (CP-PAH) indene from hydrocarbon species abundant in combustion, including benzene, phenyl, propargyl, and methyl radicals, and acetylene, in order to investigate the build-up of an additional cyclopenta moiety over the existing six-member aromatic ring. This was followed by statistical calculations of high-pressure-limit thermal rate constants in the temperature range of 300-3000 K for all reaction steps utilizing conventional RRKM and transition state (TST) theories. The HACA type mechanism, which involves the formation of benzyl radical followed by addition of acetylene, is shown to have low barriers (12-16 kcal/mol) and to be a viable candidate to account for the indene formation in combustion flames, such as the 1,3-butadiene flame, where this mechanism was earlier suggested as the major indene formation route. The mechanism of indene formation involving the addition of propargyl radical to benzene and rearrangements on the C_9H_9 PES is demonstrated to have higher barriers for all reaction steps as compared to an alternative pathway, which starts from the recombination of phenyl and propargyl radicals and then proceeds by activation of the C_9H_8 adducts by H abstraction or elimination followed by five-member ring closure in C_9H_7 and H addition to the 2-indenyl radical. The suggested pathways represent potentially important contributors to the formation of indene in combustion flames and the computed rate constants can be utilized in kinetic simulations of the reaction mechanisms leading to indene and to higher CP-PAH.

Ab initio/RRKM study of rearrangements of the C_5H_5-C_5H_4 (9-H-fulvalenyl) radical: the formation of naphthalene, azulene, and fulvalene from the recombination product of two cyclopentadienyl radicals. Chemically accurate *ab initio* Gaussian-3-type calculations of the potential energy surface for rearrangements of the 9-H-fulvalenyl radical have been performed to investigate mechanisms of formation of PAH originated by recombination of cyclopentadienyl radicals in combustion flames. Statistical theory calculations have been applied to obtain high-pressure limit thermal rate constants, followed by kinetic modeling of unimolecular reactions of C_5H_5-C_5H_4 to obtain product branching ratios at the high-pressure limit.

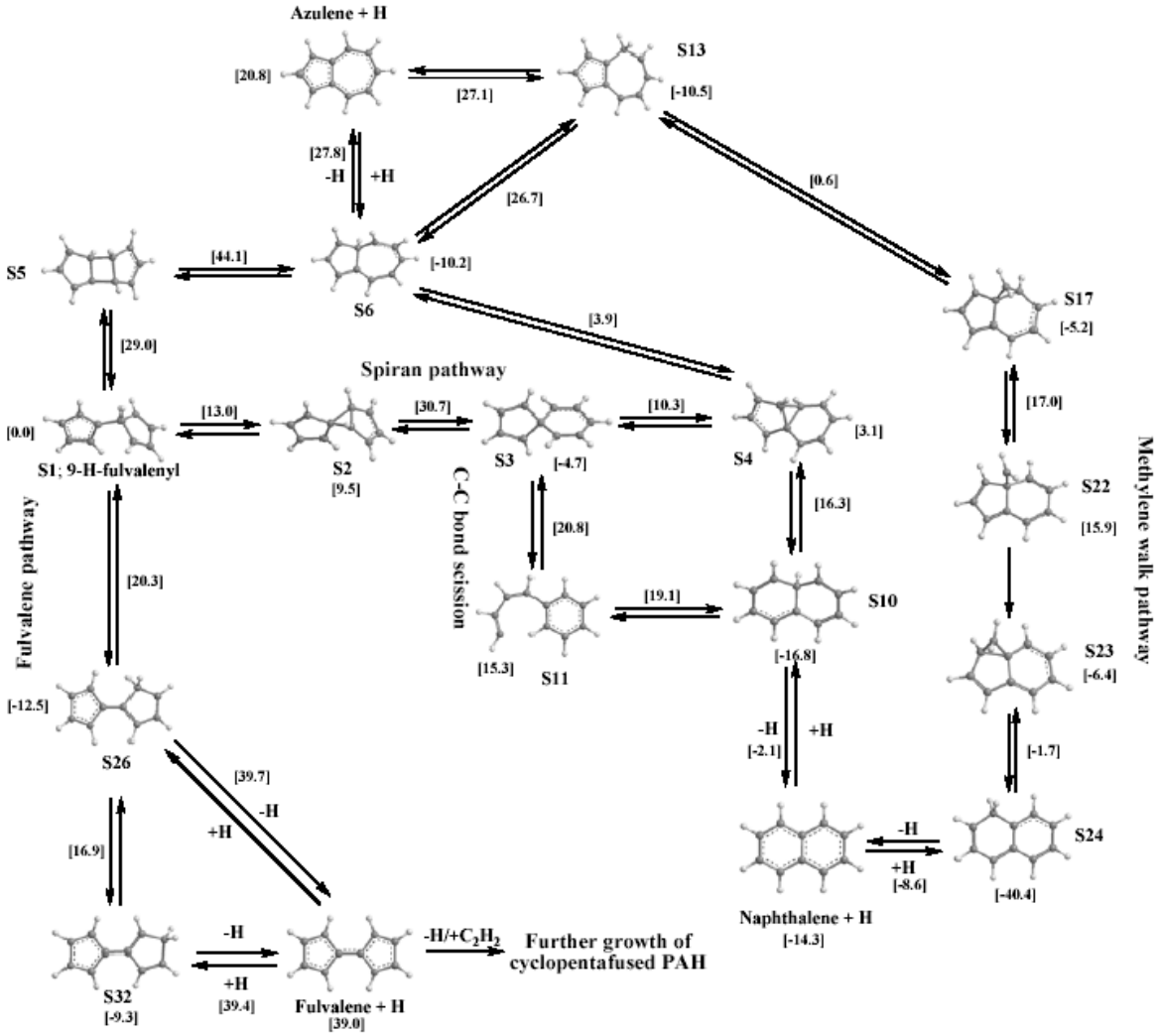

Naphthalene, fulvalene, and azulene have been shown to be the reaction products in rearrangements of the 9-H-fulvalenyl radical with relative yields depending on temperature. At low temperatures (T < 1000 K), naphthalene is predicted to be the major product, whereas at higher temperatures the naphthalene yield rapidly decreases and the formation of fulvalene becomes dominant. At T > 1500 K, naphthalene and azulene are only minor products accounting for less than 10% of the total yield. The recombination of cyclopentadienyl radicals has thus been shown to give only a small contribution to the naphthalene production at medium and high combustion temperatures. On the contrary, the high yields of fulvalene at these conditions indicate that cyclopentadienyl recombination may represent a significant source of cyclopentafused PAH, which are possible fullerene precursors. Azulene has been found to be only a minor product with branching ratios of less than 5% at all studied temperatures. The production of naphthalene at low combustion temperatures (T < 1000 K) is governed by the spiran mechanism originally suggested by Melius et al. At higher temperatures, the alternative C-C bond scission route, which proceeds via the formation of the *cis*-4-phenylbutadienyl radical, becomes competitive with the spiran pathway. The contributions of the methylene walk pathway to the production of naphthalene from unimolecular transformations of C_5H_5-C_5H_4 have been calculated to be negligible at all temperatures relevant to combustion.

Theoretical study of PESs, rate constants, and product branching ratios for the reactions of C_3 with unsaturated hydrocarbons. We have investigated PES for the reactions of tricarbon molecules with acetylene, ethylene, methylacetylene, allene, and benzene. This work was also complementary to experimental crossed molecular beam studies in Kaiser's group at the University of Hawaii at Manoa. The C_3 reaction mechanisms were found to be similar to those of the analogous C_2 reactions and to involve C_3 addition to the double, triple, or aromatic C-C bonds in unsaturated hydrocarbons followed by its insertion into the attacked carbon-carbon bond. However, on the contrary to C_2, the initial C_3 addition steps exhibit significant barriers in the range of 6-10 kcal/mol. The addition/insertion processes are followed by a variety of isomerization steps including ring opening and ring closure rearrangements and migrations of hydrogen atoms. Finally, the reaction intermediates decompose by losing an H atom or H_2. According to the results of our RRKM calculations, which are in accord with the experimental observations, the dominant reaction channel is the C_3-for-H exchange, i.e. $C_3 + C_nH_m \rightarrow C_{n+3}H_{m-1} + H$. For instance, the reaction with acetylene gives mostly the l-C_5H radical + H with overall endothermicity of 24.4 kcal/mol, the reaction with ethylene produces $H_2CCCCCCH$ (i-C_5H_3) exothermic by 13.3 kcal/mol, the reactions with the C_3H_4 isomers methylacetylene and allene yield the 1-hexene-3,4-diynyl-2 radical (C_6H_3; $H_2CCCCCCH$) with exothermicity of ~13 kcal/mol, and the reaction with benzene forms C_6H_5CCC endothermic by 25 kcal/mol. All the reactions considered were found to have a characteristic energy threshold from 10 to 25 kcal/mol and therefore can occur only at elevated or high temperatures. At high-temperature combustion conditions, the C_3 reactions with unsaturated hydrocarbons can be a significant source of hydrogen-deficient hydrocarbon RSFR, such as C_5H, C_5H_3, C_6H_3, and C_9H_5.

Future Plans

We will continue theoretical studies of the reactions of PAH formation and growth using ab initio molecular orbital and density functional calculations of PES and statistical (RRKM and TST) computations of absolute rate constants and product branching ratios. We will address the reactions of cyclopentadienyl radicals and cyclopentadiene involving the $C_{10}H_{11}$, $C_{10}H_{10}$, and $C_{10}H_9$ PES and synthesizing naphthalene, azulene, fulvalene, or indene. We will also investigate the formation mechanisms of naphthalene and indene from smaller hydrocarbons, alternative to the HACA sequences considered earlier. We will continue the studies of the related chemical reactions under single-collision conditions, which will complement experimental cross molecular beam measurements in Kasier's group. These reactions will include the cross beam reactions of singlet and triplet C_2 with C_4H_6 isomers and C_6H_6 accessing earlier unexplored regions of the C_6H_6 (benzene) and C_8H_6 (phenylacetylene) surfaces and the reactions of phenyl radical with C_3H_4, C_3H_6, and C_4H_6 occurring on the C_9H_9, C_9H_{11}, and $C_{10}H_{11}$ PES, directly linked to the indene and naphthalene formation routes.

DOE/BES sponsored publications (2005-2007)

1. L. Wang, V. V. Kislov, A. M. Mebel, X. Yang, X. Wang, "Potential energy surface and product branching ratios for the reaction of F(^{2}P) with the methyl radical: An ab initio/RRKM study," Chem. Phys. Lett. 406, 60 (2005).
2. I. V. Tokmakov, G.-S. Kim, V. V. Kislov, A. M. Mebel, M. C. Lin, "The reaction of phenyl radical with molecular oxygen: A G2M study of the potential energy surface," J. Phys. Chem. A 109, 6114 (2005).
3. V. V. Kislov, A. M. Mebel, "The $C_2H_3 + O_2$ reaction revisited: Is multireference treatment of the wave function really critical?", J. Phys. Chem. A 109, 6993 (2005).

4. V. V. Kislov, N. I. Islamova, A. M. Kolker, S. H. Lin, A. M. Mebel, "Hydrogen abstraction acetylene addition and Diels-Alder mechanisms of PAH formation: A detailed study using first principles calculations," J. Chem. Theory and Comput. 1, 908 (2005).
5. Y. A. Dyakov, C. K. Ni, S. H. Lin, Y. T. Lee, A. M. Mebel, "Photodissociation of azulene at 193 nm: Ab initio and RRKM study", J. Phys. Chem. A 109, 8774 (2005).
6. A. M. Mebel, V. V. Kislov, R. I. Kaiser, "Potential energy surface and product branching ratios for the reactions of dicarbon $C_2(X^1\Sigma_g^+)$ with methylacetylene, $CH_3CCH(X^1A_1)$: An ab initio/RRKM study", J. Phys. Chem. A 110, 2421 (2006).
7. Y. A. Dyakov, A. M. Mebel, S. H. Lin, Y. T. Lee, C. K. Ni, "Acetylene elimination in photodissociation of neutral azulene and its cation: An ab initio and RRKM study", J. Chin. Chem. Soc. 53, 161 (2006).
8. Y. A. Dyakov, C. K. Ni, S. H. Lin, Y. T. Lee, A. M. Mebel, "Ab initio and RRKM study of photodissociation of azulene cation", Phys. Chem. Chem. Phys. 12, 1404 (2006).
9. Y. Guo, X. Gu, F. Zhang, A. M. Mebel, R. I. Kaiser, "Unimolecular decomposition of chemically activated pentatetraene ($H_2CCCCCH_2$) intermediates – a crossed beams study of dicarbon molecule reactions with allene", J. Chem. Phys., 110, 10699 (2006).
10. X. Gu, Y. Guo, A. M. Mebel, R. I. Kaiser, Chemical dynamics of the formation of the 1,3-butadiynyl radical ($C_4H(X^2\Sigma^+)$) and its isotopomers, J. Phys. Chem. A, 110, 11265 (2006).
11. A. M. Mebel, V. V. Kislov, R. I. Kaiser, "Ab initio/RRKM study of the singlet C_4H_4 potential energy surface and of the reactions of $C_2(X^1\Sigma_g^+)$ with $C_2H_4(X^1A_{1g}^+)$ and $C(^1D)$ with C_3H_4 (allene and methylacetylene)", J. Chem. Phys., 125, 133113 (2006).
12. Y. Guo, X. Gu, F. Zhang, A. M. Mebel, R. I. Kaiser, "Reaction dynamics of carbon bearing radicals in circumstellar envelopes of carbon stars", Faraday Discuss., 133, 245 (2006).
13. X. Gu, Y. Guo, F. Zhang, A. M. Mebel, R. I. Kaiser, "A crossed molecular beam study of the reaction of dicarbon molecules with benzene – identification of the phenylethynyl radical (C_6H_5CC; X^2A')", Chem. Phys. Lett., 436, 7 (2007).
14. V. V. Kislov, A. M. Mebel, "An ab initio G3-type / statistical theory study of the formation of indene in combustion flames. I. The pathways involving benzene and phenyl radical", J. Phys. Chem. A, ASAP Article, DOI: 10.1021/jp067135x (2007).
15. Y. Guo, X. Gu, F. Zhang, A. M. Mebel, R. I. Kaiser, "A crossed molecular beam study on the formation of hexenediynyl radical ($H_2CCCCCCH$; C_6H_3 (X^2A')) via reactions of tricarbon molecules, $C_3(X^1\Sigma_g^+)$ with allene (H_2CCCH_2; X^1A_1) and methylacetylene (CH_3CCH; X^1A_1)", Phys. Chem. Chem. Phys., ASAP Article, DOI: 10.1039/b618179a (2007).
16. A. M. Mebel, G.-S. Kim, V. V. Kislov, R.I. Kaiser, "The reaction of tricarbon with acetylene: An ab initio/RRKM study of the potential energy surface and product branching ratios, J. Phys. Chem. A, ASAP Article, DOI: 10.1021/jp0690300 (2007).
17. A. M. Mebel, V. V. Kislov, R. I. Kaiser, "Theoretical studies of potential energy surfaces and product branching ratios for the reactions of C_2 with small unsaturated hydrocarbons (acetylene, ethylene, methylacetylene, and allene)", in Modern Gas Phase Molecular Dynamics, K. C. Lin, P. D. Kleiber, Eds., Research Signpost, in press.
18. X. Gu, Y. Guo, F. Zhang, A. M. Mebel, R. I. Kaiser, "A crossed molecular beams study on the formation and energetics of the resonantly stabilized Free i-C_4H_3(X^2A') radical and its isotopomers, Chem. Phys., in press.
19. L. Yao, A. M. Mebel, H. F. Lu, H. J. Nausser, S. H. Lin, "Anharmonic effect on unimolecular reactions with application to the photodissociation of ethylene", J. Phys. Chem. A, in press.

FLASH PHOTOLYSIS-SHOCK TUBE STUDIES

Joe V. Michael

Gas Phase Chemical Dynamics Group, Chemistry Division
Argonne National Laboratory, Argonne, IL 60439
e-mail: jmichael@anl.gov

The scope of the program is to measure high-temperature thermal rate constants for use in high-temperature combustion with the reflected shock tube technique. As described earlier, we have used a multi-pass optical system for detecting OH-radicals.[1] The new configuration is similar to that described previously.[2-4]

During the past year, the reflected shock tube technique using OH-radical absorption at 308 nm has been used to study six bimolecular reactions at path lengths between 1.57 and 5.25 m with $[OH]_t$ being determined from measured absorbance through an earlier determination[1] of the absorption cross-section at 308 nm ($\sigma_{OH} = (4.516 - 1.18 \times 10^{-3}\ T) \times 10^{-17}$ cm^2 molecule^{-1}). The present optical configuration gives an S/N ratio of ~1 at ~0.5-3.0 x 10^{12} radicals cm^{-3} depending on the number of path lengths used in a particular study.

In the first study,[5] rate constants for the primary initiation process in CH_4 oxidation

$$CH_4 + O_2 \rightarrow CH_3 + HO_2 \qquad (1)$$

were measured in reflected shock waves between 1655-1822 K using multi-pass absorption spectrometric detection of OH-radicals. After rapid dissociation of HO_2 yielding H-atoms, which are instantaneously converted to OH by $H + O_2 \rightarrow OH + O$, the temporal concentration of OH-radicals was observed as the final product from the rate controlling title reaction.

The present work utilized 18 optical passes corresponding to a total path length of 1.57 m giving an S/N ratio of one at ~3 x 10^{12} radicals cm^{-3}. Hence, kinetics experiments could be performed at conditions of low $[CH_4]_0$ (~ 70 ppm) thereby substantially reducing secondary chemistry. Possible implications due to CH_4 dissociation contributing to the OH formation rates were considered.

The present experimental results agreed with a priori variational transition state theoretical (VTST) calculations, $k_{1,th} = 3.37 \times 10^{-19}\ T^{2.745}\ \exp(-26041\ K/T)$ cm^3 molecule^{-1} s^{-1}, clearly overlapping each other within experimental error. The new values for $k_{1,th}$ obtained in this study are 8-10 times higher than the values used in the popular mechanisms GRI-Mech 3.0 and Leeds Methane mechanism version 1.5.

The reflected shock tube technique with multi-pass absorption spectrometric detection of OH-radicals with a total path length of ~4.9 m has been used to study the reactions,[6]

$$OH + C_2H_2 \rightarrow \text{products} \qquad (2)$$

and

$$OH + C_2H_4 \rightarrow C_2H_3 + H_2O \qquad (3)$$

Kinetics experiments were performed at $[OH]_0$ = ~4-20 ppm thereby minimizing secondary reactions. OH was produced rapidly from the dissociations of either CH_3OH or NH_2OH (hydroxylamine). A mechanism was then used to obtain profile fits that agreed with the experiment to within <±5 %. The derived Arrhenius expressions, in units of cm^3 $molecule^{-1}$ s^{-1} are:

$$k_2 = (1.03 \pm 0.24) \times 10^{-10} \exp(-7212 \pm 417 \text{ K/T}) \text{ for } 1509\text{-}2362 \text{ K} \quad (4)$$

and

$$k_3 = (10.2 \pm 5.8) \times 10^{-10} \exp(-7411 \pm 871 \text{ K/T}) \text{ for } 1463\text{-}1931 \text{ K} \quad (5)$$

The present study is the first ever direct measurement for reaction (2) at temperatures >1275 K while the present results extend the temperature range for (3) by ~700 K. These values are compared with earlier determinations and with recent theoretical calculations by Senosiain et al.[7,8] As seen in Figs. 1 and 2, the theoretical calculations agree with the present data for both reactions to within ±10% over the entire T-range.

The reflected shock tube technique with multi-pass absorption spectrometric detection of OH-radicals using either 36 or 60 optical passes corresponding to total path lengths of 3.15 or 5.25 m, respectively, were used to study the bimolecular reactions[9]

$$OH + CF_3H \rightarrow CF_3 + H_2O \quad (6)$$

$$CF_3 + H_2O \rightarrow OH + CF_3H \quad (-6)$$

between 995 and 1663 K. During the course of the study, estimates of rate constants for

$$CF_3 + OH \rightarrow \text{products} \quad (7)$$

were also determined. Experiments on reaction (-6) were transformed through equilibrium constants[10] to k_6 giving the Arrhenius expression

$$k_6 = (9.7 \pm 2.1) \times 10^{-12} \exp(-4398 \pm 275 \text{ K/T}) \text{ cm}^3 \text{ molecule}^{-1} \text{ s}^{-1} \quad (8)$$

Over the temperature range, 1318 to 1663 K, the results for reaction (7) were constant at

$$k_7 = (1.5 \pm 0.4) \times 10^{-11} \text{ cm}^3 \text{ molecule}^{-1} \text{ s}^{-1} \quad (9)$$

Reactions (6) and (-6) were also studied with variational transition state theory (VTST) employing QCISD(T) properties for the transition state. These a priori VTST predictions are in good agreement with the present experimental results, but are too low at the lower temperatures of earlier experiments, suggesting that either the barrier height is overestimated by about 1.3 kcal/mol, or that the effect of tunneling is greatly underestimated. The present experimental results have been combined with the most accurate earlier studies to derive an evaluation over the extended temperature range of 252-1663 K. The three-parameter expression

$$k_6 = 2.08 \times 10^{-17}\ T^{-1.5513} \exp(-1848\ K/T)\ cm^3\ molecule^{-1}\ s^{-1} \quad (10)$$

describes the rate behavior over this temperature range. Alternatively, the expression

$$k_{6,th} = 1.78 \times 10^{-23}\ T^{3.406} \exp(-837\ K/T)\ cm^3\ molecule^{-1}\ s^{-1} \quad (11)$$

obtained from empirically adjusted VTST calculations over the 250 to 2250 K range, agreed with the experimental evaluation to within a factor of 1.6. Reaction (7) was also studied with direct CASPT2 variable reaction coordinate transition state theory. The resulting predictions for the capture rate are found to be in good agreement with the mean of the experimental results and can be represented by the expression

$$k_{2,th} = 2.42 \times 10^{-11}\ T^{-0.0650} \exp(134\ K/T)\ cm^3\ molecule^{-1}\ s^{-1} \quad (12)$$

over the 200 to 2500 K temperature range. The products of this reaction are predicted to be CF_2O + HF.

We also have completed work on the thermal decompositions of NH_2OH and CF_3-radicals. Additional atom and radical with molecule reaction studies (e. g. Cl + hydrocarbons, OH + hydrocarbons, CF_2 + O_2, CF_2 + OH, etc.) and, also, thermal decomposition investigations (e. g. C_2H_5, C_2H_3, etc.) are in the planning stage at the present time.

This work was supported by the U. S. Department of Energy, Office of Basic Energy Sciences, Division of Chemical Sciences, Geosciences, and Biosciences, under Contract No. DE-AC02-06CH11357.

References

1. Srinivasan, N. K.; Su, M.-C.; Sutherland, J. W.; Michael, J. V. *J. Phys. Chem. A* **2005**, *109*, 1857.
2. Su, M.-C.; Kumaran, S. S.; Lim, K. P.; Michael, J. V. *Rev. Sci. Inst.* **1995**, *66*, 4649.
3. Su, M.-C.; Kumaran, S. S.; Lim, K. P.; Michael, J. V.; Wagner, A. F.; Dixon, D. A.; Kiefer, J. H.; DiFelice, J. *J. Phys. Chem.* **1996**, *100*, 15827.
4. Su, M.-C.; Kumaran, S. S.; Lim, K. P.; Michael, J. V.; Wagner, A. F.; Harding, L. B.; Fang, D.-C. *J. Phys. Chem. A* **2002**, *106*, 8261.
5. Srinivasan, N. K.; Michael, J. V.; Harding, L. B.; Klippenstein, S. J. *Combust. Flame* **2007**, *149*, 104.
6. Srinivasan, N. K.; Su, M.-C.; Michael, J. V. *Phys. Chem. Chem. Phys.* **2007**, in press.
7. Senosiain, J. P.; Klippenstein, S. J.; Miller, J. A. *J. Phys. Chem. A* **2005**, *109*, 6045.
8. Senosiain, J. P.; Klippenstein, S. J.; Miller, J. A. *J. Phys. Chem. A* **2006**, *110*, 6960.
9. Srinivasan, N. K.; Su, M.-C.; Michael, J. V.; Klippenstein, S. J.; Harding, L. B. *J. Phys. Chem. A* **2007**, in press.
10. Ruscic, B., private communication of unpublished results obtained from Active Thermochemical Tables 1.25 and the Core (Argonne) Thermochemical Network 1.049 (2005) Tables.

PUBLICATIONS FROM DOE SPONSORED WORK FROM 2005-2007

- *Reflected Shock Tube Studies of High-Temperature Rate Constants for OH + CH_4 → CH_3 + H_2O and CH_3 + NO_2 → CH_3O + NO*, N. K. Srinivasan, M.-C. Su, J. W. Sutherland, and J. V. Michael, J. Phys. Chem. A **109**, 1857 (2005).
- *Reflected Shock Tube Studies of High-Temperature Rate Constants for CH_3 + O_2, H_2CO + O_2, and OH + O_2*, N. K. Srinivasan, M.-C. Su, J. W. Sutherland, and J. V. Michael, J. Phys. Chem. A **109**, 7902 (2005).
- *The Thermal Decomposition of Water*, N. K. Srinivasan and J. V. Michael, Int. J. Chem. Kinet. **38**, 211 (2006).
- *Active Thermochemical Tables: Accurate Enthalpy of Formation of Hydroperoxyl*

Radical, HO_2, B. Ruscic, R. E. Pinzon, M. L. Morton, N. K. Srinivasan, M.-C. Su, J. W. Sutherland, and J. V. Michael, J. Phys. Chem. A **110**, 6592 (2006).

- *Reflected Shock Tube Studies of High-Temperature Rate Constants for $OH + NO_2 \rightarrow HO_2 + O_2$ and $OH + HO_2 \rightarrow H_2O + O_2$*, N. K. Srinivasan, M.-C. Su, J. W. Sutherland, J. V. Michael, and B. Ruscic,, J. Phys. Chem. A **110**, 6602 (2006).
- *Experimental and Theoretical Rate Constants for $CH_4 + O_2 \rightarrow CH_3 + HO_2$*, N. K. Srinivasan, J. V. Michael, L. B. Harding, and S. J. Klippenstein, Combust. Flame, **149**, 104-111 (2007).
- *High-Temperature Rate Constants for $CH_3OH + Kr \rightarrow$ Products, $OH + CH_3OH \rightarrow$ Products, $OH + (CH_3)_2CO \rightarrow CH_2COCH_3 + H_2O$*, and *$OH + CH_3 \rightarrow CH_2 + H_2O$*, N . K. Srinivasan, M.-C. Su, and J. V. Michael, J. Phys. Chem. A, in press, ASAP.
- *Reflected Shock Tube and Theoretical Studies of High-Temperature Rate Constants for $OH + CF_3H \leftrightarrows CF_3 + H_2O$ and $CF_3 + OH \rightarrow$ Products*, N. K. Srinivasan, M.-C. Su, J. V. Michael, S. J. Klippenstein, and L. B. Harding, J. Phys. Chem. A, in press.
- *Reflected Shock Tube Studies of High-Temperature Rate Constants for $OH + C_2H_2$ and $OH + C_2H_4$*, N. K. Srinivasan, M.-C. Su, and J. V. Michael, Phys. Chem. Chem. Phys., in press.
- *The Thermal Decomposition of CF_3-radicals in Reflected Shock Waves*, N. K. Srinivasan, M.-C. Su, J. V. Michael, S. J. Klippenstein, and L. B. Harding, J. Phys. Chem. A, submitted.
- *Reflected Shock Tube Studies of the Thermal Decomposition of NH_2OH and Rate Constants for $OH + NH_2OH \rightarrow$ Products and $OH + NH_2 \rightarrow NH + H_2O$*, N. K. Srinivasan, M.-C. Su, J. V. Michael, S. J. Klippenstein, and L. B. Harding, J. Phys. Chem. A, submitted.

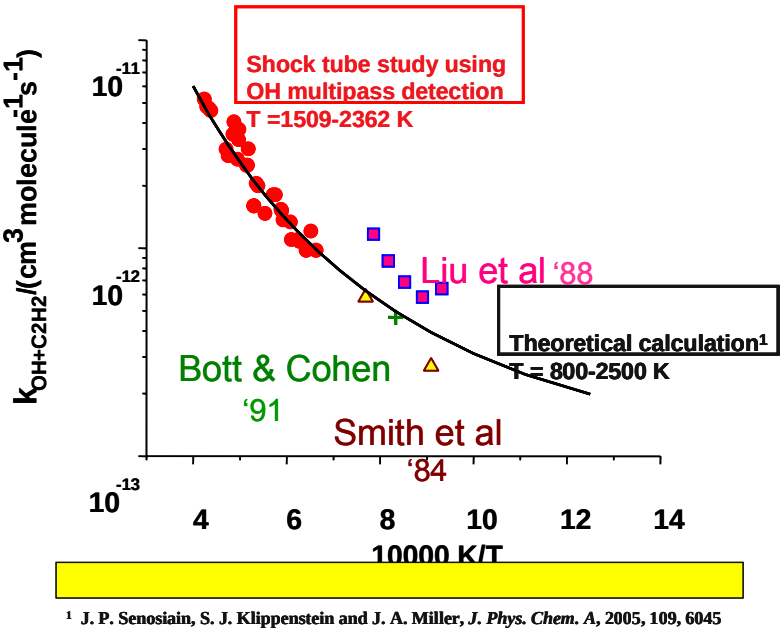

[1] J. P. Senosiain, S. J. Klippenstein and J. A. Miller, *J. Phys. Chem. A*, 2005, 109, 6045

Fig. 1

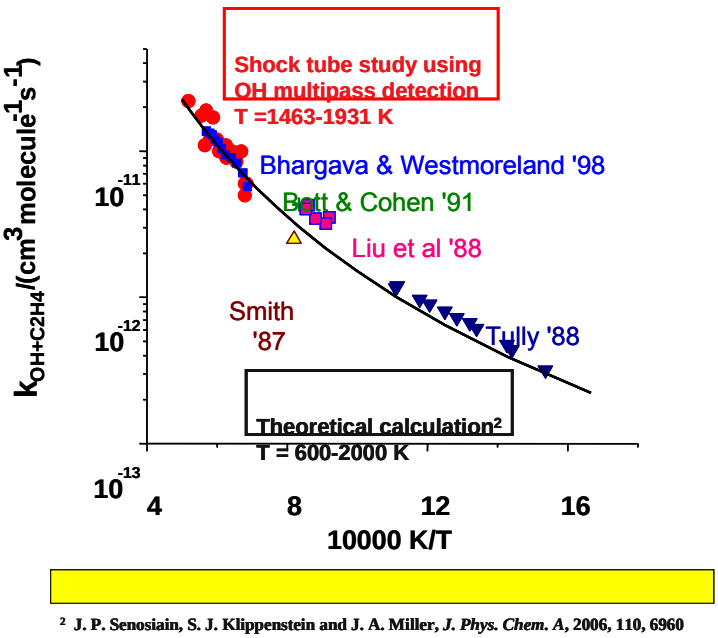

[2] J. P. Senosiain, S. J. Klippenstein and J. A. Miller, *J. Phys. Chem. A*, 2006, 110, 6960

Fig. 2

Multiphase Combustion Diagnostics Development

H. A. Michelsen
Sandia National Labs, MS 9055, P. O. Box 969, Livermore, CA 94551
hamiche@sandia.gov

1. Program Scope

Combustion in practical combustors, such as internal combustion engines, frequently evolves through multiple phases. Liquid fuels injected into such combustors are generally vaporized and mixed with a gas-phase oxidizer. Combustion processes often produce solid carbon particles, i.e., soot. These particles may be oxidized to form gas-phase species or released into the exhaust stream, where they can be coated with liquid coatings. These coatings can be comprised of any of a number of components, including unburned fuel, lube oil, sulfuric acid, water, and other combustion by-products.[1,2] The research program described here focuses on the development of optical diagnostics for soot particles in combustion environments and combustion exhaust plumes. The goal of this work is *in situ* measurements of volume fraction, size, composition, and morphology of combustion-generated particles with fast time response and high sensitivity. Future work will expand the scope of this program to include optical diagnostics development for studies of the structure and evolution of liquid-jet sprays.

2. Recent Progress

Our work has focused on developing a detailed understanding of the chemical and physical mechanisms that influence the applicability of laser-induced incandescence (LII) for soot detection under a wide range of conditions. In order to understand these mechanisms, we have coupled experimental studies with the development of a model that predicts the temporal behavior of LII from soot on a nanosecond time scale. The model accounts for particle heating by laser absorption, oxidation, and annealing and cooling by sublimation, conduction, and radiation. The model also includes mechanisms for convective heat and mass transfer, melting, and nonthermal photodesorption of carbon clusters.[3]

In our recent work we have studied the effects of laser radiation on the morphology and fine structure of dry soot aggregates. We have performed these studies in collaboration with Mary Gilles and Alexei Tivanski at the Lawrence Berkeley National Laboratory Advanced Light Source (ALS) and with Peter Buseck and Laura van Poppel at Arizona State University (ASU).

We have also performed experiments designed to isolate fast (picosecond timescale) laser-particle mechanisms from processes that are expected to evolve over longer (nanosecond) timescales. Fast processes, such as laser absorption and photolytic desorption, can have an influence on LII and elastic laser scattering (ELS). These experiments were performed using a Nd:YAG laser with a pulse duration at 532 nm of ~65 ps and a streak camera with a temporal resolution of ~8 ps. These measurements have been compared with those made using a Nd:YAG laser with a 6.9-ns pulse duration to heat the particles. The results will be used to improve our understanding of the mechanisms involved in LII detection.

2.1. The effects of laser radiation on the morphology and fine structure of soot aggregates.

Soot is composed of branched-chain aggregates of small (15-50 nm diameter) carbon spheroids called primary particles. Previous work has suggested that, during laser irradiation, these aggregates can break apart into primary particles.[4,5] Transmission electron microscopy (TEM) images of laser-heated soot, however, have demonstrated substantial changes to particle fine structure and morphology without the appearance of small fragments.[6,7] This result suggests that either mass loss occurred via laser-induced sublimation of carbon clusters or that any primary particles lost from the aggregates were not retained on the grids.

In collaboration with Peter Buseck and his group at ASU and Mary Gilles and her group at the ALS, we have used particle electric mobility sizing, TEM techniques, and near edge X-ray absorption fine structure (NEXAFS) spectroscopy to investigate the physical and chemical changes induced in soot aggregates exposed to laser radiation at 532 and 1064 nm. In these experiments, soot particles were measured with a scanning mobility particle sizer (SMPS) and were concurrently collected on TEM grids and Si_3N_4 windows prior to and following exposure to laser radiation over a wide range of laser fluences (0.01-1 J/cm^2).

The initial soot particles produced by the flame during these experiments were polydisperse and followed a log-normal size distribution with a median electric mobility diameter of ~100 nm. TEM images of these particles revealed typical fractal-like branched-chain aggregates consisting of approximately 50 spherical primary particles. The average geometric diameter of the primary particles was 25 nm. The aggregate fractal dimension was $d_f = 1.7$, which is typical of dry, mature soot.

No change in particle electric mobility diameter, morphology, fine structure, or chemical structure (carbon hybridization) was observed when the particles were exposed to laser radiation at low fluences (<~0.12 J/cm^2 at 532 nm and <~0.22 J/cm^2 at 1064 nm). At higher fluences, a new size mode (centered at 8 – 20 nm in electric mobility diameter) was observed. These smaller particles grew in size and particle number density with increasing fluence. NEXAFS showed predominantly graphitic (sp^2-hybridized) carbon in the non-irradiated particles and a mixture of sp^2- and sp^3-hybridized carbon (consistent with amorphous carbon) in the irradiated particles. In TEM images small (~30 nm diameter) particles produced by irradiation of soot consisted of extended regions without any obvious long-range order and smaller isolated regions of carbon with significant long-range order. These ordered regions contain small graphite crystallites or partially annealed carbon that forms small, layered carbon rings or ribbons. Large particles (~100 nm diameter) irradiated at fluences above the threshold fluence for new particle formation consist of primary particles that appear to be similar in size and structure to the non-irradiated primary particles. These large particles can also include primary particles with denser layered carbon rings, which may result from partial annealing.

These results suggest that particle growth proceeds through recondensation of small carbon clusters (e.g., C, C_2, and C_3) by homogeneous nucleation, heterogeneous nucleation onto graphitic fragments of primary particles, or a combination of both homogeneous and heterogeneous nucleation. Nanoparticle growth via homogeneous or heterogeneous nucleation of small carbon clusters is consistent with model predictions of the onset and extent of carbon volatilization by sublimation and photodesorption mechanisms. The efficiency for laser-induced nanoparticle production was significantly smaller at 1064 nm than at 532 nm at all fluences above 0.12 J/cm^2. Reduced efficiency of new particle formation at the longer wavelength is likely due to a smaller absorption coefficient and lower photodesorption efficiency at the longer wavelength. These results are consistent with previous studies of laser irradiation of soot particles and bulk graphite. The onset of soot fragmentation at 0.12 J/cm^2 at 532 nm is consistent with energetic requirements for carbon sublimation observed experimentally and predicted by the LII model.[3]

2.2. Laser-induced incandescence on a picosecond timescale.

LII involves heating the soot particles with a high-power pulsed laser to temperatures (2500-4000 K) at which they incandesce and measuring the emitted light. Interpretation of LII signals for quantitative measurements is hampered by an incomplete understanding of the physical mechanisms that influence signal evolution during and after the laser pulse. Previous experimental work has shown that, at low fluences (<~0.15 J/cm^2), temporally resolved LII signals increase during the laser pulse and slowly decay with decay times on the order of a few hundred nanoseconds at atmospheric pressure and flame temperatures.[3,8-12] Decay times decrease with increasing fluence, particularly at

fluences above 0.2 J/cm^2.[3,4,8-10,13,14] These studies were performed using laser systems with pulse durations in the range of 7-8 ns.

Because the LII signal is approximately proportional to T^5, particle cooling leads to a decrease in signal. LII signals also depend on particle size and decrease approximately linearly with a decrease in particle volume. Model results suggest that, on nanosecond to microsecond timescales, laser-heated soot particles cool predominantly by sublimation and conduction to the surrounding atmosphere.[3,4,11,12,14-18] Sublimation also causes particles to shrink. Further evidence indicates that an unknown mechanism leads to a significant loss of signal within the first few nanoseconds of the laser pulse at fluences above ~0.2 J/cm^2.[3,10] In order to gain an understanding of this latter process, experiments were performed on a picosecond timescale with a picosecond laser to heat the soot and a streak camera to collect the emitted light.

Soot was produced in an atmospheric laminar co-flow diffusion flame and was heated with the 532-nm output from a picosecond Nd:YAG laser with a pulse duration of 65 ps. The signal was recorded on a streak camera with a temporal resolution of ~8 ps. Similar measurements were made using the 532-nm output from a Nd:YAG with a 6.9-ns pulse duration to heat the soot and a photodiode with a rise time of <0.3 ns to record the signal. Relative to the laser timing, the temporal characteristics of the picosecond and nanosecond signals are qualitatively very similar.

The results of both experiments were compared with an LII model that has been optimized using data from a nanosecond LII system. As has been demonstrated previously,[3,10] the LII model gives good agreement with the nanosecond data at fluences ≤0.2 J/cm^2 and underpredicts the signal decay rates at higher fluences. The model does not agree as well with the picosecond data. The picosecond temporal profiles increase significantly faster and earlier in the laser pulse than predicted by the model. This disagreement between the model and picosecond LII data may be attributable to perturbations to the signal by laser-induced fluorescence (LIF) from polycyclic aromatic hydrocarbons (PAHs) or other class of large organic species that fluoresces in the range of 633-900 nm in which the signal was detected. The power dependence of the signal enhancement suggests that the excited state or states responsible for this fluorescence are accessed via a two-photon transition, which would explain the enhanced sensitivity to this interference with the shorter pulse duration. These states are short-lived and are estimated to have an effective lifetime of ~55 ps.

3. Future plans

Current work builds on these results and extends it to combustion-generated particles with inorganic and organic coatings representative of particles found in exhaust plumes. In order to simulate exhaust-plume particulates, we have modified our flow-tube system to allow controlled deposition of a coating with low volatility on flame-generated soot. The thickness of the coating can be varied and the particles collected for analysis by TEM and NEXAFS. Coatings investigated to date have been selected for diagnostic development for diesel exhaust and include sulfuric acid, heptamethylnonane, and oleic acid. These experiments are currently limited by our inability to determine the mass loading of particle coatings. Developing an understanding of the cause and magnitude of the effects of coatings will require characterization of the particle coatings. Coating the particles increases the mean aggregate size as measured by the SMPS, but measurements of electric mobility diameter provided by the SMPS do not provide a quantitative measure of the volatile coating fraction either by volume or by mass. In order to measure the volatile fraction, we will build a chamber that includes a temperature-controlled oscillating crystal microbalance for differential mass measurements on coated and evaporatively dried particles.

We will also extend our studies of fast processes that are important during laser heating of soot. In order to identify the source of the fast signal seen in the picosecond experiments, we will perform these experiments at 1064 nm, which would reduce any contribution from a multiphoton LIF process.

4. References

(1) Kittelson, D. B. *J. Aerosol Sci.* **1998**, *29*, 575.
(2) Lighty, J. S.; Veranth, J. M.; Sarofim, A. F. *J. Air Waste Manage. Assoc.* **2000**, *50*, 1565.
(3) Michelsen, H. A. *J. Chem. Phys.* **2003**, *118*, 7012.
(4) Filippov, A. V.; Markus, M. W.; Roth, P. *J. Aerosol Sci.* **1999**, *30*, 71.
(5) Beyer, V.; Greenhalgh, D. A. *Appl. Phys. B* **2006**, *83*, 455.
(6) Vander Wal, R. L.; Ticich, T. M.; Stephens, A. B. *Appl. Phys. B* **1998**, *67*, 115.
(7) Vander Wal, R. L.; Choi, M. Y. *Carbon* **1999**, *37*, 231.
(8) Ni, T.; Pinson, J. A.; Gupta, S.; Santoro, R. J. *Appl. Opt.* **1995**, *34*, 7083.
(9) Witze, P. O.; Hochgreb, S.; Kayes, D.; Michelsen, H. A.; Shaddix, C. R. *Appl. Opt.* **2001**, *40*, 2443.
(10) Michelsen, H. A.; Witze, P. O.; Kayes, D.; Hochgreb, S. *Appl. Opt.* **2003**, *42*, 5577.
(11) Snelling, D. R.; Liu, F.; Smallwood, G. J.; Gülder, Ö. L. *Combust. Flame* **2004**, *136*, 180.
(12) Schittkowski, T.; Mewes, B.; Brüggemann, D. *Phys. Chem. Chem. Phys.* **2002**, *4*, 2063.
(13) Vander Wal, R. L.; Weiland, K. J. *Appl. Phys. B* **1994**, *59*, 445.
(14) Allouis, C.; Beretta, F.; D'Alessio, A. *Exp. Thermal Fluid Sci.* **2003**, *27*, 455.
(15) Weeks, R. W.; Duley, W. W. *J. Appl. Phys.* **1974**, *45*, 4661.
(16) Eckbreth, A. C. *J. Appl. Phys.* **1977**, *48*, 4473.
(17) Melton, L. A. *Appl. Opt.* **1984**, *23*, 2201.
(18) Liu, F.; Smallwood, G. J.; Snelling, D. R. *J. Quant. Spectrosc. Radiat. Transfer* **2005**, *93*, 301.

5. BES-supported, peer-reviewed publications

H. A. Michelsen et al., "Modeling laser-induced incandescence of soot: A summary and comparison of LII models", *Appl. Phys. B*, in press (2007).

L. Nemes, A. M. Keszler, C. G. Parigger, J. O. Hornkohl, H. A. Michelsen, and V. Stakhursky, "On spontaneous emission from the C_3 radical in carbon plasma", *Appl. Opt.*, in press (2007).

H. A. Michelsen, A. V. Tivanski, M. K. Gilles, L. H. van Poppel, M. A. Dansson, and P. R. Buseck, "Particle formation from pulsed laser irradiation of soot aggregates studied with a scanning mobility particle sizer, a transmission electron microscope, and a scanning transmission x-ray microscope", *Appl. Opt.* **46**, 959-977 (2007).

C. Schulz et al., "Laser-induced incandescence: Recent trends and current questions", *Appl. Phys. B* **83**, 333-354 (2006).

H. A. Michelsen, "Laser-induced incandescence of flame-generated soot on a picosecond timescale", *Appl. Phys. B* **83**, 443-448 (2006).

L. Nemes, A. M. Keszler, C. G. Parigger, J. O. Hornkohl, H. A. Michelsen, and V. Stakhursky, "The C_3 puzzle: Formation of and spontaneous emission from the C_3 radical in carbon plasmas", *Int. Elect. J. Mol. Design* **5**, 150-167 (2006).

P. O. Witze, M. Y. Gershenzon, and H. A. Michelsen, "Dual-laser LIDELS: An optical diagnostic for time-resolved volatile fraction measurements of diesel particulate emissions", *Proc. SAE*, SAE paper #2005-01-3791 (2005).

B. K. Pun, C. Seigneur, and H. A. Michelsen, "Atmospheric Transformations", in *Air Pollution Modeling: Theories, Computational Methods, and Available Software, 2nd edition, Vol. 2*, P. Zannetti, Ed., Van Nostrand Reinhold, New York, Chapter 12 (2005).

Chemical Kinetics and Combustion Modeling

James A. Miller

Combustion Research Facility, Sandia National Laboratories
MS 9055, Livermore, CA, 94551-0969
email: jamille@sandia.gov

Program Scope

The goal of this project is to gain qualitative insight into how pollutants are formed in combustion systems and to develop quantitative mathematical models to predict their formation and destruction rates. The approach is an integrated one, combining theory, modeling, and collaboration with experimentalists to gain as clear a picture as possible of the processes in question. My efforts and those of my collaborators are focused on problems involved with the nitrogen chemistry of combustion systems and the formation of soot and PAH in flames, as well as on general problems in hydrocarbon combustion. Current emphasis is on determining phenomenological rate coefficients from the time-dependent, multiple-well master equation for reactions involved in the pre-cyclization and cyclization chemistry of flames burning aliphatic fuels.

Recent Results

The Reactions of Normal and Iso- C_4H_5 Radicals with Acetylene (with Juan Senosiain)

In this work we analyzed in detail the reactions of i-C_4H_5 and n-C_4H_5 with acetylene. Both have been proposed as possible cyclization steps, forming benzene or fulvene, in rich flames burning aliphatic fuels. The relevant parts of the potential energy surface were determined from rQCISD(T) calculations extrapolated to the infinite-basis-set limit. Using this information in an RRKM-based master equation, we calculated thermal rate coefficients and product distributions for both reactions as a function of temperature and pressure. The results are cast in forms that can be used in modeling. For both reactions the initial adducts close relatively easily into five- and six-membered rings, so that the thermal rate coefficient is largely determined by the rate of association. In the n-C_4H_5+C_2H_2 reaction both five- and six-membered rings are formed, leading to both fulvene + H and benzene + H; i-C_4H_5+C_2H_2 produces only fulvene + H. The rate coefficient for n-C_4H_5 + C_2H_2 is considerably larger than that for i-C_4H_5 + C_2H_2. However, because the n- isomer is relatively easily converted to the i- form by H-atom-assisted isomerization in rich flames, it is the i-C_4H_5 + C_2H_2 reaction that plays the more important role in flame chemistry. We have used our rate coefficients in some preliminary modeling of a series of low-pressure flames (acetylene, ethylene, allene, propyne, propene, and 1,3-butadiene) previously studied experimentally by others, all near the sooting limit. In the 1,3-butadiene flame, i-C_4H_5 + C_2H_2 accounts for virtually all the fulvene produced in the flame and, indirectly through the H-assisted isomerization of fulvene to benzene, perhaps as much as 30 per cent of the benzene. The remainder, of course, comes from the C_3H_3 + C_3H_3 recombination. The contributions of i-C_4H_5+C_2H_2 are considerably less in the other flames, and the contribution of n-C_4H_5 + C_2H_2 to forming cyclic products is largely negligible in all the flames.

Association Rate Constants for Reactions between Resonantly Stabilized Radicals: C_3H_3 + C_3H_3, C_3H_3 + C_3H_5, and C_3H_5 + C_3H_5 (with Yuri Georgievski and Stephen Klippenstein)

Reactions between resonantly stabilized radicals play an important role in the formation of polycyclic aromatic compounds and soot in flames burning aliphatic fuels. The theoretical prediction of rate coefficients and product distributions for such reactions is complicated by the fact that the initial

complex-formation steps and some dissociation steps are barrierless. In this work direct variable-reaction-coordinate transition state theory (VRC-TST) was used to predict accurately the association rate constants for the self and cross reactions of propargyl and allyl radicals. For each reaction, a set of multifaceted dividing surfaces was used to account for the multiple possible addition channels. Because of their resonant character the geometric relaxation of the radicals is important. Here, the effect of this relaxation is explicitly calculated with the UB3LYP/cc-pvdz method for each mutual orientation encountered in the configurational integrals over the transition state dividing surfaces. The final energies are obtained from CASPT2/cc-pvdz calculations with all π-orbitals in the active space. Evaluations along the minimum energy path suggest that basis set corrections are negligible. The VRC-TST approach was also used to calculate the association rate constant and the corresponding number of states for the $C_6H_5 + H \rightarrow C_6H_6$ exit channel of the $C_3H_3 + C_3H_3$ reaction, which is also barrierless. For this reaction, the interaction energies were evaluated with the CASPT2(2e,2o)/cc-pvdz method and a one –dimensional correction is included on the basis of CAS+1+2+QC/aug-cc-pvtz calculations for the $CH_3 + H$ reference system. For the $C_3H_3 + C_3H_3$ reaction, the VRC-TST results for the energy and angular momentum resolved numbers of states in the entrance channels and in the $C_6H_5 + H$ exit channel are incorporated in a master equation analysis to determine the temperature and pressure dependence of the phenomenological rate coefficients. The rate constants for the $C_3H_3 + C_3H_3$ and $C_3H_5 + C_3H_5$ self-reactions compare favorably with the available experimental data. To our knowledge there are no experimental rate data for the $C_3H_3 + C_3H_5$ reaction.

Theoretical Analysis of the Reactions $H + O_2 \rightarrow HO_2$, $H + OH \rightarrow H_2O$, and $OH + OH \rightarrow H_2O_2$ at High Pressure (with Stig Rune Sellevag and Yuri Georgievski)

Fossil fuel use since the pre-industrial period has significantly increased the atmospheric concentration of carbon dioxide and contributed to an unequivocal warming of the climate system. Therefore there is a growing interest in using hydrogen (H_2) for power production. Utilization of H_2 as fuel in gas turbine combustors requires accurate description of the combustion process at elevated pressures. However, even apparently small differences between the available chemical mechanisms for H_2 combustion can have significant effect on predicted flame properties. Thus, although significant progress has been made to provide a detailed description of the chemical kinetics involved at these conditions, some uncertainties still remain.

We have initiated a theoretical investigation of the reactions $H + O_2 \rightarrow HO_2$ (I), $H + OH \rightarrow H_2O$ (II), and $OH + OH \rightarrow H_2O_2$ (III). In the first part of this work, potential energy surfaces involved in the reactions I-III have been characterized using complete active space second-order multireference perturbation theory (CASPT2) and aug-cc-pV*X*Z (*X* = D, T, Q) basis sets. High-pressure limiting rate coefficients for reactions I and II have been calculated using variable-reaction-coordinate transition state theory (VRC-TST). Over the temperature range 300-3000 K the following expressions were obtained: $k_\infty(H+O_2) = (25T^{-0.367} + 7.5 \times 10^{-2}T^{0.702}) \times 10^{-11}$ and $k_\infty(H+OH) = 4.17 \times 1^{11}T^{0.234}\exp(57.5/T)$ cm^3 $molecule^{-1}$ s^{-1}. The dynamics of reaction III are complicated by the presence of two equivalent hydrogen-bonded adducts involving the two OH radicals. At the CASPT2/aug-cc-pVTZ level of theory, the $^1A'$ hydrogen-bonded dimer is stabilized by 3.88 kcal mol^{-1} relative to the OH + OH reactants, while the transition state connecting the $^1A'$ dimer and H_2O_2 lies 3.53 kcal mol^{-1} below the energy of the OH + OH reactants. Due to the presence of this potential well connected by an “outer” and an “inner” transition state, the capture rate coefficient of reaction III is not well described using VRC-TST. It is likely that the recent two-transition-state model developed by Georgievskii and Klippenstein will provide a better description of reaction III. This work is currently in progress.

Future Directions

We shall continue our work on the chemical kinetics of rich flames of aliphatic fuels, particularly that concerned with the formation of the first aromatics containing one or two rings. In the next year or 2 we expect to focus attention on the reaction of allyl with propargyl, on the reaction of OH with propargyl, and on a number of reactions on the C_3H_5 potential, particularly allyl dissociation. The work on allyl + propargyl is being pursued in collaboration with Wesley Allen and co-workers at the University of Georgia. We shall continue to develop our chemical kinetic model, particularly in conjunction with the flame experiments at the Advanced Light Source. We shall also continue to maintain our interest in the nitrogen chemistry of combustion, particularly that concerned with NO_x control technologies such as reburning, Thermal De-NO_x, and RAPRENO$_x$.

Publications of James A. Miller
2005-2007

- Y. Georgievski, S. J. Klippenstein, and J. A. Miller, "Association Rate Constants for Reactions between Resonance Stabilized Radicals: C_3H_3+C_3H_3, C_3H_3+C_3H_5, and C_3H_5+C_3H_5," *Phys. Chem. Chem. Phys.*, in press (2007)

- J.A. Miller and S.J. Klippenstein, "Master Equation Methods in Gas Phase Chemical Kinetics", feature article for *J. Phys. Chem. A* **110**, 10528-10544 (2006)

- A.Fernandez-Ramos, J.A. Miller, S.J. Klippenstein, and D.G. Truhlar, "Modeling the Kinetics of Bimolecular Reactions," *Chemical Reviews* **106**, 4518-4584 (2006)

- J.P. Senosiain and J.A. Miller, "The Reaction of Normal and Iso-C_4H_5 Radicals with Acetylene," *J. Phys. Chem. A*, in press (2007)

- J.P. Senosiain, S.J. Klippenstein, and J.A. Miller, "The Reaction of Ethylene with Hydroxyl Radicals: A Theoretical Study", *J. Phys. Chem. A* **110**, 6960-6970 (2006)

- J.P. Senosiain, S.J. Klippenstein, and J.A. Miller, "Oxidation Pathways in the Reaction of Diacetylene with OH Radicals", *Proc. Combust. Inst.* **31**, 185-192 (2007)

- N. Hansen, J. A. Miller, J. Wang, T. A. Cool, M.E. Law, P. R. Westmoreland, T. Kasper, and K. Kohse-Höinghaus, " Photoionization Mass Spectrometric Studies and Modeling of Fuel-Rich Allene and Propyne Flames," *Proc. Combust. Inst.* **31**, 1157-1164 (2007)

- N. Hansen, S. J. Klippenstein, J. A. Miller, J. Wang, T. A. Cool, M.E. Law, P. R. Westmoreland, T. Kasper, and K. Kohse-Höinghaus, "Identification of C_5H_x (x=3-6,8) Isomers in Fuel-Rich Flames by Photoionization Mass Spectrometry and Electronic Structure Calculations", *J. Phys. Chem. A* **110**, 4376-4388 (2006)

- J.P. Senosiain, S.J. Klippenstein, and J.A. Miller, "Pathways and Rate Coefficients for the Decomposition of Vinoxy and Acetyl Radicals", *J. Phys. Chem. A* **110**, 5772-5781 (2006)

- C.A. Taatjes, N. Hansen, J.A. Miller, T.A. Cool, J. Wang, P.R. Westmoreland, M.E. Law, T.

Kasper, and K. Kohse-Höinghaus, "Combustion Chemistry of Enols: Possible Ethenol Precursors in Flames", *J. Phys. Chem. A* **110**, 3254-3260 (2006)

- N. Hansen, S. J. Klippenstein, C. A. Taatjes, J. A. Miller, J. Wang, T. A. Cool, F. Qi, M.E. Law, and P. R. Westmoreland, "The Identification and Chemistry of C_4H_3 and C_4H_5 Isomers in Fuel-Rich Flames", *J. Phys. Chem. A* **110**, 3670-3678 (2006)

- J.A. Miller, M.J. Pilling, and J. Troe, "Unravelling Combustion Mechanisms Through a Quantitative Understanding of Elementary Reactions", *Proc. Combust. Inst.* **30**, 43-88 (2005)

- S.J. Klippenstein and J.A. Miller, "The Addition of Hydrogen Atoms to Diacetylene and the Heats of Formation of i-C_4H_3 and n-C_4H_3", *J. Phys. Chem. A* **109**, 4285-4295 (2005)

- J.P. Senosiain, S.J. Klippenstein, and J.A. Miller, "The Reaction of Acetylene with Hydroxyl Radicals", *J. Phys. Chem. A* **109**, 6045-6055 (2005)

- C.A. Taatjes, N. Hansen, A. McIlroy, J.A. Miller, J.P. Senosiain, S.J. Klippenstein, F. Qi, L. Sheng, Y. Zhang, T.A. Cool, J. Wang, P.R. Westmoreland, M.E. Law, T. Kasper, and K. Kohse-Höinghaus, "Enols are Common Combustion Intermediates in Hydrocarbon Oxidation", *Science* **308**, 1887-1889 (2005)

- C. A. Taatjes, S. J. Klippenstein, N. Hansen, J. A. Miller, T. A. Cool, J. Wang, M.E. Law, and P. R. Westmoreland, "Synchrotron Photoionization Measurements of Combustion Intermediates: Photoionization Efficiency and Identification of C_3H_2 Isomers", *Phys. Chem. Chem. Phys.* **7**, 806-813 (2005)

- J.P. Senosiain, S.J. Klippenstein, and J.A. Miller, "A Complete Statistical Analysis of the Reaction Between OH and CO," *Proc. Combust. Inst.* **30**, 945-953 (2005)

Detection and Characterization of Free Radicals Relevant to Combustion Processes

Terry A. Miller
Laser Spectroscopy Facility, Department of Chemistry
The Ohio State University, Columbus OH 43210, email: tamiller+@osu.edu

1 Program Scope

While combustion processes have been studied for many years, the chemistry is so complex that it is yet to be fully understood under a variety of conditions. Modern computer codes for its modelling typically employ hundreds of reaction steps with a comparable number of chemical intermediates. Nonetheless the predictions of such models can be no better than the fundamental dynamical and mechanistic data that are their inputs. Spectroscopic identifications and diagnostics for the chemical intermediates in the reaction mechanisms constitute an important experimental verification of the models, as well as provide molecular parameters that are experimental "gold standards" against which quantum chemistry computations of molecular properties may be judged.

Our spectroscopic work, therefore, has recently centered upon the peroxy family of reactive, organic radical intermediates (RO_2), which are known to be of key importance in combustion processes. While we have also studied the corresponding alkoxy radicals (RO) in the past, we will focus in this report on our cavity ringdown spectroscopy (CRDS) of various RO_2 radicals.

2 Recent Progress

Given that peroxy radicals are involved in many complex reaction mechanisms, whose rates can be greatly affected by the structural form of the radical, it is desirable to have a diagnostic technique that can distinguish between different peroxy radicals (RO_2 and $R'O_2$), as well as between different isomers and conformers of the same RO_2. Historically, spectroscopic studies of these species and their reaction chemistry have centered around the $\widetilde{B} - \widetilde{X}$ transition, generally located in the ultraviolet (UV) region of the spectrum. While this approach benefitted from the strong UV absorption cross-section, it was limited by the fact that the $\widetilde{B}$ state is repulsive and hence most RO_2 radicals have a broad absorption centered around 240 nm that is largely independent of the R group. More recently, therefore, spectroscopic studies of peroxy radicals have shifted to the much weaker $\widetilde{A} - \widetilde{X}$ electronic transition, which is located in the near infrared (NIR). Our expectations that transitions to this bound $\widetilde{A}$ state should yield sharp, structured spectra that would be distinguishable for different R groups, have now been realized.

To put matters in perspective we initially review briefly our progress on the NIR CRDS studies of RO_2 radicals, supported by DOE prior to this past year. We then discuss results of two particular studies this past year in some detail. Finally, we overview on-going work aimed at developing relationships between the radical's structure, i.e. empirical formula, isomer, and conformer, and the characteristics of their observed $\widetilde{A} - \widetilde{X}$ electronic spectra.

Our first studies of methyl peroxy (CH_3O_2) and ethyl peroxy ($C_2H_5O_2$) confirmed that their NIR electronic spectra were distinctive, demonstrating that the $\widetilde{A} - \widetilde{X}$ transition is a selective diagnostic for these species. In our studies [1,3,4] of propyl peroxy ($C_3H_7O_2$) and butyl peroxy ($C_4H_9O_2$), we confirmed that not only can this transition be used to distinguish between different alkyl peroxy radicals (RO_2 vs. $R'O_2$), but it can also distinguish between isomers and conformers of the same RO_2. This past year we have extended our NIR CRDS studies to include pentyl peroxy radical ($C_5H_{11}O_2$), allowing a more global understanding of the spectroscopy of these alkyl peroxy species and how their structure affects their electronic spectra.

Pentyl peroxy radical presents the most structurally diverse alkyl peroxy radical studied to date, since it has eight isomeric forms (see Fig. 1) and numerous conformeric forms for each isomer. Based on the spectroscopic results for $C_3H_7O_2$ and $C_4H_9O_2$, we expected to resolve unique electronic spectra for each of the isomers and some of the conformers of $C_5H_{11}O_2$. We present in Fig. 2, as an example, the unique NIR CRDS spectra [7] for the four primary pentyl peroxy isomers, 1-pentyl peroxy, 2-methylbutyl peroxy, 3-methylbutyl peroxy, and neopentyl peroxy. All four spectra clearly show unique features, but also do possess similarities in that three peaks, labelled A, B, and C, are clearly resolved. Given that this pattern was also observed in the spectra of 1-propyl peroxy and 1-butyl peroxy, we can extrapolate the assignments of these peaks in the smaller alkyl peroxy spectra to our more complicated pentyl peroxy results.

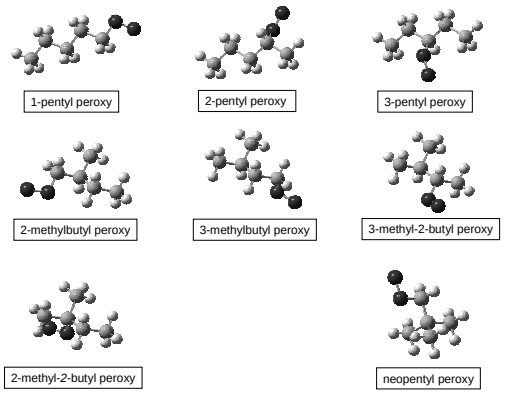

Figure 1: The eight isomers of pentyl peroxy radical. There are four primary pentyl peroxies, three secondary, and one tertiary.

We believe that the spectral structure shown in each trace of Fig. 2 arises from the origin transitions of different conformers of each of the 4 isomers of primary pentyl peroxy. Conformers of a given primary pentyl peroxy isomer originate firstly from the change in dihedral angle between the O-O-C and O-C-C planes in the molecule. Quantum chemistry calculations for 1-$C_3H_7O_2$ indicate that a 0° dihedral angle (labelled *trans* or T), as well as ±120° (labelled *gauche* or G) yield stable conformers, which should all be populated at room temperature. In addition, different T and G orientations of other dihedral angles further down the hydrocarbon chain in the larger alkyl peroxy radicals yield more possible stable conformers of a given radical, approximately 170 in total for pentyl peroxy. Based upon empirical extrapolation of the spectra and extensive quantum chemical calculations, the following assignments were made to the three corresponding peaks in the spectrum of 1-propyl peroxy: peak A was assigned to the overlap of T_1T_2 and T_1G_2 conformer origins, peak B to the origin of G_1G_2, and peak C to the overlap of G_1T_2 and $G_1'G_2$ conformer origins, with T_1/G_1 indicating the orientation of the dihedral angle between the O-O-C and O-C-C planes and T_2/G_2 indicating the angle between the O-C-C and C-C-C planes. Extending these assignments to the primary pentyl peroxy spectra in Fig. 2, we can assign peak A to an unresolved overlap of T_1 conformer origins and peaks B and C to transitions corresponding to two sets of G_1 conformer origins, with numerous conformeric changes further down the hydrocarbon chain making contributions to both peak B and C.

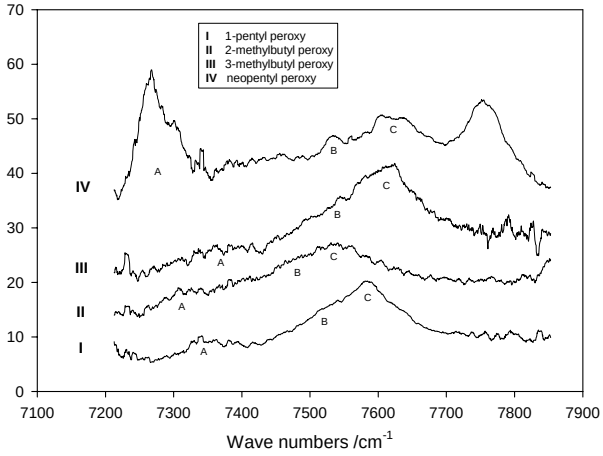

Figure 2: CRDS spectra of the primary pentyl peroxy radicals. The spectra have been manually offset from one another for a better view. Peaks A, B, and C are assigned to overlaps of different conformer origins for a given isomer.

While the structural pattern is similar for all four primary pentyl peroxy isomers, it should be noted that the intensity ratio of these three peaks is clearly different for neopentyl peroxy (trace IV in Fig. 2). For the other primary pentyl peroxy radicals, the intensity order for the three peaks, from smallest to largest, is A:B:C. This intensity order was likewise observed in the origin spectra of 1-$C_3H_7O_2$ and 1-$C_4H_9O_2$; however, for neopentyl peroxy, the intensity order from smallest to largest is B:C:A. This change in intensity is partially explained by an energy re-ordering of the conformer ground states that give rise to the A, B, and C peaks. In 1-$C_5H_{11}O_2$, like 1-$C_3H_7O_2$, the G_1 conformers are predicted by *ab initio* calculations to have lower $\widetilde{X}$ state energies than the T_1 conformers, yielding a higher population of the G_1 vs T_1

conformers in the ground state and hence a higher intensity of B and C versus A peaks. In neopentyl peroxy, however, calculations predict that the T_1 conformers have lower $\widetilde{X}$ state energies than the G_1 conformers.

Although not shown in Fig. 2 we have observed structure to the blue of the origin region for both neopentyl peroxy and 2-methyl-2-butyl peroxy, which is assigned to fundamental transitions in the COO bend and O-O stretching vibrations. We have also recorded the origin spectra for all the secondary and tertiary pentyl peroxy radicals. Additional details are found in a forthcoming paper. [7]

In developing a global picture relating structure and $\widetilde{A}-\widetilde{X}$ spectra for the RO_2 radicals we found a need to re-investigate ethyl peroxy radical. While $C_2H_5O_2$ has only one possible isomer, our quantum chemistry calculations indicate there are two stable minima in the potential, namely the *trans* (T) and *gauche* (G) conformations corresponding respectively to O-O-C and O-C-C dihedral angles of 0° and ±120° respectively (spectrally unresolvable G± enantiomers). However our previous NIR $\widetilde{A}-\widetilde{X}$ spectral observations identified bands associated with only a single conformer.

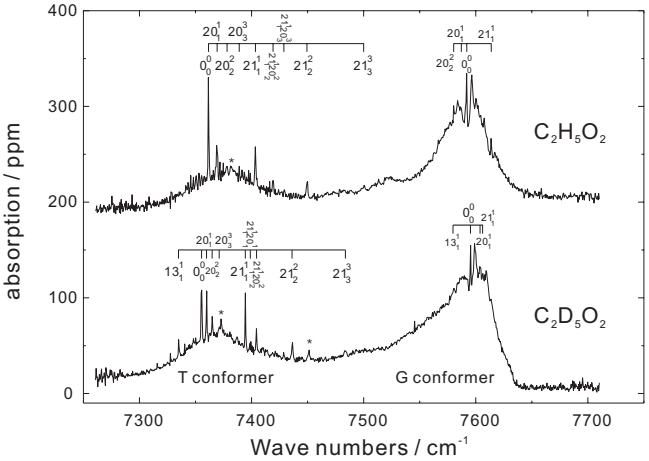

Figure 3: CRDS spectra of the ethyl peroxy radical (upper trace) and its deuterated isotopomer (lower trace). The spectrum of $C_2H_5O_2$ has been manually offset for a better view. Hot bands are labelled according to the $N^{v'}_{v''}$ notation, where v''/v', respectively, are $\tilde{X}/\tilde{A}$ excitation level in vibration N. The three peaks labelled with an asterisk belong to methyl peroxy and its perdeuterated analogue, respectively.

We have recorded [5] new NIR CRDS spectra for ethyl peroxy, both the normal and fully deuterated isotopomers, which are presented in Figure 3. The lower energy feature is assigned to the T conformer origin, while the previously reported higher energy feature is assigned to the G conformer. These assignments are based on several reasons. Foremostly, the experimentally observed, quite different rotational contours for the two bands were well matched by simulations based upon quantum chemistry calculations of the T and G conformer geometries, respectively. Secondarily these calculations predict the T conformer's adiabatic transition frequency to be lower in energy than that of the G by >100 cm^{-1} for both the normal and deuterated isotopomers. This agrees well with the actual separations of 230 cm^{-1} and 240 cm^{-1} respectively. Finally, the observed intensity ratio of the two conformer origins is in qualitative agreement with what is predicted from calculations for the T and G energies.

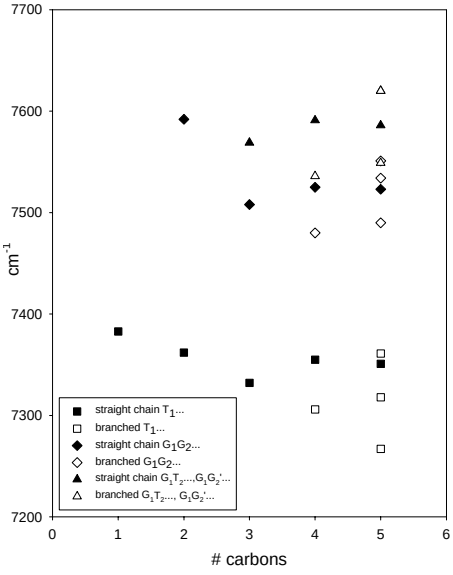

Figure 4: Plot of the observed $\widetilde{A}-\widetilde{X}$ transition frequencies vs. number of carbons for the primary alkyl peroxy radical isomers and conformers.

In addition to assigning the two conformer origins of $C_2H_5O_2$ and $C_2D_5O_2$, there are additional peak assignments in Figure 3, which can be generally categorized as sequence band structure. Ethyl peroxy has several low-lying vibrations, which are reasonably populated at room temperature, and therefore transitions involving these vibrations are likely to be observed. These vibrations correspond to the CCO bend (ν_{13}), CH_3 torsional (ν_{20}) and CO torsional (ν_{21}) motions. While not shown here, fundamental transitions in the COO bend, O-O stretch, and CCO bend vibrations were also observed to the blue for both the T and G conformers of $C_2H_5O_2$.

The combination of the ethyl and pentyl peroxy data with our previous spectroscopic work allows us to realize a sufficient data set to develop structure/spectral relationships for the alkyl peroxy radicals. These include correlations between the $\widetilde{A}-\widetilde{X}$ electronic origin frequencies and a number of structural characteristics including: (i) number of carbon atoms, (ii) site (primary, secondary, tertiary) of O_2 substitution, (iii) isomeric

branching of the hydrocarbon chain at the β carbon and beyond, (iv) T_1 vs G_1 conformation of OOC-OCC dihedral angle, (v) T_2 vs $G_2^{(\prime)}$ conformation of OCC-CCC dihedral angle and configurations ($T_{n>2}$,$G_{n>2}^{(\prime)}$) down the hydrocarbon chain.

Fig. 4 is an example of several plots that illustrate these correlations; an invited review article [8] in preparation discusses several additional such plots. In Fig. 4 we plot the origin frequencies of the various isomers and conformers of the primary alkyl peroxy radicals, $C_nH_{2n+1}O_2$, vs the number of C atoms, n. It is clear that the origin bands fall into two clearly separated groups, depending upon the T_1 or G_1 conformations. Furthermore there is a large frequency shift (in the range of +200 cm^{-1} on average) between T_1 and G_1 origins. Changing dihedral angles, denoted as (T_2..., G_2...) further down the hydrocarbon chain has an average shift of 60 cm^{-1} or less. Looking at the n=4 and 5 points in Fig. 4 we see that the branching of the hydrocarbon causes a small but clear shift in the origin frequency. For example, the T conformers of a branched butyl or pentyl peroxy, on average, have lower origin frequencies than the straight chain T conformers. In general we observe red shifts as the number of carbon atoms increase, but we also observe a slight dip in the origin frequency for the straight chain primary alkyl peroxy radicals at n=3. This is particularly noticeable in the T conformer group. This effect is not yet understood, but given that it is also repeated in the G conformers, it appears to be real.

Before closing we should point out that during the past year we have also recorded the full $\widetilde{A} - \widetilde{X}$ electronic spectrum for methyl peroxy. Previously, as the first peroxy radical studied with our NIR CRDS apparatus, we had only recorded the origin region of its electronic spectrum to prove that our spectroscopic diagnostic could distinguish between RO_2 species containing different R. In looking at the full spectrum, we have now observed much more structure than was originally anticipated, which has since been assigned to large amplitude vibrational motion in the CH_3 torsional mode. These results are reported in more detail in a just submitted paper. [6]

3 Future Plans

The immediate future work is to complete a global picture of the structure/spectral relationships for the alkyl peroxy radicals. We next plan to investigate a new homologous series of peroxy radicals, namely the unsaturated alkyl peroxy radicals. We have already observed the $\widetilde{A}-\widetilde{X}$ electronic spectrum of phenyl peroxy [2] radical with our NIR CRDS apparatus. We wish to continue by studying non-aromatic unsaturated alkyl peroxy radicals. Our immediate goal is vinyl peroxy, with propargyl peroxy and other unsaturated radicals thereafter. The long term goal is to build similar data sets for other types of peroxy radicals, much like that which we have produced for the alkyl peroxy radicals.

List of Publications Supported by DOE

[1] "Conformational Analysis of the 1- and 2-Propyl Peroxy Radicals," G. Tarczay, S. Zalyubovsky, and T. A. Miller, *Chem. Phys. Lett.* **406**, 81 (2005).

[2] "Cavity Ringdown Spectroscopy of the $\widetilde{A} - \widetilde{X}$ Electronic Transition of the Phenyl Peroxy Radical," G. M. P. Just, E. N. Sharp, S. J. Zalyubovsky, and T. A. Miller, *Chem. Phys. Lett.* **417**, 378 (2006).

[3] "Near-IR Cavity Ringdown Spectroscopy and Kinetics of the Isomers and Conformers of the Butyl Peroxy Radical," B. G. Glover and T. A. Miller, *J. Phys. Chem. A* **109**, 11191 (2005).

[4] "Spectroscopic Probing and Diagnostics of the Geometric Structure of the Alkoxy and Alkyl Peroxy Radical Intermediates," T. A. Miller, *Mol. Phys.* **104**, 2581 (2006).

[5] "Investigation of Ethyl Peroxy Radical Conformers Via Cavity Ringdown Spectroscopy of the $\tilde{A} - \tilde{X}$ Electronic Transition," P. Rupper, E. N. Sharp, G. Tarczay, and T. A. Miller, *J. Phys. Chem. A* **111**, 832 (2007).

[6] "Rovibronic Bands of the $\widetilde{A} \leftarrow \widetilde{X}$ Transition of CH_3OO and CD_3OO Detected with Cavity Ringdown Absorption Near 1.2-1.4 μm," C.-Y. Chung, C.-W. Cheng, Y.-P. Lee, H.-Y. Liao, E. N. Sharp, P. Rupper, and T. A. Miller, *J. Chem. Phys.* (submitted).

[7] "Observation of the $\widetilde{A}-\widetilde{X}$ Electronic Transition of the Isomers and Conformers of Pentyl Peroxy Radical Using Cavity Ringdown Spectroscopy," E. N. Sharp, P. Rupper, and T. A. Miller, (in preparation).

[8] "Spectra and Structure of Alkyl Peroxy Radicals," P. Rupper, E. N. Sharp, and T. A. Miller, *Phys. Chem. Chem. Phys.* (invited review, in preparation).

Reaction Dynamics in Polyatomic Molecular Systems

William H. Miller

Department of Chemistry, University of California, and
Chemical Sciences Division, Lawrence Berkeley National Laboratory
Berkeley, California 94720-1460
millerwh@berkeley.edu

Program Scope or Definition

The goal of this program is the development of theoretical methods and models for describing the dynamics of chemical reactions, with specific interest for application to polyatomic molecular systems of special interest and relevance. There is interest in developing the most rigorous possible theoretical approaches and also in more approximate treatments that are more readily applicable to complex systems.

Recent Progress

There are only a few computational methodologies that are available for treating molecular systems with *many degrees of freedom*, primarily methods based on integrating the classical equations of motion (i.e., classical trajectory calculations ≡ molecular dynamics simulations), and those based on evaluating Feynman path integrals (by Monte Carlo or other statistical sampling methods) for the Boltzmann operator, $\exp(-\beta\hat{H})$. This research program has been focusing in recent years on developing theoretical approaches to chemical dynamics that leverage these two computational methodologies.

The ability to evaluate the Boltzmann operator, $\exp(-\beta\hat{H})$, fully quantum mechanically, for large molecular systems, motivated the development of the *quantum instanton* (QI) model for thermal rate constants for chemical reactions, k(T). The name is due to the relation to a much older semiclassical (SC) approximation[1] for thermal rates that came to be known as the instanton model. The SC instanton model has many qualitatively correct features and insights, but the SC approximation to the Boltzmann operator that is inherent to it was not sufficiently quantitative in early test calculations.[2] The present QI model incorporates the physical ideas of the SC instanton model but is expressed wholly in terms of the *quantum* Boltzmann operator, thus alleviating most of the quantitative deficiencies of the SC version. It's evaluation thus involves (Monte Carlo) evaluation of the path integral expression for the Boltzmann operator, but no real time dynamics. The basic result for the thermal reaction rate is

$$k(T) = Q_r^{-1} \; \frac{\hbar\sqrt{\pi/2}}{\Delta H(T)} \; C_{ff}(0) \; , \tag{1a}$$

where $C_{ff}(0)$ is the zero time flux-flux autocorrelation function

$$C_{ff}(0) = tr\left[e^{-\beta\hat{H}/2} \, \hat{F} \, e^{-\beta\hat{H}/2} \, \hat{F} \right] , \tag{1b}$$

and $\Delta H(T)$ is a particular kind of energy variance (also expressed wholly in terms of the Boltzmann operator). The important practical aspect of Eq. (1) is that its evaluation only requires that of the Boltzmann operator and quantities related to it, and as emphasized above, this can be performed fully quantum mechanically for quite large molecular systems. Most of the papers in the 2004-2006 list below have to do with technical developments related to evaluating the QI rate expression and to its applications to various test reactions.

Paper 2 describes the application to a model of proton transfer in a polar solvent, $AH + B \rightarrow A^- + H^+B$ solvated by 255 methyl chloride molecules (the Azzouz-Borgis model[3]), this calculation also being carried out using the 3d Cartesian coordinates of all the atoms. Of particular interest here, too, is the isotope effect in the rate constant upon replacement of the H atom by D. This model problem is important since it is characteristic of H atom transfer reactions in condensed phases, and also because many different theoretical approaches has been applied to it. Unfortunately, the results of the various approaches differ from each other in various respects, so even though we believe the QI calculations to be the most accurate to date, there is no way at present to be certain of this, for this non-trivial example lies beyond the possibility of a brute-force 'exact' calculation.

Papers 7 and 8 show how the QI rate theory can be put into a particularly convenient form for calculating *kinetic isotope effects* (such as the $H \rightarrow D$ isotope effect noted above in paper 6). This makes use of free-energy perturbation methods in Monte Carlo simulation technology, and it yields an approach for calculating the *ratio* of two rate constants for different isotopic species that is much more efficient than the calculation of the rate constant for either species alone. This should be a particularly useful feature of the QI model.

Papers 4 and 10 deal with the important problem in any transition state-type theory of reaction rates (of which the QI model is one), namely how to choose the best *dividing surface* (DS) for defining the flux operators that appear in the rate expression. Paper 10 shows how the one parameter family of DS's that are normal to the MEP at various distances along it can by used in the QI model. This is a simple but general approach that should be applicable to a wide range of polyatomic systems. It should be emphasized that in this approach the MEP is used solely for the purpose of defining a family of DS's; the dynamical coordinates in which the path integrals are evaluated are still the Cartesian coordinates of all the atoms. Thus the "reaction coordinate", the distance along the MEP, is simply a *parameter* that specifies the particular DS, and is not one of the dynamical coordinates of the system.

Further progress has also been made in developing the initial value representation (IVR) of semiclassical (SC) theory into a practical way of adding quantum effects to classical molecular dynamics (MD) simulations of molecular systems large and small. The simplest version of the SC-IVR is the 'linearized' approximation to it (LSC-IVR), which reduces it to essentially a classical calculation with Wigner distribution functions. Calculating the Wigner function for the Boltzmann operator is thus the hardest part in applying the LSC-IVR, and paper 12 describes how this is greatly simplified by using the thermal Gaussian approximation (TGA) for the Boltzmann operator. Applications to several test problems showed how well this combined TGA-LSC-IVR approach works. It was then used to calculate the velocity-velocity

autocorrelation function for liquid neon, demonstrating that it is indeed possible to implement this approach for large molecular systems.

Paper 15 describes an even more accurate version of the SC-IVR, one that essentially entails no approximation other than the basic SC-IVR approximation itself, and yet it has no more inherent complexity than the LSC-IVR noted above. Applications to several model problems, and to the calculation of flux-flux autocorrelation functions (to give thermal rate constants for chemical reaction), demonstrate the increased accuracy of this approach.

Future Plans

Future efforts are planned to focus on the SC-IVR approach for including quantum effects in classical MD simulations. This is a completely general dynamical framework that allows one to calculate thermal reaction rates, or any other dynamical quantity. It is thus a *complete* dynamical theory, the main goal now being to make it as generally applicable as possible.

References

1. W. H. Miller, J. Chem. Phys. **62**, 1899 (1975).
2. S. Chapman, B. C. Garrett, and W. H. Miller, J. Chem. Phys. **63**, 2710 (1975).
3. H. Azzouz and D. Borgis, J. Chem. Phys. **98**, 7361 (1993); J. Mol. Liq. **61**, 17 (1994); **63**, 89 (1995).

2005 - 2007 (to date) DOE Publications

1. Y. Li and W. H. Miller, "Different Time Slices for Different Degrees of Freedom in Feynman Path Integration," Molec. Phys. **103**, 203-208 (2005). LBL-56194.
2. T. Yamamoto and W. H. Miller, "Path Integral Evaluation of the Quantum Instanton Rate Constant for Proton Transfer in a Polar Solvent," J. Chem. Phys. **122**, 044106.1-13 (2005). LBNL-56319.
3. M. Ceotto, S. Yang and W. H. Miller, "Quantum Reaction Rate from Higher Derivatives of the Thermal Flux-Flux Autocorrelation Function at Time Zero," J. Chem. Phys. **122**, 044109.1-7 (2005). LBNL-56546.
4. C. Predescu and W. H. Miller, "Optimal Choice of Dividing Surface for the Computation of Quantum Reaction Rates," J. Phys. Chem. J. Phys. Chem. B **109**, 6491-6499 (2005). LBNL-56195.
5. W. H. Miller, "Quantum Dynamics of Complex Molecular Systems", Proceedings of the National Academy of Sciences **102**, 6660-6664 (2005). LBNL-56664.
6. M. S. Small, C. Predescu and W. H. Miller, "Quantifying the Extent of Recrossing Flux for Quantum Systems," Chem. Phys. **322**, 151-159 (2006). LBNL-57467.
7. J. Vanicek, W. H. Miller, J. F. Castillo and F. J. Aoiz, Quantum Instanton Evaluation of the Kinetic Isotope Effects, J. Chem. Phys. **123**, 054108.1-14 (2005). LBNL-57468.
8. J. Vanicek and W. H. Miller, "Path Integral Evaluation of the Kinetic Isotope Effects Based on the Quantum Instanton Approximation," in Proceedings of the 8th International Conference on "Path Integrals, from Quantum Information to Cosmology," (JINR Publishing, Dubna, Moscow, Russia) pp. 1-10 (2005). LBNL-58733.

9. S. Yang, T. Yamamoto, and W. H. Miller, "Path-Integral Virial Estimator for Reaction Rate Calculation Based on the Quantum Instanton Approximation," J. Chem. Phys. **124**, 84102.1-9 (2006). LBNL-59146.
10. Y. Li and W. H. Miller, "Using a Family of Dividing Surfaces Normal to the Minimum Energy Path for Quantum Instanton Rate Constants," J. Chem. Phys. **125**, 064104.1-8 (2006). LBNL-59735.
11. W. H. Miller, "Including quantum effects in the dynamics of complex (i.e., large) molecular systems," J. Chem. Phys. **125**, 132305.1-8 (2006). LBNL-60078.
12. J. Liu and W. H. Miller, "Using the thermal gaussian approximation for the Boltzmann operator in semiclassical initial value time correlation functions," J. Chem. Phys. **125**, 224104.1-13 (2006). LBNL-61564.
13. C. Predescu, "Spatially-discretized high-temperature approximations and their *O(N)* implementation on a grid," J. Theor. Comput. Chem. 5, 255 (2006). LBNL-62197.
14. C. Predescu, "Highly optimized fourth-order short-time approximation for path integrals," J. Phys. Chem. B 110, 667 (2006). LBNL-62198.
15. C. Venkataraman and W. H. Miller, "Chemical reaction rates using the semiclassical Van-Vleck Initial Value Representation," J. Chem. Phys. **126**, 094104.1-8 (2007). LBNL-62085.
16. T. F. Miller and C. Predescu, "Sampling diffusive transitions paths," J. Chem. Phys. (accepted). LBNL-62178.

GAS-PHASE MOLECULAR DYNAMICS: Theoretical Studies of Combustion-Related Chemical Reactons and Molecular Spectra

James T. Muckerman (muckerma@bnl.gov)
Chemistry Department, Brookhaven National Laboratory, Upton, NY 11973-5000

Program Scope

This project explores the energetics, dynamics and kinetics of chemical reactions resulting from molecular collisions in the gas phase. The goal of this work is a fundamental understanding of chemical processes related to combustion. We are interested in the microscopic factors affecting the structure, dynamics and reactivity of short-lived intermediates such as free radicals in gas-phase reactions. There is a very strong coupling between the theoretical and experimental efforts in all of the group's work. From the phenomenon of axis-switching in halocarbenes, dynamical aspects of the rovibronic spectrum of methylene to the spectroscopy of coordinatively unsaturated transition-metal-containing species, the interplay between state-of-the-art theory and experiment has provided deep new insights. The theoretical work in spectroscopy seeks to generate extremely accurate benchmark calculations of the electronic structure of systems at the small end of the size scale of interest for comparison with (and as a guide to) high-resolution experimental studies carried out in this program. There is also a strong focus in the theoretical work on the direct dynamics of the reactions of polyatomic molecules involving species being studied in the experimental part of the program.

Recent Progress

Vibronic spectrum calculation of HCCl and DCCl in three low-lying states

We have carried out a combined experimental and theoretical study on the vibronic energies and transition intensities of the $A\ ^1\mathrm{A}''$–$X\ ^1\mathrm{A}'$ bands. The theoretical calculations were carried out on our MRCI/aug-cc-pVTZ dipole moment and potential energy surfaces. These surfaces were interpolated using a general DVR interpolation technique from thousands of grid points. The quantum dynamics (QD) problem of nuclei was solved using a variational *K*-dependent QD approach in hyperspherical coordinates including the Renner-Teller effect.

The experimental and theoretical results have revealed that the C-Cl stretching vibration in the excited state was previously mis-assigned. The revised frequency corrects an anomalously large apparent anharmonicity in this mode and permitted a recalibration of the *ab initio* potential energy surface for the state. This, in turn, allowed the assignment of many shorter wavelength bands observed by other workers and an accurate calculation of vibronic band positions and intensities in this spectrum. Intensity was also found for transitions involving C-H stretching (ν_1) excitation in the ground state due to an anharmonic resonance between $X(100)$ and $X(012)$.

Similarly, the spin-orbit couplings between the $X\ ^1\mathrm{A}'$ and $a\ ^3\mathrm{A}''$ states of HCCl/DCCl have been further studied. The relative position of the triplet state of HCCl to the singlet ground state is predicted to be 2122 cm^{-1}. This prediction was just confirmed by Reid et al. (with Sears & Yu).

Calculation of ground and excited states of transition metal species

We have calculated the energies, spectroscopic constants and dipole moments for the low-lying electronic states of several first transition metal series hydrides at a very high level of theory (MRCI-SD from a very large CASSCF reference function). As pointed out by Walch and Bauschlicher, Fe and V are complicated by the fact that the low-lying $(3d)^{n+1}(4s)^1$ excited configuration of the atom is nearly degenerate with the $(3d)^n(sp)^1(\overline{sp})^1$ sp-hybrid state required for bonding with H, thereby mixing electronic configurations in the lowest states of the FeH and VH molecules. The results for FeH were compared to the experimental results in order to calibrate the level of theory required to obtain a sufficiently accurate description of its electronic states. In particular, we systematically expanded the full-valence active space in order to obtain

the correct ordering of the $^6\Delta$ and ground $^4\Delta$ states at both the MRCI and MRCI+Q levels of theory using a large basis set. The addition of what amounts to the 5s and 5p Fe orbitals to the active space allows for both a polarizing dπ orbital and a 4pπ orbital in the molecular configurations (otherwise the 4pπ orbital would be missing). Analogous calculations on VH predict a similarly complicated set of low-lying states. Related experimental work directed toward the detection of the electronic spectrum is described above. (with Sears & Wang)

Multi-reference configuration interaction calculations of the low-lying states of TiC_2 and the ground electronic state of Ti_8C_{12}

Using a recently acquired 64-bit AMD Opteron Linux cluster with very large memory, we have finished a project involving multi-reference configuration interaction (MRCI) calculations on the electronic structure and properties of the metcar precursor molecule TiC_2 with no restrictions on the reference function. We have also carried out a corresponding series of CCSD geometry optimizations and single-point CCSD(T) calculations to corroborate our MRCI and MRCI+Q results in view of our discovery of a plethora of conical intersections involving the four lowest (triplet) states of TiC_2 in the vicinity of the (nested) equilibrium structures.

We have also employed MRCI calculations to determine whether the ground electronic state of the Ti_8C_{12} "metcar" is a singlet or a triplet state. Spin-polarized (spin-unrestricted) DFT calculations predict a triplet ground state, while our earlier MP2 and QCISD calculations correlating all 80 valence electrons predicted a singlet ground state. The answer is of great importance to the question of whether this metcar will be stable when deposited on a support, *i.e.*, whether it will disproportionate or polymerize rather than retain its structural and chemical integrity.

Energetics and dynamics of the reaction of O_2 with HOCO

The important combustion reaction of O_2 with HOCO has been studied using an *ab initio* direct dynamics method based on the UB3PW91 density functional theory (DFT). This DFT method is selected by minimizing the errors of the relative energies of the stationary points on the ground-state electronic surface of $HOC(O)O_2$ with respect to the best *ab initio* values of Poggi and Francisco. Results show that the reaction can occur *via* two mechanisms: direct hydrogen abstraction and an addition reaction through a short-lived $HOC(O)O_2$ intermediate. The lifetime of the intermediate is predicted to be 660±30 fs. Although it is an activated reaction, the activation energy is only 0.71 kcal/mol. The thermal rate coefficients are calculated over the temperature range 200-1000 K. The values vary from 1.36×10^{-12} $cm^3molec^{-1}s^{-1}$ at 200K to 7.08×10^{-12} $cm^3molec^{-1}s^{-1}$ at 1000 K. At room temperature, the obtained thermal rate coefficient is 2.1×10^{-12} $cm^3molec^{-1}s^{-1}$, which is in good agreement with the experimental results of 1.44×10^{-12}-1.90×10^{-12} $cm^3molec^{-1}s^{-1}$. Compared to the OH + HOCO reaction, this reaction is about an order of magnitude slower (with Yu).

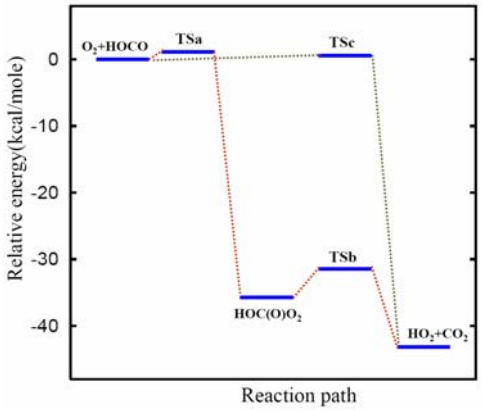

A B3PW91 energy diagram for the O_2 + OCO reaction

Future Plans

Kinetics and dynamics study of the reaction of HOCO with atomic oxygen

We will apply our direct *ab initio* molecular dynamics program for studying some important combustion reactions. Currently, of particular interest is the reactivity of the HOCO radical reaction with oxygen atom and molecule. For the O + HOCO reaction, in collaboration with J. Francisco (Purdue), we will address the energies, geometries, and vibrational frequencies of the stationary points on the ground-state doublet

potential energy surface, and the reaction mechanism by using a SAC/UCCD method. Besides the kinetics and dynamics studies of the reaction, we also hope to predict the lifetime of the HOC(O)O intermediate produced through the reaction course. The temperature dependence of the thermal rate constants will be calculated (with Yu & J. Francisco).

Spectroscopy and structure of transition metal-containing species

Following the initial work on transition metal hydrides described above, work in this area is proposed along two main fronts. Both are directed toward the detection and characterization of intermediates postulated to be important in heterogeneous catalysis systems as well possessing intrinsic chemical interest. Coordinated experimental and theoretical studies of small transition metal-containing species in the gas phase will continue with new focus on VN, RhN, IrN and TiC_2. (with Sears and Wang)

Triplet channel in CH_2 + HCCH

One aspect of the reaction of methylene with acetylene that was neglected in the previous quantum force trajectory studies is the possible role of the triplet state of the adduct. Reaction dynamics were computed under the influence of the ground singlet surface, yet the triplet state of the biradical obtained by transient ring-opening of the cyclopropene intermediate is known to be lower in energy than the singlet biradical, as is the asymptotic $^3CH_2$ + HCCH channel lower in energy than the $^1CH_2$ + HCCH asymptote. It is unclear where the surface crossings occur or what influence they may have on this reaction. Further investigation of this reaction is warranted by both experimental and computational means. Experimentally, the marginal effect of added HCCH on the double-exponential decays of singlet methylene in rare gas can probe the $^3CH_2$ channel. Theoretically, the stationary points of the lowest triplet potential energy surface will be computed at a high level of theory and their relative energies fit with a cheaper method with analytic gradients by scaling the computed correlation energy by a global constant. New direct dynamics (QFMD) trajectories will then be computed on the singlet surface and the energies of both the singlet and triplet surface will be monitored along each trajectory to determine where crossings occur. Finally, we will compute surface-hopping trajectories to estimate the importance of non-adiabatic effects due to spin-orbit coupling in the dynamics of the reaction. (with Yu and Hall)

Acknowledgment

This work was performed at Brookhaven National Laboratory under Contract DE-AC02-98CH10886 with the U.S. Department of Energy and supported by its Division of Chemical Sciences, Office of Basic Energy Sciences.

Publications since 2005

Ab initio and direct dynamics studies of the reaction of singlet methylene with acetylene, and the lifetime of the cyclopropene complex, H.-G. Yu and J.T. Muckerman, J. Phys. Chem. A **109**, 1890-1896 (2005).

Product Study of the Reaction of CH_3 with OH Radicals at Low Pressures and Temperatures, C. Fockenberg, R.A. Weston, Jr. and J.T. Muckerman, J. Phys. Chem. B **109**, 8415-8427 (2005).

Direct Ab Initio Dynamics Study of the OH + HOCO Reaction, H.-G. Yu, J.T. Muckerman and J.S. Francisco, J. Phys. Chem. A **109**, 5230-5236 (2005).

Potential energy surfaces and vibrational energy levels of DCCl and HCCl in three low-lying states, H.-G. Yu, T.J. Sears and J.T. Muckerman, Mol. Phys. **104**, 47 (2006).

Quantum molecular dynamics study of the reaction of O_2 with HOCO, H.-G. Yu and J.T. Muckerman, J. Phys. Chem. A **111**, 5312 (2006).

Multi-reference configuration interaction calculations of the low-lying states of iron and vanadium monohydride, FeH and VH, Z. Wang, T. J. Sears and J. T. Muckerman, J. Chem. Phys. (submitted).

Related publications in Nanocatalysis and the Hydrogen Fuel Initiative

Sulfur Adsorption and Sulfidation of Transition Metal Carbides as Hydrotreating Catalysts, P. Liu, J.A. Rodriguez and J.T. Muckerman, J. Mol. Catal. A: Chem. **239**, 116-124 (2005).

First-principles study of Ti-catalyzed hydrogen chemisorption on an Al surface: A critical first step for reversible hydrogen storage in $NaAlH_4$, S. Chaudhuri and J.T. Muckerman, J. Phys. Chem. B **109**, 6952 (2005).

Hydrogen Oxidation and Production Using Nickel-Based Molecular Catalysts with Positioned Proton Relays, A.D. Wilson, R.H. Newell, M.J. McNevin, J.T. Muckerman, M. Rakowski DuBois, and D.L. DuBois, J. Am. Chem. Soc. **128**, 358-366 (2006).

Kinetic Studies of the Photoinduced Formation of Transition Metal-Dinitrogen Complexes Using Time-Resolved Infrared and UV-vis Spectroscopy, D.C. Grills, K.-W. Huang, J.T. Muckerman and E. Fujita, Coord. Chem. Rev. **250**, 1681 (2006).

Transition State Characterization for the Reversible Binding of Dihydrogen to Bis(2,2´-bipyridine)rhodium(I) from Temperature- and Pressure-Dependent Experimental and Theoretical Studies, E. Fujita, B.S. Brunschwig, C. Creutz, J.T. Muckerman, N. Sutin, D. Szalda and R. van Eldik, Inorg. Chem. **45**, 1595 (2006).

Adsorption of platinum on the stoichiometric $RuO_2(110)$ surface, P. Liu, J.T. Muckerman and R.R. Adzic, J. Chem. Phys. **124**, 141101 (2006).

Reaction of thiophene with metcar $Ti_8C_{12}^+$ nanoparticles, P. Liu, J.M. Lightstone, J.A. Rodriguez, J.T. Muckerman and M.G. White, J. Phys. Chem. B **110**, 7449 (2006).

Direct Measurements of Rate Constants and Activation Volumes for the Binding of H_2, D_2, N_2, C_2H_4 and CH_3CH to $W(CO)_3(PCy_3)_2$: Theoretical and Experimental Studies with Time-Resolved Step-Scan FTIR and UV-Vis Spectroscopy, J. Am. Chem. Soc. **128**, 15728-15741 (2006).

Understanding the role of Ti in reversible hydrogen storage as sodium alanate: A combined experimental and first-principles theoretical approach, S. Chaudhuri, J. Graetz, A. Ignatov, J.T. Reilly and J.T. Muckerman, J. Am. Chem. Soc. **128**,11404 (2006).

Pressure-induced structural and electronic changes in α-AlH_3, J. Graetz, S. Chaudhuri, Y. Lee, T. Vogt, J.T. Muckerman and J.J. Reilly, Phys. Rev. B **74**, 214114 (2006).

Nature of hydrogen interactions with Ni(II) complexes containing cyclic phosphine ligands with pendant nitrogen bases, A.D. Wilson, R.K. Shoemaker, A. Miedaner, J.T. Muckerman, D. L. DuBois and M. Rakowski DuBois, Proc. Natl. Acad. Sci. USA, online (2007).

Photochemical and Radiolytic Production of Organic Hydride Donor with Ru(II) Complex Containing an NAD^+ Model Ligand, D. Polyansky, D. Cabelli, J.T. Muckerman, E. Fujita, T. Koizumi, T. Fujushima, T. Wada and K. Tanaka, Angew. Chem. Int. Ed. (in press).

Electronic Structure of ZnO Nanowire, X. Shen, M.R. Pederson, J.-C. Zheng, J.W. Davenport, J.T. Muckerman and P.B. Allen, Phys. Rev. B (submitted).

First-Principles Studies on the Structural and Electronic Properties of $(Ga_{1-x}Zn_x)(N_{1-x}O_x)$ Solid Solution Photocatalyst, L. Zhao, J.T. Muckerman and M.D. Newton, J. Phys. Chem. C (submitted).

Wire versus Tube: Stability of Small One-Dimensional ZnO Nanostructures, X. Shen, P.B. Allen, J.T. Muckerman, J.W. Davenport and J.-C. Zheng, Nanolett. (submitted).

Theoretical Investigation of the Binding of Small Molecules and the Intramolecular Agostic Interaction at Tungsten Centers with Carbonyl and Phosphine Ligands, J.T. Muckerman, E. Fujita, C.D. Hoff and G.J. Kubas, J. Phys. Chem. B (submitted).

Dynamics of Activated Molecules

Amy S. Mullin
Department of Chemistry and Biochemistry, University of Maryland, College Park, Maryland, 20742
Email: mullin@umd.edu

Program Scope

Hydrocarbons are primary constituents of combustion fuels and their chemistry under high temperature conditions is determined in part by their reactivity and in part by their collisional behavior. High energy molecules play important roles in the chemical and physical processes in combustion, both as reactive species and as energy transporters through collisions. Understanding the behavior of high energy molecules poses significant challenges, in part because of their transient natures, the large number of states involved and our lack of knowledge as to how they interact with neighboring species. Currently most efforts to model complex reactive environments account for the effect of collisions on multi-component multi-reaction rates using average energy transfer values. This approach works reasonably well for some reactions but is inadequate for many practical combustion processes such as bimolecular reactions that take place over deep potential wells. For these reactions, rate coefficient calculations are sensitive to the shape of the energy transfer distribution function and require a more accurate description of energy transfer. A goal of my research program is to develop a better understanding of energy transfer of large molecules under combustion conditions.

The focus of my research program is to investigate the physical and chemical properties of molecules with large amounts of internal energy using novel experimental and theoretical approaches in order to gain new insights into the microscopic details of relatively large complex molecules at high energy. To overcome the inherent difficulties of developing a molecular level understanding of high energy molecules, we use high resolution transient IR probing to measure energy gain in small collision partners or reaction products that result from collisions of high energy molecules. Using this technique, we have preformed in-depth spectroscopic studies that provide a greater understanding of high energy molecules and their collisional energy transfer.

Recent Progress

Energy dependence of strong collisions: azulene (E=19,700 and 38,500 cm^{-1}) with CO_2

We have measured the dynamics of strong collisions of vibrationally excited azulene and CO_2 in order to explore the energy dependence of strong collisions. In these studies, azulene was excited with λ=532 and 266 nm to prepare highly excited molecules with E_{vib}~19,700 and 38,500 cm^{-1} respectively. Previously we investigated the state-resolved energy-dependent quenching of hot donor molecules over smaller ranges of initial energy. Pyrazine (E_{vib}=32000 to 41000 cm^{-1}) and pyridine (E_{vib}=37000 to 41000 cm^{-1}) were quenched with CO_2 and the strong collisions were characterized for 6-10 energies over the range of donor energies. We found that the scattered CO_2 rotational and translational energy distributions are invariant to changes in donor energy with the exception that for pyrazine a step-wise increase is seen near a threshold energy of E_{vib}= 37000 cm^{-1}. For pyrazine, the energy transfer rates increase monotonically with increasing donor energy and as the initial energies increase above the threshold, the rate increase becomes more pronounced. For pyridine, both the energy distributions and energy transfer rates are insensitive to changes in the donor energy. These results were surprising because physical intuition suggests that the distribution of transferred energy must depend on the donor's internal energy. For the high internal energies of pyrazine studied, the CO_2 energy gain distributions extend beyond ΔE~10,000 cm^{-1}. After the hot donor has undergone collisional relaxation and come to thermal equilibrium with the bath, we expect the energy transfer distribution function to have much lower probabilities for the large ΔE collisions. Yet our results showed that the strong collisions were not particularly sensitive to a 25% decrease in donor energy. These observations motivated us to study a molecule for which a broader range of initial energies could be prepared.

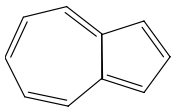

Azulene

Our energy-dependent studies on azulene(E_{vib}):CO_2 supercollision dynamics reveal that the amount of energy transferred through single strong collisions scales approximately linearly with the azulene vibrational energy. The rotation and (center-of-mass) translational energies for the scattered CO_2 increase as a function of azulene energy, as shown here. For a doubling of donor energy, the average rotational energy of the scattered high-J CO_2 molecules increases by a factor of 1.7 and the average translational energy increases by a factor of 1.8. The average changes in CO_2 rotational energy $\langle \Delta E_{rot} \rangle = k_B (T_{rot} - T_0)$ and translational energy $\langle \Delta E_{trans} \rangle = k_B (T_{trans} - T_0)$ increase by a factor of ~3 for a doubling a donor energy, based on T_0=300 K. The energy transfer probability for energy gain into high-J CO_2 has an energy dependence that is stronger than linear with respect to donor energy, with energy transfer rate increasing by a factor of 4 for a doubling of the donor energy.

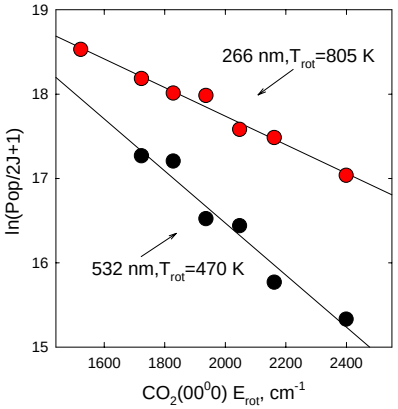

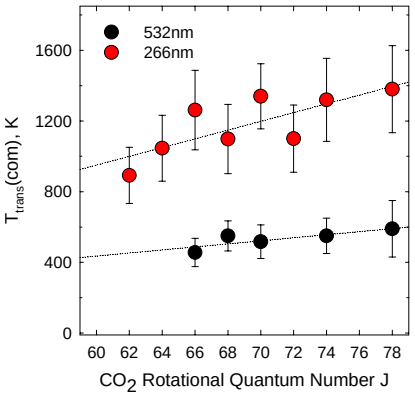

We have used our azulene results to determine the energy transfer distribution function P(ΔE) for the strong collisions of azulene with CO_2 at both excitation energies. Previously in other work, we showed that in the strong collisions of methylated pyridines with CO_2, the curvature of P(ΔE) correlates with the energy dependence of the donor's vibrational state density ρ. We explained this observation using ideas based on Fermi's Golden Rule. As an aside, our azulene energy-dependent data agree extremely well with predictions from our model. It is noteworthy that the energy dependence observed for azulene is consistent with the apparent lack of energy dependence for pyrazine and pyridine relaxation. The range of excitation energies used in the pyrazine and pyridine studies was such that the state-density energy dependence did not change by an appreciable amount and hence did not have much of an effect on the curvature in the energy transfer distribution function. In this situation, the energy transfer distribution function does not change its curvature. However, the difference in excitation energies in the azulene study is large enough so that the state-density energy dependence is appreciably different and the energy transfer shows a substantial dependence on the donor energy.

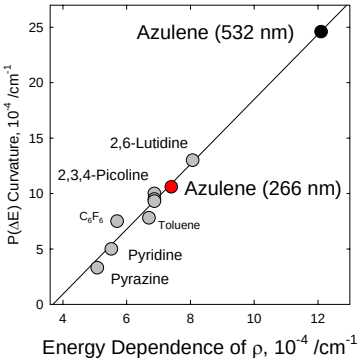

Dynamics of strong collisions of highly excited alkylated pyridines with CO_2

We have performed a series of experiments designed to test how alkylation of hot donor molecules affects their strong collisional relaxation. We used CO_2 to quench highly excited ethyl- and n-propyl-pyridine initially prepared with E_{vib}~38,500 cm^{-1} and measured the state-resolved energy gain dynamics for high J states of CO_2. The results are compared with earlier work on pyridine and methyl-pyridine. We find that the strong collisions impart to CO_2 rotational and translational energy that generally decreases with increasing alkyl chain length. The energy exchanged through strong collisions is most sensitive to replacement of the H atom with an alkyl group and of these donors, pyridine imparts the most energy to CO_2. The CO_2 rotational energy gain from

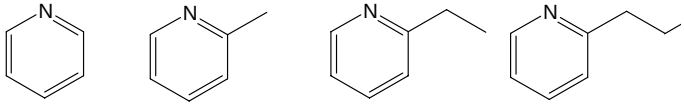

Pyridine (Pyd) | 2-Methylpyridine (2MP) | 2-Ethylpyridine (2EP) | 2-Propylpyridine (2PP)

collisions with pyridine is 25% larger than for the alkylated donors and the CO_2 translational energy gain from pyridine is approximately twice that of the alkylated donors. The prevalence of strong collisions for pyridine is apparent from a comparison of the energy transfer distribution functions. We see that the probability of strong collisions decreases with increasing donor size for pyridine, methyl pyridine and ethylpyridine but increases for propylpyridine relative to ethylpyridine. Dynamical effects such as large amplitude motion of the longer chain alkyl groups or ring closing mechanisms may be responsible for this observation. Statistically, the strong collisions will be reduced for donors with longer alkyl chains since the average energy per mode is smaller. Dynamically, however, the longer chains have increased flexibility and higher state densities in those floppy modes that may enhance energy loss via strong collisions. It is also possible that the vibrational energy distribution between the aromatic ring and the propyl chain is nonstatistical.

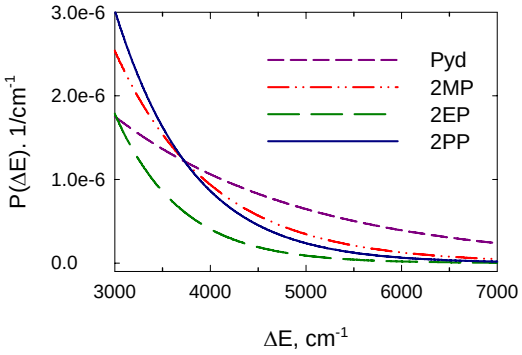

Measuring dynamics of weak collisions

Collisional energy transfer of large molecules containing sizable amounts of energy poses major challenges to the experimentalist. Strong collisions scatter bath molecules into states that are well removed from ambient background population in final states that can be readily identified. However, the probability for strong collisions is generally much smaller than that for weak collisions, so the signal levels are small. Weak collisions are more likely to occur than strong collisions, so weak collisons generally have large signals, but because they impart only modest energy changes to the bath molecules, detection of their energy partitioning must somehow be extracted from the ambient population of the bath molecule. In this funding cycle we have performed key experiments with DOE support that have allowed us to uniquely characterize the weak collisions of pyrazine (E_{vib}=38,000 cm^{-1}) with HOD. Prior to being awarded our DOE funding, we collected transient linewidth data for low J states of HOD (000). The line profiles are characterized by double Gaussian functions that include appearance of scattered molecules and depletion of absorption from the ambient background. The appearance profiles are broadened relative to the depletion profiles and unique fits to the data are found. However, without further information, the appearance data could not unequivocally be assigned to V–RT collisional energy transfer from hot pyrazine. Two additional collisional processes could impact the measured appearance of HOD molecules. Isotope exchange reactions of vibrationally hot pyrazine with D_2O could lead to formation of HOD and V–V collisional energy transfer could produce vibrationally excited HOD in the (001) state that would interfere with absorption measurements that use the 000→001 probe transition. With DOE support, we addressed both of these issues and found no evidence for either the H/D exchange reactions or for vibrational excitation of the HOD (001) state. Because the absorption data are collected at short times relative to the average collision time, the appearance and depletion signals correspond to distinct populations of molecules and the net signal is a sum of the two sub-populations. This approach leads to an absolute measurement of the appearance of scattered molecules in low J states and complements our studies on the strong collisions of HOD.

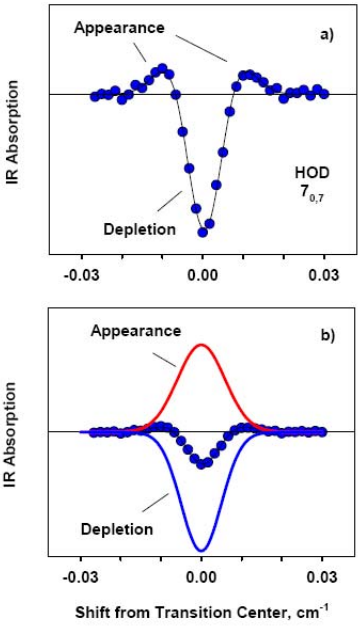

The low-J appearance data provides a trove of interesting information. 1) Nascent population data for the appearance of low J states have nearly the same rotational distribution as the high J data with

T_{rot} =430 K for the entire distribution, falling within 3% of that for the high-data alone. As far as we know, these data are the first case in which both the weak and strong collisions have been characterized for high-energy molecules. 2) The center of mass velocity distributions of the scattered HOD molecules in all states measured (high-J and low-J) have translational temperatures near 500 K, irrespective of rotational state and angular momentum relative to the molecular axes. 3) The transient depletion lineshapes for the low-J states are a measure of the J-dependent velocity distributions for molecules that are among the most likely to be involved in collisional energy transfer. We find that the depletion lineshapes are well described with translational temperatures near T_{trans}~300 K, which is the ambient cell temperature. This result provides insight into the initial distribution of HOD molecules involved in collisional energy transfer with high energy molecules.

Collision rates from transient IR absorption studies

The ability to characterize the outcome of weak collisions is a major step toward understanding the collisional energy transfer of large molecules. Combining population data for the nascent low energy rotational states of HOD with the strong collision data yields an excellent description of the scattered HOD molecules from which we directly determine the collision rate.

For a discrete set of states indexed by J, the average energy for these states is the sum of the fractional population f_J times the energy E_J of each state.

$$\langle E_{rot}\rangle_{obs} = \sum_J f_J E_J = \sum_J \frac{g_J e^{(-E_J/k_B T_{rot})}}{Q_{rot}} E_J = 438 \pm 56 \text{ cm}^{-1} = \sum_J \frac{k_J}{k_{col}} E_J$$

The fractional HOD population f_J for each state is equivalent to the ratio of the appearance rate constant k_J to the collision rate k_{col}. Using experimental measurements of the appearance rates (k_J) and the rotational distribution (T_{rot}) of the scattered molecules, we find that the collision rate for pyrazine(E) with HOD is $k_{col}=1.7\times10^{-9}$ cm^3 molecule^{-1} s^{-1}. This value is 1.7 times larger than the Lennard-Jones collision rate and 3 times larger than the hard sphere rate. It is important to recognize that our collision rate accounts for all collisions that lead to formation of HOD(000). It is possible that the bending mode near 1600 cm^{-1} is also excited through collisions to generate the (010) state, but estimates based on data for collisional excitation of the bend in H_2O suggest that the V–V energy transfer in water is a relatively low probability pathway. Whether the observed collision rate depends on the amount of vibrational energy in the highly excited donor remains to be determined.

Future Plans

Future plans include energy-dependent measurements of supercollision energy transfer, investigations of weak collisional energy transfer for other donor:acceptor pairs including DCl, HCl, CH_4, CD_4 and D_2O, and studies of reactions of highly vibrationally excited molecules with OH radicals.

Publications supported by DOE 2005-2007

1. "Trajectory study of supercollision relaxation in highly vibrationally excited pyrazine and CO_2" Ziman Li, Rebecca Sansom, Sara Bonella, David Coker and Amy Mullin, Journal of Physical Chemistry A. **109**, 7658-7666 (2005).
2. "Quenching dynamics of highly excited azabenzenes with DCl: The role of the energy acceptor," Ziman Li, E. Korobkova, K. Werner, L. Shum, A. S. Mullin, Journal of Chemical Physics **123**, 174306 (2005).
3. "Relaxation dynamics of highly vibrationally excited picoline isomers (E_{vib} =38300 cm^{-1}) with CO_2: The role of state density in impulsive collisions," Elisa M. Miller, Liat Murat, Nicholas Bennette, Mitchell Hayes, and Amy Mullin, Journal of Physical Chemistry A. 110, 3266-3272 (2006).
4. "Direct determination of collision rates beyond the Lennard-Jones model through state-resolved measurements of strong and weak collisions," D. K. Havey, Q. Liu, Z. Li, M. S. Elioff, M. Fang, J. Neudel and A. S. Mullin, Journal of Physical Chemistry A 111, 2458 (2007).
5. Alkylation Effects on Strong Collisions of Highly Vibrationally Excited Alkylated Pyridines (E_{vib}~38800 cm^{-1}) with CO_2" by Qingnan Liu, Juan Du, Daniel K. Havey, Ziman Li, Elisa M. Miller and Amy S. Mullin, Journal of Physical Chemistry A, in press (2007).

Reacting Flow Modeling with Detailed Chemical Kinetics

Habib N. Najm

Sandia National Laboratories
P.O. Box 969, MS 9051, Livermore, CA 94551
hnnajm@sandia.gov

1 Program Scope

The purpose of this research program is to improve our fundamental understanding of reacting flow, thereby advancing the state of the art in predictive modeling of combustion. The work involves: (1) Using computations to investigate the structure and dynamics of flames in unsteady vortical flows; (2) Developing techniques for analysis of multidimensional reacting flow; (3) Developing numerical methods for discretizing reacting flow systems of equations with detailed kinetics and transport; (4) Developing massively parallel codes for computing large scale reacting flow with detailed kinetics; and (5) Developing means for uncertainty quantification in reacting flow computations, including Bayesian methods for construction of uncertain chemical models from experimental data.

2 Recent Progress

2.1 Reacting Flow Computations, Analysis, and Model Reduction

We have continued to use targeted one and two-dimensional (1D/2D) reacting flow computations with detailed chemical kinetics as benchmarks for the examination of *a-posteriori* accuracy of simplified chemical models. These studies focus on hydrocarbon fuels, hitherto including methane and n-heptane flames. The model simplification/reduction strategy is based on Computational Singular Perturbation (CSP) theory. We use CSP to analyze precomputed reacting flow databases, to identify low dimensional manifolds of specific chemical systems, and to generate corresponding simplified chemical models. Using 1D premixed methane-air flame studies starting with GRImech3.0, we examined the errors in computed flame structure from a range of simplified models corresponding to various choices of the CSP error tolerance and the choice of kernel species in the reduction strategy. We find general convergence trends with decreased tolerance thresholds, and a controlled level of accuracy on the specific choice of kernel species. We have continued *a-posteriori* accuracy studies in transient 2D flame-vortex interactions, and have also further developed our code-base to allow computations of edge flames stabilized against prescribed mixing layers. We computed methane-air edge flames using GRImech3.0 with fuel and air streams with varying degrees of N_2-dilution, and equivalence ratio gradients. We analyzed the computed edge flame structure using CSP. The results identified the spatial structure of the underlying low dimensional manifolds, via the spatial distribution of the driving timescale τ_{M+1}, and the number of exhausted modes M. We find generally low values of τ_{M+1} and M within the edge flame and the trailing non-premixed flame, a general indication of the locally high degree of chemical activity. However, we also find non-trivial topology of these fields within the flame structure. Results were used to generate simplified chemical mechanisms corresponding to different regions of the edge flame structure, as well as comprehensive models for the overall system. We have also used CSP analysis for the study of chemical systems exhibiting oscillatory behavior. Such systems are characterized by alternating time periods of growth and relaxation behavior. The analysis results allowed probing of the underlying manifold structure, when such manifolds exist, during different phases of the dynamics, thereby elucidating the driving aspects of the dynamics in each phase.

2.2 Model Construction

The construction of models from empirical data, whether in terms of model structure or parameter values, is a classic inverse problem. Bayesian inference provides an attractive setting for the solution of inverse problems, where detailed accounting of uncertainties in the resulting models is of interest. Measurement errors, forward model uncertainties, and complex prior information can all be combined to yield a rigorous and quantitative assessment of uncertainty in the inverse solution. However, obtaining useful information from the posterior density may be computationally expensive. For complex forward models, the cost of likelihood evaluations may render

the Bayesian approach prohibitive. We have continued to develop constructions designed to accelerate Bayesian inference in computationally intensive inverse problems using Polynomial Chaos (PC) representations of random variables/fields, and associated spectral methods for efficient uncertainty propagation. Uncertain inputs that span the range of the prior define a stochastic forward problem; a Galerkin solution of this problem with the PC basis yields a spectral representation of uncertain forward model predictions. Evaluation of integrals over the unknown parameter space is then recast as sampling of the random variables underlying the PC expansion, with significant speedup. We had previously demonstrated this strategy for efficient inference of discrete model parameters, formulated as random variables. More recently, we extended this approach to systems where inference of field quantities is of primary interest. Such problems can be especially taxing from a computational perspective due to high dimensionality. Thus, for example, the naive representation of field quantities in terms of their discretized values on a computational mesh leads to exceedingly high dimensional inverse problems that are computationally taxing in the deterministic context, let alone the stochastic Bayesian context. In this regard, we employed means of dimensionality reduction, using the Karhunen-Loéve (KL) representation of the random fields in question. Such means of representation of field quantities are effective because of the underlying regularity of these fields. As a result, a few KL modes can be sufficient for representation of the relevant spatial content of a typical random field quantity. Using KL representations in the Bayesian context enabled an order of magnitude reduction in computational expense in 1D inverse problems. Further, coupling KL with PC constructions allowed achievement of yet another order of magnitude speedup in this class of problem.

We have also continued our work on Bayesian parameter estimation using T. Settersten's experimental measurements of the rate of quenching of NO $A^2\Sigma^+(v'=0)$ probed by two-photon laser-induced fluorescence using a picosecond laser. The goal is to arrive at rigorous estimates of uncertainties in quenching-rate parameter values inferred from data. Besides their inherent value, these uncertainties, particularly when formulated probabilistically, are key pre-requisites for subsequent uncertainty quantification studies that rely on models built with empirically-estimated parameters. Our recent progress in this context focused on detailed comparisons with traditional root-mean-square (RMS) estimation of parameter values and associated uncertainties. We found that, when the detailed aspects of instrument noise are neglected, presuming noise levels independent of signal amplitude, then the RMS means and standard deviations were consistent with marginal parametric probability density functions available from the Bayesian analysis. On the other hand, significant differences in parametric uncertainties were evident when using the true error model of the instrument in the Bayesian analysis. Comparisons with weighted least-squares methods should exhibit agreement in this latter context. Further, in an effort to make the Bayesian analysis more easily accessible to non-experts, we have assembled a C-library that facilitates the utilization of Bayesian inference for discrete parameter estimation problems, and are promoting its use by experimental investigators.

2.3 High-Order Structured Adaptive Mesh Refinement

We have continued scalability studies using high-order uniform/adaptive mesh constructions for reacting flow computations. Mesh partitioning strategies are key to achieving scalability, and are therefore an important feature of our work. The main thrust of our load partitioning philosophy is the construction of a meta-partitioner - a control system that maps a certain characterization of a Grid Hierarchy (GH) to a set of partitioner configuration parameters for optimal partitioning. This requires us (1) to characterize an incoming GH for its amenability for load-balance or communication-efficiency, (2) to characterize a GH for its amenability to be partitioned for reduction of data migration, and (3) to have a characterization of the partitioner with respect to its configuration parameters i.e. a sensitivity study. We have progressed in each of these areas. We developed an analytical approach by which a given GH could be characterized for its *amenability* for domain-based or patch-based partitioning. This amenability places the GH in a continuous spectrum between patch- and domain-based methods. We have also developed a quantitative theory that identifies the potential load balance gain by migrating certain patches. We also addressed the minimization of data migration costs as we try to realize a recommended partitioner. We also conducted a preliminary sensitivity study of salient parameters of a partitioner library that can accomodate both domain- and patch-based approaches.

Our operator-split construction with implicit chemistry integration leads to an uneven computational load across grid cells, with the flame region accounting for the bulk of the load. We conducted a study where partitioning was done purely based on chemistry-integration loads; however scalability improvements over the default partitioner were modest. The principal reasons were (1) the chemisty-integration load was only 2-3 times larger than transport (i.e. one could not ignore transport completely) and (2) the chemistry load was concentrated in the flame region, which also had the largest grid cell density (and thus transport-integration load). Consequently,

both geometric and chemistry-load based partitioning strategies yielded similar grid partitions and scalability. This study indicated that a more sophisticated approach, including both chemistry and transport integration costs, would be required to deliver scalability.

2.4 CSP/PRISM Adaptive Chemistry

We have developed a tabulation strategy for the numerical integration of chemically reacting flow processes on the basis of a non-stiff system of equations. Both the tabulation and the identification of the non-stiff system are adaptive and are based on CSP. The tabulation strategy is implemented in order to store and reuse the CSP quantities required for the construction of the local non-stiff model. Our tabulation borrows from M. Frenklach's "Piecewise Reusable Implementation of Solution Mapping" (PRISM) technique the utilization of hypercubes in the chemical configuration space and the polynomial regression of response surfaces, and adapts them to address the specific challenges of CSP, while exploiting the reduction of dimensionality offered by CSP.

Our approach involves (1) a table construction phase, where the distribution and sizes of individual hypercubes are determined, along with the assessment of optimal local manifold dimensionality and the response surface representation of CSP quantities; and (2) a time integration phase using the tabulated information. One particular feature of our algorithm is the CSP "homogeneous correction", which allows for an accurate and efficient identification of the manifold on which the solution moves according to the slow time scales. This correction can be used to project any state vector picked at random in an N-dimensional hypercube onto a neighborhood of an $(N-M)$-dimensional manifold, and is used in the determination of manifold dimensionality during the table construction phase. Moreover, by projecting the state vector onto the manifold during the integration phase, computational savings can be achieved, since the exhausted fast scales are eliminated and the number of time steps needed to accurately integrate the slow dynamics of the original system of differential equations is significantly smaller. We have demonstrated, using a 3-dimensional analytical model system, the improved efficiency of this approach in both constructing the slow model and simulating the system dynamics along the manifold.

3 Future Plans

3.1 Reacting Flow Computations, Analysis, and Model Reduction

We plan to continue and expand ongoing work on the analysis of simplified chemical models in targeted 1D/2D reacting flow computations, including both premixed flame-vortex interactions and edge flames. These studies will span different fuels over ranges of operating conditions. We will conduct detailed analysis of computed edge flame structure using CSP. We will also continue ongoing work on the development of our reacting flow code towards a distributed parallel axisymmetric construction. Initial steps in this regard are underway, in terms of conversion of the existing rectangular code from shared memory parallelism towards a combined distributed/shared construction. This will be followed by implementation of axisymmetric discretizations.

3.2 Uncertainty Quantification in Reacting Flow

We plan to improve the utility of our existing multiwavelet-based multiresolution analysis (MRA) PC code for uncertainty quantification (UQ), by suitable code redesign in a manner that incorporates it in our UQ library. This will enable easy use of MRA PC UQ for chemical systems, and facilitate our utilization of these constructions for chemical ignition and 1D flame computations.

3.3 Model Construction

We plan to finalize our ongoing work on Bayesian inference of random fields, and begin working on the inference of chemical networks from data. This problem is quite involved, and, depending on the nature of available data, is expected to require suitably designed structural constraints for the structural inference to become feasible. The problem of inference of rate parameters for a given known network structure is much easier, and should be directly amenable to our hitherto developed algorithms.

One area of considerable interest in this context is the handling of parameter estimation problems where the fit-model has some *a-priori* uncertainty in one or more parameters. This is a typical situation where prior measurements or computations are utilized in the fit function, which is then fit to some more recent data. We plan to

investigate suitable means of handling this problem by coupling Bayesian inference procedures with PC representation of prior uncertainties in fit models. This combination should allow seamless integration of prior uncertainties with present data noise effects, arriving at well-founded overall uncertainties for the inferred parameters.

3.4 High-Order Structured Adaptive Mesh Refinement (SAMR)

We will continue ongoing testing and validation of the various software components of the high-order uniform-mesh projection-scheme momentum solver. This will be followed by testing of the coupling between the momentum and species/energy solvers, arriving at the overall adaptive mesh construction for reacting flow computations. We will also pursue further scalability testing, and the evaluation of different mesh partitioning strategies.

3.5 CSP/PRISM Adaptive Chemistry

We plan to finalize the ongoing testing of strategies for hypercube construction, including identification of low dimensional manifolds, construction of response surfaces for CSP quantities, and refinement of hypercube size. These strategies will then be implemented in code components under the common component architecture (CCA) framework and used in conjunction with existing chemistry components, arriving at a general CSP/PRISM adaptive chemistry implementation.

4 BES-Supported Published/In-Press Publications [2005-2007]

[1] Marzouk, Y.M., Najm, H.N., and Rahn, L.A., Stochastic Spectral Methods for Efficient Bayesian Solution of Inverse Problems, *J. Comput. Phys.* (2007) in press — doi:10.1016/j.jcp.2006.10.010.

[2] Le Maître, O.P., Najm, H.N., P.P. Pébay, R.G. Ghanem, and Knio, O.M., Multi-resolution analysis for Uncertainty Quantification in Chemical Systems, *SIAM J. Scientific Computing* (2007) in press.

[3] Ray, J., Kennedy, C.A., Lefantzi, S., and Najm, H.N., Using High-Order Methods on Adaptively Refined Block-Structured Meshes, *SIAM J. Sci. Comp.*, 29(1):139–181 (2007).

[4] Lee, J.C., Najm, H.N., Lefantzi, S., Ray, J., Frenklach, M., Valorani, M., and Goussis, D., A CSP and Tabulation Based Adaptive Chemistry Model, *Combustion Theory and Modeling*, 11(1):73–102 (2007).

[5] Valorani, M., Creta, F., Donato, F., Najm, H.N., and Goussis, D.A., Skeletal Mechanism Generation and Analysis for *n*-heptane with CSP, *Proc. Comb. Inst.*, 31:483–490 (2007).

[6] Goussis, D.A., and Najm, H.N., Model Reduction and Physical Understanding of Slowly Oscillating Processes: The Circadian Cycle, *Multiscale Modeling and Simulation*, 5(4):1297–1332 (2006).

[7] Valorani, M., Creta, F., Goussis, D.A., Lee, J.C., and Najm, H.N., Chemical Kinetics Simplification via CSP, *Combustion and Flame*, 146:29–51 (2006).

[8] Singer, M.A., Pope, S.B., and Najm, H.N., Operator-Splitting with ISAT to Model Reacting Flow with Detailed Chemistry, *Combustion Theory and Modelling*, 10(2):199–217 (2006).

[9] Singer, M.A., Pope, S.B., and Najm, H.N., Modeling Unsteady Reacting Flow with Operator-Splitting and ISAT, *Combustion and Flame* (2006).

[10] Goussis, D.A., and Valorani, M., An Efficient Iterative Algorithm for the Approximation of the Fast and Slow Dynamics of Stiff Systems, *J. Comp. Phys.*, 214:316–346 (2006).

[11] Najm, H.N., and Knio, O.M., Modeling Low Mach Number Reacting Flow with Detailed Chemistry and Transport, *J. Sci. Comp.*, 25(1):263–287 (2005).

[12] Valorani, M., Goussis, D.A., Creta, F., and Najm, H.N., Higher Order Corrections in the Approximation of Low Dimensional Manifolds and the Construction of Simplified Problems with the CSP Method, *J. Comput. Phys.*, 209:754–786 (2005).

[13] Lefantzi, S., Ray, J., Kennedy, C.A., and Najm, H.N., A Component-based Toolkit for Reacting Flows with Higher Order Spatial Discretizations on Structured Adaptively Refined Meshes, *Progress in Computational Fluid Mechanics*, 5(6):298–315 (2005).

[14] Goussis, D.A., Valorani, M., Creta, F., and Najm, H.N., Reactive and Reactive/Diffusive Time Scales in Stiff Reaction-Diffusion Systems, *Progress in Computational Fluid Mechanics*, 5(6):316–326 (2005).

[15] Reagan, M.T., Najm, H.N., Pébay, P.P., Knio, O.M., and Ghanem, R.G., Quantifying Uncertainty in Chemical Systems Modeling, *Int. J. Chem. Kin.*, 37(6):368–382 (2005).

"Spectroscopy, Kinetics and Dynamics of Combustion Radicals"
Grant No. DE-FG02-05ERE15961
Annual Progress Report
David J. Nesbitt
March 9, 2007

This report covers the results from the second year into a three-year program for elucidation of spectroscopy, kinetics and structural dynamics of combustion radicals. Significant progress has been achieved in each of the following areas, resulting in 4 papers already published, 1 in press and another ready to be submitted.

1) We have recently published the first high-resolution infrared spectra of jet-cooled cyclopropyl radical, specifically sampling the in-phase antisymmetric CH_2 stretch (ν_7) vibration. In addition to yielding the precise gas-phase structural information, the spectra reveal quantum level doubling into lower (+) and upper (-) states due to tunneling of the lone α-CH with respect to the CCC plane. The bands clearly reveal intensity alternation due to H atom nuclear spin statistics (6:10 and 10:6 for even:odd K_a+K_c in lower (+) and upper (-) tunneling levels, respectively) consistent with C_{2v} symmetry of the cyclopropyl-tunneling transition state. The two *ground*-state-tunneling levels fit extremely well to a rigid asymmetric rotor Hamiltonian, but there is clear evidence for both local and global state mixing in the vibrationally *excited* ν_7 tunneling levels. In particular, the upper (-) tunneling component of the ν_7 state is split by anharmonic coupling with a nearly isoenergetic dark state, which thereby acquires oscillator strength via intensity sharing with this bright state. From thermal Boltzmann analysis of fractional populations, tunneling splittings for cyclopropyl radical are estimated to be 3.2 ± 0.3 cm^{-1} and 4.9 ± 0.3 cm^{-1} in the ground and ν_7-excited states, respectively. This analysis indicates ground state stereoracemization of the α-CH radical center to be a very fast process [$k \approx 2.0(4) \times 10^{11}$ s^{-1}], with the increase in tunneling rate upon CH_2 in-phase asymmetric stretch excitation consistent with *ab initio* predictions of equilibrium vs transition-state zero-point energies. Modeling of the ground-state-tunneling splittings with high level *ab initio* 1D potentials indicates an improved $V_0 = 1115 \pm 35$ cm^{-1} barrier height for α-CH inversion through the cyclopropyl CCC plane. (F. Dong, S. Davis and D. J. Nesbitt, "Slit Discharge IR Spectroscopy of Jet-Cooled Cyclopropyl Radical: Structure and Intramolecular Tunneling Dynamics", J. Phys. Chem. A110, 3059 (2005)).

2) High resolution IR absorption spectra of supersonically cooled ethyl radicals ($T_{rot} \approx 20$K) have been obtained in a slit supersonic jet discharge expansion, revealing first rotationally resolved data for CH-stretch excitation of the methyl group. Three different vibrational bands are observed, one parallel ($k = 0 \leftarrow 0$) and two perpendicular ($|k| = 1 \leftarrow 0$), which for a nearly decoupled methyl rotor framework would correspond to symmetric and (nearly degenerate) asymmetric CH-stretch excitations. However, the splitting between the two asymmetric CH-stretch excitations is anomalously large ($\approx$125 cm^{-1}), signaling the presence of interactions between the CH_2 radical moiety and the opposing CH bond on the methyl group. This suggests an improved zeroth order vibrational description as an isolated CH stretch, strongly red shifted by hyperconjugation, with localized vibrations in the remaining CH bonds split into symmetric and asymmetric

stretches. Such a dynamical picture highlights a remarkably strong coupling between methyl CH-stretch vibrations and C–C torsional geometry and begins to elucidate discrepancies with previous matrix observations. (T. Haeber, A. C. Blair, M. D. Schuder and D. J. Nesbitt, "CH stretch/internal rotor dynamics in ethyl radical: High resolution spectroscopy in the CH_3-stretch manifold", J. Chem. Phys. 124, 54316 (2006))

3) The combination of shot noise-limited direct absorption spectroscopy with long-path-length slit supersonic discharges has been used to obtain first high-resolution infrared spectra for jet-cooled CH_2F radicals in the symmetric (ν_1) and antisymmetric (ν_5) CH_2 stretching modes. Spectral assignment has yielded refined lower- and upper-state rotational constants and fine-structure parameters from least-squares fits to the sub-Doppler line shapes for individual transitions. The rotational constants provide indications of large amplitude vibrational averaging over a low-barrier double minimum inversion-bending potential. This behavior is confirmed by high-level coupled cluster singles/doubles/triples (CCSD(T)) calculations extrapolated to the complete basis set (CBS) limit and adiabatically corrected for zero point energy. The calculations predict a nonplanar equilibrium structure ($\theta \approx 29^o$, where θ is defined to be 180^o minus the angle between the C-F bond and the CH_2 plane) with a 132 cm^{-1} barrier to planarity and a vibrational bend frequency ($\nu_{bend} \approx 276$ cm^{-1}), in good agreement with previous microwave studies by Hirota and co-workers ($\nu_{bend} = 300(20)$ cm^{-1}). The nearly 2:1 ratio of absorption intensities for the symmetric versus antisymmetric bands is in good agreement with density functional theory (DFT) calculations, but in sixfold contrast with simple local mode CH_2 bond dipole predictions of 1:3. This discrepancy arises from a surprisingly strong dependence of the symmetric stretch intensity on the inversion bend angle and provides further experimental support for a nonplanar equilibrium structure. (E. S. Whitney, F. Dong, and D. J. Nesbitt, "Jet-cooled infrared spectroscopy in slit supersonic discharges: Symmetric and antisymmetric CH_2 stretching modes of fluoromethyl (CH_2F) radical", J. Chem. Phys. 124, 054304 (2006)).

4) First high-resolution infrared spectra have been obtained for jet-cooled $CH_2{}^{35}Cl$ and $CH_2{}^{37}Cl$ radicals in the symmetric (ν_1) CH_2 stretching mode. A detailed spectral assignment yields refined lower- and upper- state rotational constants, as well as fine-structure spin rotation parameters from least-squares fits to the sub-Doppler line shapes for individual transitions. The rotational constants are consistent with a nearly planar structure, but do not exclude substantial large-amplitude-bending motion over a small barrier to planarity accessible with zero-point excitation. High level coupled cluster (singles/doubles/triples) calculations, extrapolated to the complete basis set (CBS) limit, predict a slightly nonplanar equilibrium structure ($\theta \sim 11$ degrees), with a vibrationally adiabatic treatment of the bend coordinate yielding a $v = 1 \leftarrow 0$ anharmonic frequency (393 cm^{-1}) in excellent agreement with matrix studies ($\nu_{bend} \sim 400$ cm^{-1}). The antisymmetric CH_2 stretch vibration is not observed despite high sensitivity detection (S/N > 20:1) in the symmetric stretch band. This is consistent with density functional theory (DFT) intensity calculations indicating a > 35-fold smaller antisymmetric stretch transition moment for CH_2Cl, and yet contrasts dramatically with high-resolution infrared studies of CH_2F radical, for which both symmetric and antisymmetric CH_2 stretches are observed in a nearly 2:1 intensity ratio. A simple physical model is presented based on a competition

between bond dipole and "charge sloshing" contributions to the transition moment, which nicely explains the trends in CH_2X symmetric vs asymmetric stretch intensities as a function of electron withdrawing group (X=D, Br, Cl, F). (E. S. Whitney, T. Haeber, M. D. Schuder, A. C. Blair, and D. J. Nesbitt, "High-resolution infrared studies in slit supersonic discharges: CH_2 stretch excitation of jet-cooled CH_2Cl radical", J. Chem. Phys. 124, 054303 (2006)).

5) We have the microinjection slit capability currently installed and operation for use in the slit jet discharge, which will allow us to inject reagents selectively into the post discharge region. Of greatest interest will be a general route for "rational synthesis" of alkylperoxy radicals, the first of which will be methylperoxy. Our immediate goal is the kinetics of radical removal in the slit jet, namely by monitoring loss of methyl via $CH_3^{\bullet} + O_2 \rightarrow$ products. The simultaneous pulsed injection of multiple gases into the slit region has raised interesting questions as to what partial pressures of the different species exist in the expansion, which is of course necessary for accurate analysis of the kinetics. We have therefore developed a flow model for this three way gas expansion, based on a simple electrical analog for multiple currents flowing through a network of coupled resistors. This model is proving extremely useful for quantitative prediction of appropriate backing pressures behind each of the flow orifices for achieving sufficient three body collision rates for production of the desired oxy-radical adduct.

6) We have recently obtained the high resolution CH stretching spectra of monodueterosubstituted methyl radical, i.e. CH_2D. We synthesize this radical by dissociative electron detachment of a commercially available precursor, CH_2DBr, in the slit jet discharge. We have used scaled *ab initio* calculations to predict the vibrational band origins and rotational constants and scanned the jet cooled spectrum in the corresponding symmetric CH stretch region. As this radical species has never been observed at high resolution and the rotational constants are quite large, "cracking" of the jet cooled spectrum was a challenge whose unambiguous analysis required tentative line assignment confirmed by 4-line combination differences. Each of the lines show extensive fine and hyperfine structure, which is currently being analyzed but looks to be consistent with Fermi contact and spin rotation parameters extrapolated from methyl radical. The symmetric methyl radical (D_{3h}) has no dipole moment and is invisible in the microwave, whereas the C_{2v} symmetry of CH_2D now allows a weak dipole moment. As a result, these high resolution studies in the near IR will predate and likely facilitate the first microwave studies of any gas phase methyl radical.

7) As a result of collisional collimation in the slit jet expansion, our methods yield high resolution data below the conventional Doppler limit. In addition to rovibrational characterization, such spectral resolution also provides a novel infrared window into fine (spin rotation) and hyperfine (Fermi contact, dipole-dipole) structure in doublet asymmetric top radicals. This necessitates a detailed treatment of the rovibrational Hamiltonian to account for the inhomogeneous line contours generated by the manifold of transitions, even if these are only partially resolved under slit supersonic jet conditions. To achieve such least squares fitting capabilities for these lineshapes, we have developed a detailed Hamiltonian predictor program that reflects contributions from i) asymmetric

top end over end tumbling (NK_aK_c), ii) electron spin rotation interactions ($\Sigma\varepsilon_\alpha N_\alpha S_\alpha$, and iii) a suite of hyperfine coupling terms (dipole-dipole, Fermi contact and electric quadrupole) between multiple nuclei with non-zero spin. This represents a significant computational challenge, and involved a collaborative benchmarking of our code against code developed in parallel by John Brown's group at Oxford to be sure that either code was correct. There was no previous benchmarking of energy levels for this degree of coupled angular momenta available in the literature, and thus no way to verify the veracity of the code except by development of two independent codes and direct comparison of energy level predictions. This has resulted in a paper recently submitted to the John Brown Festschrift issue of Molecular Physics. (D. J. Nesbitt, E. S. Whitney, M. Roberts, and C. Savage, "Spectroscopy in slit supersonic jet discharges: Fine and hyperfine structure calculations for asymmetric top radicals with multiple nuclear spins", Mol. Phys. (in press)).

8) We have recently completed the analysis and are currently finishing a paper to submit to J. Chem. Phys. on infrared spectroscopy of vinyl radical, H_2CCH. In this paper, first high-resolution IR spectra of jet-cooled vinyl radical in the C-H stretch region are reported. Detailed spectral assignments and least-squares fits to an A-reduction Watson asymmetric top Hamiltonian yield rotational constants and vibrational origins for three A-type bands, each corresponding to single quantum excitation of the symmetric CH_2 stretch vibration. Two of the observed bands arise from the vibrational ground state of vinyl radical, as can be unambiguously confirmed by ground state combination differences that match results from microwave studies [Kanamori et al, J. Chem. Phys. 92, 197 (1989)]. The third band has substantially different rotational constants with ground state vinyl radical, which indicates unambiguously that it is a hot band arising from a low frequency vibrationally excited state. Interestingly, the band origin of the assigned symmetric CH_2 stretch is substantially different (~200 cm^{-1} lower) than that assigned via time resolved FTIR vibrational spectroscopy by Letendre et al [J. Chem. Phys. 112, 9209 (2000)).

Although much of the vinyl spectroscopy is completely analyzed, there are nevertheless interesting questions remaining. For example, the spectra do not contain evidence for transitions out of both lower and upper tunneling levels, though both states are clearly populated in the supersonic expansion. We do see two bands out of the ground state, which would be tempting to attribute to lower and upper tunneling levels. However, none of the bands out of the ground vibrational state exhibits the anticipated 3:1 nuclear spin statistics as a function of K_a+K_c = even vs.odd that one expects for exchange of the identical methylenic hydrogen atoms. Such a lack of nuclear spin statistics would occur if the tunneling splittings were unresolved, which could be caused by two possible reasons: i) near-zero tunneling difference between the two tunneling splittings in the ground and excited states, or ii) very small tunneling splitting of vinyl radical. The former is the most likely explanation, which we hope to test via detailed *ab initio* studies of the potential surface, as discussed below.

9) The issue of barrier heights and tunneling dynamics for in plane CH motion around the radical carbon center in vinyl radical is a very interesting one – and impacts directly on

the interpretation of our jet cooled spectra. In support of our spectroscopic effort, we have therefore developed an *ab initio* surface for tunneling of the CH group, building on our experience with analysis of out of plane bending motion in CH_2F and CH_2Cl radicals. Our efforts for vinyl are based on i) high level CCSD(T) methods, ii) correlation consistent basis sets of Dunning (AVnZ, n=2,3,4), iii) extrapolation to the complete basis set limit (CBS), and iv) adiabatic correction for zero point energies in the higher frequency othorgonal coordinates. Based on our experience with similar analysis of hydronium ions, this surface this should yield tunneling barrier height estimates accurate Exploiting the large amplitude Hamiltonian methods of Rush and Wiberg, this will allow us to predict tunneling splittings in the ground and vibrationally excited states. Benchmarked against the observed microwave tunneling splittings, this should provide barrier heights in the vinyl radical system to unprecedented accuracy. Most importantly, this should be readily sufficient to test the two possible interpretations for the apparent lack of nuclear spin statistics in the high resolution IR vinyl radical spectra.

Determination of Accurate Energetic Database for Combustion Chemistry by High-Resolution Photoionization and Photoelectron Methods

C. Y. Ng

Department of Chemistry, University of California, Davis
One Shields Avenue, Davis, California 95616
E-mail Address: cyng@chem.ucdavis.edu

Program Scope:

The main goal of this project is to obtain accurate thermochemical data, such as ionization energies (IEs), 0 K dissociative photoionization thresholds or appearance energies (AEs), 0 k bond dissociation energies (D_0), and 0 K heats of formation ($\Delta H°_{f0}$'s) for small and medium sizes molecular species and their ions of relevance to combustion chemistry. Accurate thermochemical data determined by high-resolution photoionization and photoelectron studies for selected polyatomic neutrals and their ions are also useful for benchmarking the next generation of *ab initio* quantum computational procedures.

Recent Progress:

1. Kai-Chung Lau and Cheuk-Yiu Ng, "Benchmarking state-of-the-art *ab initio* thermochemical predictions with accurate pulsed-field ionization photoion-photoelectron measurements", *Accounts on Chemical Research*, **39**, 823-829 (2006).

   We have compared highly precise thermochemical data, including IEs, AEs, D_0, and 0 K heats of formation for selected radicals and molecules and their cations obtained by pulsed field ionization (PFI) measurements with theoretical predictions calculated using the current state-of-the-art wavefunction based *ab initio* computation procedures based on the combination of the complete basis set (CBS) extrapolation and the coupled cluster approach including single and double excitations plus quasi-perturbative triple excitations [CCSD(T)]. The benchmarking efforts show that the fully *ab initio* CCSD(T)/CBS procedures together with high-level corrections are capable of yielding highly reliable thermochemical predictions for small to medium size radicals and molecules and their cations of some main group elements, achieving error limits of ≤ 35 meV.

2. Juan Li, Jie Yang, Yuxiang Mo, K. C. Lau, X. M. Qian, Y. Song, Jianbo Liu, and C. Y. Ng, "A combined vacuum ultraviolet laser and synchrotron pulsed field ionization study of CH_2BrCl", *J. Chem. Phys.,* accepted.

   The PFI-PE spectrum of bromochloromethane (CH_2BrCl) in the region of 85,320-88,200 cm^{-1} has been measured using VUV laser. The vibrational structure resolved in the PFI-PE spectrum was assigned based on *ab initio* quantum chemical calculations and Franck-Condon factor predictions. At energies 0-1400 cm^{-1} above the adiabatic IE of CH_2BrCl, the Br-C-Cl bending vibration progression (ν_1^+ = 0-8) of CH_2BrCl^+ is well resolved and constitutes the major structure in the PFI-PE spectrum, whereas the spectrum at energies 1400-2600 cm^{-1} above the IE(CH_2BrCl) is found to exhibit complex vibrational features, suggesting perturbation by the low lying excited $CH_2BrCl^+(\tilde{A}\,^2A'')$ state. The assignment of the PFI-PE vibrational bands gives the IE(CH_2BrCl) = 85,612.4±2.0 cm^{-1} (10.6146±0.0003 eV) and the bending frequencies $\nu_1^+(a_1')$ = 209.7±2.0 cm^{-1} for $CH_2BrCl^+(\tilde{X}\,^2A')$. We have also examined the dissociative photoionization process, $CH_2BrCl + h\nu \rightarrow CH_2Cl^+ + Br + e^-$, in the energy range of 11.36-11.57 eV using the synchrotron based PFI-PE-photoion coincidence method, yielding the 0 K threshold or appearance energy AE(CH_2Cl^+) = 11.509±0.002 eV. Combining the 0 K AE(CH_2Cl^+) and IE(CH_2BrCl) values obtained in this study,

together with the known IE(CH_2Cl), we have determined the D_0 for CH_2Cl^+-Br (0.894±0.002 eV) and CH_2Cl-Br (2.76±0.01 eV). We have also performed CCSD(T, Full)/CBS calculations with high-level corrections for the predictions of the IE(CH_2BrCl), AE(CH_2Cl^+), IE(CH_2Cl), D_0(CH_2Cl^+-Br), and D_0(CH_2Cl-Br). The comparison between the theoretical predictions and experimental determinations indicates that the CCSD(T,Full)/CBS calculations with high-level corrections are highly reliable with estimated error limits of <17 meV.

3. Jingang Zhou, Kai-Chung Lau, Elsayed Hassanein, Haifeng Xu, Shan-Xi Tian, Brant Jones, and C. Y. Ng, "A photodissociation study of CH_2BrCl in the A-band using the time-sliced velocity ion imaging method", *J. Chem. Phys.* **124**, 034309 (2006).

   Employing a high-resolution (velocity resolution $\Delta v/v < 1.5\%$) time-sliced ion velocity imaging apparatus, we have examined the photodissociation of CH_2BrCl in the photon energy range of 448.6-618.5 kJ/mol (193.3 – 266.6 nm). Precise translational and angular distributions for the dominant Br($^2P_{3/2}$) and Br($^2P_{1/2}$) channels have been determined from the ion images observed for Br($^2P_{3/2}$) and Br($^2P_{1/2}$). In confirmation with the previous studies, the kinetic energy distributions for the Br($^2P_{1/2}$) channel are found to fit well with one Gaussian function, whereas the kinetic energy distributions for the Br($^2P_{3/2}$) channel exhibit bimodal structures and can be decomposed into a slow and a fast Gaussian component. The observed kinetic energy distributions are consistent with the conclusion that the formation of the Br($^2P_{3/2}$) and Br($^2P_{1/2}$) channels takes place on a repulsive potential energy surface, resulting in a significant fraction (0.40–0.47) of available energy to appear as translational energy for the photofragments. On the basis of the detailed kinetic energy distributions and anisotropy parameters obtained in the present study, together with the specific features and relative absorption cross sections of the excited 2A′, 1A″, 3A′, 4A′, and 2A″ states estimated in previous studies, we have rationalized the dissociation pathways of CH_2BrCl in the A-band, leading to the formation of the Br($^2P_{3/2}$) and Br($^2P_{1/2}$) channels. The analysis of the ion images observed at 235 nm for Cl($^2P_{3/2,1/2}$) provides strong evidence that the formation of Cl mainly arises from the secondary photodissociation process $CH_2Cl + h\nu \rightarrow CH_2 + Cl$.

4. K.-C. Lau and C. Y. Ng, "Accurate *ab initio* predictions of ionization energies and heats of formation for the cyclopropenylidene, propargylene and propadienylidene radicals", *Chinese Journal of Chemical Physics* (invited article), **19**, 29-38 (2006).

   The IEs of cyclopropenylidene (c-C_3H_2), propargylene (HCCCH) and propadienylidene (H_2CCC) have been computed using the CCSD(T)/CBS method. The zero-point vibrational energy correction, the core-valence electronic correction, and the scalar relativistic effect and the high level correction beyond the CCSD(T) excitations have also been made in these calculations. The CCSD(T)/CBS values for the IE(c-C_3H_2) and IE(HCCCH) of 9.164 and 8.987 eV are in good agreement with the experimental values of 9.15 ± 0.03 and 8.96 ± 0.04 eV. The CCSD(T)/CBS calculations yield the IE values of 10.477 and 10.388 eV for the ionization transitions $H_2CCC \rightarrow H_2CCC^+(^2A_1, C_{2v})$ and $H_2CCC \rightarrow H_2CCC^+(^2A', C_s)$, respectively. On the basis of the Franck-Condon factor consideration, the IE of 10.43 ± 0.02 eV determined in the previous single-photon ionization experiment most likely corresponds to the ionization threshold for the $H_2CCC \rightarrow H_2CCC^+(^2A_1, C_{2v})$ transition. Although the precision of the experimental IE measurements for c-C_3H_2, HCCCH, and H_2CCC is insufficient to pin down the accuracy of the theoretical calculations to better than ±30 meV, the excellent agreement between the experimental and theoretical IE values observed in the present study indicates that the CCSD(T)/CBS calculations together with high-order correlation corrections are capable of yielding reliable IE predictions for simple hydrocarbon carbenes and bi-radicals. We have also reported the $\Delta H°_{f0}$ and $\Delta H°_{f298}$ for c-C_3H_2/c-$C_3H_2^+$, HCCCH/$HCCCH^+$, and H_2CCC/H_2CCC^+. The available experimental $\Delta H°_{f0}$ and $\Delta H°_{f298}$ for c-C_3H_2/c-$C_3H_2^+$, HCCCH/$HCCCH^+$ are found to be in good accord with the CCSD(T)/CBS predictions after taking into account the experimental uncertainties.

5. M.-K. Bahng, X. Xing, Sun Jong Baek, X.-M. Qian, and C. Y. Ng, "A combined VUV synchrotron pulsed field ionization-photoelectron and IR-VUV laser photoion depletion study of ammonia", *J. Phys. Chem. A*, **110**, 8488-8496 (2006).

   Synchrotron based VUV-PFI-PE spectrum of ammonia (NH_3) has been measured in the energy range of 10.12-12.12 eV using a room temperature NH_3 sample. In addition to extending the VUV-PFI-PE measurement to include the v_2^+ = 0, 10, 11, 12, and 13 and the $v_1^+ + nv_2^+$ (n=4–9) vibrational bands, the present study also reveals photoionization transition line strengths for higher rotational levels of NH_3, which were not examined in previous PFI-PE studies. Here, v_1^+ and v_2^+ represent the N-H symmetric stretching and inversion vibrational modes of the ammonia cation (NH_3^+), respectively. The relative PFI-PE band intensities for $NH_3^+(v_2^+=0\text{-}13)$ are found to be in general agreement with the calculated Franck-Condon factors. However, rotational simulation indicates that rotational photoionization transitions of the P-branches, particularly those for the lower v_2^+ PFI-PE bands, are strongly enhanced by forced rotational autoionization. For the synchrotron based VUV-PFI-PE spectrum of the origin band of NH_3^+, rotational transition intensities of the P-branch are overwhelming compared to those of other rotational branches. Similar to that observed for the nv_2^+ (n=0-13) levels, the $v_1^+ + nv_2^+$ (n=4–9) levels are found to have a positive anharmonicity constant, i.e., the vibrational spacing increases as n is increased. The VUV laser PFI-PE measurement of the origin band has also been made using a supersonically cooled NH_3 sample. The analysis of this band has allowed the direct determination of the ionization energy of NH_3 as 82158.2±1.0 cm^{-1}, which is in good accord with the previous PFI-PE and photoionization efficiency measurements. Using the known $nd(v_2^+=1, 1_0 \leftarrow 0_0)$ Rydberg series of NH_3 as an example, we have demonstrated a valuable method based on two-color infrared-VUV-photoion depletion measurements for determining the rotational character of autoionizing Rydberg states.

Future Plans:

We are making excellent progress in photoionization efficiency (PIE) and PFI-PE measurements of small radicals using the VUV laser PFI apparatus established in our laboratory. In collaboration with Xu Zhang (Jet propulsion Laboratory, NASA), Barney Eillison (Univ. of Colorado, Boulder), and Branko Ruscic (Argonne National Laboratory), we have constructed and successfully used a pulsed pyrolysis radical beam source for the VUV laser PIE and PFI-PE study of radicals. We plan to continue with the VUV-PFI-PE and VUV-PIE measurement of propargyl (C_3H_3), phenyl (C_6H_5), benzyne (C_6H_4) radicals in the coming year. Efforts will also be made to measure the excited electronic bands of these hydrocarbon radicals using the PFI-photoion method.

Publications of DOE sponsored research (2005-present)

1. C. Y. Ng, "Two-color photoionization and photoelectron studies by combining infrared and vacuum ultraviolet", *J. Electron Spectroscopy & Related Phenomena* (invited review), **142**, 179-192 (2005).
2. Jie Yang, Yuxiang Mo, K. C. Lau, Y. Song, X. M. Qian, and C. Y. Ng, "A combined vacuum ultraviolet laser and synchrotron pulsed field ionization study of BCl_3", *Phys. Chem. Chem. Phys.* (Special issue for the *85th International Bunsen Discussion Meeting on Chemical Processes of Ions-Transport and Reactivity*), **7**, 1518 (2005).
3. X. N. Tang, H. F. Xu, T. Zhang, Y. Hou, C. Chang, C. Y. Ng, Y. Chiu, R. A. Dressler, D. J. Levandier, "A pulsed field ionization photoelectron secondary ion coincidence study of the $H_2^+(X, v^+=0\text{-}15, N^+=1)$ + He proton transfer reaction", *J. Chem. Phys.* **122**, 164301 (2005).
4. K. C. Lau and C. Y. Ng, "Accurate *ab initio* predictions of ionization energies of hydrocarbon radicals: CH_2, CH_3, C_2H, C_2H_3, C_2H_5, C_3H_3 and C_3H_5", *J. Chem. Phys.***122**, 224310 (2005).

5. T.-S. Chu, R.-F. Lu, K.-L. Han, X.-N. Tang, H.-F. Xu, and C. Y. Ng, "A time-dependent wave packet quantum scattering study of the reaction H_2^+(v=0-2, 4, 6; j=1) + He $\rightarrow$ HeH^+ + H", *J. Chem. Phys.* **122**, 244322 (2005).
6. X. N. Tang, Y. Hou, C. Y. Ng, and B. Ruscic, "Pulsed field ionization photoelectron-photoion coincidence study of the process N_2 + hν $\rightarrow$ N^+ + N + e^-: Bond Dissociation Energies of N_2 and N_2^+", *J. Chem. Phys.* **123**, 074330 (2005).
7. M.-K. Bahng, X. Xing, Sun Jong Baek, and C. Y. Ng, "A two-color infrared-vacuum ultraviolet laser pulsed field ionization photoelectron study of NH_3, *J. Chem. Phys*. **123**, 084311 (2005).
8. M. Hochlaf, T. Baer, X. M. Qian, and C. Y. Ng, "A Photoionization and Pulsed Field Ionization-Photoelectron Study of Cyanogen", *J. Chem. Phys.* **123**, 144302 (2005).
9. Tao Zhang, C. Y. Ng, Chow-Shing Lam, and Wai-Kee Li, "A 193 nm Laser Photofragmentation Time-of-Flight Mass Spectrometric Study of CH_2ICl", *J. Chem. Phys*. **123**, 174316 (2005).
10. M.-K. Bahng, X. Xing, Sun Jong Baek, X.-M. Qian, and C. Y. Ng, "A combined VUV synchrotron pulsed field ionization-photoelectron and IR-VUV laser photoion depletion study of ammonia", *J. Phys. Chem. A*, **110**, 8488-8496 (2006).
11. Jingang Zhou, Kai-Chung Lau, Elsayed Hassanein, Haifeng Xu, Shan-Xi Tian, Brant Jones, and C. Y. Ng, "A photodissociation study of CH_2BrCl in the A-band using the time-sliced velocity ion imaging method", *J. Chem. Phys.* **124**, 034309 (2006).
12. K.-C. Lau and C. Y. Ng, "Accurate *ab initio* predictions of ionization energies and heats of formation for the 2-C_3H_7, C_6H_5, and C_7H_7 radicals", *J. Chem. Phys.* **124**, 044323 (2006).
13. P. Wang, H. K. Woo, K. C. Lau, X. Xing, C. Y. Ng, A. S. Zyubin, and A. M. Mebel, "Infrared vibrational spectroscopy of *cis*-dichloroethene in Rydberg states", *J. Chem. Phys.* **124**, 064310 (2006). Selected as the March 2006 issue of Virtual Journal of Ultrafast Science
14. T. Zhang, X. N. Tang, K.-C. Lau, C. Y. Ng, C. Nicolas, D. S. Peterka, M. Ahmed, M. L. Morton, B. Ruscic, R. Yang, L. X. Wei, C. Q. Huang, B. Yang, J. Wang, L. S. Sheng, Y. W. Zhang, and F. Qi, "Direct identification of propargyl radical in combustion flames by VUV photoionization mass spectrometry", *J. Chem. Phys.* **124**, 074302 (2006).
15. K.-C. Lau and C. Y. Ng, "Accurate *ab initio* predictions of ionization energies and heats of formation for the cyclopropenylidene, propargylene and propadienylidene radicals", *Chinese J. Chem. Phys.* (invited article), **19**, 29-38 (2006).
16. K. C. Lau, H. K. Woo, P. Wang, X. Xing, and C. Y. Ng, "Vacuum ultraviolet laser pulsed field ionization-photoelectron study of *cis*-dichloroethene", *J. Chem. Phys*. **124**, 224311 (2006).
17. Rainer A. Dressler, Y. Chiu, D. Lavandier, X. N. Tang, Y. Hou, C. Chang, C. Houchins, H. Xu, and Cheuk-Yiu Ng, "The Study of State-Selected Ion-Molecule Reactions using the Pulsed-Field Ionization-Photoion Technique", *J. Chem. Phys.* **125**, 132306 (2006)
18. Xi Xing, M.-K. Bahng, P. Wang, K. C. Lau, S.-J. Baek, and C. Y. Ng, "Rovibrationally selected and resolved state-to-state photoionization of ethylene using the infrared-vacuum ultraviolet pulsed field ionization-photoelectron method", *J. Chem. Phys.* **125**, 1333304 (2006).
19. Cheuk-Yiu Ng, "Introduction: Chemical Dynamics", *J. Chem. Phys.* **125**, 132201 (2006).
20. Kai-Chung Lau and Cheuk-Yiu Ng, "Benchmarking state-of-the-art *ab initio* thermochemical predictions with accurate pulsed-field ionization photoion-photoelectron measurements", *Accounts on Chemical Research*, **39**, 823-829 (2006).
21. S. Stimson, M. Evans, C.-W. Hsu, and C. Y. Ng, "Rotationally Resolved Vacuum Ultraviolet Pulsed Field Ionization-Photoelectron Bands for $HD^+(X^2\Sigma_g^+, v^+=0\text{-}20)$", *J. Chem. Phys.,* accepted.
22. Juan Li, Jie Yang, Yuxiang Mo, K. C. Lau, X. M. Qian, Y. Song, Jianbo Liu, and C. Y. Ng, "A combined vacuum ultraviolet laser and synchrotron pulsed field ionization study of CH_2BrCl", *J. Chem. Phys.,* accepted.
23. X. Xing, B. Reed, K.-C. Lau, C. Y. Ng, X. Zhang. B. Ellison, "Vacuum ultraviolet pulsed field ionization-photoelectron study of allyl radical CH_2CHCH_2", *J. Chem. Phys.*, submitted.

Large Eddy Simulation of Turbulence-Chemistry Interactions in Reacting Multiphase Flows

Joseph C. Oefelein
Combustion Research Facility
Sandia National Laboratories, Livermore, CA 94551-9051
oefelei@sandia.gov

Program Scope

Application of the Large Eddy Simulation *(LES)* technique within the Diagnostics and Reacting Flows program is being conducted with two primary objectives. The first is to establish a set of high-fidelity, three-dimensional (3-D), computational benchmarks that identically match the geometry (i.e., experimental test section and burner) and operating conditions of selected experimental target flames. The second is to establish a scientific foundation for advanced model development. The goal is to provide direct one-to-one correspondence between measured and modeled results at conditions unattainable using Direct Numerical Simulation *(DNS)* by performing a series of detailed simulations that progressively incorporate the fully coupled dynamic behavior of reacting flows with detailed chemistry and realistic levels of turbulence. Our focal point is the series of flames that have been studied as part of the Experimental Reacting Flow Research program. This represents a direct extension of joint activities being pursued as part of the International Workshop on Measurement and Computation of Turbulent Nonpremixed Flames (TNF Workshop).

There are several significant aspects of our *LES* research that distinguish it from typical approaches. All of the calculations being performed reach beyond the capabilities and resources of most universities and industry and are consistent with a National Laboratory's role of using high-performance computing. We apply a single unified theoretical-numerical framework to all cases being considered. This framework has been optimized to handle high-Reynolds-number, high-pressure, real-gas and/or liquid conditions over a wide Mach operating range (from incompressible, through transonic, to supersonic conditions). The numerical algorithm is massively parallel and has been optimized to meet the strict algorithmic requirements imposed by the *LES* formalism. It is designed to handle state-of-the-art grids, complex geometries, and employs a general R-refinement adaptive mesh *(AMR)* capability. This allows us to account for the inherent effects of geometry on turbulence over the full range of relevant scales while significantly reducing the total number of grid cells required. Recent results and details are given by Oefelein *et al*, as listed under BES Sponsored Publications 2005-2007 at the end of this report.

Recent Progress

Given current research needs in the area of combustion, our goal is to be complementary, not redundant, and use the unique features of our theoretical-numerical framework to provide information that will not be available elsewhere. To achieve this goal, we are investigating two new modeling approaches. The first employs a stochastic reconstruction methodology that treats detailed chemistry directly within the *LES* formalism. This model is "science-based" in that it incorporates turbulence-chemistry interactions and

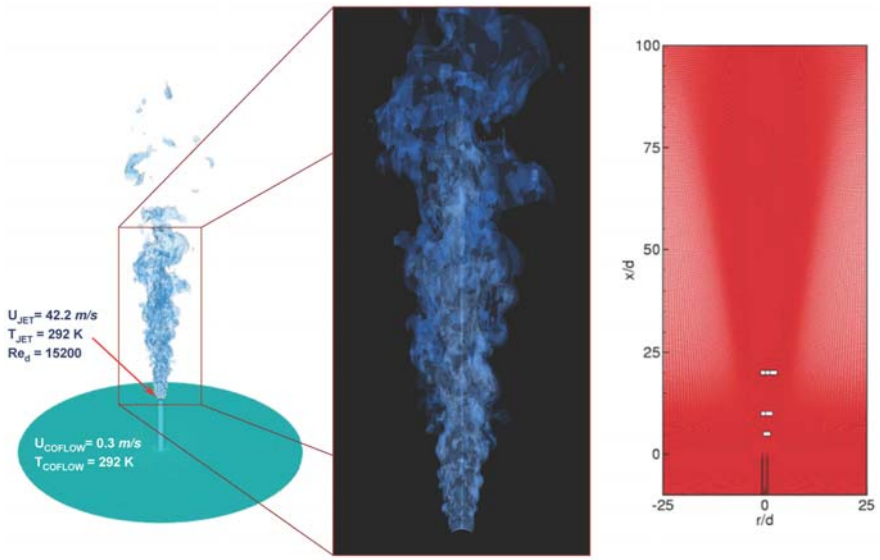

Figure 1: Computational domain used for the turbulent nonpremixed $CH_4/H_2/N_2$ jet flames with close-up of the simulated flame and cross-section of the grid topology. White boxed regions on grid highlight field of view at $x/d = 5$, 10 and 20 where 2-D Rayleigh imaging was performed.

multiple-scalar mixing in a manner consistent with the application of *DNS*. The second is "engineering-based" and employs a tabulated combustion closure based on the Linear Eddy Model (*LEM*). The stochastic reconstruction model combines the purely mathematical approximate deconvolution procedure with physical information from an assumed scalar spectrum. This allows one to invert the resolved-scale solution and provide a modeled representation of the instantaneous field (i.e., $\phi_i = \tilde{\phi}_i + \phi_i''$, where $\tilde{\phi}_i$ represents the resolved-scale contribution of an arbitrary scalar and ϕ_i'' the correlated *sgs* fluctuation). Highly accurate estimates of the *sgs* scalar variances are used as inputs to a stochastic reconstruction technique that provides a correlated approximation of both scalar and velocity fluctuations. The modeled instantaneous field, in turn, is used to evaluate the filtered chemical source terms directly. Model coefficients are evaluated locally in a manner consistent with the dynamic modeling procedure. The only adjustable parameters are the grid spacing, integration time-step, and boundary conditions.

Implementation of the stochastic reconstruction model is expensive, but in return provides a detailed description of turbulence-chemistry interactions with a minimal set of modeling assumptions. The tabulated *LEM* model, in contrast, requires far less computational resources and provides more routine turn-around of solutions and analysis. Given the need for such models and our experience with *LEM*, we have begun to investigate the merits of a new tabulated combustion closure as part of a parallel effort. Here, thermo-chemical state libraries are constructed in a manner directly analogous to the conventional flamelet-library approach. A unique difference, however, is that *LEM* simulates instantaneous realizations of the flow as a function of both the resolved and the unresolved strain-rate. Time-correlated averaged solutions of the *LEM* field can be directly parameterized and tabulated based on filtered values of mixture fraction, scalar dissipation rate, and turbulent Reynolds number. This eliminates the need to introduce additional models to link filtered quantities with instantaneous quantities.

To investigate the merits of the stochastic reconstruction model, we have performed a series of calculations of nonpremixed $CH_4/H_2/N_2$ jet flames. These flames have been studied extensively and used as a benchmark for the TNF Workshop. Emphasis has been placed on the instantaneous, small-scale features of the thermal gradients and mixture fraction. Results from extensive experimental investigations have

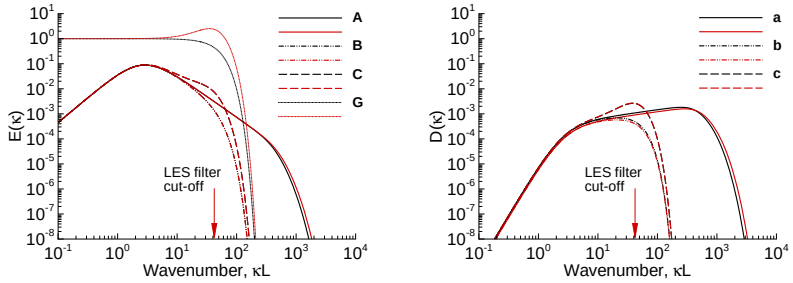

Figure 2: Representative energy (left) and dissipation (right) spectra: **A.** assumed (black) and reconstructed (red) energy spectra, **B.** theoretical (black) and actual (red) resolved-scale spectra, **C.** theoretical (black) and corrected (red) resolved-scale energy spectra, **G.** specified (black) and corrected (red) **LES** filter kernel; **a**, **b**, **c** show dissipation spectra corresponding to **A**, **B**, **C**.

provided significant insights into to the small-scale dissipative structure of these flames. One-dimensional (1-D) line Rayleigh thermometry has been used to investigate the effects of spatial resolution and noise on the thermal dissipation spectra, and two-dimensional (2-D) Rayleigh imaging has been used to investigate the detailed structure of the thermal dissipation field. Data was acquired for jet Reynolds numbers of 15200 (DLR-A) and 22800 (DLR-B).

To augment the experimental efforts, we have performed a set of highly resolved *LES* calculations of the DLR-A case with two primary objectives. The first is to validate our baseline modeling approaches. The second is to extract additional 3-D dynamic information in a manner that complements the 1-D and 2-D experimental results. Figure 1 shows the extent of the computational domain, with a close-up of the simulated flame and cross-section of the grid topology. To eliminate ambiguities associated with boundary conditions, the computational domain includes the entire experimental test section and burner geometry. The inner nozzle diameter is $8.0\ mm$. The outer nozzle surface is tapered to a sharp edge at the burner exit. The overall dimensions are 100 by 50 inner jet diameters ($80\ cm\ \times\ 40\ cm$). The flame image shows the volume rendered mixture fraction field at near stoichiometric values. The white boxed regions on the grid section highlight the field of view at $x/d\ =\ 5$, 10 and 20 where the 2-D Rayleigh imaging and 1-D line Rayleigh thermometry were performed. The total grid density is 6-million cells, with most inside the flame.

As a first step toward rigorous validation, we have performed a series of studies to determine the degree to which the scalar dissipation spectra can be reproduced using the stochastic reconstruction model. Figure 2 shows preliminary results that suggests that these spectra can be reproduced in the statistical sense with reasonable accuracy. Here, the scalar energy spectra (left) and corresponding dissipation spectra (right) are shown at conditions observed in the flame zone at $x/d\ =\ 10$. The reconstruction model was implemented using Pope's model spectrum as one of the required inputs to generate the 3-D energy spectrum for mixture fraction. Measured and reconstructed spectra are shown by curve "A." Note that the portion of the spectra to the far left of the *LES* filter cut-off are generated by fluctuations in the resolved-scales, and that to the far right are reproduced by stochastically generated *sgs* fluctuations. Curve "B" in Fig. 2 shows the distribution of energy in the resolved-scale mixture fraction that would be obtained without the model. This corresponds to the original Gaussian filter kernel (as indicated by the black dotted line designated as "G"). The assumed spectrum in the model provides the missing information required to invert the solution. This is done by correcting the energy distribution associated with the resolved scales in the manner shown by curve "C," which effectively rescales the *sgs* scalar variance in mixture fraction. The final reconstructed energy spectrum matches the assumed distribution to within 5 percent. The corresponding dissipation spectra is obtained in a similar manner and we are currently investigating the error associated with this estimation. After performing detailed validation of the model, our primary goal will be to corroborate the experimental

observations that Barlow and Frank have made with respect to the thermal and scalar dissipation fields by systematically reducing the modeled 3-D spectral information for mixture fraction and temperature to the analogous 1-D and 2-D experimental results. We will also analyze the degree to which the stochastic model can reproduce the instantaneous structure of the flow by reproducing the images of the thermal dissipation field and comparing these to the Kaiser and Frank images.

Future Plans

As our core effort, we plan to continue with the development of high-fidelity benchmark simulations in collaboration with the Experimental Flow Research program. Simulation of the DLR $CH_4/H_2/N_2$ jet flames, as described above, represents the starting point for this activity. Our goal as we progress will be to focus on the sequence of flames that are currently being studied under the TNF Workshop. We will continue to perform joint investigations of DLR flames with emphasis placed on the dynamics of scalar dissipation and provide a 3-D description of the related turbulence-chemistry interactions. We will also augment the experimental database by providing high-fidelity descriptions of turbulent boundary conditions that will be usable in a wide variety of engineering-based models. After establishing a good connection between the experimental and numerical data for the DLR flames, we will augment the effort by focusing on the series of piloted CH_4-air jet flames. This series of flames exhibits increasing degrees of localized extinction due to strong interactions between turbulence and chemistry. The degree of extinction ranges from very low levels (the Sandia-D flame) to very high levels (Sandia-E and F flames) as the jet Reynolds number is progressively increased. Understanding and controlling local extinction is a leading research issue and has significant implications for a variety of applications. There is also a link between the dynamics of scalar dissipation and its effect on local extinction and reignition. This link is not yet fully understood. The third series of flames to be considered are the bluff-body configurations that have been studied jointly by researchers at the University of Sydney and Sandia. These configurations add fluid dynamic complexity by producing recirculation zones around a central jet that stabilizes the flames.

BES Sponsored Publications, 2005 - 2007

- Oefelein, J. C., Sankaran, V. and Drozda T. G. (2006). Large eddy simulation of swirling particle-laden flow in a model axisymmetric combustor, *Proceedings of the Combustion Institute*, **31**: 2291-2299.
- Oefelein, J. C., Drozda T. G. and Sankaran, V. (2006). Large Eddy Simulation of Turbulence-Chemistry Interactions in Reacting Flows: The Role of High-Performance Computing and Advanced Experimental Diagnostics (**invited**). *Journal of Physics*, **46**: 16-27.
- Oefelein, J. C. (2006). Large eddy simulation of turbulent combustion processes in propulsion and power systems (**invited topical review**). *Progress in Aerospace Sciences*, **42**: 2-37.
- Oefelein, J. C., Schefer, R. W. and Barlow, R. S. (2006). Toward validation of large eddy simulation for turbulent combustion (**invited**), *AIAA Journal*, **44**(3): 418-433.
- Oefelein, J. C. (2006). Mixing and combustion of cryogenic oxygen-hydrogen shear-coaxial jet flames at supercritical pressure (**invited**). *Combustion Science and Technology*, **178**(1-3): 229-252.
- Oefelein, J. C. (2005). Thermophysical characteristics of LOX-H2 flames at supercritical pressure. *Proceedings of the Combustion Institute*, **30**: 2929-2937.
- Special triple issue on Supercritical Fluid Transport and Combustion by J. C. Oefelein and V. Yang (guest editors). *Combustion Science and Technology*, **178**(1-3), 1-621 (20 topical papers), 2006.
- Special sections on Combustion Modeling and Large Eddy Simulation, Development and Validation Needs for Gas Turbines by F. F. Grinstein, N.-S. Liu and J. C. Oefelein (guest editors). *AIAA Journal*, **44**(3), 417-468 and **44**(4), 673-750 (20 topical papers), 2006.

KINETICS AND DYNAMICS OF COMBUSTION CHEMISTRY

David L. Osborn
Combustion Research Facility, Mail Stop 9055
Sandia National Laboratories
Livermore, CA 94551-0969
Telephone: (925) 294-4622
Email: dlosbor@sandia.gov

PROGRAM SCOPE

The goal of this program is to elucidate mechanisms of elementary combustion reactions through the use of optical spectroscopy and mass spectrometry. We employ time-resolved Fourier transform spectroscopy (TR-FTS) to probe multiple reactants and products with broad spectral coverage (> 1000 cm^{-1}), moderate spectral resolution (0.1 cm^{-1}), and a wide range of temporal resolution (ns – ms). The inherently multiplexed nature of TR-FTS makes it possible to simultaneously measure product branching ratios, internal energy distributions, energy transfer, and spectroscopy of radical intermediates. Together with total rate coefficients, this additional information provides further constraints upon and insights into the potential energy surfaces that control chemical reactivity. Because of its broadband nature, the TR-FTS technique provides a global view of chemical reactions and energy transfer processes that would be difficult to achieve with narrow-band, laser-based detection techniques.

In addition, photoionization mass spectrometry (PIMS) is used to sensitively and selectively probe unimolecular and bimolecular reactions. In the last two years, we have developed a new apparatus, the Multiplexed Chemical Kinetics Photoionization Mass Spectrometer. This apparatus utilizes tunable vacuum ultraviolet light from the Advanced Light Source synchrotron at Lawrence Berkeley National Laboratory for sensitive, isomer-specific ionization of reactant and product molecules in chemical reactions.

RECENT PROGRESS

Acetaldehyde photodissociation; contributions from roaming mechanisms

The growing experimental and theoretical evidence that roaming mechanisms can play a role in both unimolecular and bimolecular reaction is an exciting development in chemical physics.[1-3] A roaming mechanism is characterized by an activated complex in which an atom or functional group (such as CH_3) is loosely bound to the core of the complex by a potential that is relatively flat. In this region of the potential, where forces are small, the roaming moiety may execute large amplitude motion until it more-or-less randomly finds an entrance valley on the potential surface that facilitates abstraction of part of the core. These pathways do not pass through traditional transition states and represent a departure from this paradigm.

In collaboration with Scott Kable, we have recently studied the photodissociation of acetaldehyde (CH_3CHO), the largest molecule for which a roaming mechanism has been proposed. In analogy to its smaller cousin formaldehyde (H_2CO), acetaldehyde's photodissociation dynamics after $S_1 \leftarrow S_0$ excitation in the ultraviolet region are characterized by

fast non-radiative decay to the T_1 and S_0 electronic states. Two photodissociation channels have been observed with 308 nm ($h\nu$ = 92.8 kcal/mol) excitation:

$CH_3CHO \rightarrow CH_3 + HCO$ (radical channel) ΔH = +83.6 kcal/mol
$\rightarrow CH_4 + CO$ (molecular channel) ΔH = -3.6 kcal/mol

There is a well-defined transition state on the S_0 surface for the formation of the molecular channel.

Employing VUV laser-induced fluorescence, Kable and Houston[3] observed little vibrational excitation and a bimodal rotational distribution of CO, implying the existence of two distinct mechanisms in this photodissociation. They attributed the rotationally-colder CO to a roaming mechanism, in which the methyl group roams around an HCO core until it abstracts the H atom, forming CH_4 + CO. They concluded from their measurements of CO that 87% of the available energy should be deposited in the methane product.

We have made measurements of the time-resolved infrared emission of this system using 248 and 308 nm excitation. All four of the products are observed. The methane product is highly internally excited in agreement with the roaming channel. A quantitative analysis of the data to extract nascent vibrational distributions is ongoing.

The multiplexed chemical kinetics photoionization mass spectrometer

In collaboration with Craig Taatjes, Stephen Leone, Simon North, Askar Fahr, and Vadim Knyazev, we have recently completed the second year of experiments on a new photoionization mass spectrometer at the Chemical Dynamics Beamline of the Advanced Light Source (ALS) of LBNL. The chemical reactor is based on the Gutman design,[4] which allows the study of photodissociation and bimolecular reactions at pressures of ~ 3 – 10 Torr and temperatures up to 1000 K.

While the study of chemical kinetics using PIMS is well-established, this apparatus has two unique features that make it especially powerful for chemical kinetics. First, the widely tunable, intense VUV radiation from the ALS enables isomer specific ionization of product species. As an example, we have recently studied the isomer-resolved products of the C_2H + CH_2CCH_2 reaction, measuring the branching ratios for three different C_5H_4 isomers.

The second unusual feature of this experiment is the mass spectrometer. We employ a small magnetic sector instrument coupled to a time- and position-sensitive single-ion counting detector. This approach creates a mass spectrometer with 100% duty cycle (like a quadrupole instrument) and the multiplex advantage of measuring a broad range of masses simultaneously (as in time-of-flight spectrometry). This detector also measures the time dependence of each observed reactant and product molecule, which provides kinetic information on the reaction.

Our initial experiments investigated the CH_3 + O_2 and C_2H_5 + O_2 reactions. We have made the first measurement of the ionization energy of the CH_3OO radical, and determined a new heat of formation of $\Delta_f H_0°(CH_3OO)$ = 5.35 ± 1.2 kcal/mol. In the case of the C_2H_5 + O_2 reaction, the C_2H_5OO radical undergoes only dissociative ionization: its parent cation is not

stable. The weakening of the OO–C_2H_5 bond in the cation is consistent with the effects of hyperconjugation between the $\sigma(C_\alpha\text{-}O)$ orbital and the $\sigma(C_\beta\text{-}H)$ orbital that lies in the same plane.

The $C_3H_3 + C_3H_3 \rightarrow C_6H_6$ reaction

A topic of substantial current interest is the formation of the first benzene ring in flames, or more generally, the formation of different C_6H_6 isomers. The $C_3H_3 + C_3H_3$ reaction is believed to be one of the most important reactions involved in the formation of the first aromatic rings in combustion. This reaction has been the focus of several experimental[5-7] and theoretical studies.[8,9] In this reaction many isomeric forms of C_6H_6 are energetically feasible (e.g., benzene, fulvene, 1,2 dimethylenecyclobutene, etc.), and the energy landscape that connects them has been explored theoretically. It is important to know which isomers are produced in each reaction step because some isomers are more reactive than others, and therefore affect downstream chemistry in different ways. By determining which C_6H_6 isomers are formed as a function of temperature and pressure, we can place experimental constraints on the size of barriers separating the many wells on this multi-dimensional potential surface.

We have measured the propargyl recombination reaction over the pressure and temperature ranges of 1 – 8 Torr and 305 – 500 K using the new PIMS apparatus at the ALS. This experiment provides the first direct, time-resolved measurements of the isomer distribution of C_6H_6 produced in this key reaction. To derive quantitative C_6H_6 isomer branching ratios from the photoionization efficiency measurements, we have synthesized and measured absolute photoionization cross sections of the isomers fulvene and dimethylenecyclobutene. We will continue this work with several more C_6H_6 isomers to complete the data analysis. Qualitatively, the experiments are in agreement with the predictions of Miller and Klippenstein.

Future Directions

Using TR-FTS, we will investigate reactions of the vinyl (C_2H_3) and propargyl (C_3H_3) radicals to determine product channel identities and energy disposal. We will employ higher spectral resolution to make more definitive measurements of the energy disposal in acetaldehyde photodissociation.

One interesting problem to explore using the multiplexed chemical kinetics mass spectrometer apparatus instrument is the reaction $C_3H_3 + C_2H_2$. Previous work by Knyazev and Slagle[10] has shown that the initial product (C_5H_5) can react with excess acetylene to form C_7H_7. This process continues to form C_9H_8 and perhaps larger species. Measuring the isomeric forms of these products will provide information critical to the reaction mechanism for this molecular weight growth process.

BES sponsored publications, 2005 - present

"Exploring multiple reaction paths to a single product channel" D. L. Osborn, Advances in Chemical Physics, in press (2007).

"Direct detection of polyynes formation from the reaction of ethynyl radical (C_2H) with propyne (CH_3–C≡CH) and allene (CH_2=C=CH_2)" F. Goulay, D. L. Osborn, C. A. Taatjes, P. Zou, G. Meloni, and S. R. Leone, Physical Chemistry Chemical Physics, in press (2007).

"Energy-resolved photoionization of alkylperoxy radicals and the stability of their cations" G. Meloni, P. Zou, S. J. Klippenstein, M. Ahmed, S. R. Leone, C. A. Taatjes, and D. L. Osborn, Journal of the American Chemical Society, **128**, 13559 (2006)

"Time-dependent infrared emission following photodissociation of nitromethane and chloropicrin" E. A. Wade, K. E. Reak, S. L. Li, S. M. Clegg, P. Zou, and D. L. Osborn, Journal of Physical Chemistry A, **110**, 4405 (2006).

"Measurement of the sixth overtone band of nitric oxide, and its dipole moment function, using cavity-enhanced frequency modulation spectroscopy" J. Bood, A. McIlroy, and D. L. Osborn, Journal of Chemical Physics, **124**, 084311 (2006).

"The vinyl + NO reaction: determining the products with time-resolved Fourier transform spectroscopy," Peng Zou, Stephen J. Klippenstein, and David L. Osborn, Journal of Physical Chemistry A, **109**, 4921 (2005).

References

[1] T. P. Marcy, R. R. Diaz, D. Heard, S. R. Leone, L. B. Harding, and S. J. Klippenstein, *J. Phys. Chem. A* **105**, 8361 (2001).

[2] D. Townsend, S. A. Lahankar, S. K. Lee, S. D. Chambreau, A. G. Suits, X. Zhang, J. Rheinecker, L. B. Harding, and J. M. Bowman, *Science* **306**, 1158 (2004).

[3] P. L. Houston and S. H. Kable, *Proc. Nat. Acad. Sci.* **103**, 16079 (2006).

[4] I. R. Slagle and D. Gutman, *J. Am. Chem. Soc.* **107**, 5342 (1985).

[5] E. V. Shafir, I. R. Slagle, and V. D. Knyazev, *J. Phys. Chem. A* **107**, 8893 (2003).

[6] W. Y. Tang, R. S. Tranter, and K. Brezinsky, *J. Phys. Chem. A* **109**, 6056 (2005).

[7] P. T. Howe and A. Fahr, *J. Phys. Chem. A* **107**, 9603 (2003).

[8] J. A. Miller and S. J. Klippenstein, *J. Phys. Chem. A* **105**, 7254 (2001).

[9] J. A. Miller and S. J. Klippenstein, *J. Phys. Chem. A* **107**, 7783 (2003).

[10] V. D. Knyazev and I. R. Slagle, *J. Phys. Chem. A* **106**, 5613 (2002).

Large amplitude motion and the birth of novel modes of vibration in energized molecules

David S. Perry, Principal Investigator
Department of Chemistry, The University of Akron
Akron OH 44325-3601
DPerry@UAkron.edu

Introduction

In the presence of large amplitude motion, a molecular system no longer remains close to a well-defined reference geometry, which challenges the concepts of the traditional theory of molecular vibrations. Among the challenged concepts are normal modes and point group symmetry. The large amplitude coordinate may take on the character of a reaction coordinate along which one must continuously redefine the remaining "normal" coordinates. The consequences are that large amplitude motion can result in novel energy level structures and it can promote coupling between vibrations and hence accelerate intramolecular vibrational energy redistribution (IVR).

In this project, we examine the vibrational level structure and dynamics of molecules with a single internal rotor including methanol, nitromethane, and methylamine. Vibrational fundamental and overtone spectra of the jet-cooled molecules are examined by cavity ringdown, FTIR spectroscopy, and photofragment spectroscopy (IRLAPS). The ringdown experiments are done in our lab in Akron; the jet-FTIR is done in collaboration with Robert Sams at Pacific Northwest Labs (PNNL); the IRLAPS experiments are done in Thomas Rizzo's lab at the EPFL in Switzerland. To understand the level structures and the vibrational mode coupling, we analyze high-resolution spectra, develop quantum mechanical models of the nuclear motion, and probe the potential surface with *ab initio* calculations.

A. Diabatic, Adiabatic, and Non-Adiabatic behaviors in the CH Stretch – Torsion Manifold of Methanol.

In previous work under this project,[1] we discovered the inverted torsional tunneling splitting in the asymmetric CH stretch vibrational states (ν_2=1 and ν_9=1). These results were successfully explained by our 4-dimensional model calculation that included the three CH stretch coordinates and the torsion.[2] Torsional motion interchanges the identities of the CH bonds *anti* and *gauche* to the OH, and the CH bonds in these positions have different force constants. A single lowest-order coupling term with the required symmetry (A_1 in G_6) was sufficient to reproduce the observed torsional structure. The inverted torsional structure is a general phenomenon that derives from molecular symmetry and the single coupling term results in many mixed vibrational states throughout the CH stretch-torsion manifold. Subsequent spectroscopic reports[3] of other asymmetric vibrations have confirmed the generality of the effect, and a number of theoretical studies,[4-8] including the adiabatic treatment of Fehrensen et al.[9] have contributed to our understanding. With the aid of our new CH overtone data [2], we have been able to extend the model to treat the CH overtones and the torsional states built on them.

Just as the Born-Oppenheimer approximation is an invaluable tool for obtaining approximate solutions to the electronic-nuclear problem, so too in the case of coupled nuclear motions, we would like to have an approximate separation of the large-amplitude motion (e.g., torsion) from the small amplitude vibrations. In the case of methanol, we have able to use our fully coupled 4-D model to test the range of applicability of adiabatic and diabatic separations and to explore the non-adiabatic effects, such as IVR [3].

In the present adiabatic approximation, the CH stretches are the "fast" degrees of freedom solved at each torsional angle, and the "slow" degree of freedom is torsion motion in the effective potential defined by the CH stretch vibrations. By definition, such an approximation does not allow exchange of energy between the torsion and the CH stretch vibrations. Such energy transfer (IVR) is therefore a non-adiabatic effect. Even though our model contains only a single coupling term in the local-mode – free-rotor basis, the same Hamiltonian, when expressed in the adiabatic basis, contains a myriad of off-diagonal IVR coupling matrix elements. In agreement with Pearman and Gruebele[10], we find that the scaling behavior of torsionally-mediated IVR is such that the coupling strength falls off only slowly ($a = 0.3 – 0.5$) with increasing coupling order. This scaling behavior dictates a more important role for direct high-order coupling in the presence of large-amplitude torsional motion than in more rigid molecules. Our model calculations indicate that the extended high-order coupling derives fundamentally from the form of the torsional potential and the nature of the 1-dimensional torsional motion and is therefore expected to be general property of torsional molecules.

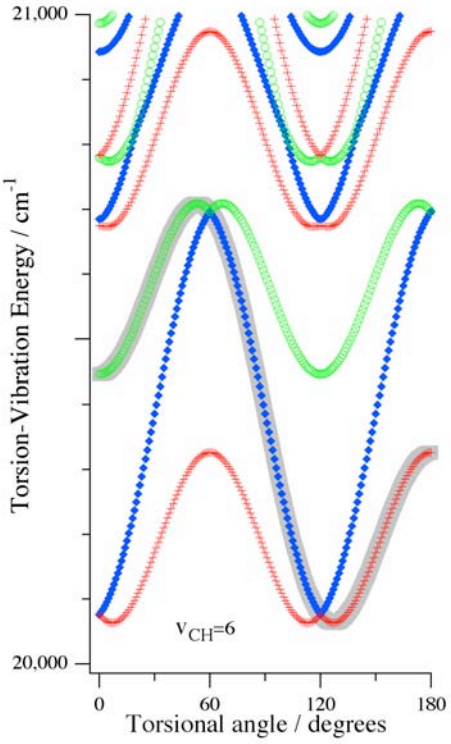

Fig. 1. In the ν_{CH}=6 region of methanol, the adiabatic curves for the torsional potential have very narrowly avoided crossings. One diabatic curve is indicated in grey.

At high energies, our model reveals new patterns of approximate torsion-vibration degeneracies: (i) At high torsional energy but low CH stretch excitation, the ν_2 and ν_9 normal modes merge into an E-type degenerate asymmetric stretch, which is combined with the degenerate free internal rotation. (ii) At high CH stretch but low torsion, torsional tunneling is quenched (Fig. 1) and the three CH normal modes morph into two distinct local modes ν_a and ν_b. (iii) When both are highly excited, the two local CH stretches converge to a triply degenerate local mode that combines with free internal rotation to yield six-fold near-degeneracies. The fully coupled torsional structure of the local CH stretch overtones is consistent with torsional structure on a diabatic potential of C_S symmetry (Fig. 1). The differing behavior in four regions of the CH-stretch-torsion phase space is summarized in Fig. 2.

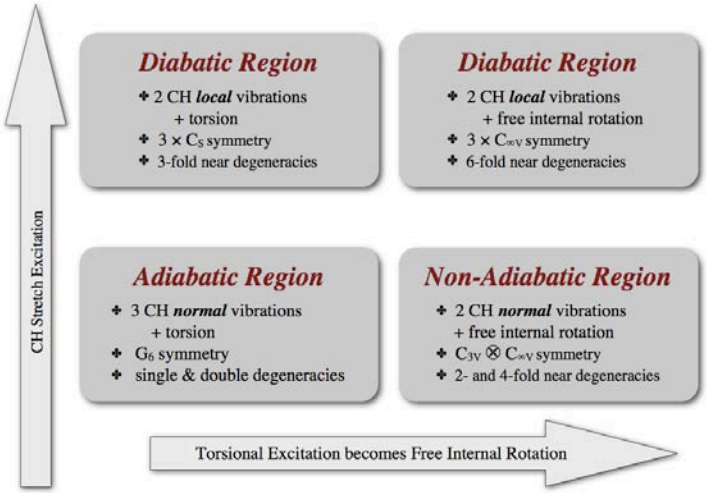

Fig. 2. Approximate CH stretch-torsion behaviors in methanol.

B. Multistage Torsion-Vibration-Rotation Coupling in the ν_6 NO Stretch of Nitromethane

In nitromethane (CH_3NO_2), the planarity of the heavy atoms results in a very low (2 cm^{-1}) 6-fold torsional barrier. Thus, we have the opportunity to extend the stretch-torsion model discussed above to

this new situation. Slit-jet FTIR spectra from PNNL have enabled detailed rotational assignments of the lowest 4 internal-rotation states of the ν_6 asymmetric NO stretch. The comparison of the observed pattern of the torsional levels with our model calculation indicates that the torsion-vibration coupling parameter in nitromethane is much smaller than in methanol. We also find that the rotational lines of lowest torsional state (m=0) are each fragmented into clumps of 3 – 6 transitions, which are the spectroscopic signature of IVR. Because of a favorable combination of spectroscopic parameters, we are able to follow each IVR interaction as a function of J, K_a, and K_c, and thereby assign each as anharmonic or Coriolis type a, b, or c. Three stages of vibration-torsion-rotation coupling are identified: (i) sub-picosecond c-axis Coriolis coupling to a torsionally excited state dark vibration ($\nu_7+\nu_{10}$ or ν_5), (ii) c-axis Coriolis coupling of the dark vibration back to dark rotational states of the ν_6 N-O stretch, and (iii) at J'=8 and higher an additional strong coupling to a second torsionally excited dark vibration.

C. Conformational Dependence of IVR in Methanol

Methanol molecules with one or two quanta of torsional excitation have a significant probability of being at or near the eclipsed conformation, whereas molecules without torsional excitation have geometries near the minimum energy (staggered) conformation. In previous work,[11] we have recorded and assigned IRLAPS spectra representing the direct excitation of torsionally excited states in the OH manifold. This capability has made it possible to study the conformational dependence of IVR in the OH overtone manifold of methanol. Results for staggered and partially eclipsed methanol excited to the OH stretch overtone $5\nu_1$ are presented in Fig. 3 [4].

Our previous IRLAPS spectra of the OH overtones (Fig. 3(c)) showed structure on three frequency scales, which was interpreted in terms of three IVR timescales. The fastest timescale, which corresponds to the 46 cm^{-1} splitting in Fig 3(c), is the coupling of the OH overtone $5\nu_1$ with the CH combination $4\nu_1+\nu_2$. In the partially eclipsed conformation (Fig. 3(b)), the splitting is reduced to 36 cm^{-1}, which means that the OH – CH coupling has become slower than in the staggered conformation. We believe that this change can be explained by the misalignment of the atomic orbitals involved in coupling the OH bond to the *anti* CH bond. In contrast, the narrowest features in the partially eclipsed methanol spectra are broader than in staggered methanol. This indicates that the third timescale, which corresponds to coupling to a dense manifold of dark vibrational states, is faster.

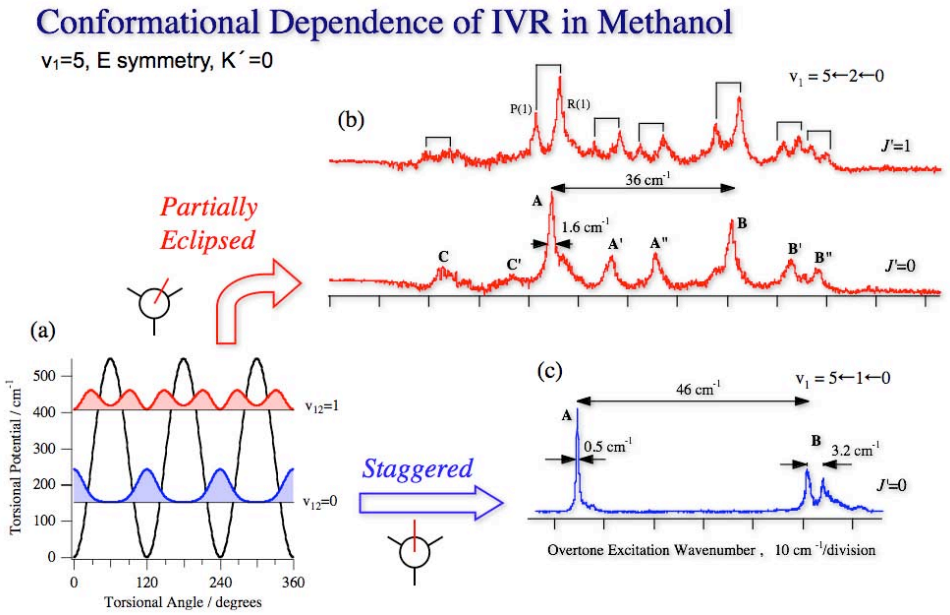

Fig. 3. (a) Calculated torsional angle probability distribution of the lowest two torsional states in methanol in the ν_1=5 vibrational state.
(b) Spectra of partially eclipsed methanol.
(c) Spectra of staggered methanol. [4]

Plans for the Next Year

Our continuous-wave cavity ringdown technique (CW-CRDS) was developed and tested on the OH (ν_1) + CH (ν_3) stretch combination band of methanol between 6510 and 6550 cm^{-1} [1]. In order to test and extend the concepts presented in section A. above at a higher level of CH stretch excitation, our high resolution CW-CRDS technique will be extended to the $2\nu_{CH}$ region. For this purpose a new laser source, a CW PPLN OPO, has been acquired and a CW slit jet has been constructed. The PPLN OPO has both broader tunability and narrower bandwidth than the previously used external cavity diode laser; however scanning and control are much more complicated and the requisite developmental effort is in progress. Analysis of the data outlined in the sections above will continue and manuscripts will be prepared for publication.

Cited References

1 L.-H. Xu, X. Wang, T. J. Cronin, D. S. Perry, G. T. Fraser, and A. S. Pine, *J. Mol. Spectrosc.* **185**, 158 (1997).

2 X. Wang and D. S. Perry, *J. Chem. Phys.* **109**, 10795 (1998).

3 R. M. Lees and L.-H. Xu, *Phys. Rev. Let.* **84**, 3815 (2000).

4 J. T. Hougen, *J. Mol. Spectrosc.* **181**, 287 (1997).

5 J. T. Hougen, *J. Mol. Spectrosc.* **207**, 60 (2001).

6 M. A. Temsamani, L.-H. Xu, and D. S. Perry, *Can. J. Phys.* **79**, 467 (2001).

7 E. L. Sibert, III and J. Castillo-Chara, *J. Chem. Phys.* **122**, 194306/1 (2005).

8 J. Castillo-Chara and E. L. Sibert, III, *J. Chem. Phys.* **119**, 11671 (2003).

9 B. Fehrensen, D. Luckhaus, M. Quack, M. Willeke, and T. R. Rizzo, *J. Chem. Phys.* **119**, 5534 (2003).

10 R. Pearman and M. Gruebele, *Z. Phys. Chem. (Muenchen)* **214**, 1439 (2000).

11 D. Rueda, O. V. Boyarkin, T. R. Rizzo, I. Mukhopadhyay, and D. S. Perry, *J. Chem. Phys.* **116**, 91 (2002).

Publications from this Project, 2004-2007

[1] Shucheng Xu, Jeffrey J. Kay, and David S. Perry, Doppler-limited CW infrared cavity ringdown spectroscopy of the $\nu_1+\nu_3$ OH+CH stretch combination band of jet-cooled methanol, *J. Mol. Spectrosc.* **225**, 162-173 (2004).

[2] David Rueda, Oleg V. Boyarkin, Thomas R. Rizzo, Andrei Chirokolava and David S. Perry, Vibrational overtone spectroscopy of jet-cooled methanol from 5,000 to 14,000 cm^{-1}, *J. Chem. Phys.*, **122**, 044314 (2005). (8 pages)

[4] Trocia N Clasp and David S Perry, Torsion-vibration coupling in methanol: The adiabatic approximation and IVR scaling, *J. Chem. Phys.*, **125**, 104313 (2006). (9 pages)

[5] Pavel Maksyutenko, Oleg V. Boyarkin, Thomas R. Rizzo and David S. Perry, Conformational dependence of intramolecular vibrational redistribution in methanol, *J. Chem. Phys.*, **126**, 044311 (2007). (6 pages)

Chemical Kinetic Modeling of Combustion Chemistry

William J. Pitz and Charles K. Westbrook
L-327, P.O. Box 808
Lawrence Livermore National Laboratory
Livermore, CA 94551
pitz1@llnl.gov

Program Scope

Our research project focuses on developing detailed chemical kinetic reaction mechanisms for the combustion of a wide variety of hydrocarbon and other chemical species. These reaction mechanisms are intended to be applicable over extended ranges of operating conditions, including temperature, pressure, and fuel/oxidizer ratio, making them so-called "comprehensive" reaction mechanisms. They can then be systematically reduced in size and complexity as needed for specific types of modeling applications. We also use these detailed kinetic mechanisms to carry out modeling studies of practical combustion systems, and we also contribute to basic chemical information on thermochemical and kinetic data.

Recent Progress

During the past year, we have developed detailed kinetic mechanisms and carried out kinetic modeling studies in several interconnected areas, including kinetics of low temperature hydrocarbon oxidation of chemical species that are present in transportation fuels for gasoline, diesel and homogeneous charge, compression ignition (HCCI) engines. In addition, we have examined kinetics of reactions of chemical species expected to be important in fuels derived from new fuel sources such as oil sands and biological materials.

An important new source of petroleum for transportation and other uses is the enormous reserves in Canada that exists in the form of oil sands. This petroleum, when refined for diesel fuel, contains unusually high levels of polycyclic paraffins, and previous and present kinetic models for practical fuels have never taken this class of hydrocarbons into account. To solve this problem, we have been developing full-range kinetic reaction mechanisms for representative cyclic paraffins. Our previous study of ignition kinetics of methyl cyclohexane revealed some important difference between rates of key low temperature, alkylperoxy radical reactions for cyclic alkanes and their acyclic analogs, and during the past year we addressed the related species cyclohexane, which has no methyl side chains and thus is significantly simpler than methyl cyclohexane.

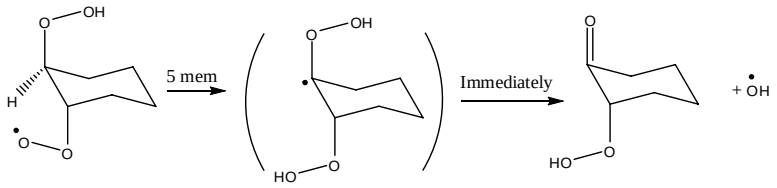

Rate expressions for processes such as formation of ketohydroperoxide intermediate species via isomerization steps like that shown above were found to be much different from comparable reaction steps in fuels modeled previously such as n-heptane and iso-octane. Since new fuels derived from oil sands are expected to contain high levels of cyclic paraffins, these discoveries may have significant practical implications.

The relative simplicity of cyclohexane permitted us to focus on those kinetic features which depend particularly on its cyclic nature. A potential energy diagram was developed for the reaction of the cyclohexyl radical with molecular oxygen, as shown below which incorporates important experimental and theoretical research of Taatjes and Klippenstein at Sandia, dealing with direct production of HO_2 from these reactants, as well as the cyclohexylperoxy radical isomerization reactions.

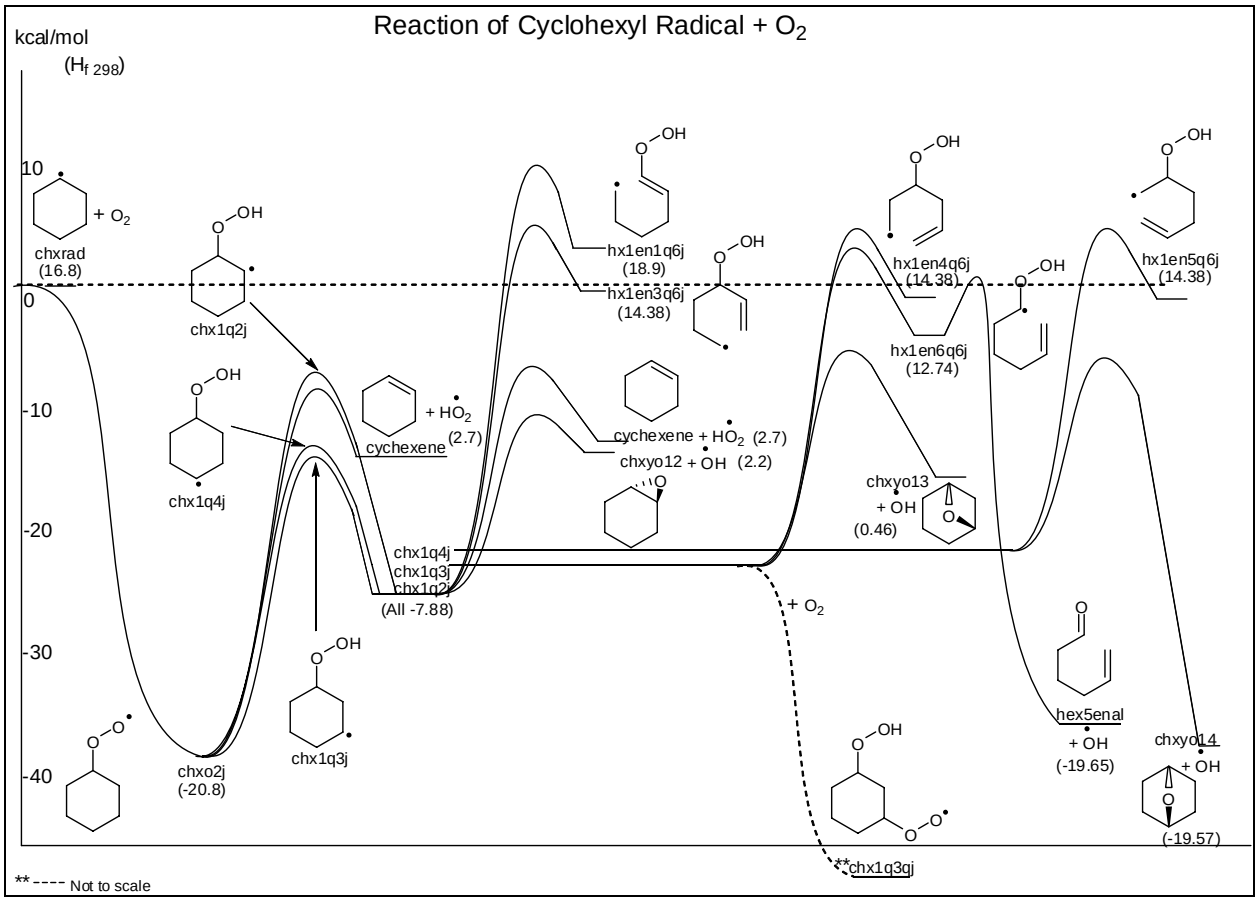

Development of a chemical kinetic model for cyclohexane showed the importance of including what we term “alternative” hydroperoxy-cyclohexyl radical isomerisations. These reactions result in the formation of dihydroperoxy-cyclohexyl radicals which ultimately decompose to a different set of products than those obtained from a conventional isomerisation to ketohydroperoxide and hydroxyl radical. The inclusion of the alternative isomerisations was found to be essential for the predictive capability of our model. Results of our chemical kinetic model of cyclohexane were compared to experimental results from the literature, incorporating a wide range of temperature,

pressures and equivalences ratios. The model was able to correctly reproduce the negative temperature coefficient region observed in a rapid compression machine (RCM), which is characteristic low temperature hydrocarbon combustion. Also, it correctly simulated many the species profiles measured in the RCM and a stirred reactor. Of particular interest is the production of benzene which is a soot precursor. Benzene was predicted quite well at stirred reactor conditions, but under predicted at RCM conditions. In addition, we have better established a methodology for addressing cyclic hydrocarbon species that can be used in future mechanism development for other cyclic species.

Future Plans

We will continue to carry out chemical kinetic modeling studies of a wide variety of combustion problems, developing new kinetic reaction mechanisms when they do not already exist. A major new feature of our kinetic modeling research involves development of kinetic mechanisms for methyl ester species typical of those in practical biodiesel fuels. Our past experience with models for a C_4 methyl ester, methyl butanoate, showed that this species was too small to reproduce important features of diesel ignition, so our new efforts are directed towards production of a C_{10} saturated methyl ester, methyl decanoate. Subsequent attention will be given to unsaturated related methyl ester species and to larger biodiesel components with 16-18 carbon atoms, characteristic of commercially viable fuels including soy biodiesel and canola biodiesel fuels.

We will also continue to refine hydrocarbon mechanisms for important low temperature reaction pathways of practical fuel components, with particular attention for how molecular structure affects such processes as alkylperoxy radical isomerization.

References to publications of DOE sponsored research in 2005-2007

1. Jayaweera, T.M., Melius, C.F., Pitz, W.J., Westbrook, C.K., Korobeinichev, O.P., Shvartsberg, V.M., Shmakov, A.G., Rybitskaya, I.V., and Curran, H.J., "Flame Inhibition by Phosphorus-Containing Compounds over a Range of Equivalence Ratios", Combust. Flame 140, 103-115 (2005).

2. Korobeinichev, O.,P., Shvartsberg, V.M., Shmakov, A.G., Bolshova, T.A., Jayaweera, T.M., Melius, C.F., Pitz, W.J., and Westbrook, C.K., "Flame Inhibition by Phosphorus-Containing Compounds in Lean and Rich Propane Flames", Proc. Combust. Inst. 30, 2350-2357 (2005).

3. Glaude, P.-A., Pitz, W.J., and Thomson, M.J., "Chemical Kinetic Modeling of Dimethyl Carbonate in an Opposed-Flow Diffusion Flame", Proc. Combust. Inst. 30, 1111-1118 (2005).

4. Zheng, X.L., Lu, T.F., Law, C.K., Westbrook, C.K., and Curran, H.J., "Experimental and Computational Study of Nonpremixed Ignition of Dimethyl Ether in Counterflow", Proc. Combust. Inst. 30, 1101-1109 (2005).

5. Westbrook, C.K., Mizobuchi, Y., Poinsot, T., Smith, P.A., and Warnatz, J., "Computational Combustion", Proc. Combust. Inst. 30, 125-157 (2005).

6. Naik, C.V., Pitz, W.J., Sjöberg, M., Dec, J.E., Orme, J., Curran, H. J., Simmie, J. M., and Westbrook, C.K., "Detailed Chemical Kinetic Modeling of Surrogate Fuels for Gasoline and Application to an HCCI Engine", SAE 2005 Transactions of Fuels and Lubricants, SAE paper 2005-01-3742.

7. Westbrook, C.K., Pitz, W.J., and Curran, H.J., "Chemical Kinetic Modeling Study of the Effects of Oxygenated Hydrocarbons on Soot Emissions from Diesel Engines", J. Phys. Chem. A 110, 6912-6922 (2006).

8. Pitz, W.J., Naik, C.V., Ni Mhaoldúin, T., Westbrook, C.K., Curran, H.J., Orme, J.P., and Simmie, J.M., "Modeling and Experimental Investigation of Methylcyclohexane Ignition in a Rapid Compression Machine", Proc. Combust. Inst. 31, 267-275 (2007).

9. Metcalfe, W.K., Pitz, W.J., Curran, H.J., Simmie, J.M., and Westbrook, C.K., "The Development of a Detailed Chemical Kinetic Mechanism for Diisobutylene and Comparison to Shock Tube Ignition Times", Proc. Combust. Inst. 31, 377-384 (2007).

10. Pitz, W.J., and Westbrook, C.K., "A Detailed Chemical Kinetic Model for Gas Phase Combustion of TNT", Proc. Combust. Inst. 31, 2343-2351 (2007).

11. Saylam, A., Ribaucour, M., Pitz, W. J., and Minetti, R., "Reduction of Large Detailed Chemical Kinetic Mechanisms for Autoignition Using Joint Analyses of Reaction Rates and Sensitivities", International Journal of Chemical Kinetics, 39 181-196 (2007).

12. W. J. Pitz, N. P. Cernansky, F. L. Dryer, F. Egolfopoulos, J. T. Farrell, D. G. Friend and H. Pitsch, "Development of an Experimental Database and Kinetic Models for Surrogate Gasoline Fuels," 2007 SAE World Congress, SAE Paper 2007-01-0175, Detroit, MI, 2007.

13. Silke, E.J., Pitz, W.J., Westbrook, C.K., and Ribaucour, M., "Detailed Chemical Kinetic Modeling of Cyclohexane Oxidation", J. Phys. Chem. A, in press (2007).

INVESTIGATION OF NON-PREMIXED TURBULENT COMBUSTION

Grant: DE-FG02-90ER14128

Stephen B. Pope
Sibley School of Mechanical & Aerospace Engineering
Cornell University
Ithaca, NY 14853
pope@mae.cornell.edu

1 Scope of the Research Program

The focus of the current work is on the development of computational approaches which allow our detailed knowledge of the chemical kinetics of combustion to be applied to the modeling and simulation of combustion devices. In the past year, the work has been focused in three general areas: Lagrangian investigations of the competition between mixing and reaction in turbulent non-premixed flames; the development of a methodology for sensitivity analysis in PDF methods for turbulent combustion; and, an investigation of dimension reduction of a large chemical kinetics mechanism for n-heptane.

2 Recent Progress

The principal research results from this program are described in the publications listed in the final Section. Some of these results are highlighted in the following subsections.

2.1 Lagrangian investigation of local extinction, re-ignition and auto-ignition in turbulent flames

Lagrangian PDF investigations are performed of the Sandia piloted flame E and the Cabra H_2/N_2 lifted flame to help develop a deeper understanding of local extinction, re-ignition and auto-ignition in these flames, and of the PDF models' abilities to represent these phenomena (Wang & Pope 2007). Lagrangian particle time series are extracted from the PDF model calculations and are analyzed.

The PDF calculations are based on the modeled transport equation for the joint PDF of velocity, turbulent frequency and composition. The three commonly used mixing models—IEM, modified Curl, and EMST—are investigated, but only the EMST results are reported here. For flame E, the GRI 3.0 mechanism is used to describe the methane chemistry, whereas for the Cabra flame the Li mechanism for hydrogen is used.

The modeled PDF equation is solved using a particle method, and the Lagrangian particle time series are extracted for post-processing. Figure 1 shows selected particle trajectories for the Barlow & Frank flame E. Each plot shows the particle trajectories on the mixture fraction (ξ) temperature plane, up to the indicated axial distance (x/D). The upper dashed line corresponds to a mildly strained laminar flame, and the lower dashed line to a strongly strained laminar flame profile, shifted down by 300K. A particle below this line is deemed to correspond to extinguished mixture. The particles shown originate from the fuel stream and, at some point, are extinguished.

As may be seen from the figure, extinction generally occurs on the rich side ($\xi \approx 0.6$) as might be expected. There are two different re-ignition scenarios. At $x/D = 18$ particles are observed which reignite around stoichiometric ($\xi \approx 0.35$). But other particles move to the lean side (e.g., $\xi \approx 0.2$ at $x/D = 22$) and there achieve the fully burnt state.

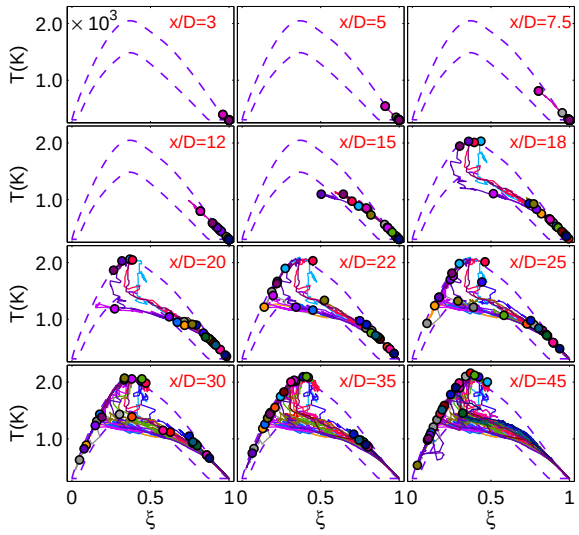

Figure 1: Trajectories in the mixture fraction-temperature plane of "extinguished" particles originating from the fuel stream in PDF calculations of the Barlow & Frank flame E.

In the paper by Wang & Pope (2007), these types of results are used to understand the behavior of the three mixing models in representing local extinction and re-ignition in the Barlow & Frank flame E, and auto-ignition in the Cabra flame.

2.2 Sensitivity calculations in PDF methods

In combustion modeling, it is desirable to know how sensitive the predictions are to certain parameters in the model formulation. In chemical kinetics and laminar flames, sensitivity analysis has been widely used in examining quantitatively the relationship between the parameters and the output of the model, and has thereby been used to improve chemical kinetic models and in uncertainty analysis. In these fields, tools for sensitivity analysis (e.g., SENKIN) are well developed.

For turbulent combustion calculations, it would be equally valuable to perform sensitivity analysis, but the tools are less well developed. In the past, somewhat crude analyses have been performed to evaluate sensitivity by repeating a calculation with a single parameter changed by a small amount. Ren & Pope (2007) developed a methodology for the accurate computation of sensitivities in PDF calculations of turbulent combustion. The method enables the computation of the sensitivities for each particle. These particle-level sensitivities are very revealing. For example, in a region of significant local extinction, one can examine the particles with the largest sensitivities, and the corresponding compositions reveal the sensitive region in the composition space. By ensemble averaging the particle sensitivities, sensitivities of mean (or conditional mean) quantities can be determined.

The method has been applied to a partially-stirred reactor (PaSR) burning a hydrogen-air mixture with different existing mixing models (i.e., IEM, MC and EMST). The PaSR is continuously fed by two inlets, which inject cold non-premixed fuel (diluted hydrogen) and oxidant (air) into the reactor. Ren & Pope (2007) calculated the sensitivities of the PDF calculation to the mixing time τ_{mix}, and to the pre-exponential constants for the following three important chain reactions:

$$
\begin{aligned}
R1 \quad & \mathrm{O_2 + H \Leftrightarrow OH + O} \\
R2 \quad & \mathrm{H_2 + O \Leftrightarrow OH + H} \\
R3 \quad & \mathrm{H_2 + OH \Leftrightarrow H_2O + H.}
\end{aligned}
$$

In the mixture fraction space, Fig. 2 shows the scatter plots of temperature T and the sensitivities of H_2O to the mixing time τ_{mix}. Figure 2 shows the qualitatively different behavior of two of the mixing models in both the composition and the sensitivities. For the IEM model, the most sensitive region in composition space evolves with the residence time. When τ_{res} is reduced toward global extinction, the most

sensitive region in composition space moves towards stoichiometric. In contrast, for the EMST model, the shape of the sensitivity distribution and the most sensitive region in composition space remain almost the same over a wide range of residence times.

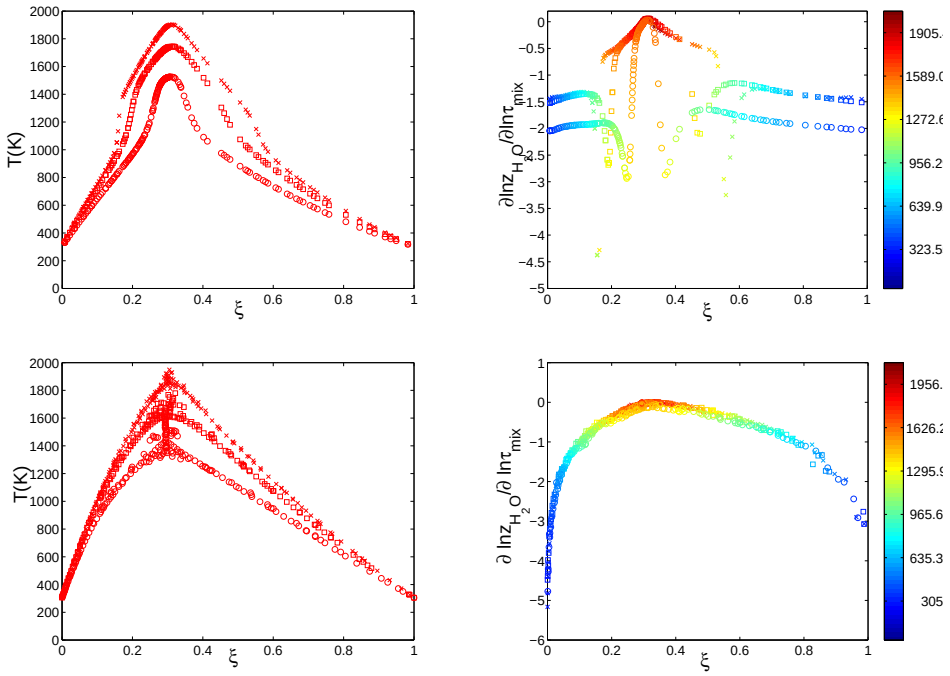

Figure 2: In the mixture fraction space, scatter plots of temperature T and sensitivities of H_2O (colored by particle temperature) to the mixing time τ_{mix} for different mixing models with different values of τ_{res} and $\tau_{mix}/\tau_{res} = 0.25$. Symbol $\times$: $\tau_{res} = 2 \times 10^{-3}$ (s); symbol $\square$: $\tau_{res} = 3 \times 10^{-4}$ (s); symbol $\circ$: $\tau_{res} = 8 \times 10^{-5}$ (s). Top row, results from the IEM model; bottom row, results from the EMST model.

Figure 3 shows the sensitivities of the burning index (BI) to the mixing time τ_{mix} and the pre-exponential factors of the three chain reactions against residence time. The burning index (BI) is defined as the ratio of the conditional mean mass fraction of H_2O (conditioned on stoichiometric mixture fraction) to the chemical equilibrium value of H_2O at stoichiometry. The figure shows that for large residence time (where combustion is controlled by the mixing process), as expected, for all the mixing models, BI is insensitive to the pre-exponential factors of the chain reactions, i.e., insensitive to the chemistry. When τ_{res} is reduced close to global extinction, the sensitivities of BI (i.e., the sensitivity of the combustion process) both to the mixing time and to the chemistry increase (in magnitude) dramatically. The counter effect of mixing and the three chain reactions is due to the fact that increasing mixing fosters extinction whereas increasing rates in chain reactions defers extinction. At the same residence time, the BI from EMST is less sensitive to the mixing time than the BIs from IEM and MC. In other words, the combustion around stoichiometry using EMST is less sensitive to the mixing time compared to IEM and MC.

3 Future Plans

The focus of current and future work is on the development of a computationally-efficient implementation of "local" turbulent mixing models. There are several such models (e.g., VCIEM and MMC) which provide a superior physical description of the process of molecular mixing, but their use in practice has been extremely limited because of the lack of an acceptably efficient computational implementation. This work is progressing well, and publications describing the algorithm developed are expected in the coming year.

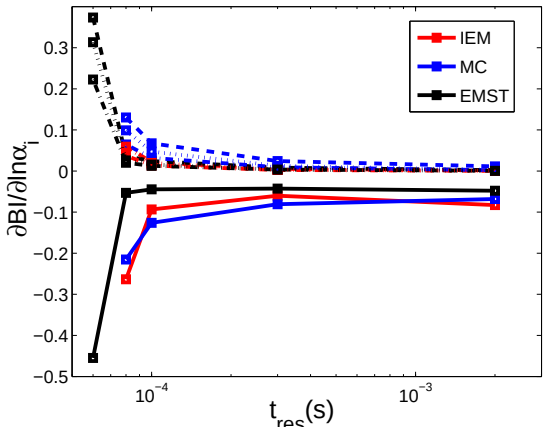

Figure 3: Sensitivities of the burning index (BI) to the mixing time τ_{mix} and to the pre-exponential factors of the three chain reactions against residence time with $\tau_{mix}/\tau_{res} = 0.25$. Solid line: sensitivities to the mixing time; dashed line: sensitivities to the pre-exponential factor of $R1$; dashed-dotted line: sensitivities to the pre-exponential factor of $R2$; dotted line: sensitivities to the pre-exponential factor of $R3$. Red lines: IEM results; blue lines: MC results; black lines: EMST results.

4 Publications from DOE Research 2005-2007

1. R.W. Bilger, S.B. Pope, K.N.C. Bray and J.F. Driscoll (2005) "Paradigms in Turbulent Combustion Research," Proceedings of the Combustion Institute, **30**, 21–42. (Plenary lecture at the Thirtieth International Symposium on Combustion.)

2. R. Cao and S.B. Pope (2005) "The influence of chemical mechanisms on PDF calculations of nonpremixed piloted jet flames," Combustion and Flame **143**, 450–470.

3. R.R. Cao, H. Wang and S.B. Pope (2007) "The effect of mixing models in PDF calculations of piloted jet flames," Proceedings of the Combustion Institute, **31**, 1543–1550.

4. B.J.D. Liu and S.B. Pope (2005) "The Performance of *In Situ* Adaptive Tabulation in Computations of Turbulent Flames," Combustion, Theory & Modelling **9**, 549–568.

5. K. Liu, S.B. Pope and D.A. Caughey (2005) "Calculations of Bluff-Body Stabilized Flames using a Joint PDF Model with Detailed Chemistry," Combustion and Flame **141**, 89–117.

6. S.B. Pope (2005) "Computational modeling of turbulent flames," in *Frontiers of Computational Fluid Dynamics 2006*, World Scientific Publishing.

7. Z. Ren and S.B. Pope (2007) "Sensitivity calculations in PDF methods," Combustion and Flame (in preparation).

8. Z. Ren and S.B. Pope (2005) "Species reconstruction using pre-image curves," Proceeding of the Combustion Institute, **30**, 1293–1300.

9. Z. Ren and S.B. Pope (2006) "The geometry of reaction trajectories and attracting manifolds in composition space," Combustion Theory and Modelling, **10**, 361–388.

10. M.A. Singer, S.B. Pope and H.N. Najm (2006a). "Operator-Splitting with ISAT to Model Reacting Flow with Detailed Chemistry," Combustion, Theory & Modelling, **10**, 199–217.

11. M.A. Singer, S.B. Pope and H.N. Najm (2006b) "Modeling unsteady reacting flow with operator-splitting and ISAT," Combustion and Flame, **147**, 150–162.

12. H. Wang and S.B. Pope (2007) "Lagrangian investigation of local extinction, re-ignition and auto-ignition in turbulent flames," Combustion Theory and Modelling (to be submitted).

OPTICAL PROBES OF ATOMIC AND MOLECULAR DECAY PROCESSES

S.T. Pratt
Building 200, B-125
Argonne National Laboratory
9700 South Cass Avenue
Argonne, Illinois 60439
E-mail: stpratt@anl.gov

PROJECT SCOPE

Molecular photoionization and photodissociation dynamics can provide considerable insight into how energy and angular momentum flow among the electronic, vibrational, and rotational degrees of freedom in isolated, highly energized molecules. This project involves the study of these dynamics in small polyatomic molecules, with an emphasis on understanding the mechanisms of intramolecular energy flow and determining how these mechanisms influence decay rates and product branching ratios. It is also aimed at understanding how internal energy can influence photoionization cross sections and dissociative ionization processes. The experimental approach combines double-resonance laser techniques, which are used to prepare selected highly excited species, with mass spectrometry, ion-imaging, and high-resolution photoelectron spectroscopy, which are used to characterize the decay of the selected species. Four-wave mixing techniques to generate vacuum ultraviolet (vuv) light for single-photon ionization studies are also employed.

RECENT PROGRESS

We have continued to focus on using a combination of ion imaging and vuv single-photon ionization to probe the internal energy dependence of the relative photoionization cross sections and dissociative ionization of a number of small free radicals. This work is important because vuv photoionization is increasingly being used to detect products of photodissociation and reactive scattering, and to characterize species in flames, and because the internal energy dependence of the ionization cross sections has not been characterized. In addition, the dissociation energies for many ions are considerably smaller than the values for corresponding neutral radicals, making it essential to characterize the dissociative ionization processes to avoid misassigning the processes under study.

In the past year, we have performed a systematic series of experiments on the dissociative ionization of the C_3H_5 allyl and 2-propenyl radicals produced by the photodissociation of allyl chloride, allyl bromide, allyl iodide, and 2-propenyl chloride. The different allyl halides produce allyl radicals with different distributions of internal energy, and the radicals show varying amounts of dissociative ionization. Dissociative ionization in all cases leads to the production of $C_3H_3^+ + H_2$, and the fraction of dissociative ionization at ~10.5 eV is considerably larger for the 2-propenyl radical than for the allyl radical. Theoretical calculations indicate that there is an electronically excited state of 2-propenyl ion that can be populated at 9.82 eV, and it is likely that this excited state is responsible for the increased dissociative ionization yield. Tuning the photoionization energy to 9.5 eV, i.e., below the threshold for the excited state of the ion, results in a considerably smaller fraction of dissociative photoionization (64% vs. 88% at 10.5 eV). Overall, this work shows that, in general, a significant fraction of the internal energy of the neutral radical is retained upon photoionization, and that the photoionization process itself can produce ions with more internal energy than in the neutral. As a result, if the radicals of interest have significant internal energy, fragmentation can be important even close to their adiabatic ionization threshold.

The photodissociation of allyl iodide was examined using a combination of vuv photoionization, two-photon resonant, three-photon ionization, and velocity map ion imaging. The results were largely consistent with the earlier translational spectroscopy results of Szpunar et al.,[1,2] in that a significant fraction of the allyl radicals with internal energies greater than barrier to dissociation were found to be stable. As in the previous study, this stability was ascribed to the effects of rotational excitation in the allyl radical: the conservation of angular momentum and the small change in rotational constants between the radical and the transition state for H loss result in the approximate conservation of rotational energy between the allyl radical and the C_3H_4 fragment. Thus, rotational energy is not available for overcoming the dissociation barrier. It is expected that the dissociation process results in considerable rotational excitation in the radicals, leaving them insufficient vibrational energy to dissociate. This conclusion was also reconciled with the seemingly contradictory conclusions of Castiglioni et al.[3] Our results also suggested that some allyl radicals in both the I* and I channels are stable at energies greater than the dissociation threshold, and that the I* channel is more important than previously suspected. This last conclusion could not be tested in these experiments because the translational energy distributions for both the I and I* channels were very similar. Indeed, in the photodissociation of hydrocarbon halides, the translational energy distributions for the $R + X(^2P_{3/2})$ and $R + X^*(^2P_{1/2})$ channels are often overlapped, making it difficult to determine the branching fractions for the two channels. One approach to this difficulty is to use resonance enhanced multiphoton ionization to determine the ion signal from the two channels, and then correct these intensities with the relative linestrengths for the multiphoton process. However, these linestrengths can be power dependent, requiring careful calibration. We have developed two complementary approaches based on the photoionization of the halogen atom, using the wavelength and electric field dependence of the photoionization cross section near the $^2P_{3/2}$ threshold. We have applied these methods to the determination of the spin-orbit branching fractions in the photodissociation of isopropyl iodide and allyl iodide, two molecules in which the translational energy distributions are strongly overlapped. The result for isopropyl iodide is consistent with previous determinations of the branching fraction using different techniques, while the determination for allyl iodide is the first to be reported. The latter measurement confirmed our conclusion that the I* branching fraction at 193 nm was significant, with a value of 0.6 ± 0.1.

We have also used single-photon ionization to study the C_3H_5 and C_3H_4 fragments produced by the 193-nm photodissociation of allyl chloride. Morton et al.[4] had previously studied the photodissociation of allyl chloride at 193 nm and found a significant amount of hot C_3H_4 fragments that could be photoionized well below the ionization threshold of either allene or propyne, and we were interested in determining the vuv-energy dependence of the images resulting from this species. Contrary to our expectations, however, we observed a negligible amount (< 2-3%) of C_3H_4 in our experiments, even when the vuv energy was tuned well above the ionization energies of allene and propyne. Our results appear to indicate that the primary dissociation process is C-Cl bond fission, and, in contrast to the earlier experiments, that very little of the initial population finds its way to the ground state surface with subsequent dissociation to $C_3H_4 + HCl$. We do not believe that our observations are due to our inability to detect C_3H_4 efficiently, as the photoionization cross sections for allene and propyne at the chosen wavelengths are significantly larger than that of allyl, which is detected, and because we observe C_3H_4 in the photodissociation of 2-chloropropene and 2-bromopropene. We are currently working to understand our results through the use of recent theoretical results and new experimental data.

We have begun performing time-resolved experiments on the secondary dissociation of 2-propenyl radicals formed by the photodissociation of 2-chloropropene and 2-bromopropene at 193 nm. In these experiments, images are recorded for different delays between the photodissociation laser pulse and the vuv ionization pulse. If the C_3H_5 radical dissociates before the vuv pulse, the fragment C_3H_4 will be photoionized and detected, whereas if the dissociation is slower, the C_3H_5 will be photoionized and detected. These experiments are very similar (but on a longer timescale) to the femtosecond time-resolved imaging studies of the acetyl (CH_3CO) radical by Suzuki and coworkers.[5] The $P(E_T)$ curves for both 2-halopropenes indicate that the 2-propenyl radicals are formed with ranges of internal energies that span the secondary dissociation threshold for the 2-propenyl radical to dissociate to H + C_3H_4 (allene or propyne). Although we are using lasers with ~10 ns pulse durations, RRKM calculations by Miller[6] indicate that there is a range of ~5 kcal/mol above the dissociation threshold over which the dissociation rate is less than ~10^8 s^{-1}. Thus, the $C_3H_5^+$ and $C_3H_4^+$ images are expected to show complementary time dependences over this small range of internal energies, or E_T values. This time-dependence has been observed, and we are currently in the process of analyzing our results and recording the corresponding images for Cl and Br by using resonantly enhanced multiphoton ionization.

FUTURE PLANS

We plan on extending our time-resolved studies to the primary dissociation of state-selected radicals prepared by using a jet-cooled photolysis or pyrolysis source to produce cold radicals. These studies will build on the work of Chen and co-workers, who studied the time dependence of the dissociation of allyl[7] (C_3H_5) radicals and propargyl[8] (C_3H_3) radicals by using H atom detection on the ns timescale. By incorporating an imaging detector and looking at the radicals, we expect to be able to provide additional insight into the dissociation of radicals. For example, in their study of allyl radicals, Deyerl et al.[7] found a bi-exponential growth of the H atom signal. They assigned the faster rate to dissociation from allyl isomer and the slower rate to the isomerization to the 2-propenyl radical followed by dissociation. While this explanation is reasonable, it would be nice to have experimental confirmation for it. Images of the C_3H_4 fragment are expected to show different behavior for the two mechanisms, and thus the time dependence of the C_3H_4 signal should provide this confirmation. While our initial experiments will again focus on C_3H_5 radicals (both allyl and 2-propenyl), the approach should be applicable to the primary dissociation processes of a number of free radicals.

Before the end of the year, we expect to return to experiments using photoelectron spectroscopy to probe the photoionization dynamics of some smaller stable molecules and simple radicals. The latter will employ the cold radical sources developed for the photodissociation studies. Imaging studies of superexcited states that undergo both autoionization and predissociation are also planned, and the ability to examine both the ionization and dissociation processes in a complementary manner should be particularly revealing.

Finally, I am continuing to collaborate with Christian Jungen on theoretical models of vibrational autoionization in polyatomic molecules. We continue to work on extending our earlier study of simple polyatomic molecules to situations involving degenerate electronic states. In particular, a manuscript is nearly completed that shows how to extract information about autoionization rates for triatomic molecules from spectroscopic information on the Renner-Teller interactions in low-lying Rydberg states.

References

1. D. E. Szpunar, M. L. Morton, L. J. Butler, and P.M. Regan, J. Phys. Chem. B **106**, 8086 (2002).

2. D. E. Szpunar, Y. Liu, M. J. McCullagh, L. J. Butler, and J. Shu, J. Chem. Phys. **119**, 5078 (2003).
3. L. Castiglioni, A. Bach, and P. Chen, J. Phys. Chem. A **109**, 962 (2005).
4. M. L. Morton, L. J. Butler, T. A. Stephenson, and F. Qi, J. Chem. Phys. **116**, 2763 (2002).
5. T. Shibata, H. Li, H. Katayanagi, and T.Suzuki, J. Phys. Chem. A **102**, 3643 (1998).
6. J. A. Miller, private communication.
7. H. J. Deyerl, I. Fischer, and P. Chen, J. Chem. Phys. **110**, 1450 (1999).
8. H. J. Deyerl, I. Fischer, and P. Chen, J. Chem. Phys. **111**, 3441 (1999).

This work was supported by the U.S. Department of Energy, Office of Science, Office of Basic Energy Sciences, Division of Chemical Sciences, Geosciences, and Biological Sciences under contract No. DE-AC02-06CH11357.

DOE-SPONSORED PUBLICATIONS SINCE 2005

1. S. T. Pratt
VIBRATIONAL AUTOIONIZATION IN POLYATOMIC MOLECULES
Ann. Rev. Phys. Chem., **56**, 281-308 (2005).

2. F. Aguirre and S. T. Pratt
PHOTOIONIZATION OF VIBRATIONALLY HOT CH_3 AND CF_3
J. Chem. Phys. **122**, 234303 (2005).

3. Haiyan Fan and S. T. Pratt
PHOTOIONIZATION OF HOT RADICALS: C_2H_5, n-C_3H_7, and i-C_3H_7
J. Chem. Phys. **123**, 204301 (2005).

4. L. R, McCunn, D. I. G. Bennett, L. J. Butler, H. Fan, F. Aguirre, and S. T. Pratt
PHOTODISSOCIATION OF PROPARGYL CHLORIDE AT 193 NM
J. Phys. Chem. A. **110**, 843-850 (2006).

5. Haiyan Fan and S. T. Pratt
NEAR THRESHOLD PHOTOIONIZATION OF HOT ISOPROPYL RADICALS
J. Chem. Phys. **124**, 114312 (2006).

6. Haiyan Fan and S. T. Pratt
PHOTODISSOCIATION OF PROPARGYL BROMIDE AND PHOTOIONIZATION OF PROPARGYL RADICAL
J. Chem. Phys. **124**, 144313 (2006).

7. Haiyan Fan and S. T. Pratt
THE STABILITY OF ALLYL RADICALS FOLLOWING THE PHOTODISSOCIATION OF ALLYL IODIDE AT 193 NM
J. Chem. Phys. **125**, 144302 (2006).

8. Haiyan Fan and S. T. Pratt
DETERMINATION OF SPIN-ORBIT BRANCHING FRACTIONS IN THE PHOTODISSOCIATION OF HALOGENATED HYDROCARBONS
J. Phys. Chem. A, in press (2007).

9. H. Fan, L. B. Harding, and S. T. Pratt
DISSOCIATIVE IONIZATION OF HOT C_3H_5 RADICALS
Mol. Phys., in press (2007).

Photoinitiated Reactions of Radicals and Diradicals in Molecular Beams

Hanna Reisler
Department of Chemistry, University of Southern California
Los Angeles, CA 90089-0482
reisler@usc.edu

Program Scope

Open shell species such as radicals and diradicals are central to reactive processes in combustion and environmental chemistry. Hydroxyalkyl radicals and carbenes are important, because cleavage of C-H and O-H bonds is implicated in reactions of atoms and radicals with alcohols and alkanes. For the alkoxy ↔ hydroxyalkyl and hydroxycarbene ↔ aldehyde structural isomers, competition between isomerization and dissociation on the ground potential energy surface may be significant. Our long-term goal is to investigate the dynamics of pre-dissociation of free radicals and diradicals for which multiple pathways, including molecular rearrangements, compete. The chosen systems are amenable to treatment by high-level theory. The detailed measurements on simple systems will serve as benchmarks that will be extended to larger systems in a homologous series.

Recent Progress

Photoelectron Imaging and REMPI Spectroscopy of Diazomethane

Methylene is the simplest diradical containing carbon. Yet, little is known experimentally about its excited state dynamics because of difficulty in preparing it cleanly in molecular beams. After unsuccessful attempts with several precursors, we are now considering diazomethane as a candidate for pyrolytic preparation of methylene. The first step was to develop a procedure for safe preparation of diazomethane and its delivery to the molecular beam without decomposition. This was achieved with the help of Dr. Karl Christe at USC, an expert in the synthesis of unstable nitrogen compounds. The next step was to develop reliable and sensitive diagnostics of diazomethane by using 2+1 REMPI via a Rydberg state. In order to assign the spectroscopy and understand the excited state dynamics we collaborated with Prof. Krylov's group at USC, and their electron structure calculations are described by her. Below we summarize briefly our experimental results on the vibronic spectroscopy of Rydberg states of diazomethane and its isotopic analogs.

The electronic transitions of diazomethane in the region 6.32 – 7.30 eV were examined experimentally using a combination of 2 + 1 REMPI spectroscopy and photoelectron imaging in a molecular beam. In the examined region, three Rydberg states of 3p character contribute to the transitions, $2^1A_2(3p_y \leftarrow \pi)$, $2^1B_1(3p_z \leftarrow \pi)$, and $3^1A_1(3p_x \leftarrow \pi)$. The former two states are of mostly pure Rydberg character and exhibit a resolved *K* structure in their spectra, whereas the $3^1A_1(3p_x \leftarrow \pi)$ state is mixed with the valence $2^1A_1(\pi^* \leftarrow \pi)$ state, which is unbound, and is strongly predissociative.

We assign most of the observed 2+1 REMPI bands to the $2^1A_2 \leftarrow 1^1A_1$ $(3p_y \leftarrow \pi)$ Rydberg transition, which is allowed only in two-photon absorption. Moreover, we obtained for the first time photoelectron spectra from excited states of diazomethane. The REMPI spectrum of diazomethane in the region near the origin of the $2^1A_2 \leftarrow 1^1A_1$ $(3p_y \leftarrow \pi)$ transition is shown in

Fig. 1. The accompanying high-level electronic structure calculations carried out by the Krylov group determine ground, Rydberg, and ionic state geometries and vertical transition energies. Combined with experiments, they enable us to characterize the nature of the excited electronic states and their interactions.

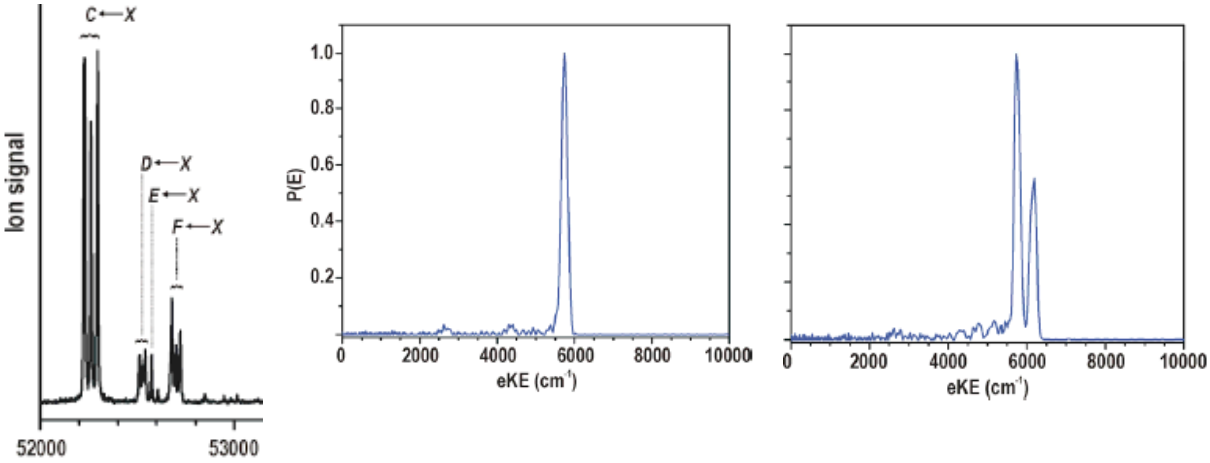

Fig.1. Left panel: REMPI spectra of diazomethane in the region of the $2^1A_2 \leftarrow 1^1A_1$ ($3p_y \leftarrow \pi$) origin band. Each of the C-F bands shows *K* structure. The other panels show photoelectron kinetic energy (eKE) distributions obtained by pumping in the C band (middle panel) and the D band (right panel).

In order to assign the peaks marked C-F in Fig. 1, we obtained photoelectron images from the excited states from which electron kinetic energy (eKE) distributions were derived. Representative examples for peaks C and D are shown in Fig. 1. Photoelectron spectra in band C have a single narrow peak (see middle panel), and are typical of eKE distributions of unperturbed Rydberg states. The C band is assigned as the origin band of the $2^1A_2 \leftarrow 1^1A_1$ ($3p_y \leftarrow \pi$) transition (52,227 - 52,295 cm^{-1}), a transition which is not seen in one-photon absorption.[1] From the eKE distribution shown in the middle panel, we conclude that the $CH_2N_2^+$ ions are generated in the vibrational ground state. The onset of this transition is close to the calculated one and its quantum defect ($\delta = 0.68$) is typical of a Rydberg p state.[2]

The next three groups of bands at 52,513 - 52,541 cm^{-1} [D($^1B_1$)], 52,574 cm^{-1} [E($^1B_2$)], and 52,679 - 52,722 cm^{-1} [F($^1B_1$)] were observed also in one-photon absorption and assigned to three different electronic states,[1] but according to ab initio calculations,[2] there exist only two electronic states [$2^1B_1(3p_z)$ and $2^1A_2(3p_y)$] in this energy region.

The photoelectron images can aid in assigning these bands. The eKE distributions of the D and F bands are similar and assigned as mixed bands composed of the 9_0^1 transition to the $2^1A_2(3p_y)$ state and the band origin of the $2^1B_1(3p_z) \leftarrow 1^1A_1$ transition. This assignment is based on the two-peak structure in the corresponding eKE distributions, and the one for the D band is shown in the right panel of Fig. 1. It has two prominent peaks: a high-energy peak of lower intensity, and a lower energy peak of higher intensity. The eKE distribution of band F is its mirror image, only this time the higher energy peak is of greater intensity. The two peaks display different angular distributions. Comparing the two eKE distributions, which have equal energy separations but different peak heights, suggests coupling of two electronic states. The D and F bands are also seen in Merer's 300 K absorption experiments.[1] Our interpretation is that the one-photon optically forbidden 9_0^1 band of the $2^1A_2(3p_y) \leftarrow 1^1A_1$ transition becomes allowed by vibronic coupling to the $2^1B_1(3p_z)$ state mediated by the non-totally symmetric $\nu'_9(b_2)$ vibra-

tion. We used a two state approximation to obtain the energy of the deperturbed states and the coupling matrix elements. Our analysis shows that the adiabatic origin of the $2^1B_1(3p_z)$ state is at 52,638 cm^{-1}, and its associated quantum defect, $\delta = 0.65$, is typical of a Rydberg p state. The coupling matrix element between the two states is estimated at 83 cm^{-1}.

All the other bands in the 52,000 - 55,000 cm^{-1} region are fairly sharp and have a typical triad *K* structure. They are assigned to unperturbed transitions to the $2^1A_2(3p_y \leftarrow \pi)$ state, because their photoelectron spectra display single peaks corresponding to the ion's vibrational levels. A detailed analysis of the REMPI vibronic spectrum and photoelectron images allows us to assign vibrational states of the $2^1A_2(3p_y \leftarrow \pi)$ neutral state and the ground state of the ion. Our assignments are supported by corresponding measurements of the isotopologs of diazomethane (Fig. 2) and by theory.[2,3] The 2^1A_2 vibrational levels are: ν_1 = CD stretch, ν_2 = NN stretch, ν_3 = CH_2 sym-bend (or CHD, CD), ν_4 = CN stretch, ν_5 = CNN bend (out-of-plane), and ν_9 = CNN bend (in-plane).

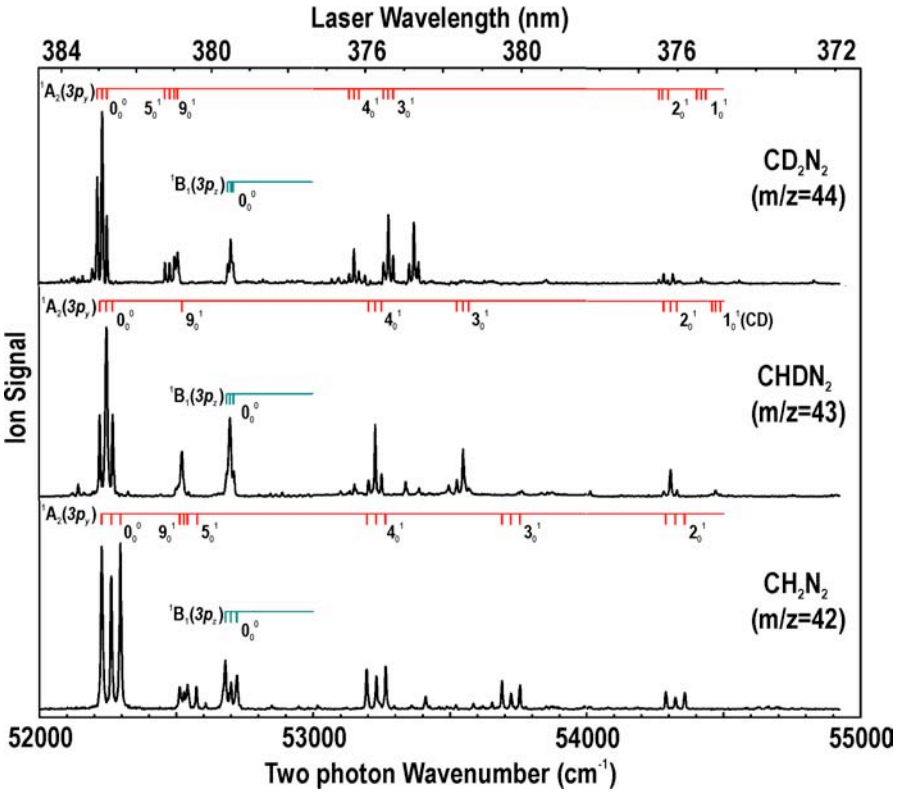

Fig. 2. 2+1 REMPI spectra of CH_2N_2, $CHDN_2$ and CD_2N_2.

In summary, in the investigated region we find that three Rydberg 3p states are excited, the $2^1A_2(3p_y \leftarrow \pi)$, $2^1B_1(3p_z \leftarrow \pi)$, and $3^1A_1(3p_x \leftarrow \pi)$. The former two states are of mostly pure Rydberg character, whereas the $3^1A_1(3p_x \leftarrow \pi)$ state is mixed with the valence $2^1A_1(\pi^* \leftarrow \pi)$ state and is strongly predissociative. We find that the ground vibrational level of the $2^1B_1(3p_z)$ state is mixed with the $2^1A_2(3p_y)$ ν_9 level, which is of B_1 vibronic symmetry. The other $2^1A_2(3p_y)$ vibronic states predissociate slowly and generate ions in single vibrational states. Thus, this state can serve both as a sensitive and state-specific two-photon diagnostic for diazomethane and as a gateway state for preparation of diazomethane ions in specific vibrational levels. The two-photon excitation scheme used here excited vibronic levels in the $2^1A_2(3p_y)$ state efficiently, whereas vibronic levels of the $2^1B_1(3p_z)$ state are best accessed by one-photon absorption. The experi-

mental and theoretical results agree very well and help explain the differences in vibrational levels of the three Rydberg p states in terms of interactions of the Rydberg electron density with the core.

Future Work

Currently, we are finishing our work on the dynamics of the hydroxyethyl radical, CH_3CHOH, on the ground and excited electronic states. For these studies we use partially deuterated hydroxyethyl radicals. Our results so far show that near the origin of the transition to the 3s Rydberg state, only the OH bond is broken, whereas at higher energies, the C-H bond is broken as well. We do not see any evidence for isomerization to ethoxy. We plan to extend the work to other hydroxyalkyl radicals, such as CH_2CH_2OH and hydroxypropyl. We will then start work on the photodissociation dynamics of small carbenes such as $^3CH_2$ and HCOH.

References

1. A. Merer, J. Can. J. Phys. 42, 1242 (1964).

2. I. Fedorov, L. Koziol, G. Li, J. A. Parr, A. I. Krylov, and H Reisler, J. Phys. Chem. A, in press.

3. L. Koziol I. Fedorov, , G. Li, J. A. Parr, H Reisler, and A. I. Krylov, J. Phys. Chem. A, in preparation.

Recent Publications

Theoretical and Experimental Investigations of the Electronic Rydberg States of Diazomethane: Assignments and State Interactions, I. Fedorov, L. Koziol, G. Li, J. A. Parr, A. I. Krylov, and H Reisler, J. Phys. Chem. A, (in press).

Unimolecular processes in CH_2OH below the dissociation barrier: O-H stretch overtone excitation and dissociation, J. Wei, B. Karpichev, and H. Reisler, J. Chem. Phys. **125**, 34303, (2006).

Competitive C–H and O–D bond fission channels in the UV photodissociation of the deuterated hydroxymethyl radical (CH_2OD), L. Feng, A. V. Demyanenko, and H. Reisler, J. Chem. Phys.**120**, 6524-6530 (2004).

Rotationally resolved infrared spectroscopy of the hydroxymethyl radical (CH_2OH), L. Feng, J. Wei, and H. Reisler, J. Phys. Chem. A, **108**, 7903 (2004).

Photodissociation of the $3p_z$ state of the hydroxymethyl radical (CH_2OH): CH_2O and HCOH products, L. Feng and H. Reisler, J. Phys. Chem. A., **108** (45): 9847-9852 (2004).

Accurate Calculations and Analyses of Electronic Structure, Molecular Bonding and Potential Energy Surfaces

Klaus Ruedenberg
Ames Laboratory USDOE, Iowa State University, Ames, Iowa, 50011
ruedenberg@iastate.edu

Scope

Essential for the theoretical treatment of molecular reactions, dynamics, kinetics, spectra etc is an accurate knowledge of potential energy surfaces, not only at equilibrium geometries but also in other coordinate space regions that are traversed during reactive geometry changes. The major difficulty is achieving a sufficiently accurate description of the non-relativistic electron correlations. This is because the effectiveness of most methods is tied to the *dominance of a single configuration* in the wavefunction, a feature that is lost on many reaction paths and transition states. A substantive advance in dealing with this problem has been the *correlation energy extrapolation by intrinsic scaling (CEEIS)* developed in this group.

The complexity of accurate ab-initio electronic wavefunctions and energies presents a challenge to extracting a legitimate and valid identification of the physical reasons for the calculated electronic structure rearrangements and energy changes. A substantive advance in dealing with this problem has been the *exact* representation of accurate *molecular* density matrices in terms of chemically deformed and oriented *atomic* minimal basis set orbitals developed in this group.

Recent Work

An ab-initio potential energy curve has been determined for the F_2 molecule that yields an accurate full vibration rotation spectrum. It is the first full potential energy curve for any 18 electron system accurate enough for theoretically recovering the vibrational spectrum.

The CEEIS method has been used to calculate the non-relativistic electron correlations in the valence shell at 13 internuclear distances along the ground state potential energy curve. Using Dunning's correlation-consistent double-, triple- and quadruple-zeta basis sets, the full configuration interaction energies are determined, with an accuracy of about 0.2 millihartree, by successively generating up to eight-tuple excitations *with respect to multiconfigurational reference functions that strongly change along the reaction path*. The energies are then extrapolated to their complete basis set limits. These nonrelativistic, valence-shell-only-correlated energies are complemented by the energy contributions that arise from electron correlations involving core electrons, from spin-orbit coupling and from scalar relativistic effects.

The dissociation curve is found to rise rather steeply towards the energy of the dissociated atoms, exhibiting a Gaussian decay. This is because, at larger distances, the repulsion of the coaxially aligned atomic quadrupoles as well as the repulsion due to the loss of spin-orbit coupling are found to counteract the attractive contributions from incipient covalent binding and correlation forces, including dispersion.

An expansion in terms of eventempered Gaussian exponentials is found to fit the *ab initio* energies with a mean absolute deviation of about 0.05 millihartree, furnishing an accurate analytical representation for the potential energy curve.

With this analytical potential energy curve, the full vibrational and rotational energy spectrum of F_2 is calculated using the discrete-variable-representation. The mean absolute deviation of the theoretical levels from the experimental levels, which had been measured in the Herzberg Institute by high-resolution electronic spectroscopy, is about 5 cm^{-1} over the full spectrum of 22 vibrational levels. The mean absolute deviation of the rotational constants B_v is 0.002 cm^{-1}.

The Dunham analysis of the theoretical spectrum is found to be very accurate and its coefficients converge to unique values. The convergence problems encountered in deducing spectroscopic constants from the experimental spectrum are due to the measurement accuracy of 1 cm^{-1} being insufficient for an unambiguous determination of Dunham coefficients by least mean squares fitting. An improved approach to this problem is developed and modified spectroscopic constants of F_2 in Huber and Herzberg are proposed.

The dissociation energy with respect to the lowest vibrational energy is calculated within 10 cm^{-1} of the experimental value of 12920 ± 50 cm^{-1}.

The agreement of the theoretical spectrum and dissociation energy with the experimental values is found to be contingent upon the inclusion of the effects of electron correlations involving the core and of spin orbit coupling. The results establish the effectiveness of the CEEIS method along a reaction path even when strongly multi-configurational reference functions change strongly.

To extract the model of atoms linked by bonds *quantitatively* from ab-initio quantum chemistry is difficult because fundamental rigorous physical theory is built on the many-electron-many-nuclei model. Past attempts to identify atoms in molecules have not furnished an *exact, intrinsic, basis-set-independent* resolution of accurate molecular electronic wavefunctions in terms of local constituents.

We have developed a coherent, intrinsic, basis-set-independent analysis for the invariants of the first-order density matrix of an accurate molecular electronic wavefunction. From the hierarchical ordering of the natural orbitals, the zeroth-order orbital space is deduced, which generates the zeroth-order wavefunction, typically an MCSCF function in the full valence space. It is shown that intrinsically embedded in such wavefunctions are elements that are local in bond regions and elements that are local in atomic regions. Basis-set-independent methods are given that extract and exhibit the intrinsic bond orbitals and the intrinsic minimal-basis *quasi-atomic* orbitals in terms of which the wavefunction can be *exactly* constructed. The quasi-atomic orbitals are furthermore *oriented* by a basis-set independent criterion in terms of the off-diagonal density matrix elements so as to exhibit the chemical interactions. The unbiased nature of the method allows for the adaptation of the localized and directed orbitals to changing geometries. Analyses of the molecules FOOH, H_2CO, $H_2BH_2BH_2$ and of the isomerization $HNO \rightarrow NOH$ in terms of such intrinsic, oriented quasi-atomic orbitals, extracted from full-valence MCSCF wavefunctions, brings to light the essentials of the bonding interactions. Insights are gained regarding the hyper-conjugation between lone pairs and nearby antibonding orbitals in FOOH and H_2CO, regarding the three-center bonding in diborane, and regarding the transition state structure in HNO.

It has been shown that an understanding of the physical reasons for covalent binding is only possible on the basis of the variation principle. A rigorous analysis of a highly accurate wavefunction of H_2^+ has shown that the energy of the molecule is lower because, in the variational competition between the kinetic and the potential energy functional, the strength of the kinetic functional is weakened by the delocalization of the electron over two attractive centers.

Future Work

The CEEIS method will be applied to reaction paths of other dissociations and reactions. The method will be adapted to the treatment of core-related correlations. The use of localized orbitals will be developed for the treatment of larger reactive systems. The energetic implications of the resolution in terms of quasi-atomic orbitals will be quantified.

Publications in 2005, 2006, 2007

Correlation Energy Extrapolation Through Intrinsic Scaling. IV. Accurate Binding Energies of the Homonuclear Diatomic Molecules C_2, N_2, O_2 and F_2.

L. Bytautas and K. Ruedenberg

J. Chem. Phys. **122**, 154110 (2005)

Transferabiliy of the Slater-Koster Tight-Binding Scheme from a First-Principles Perspective.

W. C. Lu, C. Z. Wang, K. Ruedenberg and K. M. Ho,

Phys. Rev. B **72**, 205123 (2005).

Correlation Energy Extrapolation Through Intrinsic Scaling. V. Electronic Energy, Atomization Energy and Enthalpy of Formation of Water.

L. Bytautas and K. Ruedenberg

J. Chem. Phys., **124**, 174304 (2006)

Scalable Correlated Electronic Structure Theory.

Mark S. Gordon, Klaus Ruedenberg, Michael W. Schmidt, Laimis Bytautas, Timothy J. Dudley, Takeshi Nagata, Ryan Olson, Sergey Varganov,

J. of Physics: Conference Series 46, 229-233 (2006).

Why Does Electron Sharing Lead to Covalent Bonding? A Variational Analysis.

Klaus Ruedenberg and Michael W. Schmidt.

J. Comp. Chem., 28, 391-410 (2007).

Toward a Physical Understanding of Electron-Sharing Two-Center Bonds. I. General Aspects.

T. Bitter, K. Ruedenberg, W.H.E. Schwarz,

J. Comp. Chem., 28, 411-422 (2007).

Economical Description of Electron Correlation,

L. Bytautas and K. Ruedenberg,

Advances in Electron Correlation Methodology (A. K. Wilson and K. A. Peterson Edtrs), ACS Symposium Series Volume 958, March 2007.

Intrinsic Local Constituents of Molecular Electronic Wave Functions. I. Exact Representation of the Density Matrix in terms of Chemically Deformed and Oriented Atomic Minimal Basis Set orbitals.

J. Ivanic, G. J. Atchity and K. Ruedenberg,

Theor. Chem. Acc, accepted

Intrinsic Local Constituents of Molecular Electronic Wave Functions. II. Electronic Structure Analyses in terms of Intrinsic Oriented Quasi-Atomic Molecular Orbitals for the Molecules FOOH, $H_2BH_2BH_2$, H_2CO and the Isomerization HNO → NOH.

J. Ivanic and K. Ruedenberg,

Theor. Chem. Acc, accepted .

Figure below: Oriented quasi-atomic ***molecular*** orbitals for B_2H_6. Occupation numbers next to the orbital labels. Large bond orders between arrows pointing to involved orbitals.

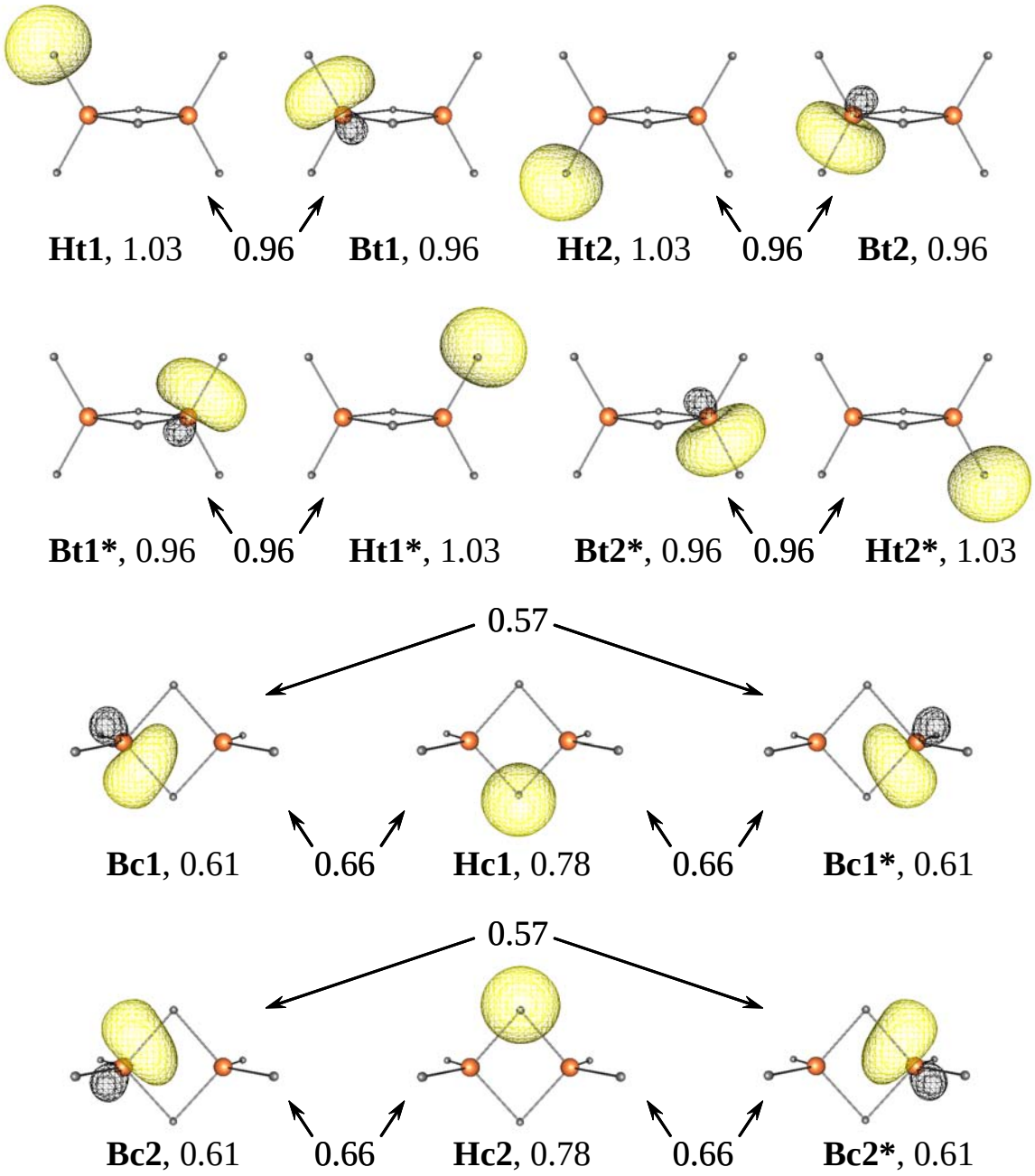

Active Thermochemical Tables – Progress Report

Branko Ruscic
Chemistry Division, Argonne National Laboratory,
9700 South Cass Avenue, Argonne, IL 60439
ruscic@anl.gov

Program Scope

The *spiritus movens* of this program is the need to provide the scientific community with accurate and reliable thermochemical, spectroscopic, and structural information on chemical species that are relevant in energy–producing processes, such as combustion, or play prominent roles in the related post–combustion environmental chemistry, thus contributing to the global comprehension of the underlying chemical reactions and/or providing reliable benchmark values for development and testing of state–of–the–art theoretical approaches. This program has recently developed a novel approach that is capable of optimally extracting the knowledge content from thermochemically relevant measurements and hence produces not only *the best currently available* thermochemical values for the target species, but also provides *critical tests of new experimental or theoretical data* and develops *pointers to future determinations that will most efficiently improve the thermochemical knowledge base*. The effort of this program is coordinated with related experimental and theoretical efforts within the Argonne Chemical Dynamics Group to provide a broad perspective of this area of science.

Recent Progress

Development of Active Thermochemical Tables and the Core (Argonne) Thermochemical Network

Active Thermochemical Tables (ATcT) are a new paradigm of how to derive accurate, reliable, and internally consistent thermochemical values for stable, reactive, and transient chemical species. Availability of high-quality thermochemical values, accompanied by properly quantified uncertainties, is central to chemistry, and critical in many areas of physical chemistry, including, for example, interpretation of kinetic data, development of realistic predictive multi–scale models of complex chemical environments that occur in combustion processes or in the atmosphere, or development of new sophisticated high–fidelity electronic structure computational treatments.

As opposed to traditional sequential thermochemistry, which – in the age of sophisticated computer technologies – appears to be a highly inadequate and outdated option, ATcT is based on the Thermochemical Network (TN) approach, thus overcoming serious limitations of the legacy method. The TN approach involves the construction, manipulation, statistical evaluation, and optimization of the TN Graph, which is then followed by a simultaneous solution providing consistent thermochemistry for all target species described by the TN. The TN Graph is constructed by incorporating all available thermochemically–relevant experimental determinations, and further complemented both by existing and new (custom–computed) high–quality theoretical results, as well as new (custom-conducted) experiments. The constructed TN Graph explicitly exposes to analysis the maze of inherent thermochemical interdependencies between various chemical species, which is normally completely ignored or – at best – heavily underutilized by conventional treatments. The ATcT approach allows, *inter alia*, a thorough statistical analysis of the individual experimental and theoretical measurements that define the TN, critically examining the self-consistency of the TN Graph. The goal of the statistical analysis is to isolate "optimistic" uncertainties that invariably occur with some of the original determinations (both experimental and theoretical), and which, if left unchecked, would skew the resulting thermochemistry and thus adversely affect the quality of the resulting knowledge. The statistical evaluation of the individual determinations present in the TN is made possible by the manifold of thermochemical interdependencies described by the TN Graph, which inherently offers a considerable degree of redundancy, such as the presence of competing determinations of the same thermochemical interdependency, and the existence of alternate thermochemical cycles within the TN Graph. Once the TN is statistically evaluated and adjusted to be self-consistent, it is utilized by ATcT to simultaneously

produce the thermochemistry of all the target chemical species. The end result is the extraction of *best possible thermochemical values* for all chemical species described by the TN, based on optimal use of *all the available knowledge*, hence making conventional tabulations of thermochemical values obsolete.

In addition to providing a new approach to deriving accurate, reliable, and consistent thermochemical values for the target chemical species, ATcT introduces a number of features that are neither present nor possible in the traditional sequential approach. An important new aspect of the ATcT approach is that new thermochemically–relevant determinations can be simply added to the existing TN Graph as they become available, and thus painlessly propagated through all affected thermochemical values, hence providing at all times an updated and internally consistent set of thermochemical values that always reflects the latest incorporated knowledge. Not less importantly, ATcT also allows hypothesis testing and evaluation ("what if" experiments), as well as discovery of "weak links" in the TN. The latter provide pointers to new experimental or theoretical determinations that can most efficiently improve the underlying thermochemical body of knowledge, and are thus *ipso facto* a new paradigm of how to make best use of available experimental resources and theoretical capabilities. In addition, the ATcT approach provides the full covariance matrix (so far unavailable in thermochemistry, but very important in recovering the proper uncertainties associated with the overall thermochemistry of various chemical reactions), as well as additional correlation maps between various thermochemical properties that augment the information content available in the covariance elements, etc.

The development of ATcT has two related, though distinct components. One component is the conceptual development of the TN approach to thermochemistry (and its various facets, such as the manipulation and analysis of the TN Graph), which subsequently drives the development of the associated software (the ATcT Kernel). A second very important component is the development of the underlying data libraries that define, *inter alia*, the TN Graph, and are the *de facto* source of new thermochemical knowledge.

While we are constantly advancing the conceptual development of the TN approach to thermochemistry, and have developed an extensive list of features and commodities that we intend to implement, the current ATcT Kernel is at a sufficiently mature stage to perform the necessary manipulations of the TN Graph and produce new thermochemistry. Thus, the bulk of the effort in the recent past has focused on further developing the TN Graph described by the Core (Argonne) Thermochemical Network, C(A)TN. During the past year, C(A)TN (current ver. 1.062) has grown to encompass ~800 species linked by ~8000 thermochemically relevant determinations. The central focus of our effort was both on expanding the coverage of the TN Graph and on fortifying and polishing its knowledge content. A substantial fraction of newly added edges in the TN Graph comes not only from experimental determinations, but also from targeted composite theoretical computations that are in non–pathological cases of good quality and are conveniently available using commodity computers (G3, G3//B3LYP, G3X, CBS-Q, CBS-QB3, CBS-APNO, W1). These computations currently serve as the routine 0^{th} order definition for most gaseous species in C(A)TN, enhancing the span of the TN manifold and complementing the information content for species that are plagued either by otherwise unverifiable reliability or paucity of experimental data.

Among various projects carried out during the past year, we have now essentially completed the extensive H_xO_y TN manifold. Using the resultant ATcT thermochemistry for HO_2 and for several other related species, such as OH, NO, and NO_2, we have concluded that the previous equilibrium constant for NO + $HO_2 \rightarrow$ OH + NO_2 was underestimated by a factor of ~2, and thus, if it were to be used in the traditional manner (i.e. outside a TN Graph), it would imply unrealistic thermochemistry for HO_2. The arguments utilizing the latest ATcT enthalpies of formation have been additionally augmented by thermochemical arguments leveraging from the underlying knowledge of the partition functions for these species and also provided by ATcT. This realization has resulted in an additional collaborative experimental study (J. V. Michael, ANL), that remeasured the OH + NO_2 rate, fully validating the ATcT conclusion. These results have now been now published. In preparation for publishing the thermochemistry of the remaining H_xO_y species, we are currently performing a final ATcT analysis of the relevant portions of C(A)TN.

We have currently several other projects that we are trying to finalize. One of these is an intense effort to provide a new value for the enthalpy of formation of carbon atom. This important quantity is one of the

"key" values in the CODATA list, and is also crucial in converting theoretical atomization energies to enthalpies of formation, where inaccuracies in the used enthalpy of formation of C directly affect the accuracy of numerous high–level theoretical approaches (e.g, G*n*, W*n*, and HEAT families). The essential difficulty in delivering a reliable value is in accumulating a "critical mass" of information in the TN Graph. Namely, earlier on, the ATcT discovery of a "weak link" in the TN and the resulting reinterpretation of the spectroscopic measurements has shown that the currently accepted enthalpy of formation of C is inadequate for critical applications, but we were unable to provide a reliable "definitive" value using previous, less extensive versions of C(A)TN. We now believe that the knowledge content of C(A)TN is nearing the point where an accurate value for this quantity is at hand.

In a parallel effort, accurate ATcT benchmark values guided the development and provided validation for the new W4 approach (J. M. L. Martin, Weizmann). This state–of–the–art electronic structure approach is capable of delivering computed thermochemistry for small species that is consistently accurate to sub–kJ mol^{-1}. We are now engaged in collaboratively exploring post–W4 approaches. ATcT is also currently contributing to the development of the latest version of the HEAT approach (J. Stanton, UT Austin). In both cases the developers tried initially to use benchmarks from traditional thermochemical tabulations and rejected them unreliable and/or insufficiently accurate, turning to ATcT for help.

In collaboration with NIST, we are currently examining the thermochemistry of "key" S-containing species. The ATcT analysis has so far uncovered very serious discrepancies in the existing thermochemistry of even the most fundamental species, which propagates to almost all other S–containing species. The initial discovery of "weak links" at the foundation of the S manifold of C(A)TN is being currently pursued through additional collaborations with several leading researchers (J. M. L. Martin, Weizmann; J. Hougen, NIST; J. Boggs, UT Texas; D. Yarkony, Hopkins).

We have also numerous ongoing collaborations with other members of the Argonne Chemical Dynamics Group, where we are developing and providing ATcT thermochemistry that is crucial in evaluating and correcting the computed potential energy surfaces, or is needed as auxiliary thermochemical data in interpreting current experimental results.

Other progress

As part of the IUPAC Task Group on Thermochemistry of Radicals (where the Argonne effort is central to the success of the project), we are in the process of performing critical and meticulous evaluations of the thermochemistry of a number of small radicals and intermediate species that are important in combustion and atmospheric chemistry. The resulting "IUPAC recommended values" are being published in a series of papers. We have ongoing long–term collaboration with C.-Y. Ng (U. C. Davis) and T. Baer (UNC Chapel Hill) to perform thermochemically relevant photoionization measurements, which are driven by deficiencies or inconsistencies that are being uncovered as we are building and analyzing the Core (Argonne) Thermochemical Network. We have an ongoing long–term collaboration with J. Stanton and J. Boggs (U. Texas Austin), A. Csaszar (Eötvös U. Budapest), and J. M. L. Martin (Weizmann) on developing new and improved high–fidelity theoretical methods (where the benchmark data is developed via ATcT), as well as on computing critical thermochemistry for small radicals via state–of–the–art theory (where the selection of targets is via ATcT). We have also an ongoing collaboration with the group of T. Turany (Eötvös U. Budapest) on extending the ATcT approach toward Monte Carlo analysis of reaction mechanisms, and with A. Burcat (Technion) in refining the largest existing polynomialized thermochemical database and coupling it to ATcT.

Future Plans

Future plans of this program pivot around further developments and expansive use of Active Thermochemical Tables, driving targeted theoretical and laboratory experimental investigation of radicals and transient species that are intimately related to combustion processes. The final goal is to achieve a reliable thermochemical characterization of chemical species that are crucial in understanding and modeling the combustion processes of alternative (as well as conventional) fuels, or are implicated in

subsequent atmospheric chemistry.

This work is supported by the U.S. Department of Energy, Office of Basic Energy Sciences, Division of Chemical Sciences, Geosciences, and Biosciences, under Contract No. DE–AC02–06CH11357.

Publications resulting from DOE sponsored research (2005 - present)

- *IUPAC Critical Evaluation of Thermochemical Properties of Selected Radicals: Part I*, B. Ruscic, J. E. Boggs, A. Burcat, A. G. Csaszar, J. Demaison, R. Janoschek, J. M. L. Martin, M. L. Morton, M. J. Rossi, J. F. Stanton, P. G. Szalay, P. R. Westmoreland, F. Zabel, and T. Berces, *J. Phys. Chem. Ref. Data* **34**, 573 (2005).
- *Pulsed Field-Ionization Photoelectron-Photoion Coincidence Study of the Process $N_2 + h\nu \rightarrow N^+ + N + e^-$: Bond Dissociation Energies of N_2 and N_2^+*, X. Tang, Y. Hou, C. Y. Ng, and B. Ruscic, *J. Chem. Phys.* **123**, 074330 (2005).
- *A Collaborative Informatics Infrastructure for Multi-scale Science*, J. D. Myers, T. C. Allison, S. Bittner, B. Didier, M. Frenklach, W. H. Green, Jr., Y.-L. Ho, J. Hewson, W. Koegler, C. Lansing, D. Leahy, M. Lee, R. McCoy, M. Minkoff, S. Nijsure, G. von Laszewski, D. Montoya, L. Oluwole, C. Pancerella, R. Pinzon, W. Pitz, L. A. Rahn, B. Ruscic, K. Schuchardt, E. Stephan, A. Wagner, T. Windus, and C. Yang, *Cluster Computing* **8**, 243 (2005).
- *Third Millennium Ideal Gas and Condensed Phase Thermochemical Database for Combustion with Updates from Active Thermochemical Tables*, A. Burcat and B. Ruscic, ANL-05/20, Argonne National Laboratory, Argonne, IL, USA, and TAE 960, Technion – Israel Institute of Technology, Haifa, Israel (2005).
- *Active Thermochemical Tables: Thermochemistry for the 21st Century*, B. Ruscic, R. E. Pinzon, G. von Laszewski, D. Kodeboyina, A. Burcat, D. Leahy, D. Montoya, and A. F. Wagner, *J. Phys. Conf. Ser.* **16**, 561 (2005).
- *Theoretical Calculations on the Reaction of Ethylene with Oxygen*, H. Hua, B. Ruscic, and B. Wang, *Chem. Phys.* **311**, 335 (2005).
- *Direct Identification of Propargyl Radical in Combustion Flames by VUV Photoionization Mass Spectrometry*, T. Zhang, X. N. Tang, K.-C. Lau, C. Y. Ng, C. Nicolas, D. S. Peterka, M. Ahmed, M. L. Morton, B. Ruscic, R. Yang, L. X. Wei, C. Q. Huang, B. Yang, L. S. Sheng, Y. W. Zhang, and F. Qi, *J. Chem. Phys.* **124**, 074302 (2006).
- *Active Thermochemical Tables: Accurate Enthalpy of Formation of Hydroperoxyl Radical, HO_2*, B. Ruscic, R. E. Pinzon, M. L. Morton, N. K. Srinivasan, M.-C. Su, J. W. Sutherland, and J. V. Michael, *J. Phys. Chem.* **110**, 6592 (2006).
- *Reflected Shock Tube Studies of High-Temperature Rate Constants for $OH + NO_2 \rightarrow HO_2 + NO$ and $OH + HO_2 \rightarrow H_2O + O_2$*, N. K. Srinivasan, M.-C. Su, J. W. Sutherland, J. V. Michael, and B. Ruscic, *J. Phys. Chem.* **110**, 6602 (2006).
- *The Origin of Systematic Error in the Standard Enthalpies of Formation of Hydrocarbons Computed via Atomization Schemes*, G. Tasi, R. Izsak, G. Matisz, A. G. Csaszar, M. Kallay, B. Ruscic, and J. F. Stanton, *Chem. Phys. Chem.* **7**, 1664 (2006).
- *W4 Theory for Computational Thermochemistry: In Pursuit of Confident sub-kJ/mol Predictions*, A. Karton, E. Rabinovich, J. M. L. Martin, and B. Ruscic, *J. Chem. Phys.* **125**, 144108 (2006).
- *Unimolecular Thermal Fragmentation of ortho-Benzyne*, X. Zhang, A. T. Maccarone, M. R. Nimlos, S. Kato, V. M. Bierbaum, B. K. Carpenter, G. B. Ellison, B. Ruscic, A. C. Simmonett, W. D. Allen, and H. F. Schaefer III, *J. Chem. Phys.* **126**, 044312 (2007).
- *Kinetics of the Reaction of Methyl Radical with Hydroxyl Radical and Methanol Decomposition*, A. W. Jasper, S. J. Klippenstein, L. B. Harding, and B. Ruscic, *J. Phys. Chem. A* **111**, xxxx (2007), in press [doi:10.1021/jp067585p].
- *Benchmark Atomization Energy of Ethane: Importance of Accurate Zero-point Vibrational Energies and Diagonal Born-Oppenheimer Corrections for a 'Simple' Organic Molecule*, A. Karton, B. Ruscic, and J. M. L. Martin, *J. Mol. Struct. (Theochem)*, in press (2007) [doi:10.1016/j.theochem.2007.01.013].

Theoretical Studies of Elementary Hydrocarbon Species and Their Reactions

Henry F. Schaefer III and Wesley D. Allen
Center for Computational Chemistry
University of Georgia, Athens, GA 30602-2525
E-mail: hfs@uga.edu and wdallen@uga.edu; Phone: (706) 542-2067

Thermochemistry of Key Soot Formation Intermediates: C_3H_3 Isomers

Unraveling the complex mechanisms of soot formation stands at the forefront of modern combustion research. A primary focus is the formation and growth of polycyclic aromatic hydrocarbons (PAHs), which are the primary precursors to soot particles. The rate-limiting step in PAH formation is thought to be the formation of the first aromatic compounds (benzene or naphthalene) from smaller precursors. Although both C3 and C4 species have been hypothesized to play important roles in ring formation (via the so-called odd- and even-carbon-atom pathways), it is now generally accepted that the dominant reaction leading to the formation of benzene during combustion of aliphatic fuels is the self-reaction of the resonance-stabilized propargyl radical (2-propynyl, **1)**.

Several other isomeric forms of C_3H_3 are also energetically accessible during combustion, including the 1-propynyl (**2**), cycloprop-1-enyl (**3**), and cycloprop-2-enyl (**4**) radicals, though propargyl is universally accepted to be the lowest energy isomer. Canonical Lewis structures for species **1** - **4** are shown below. The propargyl radical is often not the initial isomer formed under typical combustion conditions: for example, the addition of CH to acetylene initially yields (**4**), rather than (**1**) directly, while the reaction of C(^3P) with vinyl radical passes through (**3**) before settling into the propargyl radical potential energy well. Pathways connecting C_3H_3 isomers **1** - **4** were previously explored using density functional theory (DFT), and details of the associated isomerization energy surface play a vital role in the lifetime and kinetics of the propargyl radical during combustion. Additional C_3H_3 isomers also exist (2-propen-1-yl-3-ylidene and 1-propen-1-yl-3-ylidene), though these alternative isomers are kinetically unstable with respect to isomerization to structures **1** - **4**.

Despite the central role of C_3H_3 radicals in the formation of aromatic rings during combustion, there are few high-level, purely *ab initio* predictions of the relative energies of C_3H_3 species available in the literature. Previous studies to characterize **1** - **4** have almost universally relied on density functional theory for the optimization of geometries. However, DFT, and in particular the popular B3LYP functional, is known to perform poorly for some unsaturated hydrocarbon radicals, giving qualitatively incorrect geometries.

State-of-the-art focal point analyses have been executed to determine very accurate enthalpies of formation for allene and propyne, as well as the propargyl (**1**), 1-propynyl (**2**), cycloprop-1-enyl (**3**), and cycloprop-2-enyl (**4**) radicals. Our extrapolations incorporate explicit computations as large as cc-pV6Z ROHF, cc-pV6Z MP2 or ZAPT2, cc-pV5Z CCSD and CCSD(T), cc-pVTZ CCSDT, and cc-pVDZ CCSDT(Q). Separate focal point analyses of core correlation effects employed computations through the cc-pCVQZ CCSD(T) level. Zero-point vibrational energies were determined via VPT2 with ANO4321 CCSD(T) harmonic frequencies appended with anharmonicities from ANO4321 MP2 quartic force fields. The diagonal Born-Oppenheimer correction (DBOC) and scalar relativistic effects were also accounted for with correlated electronic structure methods. Our approach is competitive with the HEAT 345-(Q) protocol, which for a standard test suite of small molecules yields atomization energies with errors no larger than 0.17 kcal mol^{-1}. The key methodological improvement in the focal point scheme employed here is the use of CCSDT(Q) computations to account perturbatively for connected quadruple excitations

in coupled cluster theory. Accordingly, the realm of subchemical accuracy (near 0.1 kcal mol^{-1}) in computational thermochemistry has been reached here for systems with three heavy atoms and three or four hydrogens.

By means of isodesmic reactions involving methyl, methane, acetylene, ethylene, and ethane, we determine $\Delta_f H_0^\circ$ (allene) = 47.41, $\Delta_f H_0^\circ$ (propyne) = 46.33, $\Delta_f H_0^\circ$ (propargyl) = 84.76, $\Delta_f H_0^\circ$ (1-propynyl) = 126.60, $\Delta_f H_0^\circ$ (cycloprop-1-enyl) = 126.28, and $\Delta_f H_0^\circ$ (cycloprop-2-enyl) = 117.36 kcal mol^{-1}. By comparison, use of our *ab initio* data in a direct atomization energy approach gives $\Delta_f H_0^\circ$ = 47.20, 46.14, and 84.48 kcal mol^{-1} for allene, propyne, and propargyl, respectively. Based on this comparison, the existing standardizations for the HEAT 345-(Q) method, and the small inconsistencies observed among various thermochemical routes, we estimate the errors in our recommended enthalpies of formation to be no larger than 0.3 kcal mol^{-1}. There is recent evidence that $\Delta_f H_0^\circ$ of the gaseous carbon atom should be revised upward by about 0.1 kcal mol^{-1}, a shift that would alter virtually the entire thermochemical database of hydrocarbon compounds. Any future changes that might be necessitated in the enthalpies of formation for our reference compounds can be applied readily to our final results. Immediate results of our thermochemical recommendations are the C-H bond dissociation energies of propyne and allene: $D_0(HCCCH_2–H)$ = 90.1, $D_0(H–CCCH_3)$ = 131.9, and $D_0(H_2CCCH–H)$ = 89.0 kcal mol^{-1}. Our enthalpies of formation are the most reliable values available for the C_3H_3 isomers **1** – **4** and should be incorporated into detailed kinetic models of soot formation. Additionally, our computed energy of allene relative to propyne is a suitable benchmark against which DFT methods can be tested, since this system poses a difficulty for many popular DFT functionals.

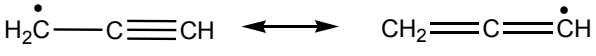

2-propynyl radical (propargyl, **1**)

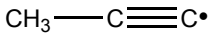

1-propynyl radical (**2**)

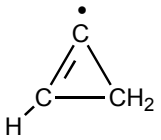

cycloprop-1-enyl radical (**3**)

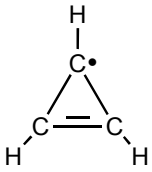

cycloprop-2-enyl radical (**4**)

In Search of the Elusive NCCO Radical

The NCCO radical is thought to be an important intermediate in combustion chemistry, but no gas-phase IR signatures of this species have ever been detected unambiguously. This absence of information is not through a lack of attention, as a number of experimental and theoretical studies concerning NCCO have been published in the literature. Generation of NCCO from various precursors has been well documented by mass spectrometry, reinforcing the viability of this radical in combustion processes. Such parent compounds include carbonyl cyanide [$CO(CN)_2$], pivaloyl cyanide [$NCC(O)C(CH_3)_3$], methyl cyanoformate [$NCC(O)OCH_3$], and acetyl cyanide [$CH_3C(O)CN$]. McNavage, Dailey, and Dai [Can. J. Chem. **82,** 925 (2004)] photodissociated the first three compounds in an effort to achieve the first vibrational characterization of the NCCO radical. The photolysis species were probed by means of time-resolved Fourier transform infra-red emission spectroscopy (TR-FTIRES). The spectra emanating from the different precursors were disentangled by means of two-dimensional cross-spectra correlation analysis, devised to elucidate the features due to NCCO; this analysis yielded (ν_1, ν_2) stretching fundamentals of (2093, 1774) cm^{-1}. Following this research, Hershberger and co-workers intended to use these characteristic frequencies to monitor the NCCO radical via infrared diode laser absorption spectroscopy in order to study the kinetics of its reactions with NO_x species. Despite using methyl

cyanoformate and acetyl cyanide precursors, which have proved to be reliable sources of NCCO, no signals were observed that could be definitively ascribed to the ν_1 mode of the NCCO radical.

In order to establish definitive signatures of the elusive NCCO radical, we have pinpointed its fundamental vibrational frequencies by applying second-order vibrational perturbation theory (VPT2) to the complete quartic force field computed at the all-electron (AE) coupled cluster singles, doubles, and perturbative triples level [CCSD(T)] with the large correlation-consistent, polarized core-valence quadruple-zeta (cc-pCVQZ) basis set. This rigorous methodology provides highly accurate predictions of both the harmonic vibrational frequencies and their associated anharmonicities without any empirical scaling. As a point of calibration, our procedure gives (ω_e, $\omega_e x_e$) = (2173.6, 13.1) cm^{-1} for diatomic CO, in excellent agreement with the experimental values of (2169.8, 13.3) cm^{-1}. Our AE-CCSD(T)/cc-pCVQZ computations determine that NCCO is a planar molecule with a $^2A'$ electronic ground state and the equilibrium geometric parameters r_e(N-C) = 1.1623 Å, r_e(C-C) = 1.4370 Å, r_e(C-O) = 1.1758 Å, θ_e(N-C-C) = 168.55°, and θ_e(C-C-O) = 132.22°. The CCSD(T)/cc-pCVQZ values of the characteristic stretching frequencies ν_1(C≡N) and ν_2(C=O) are 2171 cm^{-1} and 1898 cm^{-1}, respectively, substantially removed from the previous experimental assignments of 2093 cm^{-1} and 1774 cm^{-1}. Our definitive results should greatly aid efforts to characterize the NCCO radical by high-resolution vibrational spectroscopy.

Key energetic quantities for the NCCO radical were determined by focal-point extrapolations using correlation-consistent basis sets cc-pV*X*Z (*X* = D,T,Q,5,6) and electron correlation treatments as extensive as full coupled cluster singles, doubles, and triples (CCSDT) with perturbative accounting of quadruple excitations [CCSDT(Q)]. The converged vibrationless barrier to linearity of NCCO is 8.4 kcal mol^{-1}, and the dissociation energy (D_0) of NCCO → NC + CO is 26.5 kcal mol^{-1}, an unusually small bond energy. Using our precisely determined dissociation energy, we ascertain a new enthalpy of formation for NCCO of $\Delta_f H_0^\circ = 50.9 \pm 0.3$ kcal mol^{-1}.

Next-generation, explicitly correlated electronic structure methods

All common wavefunction methods of electronic structure theory have a fundamental and troublesome flaw: the inability to correctly describe the exact mathematical cusp behavior of many-electron wavefunctions in the vicinity of coalescence points (Coulomb singularities), and hence to fully account for instantaneous, short-range correlation among electrons. Achieving high thermochemical accuracy requires *next-generation* methodologies that solve the electron cusp problem by explicitly incorporating interelectronic variables (r_{12}) into molecular wavefunctions. We have continued to pursue a long-term research program to further develop highly accurate *explicitly correlated* methods, to create attendant state-of-the-art computer codes, to undertake practical chemical applications of unprecedented size, and to disseminate such expertise to the scientific community. Our computer codes have been used in numerous chemical applications that conjoin conventional CCSD(T) and explicitly correlated MP2 methods within a focal point extrapolation scheme for pinpointing the *ab initio* limit of electronic structure theory. Unprecedented accuracy has thus been achieved for contemporary problems in combustion and other areas. Most recently we have programmed R12 second-order perturbation theory methods for explicitly-correlated computations on *open-shell* molecules in both unrestricted (UHF) and restricted (ROHF) formalisms. Our codes use a full integral-direct approach and are multithreaded, allowing parallel processing on SMP machines. Open-shell R12 computations with over a thousand basis functions are thus routine. An era is approaching in which explicitly-correlated computations with atomic orbital basis sets as small as cc-pVDZ will commonly deliver results as accurate as conventional computations with a cc-pVQZ basis set, thus providing better than chemical accuracy for increasingly larger chemical systems.

Publications Supported by DOE: 2004, 2005, 2006

1. K. W. Sattelmeyer, Y. Yamaguchi, and H. F. Schaefer, "Energetics of the Low-Lying Isomers of HCCO," *Chem. Phys. Lett.* **383**, 266 (2004).
2. L. D. Speakman, B. N. Papas, H. L. Woodcock, and H. F. Schaefer, "A Reinterpretation of Microwave and Infrared Spectroscopic Studies of Benzaldehyde," *J. Chem. Phys.* **120**, 4247 (2004).
3. R. L. DeKock, M. J. McGuire, P. Piecuch, W. D. Allen, H. F. Schaefer, K. Kowalski, S. A. Kucharski, M. Musial, A. R. Bonner, S. A. Spronk, D. B. Lawson, and S. L. Laursen, "The Electronic Structure and Vibrational Spectrum of *trans*-HNOO," *J. Phys. Chem. A* **108**, 2893 (2004).
4. M. Schuurman, S. Muir, W. D. Allen, and H. F. Schaefer, "Toward Subchemical Accuracy in Computational Thermochemistry: Focal Point Analysis of the Heat of Formation of NCO and [H, N, C, O] Isomers," *J. Chem. Phys.* **120**, 11586 (2004).
5 Y. Yamaguchi and H. F. Schaefer, "The Diazocarbene (CNN) Molecule: Characterization of the $\tilde{X}^3\Sigma^-$ and $\tilde{A}^3\Pi$ Electronic States," *J. Chem. Phys.* **120**, 9536 (2004).
6. S. E. Wheeler, W. D. Allen, and H. F. Schaefer, "Thermochemistry of Disputed Soot Formation Intermediates C_4H_3 and C_4H_5," *J. Chem. Phys.* **121**, 8800 (2004).
7. R. K. Sreeruttun, P. Ramasami, G. Yan, C. S. Wannere, P.v. R. Schleyer, and H. F. Schaefer, "The Alkylethynyl Radicals, $\bullet C{\equiv}C{-}C_nH_{2n+1}$($n$ = 1-4), and their Anions," William L. Hase Special Issue, *Int. J. Mass Spec.* **241**, 295 (2005).
8. M. S. Schuurman, W. D. Allen, P. v. R. Schleyer, and H. F. Schaefer, "The Highly Anharmonic BH_5 Potential Energy Surface Characterized in the *Ab Initio* Limit," *J. Chem. Phys.* **122**, 104302 (2005).
9. M. S. Schuurman, W. D. Allen, and H. F. Schaefer, "The *Ab Initio* Limit Quartic Force Field of BH_3," *J. Comput. Chem.* **26**, 1106 (2005).
10. A. V. Sergeev, D. Z. Goodson, S. E. Wheeler, and W. D. Allen, "On the Nature of the Møller-Plesset Critical Point," *J. Chem. Phys.* **123**, 064105 (2005).
11. B. N. Papas and H. F. Schafer, "Concerning the Precision of Standard Density Functional Programs: GAUSSIAN, MOLPRO, NWCHEM, QCHEM, and GAMESS," *J. Mol. Struct.* **768**, 175 (2006).
12. X. Zhang, Q. Li, J. B. Ingels, A. C. Simmonett, S. E. Wheeler, Y. Xie, R. B. King, H. F. Schaefer, and F. A. Cotton, "Remarkable Electron Accepting Properties of the Simplest Benzenoid Cyanocarbons: Hexacyanobenzene, Octacyanonaphthalene, and Decacyanoanthracene," *J. Chem. Soc. (London) Chem. Comm.* **758** (2006).
13. N. C. Handy, S. Carter, Y. Yamaguchi, S. Li, and H. F. Schaefer, "Rovibrational Energy Levels for the Electronic Ground State of AlOH," *Chem. Phys. Lett.* **427**, 14 (2006).
14. D. Moran, A. C. Simmonett, F. E. Leach III, W. D. Allen, P. v. R. Schleyer, and H. F. Schaefer, "Popular Theoretical Methods Predict Benzene and Arenes to be Nonplanar," *J. Am. Chem. Soc.* **128**, 9342 (2006), communication. See highlight in Editor's Choice, *Science* **313**, 149 (July 14, 2006 issue).
15. X. Zhang, A. T. Maccarone, M. R. Nimlos, S. Kato, V. M. Bierbaum, G. B. Ellison, B. Ruscic, A. C. Simmonett, W. D. Allen, and H. F. Schaefer, "Unimolecular thermal fragmentation of *ortho*-benzyne," *J. Chem. Phys.* **126**, 044312 (2007).
16. S. E. Wheeler, K. A. Robertson, W. D. Allen, H. F. Schaefer, Y. J. Bomble, and J. F. Stanton, "Thermochemistry of Key Soot Formation Intermediates: C_3H_3 Isomers," Jim Miller Festschrift, *J. Phys. Chem. A*, web release April 3, 2007.
17. V. Kasalova, W. D. Allen, H. F. Schaefer, E. D. Pillai, and M. A. Duncan, "Model Systems for Probing Metal Cation Hydration," Roger E. Miller Memorial Issue, *J. Phys. Chem. A.*, in press (2007).
18. A. C. Simmonett, F. A. Evangelista, W. D. Allen, and H. F. Schaefer, "In Search of Definitive IR Signatures of the Elusive NCCO Radical," *J. Chem. Phys.,* submitted (2007).
19. R. K. Sreeruttun, P. Ramasami, C. S. Wannere, and H. F. Schaefer, "The π-PhenylethynylRadical and its Isomers *o*-, *m*-, and *p*-Ethynylphenyl: Structures, Energetics, and Electron Affinities," *J. Org. Chem.*
20. L. Belau, S. E. Wheeler, B. W. Ticknor, M. Ahmed, S. R. Leone, W. D. Allen, H. F. Schaefer, and M. A. Duncan, "Ionization Thresholds of Small Carbon Clusters: Tunable VUV Experiments and Theory," *J. Am. Chem. Soc.*, submitted (2007).

Gas-Phase Molecular Dynamics: Spectroscopy and Dynamics of Transient Species

Trevor J. Sears (sears@bnl.gov),
Department of Chemistry, Brookhaven National Laboratory, Upton, NY 11973-5000

Program Scope

This research is carried out as part of the Gas-Phase Molecular Dynamics program in the Chemistry Department at Brookhaven National Laboratory. High-resolution spectroscopy, augmented by theoretical and computational methods, is used to investigate the structure and reactivity of chemical intermediates in the elementary gas-phase reactions involved in combustion chemistry and in chemical processes occurring at or near surfaces of heterogeneous catalysts. Techniques to improve the sensitivity of laser spectroscopy are developed as are models of intra-and inter-molecular interactions in molecular free radicals and other reactive species. The results lead to improved understanding and modeling of processes involving these species and are applicable to a wide variety of practical problems.

Recent Progress

CH_2 c-state double resonance measurements

We have extended our optical-optical double resonance studies of CH_2 in its a^1A_1, b^1B_1 and c^1A_1 states to other vibronic levels and have very recently demonstrated a more convenient and less obvious double resonance scheme. For experimental reasons it is desirable to employ a more easily scanned pulsed laser system to search for unknown transitions. Yet if the sequence of fixed and scanning lasers is reversed, using a cw laser on a fixed *a–b* transition, while scanning a pulsed laser in search of *b–c* resonances, one might not anticipate any observable signal to mark the double resonance condition, since the first transition is not strongly pumped and the *b* state population is negligible. However, we have recently shown that AC Stark level shifts and broadening induced by moderate-power (~5 mJ), unfocused, nanosecond laser pulses can be sensitively detected by the cw probe laser beam monitoring the known *b–a* transition. The distinctive observed lineshapes are well modeled by sub-Doppler, pump-frequency-dependent broadening and shifting of the *a–b* resonance, as the pump laser is tuned through the *b–c* resonance. This new scheme for detecting optical-optical double resonance spectra has several immediately exciting potential applications, some of which are discussed below.

New spectra of CH_2 at 1.3 microns.

Near infrared spectra of CH_2 at 1.3 micron wavelengths have characterized ro-vibronic levels at energies at and below the barrier to linearity of the two lowest singlet states. The data also provide much new information on the rotational structure of the bending excited lower $a\ ^1A_1$ state which is being used to determine a more precise and complete set of rotational term values for this vibronic state. Perturbations due to background $X\ ^3B_1$ levels are smaller in (010) than (000), but some relatively weakly perturbed levels have been identified. Rotational levels in (040) of the *X* state are the most likely candidates for the perturbers and, for the first time, one specific triplet interacting level has been identified.

The diffuse structure in ultraviolet spectra of the $GeCl_2$ A–X transition

There has been controversy in the literature since the first observation by Karolczak et al. in 1993 of an extended diffuse section in the spectrum of $GeCl_2$. The diffuse structure begins at approximately 31630 cm^{-1} (316 nm vacuum wavelength) and extends to shorter wavelengths. We have explored the hypothesis that this diffuse structure arises from the LIF spectrum of the $GeCl_2$…$GeCl_2$ van der Waals dimer complex based on our CIS(D)/cc-pVTZ calculations. Three isomers on the ground-state potential energy surface were characterized. The most stable dimer has a dissociation energy of 0.74 eV and has a trans-

$(GeCl_2)_2$ structure. There is also a related, less stable, cis-minimum. These isomers are not responsible for the diffuse spectra in $GeCl_2$ as they have zero Frank-Condon intensity to the first excited singlet electronic state. A third, C_i symmetry, isomer has a binding energy of 0.31 eV. It is found that this C_i isomer has substantial dipole transition strength to the first excited singlet state of the dimer with a vertical excitation energy of 3.33 eV. The transition energy (T_0) between this C_i isomer and the van der Waals complex on the singlet excited state is predicted to be 4.007 eV, or a 1104 cm^{-1} blue shift with respect to that of the $GeCl_2$ *A–X* transition, closely matching the experimental observation. We have therefore proposed that dimer absorption and emission can explain the diffuse structure that has been observed in the ultraviolet spectra of $GeCl_2$.

Laser Induced Fluorescence of transition metal-containing radicals

The spectroscopy of transition metal-containing radical species is being investigated using a laser ablation source coupled with a supersonic molecular beam source and laser-induced fluorescence. Such species provide extreme tests of current computational models due to the presence of multiple low-lying electronic states and complete breakdown of the Born-Oppenheimer approximation. Particular interest lies in molecular species related to the intermediates occurring at the gas-surface interface in catalytically active systems and building blocks for unusually stable met-car complexes. New spectra have been observed in the La + alkane and alkene systems that, by analogy with known YC_2 spectra, are possibly due to LaC_2. Much additional spectroscopic work is required before the spectra can be understood, however it appears that they must be due to larger than diatomic species.

Future Plans

Severe breakdown of the Born-Oppenheimer approximation in CCX species

Ethynyl and substituted ethynyl radicals are particularly interesting species because the ground and first excited electronic states lie exceptionally close in energy. The best characterized is CCH, where the ground $X\ ^2\Sigma$ and first excited $A\ ^2\Pi$ states are separated by only about 3000 cm^{-1}. The chloro- and bromo-compounds are potentially even more pathological: the state separation is only on the order of 200 cm^{-1}, the vibronic absorption spectrum extends through the near-IR, and the spectroscopic transitions cannot be simply assigned as either vibrational or electronic in character. The vibronic structure of these species has very recently been examined using some of the most advanced theoretical and computational techniques currently available including the Breit-Pauli approximation of the relativistic Hamiltonian and both bending and stretching vibrational motion. Some years ago, we recorded new spectral bands in a photolytic $HCBr_3$ system that we tentatively attributed to CCBr. The secondary chemistry in bromoform photolysis is complex and known to make C_2 species, and the observed isotopic splitting structure was consistent with a single Br atom. Although rotational branches were assigned at the time, and the rotational constant derived from them is consistent with that expected for the molecule, we were not able to make any further progress assigning the spectrum. With the new theoretical advances, it has been possible to make some further progress and the observed structure of our old spectra is now understood. We will attempt to record the CCBr spectrum in absorption at longer wavelengths than our previous data (near 1 micron) by mixing one of our c.w. Ti:sapphire lasers with a new c.w. YAG or fiber amplified extended cavity diode laser system in periodically-poled lithium niobate, to access wavelengths as long as 3.5 microns. Other new high-resolution laser systems based on mixing of fiber-amplified, extended cavity diode lasers are also becoming available, and it is unclear at present which type of system is to be preferred, particularly as ultra-precise frequency-comb-referenced laser sources also become commercially available.

Spectroscopic determination of ΔE_{ST} for methylene

Building on developments in OODR techniques, we will attempt a measurement of the singlet-triplet energy splitting for CH_2 to spectroscopic accuracy. While FM probing an *a-b* transition involving a level of mixed singlet-triplet character in the $a\ ^1A_1$ state, we will scan a pulsed laser source in the 3 micron

region seeking downward *a-X* transitions to levels in the $X\ ^3B_1$ state. The pump transitions obtain their intensity as vibrational overtones within the $X\ ^3B_1$ state. The bending potential in the *X* state is highly anharmonic, so the transition moment is far from negligible. Using the double resonance method with a mixed state allows a sensitive near-infrared singlet-based detection scheme to report the triplet-based vibrational resonance. The current best estimate for the singlet-triplet splitting comes from a combination of theoretical extrapolation and knowledge of specific mixed states in a $^1A_1(000)$. We hope to provide a definitive, completely experimental, value for this splitting.

Higher electronic states and predissociation in methylene

The nature of the higher vibrational levels of the *c* state of CH_2 has become a subject of recent theoretical interest. A series of surface intersections involving the *c* state have consequences for the reaction of C (^1D) with H_2 as well as predissociation thresholds of the *c* state. There is disagreement over whether the *c* state predissociation is due to direct coupling with the H+CH(*X*) continuum of the *a/b* states, or if the coupling is via higher energy Rydberg levels that form an effective adiabatic barrier to predissociation above the H+CH dissociation threshold. The highest energy bands ascribed to *c-a* transitions by Herzberg were at 332.9 nm, placing the highest observed sharp levels of the *c* state in the vicinity of both the C(^1D) $+H_2$ and the H+CH($X\ ^2\Pi$) asymptotes. Systematic investigation in the energy region of the (0,12,0), (0,13,0) and higher levels of the *c* state could provide spectroscopic clues to the predissociation and an experimental bound on the bond dissociation energy of singlet CH_2. The ac Stark detected double resonance method should continue to provide a sensitive means of observing predissociation broadened transitions from a sharp *b* state level to short-lived *c* state levels, however we have made some preliminary searches for broadened transitions without success. Direct absorption using frequency-doubled c.w. lasers (see below) will provide an alternative route. At somewhat higher energies still, there is a calculated *d* ($^1A_2$) state with an acute HCH angle that should cross the *b* ($^1B_1$) state in a conical intersection of A″ symmetry. No spectroscopic information is currently available concerning these interesting states and interactions.

AC Stark determination of dipole transition moments

The quantitative broadening and shifting of the AC Stark double resonance spectra depend in principle on the absolute electric field strength of the strong coupling laser and the transition dipole connecting the strongly coupled levels. The precision of our frequency domain measurements encourages us to attempt to develop a more rigorous theoretical description of the multilevel system that may provide a method to extract experimental electronic transition moments for radical species, without the need for calibrating absolute populations. Previous measurements of intensity-dependent Autler-Townes splitting have been used for such purposes, but limited to atoms and highly polarizable diatomic molecules. If theoretical developments warrant, we propose proof-of-principle experiments in the CN *X-A-B* system, where the spectroscopy is simpler than in CH_2, and results can be compared to previously established values.

High-resolution spectroscopy of radicals and aromatic precursors to PAHs in combustion

In the quest for renewable alternatives to fossil fuels, a number of new fuel sources including partially oxygenated hydrocarbons such as methyl esters and others containing heavier hydrocarbon fractions than traditional petroleum are being investigated. There is also renewed interest in cleaner-burning of traditional diesel fuels, in current and future compression-ignition engines. All these options will require understanding of new mechanistic pathways in combustion chemistry, involving poorly characterized intermediates. Of particular concern are larger intermediate species, including those containing multiple aromatic rings and the likelihood of increased micro- and nano-particulate soot formation resulting from their incomplete combustion. We propose a new effort to investigate these species, in particular polycyclic aromatics, and related radical intermediate precursors using very high resolution spectroscopic techniques. The new experiments will make use of absorption-based spectroscopy, including cavity ring-down, at infrared and near-uv wavelengths using compact extended-cavity diode laser sources combined with non-linear frequency generation techniques.

Publications 2005-2007

Observation of the c^1A_1 state of methylene by optical-optical double resonance
Y. Kim, A. V. Komissarov, G. E. Hall and T. J. Sears
J. Chem Phys. **123**, 024306 (2005).
Potential energy surfaces and vibrational energy levels of DCCl and HCCl in three low-lying states.
H. G. Yu, T. J. Sears and J. T. Muckerman
Molec. Phys. **104**, 47-53 (2006).
Rotationally resolved spectrum of the A(060) – X(000) band of HCBr
G. E. Hall, T. J. Sears and H. –G. Yu
J. Molec. Spectrosc. **235**, 125-131 (2006).
Hot bands in jet-cooled and ambient temperature spectra of chloromethylene
Z. Wang, R. G. Bird, H. –G. Yu and T. J. Sears
J. Chem. Phys. **124**, 074314 (2006).
Photoinduced Rydberg ionization spectroscopy of phenylacetylene: vibrational assignments of the C state of the cation
H. Xu, P. M. Johnson and T. J. Sears,
J. Phys. Chem. A. **110**, 7822-7825 (2006).
The spectrum of CH_2 near 1.36 and 0.92 microns: Re-evaluation of rotational level structure and perturbations in a(010).
K. Kobayashi, G. E. Hall and T. J. Sears
J. Chem. Phys. **124,** 184320 (2006).
State-resolved thermalization and singlet-triplet interconversion in CH_2
A. V. Komissarov, A. Lin, T. J. Sears and G. E. Hall
J. Chem. Phys. **125**, 084308 (2006).
AC Stark detection of optical-optical double resonance in CH_2
Y. Kim, G. E. Hall and T. J. Sears
Phys. Chem. Chem. Phys. **8**, 2823-2825 (2006).
A clue to the diffuse structure in ultraviolet spectra of $GeCl_2$ A-X transition
H. -G. Yu and T. J. Sears
J. Chem. Phys. **125**, 114316 (2006).
The calculation of vibrational intensities in forbidden electronic transitions
P. M. Johnson, H. Xu and T. J. Sears,
J. Chem. Phys **125**, 164330 (2006).
Photoinduced Rydberg ionization spectroscopy of the B state of benzonitrile cation
H. Xu, P. M. Johnson and T. J. Sears,
J. Chem. Phys **125**, 164331 (2006).
Observation of the $c^1A_1(0,10,0)$ state of CH_2 by optical-optical double resonance
Y. Kim, G. E. Hall and T. J. Sears
J. Molec. Spectrosc. **240** 269-271 (2006).

Picosecond Optical Diagnostics

Thomas B. Settersten
Combustion Research Facility, Sandia National Laboratories
P.O. Box 969, MS 9056
Livermore, CA 94551-0969
tbsette@sandia.gov

Program Scope

This program focuses on the development of innovative laser-based detection strategies for important combustion radicals and the investigation of the fundamental physical and chemical processes that directly affect quantitative application of these techniques. These investigations include the study of fundamental spectroscopy, energy transfer, and photochemical processes. This aspect of the research is essential to the correct interpretation of diagnostic signals, enabling reliable comparisons of experimental data and detailed combustion models. Many of these investigations use custom-built tunable picosecond (ps) lasers, which enable efficient nonlinear excitation, provide high temporal resolution for pump/probe studies of collisional processes, and are amenable to detailed physical models of laser-molecule interactions.

Recent Progress

Time-Resolved ps-LIF. A direct and accurate way to obtain quenching cross sections is to time-resolve the fluorescence signal following short-pulse laser excitation and to observe the variation of the fluorescence lifetime as a function of the quencher pressure. Using custom-built ps lasers and fast electronics for time-resolved LIF, we have measured precisely the temperature and species dependence of fluorescence quenching cross sections of CO B $^1\Sigma^+(v{=}0)$[1] and NO A $^2\Sigma^+(v{=}0)$,[2] which are the excited states that are commonly used for fluorescence detection of these species. The new quenching characterization for NO A $^2\Sigma^+(v'{=}0)$ significantly improves the calibration factors for LIF measurements of NO concentration in flames. In addition to improving the accuracy of NO imaging, the precision of our data enable, for the first time, the observation of subtle temperature dependencies in quenching cross sections, which provide new scientific insight into the mechanisms responsible for the quenching (see Ref. [2]).

In two recent experiments using time-resolved ps-LIF,[2,3] our measurements indicate that the natural lifetime of NO A $^2\Sigma^+(v'{=}0)$ is 194±2 ns. This value is within the 202 ± 14-ns range recommended by Piper and Cowles,[4] who averaged determinations of the fluorescence lifetime published prior to 1986. Our result is, however, outside the uncertainty limits assigned to the most recent determination (205±7 ns) by Luque and Crosley[5] and is consistently shorter than other direct measurements of the lifetime using time-resolved LIF.[2] An accurate lifetime measurement is important because other spectroscopic constants are linked to its value. Luque and Crosley scaled their empirically derived electronic transition moment function (ETMF) to a $v'{=}0$ lifetime of 206 ns in their determination of absolute transition probabilities for the NO A–X system. Because a shorter A($v'{=}0$) lifetime is suspect and implies increased values for all of the published Einstein A coefficients, we

verified the accuracy of our previous measurements with an independent technique (time-correlated single-photon counting) and systematically investigated experimental artifacts occurring in time-resolved LIF. We trace the source of disagreement between measurements to problems with the instrument response of *dynode-chain* photomultiplier tubes (PMT), which are commonly used for analog lifetime measurements.[6] Artifacts, which include PMT afterpulsing and a long (microseconds duration) tail, can result in a measurement bias towards longer lifetime. We eliminate these artifacts in our approach by operating a *microchannel-plate* PMT well within its linear range. We also identify a means to reduce significantly the artifacts from decays obtained with the much more affordable dynode-chain PMTs by removing the last two dynodes from the gain chain to operate it with greatly reduced gain.[6] We recently measured the A(v'=0,1,2) lifetimes with high precision, and we are using our more accurate lifetimes in a reassessment of the ETMF for the A–X system.

We focussed considerable effort on the details of experimental apparatus and data analysis to produce very accurate and precise measurements of fluorescence lifetimes. During the development of this expertise, we collaborated with Habib Najm and Youssef Marzouk (Sandia) to use Bayesian parameter estimation to analyze our experimental data.

We are extending our quenching experiments to temperatures of up to 2000 K using premixed, low-pressure flames. Initial work focused on the design and construction of a low-pressure flame facility, which is now complete. Experiments to characterize quenching of O($3p\,^3P$) are underway. These measurements are integral to the development of quantitative imaging of atomic oxygen, a diagnostic that we are collaboratively implementing in Jonathan Frank's lab (Sandia). Future experiments will characterize quenching of H(n=3), CO B, and NO A.

Two-Photon CO LIF. In collaboration with Roger Farrow, Jonathan Frank, and Rob Barlow (Sandia), we are developing a comprehensive density-matrix-based model for quantification of two-photon CO LIF. The model predicts the dependence of CO-LIF signals on the local gas composition, temperature, and pressure, and on the laser pulse width, irradiance, and excitation wavelength. The density-matrix approach enables modeling of excitation with nanosecond and subnanosecond laser pulses. The model incorporates results from experimental studies of CO photophysics and spectroscopy, many of which were funded by this BES program. These studies provide the measurements necessary to describe two-photon absorption, photoionization, Stark shift, pressure broadening and shift, photolytic interference, ground-state rotational energy transfer, and electronic quenching. Continued development and validation of the model will involve collaboration with Jonathan Frank and Rob Barlow, who routinely use the CO diagnostic in their research.

Future Plans

Fluorescence quenching. We will systematically investigate quenching in a series of low-pressure flames. A variety of premixed low-pressure flames, using various fuels, oxidizers, diluents, and flow rates will be utilized to achieve the desired conditions; working with Habib Najm, we will determine an appropriate matrix of flames. Accurate temperature characterization of the flames is essential, as flame calculations using the Sandia PREMIX code will be constrained by the experimentally measured temperature profiles to calculate the chemical composition relevant to the quenching measurements. In a continued collaboration with Habib Najm, we will apply Bayesian parameter estimation to extract temperature- and species-dependent cross sections for quenching of O($3p\,^3P$),

H(n=3), CO B, and NO A from the fluorescence lifetime measurements.

Time-resolved ps-LIF imaging. Formaldehyde is produced in the initial oxidation of hydrocarbon fuels, and high levels of CH_2O result from incomplete combustion, which is problematic for low-load operation of low-temperature combustion devices. LIF visualization of CH_2O has been used in combustion research, but quantifying CH_2O LIF is difficult because of the complex temperature and pressure dependence of quenching. We propose to investigate fluorescence lifetime imaging and the feasibility of prompt ps-LIF imaging for quenching-independent measurements of CH_2O using a fast gated intensified camera to detect the LIF signal generated by 50-ps excitation of CH_2O in flames. By using a gate width of approximately 500 ps, simple modeling indicates that signal variation due to quenching in atmospheric-pressure flames will be reduced from the 300–400% level to less than 10%.

As we develop this time-gated, ps-LIF approach, we envision potential improvements for LIF imaging of other species as well. NO and OH lifetimes, for example, are on the order of 1–3 ns in atmospheric-pressure flames. Using ∼100-ps gate times in combination with ps excitation, we should be able to produce "quench-free" images of these species. Furthermore, short-gate imaging of ps-LIF offers increased suppression of fluorescence interference for measurements where the fluorescence lifetime of the target species and that of the interfering species are much different. For example, in the measurement of CO using two-photon LIF, narrow-band detection of the CO fluorescence is often used to avoid C_2 Swan band interference produced in locally rich regions of the flame. Spectral discrimination against the C_2 interference, however, rejects most of the CO fluorescence, which is emitted in a broad vibrational progression. Because the fluorescence lifetime of CO is an order of magnitude shorter than that of C_2, gated detection of the CO fluorescence will reject most of the interference while collecting most of the CO fluorescence. A similar advantage may be possible for rejecting PAH fluorescence interference in H imaging.

Two-photon ps-LIF detection of atomic hydrogen. Atomic hydrogen plays a key role in ignition, flame propagation, and heat release because of its high reactivity and diffusivity. Although two-photon LIF can be used for sensitive, spatially resolved detection of H, its quantitative application in flames is plagued by photolytic interference and limited quenching data. Several multi-photon LIF schemes have been used in prior work, and initially we will focus on the simplest, which uses two-photon excitation at 205-nm ($3d\ ^2\mathrm{D} \leftarrow\leftarrow 1s\ ^2\mathrm{S}$) to excite fluorescence at 656 nm (n=3→n=2). One of the reasons that prior investigators used more complex excitation schemes was to reduce photolytic interference, which has been attributed to photodissociation of H_2O and CH_3. These alternative approaches require the absorption of three photons from either one or two laser beams, which significantly complicates laser-sheet corrections for quantitative imaging applications. As we demonstrated with two-photon ps-LIF detection of atomic oxygen, when compared to ns excitation, ps excitation reduces interference due to single-photon photolysis by allowing the use of reduced laser energy.[7–9] We propose to collaborate with Jonathan Frank to assess improvement offered by ps H-atom imaging by comparing directly H-atom line images excited with laser pulses of ps or ns duration. Additionally, we will characterize the photolytic interference in flames using a pump-probe technique employing a detuned, ns-duration, laser pulse to photolytically produce atomic hydrogen under different flame conditions. The photoproduct will be probed and compared to nascent H using a weak, time-delayed, ps probe.

High-Pressure Diagnostic Development. To date, our experimental efforts have focused on well-controlled environments at atmospheric pressure or below. A clear need exists for diagnos-

tic development at elevated pressures, and we propose to initiate a new research focus to explore optical diagnostics in the high-pressure regime. As a first step towards the development of diagnostic tools for high-pressure, we propose initial experiments at approximately 10 bar. This intermediate-pressure level begins to include important pressure effects on chemistry, is not as technically challenging as the higher pressures and thus provides an intermediate step for diagnostic development, and is representative of some furnace and turbine devices. Based on discoveries at 10 bar, future experiments will scale to higher pressures. We plan to design and build a high-temperature (∼1000 K), high-pressure (∼50 bar) flow cell for this work. In addition to controlled gas composition, the facility design will include a capability to seed the flow with particulate matter. The cell will provide a well-characterized collisional environment with optical access for laser-based diagnostics, including LIF, laser-induced incandescence, and wave-mixing spectroscopy. This new capability will enable pressure scaling studies of diagnostics, including the characterization of the photophysical properties of key species, and will serve as a test-bed for new optical approaches.

References

[1] T. B. Settersten, A. Dreizler, R. L. Farrow, J. Chem. Phys. **117**, 3173 (2002).

[2] T. B. Settersten, B. D. Patterson, J. A. Gray, J. Chem. Phys. **124**, 234308 (2006).

[3] T. B. Settersten, B. D. Patterson, H. Kronemayer, V. Sick, C. Schulz, J. W. Daily, Phys. Chem. Chem. Phys. **8**, 5328 (2006).

[4] L. G. Piper, L. M. Cowles, J. Chem. Phys. **85**, 2419 (1986).

[5] J. Luque, D. R. Crosley, J. Chem. Phys. **112**, 9411 (2000).

[6] B. D. Patterson, W. H. Humphries III, T. B. Settersten, "Time-domain measurement of fluorescence lifetimes: instrumental bias in analog detection with dynode-chain photomultiplier tubes," (2007), in preparation.

[7] T. B. Settersten, A. Dreizler, B.D. Patterson, P. E. Schrader, R. L. Farrow, Appl. Phys. B **76**, 479 (2003).

[8] J. H. Frank, X. Chen, B. D. Patterson, T. B. Settersten, Appl. Opt. **43**, 2588 (2004).

[9] J. H. Frank, T. B. Settersten, Proc. Combust. Instit. **30**, 1527 (2005).

BES-Supported Publications (2005-present)

J. H. Frank, T. B. Settersten,"Two-photon LIF imaging of atomic oxygen in flames with picosecond excitation," *Proc. Combust. Instit.*, **30**, 1527 (2005).

J. W. Daily, W. G. Bessler, C. Schulz, V. Sick, T. B. Settersten,"Role of non-stationary collisional dynamics in determining nitric oxide LIF spectra," *AIAA J.*, **43**, 458 (2005).

T. B. Settersten, B. D. Patterson, J. A. Gray, "Temperature- and species-dependent quenching of NO $A\,^2\Sigma^+(v'=0)$ probed by two-photon laser-induced fluorescence using a picosecond laser," *J. Chem. Phys.*, **124**, 234308 (2006).

T. B. Settersten, B. D. Patterson, H. Kronemayer,V. Sick, C. Schulz, J. Daily,"Branching ratios for quenching of nitric oxide $A\,^2\Sigma^+(v'=0)$ to $X\,^2\Pi(v''=0)$," *Phys. Chem. Chem. Phys.* **8**, 5328 (2006).

X. Chen, T. B. Settersten, "Investigation of OH X $^2\Pi$ collisional kinetics in a flame using picosecond two-color resonant four-wave-mixing spectroscopy," *Appl. Opt.* **46**(19), in press (2007).

W. D. Kulatilaka, R. P. Lucht, S. Roy, J. R. Gord, T. B. Settersten, "Detection of atomic hydrogen in flames using picosecond two-color two-photon-resonant six-wave-mixing spectroscopy," *Appl. Opt.* **46**(19), in press (2007).

C. A. Bauer, T. V. Timofeeva, T. B. Settersten, B. D. Patterson, V. H. Liu, B. A. Simmons, M. D. Allendorf, "Influence of Connectivity and Porosity on Ligand-Based Luminescence in Zinc Metal-Organic Frameworks," *J. Am. Chem. Soc.*, in press (2007).

Theoretical Studies of Potential Energy Surfaces and Computational Methods

Ron Shepard
Chemistry Division, Argonne National Laboratory, Argonne, IL 60439
[email: shepard@tcg.anl.gov]

Program Scope: This project involves the development, implementation, and application of theoretical methods for the calculation and characterization of potential energy surfaces (PES) involving molecular species that occur in hydrocarbon combustion. These potential energy surfaces require an accurate and balanced treatment of reactants, intermediates, and products. This difficult challenge is met with general multiconfiguration self-consistent-field (MCSCF) and multireference single- and double-excitation configuration interaction (MR-SDCI) methods. In contrast to the more common single-reference electronic structure methods, this approach is capable of describing accurately molecular systems that are highly distorted away from their equilibrium geometries, including reactant, fragment, and transition-state geometries, and of describing regions of the potential surface that are associated with electronic wave functions of widely varying nature. The MCSCF reference wave functions are designed to be sufficiently flexible to describe qualitatively the changes in the electronic structure over the broad range of molecular geometries of interest. The necessary mixing of ionic, covalent, and Rydberg contributions, along with the appropriate treatment of the different electron-spin components (e.g. closed shell, high-spin open-shell, low-spin open shell, radical, diradical, etc.) of the wave functions are treated correctly at this level. Further treatment of electron correlation effects is included using large scale multireference CI wave functions, particularly including the single and double excitations relative to the MCSCF reference space. This leads to the most flexible and accurate large-scale MR-SDCI wave functions that have been used to date in global PES studies.

Recent Progress: ELECTRONIC STRUCTURE CODE MAINTENANCE, DEVELOPMENT, AND APPLICATIONS: A major component of this project is the development and maintenance of the COLUMBUS Program System. The COLUMBUS Program System computes MCSCF and MR-CI(SD) wave functions, MR-ACPF (averaged coupled-pair functional) energies, MR-AQCC (averaged quadratic coupled cluster) energies, spin-orbit CI energies, analytic energy gradients, and nonadiabatic coupling. Geometry optimizations to equilibrium and saddle-point structures can be done automatically for both ground and excited electronic states. The COLUMBUS Program System is maintained and developed collaboratively with several researchers including Isaiah Shavitt (University of Illinois), Russell M. Pitzer (Ohio State University), Thomas Mueller (Central Institute for Applied Mathematics, Juelich, Germany), and Hans Lischka (University of Vienna, Austria). The nonadiabatic coupling and geometry optimizations for conical intersections is done in collaboration with David R. Yarkony (Johns Hopkins). The distributed development effort and software coordination uses the remote cvs utility. The COLUMBUS Program System of electronic structure codes is maintained on the various machines used for production calculations by the Argonne Theoretical Chemistry Group, including Macintosh personal computers, IBM RS6000 workstations, the parallel IBM SP at NERSC, and the Group's 96-CPU Linux cluster. Most recently, the codes have been ported to the 320-CPU JAZZ Teraflop facility at Argonne, and ports to the Cray X1 and to the IBM Blue Gene machines are in progress. The parallel sections of the code are based on the single-program multiple-data (SPMD) programming model with explicit message passing using the portable MPI library, and the portable Global Array Library (distributed from PNNL) is used for data distribution. These computer codes are used in the production-level molecular applications by members and visitors of the Argonne Theoretical Chemistry Group. The next major release of

This work was performed under the auspices of the Office of Basic Energy Sciences, Division of Chemical Sciences, Geosciences, and Biosciences, U.S. Department of Energy, under contract number DE-AC02-06CH11357.

the COLUMBUS codes will begin to incorporate the newer language features of F90/F95. This will facilitate future development and maintenance effort.

COMPUTATION OF EIGENVALUE BOUNDS: During the development of the Subspace Projected Approximate Matrix (SPAM) diagonalization method (described in previous years), it was necessary to compute bounds of approximate eigenvalues and eigenvectors. This work resulted in the development of a general computational procedure to compute rigorous eigenvalue bounds for general subspace eigenvalue methods. This method consists of the recursive application of a combination of the Ritz Bound, the Residual Norm Bound, the Gap Bound, and the Spread Bound. In addition to application within the SPAM method, this method may also be applied to the Davidson method as used in CI calculations and to the Lanczos method as used in the computation of vibrational eigenvalues. This software is distributed using anonymous ftp and through the *Computer Physics Communications* program library.

LINEAR COMBINATION OF PRODUCT WAVEFUNCTIONS: A new expansion basis for electronic wave functions was recently introduced [Shepard-2005]. In this approach, the wave function is written as a linear combination of *product basis functions*, and each product basis function in turn is formally equivalent to a linear combination of configuration state functions (CSFs) that comprise an underlying linear expansion space of dimension $N_{\rm csf}$. The CSF coefficients that define the basis functions are nonlinear functions of a smaller number of variables $N_\varphi \ll N_{\rm csf}$. The method is formulated in terms of spin-eigenfunctions using the Graphical Unitary Group Approach (GUGA) of Shavitt, and consequently it does not suffer from spin contamination or spin instability.

Our new method is characterized by several important features. First, open-shell functions may be included in our expansions, which are formulated directly in terms of spin-eigenfunctions. This allows our new method to be used for the reactions that are important to combustion chemistry (i.e. involving radicals and other open-shell electronic states) without introducing spin contamination. Second, we place no intrinsic restrictions on the orbital occupations, so our product functions are not restricted to only geminals or to other preselected molecular fragments, and there are no artificial excitation restrictions with respect to a reference function or reference space. Third, we use linear combinations of N_α product wave functions rather than a single expansion term. This allows our method to be used for both ground and excited electronic states, the increased wave function flexibility leads to more accurate wave functions, and it will allow the computation of transition moments, nonadiabatic coupling, and other properties that at present can only be computed reliably with MCSCF and MRCI approaches.

Efficient procedures to compute hamiltonian matrix elements and reduced one- and two-particle density matrices for this nonlinear expansion have been developed [Shepard-2006]. The effort required to construct an individual hamiltonian matrix element between two product basis functions $H_{MN} = \langle M | \hat{H} | N \rangle$ scales as $\mathcal{O}(\beta n^4)$ for a wave function expanded in n molecular orbitals. The prefactor β itself scales between N^0 and N^2, for N electrons, depending on the complexity of the underlying Shavitt Graph. The corresponding metric matrix element $S_{MN}=\langle M|N\rangle$ requires effort that scales as $\mathcal{O}(\beta n)$, the one-particle transition density $\mathbf{D}^{MN}$ requires $\mathcal{O}(\beta n^2)$ effort, the two-particle density $\mathbf{d}^{MN}$ requires $\mathcal{O}(\beta n^4)$ effort, and the gradient of the energy with respect to the nonlinear parameters requires $\mathcal{O}(\beta n^5)$ effort. There is no component of the effort or storage for matrix element computation or wave function optimization that scales as $N_{\rm csf}$. Timings with our initial implementation of this method are very promising (see Fig. 1). A hamiltonian matrix element involving product basis functions corresponding to an underlying linear expansion space dimension $N_{\rm csf}\approx 10^{25}$ requires only 10 to 15 seconds on a typical laptop or desktop computer. The computation of this same matrix element would require about a million

times the age of the universe using traditional full-CI technology. An energy-based optimization approach has been developed and applied to the nonlinear wave function parameters; this exploits *partially contracted functions* in order to reduce the dimensionality of the optimization problem at each step and to minimize the number of expensive gradients that must be computed.

Figs. 2 and 3 show some computed dissociation curves for our new method using optimized wave function parameters for the ground state $^1\Sigma_g^+$ of the N_2 molecule. It is clear from these curves that even the N_α=1 wave function does a good job of describing the bond-breaking and spin-recoupling involved in the dissociation of the N≡N triple bond. The N_α=2 curve is only slightly above the CASSCF curve, from about 0.3mh difference near R_e, increasing to about 3.1mh near R=3a_0, and then approaching 0.0mh as R→∞. The N_α=3 curve is indistinguishable from the converged CASSCF curve.

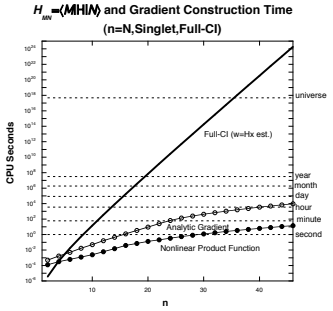

Fig. 1

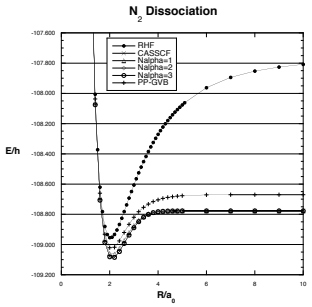

Fig. 2

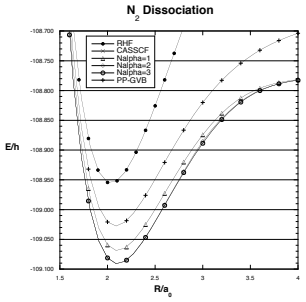

Fig. 3

PUBLIC DISTRIBUTION OF SOFTWARE: The COLUMBUS Program System is available using the *anonymous ftp* facility of the internet. The codes and online documentation are available from the web address http://www.univie.ac.at/columbus/. In addition to the source code, the complete online documentation, installation scripts, sample calculations, and numerous other utilities are included in the distribution. A partial implementation of an IEEE POSIX 1009.3 library has been developed and is available from ftp://ftp.tcg.anl.gov/pub/libpxf. This library simplifies the porting effort required for the COLUMBUS codes, and also may be used independently for other Fortran programming applications. The SPAM code described above is available from ftp://ftp.tcg.anl.gov/pub/spam. The eigenvalue bounds code described above is available from the *Computer Physics Communicstions* library and also from ftp://ftp.tcg.anl.gov/pub/bounds.

Future Plans: LINEAR COMBINATION OF PRODUCT WAVEFUNCTIONS: Most of our effort so far has been directed toward the computation of valence correlation, and our wave functions have been designed to approach the CASSCF limit. In the future, we will extend our studies to both valence and dynamical electron correlation. Figure 4 shows the convergence of the total energy toward the full-CI limit for the H_2O molecule at Re with a double-zeta bases. Convergence to 1.0 kcal/m is achieved with N_α=9 basis functions. This is encouraging because this is approximately the same rate of convergence that has been observed previously for the valence correlation of O_3.

One of the challenges with our new wave function expansion is the qualitative interpretation of the computed results. This is already a difficult process with large-scale CI expansions of size $N_{csf}=10^6$ to 10^9, and it becomes even more difficult with expansions of size 10^{20} to 10^{30}. Even if only one out of a trillion of the largest CSF coefficients were examined in such an expansion, the resulting coefficients list could not be held even on massive file servers. Other approaches are necessary that do not rely on analysis of the CSF coefficients. We have defined a novel approach based on the underlying Shavitt graph structure of our new method. We define an

arc density to be the sum of the squares of all the CSF coefficients that touch a particular arc in the graph, and we define a node density to be sum of the squares of the coefficients that touch a particular node of the graph. By exploiting the recursive nature of the product basis functions, it is trivial to compute these quantities for any wave function, regardless of the underlying CSF expansion dimension. Fig. 5 shows an initial attempt at this analysis for the dissociation of N_2 corresponding to Figs. 2-3. The quantities displayed are the differences of the density at R=10.0 and at R=2.2. The red nodes and arcs correspond to negative density (larger at 2.2 than at 10.0), and the green nodes and arcs to positive density (larger at 10.0 than at 2.2). The area of the filled circle corresponds to the magnitude of the density change. This results in a concise representation of the important orbital occupation and spin coupling differences in the molecule at these two geometries. Graph densities and difference-densities between two states, or between two wave functions describing the same state, at a given geometry may also be computed.

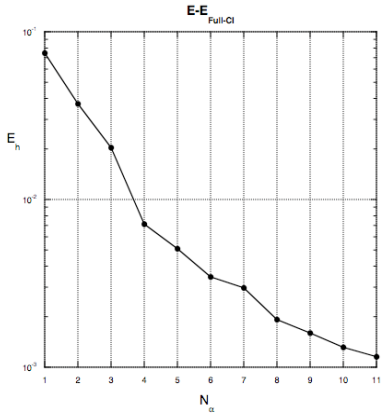

Fig. 4.

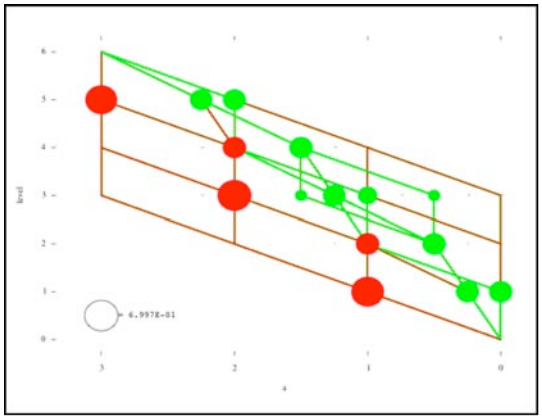

Fig. 5.

Publications:

"Computing Eigenvalue Bounds for Iterative Subspace Methods," Y. Zhou. R. Shepard, and M. Minkoff, *Computer Physics Comm.* **167**, 90-102 (2005).

"Software for Computing Eigenvalue Bounds for Iterative Subspace Methods," R. Shepard, M. Minkoff, and Y. Zhou. *Computer Physics Comm.* **170**, 109-114 (2005).

"Advanced Software for The Calculation of Thermochemistry, Kinetics, and Dynamics," D. M. Medvedev, S. K. Gray, A. F. Wagner, M. Minkoff, and R. Shepard, *J. Physics: Conf. Series* **16**, 247-251 (2005).

"A General Nonlinear Expansion Form for Electronic Wave Functions," R. Shepard, *J. Phys. Chem. A* **109**, 11629-11641 (2005).

"Hamiltonian Matrix and Reduced Density Matrix Construction with Nonlinear Wave Functions," R. Shepard, *J. Phys. Chem. A* **110**, 8880-8892 (2006).

"Optimization of Nonlinear Wave Function Parameters," R. Shepard and M. Minkoff, *Int. J. Quantum Chem.* **106**, 3190-3207 (2006).

"Advanced Software for The Calculation of Thermochemistry, Kinetics, and Dynamics," R. Shepard, A. F. Wagner, and S. K. Gray, *J. Physics: Conference Series* **46**, 239-243 (2006).

COMPUTATIONAL AND EXPERIMENTAL STUDY OF LAMINAR FLAMES

M. D. Smooke and M. B. Long
Department of Mechanical Engineering
Yale University
New Haven, CT 06520
mitchell.smooke@yale.edu

Program Scope

Our research has centered on an investigation of the effects of complex chemistry and detailed transport on the structure and extinction of hydrocarbon flames in coflowing axisymmetric configurations. We have pursued both computational and experimental aspects of the research in parallel. The computational work has focused on the application of accurate and efficient numerical methods for the solution of the boundary value problems describing the various reacting systems. Detailed experimental measurements were performed on axisymmetric coflow flames using two-dimensional imaging techniques. Spontaneous Raman scattering and laser-induced fluorescence were used to measure the temperature, and major and minor species profiles. Laser-induced incandescence has been used to measure soot volume fractions. A new approach to optical pyrometry has been developed to measure temperatures where the other techniques fail due to the presence of soot. Our goal has been to obtain a more fundamental understanding of the important fluid dynamic and chemical interactions in these flames so that this information can be used effectively in combustion modeling.

Recent Progress

The major portion of our work during the past year has focused on a combined computational and experimental study of sooting axisymmetric, laminar diffusion flames. The sooting flames can enable the investigator to understand the detailed inception, oxidation and surface growth processes by which soot is formed in hydrocarbon flames. As emissions legislation becomes more restrictive, a detailed understanding of pollutant formation in flames has become even more critical for the design of pollutant abatement strategies and for the preservation of the competitiveness of combustion related industries. It is clear that there will be continuing pressure to lower both NO_x emission indices and soot volume fractions in practical combustion devices. This is in response to the toxicological effects of small particles [1,2] and to the impact, for example, that soot can have on thermal radiation loads in combustors and on turbine blades. Moreover, soot emissions can enhance contrail formation [3] and such "man made" clouds may have an impact ultimately on the Earth's climate [4,5].

Soot and NO_x Modeling: We model the soot kinetics as coalescing, solid carbon spheroids undergoing surface growth in the free molecule limit. The particle mass range of interest is divided into sections and an equation is written for each section including coalescence, surface growth, and oxidation. For the smallest section, an inception source term is included. The transport conservation equation for each section includes thermophoresis, an effective bin diffusion rate, and source terms for gas-phase scrubbing. The gas and soot equations are additionally coupled through non-adiabatic radiative loss in the optically-thin approximation. The inception model employed here is based on an estimate of the formation rate of two- and three-ringed aromatic species (naphthalene and phenanthrene), and is a function of local acetylene, benzene, phenyl and molecular hydrogen concentrations. Oxidation of soot is by O_2 and OH. The surface growth rate is based upon that of Harris and Weiner [6] with an activation energy as suggested by Hura and Glassman [7].

Fuel and nitrogen are introduced through the center tube (4 mm id, 0.38 mm wall thickness) and air through the outer coflow. The fuel (parabolic flow profile) and oxidizer (plug flow) both have an average cold-flow velocity of 35 cm/sec to match the experiments. Flames containing 32% (68%), 40% (60%), 60% (40%) and 80% (20%) mole fractions of ethylene (nitrogen) were studied. Reactant temperatures were assumed to be 298 K. Calculations were performed on an AMD Dual Opteron 240 system.

The temperature decrease due to radiative losses in systems in which significant soot is produced can affect flame length and other temperature-dependent processes such as the formation of NO_x. Similarly, in flames in which substantial fractions of fuel carbon are converted to soot, a shift in the local H_2/H_2O and CO/CO_2 conversion ratio can affect the local heat release and the local temperature. While both NO_x and soot formation are often studied independently, there is a desire to understand their coupled relationship as a function of system parameters such as fuel type, temperature and pressure. We have begun a study to examine the interrelationship of soot formation and NO_x in coflow ethylene air diffusion flames. This analysis is performed excluding any direct NO_x-soot reactions. We examine the relationship of NO_x and soot as a function of the fuel level in these flames and the resultant effect of variable flame radiation on temperature and on NO_x formation. Specifically, the results of a computational model that includes detailed chemistry for gas-phase processes and a sectional representation for soot formation, along with optically thin radiation are compared against laser-induced fluorescence (LIF) measurements of NO. The detailed information on the temperature and species concentrations in the computed flame are combined with an NO quenching model to predict the laser-induced fluorescence signal from NO that is measured experimentally. Once the modeling technique is qualitatively validated against the data sets, computations are performed to assess the impact of soot (and related radiation) on the NO field.

Measurements of Soot and NO: Experimentally, the soot volume fraction field is determined by several different techniques. Laser extinction measurements are being coupled with laser-induced incandescence (LII) measurements in order to obtain the calibrated the soot volume fraction, and can be used as an independent measurement of the soot volume fraction profile in the future. Three-color optical pyrometry [8,9] using a color digital camera, is used to determine soot surface temperatures and also soot volume fractions. The use of the built-in color filter array (CFA) of a digital camera allows for two-dimensional imaging of flame emission at the wavelengths of the color filters. The camera was calibrated in two independent ways. Peak soot volume fractions, as well as variations in concentration across our target flames, show excellent agreement between both LII and soot pyrometry. The use of multiple measurement techniques should improve our overall confidence in the results as well as provide better estimates of the accuracy of the measurements.

For measurements of NO, the output of a dye laser is doubled, producing an ultraviolet (UV) beam near 225.8 nm that is used to excite transitions in the NO $A^2\Sigma^+$-$X^2\Pi$ (0,0) band. The $Q_1(18)$ transition is selected because it is reasonably well separated from neighboring transitions, has significant population from room temperature to the flame temperatures investigated, and causes minimal spectral interferences from other species such as O_2 [10]. Spectrally resolved fluorescence emission from NO in our target ethylene diffusion flames is imaged onto a spectrograph coupled to an intensified CCD camera. When taking data in sooty regions within the flame, a colored glass filter (Corning 7-54) is placed between the two collection lenses in order to suppress the Rayleigh scattering by the soot, which would otherwise saturate the detector. Radial images of the (0,2) vibrational band are acquired at varying axial heights, by moving the burner vertically in 0.5 mm steps, to create a two-dimensional fluorescence image. Changes in the laser

energy and any slight drift of the laser wavelength are normalized using the averaged output of the NO fluorescence from a premixed reference burner, detected by a PMT. Calibration of the experiment is obtained by imaging a nonreacting flow of 45 ppm NO in N_2 through the burner's coflow.

The presence of soot complicates the LIF experiment. The colored glass filter, used to remove scattering from the soot, makes it possible to make measurements in the sooty regions, but does not remove all interferences present in the measurement. A broadband background interference is observed, which is found to be primarily composed of C_2 fluorescence from laser vaporization of the soot, as well as from LII and PAH fluorescence. A background correction is applied using data taken with the excitation laser tuned off-peak of an NO resonance. Due to the heavy sooting within the target flames, it is difficult to characterize the flame temperature and major species and to provide an accurate quenching correction for quantitative results. Instead, a reverse-quenching [11] and Boltzmann correction is applied to the computational results in order to determine an expected fluorescence signal for comparison with experimental results.

A preliminary comparison of experimental and computational results shows good qualitative agreement of the profiles of the fluorescence signal. The fairly constant signal level in the regions above the flame, and the lower signal inside the flame/sooty areas, for example, are captured. Quantitatively, computational results are approximately 25% lower than the experimental results overall. This difference is still under investigation.

Future Plans

During the next year we hope to expand our research in several areas. We will continue our study of sooting hydrocarbon flames with the goal of understanding the interaction of soot formation and NO_x production with an emphasis on the effects of soot radiation on thermal and prompt NO_x. We also plan on including the model in our time-dependent flame systems with the goal of being able to predict soot volume fractions and NO_x as a function of time. Experimentally we will continue our work on improving the accuracy of our soot volume fraction measurements, as well as applying other diagnostic techniques that can provide information on the soot such as primary particle size and aggregation. Finally, using the same techniques that we have developed for the steady sooting flames, we will perform phase-averaged measurements in the time-varying flames.

References

1. J. Schwartz, "Particulate Air-Pollution and Chronic Respiratory-Disease," *Environmental Research*, **62**, 7-13 (1993).
2. D.W. Dockery, J.H. Ware, B.G. Ferris, F.E. Speizer, N.R. Cook and S.M. Herman, "Change in Pulmonary-Function in Children Associated with Air-Pollution Episodes," *Journal of the Air Pollution Control Association*, **32**, 937-942 (1982).
3. U. Schumann, J. Strom, R. Busen, R. Baumann, K. Gierens, M. Krautstrunk, F.P. Schroder and J. Stingl, "In situ observations of particles in jet aircraft exhausts and contrails for different sulfur-containing fuels," *Journal of Geophysical Research-Atmospheres*, **101**, 6853-6869 (1996).
4. S. Menon, J. Hansen, L. Nazarenko and Y.F. Luo, "Climate effects of black carbon aerosols in China and India," *Science*, **297**, 2250-2253 (2002).
5. J.E. Penner, D.H. Lister, D.J. Griggs, D.J. Dokken and M. McFarland, *Aviation and the Global Atmosphere, A Special Report of IPCC Working Groups I and III*. 1999: Cambridge University Press.
6. S.J. Harris and A.M. Weiner, "Surface Growth of Soot Particles in Premixed Ethylene Air Flames," *Combustion Science and Technology*, **31**, 155-167 (1983).
7. H.S. Hura and I. Glassman, *Proceedings of the Combustion Institute*, **22**, 371-378 (1988).
8. Y.A. Levendis, K.R. Estrada, H.C. Hottel, *Rev. Sci. Instrum.*, **63** (1992) 3608-3622.

9. F. Cignoli, S. De Iuliis, V. Manta, G. Zizak, *App. Opt.*, **40** (2001) 5370-5378
10. C.D. Carter and R.S. Barlow, "Simultaneous Measurements of NO, OH, and the Major Species in Turbulent Flames," *Optics Letters*, **19**, 299-301 (1994).
11. T.B. Settersten, B.D. Patterson and J.A. Gray, "Temperature-and species-dependent quenching of NO A (2)Sigma(+)(v(')=0) probed by two-photon laser-induced fluorescence using a picosecond laser," *Journal of Chemical Physics*, **124** (2006).

DOE Sponsored Publications since 2005

1. J. A. Cooke, M. D. Smooke, M. Bellucci, A. Gomez, A. Violi, T. Faravelli and E. Ranzi, "Computational and Experimental Study of a JP-8 Counterflow Diffusion Flame," *Proceedings of the Combustion Institute*, **30**, (2005).
2. V. V. Toro, A. V. Mokhov, H. B. Levinsky and M. D. Smooke, "Combined Experimental and Computational Study of Laminar, Axisymmetric Hydrogen-Air Diffusion Flames," *Proceedings of the Combustion Institute*, **30**, (2005).
3. K.T. Walsh, J. Fielding, M.D. Smooke, A. Linan and M.B. Long, "A Comparison of Computational and Experimental Lift-Off Heights of Coflow Laminar Diffusion Flames," *Proceedings of the Combustion Institute*, **30**, (2005).
4. M. Noskov and M. D. Smooke, "An Implicit Compact Scheme Solver with Application to Chemically Reacting Flows," *J. Comp. Physics*, **203**, (2005).
5. M. J. H. Anthonissen, B. A. V. Bennett and M. D. Smooke, "An Adaptive Multilevel Local Defect Correction Technique with Application to Combustion," *Comb. Theory and Modelling*, **9**, (2005).
6. S. A. Kaiser, J. H. Frank, and M. B. Long, "Use of Rayleigh Imaging and Ray Tracing to Correct for Beam-Steering Effects in Turbulent Flames," *Appl. Opt.,* **44***,* (2005).
7. J. H. Frank, S. A. Kaiser, and M. B. Long, "Multiscalar Imaging in Partially Premixed Jet Flames with Argon Dilution," *Combust. Flame,* **143***,* (2005).
8. M.D. Smooke, M.B. Long, B.C. Connelly, M.B. Colket and R.J. Hall, "Soot Formation in Laminar Diffusion Flames," *Combust. Flame* **143**, (2005).
9. M. Noskov, M. Benzi and M. D. Smooke, "An Implicit Compact Scheme Solver for Two-Dimensional Multicomponent Flows," *Comp. and Fluids*, **36**, (2006).
10. S. Dworkin, B. A. V. Bennett and M. D. Smooke, "A Mass-Conserving Vorticity-Velocity Formulation with Application to Nonreacting and Reacting Flow," *J. Comp. Phys*., **215**, (2005).
11. S. B. Dworkin, B. C. Connelly, A. M. Schaffer, M. B. Long and M. D. Smooke, "Computational and Experimental Study of a Forced, Time-Dependent, Methane-Air Coflow Diffusion Flame," *Proceedings of the Combustion Institute*, **31**, (2006).
12. A. V. Mokhov, B. A. V. Bennett, H. B. Levinsky and M. D. Smooke, "Experimental and Computational Study of C_2H_2 and CO in a Laminar Axisymmetric Methane-Air Diffusion Flame," *Proceedings of the Combustion Institute*, **31**, (2006).
13. S. Hu, P. Wang, R. W. Pitz and M. D. Smooke, "Experimental and Numerical Investigation of Non-Premixed Tubular Flames," *Proceedings of the Combustion Institute*, **31**, (2006).
14. V. Giovangigli, N. Meynet and M. D. Smooke, "Application of Continuation Techniques to Ammonium Perchlorate Plane Flames," **10**, *Comb. Theory and Modelling*, (2006).
15. G. Amantini, J. H. Frank, A. Gomez and M.D. Smooke, "Computational and Experimental Study of Standing Methane Edge Flames in the Two-Dimensional Axisymmetric Counterflow Geometry," in press, *Comb. and Flame*, (2007).
16. G. Amantini, J. H. Frank, A. Gomez and M.D. Smooke, "Computational and Experimental Study of Steady Two-Dimensional Axisymmetric Non-Premixed Methane Counterflow Flames," *Comb. Theory and Modelling*, **11**, (2007).

Universal and State-Resolved Imaging Studies of Chemical Dynamics

Arthur G. Suits
Department of Chemistry, Wayne State University
5101 Cass Ave
Detroit, MI 48202
asuits@chem.wayne.edu

Program Scope

The focus of this program is on high-resolution ion imaging experiments employing complementary approaches featuring universal and state-resolved detection techniques. The objective of these studies is to develop a molecular-level understanding of chemical phenomena, with particular emphasis on elementary reactions and mechanisms important in understanding and predicting combustion chemistry. This research is conducted using state-of-the-art molecular beam machines and vacuum ultraviolet lasers in conjunction with ion imaging technqiues to study frontier areas in photodissociation, unimolecular decomposition, and reactive scattering. An ongoing parallel effort is made to develop new tools and experimental methods with which to achieve these goals.

Recent Progress

Roaming atoms. In studies in collaboration with the Bowman group, we previously showed dramatic evidence of a novel pathway in formaldehyde ground state dissociation that avoids the region of the familiar transition state entirely. Our original report described high-resolution state-resolved CO velocity measurements that revealed the correlated H_2 internal state distribution. Low rotational levels of CO were correlated with highly vibrationally excited H_2, demonstrating this "roaming" intramolecular abstraction mechanism. Three major publications in the *Journal of Chemical Physics* have followed our initial report in *Science*.The first paper in this series exploited the remarkable resolution of the slice imaging technique to provide fully correlated product state distributions for H_2 and CO for the "conventional" molecular channel.*(7)* The photolysis energy ranged from 1800 to 4100 cm^{-1} above the molecular elimination threshold, and included the 2^14^1, 2^14^3, 2^24^1, 2^24^3, and 2^34^1 transitions to S_1. These detailed measurements allowed determination of the v_{H2}-specific CO rotational distributions even though the data was obtained in an orthogonal dimension. We find a strong correlation between H_2 vibration and CO rotation due to the dynamical influence of the highly repulsive exit channel. A simple model that estimates the impact parameters for each H_2 product vibrational level determined by calculating the molecular transition/displacement vectors at various points along the reaction coordinate can partially account for the trends in the correlated distributions. Rotational correlations between H_2 and CO products were confirmed to be very weak. In the second paper *(9)*, we explored the dynamics of the roaming intramolecular H abstraction mechanism in great detail, building on the potential surface and dynamics from the Bowman group. We showed the detailed correlated rotational distribution in the H_2 product, and used this to demonstrate that the abstraction dynamics are determined by a tendency for emission of the abstracted H atom along the original HCO bond direction regardless of the position of the roaming H atom. This work was centrally featured in an invited feature article for the *Journal of Physical Chemistry-A.(2)* Finally, in the most recent effort, we have documented *(11)* the detailed energy

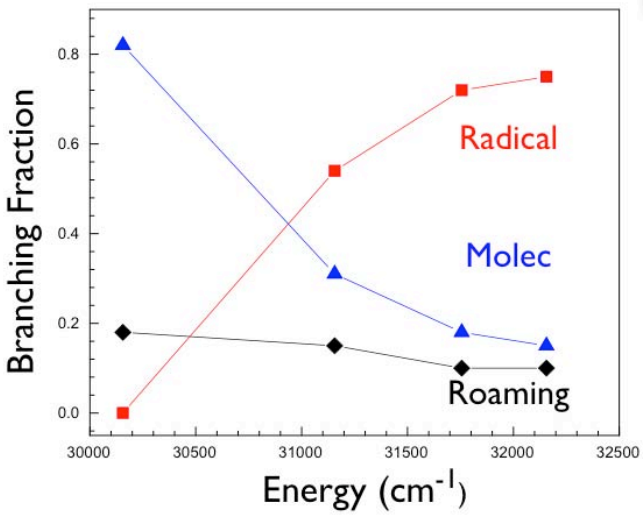

Figure 1 . Energy dependence of the multichannel branching in formaldehyde dissociation at the indicated energy. The relative branching between roaming and molecular channels were determined by slice imaging studies, and the scaling of molecular vs. radical is based on Bowman's QCT results.

dependent dynamics and branching for the roaming channel relative to the conventional molecular channel, and combined this with theoretical calculations to develop a qualitative picture of the multichannel branching in this system, a key issue in understanding the implications of the roaming mechanism for modeling combustion chemistry (Fig. 1).

State-resolved crossed-beam slice imaging. Last year we reported the development of general state-resolved crossed-beam scattering with slice imaging detection of single product rovibrational states.*(6)* In the past year we extended this investigation to a range of collision energies from 3.2 to 10.4 kcal/mol, and HCl product rotational levels from J_{HCl}=0-5, in the $Cl+C_2H_6$ system.*(8)* The center-of-mass translational energy and angular distributions obtained from the experiments were found to be strongly coupled. The angular distributions show some propensity for greater forward scattering of HCl formed in lower rotational levels, and a shift towards backward scattering for increasing rotational state up to J = 5 at the collision energy of 6.7 kcal/mol. With the collision energy increasing from 3.2 kcal/mol to 10.4 kcal/mol, the angular distribution shifts from broadly backward to broadly forward. We have observed two distinct reaction mechanisms: For the fast, forward scattered HCl products of this reaction, the venerable line-of-centers model can give a good agreement, while kinematically-controlled dynamics account well for the fast backscattered distribution. Finally, a chattering mechanism is invoked to explain the slow backscattered HCl components.

Two-color reduced-Doppler detection. We have recently developed a useful two-color reduced Doppler detection that, in many applications, offers advantages over conventional 2+1 resonance-enhanced multiphoton ionization detection.*(10)* Using counterpropagating beams of two different colors, one of which is broadband 266nm, for example, we achieve convenient and sensitive H atom detection without the need for Doppler scanning (see Fig. 2). Since the effective Doppler width of a two-photon transition is determined by the sum of the wave

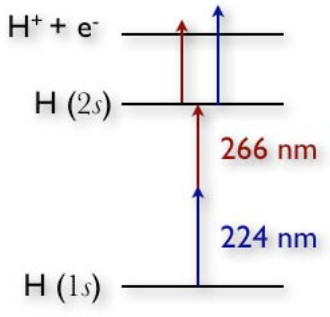

Figure 2. Two color reduced-Doppler excitation scheme for H atoms.

vectors, near Doppler-free detection can be achieved using counterpropagating beams even if the frequencies of the two beams are different. We demonstrated the approach using 224nm photodissociation of HBr and have also applied it to do related "1-color" UV dissociation, where the molecule absorbs and is dissociated by only the shorter wavelength of the two beams. This method provides a convenient and sensitive dissociation/detection method for many photochemical systems, and it may be useful for H atom excitation spectroscopy as well.

Selected Future Plans

Roaming atom reaction dynamics. We will continue DC slice imaging studies of roaming reaction mechanisms. We will examine the CO(v=1) product in formaldehyde dissociation, explore the dynamics for the molecular products in that system at energies above the triplet threshold, and explore the low energy threshold for roaming. We will also move on to other systems to investigate the generality of the roaming mechanism. This behavior has recently been reported for acetaldehyde, and we intend to examine the dynamics in formic acid dissociation, in which either H or OH could be the roaming species. Again, we will use state-resolved slice imaging detection of CO and look for the characteristic bimodal distributions and low product rotational levels to identify the roaming process.

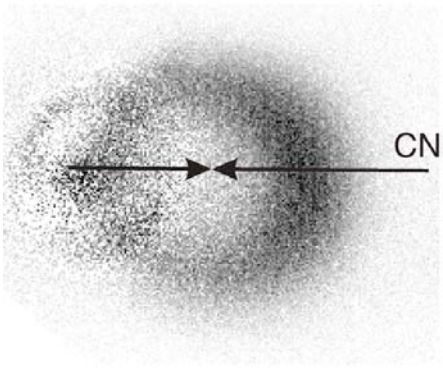

Figure 3. Raw image of 2-butyl radical from reaction of CN + C_4H_{10} with 157nm single photon ionization at a collision energy of 10.8 kcal/mol.

State-resolved and universal crossed-beam DC slice imaging. We have plans to pursue a range of studies using our crossed-beam sliced imaging approach. We have recently developed an intense CN source and have had preliminary success in crossed-beam reaction of CN with alkanes (Fig. 3). We will examine the full range of hydrocarbon reactions, both with universal VUV detection of the radical, and for the reaction CN+CH_4 we will use state resolved detection of CH_3.

State-correlated photochemistry of HCCO. We propose state-correlated imaging of the ketenyl radical, HCCO. There is a marvelous body of work on the spectroscopy and dynamics of this system. Although the dynamics measurements were obtained at fairly low translational energy resolution, they provide a roadmap for rich correlated state imaging measurements of the CO. This radical system has the advantage that metastable levels of the state may be excited state-specifically so we need not worry about contamination by dissociation of unknown species. Small changes in photolysis energy were seen to change the branching between dissociation on the doublet and quartet surfaces quite dramatically. Again, quantum state specific probing of the CO product will provide correlated internal state information on the rovibrational levels of both ground state ($X\ ^2\Pi$) and electronically excited ($a\ ^4\Sigma^-$) CH product, allowing investigation of ground state dissociation and intersystem crossing dynamics. In addition, we can examine the H loss channel, which was experimentally inaccessible in the Neumark studies.

DOE Publications 2005-present

1. S. K. Lee, D. Townsend, O. S. Vasyutinskii and A. G. Suits, "O(^{1}D) orbital orientation in the ultraviolet photodissociation of ozone," *Phys. Chem. Chem. Phys.*, **7,** 1650, (2005).

2. D. Townsend, W. Li, S. K. Lee, R. L. Gross and A. G. Suits, "Universal and State resolved imaging of chemical dynamics," (Invited feature article) *J. Phys. Chem. A*, **109**, 8661 (2005) 10.1021/jp0526086.

3. Brian D. Leskiw, Myung Hwa Kim, Gregory E. Hall and Arthur G. Suits, "Reflectron Velocity Map Ion Imaging," *Rev. Sci. Instr.* **76,** 104101 (2005); "Erratum: Reflectron Velocity Map Ion Imaging," *Rev. Sci. Instr.* **76,** 129901 (2005).

4. S. D. Chambreau, D. Townsend, S. A. Lahankar, S. K. Lee and A. G. Suits, "Novel molecular elimination mechanism in formaldehyde photodissociation: The roaming H atom pathway," *Phys. Scr.* **73** C89-C93 (2006).

5. W. Li, C. Huang, M. Patel, D. Wilson and A. G. Suits, "State-Resolved Reactive Scattering by Slice Imaging: A New View of the Cl+C_2H_6 Reaction," *J. Chem. Phys.* **124,** 011102 (2006).

6. A. Komissarov, M. Minitti, A. G. Suits and G. E. Hall, "Correlated product distributions from ketene dissociation measured by dc sliced ion imaging" *J. Chem. Phys.* **124,** 014303 (2006).

7. S. D. Chambreau, S. A. Lahankar, and A. G. Suits, "Correlated ν_{H2} and j_{CO} product states from formaldehyde photodissociation: Dynamics of molecular elimination," *J. Chem. Phys.* **125** 044303 (2006).

8. C. Huang, W. Li and A. G. Suits, "Rotationally-Resolved Reactive Scattering: Imaging Detailed Cl + C_2H_6 Reaction Dynamics," *J. Chem. Phys.* **125**, 133107 (2006).

9. S. A. Lahankar, S. D. Chambreau, F. Suits, J. Farnum, X. Zhang, J. M. Bowman and A. G. Suits, "The roaming atom mechanism in formaldehyde decomposition," *J. Chem. Phys.* **125,** 044302 (2006).

10. C. Huang, W. Li, M. H. Kim, and A. G. Suits, "Two-color Reduced Doppler Ion Imaging," *J. Chem. Phys.* **125**, 121101 (2006).

11. S. A. Lahankar, S. D. Chambreau, X. Zhang, J. M. Bowman and A. G. Suits, "Energy dependence of the roaming atom mechanism in formaldehyde decomposition," *J. Chem. Phys.* **126,** 044314 (2007).

Elementary Reaction Kinetics of Combustion Species

Craig A. Taatjes
Combustion Research Facility, Mail Stop 9055, Sandia National Laboratories, Livermore, CA 94551-0969
cataatj@sandia.gov www.ca.sandia.gov/CRF/staff/taatjes.html

SCOPE OF THE PROGRAM

This program aims to develop new methods for studying chemical kinetics and to apply these methods to the investigation of fundamental chemistry relevant to combustion science. One central goal is to perform accurate measurements of the rates at which important free radicals react with stable molecules. Understanding the reactions in as much detail as possible under accessible experimental conditions increases the confidence with which modelers can treat the inevitable extrapolation to the conditions of real-world devices. Another area of research is the investigation and application of new detection methods for precise and accurate kinetics measurements. Absorption-based techniques and mass-spectrometric methods have been emphasized, because many radicals critical to combustion are not amenable to fluorescence detection. Finally, a close collaboration with Nils Hansen utilizes measurements of flame chemistry to reveal important reactions or species for individual laboratory investigation.

An important part of our strategy is using experimental data to test and refine detailed calculations (working in close cooperation with Stephen Klippenstein at Argonne and Jim Miller at Sandia), where the calculational results offer insight into the interpretation of experimental results and to guide new measurements that will probe key aspects of potential energy surfaces. This methodology has been applied in our investigations of the reactions of alkyl radicals with O_2, where the combination of rigorous theory and validation by detailed experiments has made great strides toward a general quantitative model for alkyl oxidation. Reactions of unsaturated hydrocarbon radicals that may play a role in soot formation chemistry, and reactions that may produce or consume enols in flames are also targets of investigation.

PROGRESS REPORT

The current efforts of the laboratory center on developing high-sensitivity absorption-based techniques for kinetics measurements, and on applying these techniques to investigate important combustion reactions. We continue to apply infrared frequency-modulation (FM) and direct absorption spectroscopy to measurements of product formation in reactions of alkyl radicals with O_2 and kinetics of unsaturated hydrocarbon radicals. The multiplexed photoionization mass spectrometric reactor at the Advanced Light Source, operated in collaboration David Osborn, is a key part of our investigations

of the kinetics of enol formation and of low-temperature hydrocarbon oxidation chemistry. Several highlights of the recent work are described briefly below.

Enols as Combustion Intermediates. Enol formation in low-pressure flames takes place in the preheat zone and its precursors are most likely fuel species or the early products of fuel decomposition. We have begun measurements on enol formation in the reactions of OH with alkenes. Specifically, we have observed ethenol from the reaction of OH with ethene, propenol from the reaction of OH with propene, and but-1,3-dien-1-ol from the reaction of OH with 1,3-butadiene. Quantification of the yields of these products is the subject of ongoing work in the ALS machine. Interestingly, the $m/z = 44$ product from the reaction of OH with propene, observed previously by Hoyermann (Hoyermann and Sievert 1979) is predominantly acetaldehyde rather than ethenol.

Measurements of Product Formation in Alkyl + O_2 Reactions. We have continued investigating the key alkylperoxy chemistry that underlies autoignition. The oxidation of neopentyl radicals is important because the lack of a conjugate alkene focuses the reaction on the key $RO_2 \rightarrow QOOH$ isomerization. Reactions of cycloalkyl radicals with O_2 are becoming increasingly important as the fuel stream contains more naphthenes derived from heavier crude oil from non-traditional sources.

Neopentyl + O_2. The reaction of the neopentyl radical with oxygen was studied earlier in our laboratory, and we have revisited the OH formation in this reaction, measuring the OH by a laser photolysis / cw absorption method at 673, 700 and 725 K. The absorption method allows the absolute concentration of the OH radical to be measured, improving the reliability of modeling the system. In a collaboration with Bill Green, the MIT Reaction Mechanism Generator (RMG) was used to automatically generate a comprehensive model for this system, and the predicted OH concentration profiles compared to experimental results. We found that the experimental data provide useful constraints on the rate coefficient for the formally direct chemical activation reaction of neopentyl radical with O_2 to form OH. Absolute absorbance measurements on OH and I indicate that the branching ratio for R + O_2 to directly form OH is about 0.03 under the relatively low-pressure conditions (<100 Torr) of these experiments.

Cyclohexyl + O_2. New experimental measurements of HO_2 and OH formation in pulsed-photolytically initiated oxidation of cyclohexane have been compared to detailed ab initio calculations of stationary point energies and master-equation simulation of the multiple-well kinetics of the cyclohexyl + O_2 system, carried out by Stephen Klippenstein (Argonne) and Carlo Cavallotti (Milan). As in previous investigations, adjustment of the energies of the stationary points within the estimated uncertainty of the ab initio calculations is used to bring the model into agreement with the body of experimental data. Chemical activation and “formally direct” reactions are important in this system, as seen in other alkyl + O_2 systems. Formation of OH is substantially more prominent in the reaction of cyclohexyl with O_2 than in many other R + O_2 reactions.

Laser Photolysis/cwLPA Measurements of C_2H_3 Reactions. Reactions of vinyl radicals with unsaturated hydrocarbons are being investigated in collaboration with Bill Green's group at MIT; measurements of vinyl + ethene and vinyl + propene have been carried out in the MIT Combustion Dynamics Laboratory with the participation of members of our laboratory. The measured rate coefficients for the reaction of vinyl with ethene are in good agreement with measurements at higher temperature by Knyazev and coworkers (Shestov et al. 2005). RRKM master equation calculations predict that the formation of resonance-stabilized 1-methylallyl product is minor except at low pressures.

FUTURE DIRECTIONS

Characterization of R + O_2 reactions will continue, both in the infrared absorption work and in the new PIMS apparatus. The ability to simultaneously probe various reactants and products will play a key role in extending these measurements. One important extension of the deuterated alkane oxidation work will be to probe OD formation. Because the reaction coordinate for the internal isomerization to QOOH (the precursor to OH formation) involves a large degree of H-atom motion, the deuterium kinetic isotope effect may be larger for OH formation than for HO_2 formation. Further in the future, oxidation of selectively deuterated alkanes may make it possible to distinguish among different internal abstraction pathways in R + O_2 reactions. Interpretation of isotopic labeling experiments will require detection of both HO_2 and DO_2 and an understanding of the kinetic isotope effects on the overall reaction. In the long term, detection of the hydroperoxy radical intermediate in the R + $O_2 \rightarrow RO_2 \rightarrow QOOH \rightarrow QO$ + OH mechanism might be possible in the infrared or conceivably by photoionization.

The application of synchrotron photoionization mass spectrometry to chemical kinetics will continue. The ready tunability of the ALS photon energy permits isotopic discrimination similar to that enjoyed in the current ALS flame experiments, and the kinetics measurements will be exploit this capability. Further characterization of enol formation in reactions of OH with alkenes, kinetics of reactions of combustion radicals with ethenol, addition reactions of propargyl radicals with unsaturated hydrocarbons, and oxidation of other cycloalkyl radicals are possible targets of future investigations.

REFERENCES:

Hoyermann, K. and R. Sievert (1979). "Reaction of OH-radicals with propene. 1. Determination of the primary products at low pressures" Ber. Bunsen-Ges. Phys. Chem. **83**(9): 933-939.

Shestov, A. A., K. V. Popov, I. R. Slagle and V. D. Knyazev (2005). "Kinetics of the reaction between vinyl radical and ethylene." Chem. Phys. Lett. **408**: 339–343.

Publications acknowledging BES support 2005-present

1. Terrill A. Cool, Koichi Nakajima, Craig A. Taatjes, Andrew McIlroy, Phillip R. Westmoreland, Matthew E. Law and Aude Morel, "Studies of a Fuel-Rich Propane Flame with Photoionization Mass Spectrometry," *Proc. Combust. Inst.* **30**, 1631-1638 (2005).
2. Craig A. Taatjes, Stephen J. Klippenstein, Nils Hansen, James A. Miller, Terrill A. Cool, Juan Wang, Matthew E. Law, and Phillip R. Westmoreland, **"**Synchrotron Photoionization Measurements of Combustion Intermediates: Photoionization Efficiency of C_3H_2 Isomers," *Phys. Chem. Chem. Phys.* **7**, 806-813 (2005).
3. Edgar G. Estupiñán, Stephen J. Klippenstein, and Craig A. Taatjes, Measurements and Modeling of HO_2 Formation in the Reactions of *n*-C_3H_7 and *i*-C_3H_7 Radicals with O_2," *J. Phys. Chem. B* **109**, 8374-8387 (2005).
4. Craig A. Taatjes, Nils Hansen, Andrew McIlroy, James A. Miller, Juan P. Senosiain, Stephen J. Klippenstein, Fei Qi, Liusi Sheng, Yunwu Zhang, Terrill A. Cool, Juan Wang, Phillip R. Westmoreland, Matthew E. Law, Tina Kasper, and Katharina Kohse-Höinghaus, "Enols are Common Intermediates in Hydrocarbon Oxidation," *Science*, 308, 1887-1889, published online May 12, 2005 [DOI: 10.1126/science.1112532] (2005).
5. Terrill A. Cool, Juan Wang, Koichi Nakajima, Craig A. Taatjes, and Andrew McIlroy, "Photoionization Cross Sections for Reaction Intermediates in Hydrocarbon Combustion," *Int. J. Mass. Spectrom.* **247**, 18-27 (2005).
6. John D. DeSain, Leonard E. Jusinski, and Craig A. Taatjes, "Temperature Dependence and Deuterium Kinetic Isotope Effects in the HCO + NO Reaction," *J. Photochem. Photobiol. A: Chem.,* **176**, 149-154 (2005)
7. Craig A. Taatjes, Nils Hansen, James A. Miller, Terrill A. Cool, Juan Wang, Phillip R. Westmoreland, Matthew E. Law, Tina Kasper, Katharina Kohse-Höinghaus, "Combustion Chemistry of Enols: Possible Ethenol Precursors in Flames," *J. Phys. Chem. A* **110**, 3254-3260 (2006).
8. Nils Hansen, Stephen J. Klippenstein, Craig A. Taatjes, James A. Miller, Juan Wang, Terrill A. Cool, Bin Yang, Rui Yang, Lixia Wei, Chaoqun Huang, Jing Wang, Fei Qi, Matthew E. Law and Phillip R. Westmoreland, "The Identification and Chemistry of C_4H_3 and C_4H_5 Isomers in Fuel-Rich Flames," *J. Phys. Chem. A* **110**, 3670- (2006).
9. Craig A. Taatjes, "Uncovering the Fundamental Chemistry of Alkyl + O_2 Reactions via Measurements of Product Formation," *J. Phys. Chem. A* **110**, 4299-4312 (2006).
10. John D. DeSain, Leonard E. Jusinski, and Craig A. Taatjes, "Ultraviolet Absorption Cross Section of Vinyl Trichlorosilane and Allyl Trichlorosilane and the Branching Fraction of the Vinyl Radical and Allyl Radical Channels in 193 nm Photolysis," *Phys. Chem. Chem. Phys*. **8**, 2240–2248 (2006).
11. Eric R. Hudson, Christopher Ticknor, Brian Sawyer, Craig A. Taatjes, Heather J. Lewandowski, Jason Bochinski, John Bohn, and Jun Ye, "Stark-deceleration of formaldehyde molecules for high resolution studies of hydrogen atom abstraction reaction dynamics," *Phys. Rev. A* **73**, 063404 (2006).
12. Arjan Gijsbertsen, Harold V. Linnartz, Craig A. Taatjes and Steven Stolte, "Quantum Interference as the Source of Steric Asymmetry and Parity Propensity Rules in NO-Rare Gas Inelastic Scattering," *J. Am. Chem. Soc.* **128**, 8777-8789 (2006).
13. Giovanni Meloni, Peng Zou, Stephen J. Klippenstein, Musahid Ahmed, Stephen R. Leone, Craig A. Taatjes, and David L. Osborn, "Energy-resolved photoionization of alkylperoxy radicals and the stability of their cations," *J. Am. Chem. Soc.* **128**, 13559-13567 (2006).
14. John D. DeSain, Linda Valachovic, Leonard E. Jusinski and Craig A. Taatjes, "The Reaction of Chlorine Atom with Trichlorosilane from 296 K to 473 K," *J. Chem. Phys.,* **124**, 224308 (2006).
15. Ph. R. Westmoreland, M. E. Law, T. A. Cool, J. Wang, A. McIlroy, C. A. Taatjes, and N. Hansen, "Analysis of Flame Structure by Molecular-Beam Mass Spectrometry Using Electron-Impact and Synchrotron-Photon Ionization," *Combustion, Explosion, and Shock Waves* **42**, 672-677 (*Fizika Goreniya i Vzryva* **42**, 58-63) (2006).
16. Matthew E. Law, Phillip R. Westmoreland, Terrill A. Cool , Juan Wang, Nils Hansen, Craig A. Taatjes, and Tina Kasper, "Benzene Precursors and Formation Routes in a Stoichiometric Cyclohexane Flame," *Proc. Combust. Inst.* **31**, 565-573 (2007).
17. Katharina Kohse-Höinghaus, Patrick Oßwald, Ulf Struckmeier, Tina Kasper, Nils Hansen, Craig A. Taatjes, Juan Wang, Terrill A. Cool, Saugata Gon and Phillip R. Westmoreland, "The influence of ethanol addition on a premixed fuel-rich propene-oxygen-argon flame," *Proc. Combust. Inst.* **31**, 1119-1127 (2007).
18. Nils Hansen, James A. Miller, Craig A. Taatjes, Juan Wang, Terrill A. Cool, Matthew E. Law, Phillip R. Westmoreland, Tina Kasper and Katharina Kohse-Höinghaus, "Photoionization Mass Spectrometric Studies and Modeling of Fuel-Rich Allene and Propyne Flames," *Proc. Combust. Inst.* **31**, 1157-1164 (2007).
19. Fabien Goulay, David L. Osborn, Craig A. Taatjes, Peng Zou, Giovanni Meloni and Stephen R. Leone, "Direct detection of Polyynes Formation from the Reaction of Ethynyl Radical (C_2H) with Methylacetylene ($CH_3{-}C{\equiv}CH$) and Allene ($CH_2{=}C{=}CH_2$)," *Phys. Chem. Chem. Phys.* in press (2007).
20. N. Hansen, T. Kasper, S. J. Klippenstein, P. R. Westmoreland, M. E. Law, C. A. Taatjes, K. Kohse-Höinghaus, J. Wang, and T. A. Cool, "Initial Steps of Aromatic Ring Formation in a Laminar Premixed Fuel-Rich Cyclopentene Flame," *J. Phys. Chem. A*, in press (2007) (J. A. Miller festschrift).
21. Edgar G. Estupiñán, Jared D. Smith, Atsumu Tezaki, Stephen J. Klippenstein, and Craig A. Taatjes, "Measurements and Modeling of DO_2 Formation in the Reactions of C_2D_5 and C_3D_7 Radicals with O_2," *J. Phys. Chem. A*., in press (2007) (J. A. Miller festschrift).
22. Sarah V. Petway, Huzeifa Ismail, William H. Green Jr., Edgar G. Estupiñán, Leonard E. Jusinski, and Craig A. Taatjes, "Measurements and Automated Mechanism Generation Modeling of OH Production in Photolytically-Initiated Oxidation of the Neopentyl Radical," *J. Phys. Chem. A*., in press (2007) (J. A. Miller festschrift).
23. Craig A. Taatjes, "How Does the Molecular Velocity Distribution Affect Kinetics Measurements by Time-Resolved Mass Spectrometry?," *Int. J. Chem. Kinet.*, in press (2007).
24. Craig A. Taatjes, Arjan Gijsbertsen, Marc J. L. de Lange, and Steven Stolte, "Measurements and Quasi-Quantum Modeling of the Steric Asymmetry and Parity Propensities in State-to-State Rotationally Inelastic Scattering of NO ($^2\Pi_{½}$) with D_2," *J. Phys. Chem. A,* in press (2007) (R. E. Miller festschrift).

Theoretical Chemical Dynamics Studies of Elementary Combustion Reactions

Donald L. Thompson
Department of Chemistry, University of Missouri, Columbia, MO 65211
thompsondon@missouri.edu

Program Scope

The speed with which quantum chemistry calculations can now be done makes the direct use of *ab initio* forces in MD simulations feasible. However, high-level quantum calculations are often too costly in computer time for practical applications and the levels of theory that must be used are often inadequate for reactions. Thus, among the immediate pressing problems are the efficiency in using expensive high-level quantum chemistry methods (which may not provide the necessary gradients directly) and new ways to correct the errors in *ab initio* energies when necessary. A critical part of the solution is better methods for fitting global potential energy surfaces (PESs) and techniques for making direct dynamics more efficient (e.g., reducing the number of points that must be computed). Within the context of modern quantum chemistry capabilities it is sensible to focus on local fitting schemes. The first attempts at developing these approaches were based on cubic splines,[1,2] but have proven not to be the best approach, and thus various other approaches are being vigorously investigated. Those attracting most of the effort are modified-Shepard (MS)[3-5] interpolating moving least-squares (IMLS),[6-16] distributed approximating functionals (DAF),[17-20] and neural networks (NN).[21-25] We are exploring higher-order IMLS, which does not require derivatives, and thus can be used with the highest-level quantum chemistry methods for which forces may not be directly obtainable. The goal is to develop efficient methods for generating global PESs with a long-term goal of developing methods in which software for rate calculations direct quantum chemistry codes to produce *ab initio* predictions of reaction rates and related dynamics quantities.

Recent Progress

The IMLS method uses a weighted least-squares fit to the collection of available *ab initio* points. The weight function is peaked about the evaluation point implying that only local *ab initio* points strongly influence the value of the fit. The fact that the weights vary with the evaluation point also implies that every fit evaluation involves a least squares fit. In our initial studies,[8-13] we explored the basic properties of IMLS fits of energy values alone to generate PESs of chemical accuracy (rms fitting errors of ~1 kcal/mol). This includes automatically growing a PES with no human intervention from an initial small number of seed points. We found that fitting basis sets of relatively low degree (second or third degree) could achieve chemical accuracy over a large dynamic range (~100 kcal/mol) with a few hundred points for triatomic PESs and 1000 – 2000 points for simple tetra-atomic PESs. After the PESs have been fit using N *ab initio* points, the cost of evaluating the IMLS fit goes as NM^2, where M is the number of basis functions. We explored cutoff strategies that reduce the effective value of N and the selective elimination of basis function cross terms that reduce the value of M.

In recent studies, we have:

- extended our IMLS fits down to spectroscopic accuracy (rms fitting errors of ~1 cm^{-1}) by using much larger basis sets. Figure 1 shows the expected power-law convergence observed over more than three orders of magnitude variation in the RMS error measure for a test fit to an already determined HCN PES.[26]

- incorporated gradients and Hessians into the IMLS formalism and observed a more rapid convergence of the PES fitting error with the number of *ab initio* points.[15,16]
- developed a dual method in which a set of inexpensive electronic structure calculations defines an IMLS fit which is then upgraded by an IMLS fit to a difference surface developed from expensive but much more accurate electronic structure calculations. This approach was applied to the H_2CN PES and only a few hundred expensive calculations were need to converge both a 6D fit and the trajectory-calculated dissociation rate constants.

This last study along with earlier studies confirms that IMLS fits take a relatively long time to evaluate, making trajectory calculations very expensive. Even with careful management of N and M, the NM^2 cost of doing least squares calculations at every evaluation is too high.

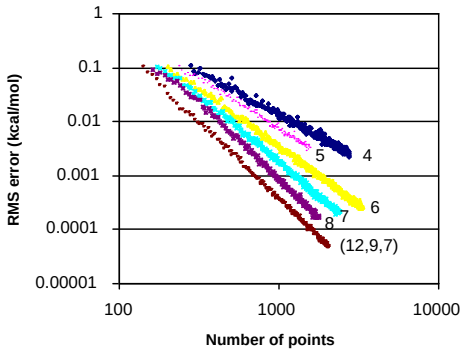

Fig. 1: Observed power-law behavior of RMS error during automatic surface generation of 3-D PES (HCN). The numbers indicate the degree of the basis. The (12,9,7) indicates a mixed basis, with d=12 for the diagonal terms, d=9 and 7 for terms with 2 and 3 coordinates, respectively.

In our most recent work, we have discovered that the solution to this problem is local IMLS or L-IMLS, an idea suggested early in the development of IMLS. L-IMLS is a variant of a local approximates method of evaluating a fit. In this approach, each member of a set of expansions centered around a scattering of points is used to estimate the energy at some evaluation point. A weighted average of these estimates gives the final estimated value where the weight is peaked at the evaluation point. Each expansion is called a local approximate and the weight functions heavily weighs only those local approximates centered on points near the evaluation point. Modified Shepard is a theory of this sort where the local approximate is a second order Taylor series expansion. L-IMLS uses IMLS expansions around a scattering of points as the local approximate. Each local approximate needs a least squares evaluation to set the basis set coefficients but these coefficients are saved and reused each time a local approximate is asked to estimate the energy at another evaluation point. The MS approach requires gradients and Hessians to define the Taylor series coefficients but L-IMLS does not need that information if it is not available. The evaluation of L-IMLS goes approximately as NM, the same cost as a Modified Shepard approach if M were that for a second order basis set. However, M can be much larger, with generally a decrease in the effective N, and no higher order derivatives are required. Figure 2 shows an application to a 6D

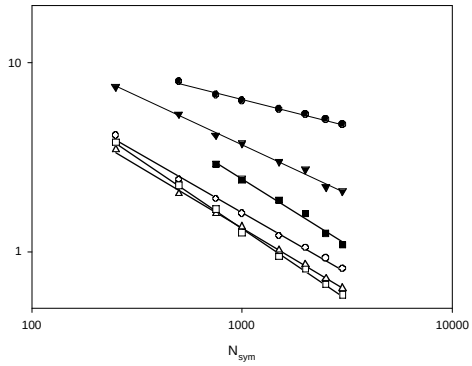

Fig. 2: The rms error vs. N_{sym} (the number of *ab initio* points) for L-IMLS fits using second, third, and fourth degree basis sets with augmented higher order diagonal terms. Random point selection is indicated by filled circles while automatic point selection is indicated by open circles.

HOOH PES[27] where chemical accuracy is achieved over a 100 kcal/mol dynamic range with an augmented 4th-degree basis set with ~1500 points. There are several variants on this approach all of which produce fits that can be evaluated reasonably quickly yet require a very sparse set of *ab initio* points.

Future Work

We are currently pursuing two projects.

- First, we are applying the L-IMLS approach to refit 5 and 6 atom analytic PESs drawn from PES libraries such as POTLIB.[28] In effect, we are using the POTLIB PESs as cheap electronic structure calculations to test and perfect our automatic surface generation techniques and to understand the scaling properties of L-IMLS.
- Second we are marrying L-IMLS technology with common electronic structure codes like Gaussian or COLUMBUS so as to produce scripts that use IMLS to drive electronic structure calculations in the automatic generation of PESs.

When these are complete, we intend to extend our IMLS efforts to direct dynamics studies and to fitting a series of PESs involving the reactions of propargyl radicals with atomic, diatomic, triatomic, and polyatomic radicals and molecules. With this series of PESs we hope to use classical trajectories to study important dynamical issues and improve the understanding of precursor reactions to soot formation.

This work is being done in collaboration with Drs. A. Wagner and M. Minkoff (retired) at ANL.

References

1 D. L. Thompson and D. R. McLaughlin, *J. Chem. Phys*. **62**, 4284 (1975).

2 N. Sathyamurthy, R. Rangarajan, and L. M. Raff, *J. Chem. Phys*. **64**, 4606 (1976).

3 J. Ischtwan and M. A. Collins, *J. Chem. Phys*. **100**, 8080 (1994).

4 T. Ishida and G. C. Schatz, *Chem. Phys. Lett*. **314**, 369 (1999).

5 M. Yang, D. H. Zhang, M. A. Collins, and S.-Y. Lee, *J. Chem. Phys*. **114**, 4759 (2001).

6 D. H. McLain, *Comput. J*. **17**, 318 (1974).

7 R. Farwig, in *Algorithms for Approximation*, edited by J. C. Mason and M. G. Cox (Clarendon, Oxford, 1987).

8 G. G. Maisuradze and D. L. Thompson, *J. Phys. Chem. A* **107**, 7118 (2003).

9 G. G. Maisuradze, D. L. Thompson, A. F. Wagner, and M. Minkoff, *J. Chem. Phys*. **119**, 10002 (2003).

10 A. Kawano, Y. Guo, D. L. Thompson, A. F. Wagner, and M. Minkoff, *J. Chem. Phys.* **120**, 6414 (2004).

11 Y. Guo, A. Kawano, D. L. Thompson, A. F. Wagner, and M. Minkoff, *J. Chem. Phys.* **121** (11), 5091 (2004).

12 G. G. Maisuradze, A. Kawano, D. L. Thompson, A. F. Wagner, and M. Minkoff, *J. Chem. Phys.* **121**, 10329 (2004).

13 A. Kawano, I.V. Tokmakov, D. L. Thompson, A. F. Wagner, and M. Minkoff, *J. Chem. Phys.* **124**, 54105 (2006).

14 Y. Guo, L. B. Harding, A. F. Wagner, M. Minkoff, and D. L. Thompson, *J. Chem. Phys.* 126, 104105 (2007).

[15] I. Tokmakov, A. F. Wagner, M. Minkoff, and D. L. Thompson, "Interpolating Moving Least-Squares Methods for Fitting Potential Energy Surfaces: Gradient Incorporation in One-Dimensional Applications," *J. Theor. Chem. Accts.*, in press.

[16] R. Dawes, D. L. Thompson, Y. Guo, A. F. Wagner, and M. Minkoff, "Interpolating Moving Least-Squares Methods for Fitting Potential Energy Surfaces: Computing High-Density PES Data from Low-Density *ab initio* Data Points," *J. Chem. Phys*., in press.

[17] A. M. Frishman, D. K. Hoffman, R. J. Rakauskas, and D. J. Kouri, *Chem. Phys. Lett*. **252**, 62 (1996).

[18] D. K. Hoffman, A. M. Frishman, and D. J. Kouri, *Chem. Phys. Lett*. **262**, 393 (1996).

[19] A. M. Frishman, D. K. Hoffman, and D. J. Kouri, *J. Chem. Phys.* **107**, 804 (1997).

[20] V. Szalav, *J. Chem. Phys*. **111**, 8804 (1999).

[21] B. G. Sumpter and D. W. Noid, *Chem. Phys. Lett*. **192**, 455 (1992).

[22] T. B. Blank, S. D. Brown, A. W. Calhoun, and D. J. Doren, *J. Chem. Phys*. **103**, 4129 (1994).

[23] D. F. R. Brown, M. N. Gibbs, and D. C. Clary, *J. Chem. Phys*. **105**, 7497 (1996).

[24] D. I. Doughan, L. M. Raff, M. G. Rockley, H. Hagan, P. M. Agrawal, and R. Komanduri, *J. Chem. Phys*. **124** 054321 (2006); *ibid*. 125, 079901 (2006).

[25] S. Manzhos, X. Wang, R. Dawes, and T. Carrington, Jr., *J. Phys. Chem. A* **110**, 5295 (2006).

[26] J. M. Bowman and B. Gazdy, *J. Phys. Chem. A* **101**, 6384 (1997).

[27] B. Kuhn, T. R. Rizzo, D. Luckhaus, M. Quack, and M. A. Suhm, J. Chem. Phys. **111**, 2565 (1999).

[28] R. J. Duchovic, Y. L. Volobuev, G. C. Lynch, D. G. Truhlar, T. C. Allison, A. F. Wagner, B. C. Garrett, and J. C. Corchado, *Comp. Phys. Comm.* **144,** 169 (2002).

Publications (2005-present):

(1) D. M. Medvedev, S. K. Gray, A. F. Wagner, M. Minkoff, and R. Shepard, "Advanced Software for the Calculation of Thermochemistry, Kinetics, and Dynamics," *J. Physics: Conference Series* **16**, 247-251 (2005).

(2) D. L. Thompson, A. F. Wagner, and M. Minkoff, "Advanced Computational Methods for Simulating Chemical Reactions," *J. Physics: Conference Series* **16**, 252-256 (2005).

(3) A. Kawano, I. V. Tokmakov, D. L. Thompson, A. F. Wagner, and M. Minkoff, "Interpolating Moving Least-Squares Methods for Fitting Potential-Energy Surfaces: Further Improvement of Efficiency via Cutoff Strategies," *J. Chem. Phys.* **124**, 54105 (2006).

(4) D. L. Thompson, A. F. Wagner, and M. Minkoff, "Advanced Computational Methods for Simulating Chemical Reactions," *Journal of Physics: Conference Series* **46**, 234-238 (2006).

(5) Y. Guo, L. B. Harding, A. F. Wagner, M. Minkoff, and D. L. Thompson, "Interpolating Moving Least-Squares Methods for Fitting Potential Energy Surfaces: An Application to the H_2CN Unimolecular Reaction," *J. Chem. Phys.* 126, 104105(1-9) (2007).

(6) I. Tokmakov, A. F. Wagner, M. Minkoff, and D. L. Thompson, "Interpolating Moving Least-Squares Methods for Fitting Potential Energy Surfaces: Gradient Incorporation in One-Dimensional Applications," *J. Theor. Chem. Accts.*, in press.

(7) R. Dawes, D. L. Thompson, Y. Guo, A. F. Wagner, and M. Minkoff, "Interpolating Moving Least-Squares Methods for Fitting Potential Energy Surfaces: Computing High-Density PES Data from Low-Density *Ab Initio* Data Points," *J. Chem. Phys*., in press.

Elementary Reactions of PAH Formation

Robert S. Tranter
Chemistry Division
Argonne National Laboratory
Argonne, Il-60439
tranter@anl.gov

Program scope

This program is focused on the experimental determination of kinetic and mechanistic parameters of elementary reactions, in particular those involved in the formation and destruction of the building blocks for aromatic species. The approach involves the development of a low pressure, fast flow, reactor equipped with a quadrupole MS and a shock tube (ST) equipped with laser schlieren (LS) and a time-of-flight mass spectrometer (TOF-MS). The combination of these techniques permit a wide range of reaction temperatures and pressures to be accessed. Recently, efforts have been primarily devoted to the ST/TOF-MS apparatus to ensure that both kinetic and mechanistic data can be accurately obtained with the instrument. To this end a series of unimolecular reactions have been studied prior to starting the more complex systems such as reactions of the propargyl and phenyl radicals.

Recent Progress

ST/TOF-MS: Considerable progress has been made with the ST/TOF-MS and it can be considered fully functional, in that accurate kinetic and mechanistic data are now routinely obtained with the apparatus. Previously, studies of HF elimination in 1,1,1-trifluoroethane (TFE) and vinyl fluoride (VF), and the dissociation of cyclohexene had yielded rate coefficient's that were considerably lower than literature data at comparable reaction conditions. Two potential sources for this discrepancy were identified: 1) the actual reflected shock conditions being different to those calculated from the initial conditions and incident shock velocity; 2) the gases flowing from the sampling orifice to the TOF-MS not accurately reflecting the concentrations in the shock heated zone. The first case was addressed by measuring the incident shock velocity close to the sampling orifice in the end wall of the driven section to minimize the effect of attenuation of the shock wave on the calculated post shock conditions. The second problem is more complicated and was addressed by a detailed investigation of the nozzle / skimmer sampling system that transports species from the rapidly changing environment in the shock tube to the TOF-MS.

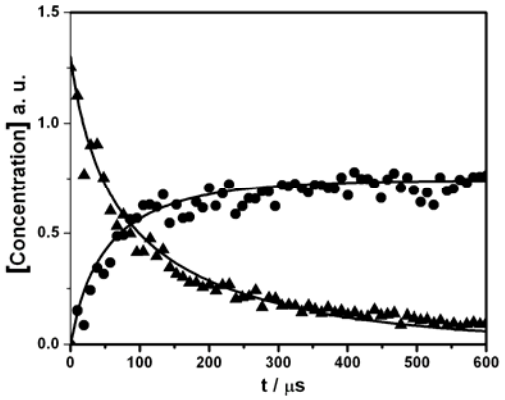

Figure 1: Concentration time profile from a ST/TOF-MS experiment on $C_6H_{10} = C_4H_6 + C_2H_4$, $P_5 = 619$ torr, $T_5 = 1424$ K; (▲) cyclohexene; (●) ethylene; (—) simulation. Ion source pulsed at 105 kHz (9.52 μs)

Following reflection of the shock wave a cold thermal boundary layer (TBL) develops at the end wall of the shock tube where the sampling orifice is located. To make reliable kinetic and mechanistic measurements it is critical that gases from the TBL do not enter the mass spectrometer as the reaction history in the TBL is completely different to that in the homogeneous reaction zone behind the reflected shock wave. The majority of previous ST/TOF-MS apparatuses were constructed without a skimmer and just a small orifice between the shock tube and MS. Typically, the orifice (<0.1mm diameter) was located at the apex of a conical nozzle that protruded into the shock tube and in principle increased the sampling time before the TBL engulfed the nozzle. We have tested many styles of nozzle and find that the most reliable data are obtained using a differentially pumped nozzle /skimmer arrangement with a large

(0.4mm diameter) divergent nozzle that does not protrude into the shock tube. On the time scale of the experiment (<2ms) the flow through the nozzle tends to confine the TBL gases to the outer streamlines of the expanding jet and the skimmer ensures that only gases on the centerline, drawn from the homogenous reaction zone, enter the TOF-MS. These improvements to the apparatus coupled with sampling the molecular beam at up to105 kHz in the ion source, and improved analysis software, generate concentration / time profiles, figure 1, from which accurate rate coefficients can be determined. The performance of the ST/TOF-MS was tested by studying the dissociation of cyclohexene to 1,3 butadiene and ethylene (T5= 1260 to 1430 K, P5 = 600 and 1300 torr). The recovered rate coefficients are in very good agreement with the literature data for this reaction however the time resolution tends to limit the maximum rate coefficients that can be reliably measured. Subsequently, a number of reactions have been investigated with the apparatus, often in conjunction with LS studies. The TOF-MS and LS methods provide complimentary, overlapping datasets and together expand the experimentally accessible range of conditions. Some of these studies are discussed below.

Fluoroethanes: An ongoing project with John Kiefer, UIC, has been the elimination of HF from fluorinated ethanes which was stimulated by a series of LS experiments on TFE dissociation. These data showed an anomalous falloff behavior that could not be explained by RRKM theory. The LS experiments were the only high temperature, low pressure data available for TFE dissociation and due to the peculiar pressure dependence the reliability of the data had been questioned. Consequently, a separate ST/TOF-MS study (T5=1500 to 1840 K and P5 =600 and 1200 torr) of TFE dissociation has been performed to both measure rate coefficients and determine if there are any chain reactions occurring in addition to the molecular elimination, suggested as a source of error in the LS experiments. The resulting rate coefficients are shown in figure 2 where they are compared with the earlier LS data and the agreement is very good. As well as the kinetic data the mass spectra obtained in the TOF-MS work clearly show that the only products in the region of overlap with the LS experiments are 1,1,-difluoroethene and HF indicating that only molecular elimination of HF occurs. Additionally, the new LS apparatus at Argonne has been used to repeat some of the earlier LS work (P2= 50 and 200 torr) and shows excellent agreement with the earlier data from Kiefer's laboratory, figure 2. Thus the experimental data on TFE dissociation appears to be quite consistent even though an adequate theoretical treatment is still being sought.

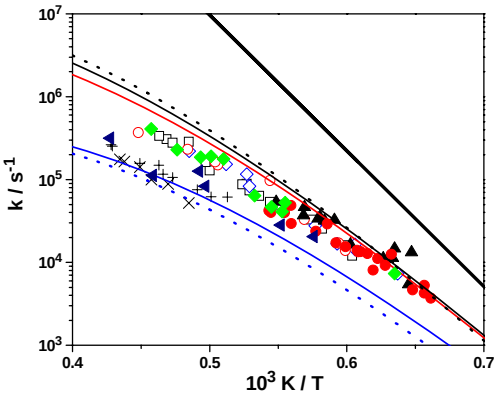

Figure 2:Results of experiments on TFE dissociation and comparison with RRKM calculations. TOF-MS: (●) 600 torr; (▲) 1200 torr. LS-ANL LS: (◀) 50 torr, (♦) 200 torr. LS- Kiefer et al. *(JPCA,108, 2443, 2004)* (□) 100 torr, (◊) 350 torr, (○) 550 torr, (+) 35 torr, (×) 15 torr.. (—) theoretical k_∞. Non-RRKM calculations: (–) 35 torr, (–) 600 torr, (–) 1200 torr. RRKM calculations: (…) 35 torr, (…) 1200 torr.

Of the remaining fluoroethanes only 1,1-difluoroethane (DFE) both dissociates by simple HF elimination and also has sufficient heat of reaction for study by LS. At the reaction conditions where DFE dissociation occurs vinyl fluoride, the organic product from DFE, readily eliminates HF to form acetylene. This subsequent reaction influences the later portion of the DFE LS profiles and thus needs to be accounted for in the interpretation of the DFE data. Furthermore, the HF elimination from VF has been suggested to occur by both a four center transition state across the double bond and a 3 center transition state froma singlecarbon atom. The later route initially forms vinylidene which rapidly rearranges to acetylene. G3B3 calculations have shown that the two transition states lie within 1.5 kcal of each other suggesting that both pathways may be almost, equally likely. Both LS (performed at UIC and Argonne) and ST/TOF-MS studies have been made of VF dissociation, with the combination of the two techniques giving access to a much larger experimental range than either method alone would permit. The results of these studies are shown in figure 3 along with the results of RRKM calculations that incorporate the two decomposition pathways. Clearly, the two sets of LS experiments are in good agreement with each other and the ST/TOF-MS data. Furthermore the RRKM calculations are in good agreement with the experimental data although a

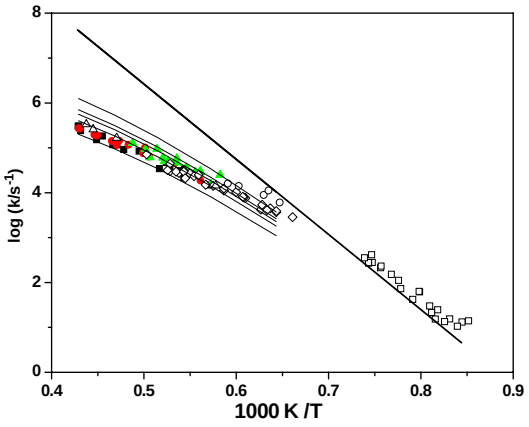

Figure 3: Results from the ST/LS and ST/TOF-MS experiments for vinyl fluoride dissociation showing the comparison with the literature data and the results of RRKM calculations. ST/LS experiments: 10% $CHF=CH_2$/Kr: [■] 75-140 torr, [●] 206-300 torr, [▲] 311-482 torr; 4% $CHF=CH_2$/Kr, [▵] 459 to 652 torr. ST-TOF/MS experiments: [◊] 4% $CHF=CH_2$/Kr, 516 - 633 torr, [○] 1210 - 1373 torr.. Here the collision efficiency, $\langle\Delta E\rangle_{down} = 9775(T/298)^{-1}$ cm^{-1}, was chosen to produce a best fit. The heavy, steep line at the top shows the sum of k_∞ for reactions (**2**) and (**3**) taken from the TST calculations. RRKM calculations: thin black lines 100, 250, 400, 550 and 1250 torr. Single-pulse experiments [□] of Simmie et al. (*JPC 74, 992, 1970*, 2800-3600 torr.

rather large value of $\langle\Delta E\rangle_{down}$ was required. Ongoing work suggests that a more reasonable value of $\langle\Delta E\rangle_{down}$ gives an improved fit to the data if the activation barrier is also lowered by a couple of kcal/mol.

Finally, only the ST/TOF-MS method has been applied to the dissociation of 1-fluoroethane (T5=1207 to 1711 K, P5 = 500 and 1200 torr) because the enthalpy of reaction is too small to produce measurable density gradients with LS. Similar to the DFE work the results show fall-off which is adequately described by a standard RRKM calculation. Thus of the fluoroethanes that we have been able to study so far, the only one showing an anomalous fall-off behavior is TFE. We intend to use the ST/TOF-MS to continue the study of fluoroethanes that are not amenable to LS study.

1,4-Dioxane: The dissociation of 1,4-dioxane is interesting as an analogue for the dissociation of cyclohexane. The literature data on the high temperature dissociation of 1,4-dioxane is sparse and has typically been conducted in static reactors which may be susceptible to wall effects. However, they indicate that C2H4, HCHO, CO and H2 are the major products, of the minor products small amounts (<2%) of acetaldehyde and (<3%) 1-propenaldhyde were observed (Battin et al. J. Anal. App. Pyrol. 16, 345, 1989) and the authors have proposed a free radical mechanism to explain their results at 510 oC and 552 oC.

From the mass spectral point of view the dissociation of 1,4-dioxane is challenging because fragmentation of the parent molecule in the ion source yields mass peaks that are the same as those seen in many of the likely products. Furthermore, the products also fragment complicating concentration measurements and species identifications. However, a strong, unique peak is seen from the parent ion of 1,4-dioxane which allows a rate coefficient to be determined for the dissociation reaction and examination of the mass peak distributions gives valuable information regarding the product identities. Ideally, a softer, more specific ionization technique than electron impact would be used thereby reducing fragmentation. However, this is currently not possible. The challenges involved in interpreting these spectra are similar to those that will arise in the study of elementary reactions involved in PAH formation/destruction and the study of 1,4-dioxane also provides a good stepping stone to more complex reaction systems.

Similar to the work on fluoroalkanes 1,4-dioxane has been studied with both LS, Kiefer, and ST/TOF-MS at Argonne. At low reaction temperatures the LS and ST/TOF-MS experiments give good agreement for the initial dissociation of 1,4-dioxane. However as the temperature increases the LS data start to show a strong negative density gradient that is characteristic of exothermic reaction. The most likely source of this gradient is due to the subsequent reaction of products from the dissociation of acetaldehyde, formed from 1,4-dioxane pyrolysis. Incorporating an acetaldehyde submechanism in the simulation of the LS data gives reasonable agreement with the experimental data. However, even at low temperatures the TOF-MS experiments show no indication of acetaldehyde which has a unique peak, m/z=44, from the parent ion. The simulations performed with the LS experiments indicate that sufficient acetaldehyde should be formed to give a strong m/z=44 peak, particularly at low temperatures where the dissociation of acetaldehyde is slow. Furthermore, the static reactor work indicates that acetaldehyde is a minor product and as such would not produce the strong exothermic density gradients observed in the LS work. However, simulation of the LS profiles will be challenging without including acetaldehyde dissociation. The only other species present that could produce the negative gradient is HCHO which should not dissociate until

much higher temperatures than in the current work. .Currently, a ST/TOF-MS study of acetaldehyde pyrolysis is being conducted to compliment the 1,4-dioxane work. In addition the 1,4-dioxane studies are being extended to lower temperatures where acetaldehyde should be unreactive and higher concentrations to enhance the mass spectra. Furthermore the initial interpretation of the TOF-MS data indicate the C2H4, H2 and H2CO are the main products similar to the static reactor experiments.

Future Plans

Several studies are planned for the ST/TOF-MS now that it is producing reliable data. These include investigation of HF elimination in the remaining fluoroalkanes that cannot be studied with LS and planned improvements to the apparatus should increase the upper limit of rate coefficients that can be measured in these systems. Combined LS and ST/TOF-MS studies are underway or will be started soon on the reactions of the propargyl radical and phenyl radical. Of particular interest is the formation of biphenyl from phenyl radicals a reaction for which there is little direct experimental data and that which exists is in poor agreement with recent theoretical calculations by Harding and Klippenstein. Characterization of the decomposition of precursors for both propargyl and phenyl has been started and provides the necessary data for the planned studies of these species. Additionally, the experiments on cyclic species will be extended to include 1,3-dioxane and cyclohexane.

In addition to the chemical studies effort will also be devoted to completing the low pressure, fast flow reactor which is particularly valuable for radical/molecule studies. Several improvements to the ST/TOF-MS are currently being made. Amongst these are modifications to the detector to enhance the sensitivity and dynamic range of the MS, implementation of ion gating to prevent unwanted species reaching the detector and converting the shock tube to a diaphragmless apparatus. The 1,4-dioxane experiments have highlighted the limitations of the current electron impact ionization method and alternative ionization schemes are being investigated for the TOF-MS.

Publications

1. Saxena S., Kiefer J. H. and Tranter R. S., “Relaxation, Incubation, and Dissociation in CO2”, J. Phys. Chem. A, DOI: 10.1021/jp066717b.
2. Tranter R. S., Giri B. G. and Kiefer J. H., “Coupling of a Shock Tube to a Time-of-Flight Mass Spectrometer for High Temperature Kinetic Studies” Rev. Sci. Instrum., 78, 034101, 2007.
3. Giri B.R. and Tranter R. S., “Dissociation of 1,1,1-Trifluoroethane Behind Reflected Shock Waves: Shock Tube/Time-of-Flight Mass Spectrometry Experiments” J. Phys. Chem. A, 111(9), 1585 – 1592, 2007.
4. Sivaramakrishnan R, Comandini A, Tranter R. S., Brezinsky K., Davis S. G. and Wang H., “Combustion of CO/H2 Mixtures at Elevated Pressures”, Proc. Combust. Inst., 31, 167-174, 2007
5. Sivaramakrishnan R., Tranter R. S. and Brezinsky K.,“High Pressure Pyrolysis of Toluene. 2. Modeling Benzyl Decomposition and Formation of Soot Precursors”, J. Phys. Chem. A110(30), 9400-9404, 2006
6. Sivaramakrishnan R., Tranter R. S., Brezinsky K., “High Pressure Pyrolysis of Toluene. 1. Experiments and Modeling of Toluene Decomposition”, J. Phys. Chem. A 110(30), 9388-9399, 2006
7. Gupte K. S., Kiefer J. H., Tranter R.S., Klippenstein S. J. and Harding L. B., “Decomposition of Acetaldehyde: Experiment and Detailed Theory”, Proc. Combust. Inst. 31, 429-437, 2007
8. Miller, C. H., Tang W., Tranter R.S. and Brezinsky K., “Shock tube pyrolysis of 1,2,4,5-hexatetraene”, J. Phys. Chem. A 110, 3605-3613, 2006.
9. Sivaramakrishnan R., Vasudevan H., Tranter R. S. and Brezinsky K., “A Shock Tube Study of the High Pressure Thermal Decomposition of Benzene”, Combustion Science and Technology, 178, 285-305, 2006
10. Tang W., Tranter R. S. and Brezinsky K., “An optimized semi-detailed sub-mechanism of benzene formation from propargyl recombination”, J. Phys. Chem. A, 110, 2165-2175,2006.
11. Sivaramakrishnan R., Tranter R. S., Brezinsky K., “A High Pressure Model for the Oxidation of Toluene”, Proceedings of the Combustion Institute, 30, 1165-1173, 2005.

VARIATIONAL TRANSITION STATE THEORY

Principal investigator, mailing address, and electronic mail

Donald G. Truhlar
Department of Chemistry, University of Minnesota, 207 Pleasant Street SE,
Minneapolis, Minnesota 55455
truhlar@umn.edu

Program scope

This project involves the development of variational transition state theory (VTST) with optimized multidimensional tunneling (OMT) contributions and its application to gas-phase reactions. The further development of VTST/OMT as a useful tool for combustion kinetics also involves developing and applying new methods of electronic structure calculations for the input potential energy surface, which is typically an implicit surface defined by a level of electronic structure theory, and methods to interface reaction-path and reaction-swath dynamics calculations with electronic structure theory. The project also involves the development and implementation of practical techniques and software for applying the theory to various classes of reactions and transition states and applications to specific reactions, with special emphasis on combustion reactions and reactions that provide good test cases for methods needed to study combustion reactions.

Recent progress

A theme that runs through our current work is the development of improved electronic structure methods and their use for rate constant calculations. One class of new methods involves wave function theory, especially generally defined electronic wave function methods with empirical elements ("semiempirical model chemistries," in the language of late John Pople), such as methods based on extrapolating the correlation energy to complete configuration interaction; another class of methods is based on new density functionals. These methods are then used in direct dynamics calculations or with efficient interpolation schemes. Direct dynamics denotes that, instead of using a pre-defined potential energy function, all required energies and forces for each geometry that is important for evaluating dynamical properties are obtained directly from electronic structure calculations. Density functional theory is very attractive as an electronic structure method for direct dynamics because of its relatively low cost and the availability of analytic gradients and Hessians. Development of improved exchange and correlation functionals is an active research area in theoretical chemistry and physics, but most of this research has neglected the important issues of barrier height prediction and noncovalent interactions, and as a consequence the functionals have not been accurate for quantitative kinetics. We have now developed new functionals, especially the M06-2X functional (Minnesota 2006 functional with double nonlocal exchange), that are quite accurate for these properties, and we have also developed multi-coefficient correlation methods for using wave function theory for these properties.

In order to generate reactive potential energy surfaces with minimal computational effort, we have introduced an algorithm called multiconfiguration molecular mechanics (MCMM). MCMM describes polyatomic potential energy surfaces by interacting molecular mechanics (MM) configurations (each of which is the analog of a valence bond configuration) and can thus be viewed as an extension of standard MM to chemical reactions or as an extension of

semiempirical valence bond theory to be systematically improvable. MCMM fitting is accomplished by combining molecular mechanics potentials for the reactant and product wells with electronic structure data (energy, gradient, and Hessian) at the saddle point and a small number of non-stationary points. We developed a general strategy for placement of the non-stationary points for fitting potential energy surfaces in the kinetically important regions and for calculating rate constants for atom transfer reactions by variational transition state theory with multidimensional tunneling. Then we improved the efficiency of the MCMM method by using electronic structure calculations only for certain critical elements of the Hessians at the non-stationary points and by using interpolation for the other elements at the non-stationary points. We tested this new MCMM strategy for a diverse test suite of reactions involving hydrogen-atom transfer. The new method yields quite accurate rate constants as compared with straight (uninterpolated) direct dynamics calculations at the same electronic structure level.

Software distribution

We have developed several software packages for applying variational transition state theory with optimized multidimensional tunneling coefficients to chemical reactions and for carrying out MCCM calculations, density functional theory calculations with new density functionals, direct dynamics, and MCMM applications. The URL of our software distribution site is comp.chem.umn.edu/Truhlar. The license requests that we fulfilled during the period Jan. 1, 2005–Mar. 30, 2007 for software packages developed wholly or partially under DOE support is as follows:

	Total	*academic*	*government/DoD*	*industry*
POLYRATE	185	167	9	9
GAUSSRATE	66	63	2	1
GAMESSPLUS	61	55	3	3
HONDOPLUS	37	31	4	2
9 others	86	80	6	0

Future plans

We have several objectives for the next few years: (1) incorporation of dividing surfaces appropriate for association reactions into POLYRATE, and integration of these methods with master equation solvers to treat the stabilization of intermediate complexes by energy transfer collisions; (2) integration of the above methods with tight transition state methods to treat multiwell reactions and reactions with inner and outer dynamical bottlenecks; (3) further improvement of density functionals and multi-coefficient correlation methods for potential energy surfaces, especially for saddle point geometries, barrier heights, and vibrational frequencies at saddle points; (4) further development of the multi-configuration molecular mechanics approach as an efficient tool for the semiautomatic fitting of complex-system potential energy surfaces; (5) development of more reliable methods for including anharmonicity at variational transition states, especially for torsions and mode-mode coupling; (6) calculation of reaction rates of peroxides and enols; (7) enhancement of our user-friendly packages to allow more researchers to carry out calculations conveniently by the new methods.

Publications, 2005-present

Journal articles

1. "Use of Block Hessians for the Optimization of Molecular Geometries," Journal of Computational and Theoretical Chemistry **1**, 54-60 (2005).

2. "The 6-31B(d) Basis Set and the BMC-QCISD and BMC-CCSD Multi-Coefficient Correlation Methods," B. J. Lynch, Y. Zhao, D. G. Truhlar, Journal of Physical Chemistry A **109**, 1643-1649 (2005).
3. "Multi-Coefficient Extrapolated Density Functional Theory for Thermochemistry and Thermochemical Kinetics," Y. Zhao, B. J. Lynch, D. G. Truhlar, Physical Chemistry Chemical Physics **7**, 43-52 (2005).
4. "Benchmark Calculations of Reaction Energies, Barrier Heights, and Transition State Geometries for Hydrogen Abstraction from Methanol by a Hydrogen Atom," and D. G. Truhlar, Journal of Physical Chemistry A **109**, 773-778 (2005).
5. "Benchmark Database of Barrier Heights for Heavy Atom Transfer, Nucleophilic Substitution, Association, and Unimolecular Reactions and Its Use to Test Theoretical Methods," Y. Zhao, N. González-García, D. G. Truhlar, Journal of Physical Chemistry A **109**, 2012-2018 (2005).
6. "Temperature Dependence of Carbon-13 Kinetic Isotope Effects of Importance to Global Climate Change," H. Lin, Y. Zhao, B. A. Ellingson, J. Pu, D. G. Truhlar, Journal of the American Chemical Society **127**, 2830-2831 (2005).
7. "Redistributed Charge and Dipole Schemes for Combined Quantum Mechanical and Molecular Mechanical Calculations," H. Lin, D. G. Truhlar, Journal of Physical Chemistry A **109**, 3991-4004 (2005).
8. "Benchmark Databases for Nonbonded Interactions and Their Use to Test Density Functional Theory," Y. Zhao D. G. Truhlar, Journal of Chemical Theory and Computation **1**, 415-432 (2005).
9. "Databases for Transition Element Bonding: Metal–Metal Bond Energies and Bond Lengths and Their Use to Test Hybrid, Hybrid Meta, Meta Density Functionals and Generalized Gradient Approximations," N. E. Schultz, Y. Zhao, D. G. Truhlar, Journal of Physical Chemistry A **109**, 4388-4403 (2005).
10. "Design of Density Functionals that are Broadly Accurate for Thermochemistry, Thermochemical Kinetics, and Nonbonded Interactions," Y. Zhao, D. G.. Truhlar, Journal of Physical Chemistry A **109**, 5656-5667 (2005).
11. "Multi-Coefficient Extrapolated DFT Studies of π···π Interactions: The Benzene Dimer," Y. Zhao, D. G. Truhlar, Journal of Physical Chemistry A **109**, 4209-4212 (2005).
12. "How Well Can New-Generation Density Functional Methods Describe Stacking Interactions in Biological Systems?" Y. Zhao, D. G. Truhlar, Phys . Chem. Chem. Phys **7**, 2701-2705 (2005).
13. "Infinite-Basis Calculations of Binding Energies for the Hydrogen Bonded and Stacked Tetramers of Formic Acid and Formamide and Their use for Validation of Hybrid DFT and Ab Initio Methods," Y. Zhao, D. G. Truhlar, Journal of Physical Chemistry A **109**, 6624-6627 (2005).
14. "How Well Can Density Functional Methods Describe Hydrogen Bonds to Pi Acceptors?" Y. Zhao, O. Tishchenko, D. G. Truhlar, Journal of Physical Chemistry B **109**, 19046-19051 (2005).
15. "A New Algorithm for Efficient Direct Dynamics Calculations of Large-Curvature Tunneling and Its Application to Radical Reactions with 9–15 Atoms," A. Fernández-Ramos, D. G. Truhlar, Journal of Chemical Theory and Computation **1**, 1063-1078 (2005).
16. "Density Functionals for Inorganometallic and Organometallic Chemistry," N. E. Schultz, Y. Zhao, D. G. Truhlar, Journal of Physical Chemistry A **109**, 11127-11143 (2005).
17. "Combined Valence Bond-Molecular Mechanics Potential Energy Surface and Direct Dynamics Study of Rate Constants and Kinetic Isotope Effects for the H + C_2H_6 Reaction," A. Chakraborty, Y. Zhao, H. Lin, D. G. Truhlar, Journal of Chemical Physics **124**, 044315/1-044315/14 (2006).
18. "Design of Density Functionals by Combining the Method of Constraint Satisfaction with Parametrization for Thermochemistry, Thermochemical Kinetics, and Noncovalent Interactions," Y. Zhao, N. E. Schultz, D. G. Truhlar, Journal of Chemical Theory and Computation **2**, 364-382 (2006).

19. “Searching for Saddle Points by Using the Nudged Elastic Band Method: An Implementation for Application to Gas-Phase Systems,” N. Gonzalez-Garcia, J. Pu, A. Gonzalez-Lafont, J. M. Lluch, D. G. Truhlar, Journal of Chemical Theory and Computation **2**, 895-904 (2006).
20. “Modeling of Bimolecular Reactions,” A. Fernández-Ramos, J. A. Miller, S. J. Klippenstein, D. G. Truhlar, Chemical Reviews **106**, 4518-4584 (2006).
21. "Statistical Thermodynamics of Bond Torsional Modes. Tests of Separable and Almost-Separable Approximations Applied to H2O2, HOOD, D2O2, H218O2, H18OOH, D18OOH, and H18OOD," B. A. Ellingson,, V. A. Lynch, B. A. Ellingson, S. L. Mielke, and D. G. Truhlar, Journal of Chemical Physics 125, 84305/1-17 (2006).
22. "Assessment of Density Functionals for Pi Systems: Energy Differences Between Cumulenes and Poly-ynes and Proton Affinities, Bond Length Alternation, and Torsional Potentials of Conjugated Polyenes, and Proton Affinities of Conjugated Schiff Bases," Y. Zhao and D. G. Truhlar, Journal of Physical Chemistry A 110, 10478-10486 (2006).
23. "Optimizing the Performance of the Multiconfiguration Molecular Mechanics Method," O. Tishchenko and D. G. Truhlar, Journal of Physical Chemistry A 110, 13530-13536 (2006).
24. "A New Local Density Functional for Main Group Thermochemistry, Transition Metal Bonding, Thermochemical Kinetics, and Noncovalent Interactions," Y. Zhao and D. G. Truhlar, Journal of Chemical Physics 125, 194101/1-18 (2006).
25. "Representative Benchmark Suites for Barrier Heights of Diverse Reaction Types and Assessment of Electronic Structure Methods for Thermochemical Kinetics," J. Zheng, Y. Zhao, and D. G. Truhlar, Journal of Chemical Theory and Computation 3, 569-582 (2007).
26. "Global Potential Energy Surfaces with Correct Permutation Symmetry by Multi-Configuration Molecular Mechanics," O. Tishchenko and D. G. Truhlar, Journal of Chemical Theory and Computation, accepted Jan. 27, 2006.
27. “The M06 Suite of Density Functionals for Main Group Thermochemistry, Thermochemical Kinetics, Noncovalent Interactions, Excited States, and Transition Elements: Two New Functionals and Systematic Testing of Four M06 Functionals and Twelve Other Functionals,” Y. Zhao and D. G. Truhlar, Theoretical Chemistry Accounts, accepted Feb. 13, 2007. (Mark S. Gordon 65th Birthday Issue)
28. “Thermochemical Kinetics of Hydrogen-Atom Transfers Between Methyl, Methane, Ethynyl, Ethyne, and Hydrogen,” J. Zheng, Y. Zhao, and D. G. Truhlar, Journal of Physical Chemistry A, accepted March 27, 2007.

Book chapters

1. “Variational Transition State Theory and Multidimensional Tunneling for Simple and Complex Reactions in the Gas Phase, Solids, Liquids, and Enzymes,” D. G. Truhlar, in *Isotope Effects in Chemistry and Biology*, edited by A. Kohen and H.-H. Limbach (Marcel Dekker, Inc., New York, 2006), pp. 579-620.
2. “Multilevel Methods for Thermochemistry and Thermochemical Kinetics,” B. J. Lynch, D. G. Truhlar, in *Recent Advances in Electron Correlation Methodology*, edited by A. K. Wilson and K. A. Peterson (American Chemical Society Symposium Series, Washington, DC, 2007), in press.
3. "Variational Transition State Theory in the Treatment of Hydrogen Transfer Reactions, " D. G. Truhlar and B. C. Garrett, in *Hydrogen Transfer Reactions*, edited by J. T. Hynes, J. P. Klinman, H.-H. Limbach, and R. L. Schowen (Wiley-VCH, Weinheim, Germany, 2007), Vol. 2, pp. 833-874.
4. “Variational Transition State Theory,” B. C. Garrett, D. G. Truhlar, in *Theory and Applications of Computational Chemistry: The First Forty Years*, edited by C. E. Dykstra, G. Frenking, K. Kim, and G. Scuseria (Elsevier, Amsterdam, 2005), pp. 67-87.
5. “Variational Transition State Theory with Multidimensional Tunneling,” A. Fernandez-Ramos, B. A. Ellingson, B. C. Garrett, D. G. Truhlar, in *Reviews in Computational Chemistry*, Vol. 23, edited by K. B. Lipkowitz and T. R. Cundari (Wiley-VCH, Hoboken, NJ, 2007), pp. 125-232.

Chemical Kinetic Data Base for Combustion Modeling

Wing Tsang
National Institute of Standards and Technology
Gaithersburg, MD 20899
Wing.tsang@nist.gov

Program Scope or Definition: Combustion is the consequence of the complex interplay between fluid dynamics and chemical kinetics. As a result it has been difficult to apply modern simulation techniques in the design process. The improvements in the capability of CFD codes to handle increasing amounts of chemistry[1] may change this situation. It will become possible to simulate the behavior of real devices burning real fuels. The focus of this project is to aid in the development of the chemical kinetic databases necessary for such efforts with particular emphasis on liquid transportation fuels.

A complete chemical kinetic database for combustion applications must contain information on chemical transformation across the entire range of possible fuel mixtures, stoichiometries, pressures and temperatures. Most of the existing chemical kinetic databases have been limited to near stoichiometric conditions for single compound fuels. Properties such as ignition delay can be predicted in a semi-quantitative manner. This is a demonstration of the feasibility of such an approach. The next step is to be able to extend this promising beginning.

Real transportation fuels are complex mixtures of C_5 to C_{20} hydrocarbons. Without specification of the nature of these compounds, it is impossible to carry out molecule based simulations. There has been general agreement that most of the features of the combustion of a real fuel can be captured with a suitable mixture of surrogate compounds[2]. Our work is designed to support this program. We seek to extend the stoichiometric range covered to richer mixtures. This is particularly important in view of current interest in PAH/SOOT formation chemistry. Finally, we seek to develop this database on a more fundamental and internally consistent manner. This is necessary since with future applications based on mixtures, internal consistency becomes especially important.

The focus of our work is on the unimolecular decomposition and isomerization of intermediate size fuel radicals in the most general sense. The pyrolysis reactions represent processes that have been neglected in existing data bases since the earlier focus was largely on oxidative processes. Our approach has been to collect and evaluate experimental results that are related to the rate constants of interest. This includes not only direct measurements but also those that are related through detailed balance, from chemical activation experiments and data on related compounds. We then apply unimolecular rate theory to the data and derive high pressure rate constants that are consistent with the experimental measurements. With this as a basis we derive rate expressions over all combustion conditions. .

Recent Progress: Work during the past year continue to be focussed on the unimolecular degradation of organic fuels. In this report we concentrate on the pyrolytic aspects since this is largely completed. They also illustrate the problems with the proper description of multichannel processes if realistic fuels are to be considered. The present discussion will concenetrate on cyclohexyl and the 1-hexenyl radicals since the 1-hexenyl radicals are formed through the sequence of reactions

hydrocarbon fuel $\rightarrow$ Fuel radical $\rightarrow$ smaller radical + 1-olefin $\rightarrow$ 1-olefinyl radical $\rightarrow$ dienes

It is a natural consequence of the breakdown of any hydrocarbon fuel with more than 8 linear carbons. An even more interesting consequence is the cyclization reactions that leads to the formation of cyclohexyl Cyclohexyl radicals can be formed from cyclohexane. Cyclanes are relatively unimportant components of traditional fuel mixtures. However, with increasing contributions of fuels from tar sands there will be

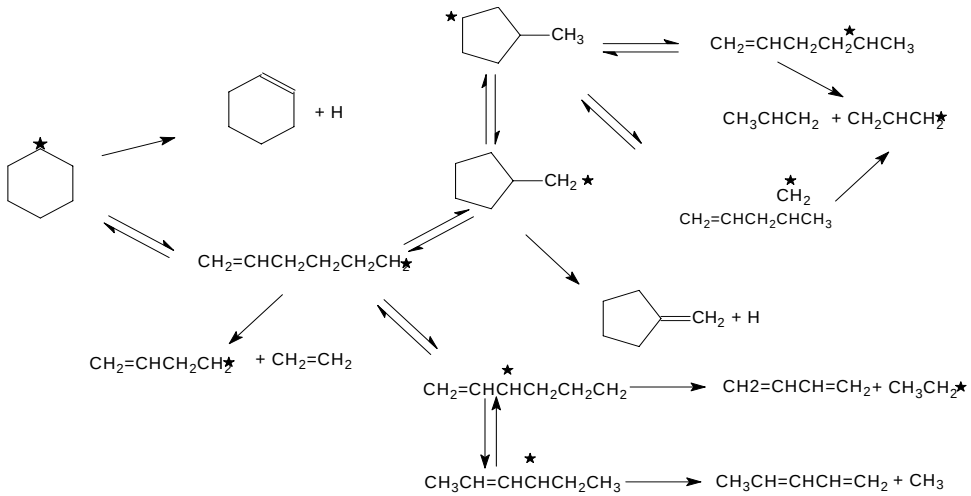

Figure 1: Mechanism for the decomposition of 1-hexenyl, cyclohexyl and cyclopentylmethyl radicals

larger amounts of cyclic compounds in future fuel mixtures. It is therefore important to develop some understanding of the mechanism and rate constants of the breakdown processes for such compounds and their differences and similarities to non-cyclic compounds.

The mechanism for the isomerization and decomposition processes of interest can be found in Figure 1, The connection between the 1-hexenyl and cyclohexyl radicals is manifest. The additional complication arises from the contribution of cyclization and decyclization processes in addition to the decomposition and H-transfer isomerization that is characteristic of fuels with an non cyclic structure.

There are very little data in the literature on the rate constants for the reactions summarized in Figure 1. Stein and Rabinovitch[3] have reported on the chemically activated isomerization of cyclohexyl radicals generated by H-atom addition to cyclohexene at room temperature and over large pressure ranges. The competition between terminal and nonterminal addition was observed. At lower temperatures, the cyclization process is much more important than the decomposition and. isomerization of the linear radical. These conclusions are supported in a qualitative fashion by the observations of Hanford-Styring and Walker[4] on the effects of introducing cyclohexane into their H_2-O_2 reacting system.

With the support of SERDP and the AFOSR we have determined the cracking pattern resulting from the introduction of cyclohexyl and 1-hexenyl-6 in the high temperature reacting system generated in a single pulse shock tube[5]. Results in terms of the ratio of a particular product and butadiene can be found in Figure 2 for the former and Figure 3 for the latter. At the higher temperatures of the shock tube experiments we have now accessed the processes involved in the breaking of the 1-hexenyl-6 radical. 1,3-Butadiene is an important product. Particularly interesting is that except for cyclohexene the cracking pattern for 1-hexenyl-6 decomposition is the same as that for cyclohexyl decomposition. For cyclohexene the yields are a factor of two higher for cyclohexyl radical as the precursor. This is indicative of the shock tube results being in the kinetically controlled regime. The lines in Figures 2 and 3 are based on the same set of rate constants and is thus confirmatory of the assignments. Finally, we show in Figure 4 our fit of the results of the chemically activated decomposition of cyclohexyl from Stein and Rabinovitch at room temperature using the same set of rate expressions as for the shock tube studies and a step size down for hydrogen used in 1-pentenyl–5 decomposition [6]. An important consequence of this study is that the rate constants for hydrogen isomerization involving a five member cyclopentyl structure is much smaller than those for a linear alkyl structure. The necessity of including cyclohexyl radical into the 1-hexenyl radical decomposition and isomerization pathways was expected. The inclusion of more isomerization channels leads to added uncertainties in the assignment of rate constants. Without the chemically activated work on

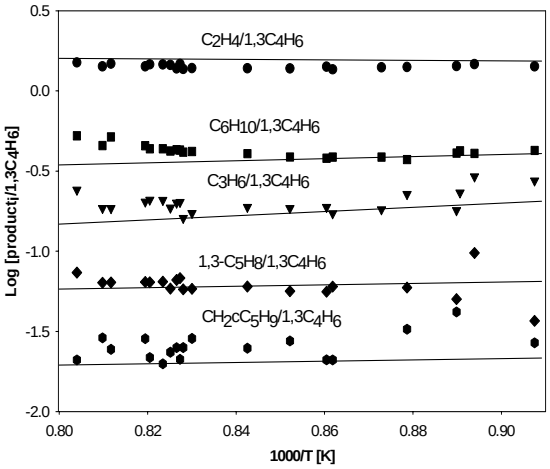

Figure 2: Ratio of products to butadiene formed as a consequence of cyclohexyl decomposition at 4 bar pressure. The lines are best fits based on rate expressions used to fit data from cyclohexyl decomposition

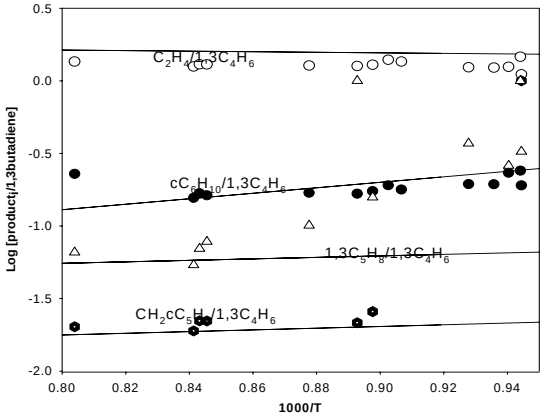

Figure 3: Ratio of products to butadiene formed as a consequence of 1-hexenyl-6 decomposition at 4 bar pressure. The lines are best fits based on rate expressions used to fit data from cyclohexyl decomposition

cyclohexyl radical decomposition, the magnitude of the differences for the relative importance of internal and terminal additions could not be deduced. Without the direct measurements at high temperatures and pressures of the branching ratios summarized in Figures 2 and 3 the predictions of product yields will have very large uncertainties. The description of this system requires seven beta bond scissions and seven reversible isomerizations. The rate constants that we have determined may have larger than the usual uncertainties.. A serious problem is the uncertainties in the thermodynamic properties of the cyclic radicals. It would be extrememly useful if there is a formalism similar to that developed by Benson for treating linear radicals. The problem here is not the enthalpies of the radicals but their entropies. We are uncertain of the accuracy of the later derived purely on the basis of Gaussian calculations. Actually, for high temperatures, the branching ratios obtained here is all that is needed since decomposition of radicals will be so fast that oxidation reactions cannot interfere except under the leanest conditions

Much effort has been devoted to collecting and examining data required to make estimates for rate expressions for oxidative processes. These are chemically activated systems that have not been treated in this fashion in existing kinetic databases. Unfortunately, the increased complexity of the system brought about through the addition of oxygen into the radical and the lack of mechanistically "clean" data leads to large uncertainties in any predictions for the type of fuels that we have treated under pyrolysis. The general mechanism is illustrated in Figure 5, where we compare mechanism for the decomposition of the oxidative and pyrolytic decomposition of n-propyl radical. Theoretical calculations [7-10] are now being published. Surprisingly, most do not publish the calculated transition state structure or the high pressure rate expression that are derived. Thus it is not possible to use such data to serve as a foundation for larger structures. The case of n-propyl radical in Figure 5 by Merle et al[10] is a welcome exception.

Future Work: We are at present deriving the molecular properties of all the possible oxygenated radicals of importance for this application through Gaussian calculations. We have described our procedure in last year's report. In the absence of data, this is the only possible approach. The intention is to use this to match experimental observations, beginning with the smallest species and then using the derived values to project to larger fuel molecules. With internal funding from NIST we are beginning to generate data on oxidative degradation at the higher temperatures similar to the shock tube experiments described earlier. As for the pyrolysis case, such branching ratio information can play a key role in determining relative rate constants and reducing the serious uncertainties arising from results derived purely on the basis of theory.

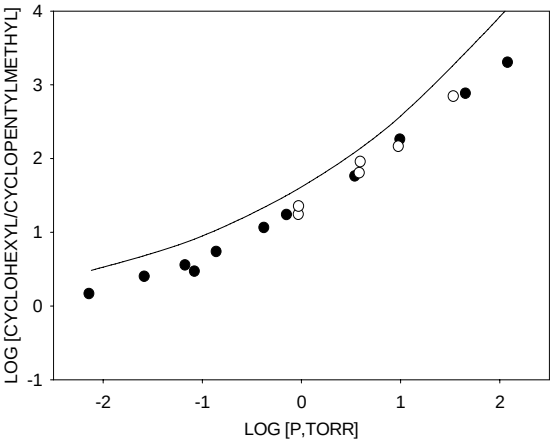

Figure 4: Comparison of calculated (line) and experimental values from the chemically activated decomposition of cyclohexyl radicals at 300 K

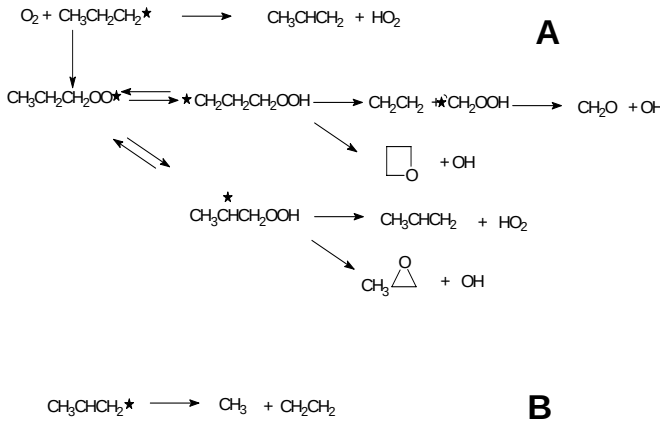

Figure 5: Mechanism for the oxidative (A) and pyrolytic (B) decomposition of n-propyl radicals

RECENT PUBLICATIONS 2005-2007

1. Baulch, DL. Bowmn, C. T., Cobos, C. J., Cox, R. A., Just, T., Kerr, J. A., Pilling, M. J., Stocker, D., Tsang, W., Walker, R. W., and Warnatz, J., "Evaluated kinetic data for combustion modeling" Supplement II, Journal of Phys. Chem Ref. Data., 4(3) 757-1397-2005

2. Tsang, W., Mechanism and rate constantsfor the decomposition of 1-pentenyl radicals.", J. Phys. Chem. A 110 (27): 8501-8509, 2006

3. Tsang, W., Walker, J. A. and Manion, J. A.,"The Decomposition of n-Hexyl Radicals", *Proc. Combust. Inst.* 2006 (in press).

4. McGivern, S., J. A. Manion, and W. Tsang, "Kinetics of the Thermal Decomposition of t-Butyl-1,3-Cyclopentadiene", J. Phys. Chem. A110 (47): 12822-12831, 2006

REFERENCES

1. Kee, R. J., Coltrin, M. E. and Glarborg, P., "Chemically Reacting Flow" Theory and Practice, Wiley, Interscience, New York, 2003
2. Colket M., Edward, C. T., Williams, S., Cernansky, N. P., Miller, D. L., Egolfopoulos, F., Lindstedt, P., Seshadri, K., Dryer F. L., Law, C. K., Friend, D., Lenhart, D. B., Pitsc, H., Sarofim, A, Smooke, M., Tsang, W., "Development of an Experimental Database and Kinetic Models for Surrogate Fuels", 45th AIAAAerospace Sciences Meeting and Exhibit, Reno, Nevada, January 9, 2007
3. Stein, S.E and Rabinovitch, B. S. J. Phys. Chem.,1975, 79, 191
4. Hanford-Styring, S. M. and Walker, R.W., Phys. Chem. Chem. Phys., 2002, 3, 204
5. Tsang, W. and Lifshitz, A., Shock Tube Methods in Chemical Kinetics" Annual Reviews of Physical Chemistry, 1990, 41, 559.
6. Tsang, W., J. Phys. Chem., A 110 8501, 2006
7. DeSain, J. D., Klippenstein, S. J. Miller, J. A. and Taatjes, C. A., J. Phys. Chem., A 107, 4415, 2003
8. Taatjes, C.A., J. Phys. Chem., A 110, 4299, 2006
9. Sun, H. , and Bozzelli, J.,J. Phys. Chem. (A) 107, 1018, 2003
10. Merle, J. A., Hayes, C. J., Zalyabovsky, S. J. Glover, B. G., Miller, T. A., and Hadad. C. ., J. Phys. Chem. (A). 109, 3637, 2005.

Time-resolved Structural Probes of Molecular Dynamics

Peter M. Weber
Department of Chemistry
Brown University, Providence, Rhode Island 02912
Peter_Weber@brown.edu

1. Program Scope

We explore new time-resolved probes of molecular dynamics, and apply them to important model systems. The two techniques that we use both rely on the interactions of electrons with molecules: time-resolved electron diffraction and time-resolved Rydberg ionization spectroscopy. In both techniques one ultimately observes the phase shift that an electron experiences as it propagates through the potential of an atom or molecule.

In the electron diffraction experiment we use ultrashort electron pulses to probe molecular structures in the Fourier plane. A laser pulse initiates a structural rearrangement, either by exciting the molecule to an excited state with a different geometry, or by inducing a chemical reaction. The electron pulse arrives some well-defined time after the pump pulse, and probes the instantaneous molecular structure, or distribution of structures. Careful consideration of the challenges of this experiment leads us to choose relativistic (megavolt) electrons for this experiment. The first demonstration experiments along this line, which are conducted in collaboration with scientists at the Stanford Linear Accelerator, have now been published.[2,5]

In the second technique, we use electrons that are loosely bound in Rydberg orbitals as structural probes. The phase shifts that Rydberg electrons encounter when passing the molecular ion core are sensitive measures of the molecular structure. The phase shifts are spectrally observed as deviations of the Rydberg peak positions from the corresponding positions of the peaks in hydrogen atoms. This leads to a method to characterize molecular structures that we call Rydberg Fingerprint Spectroscopy (RFS). One of the great advantages of RFS, discussed below, is that it is very insensitive to thermal congestion, making it a very intriguing choice for the study of molecular dynamics and combustion processes.

To implement RFS for the time-resolved determination of molecular structures, we use a pump-probe multi-photon ionization/photoelectron experiment: a first laser pulse excites the molecule to a Rydberg state, and a time-delayed probe pulse ionizes it. The photoelectron spectrum provides the binding energy of the electron, and thereby reveals the molecule's time-dependent structural fingerprint. In this abstract, several of the interesting features of RFS are highlighted.

2. Recent Progress

How much do the Rydberg states change with Methyl rotations?

Many carbohydrates, including many components of flames, have methyl groups that can rotate. Since the barriers to internal rotation are small, the methyl groups may be

freely rotating at the temperatures prevailing inflames. As a result, the 'molecular structure' of flame components is surely some average structure about such rotational degrees of freedom. Any experimental structural technique applied to combustion processes, and chemical dynamics in general, should be able to provide a measure of the molecular structure of the molecular skeleton, while not being overly sensitive toward motions such as methyl rotations.

To explore how RFS satisfies this demand, we performed experiments on a simple model system. Trimethyl amine (TMA) is useful, because it has three, possibly freely rotating, methyl groups. It also offers facile excitation to states with high internal energy. Excitation at 208 nm prepares the molecule in the 3p manifold of Rydberg states. Since TMA is pyramidal in the ground state, and planar in the excited state, excitation leads to the side of the potential energy curve, thus depositing significant energy in the molecule. Assuming equipartitioning throughout vibrational coordinates, we estimate the molecular temperature to be 650 K. The molecule quickly moves to the 3s surface, where it then has an internal effective temperature of 1170 K. Under these conditions, the barriers to internal rotation are easily crossed.

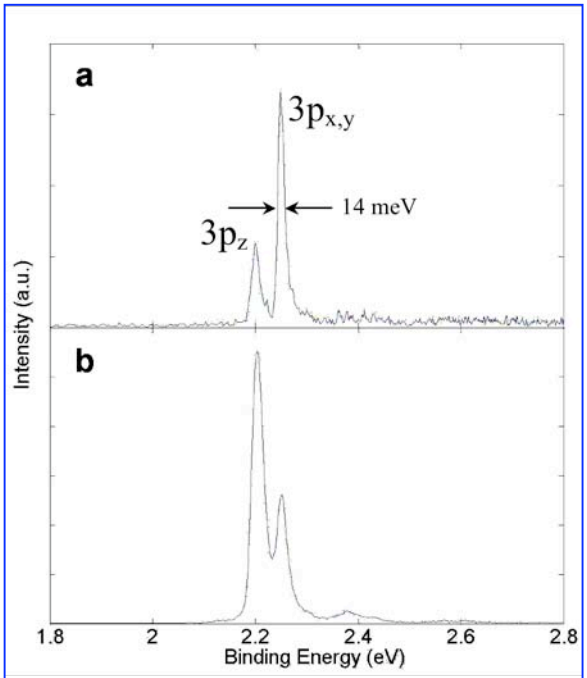

Figure 1: The binding energy spectrum of the 3p levels of trimethylamine upon one-photon and two photon excitation. a) ps pulses two-photon excitation; b) fs pulses, one-photon excitation. Ionization is with one 400 nm photon. The intensity distribution on a) includes rapid internal conversion, but the spectra show a bandwidth of 14 meV.

We excite the molecules by either one or two photon excitation and ionize using a single photon. The photoelectron spectrum is observed, and analyzed for the electron binding energy in the Rydberg level by subtracting the electron kinetic energy from the energy of the photon. Figure 1 shows two spectra that aim to explore the resolution limit: spectrum *b*, taken with femtosecond laser pulses, already shows two previously unresolved Rydberg states: $3p_{x,y}$ has a binding energy of 2.251 eV, and $3p_z$ is at 2.204 eV. Spectrum *a*, taken with a picosecond laser pulse with narrower bandwidth, shows the same peaks with higher resolution. It is evident that a spectral bandwidth of 14 meV, corresponding to a quantum defect bandwidth of 0.008, can be obtained even when the molecule is at a high internal vibrational temperature.

Conformational structures and dynamics as seen through Rydberg states

While the Rydberg spectra apparently are rather blind toward the rotation of methyl groups, they turn out to be quite sensitive toward the conformational structure of

hydrocarbon backbones. We investigated a series of aliphatic amines containing flexible hydrocarbon chains. RFS nicely separated even closely related amines such as N,N-dimethyl-2-butanamine (DM2BA) and N,N-dimethyl-1-butanamine, even though they again were at temperatures as high as 994 K.[3] In addition, by employing a time-delayed pump-probe scheme, we were able to observe the conformational dynamics of the aliphatic chains. The dynamics of the hydrocarbon backbone is induced by the laser excitation to the Rydberg states, because the amine group becomes planar and because the charge distribution changes upon excitation. Using a model of first order reversible reactions, we could use the measured equilibrium distributions and the kinetics of approach to the equilibrium, to determine both the forward and the backward reaction rates of the folding dynamics. Time constants of 66 ps and 19 ps were obtained, respectively, in DM2BA. Similar time constants in the picosecond domain were observed for the larger N,N-dimethyl-2-hexylamine. By comparing with ab initio calculations we were able to relate the Rydberg peaks of DM2BA to specific conformeric structures. Thus, all structural and dynamical parameters of the conformational dynamics at a temperature of 950 K have been determined.

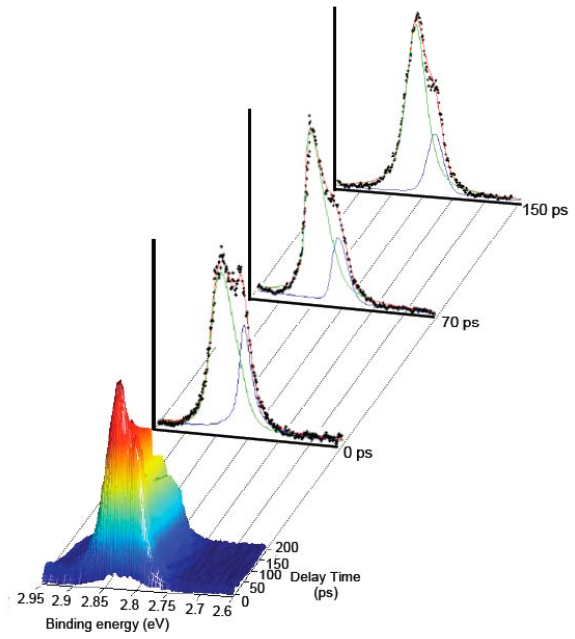

Figure 2: Time- and energy-dependent RFS spectra of the 3s region of DM2PA. The back-projected spectra are the individual slices taken at the indicated pump-probe delay times. The band can be fitted by two peaks with time-dependent intensities.

Rydberg fingerprints of components of isomeric flame components

An important question is to what extend Rydberg fingerprint spectroscopy can be applied to identify isomeric hydrocarbons in flames. Together with Dr. N. Hansen, we explored the Rydberg spectra of a number of isomeric systems with the chemical formulas C_5H_8, C_6H_8, C_7H_8, and $C_{11}H_{10}$. In all cases, we were able to obtain spectra that clearly distinguish the molecules based on their Rydberg states. For fixed laser wavelengths, separation of the spectra could be based on the structure-sensitivity of the Rydberg levels, or even simpler, on the selective access to specific Rydberg states. Remarkably, even the very similar isomers 1-methylnaphthalene and 2-methylnaphthalene can be distinguished based on the energies of the Rydberg transitions. In these test experiments no effort was made to heat the molecular sample, but since we know that high temperature does not congest the Rydberg spectra (see above), it appears that the method would be well suited to investigate combustion processes in flames.

3. Future Plans

The Rydberg fingerprint spectroscopy and the pump-probe electron diffraction provide complementary views of molecular structure. The focus of the work highlighted here was on the Rydberg spectroscopy, which is shown to be a technique with unique capabilities. It provides well-resolved spectra of even hot molecules, in the presence of methyl rotations, yet it is sensitive toward the structure of carbon backbones. Since chemical bonding is not a prerequisite, the structure sensitivity extends beyond isomers to conformers. The test with flame component molecules shows that applications to flames could be developed. We are also applying the technique to study the structural dynamics of ultrafast chemical reaction sequences.

4. Publications resulting from DOE sponsored research (2004 - 2007)

1. "Spectroscopy and femtosecond dynamics of the ring-opening reaction of 1,3-cyclohexadiene," N. Kuthirummal, F. M. Rudakov, C. Evans, and P. M. Weber, J. Chem. Phys. **125**, 133307 (**2006**).
2. "Ultrafast time-resolved electron diffraction with megavolt electron beams," J. B. Hastings, F. M. Rudakov, D. H. Dowell, J. F. Schmerge, J. Cardoza, J.M. Castro, S.M. Gierman, H. Loos, and P. M. Weber, Appl. Phys. Lett. 89, 184109 (**2006**).
3. "Rydberg Fingerprint Spectroscopy of Hot Molecules: Structural Dispersion in Flexible Hydrocarbons" M.P. Minitti, J.D. Cardoza and P.M. Weber, *J. Phys. Chem. A* **2006,** *110,* 10212-10218.
4. "The Ultrafast Photofragmentation Pathway of N,N-Dimethylisopropylamine," M.P. Minitti, J.L. Gosselin, T.I. Sølling and P.M. Weber, FemtoChemistry VII, Ed. A. W. Castleman Jr & M. L. Kimble, Elsevier (**2006**) p. 44 - 48.
5. "Megavolt electron beams for ultrafast time-resolved electron diffraction," F. M. Rudakov, J. B. Hastings, D. H. Dowell, J. F. Schmerge, and P. M. Weber, In "Shock Compression of Condensed Matter – 2005," ed. M. D. Furnish, M. Elert, T. P. Russel, and C. T. White, American Institute of Physics (**2006**).
6. "Structure sensitive photoionization via Rydberg levels," N. Kuthirummal and P. M. Weber, *J. Mol. Structure*, *787*, 163 – 166 (**2006**).
7. "Energy Flow and Fragmentation Dynamics of N, N, Dimethyl-isopropyl amine," Jaimie L. Gosselin, Michael P. Minitti, Fedor M. Rudakov, Theis I. Sølling and Peter M. Weber, *Journal of Physical Chemistry A*, **2006,** *110,* 4251-4255.
8. "Ultrafast Electron Microscopy in Materials Science, Biology, and Chemistry," Wayne E. King, Geoffrey H. Campbell, Alan Frank, Bryan Reed, John Schmerge, Bradley J. Siwick, Brent C. Stuart, and Peter M. Weber, Journal of Applied Physics, **97**, 111101 (**2005**).
9. "Rydberg Fingerprint Spectroscopy: A New Spectroscopic Tool With Local And Global Structural Sensitivity," J. L. Gosselin and Peter M. Weber, J. Phys. Chem. A, 109, pp 4899 – 4904 (**2005**).
10. "Control of local ionization and charge transfer in the bifunctional molecule 2-phenylethyl-N,N-dimethylamine using Rydberg fingerprint spectroscopy," W. Cheng, N. Kuthirummal, J. Gosselin, T. I. Sølling, R. Weinkauf, and P. M. Weber, Journal of Physical Chemistry, *109*, pp 1920 – 1925 (**2005**).

PROBING FLAME CHEMISTRY WITH MBMS, THEORY, AND MODELING

T. J. Mountziaris
Head, Department of Chemical Engineering — Phone 413-545-2507
University of Massachusetts Amherst — FAX 413-545-1647
159 Goessmann Laboratory, 686 N. Pleasant — tjm@ecs.umass.edu
Amherst, MA 01003-9303 — [Reach Prof. Westmoreland at westm@ecs.umass.edu]

Program scope

Experimental and modeling research in this project is conducted by Prof. Phillip R. Westmoreland and his students. While he is on IPA leave from the University as an NSF program officer, I am his substitute Principal Investigator, holding fiduciary responsibility during the period in which he is at NSF.

The objective of this research is obtaining kinetics of hydrocarbon combustion and molecular-weight growth in flames. Our approach combines molecular-beam mass spectrometry (MBMS) experiments on low-pressure flat flames; *ab initio* thermochemistry and transition-state structures; rate constants predicted by transition-state and chemical activation theories; and whole-flame modeling using mechanisms of elementary reactions.

MBMS is a particularly powerful technique because it can be used to measure a wide range of species quantitatively, including radicals, with minimal flame perturbation. By using two complementary instruments, we obtain remarkably complete sets of flame data that are useful for direct insights, testing of mechanistic models, and selected measurement of rate constants. Our electron-ionization quadrupole MS at UMass provides species profiles with high signal sensitivity and mass resolution. In a multi-investigator collaboration at the Advanced Light Source (ALS) at LBNL, we obtain species profiles with precise isomer resolution and identification using time-of-flight MS with VUV photoionization. We co-developed this system with fellow DOE-BES contractors Terry Cool, Andy McIlroy, Nils Hansen, and Craig Taatjes. Additional collaborators in making measurements include Katharina Kohse-Höinghaus of Universität Bielefeld, while Jim Miller, Stephen Klippenstein, Charlie Westbrook, and Fred Dryer have been collaborators in modeling thermochemistry, kinetics, and flame structure.

Recent progress

Experiments and modeling in the past year have emphasized flame studies of hydrocarbon and oxygenated fuels. The principal hydrocarbons studied have been allene, propyne [13], propene [12], cyclopentene [14], and toluene, while the oxygenates included ethanol [12], dimethyl ether [11], methyl acetate, ethyl acetate [15], and methyl formate. Highlights are described below and in Contractor Meeting reports from our ALS and modeling collaborators.

Lean toluene flame. Species identifications and composition profiles are being analyzed with new data from a lean (phi=0.9) toluene flame. They reveal evidence for oxidation paths proceeding by abstraction to benzyl and by *ipso* attack of OH, as well as molecular-weight growth happening even at the lean condition. Mapped flame species that are heavier than the toluene fuel include profiles for phenol, phenylacetylene, styrene, xylenes, benzaldehyde, benzyl alcohol, indene, and naphthalene. Further data analysis and modeling will yield insights into the growth and destruction chemistry, and a fuel-rich toluene flame has also been mapped.

Combustion chemistry of dimethyl ether. In paper [11], fuel-rich dimethyl ether flames (phi=1.2 and 1.68) were mapped. Adapting a DME combustion mechanism of the Dryer group, previously tested in their high-pressure flow reactor, initial modeling was performed at Princeton

and UMass. Agreement with the data was good, and dominant reaction pathways were inferred from the model predictions by Reaction Path Analysis.

Subsequently we have extended tests of this model against our other DME flame data at stoichiometric (phi=1.0) and more fuel-rich conditions (phi=1.75, Fig. 1). The two flames clearly reveal the dominant DME combustion path to be H abstraction; decomposition of the intermediate radical to CH_2O and CH_3; conversion of the CH_3 to CH_2O by reactions primarily with O but, to a surprising extent, with OH; and subsequent oxidation by well-known CH_2O chemistry to CHO, CO, and CO_2. Although CH_3 also forms CH_4 (in part by abstracting H from the DME fuel), CH_4 is a reactive dead end, able only to convert back to CH_3.

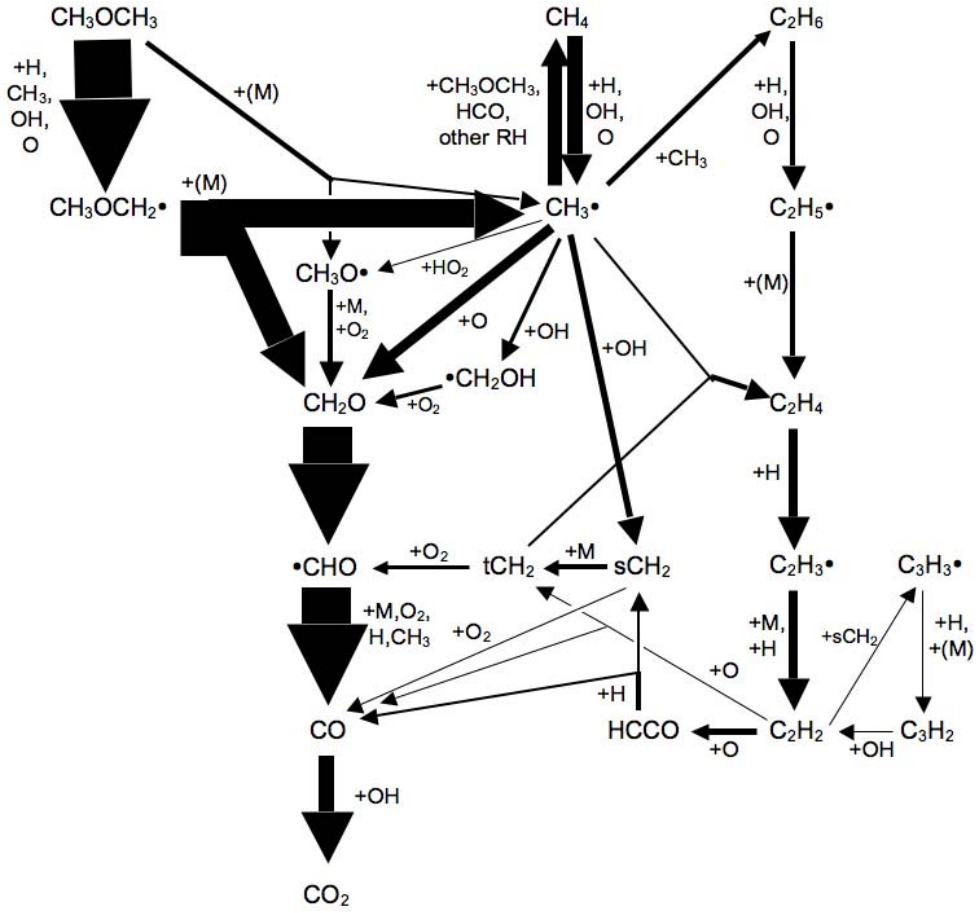

Figure 1. Dominant reactions in fuel-rich DME/O_2/Ar flame (phi=1.75).

At fuel-rich conditions, we expected to detect the chemical underpinnings of molecular-weight growth even though the flame was nonsooting. The data and modeling reveal key steps clearly. Ethane, formed by methyl combination in both flames, is reconverted to CH_3 in the stoichiometric flame but proceeds by abstractions and decompositions to C_2H_2 in the fuel-rich flame. Combination of CH_3 with triplet CH_2, formed indirectly from CH_3+OH, provides a supplementary route to C_2H_4 and thus C_2H_2. However, growth chemistry beyond C_2H_2 was minimal. Singlet CH_2, formed directly from CH_3+OH, reacted with C_2H_2 to yield C_3H_3, which produced a small amount of benzene. However, most C_3H_3 goes instead to C_3H_2 in the fuel-rich, nonsooting DME flame, and the C_2H_2 simply reforms C_2H_2.

New approaches to data dissemination. This group set up an early Web-based data archive (www.ecs.umass.edu/MBMS) that emphasizes MBMS data sets for C_2H_4 flames. Along with

temperatures where available, the archive includes composition profiles from our experiments and from the literature, usually from graphs that we digitized.

We have begun converting and submitting these files into the PrIMe collaborative data depository (www.prime.berkeley.edu), contributing to the flat-flame task force. We will also begin to enter the recent ALS data. The intents are to make these data more useful to other modelers but also to aid sharing and comparison among our collaborators. Initially, the composition data are being submitted as mole-fraction profiles, but the long-term goal is also to submit the raw data, calibrations, other ancillary information, and the data-analysis procedures and codes, allowing later re-examination of archived assumptions and procedures.

Affirmation of flame measurements of k(C_2H_4+OH). New measurements of k(C_2H_4+OH) by Joe Michael affirm the validity of the rate constants we had measured in a phi=1.9 fuel-rich C_2H_4 flame (Bhargava and Westmoreland, 1998). Our measurements had been based on determining net consumption rate of C_2H_4 from the axial derivative of the mass flux determined as the sum of convective flux (density x velocity x measured composition) and a Fickian diffusion rate, which contains the axial derivative of the measured composition. At the highest temperatures and C_2H_4 consumption rates, consumption was dominated by C_2H_4+H, which was confirmed by our *ab initio* calculations to be abstraction. Subtracting this rate from the overall consumption rate gave the rate for C_2H_4+OH; dividing by measured C_2H_4 and OH concentration gave the rate constant. These were the highest-temperature measurements of the two reactions at the time, and k(C_2H_4+OH) values were fitted well by a curved non-Arrhenius equation using these points and the earlier rate constants of Tully (1988) and Westbrook *et al.* (1988). Other reported rate constants had been higher than those data by as much as a factor of 15. The consistency of Michael's recent direct measurements supports the mutual validity of these four data sets.

Future plans

In the spring 2007 campaign at the ALS, a central target among hydrocarbon fuels will be detailed mapping of reference CH_4 flames. Conducting experiments near or above the sooting limit requires burning away probe deposits periodically, which would consume significant amounts of the limited ALS beam time. The UMass MBMS system will thus be used as the primary experiment for measuring very fuel-rich conditions, supplemented by shorter experiments at the ALS at these conditions to answer key isomer-resolution questions.

In the summer 2007 campaign, stoichiometric and fuel-rich acetylene reference flames will be mapped. Acetylene flames have been well-studied previously, but there are key uncertainties because of previous experiments' inability to resolve radical isomers. The new information will be used to characterize oxidation and molecular-weight growth. A stoichiometric acetaldehyde flame will also be targeted to address acetyl and vinoxy chemistry.

Other ALS flames picked by the collaborators emphasize oxygenated fuels and blended fuels. include alcohols, dimethyl ether, aldehydes, ketones, blended fuels like propene and ethanol, and ester fuels relevant to biodiesel, such as methyl and ethyl formate. As we steadily increase the resolving power of the instrument and develop new data-analysis techniques, we also intend to re-map selected data from our previous ALS experiments.

Our group is both modeling the data and coordinating the modeling collaborations. We are mapping temperatures and area-expansion ratios for these flames in the UMass apparatus, so we will be able to deliver more accurate modeling and to extract rate constants from the flame data.

Publications citing DOE-sponsored Research, 2005-2007

1. Hansen, J.A. Miller, T.A. Cool, J. Wang, M.E. Law, P.R. Westmoreland, "Synchrotron Photoionization Measurements of Combustion Intermediates: Photoionization Efficiency of C_3H_2 Isomers," *Phys. Chem. Chem. Phys.* **7**, 806-813 (2005).
2. Ruscic, J. E. Boggs, A. Burcat, A. G. Czàszàr, J. Demaison, R. Janoschek, J. M. L. Martin, M. L. Morton, M. J. Rossi, J. F. Stanton, P. G. Szalay, P. R. Westmoreland, F. Zabel, T. Bérces, "IUPAC critical evaluation of thermochemical properties of selected radicals - Part I," *J. Phys. Chem. Ref. Data* **34**(2), 573-656 (2005).
3. C.A. Taatjes, N. Hansen, A. McIlroy, J.A. Miller, J.P. Senosiain, S.J. Klippenstein, F. Qi, L. Sheng, Y. Zhang, T.A. Cool, J. Wang, P.R. Westmoreland, M.E. Law, T. Kasper, K. Kohse-Höinghaus, "Enols Are Common Intermediates in Hydrocarbon Oxidation," *Science* **308**(5730), 1887-1889 (2005).
4. M. E. Law, *Molecular-Beam Mass Spectrometry of Ethylene and Cyclohexane Flames*, Ph.D. Dissertation, University of Massachusetts Amherst (2005).
5. T.A. Cool, A. McIlroy, F. Qi, P.R. Westmoreland, L. Poisson, D.S. Peterka, M. Ahmed, "A Photoionization Mass Spectrometer for Studies of Flame Chemistry with a Synchrotron Light Source," *Rev. Sci. Instr.* **76,** 094102-1 to 094102-7 (Sept 2005).
6. P. R. Westmoreland, M.E. Law, T.A. Cool, J. Wang, C.A. Taatjes, N. Hansen, T. Kasper. "Analysis of Flame Structure by Molecular-Beam Mass Spectrometry Using Electron-Impact and Synchrotron-Photon Ionization," *Fizika Goreniya i Vzryva* 42(6), 58–63, November–December, 2006. / *Combustion, Explosion and Shock Waves* (English) 42(6), 672-677 (2006).
7. C.A. Taatjes, N. Hansen, J.A. Miller, T.A. Cool, J. Wang, P.R. Westmoreland, M.E. Law, T. Kasper, K. Kohse-Höinghaus. "Combustion Chemistry of Enols: Possible Ethenol Precursors in Flames," *J. Phys. Chem. A* **110**(9), 3254-3260 (2006). DOI: 10.1021/jp0547313
8. N. Hansen, S.J. Klippenstein, C. A. Taatjes, J.A. Miller, J. Wang, T.A. Cool, B. Yang, R. Yang, L. Wei, C. Huang, J. Wang, F. Qi, M.E. Law, P.R. Westmoreland, T. Kasper, K. Kohse-Höinghaus. "Identification and Chemistry of C_4H_3 and C_4H_5 Isomers in Fuel-Rich Flames," *J. Phys. Chem. A* **110**(10), 3670-3678 (2006). DOI: 10.1021/jp056769l
9. N. Hansen, S.J. Klippenstein, J.A. Miller, J. Wang, T.A.Cool, M.E.Law, P.R.Westmoreland, T. Kasper, K. Kohse-Höinghaus, "Identification of C_5H_x Isomers in fuel-rich flames by photoionization mass spectrometry and electronic structure calculations", *J. Phys. Chem. A* **110**(13), 4376-4388 (2006). DOI: 10.1021/jp0569685.
10. M.E. Law, P.R. Westmoreland, T. A. Cool, J. Wang, N. Hansen, T. Kasper. "Benzene Precursors and Formation Routes in a Stoichiometric Cyclohexane Flame," *Proceedings of the Combustion Institute* **31**, 565-573 (2007); DOI: http://dx.doi.org/10.1016/j.proci.2006.07.259
11. T. A. Cool, J. Wang, N. Hansen, P. R. Westmoreland, F. L. Dryer, Z. Zhao, A. Kazakov, T. Kasper, K. Kohse-Höinghaus. "Photoionization mass spectrometry and modeling studies of the chemistry of fuel-rich dimethyl ether flames," *Proc. Combustion Institute* **31**, 285-293 (2007); DOI: http://dx.doi.org/10.1016/j.proci. 2006.08.044
12. K. Kohse-Höinghaus, Patrick Oßwald, Ulf Struckmeier, T. Kasper, N. Hansen, C. A. Taatjes, J. Wang, T.A. Cool, S. Gon, P.R. Westmoreland. "The influence of ethanol addition on a premixed fuel-rich propene-oxygen-argon flame," *Proceedings of the Combustion Institute* **31**, 1119-1127 (2007); DOI: http://dx.doi.org/10.1016/j.proci.2006.07.007
13. N. Hansen, J.A. Miller, C. A. Taatjes, J. Wang, T.A. Cool, M.E. Law, P.R. Westmoreland. "Photoionization Mass Spectrometric Studies and Modeling of Fuel-Rich Allene and Propyne Flames," *Proc Combust Inst* **31**, 1157-64 (2007); http://dx.doi.org/10.1016/j.proci.2006.07.045
14. N. Hansen, T. Kasper, S.J. Klippenstein, P.R. Westmoreland, M.E. Law, C.A. Taatjes, K. Kohse-Höinghaus, J. Wang, T.A. Cool, "Initial steps of aromatic ring formation in a laminar premixed fuel-rich cyclopentene flame", *J Phys Chem A* (accepted, 1/2007); DOI: 10.1021/jp0683317
15. P. Oßwald, U. Struckmeier, T. Kasper, K. Kohse-Höinghaus, J. Wang, T.A. Cool, N. Hansen, P.R. Westmoreland, "Isomer-specific fuel destruction pathways in rich flames of methyl acetate and ethyl formate and consequences for the combustion chemistry of esters", *J. Phys. Chem. A* (accepted, 1/2007) ; DOI: 10.1021/jp068337w

Photoinitiated Processes in Small Hydrides

Curt Wittig
Department of Chemistry
University of Southern California
Los Angeles, CA 90089
(213) 740-7368
wittig@usc.edu

Program Scope

During the past year, we have concentrated on relativistic effects in hydrides that contain heavy atoms. In such systems, spin and electronic angular momentum cease to separately have good quantum numbers because of spin-orbit interaction. This can facilitate transitions between potential energy surfaces. Indeed, the heavy atom systems we have examined are replete with non-adiabatic processes. Moreover, relativistic effects observed in heavy atom systems often have no counterparts with lighter molecules. Our previous experimental study of H_2Te inspired us to initiate experiments with AsH_3 and SbH_3. These are described below. I expect our work with the heavy atom systems to be over by the end of 2007, at which time we will start experiments with the C_2H radical. Both the heavy-atom-hydride and C_2H systems have numerous surface crossings. Non-adiabatic processes have been central to our research program; it is the common ingredient that ties these systems together and provides much of the intellectual content of the theses that are forthcoming from this work.

Recent Progress and Future Plans

In last year's progress report, AsH_3 was mentioned, but only a short paragraph was written, as neither experimental nor theoretical data had been collected. In late summer 2006 we set about in earnest to collect experimental data on this system. It was believed that this would be easy compared to SbH_3, because AsH_3 (which is used widely in the semiconductor industry) can be handled with relative ease. Thus, AsH_3 would serve as a nice "starter project" for the students. However, one delay led to another and by years end I was frustrated, to say the least. Productivity was zero; maybe we would never get anything to work again; maybe I should just plain quit; and so on.

A first year graduate student (Bill Schroeder) told me he wanted to join the project. He advertised great enthusiasm, stating that he might not be a genius in the classroom, but he would more than make up for it in the lab. I told him to go for it: join the team, learn what must be learned about the lasers and the chambers, and then make the experiments work. By god he did it. We began taking high quality data in January, and this has continued until now. Most importantly, he resurrected an often-overlooked concept: goal-driven hard work. Yes, that's right, hard work. When the experiment is working, you do not turn it off to go home at 7 PM. You keep going: 2 AM … 4 AM … 6 AM … whatever it takes.

We now have a quite respectable amount of data and we will soon prepare a paper for publication. In our earlier work with H_2Te, we had a fruitful collaboration with a theoretical group (Aleksey Alekseyev, Wuppertal, Germany). This has now been rekindled. He has our data, and we are discussing where theory might play the most significant role. He is an expert at high-level electronic structure calculations of relativistic systems. The data are presented below, with some statements about mechanisms.

It was never my intention to devote a lot of time to AsH_3. This was a stopgap measure borne of desperation and frustration. I am now confident that we can wrap this up (experimentally) in about a month. The theory part will take longer, but this will be done mainly in Wuppertal. My students on this project will be attending a Gordon Conference in Bordeaux in June, and Bill Schroeder plans to go to Germany and, time permitting, visit Aleksey in Wuppertal. Bill also put together a synthesis apparatus for SbH_3 and we are now able to maintain samples for several hours (which is longer than sample lifetimes reported in the literature) and slight modifications will increase this to ~ a day. A few UV spectra will be shown below to make the point. This is a more interesting system that AsH_3. Nonetheless, we do not want to make a lengthy project out of it. As mentioned above, it is our intention to wrap up the heavy atom work by the end of 2007 and then devote full time to non-adiabatic effects in the C_2H radical.

Experiment and Results

Arsine dilute in H_2 (10%) was obtained commercially (Matheson). Samples were expanded into vacuum and the nozzle effluent was skimmed to form a molecular beam. The experimental arrangement for the high-*n* Rydberg time-of-flight (HRTOF) method is essentially unchanged from that used in our previous studies, so I will forego a detailed discussion of the experimental approach. Starting with AsH_3 rather than SbH_3 is sensible, as it requires no synthesis and AsH_3 has a large absorption cross-section (1.8×10^{-17} cm^2) at 193 nm. A HRTOF spectrum and the corresponding energy distribution are shown in Fig. 1.

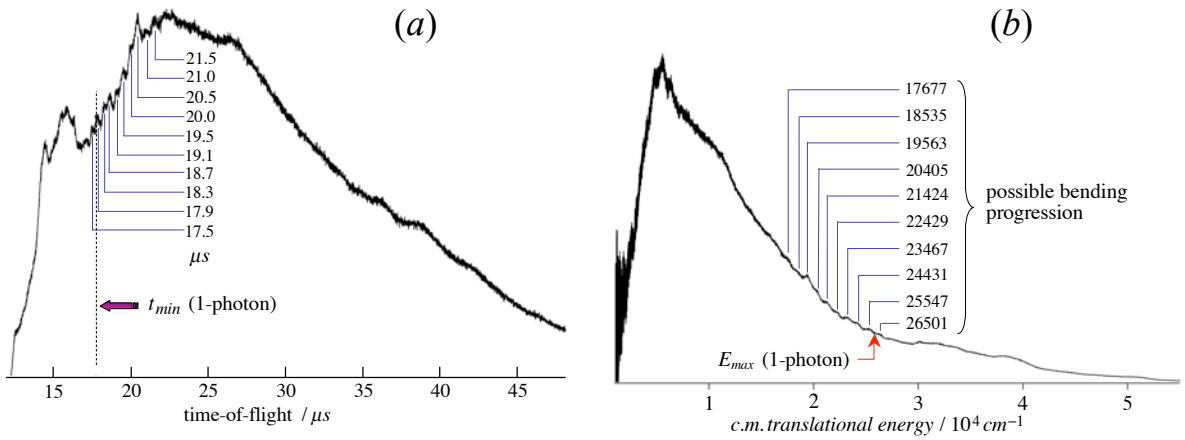

Figure 1. (*a*) The TOF spectrum contains contributions from 193 nm photodissociation of both AsH_3 and AsH_2. (*b*) The distribution in (*a*) has been transformed to the energy domain.

In systems like this, the TOF spectra lack the aesthetic appeal of those in which product quantum states are well resolved. The main reason is that the signal is distributed over too broad a range of time (or energy) to give high S/N. From Fig. 1, it is seen that the AsH_2 product has abundant internal excitation. It is also seen that AsH_2 photodissociation can be efficient, as all of the signal to the left of the t_{min} dashed line *must* arise from AsH_2 photolysis, and almost certainly a portion of the signal to the right of the t_{min} dashed line is due to AsH_2, as discussed below.

Referring to Fig. 1, there is barely discernible structure that is consistent with a vibrational progression in the AsH_2 bend (Fig. 1b). That is, this structure is due to the photodissociation of AsH_2 having a broad range of bending excitation. We are currently recording spectra over quite long periods of time (10-20 hours). On the basis of S/N improvement given by the factor: (number of traces)$^{1/2}$, the S/N is expected to increase by a factor of approximately 3 relative to the spectrum shown in Fig. 1(a).

Such a vibrational progression can arise because of motion on an excited AsH_3 surface. For example, the rapid removal of a hydrogen atom from AsH_3 (*e.g.*, direct excitation of a repulsive curve) is not expected to change the AsH_2 bond angle much from its AsH_3 equilibrium value, because for each species the equilibrium angle is approximately 90°. This is why motion on an excited PES is likely responsible for the barely discernible structure in Fig. 1. I believe that the mechanism will be revealed through comparisons between experiment and theory.

The variation of the shape of the TOF spectrum with laser fluence has been measured and this confirms the 2-photon nature of the signal at early times. In fact, it is possible to almost eliminate the 2-photon contribution by using low 193 nm fluences. It has also been possible to use polarized 193 nm radiation. This reveals a clear difference between the primary and secondary photolyses (Fig. 2). This will be explored carefully because such results enable excited PES's to be examined via their transition dipole moments.

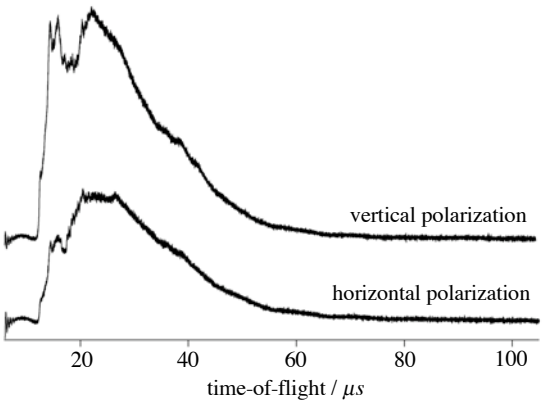

Figure 2. Primary and secondary photolyses depend differently on laser polarization.

SbH_3

One of the challenges of working with systems containing heavy atoms is that they can be unstable and SbH_3 is no exception. We have succeeded in synthesizing SbH_3 and we have carried out preliminary HRTOF experiments with 193 nm. As with (essentially) all heavy metal hydrides, sample stability is an issue. Thus, we have invested time in the synthesis. Figure 3 shows a series of UV absorbance traces taken over a 3-hour period. It is interesting

that the signal strength *increases* during the 3 hours (probably because of wall effects) but drops precipitously after that.

Once the sample issue is under control, photodissociation experiments will be carried out. With 193 nm, the energy is sufficient to break two Sb-H bonds. Calculations predict D_e values of 63.3, 55.8 and 53.9 kcal/mole for successive Sb-H bonds. Despite sample stability issues in our earlier photolysis experiments, we have observed an HRTOF signal from 193 nm photolysis.

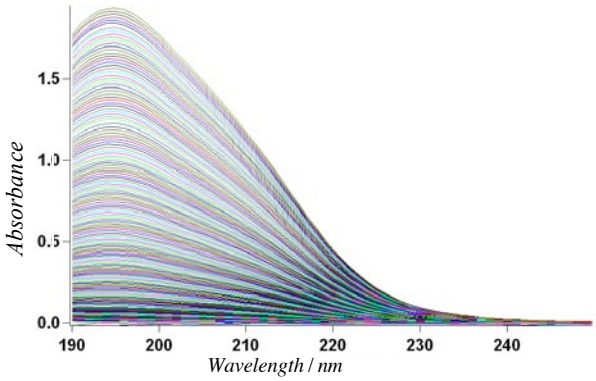

Figure 3. Traces were recorded every 30 *s* for 3 hours, with maximum absorbance at 3 hours, at which time it decreases.

Future Plans

As mentioned above, I have begun to move our effort toward C_2H. Jessica Quinn took an electronic structure course from Professor Anna Krylov and her final project was the C_2H radical. Though a few groups have carried out theoretical work, it is important that students working on the project know about the electronic structure. She and Bill Schroeder will move the project to center stage during the next year. I expect Lee-Ann to graduate by the beginning of 2008, which means that her experiments should be finished by Fall 2007. The experimental strategy for producing C_2H is straightforward: photolysis of a precursor in a short quartz or sapphire tube with a pinhole at the end; this tube is attached to the pulsed nozzle. The ultraviolet photolysis of C_2H occurs via an essentially structureless feature that makes spectroscopic identification impractical. This system is ideal, however, for the HRTOF diagnostic: The C_2 levels are sufficiently far apart that they will be resolved in the TOF spectra for all but the lowest rotational levels.

Publications supported by DOE: 2005-2007

1. J. Underwood, D. Chastaing, S. Lee, and C. Wittig, J. Chem. Phys. **123**, 84312 (2005).
2. C. Wittig, J. Phys. Chem. B **109**, 8428 (2005).
3. L. Smith-Freeman, J. Quinn, W. Schroeder, and C. Wittig, unpublished (this is the work that was presented above).

THEORETICAL STUDIES OF THE REACTIONS AND SPECTROSCOPY OF RADICAL SPECIES RELEVANT TO COMBUSTION REACTIONS AND DIAGNOSTICS

DAVID R. YARKONY
DEPARTMENT OF CHEMISTRY, JOHNS HOPKINS UNIVERSITY,BALTIMORE, MD 21218
yarkony@jhu.edu

Photoelectron/Photoionization spectra using the multimode vibronic coupling model.

Photoelectron and photoionization spectroscopies are powerful tools for describing the spectra of combustion intermediates. However the spectra become difficult to assign when they result from states that are strongly coupled by conical intersections. The spin-orbit interaction further complicates matters. We have implemented a new approach for determining photoelectron/photoionization spectra for such systems. The approach is based on the standard multimode vibronic coupling approximation[1]. In that approach a quasi diabatic Hamiltonian, is used to describe the coupled electronic states. The vibronic wave functions, the solutions to the nuclear Schrödinger equation, are then determined usually with a Lanczos algorithm[2] although time dependent approaches can also be used. From knowledge of vibronic wave functions, or the autocorrelation function in the time dependent case, the spectral intensity distribution function is determined. For many years this approach was used in the context of the linear vibronic coupling model.[1] However recent work has made it clear that all terms through second order should be included.

In our implementation the first step is the construction of a quasi diabatic Hamiltonian (excluding the spin-orbit interaction) from advanced multireference configuration interaction (MRCI) wave functions. Then this Hamiltonian is transformed to an appropriate coordinate basis, the normal modes of a reference structure, and vibronic spectrum is determined in the multimode vibronic coupling approach using a Lanczos procedure.[2] Finally the spin-orbit interaction is included using as a basis the eigenstates from the Lanczos procedure.

The principal advantages of our implementation of the multimode vibronic coupling method involve the construction of the quasi diabatic Hamiltonian, $\mathbf{H}^{(d)}$. Our algorithms require no spatial symmetry so they are generally applicable. In our implementation $\mathbf{H}^{(d)}$, is expanded about the minimum energy point of conical intersection – to better describe nonadiabatic effects - and is determined from perturbation theory using derivative coupling and energy gradient information. This provides a maximal level of quasi diabaticity and permits $\mathbf{H}^{(d)}$ to be determined, including all terms through second order, from multireference configuration interaction (MRCI) data (determined using the *COLUMBUS* suite of electronic structure codes) at a limited number of nuclear configurations. The use of *COLUMBUS* is particularly advantageous since in *COLUMBUS* the derivative couplings are determined, using analytic gradient techniques, at little additional cost, once the electronic wave functions are determined. Very recently, we have developed two ways to improve the accuracy/utility of our quadratic $\mathbf{H}^{(d)}$. A novel least squares fitting procedure can be used to improve the description of the Franck-Condon region or the region of the equilibrium structure on the ground electronic state. We have also developed an iterative procedure which can construct an $\mathbf{H}^{(d)}$ which is (i) accurate over a

larger domain, (ii) obtained using *ab initio* data at fewer nuclear configurations and (iii) can be centered around an arbitrary point in nuclear configuration space.

In the absense of spatial symmetry, for molecules with an odd number of electrons, the spin-orbit interaction cannot be chosen real-valued. To handle this situation, following Child and Longuet-Higgins,[3] we treat the total Hamiltonian (coulomb + spin-orbit terms) in the basis of eigenstates of the vibronic problem in the absence of spin-orbit coupling. This produces good results but can be limited by disk space considerations.

Representative of the above methodology, the figure below presents the predicted low energy spectrum of CH_3S obtained from photoelectron detachment of CH_3S^- (black lines) compared with the experimental results of Lineberger (red).[4] These results employed an $\mathbf{H}^{(d)}$ obtained from perturbation theory(using MRCI data at only 17 nuclear configurations) and are currently being re-evaluated using a combination of the iterative and least squares procedures.

Figure: Photoelectron spectrum of CH_3S. Electron affinity and height of one peak fixed at experimental values.

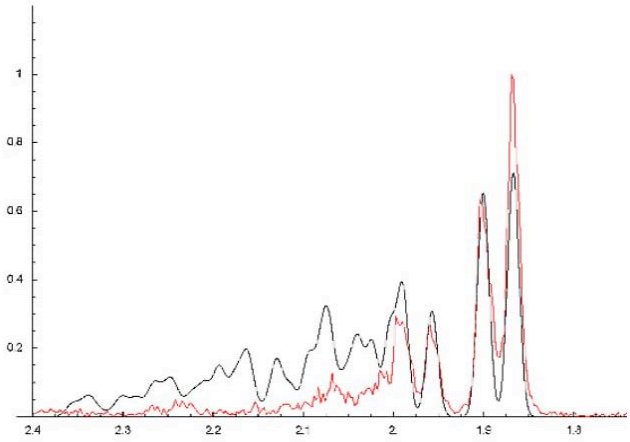

The photoelectron spectrum of C_2H_5O

The goal of this project is to understand the photoelectron spectrum of the ethoxy anion, reported previously by Lineberger's group[5] and more recently in (to be published work in) Neumark's laboratory at UC Berkeley.

The photoelectron spectrum of ethoxy anion is difficult to assign owing to nonadiabatic interactions in the ethoxy radical that is produced. The neutral radical inherits a Jahn-Teller coupling interaction (conical intersection seam) and spin-orbit coupling from the well studied methoxy radical, but not the simplifications due to C_{3v} symmetry or a limited number of internal modes (ethoxy has 18 internal modes whereas methoxy has only 9). We have determined $\mathbf{H}^{(d)}$ for ethoxy[6] - using the perturbative approach from electronic structure data a only 37 nuclear configurations - and are in the process of determining the photoelectron spectrum with and without the spin-orbit interaction. We are also evaluating this $\mathbf{H}^{(d)}$ using the least squares and iterative procedures noted above.

Although this project is ongoing an interesting result has emerged. The brightest lines in the ethoxy vibronic spectrum include the origin line and a line at 358cm^{-1}. Neumark found a much weaker line at 178 cm^{-1}, not seen by Lineberger. The three lowest lines in our

nonrelativistic (ie no spin-orbit interaction) spectrum fall at 0, 241 and 317 cm^{-1}. However the intensity of the line at 241 cm^{-1} is predicted to be zero, ie not observable in the spectrum When the spin-orbit interaction is included the lines shift slightly to 0, 245, and 325 cm^{-1} but significantly the intensity of the line at 245 cm^{-1} is now almost 8% of the remaining two lines having borrowed intensity for the origin line. This provides an explanation for Neumark's line at 178 cm^{-1}.

Nonadiabatic Dynamics involving Conical Intersections

Ab initio Multiple Spawning(AIMS)-COLUMBUS

As photoexcitation is the initial step in many detection schemes of combustion intermediates, the ultimate disposition of the excitation energy and the decomposition pathways of photoexcited states are important questions in combustion chemistry. When conical intersections are present they can have a major impact on the nuclear dynamics. To study dynamics near conical intersections, we have, in collaboration with Todd Martinez's group at University of Illinois, interfaced the *COLUMBUS* suite of electronic structure codes into Martinez's code for solving the nonadiabatic nuclear dynamics problem known as full multiple spawning (FMS),[7] to produce *ab initio multiple spawning(AIMS)-COLUMBUS*. The *AIMS-COLUMBUS* program can take advantage of *COLUMBUS*'s highly efficient analytic gradient driven algorithm for computing the interstate derivative coupling, noted above. *AIMS* is a dynamics "on the fly" algorithm which maintains a classical trajectory flavor by using centroid approximations for integrals. A trajectory necessarily explores a wide range of nuclear configurations. This can create serious technical problems resulting from requisite changes in the active space as the propagation procedes. We have addressed this problem by allowing for changes in the active space as the trajectory propagates.

Photodissociation of Ammonia and the Hydroxymethyl Radical

The photodissociation of the hydroxymethyl radical (H_2COH)

$$H_2COD(1^2A) + h\nu \rightarrow H_2COD(3^2A) \rightarrow H_2COD(2^2A) \rightarrow H_2CO(1^1A) + D \text{ or } HCOD(1^1A) + H$$

has been studied experimentally by Reislers' group.[8] We have analyzed these experiments using electronic structure methods.[9] Our analysis raises several issues concerning nonadiabatic dynamics. How does motion on the initially excited potential energy surface govern where on the seam of conical intersection the initial nonadiabatic event takes place? How does, or does, the conical intersection orient or route the nuclear motion on the lower state. Is the dynamics on the lower surface direct or quasi statistical, that is can the conical intersection route things so that the molecule dissociates with limited opportunity for energy randomization. We have begun a study of these questions using *AIMS-COLUMBUS*.

In the past we have suggested[10] an explanation for vibrational state dependence of NH_3 photodissociation

$$H_2NH(1^1A) + h\nu \rightarrow H_2NH(2^1A) \rightarrow H_2N(1^2A) + H$$

observed in Crim's group.[11] We are in the processes of studying this reaction using *AIMS-COLUMBUS*.

The Future

We plan to complete the ethoxy, NH_3 and H_2COH projects and will use the vibronic coupling code to determine photoelectron/photoionization spectra for strongly coupled electronic

states. We will further assess the utility of the least squares procedure to modify the nascent $\mathbf{H}^{(d)}$ to reproduce properties of other regions of nuclear coordinate space. The iterative procedure for obtaining a fully quadratic quasi diabatic Hamiltonians expanded around an arbitary point in nuclear coordinate space also requires further assessment. The principal limitation in our determination of vibronic spectra is the size of the expansion that is tractable in the Lanczos diagonalization. When spin-orbit coupling is not an issue, one way to avoid this bottleneck is to use the time-dependent multiconfigurational Hartree(DTMCH) method[12] with its adaptive griding. We will explore this option using the freely available DTMCH program of the Heidelberg group, which is compatible with our $\mathbf{H}^{(d)}$.

Literature Cited

1 H. Köppel, W. Domcke, and L. S. Cederbaum, Adv. Chem. Phys. **57**, 59 (1984).

2 H. Köppel, W. Domcke, and L. S. Cederbaum, in *Conical Intersections*, eds. W. Domcke, D. R. Yarkony, and H. Koppel (World Scientific, New Jersey, 2004), Vol. 15, pp. 323.

3 M. S. Child and H. C. Longuet-Higgins, Proc. P. Soc. A **245**, 259 (1961).

4 R. L. Schwartz, G. E. Davico, and W. C. Lineberger, Journal of Electron Spectrosc. and Related Phenomena **108**, 163 (2000).

5 T. M. Ramond, G. E. Davico, R. L. Schwartz, and W. C. Lineberger, J. Chem. Phys. **112**, 1158 (2000).

6 R. A. Young Jr and D. R. Yarkony, J. Chem. Phys. **125**, 234301 (2006).

7 M. Ben-Nun and T. J. Martinez, J. Phys. Chem. A **104**, 5161 (2000).

8 L. Feng, A. V. Demyanenko, and H. Reisler, J. Chem. Phys. **120**, 6524 (2004); L. Feng, A. V. Demyanenko, and H. Reisler, J. Chem. Phys. **118**, 9623 (2003).

9 B. C. Hoffman and D. R. Yarkony, J. Chem. Phys. **116**, 8300 (2002).

10 D. R. Yarkony, J. Chem. Phys. **121**, 628 (2004).

11 A. Bach, J. M. Hutchison, R. J. Holiday, and F. F. Crim, J. Chem. Phys. **116**, 4955 (2002); M. L. Hause, Y. H. Yoon, and F. F. Crim, J. Chem. Phys. **125**, 174309 (2006).

12 G. A. Worth, H.-D. Meyer, and L. S. Cederbaum, in *Conical Intersections: Electronic Structure. Dynamics and Spectroscopy*, edited by W. Domcke, D. R. Yarkony, and H. Köppel (World Scientific, New Jersey, 2004), Vol. 15, pp. 583.

PUBLICATIONS SUPPORTED BY DE-FG02-91ER14189: 2005-present

1. Statistical and Nonstatistical Nonadiabatic Photodissociation from the first excited state of the hydroxymethyl radical
   David R. Yarkony, J. Chem. Phys. **112,** 084316 (2005)
2. A Novel Conical Intersection Topography and its Consequences. The 1, 2 ^{2}A Conical Intersection Seam of the Vinoxy Radical,
   R. Andrew Young, Jr. and David R. Yarkony, J. Chem. Phys. **123**, 084315(2005).
3. *Towards a Highly Efficient Theoretical Treatment of Jahn-Teller Effects in Molecular Spectra: The 1^{2}A, 2^{2}A Electronic States of the Ethoxy Radical*
   R. Andrew Young, Jr. and David R. Yarkony, J. Chem. Phys. 125, 234301 (2006)

GAS-PHASE MOLECULAR DYNAMICS: THEORETICAL STUDIES IN SPECTROSCOPY AND CHEMICAL DYNAMICS

Hua-Gen Yu (hgy@bnl.gov)
Chemistry Department, Brookhaven National Laboratory, Upton, NY 11973-5000

Program Scope

The goal of this program is the development of computational methods for studying chemical reaction dynamics and molecular spectroscopy in the gas phase. We are interested in developing rigorous quantum dynamics algorithms for small polyatomic systems and in implementing approximate approaches for complex ones. Particular focuses are on the dynamics and kinetics of chemical reactions and on the rovibrational spectra of species involved in combustion processes. This research also explores the potential energy surfaces of these systems of interest using state-of-the-art quantum chemistry methods.

Recent Progress

Vibronic spectrum calculation of HCCl and DCCl in three low-lying states

We have carried out a combined experimental and theoretical study on the vibronic energies and transition intensities of the $A\ ^1\mathrm{A}''$–$X\ ^1\mathrm{A}'$ bands. The theoretical calculations were carried out on our MRCI/aug-cc-pVTZ dipole moment and potential energy surfaces. These surfaces were interpolated using a general DVR interpolation technique from thousands of grid points. The quantum dynamics (QD) problem of nuclei was solved using a variational *K*-dependent QD approach in hyperspherical coordinates including the Renner-Teller effect.

The experimental and theoretical results have revealed that the C-Cl stretching vibration in the excited state was previously mis-assigned. The revised frequency corrects an anomalously large apparent anharmonicity in this mode and permitted a recalibration of the *ab initio* potential energy surface for the state. This, in turn, allowed the assignment of many shorter wavelength bands observed by other workers and an accurate calculation of vibronic band positions and intensities in this spectrum. Intensity was also found for transitions involving C-H stretching (ν_1) excitation in the ground state due to an anharmonic resonance between $X(100)$ and $X(012)$.

Similarly, the spin-orbit couplings between the $X\ ^1\mathrm{A}'$ and $a\ ^3\mathrm{A}''$ states of HCCl/DCCl have been further studied. The relative position of the triplet state of HCCl to the singlet ground state is predicted to be 2122 cm^{-1}. This prediction was recently confirmed by Reid et al.

The diffuse structure in ultraviolet spectra of the $GeCl_2$ *A*–*X* transition

In 1993 Karolczak et al. reported vibrationally resolved jet-cooled laser-induced fluorescence (LIF) excitation spectra of $GeCl_2$. A diffuse section in the spectrum was observed to begin at approximately 31630 cm^{-1} (316 nm vacuum wavelength) and extend to shorter wavelengths in the ultraviolet system. In order to explain this abnormal spectrum, following the early work of Coffin et. al. on $GeBr_2$, we have explored the hypothesis that this diffuse structure arises from the LIF spectrum of the $GeCl_2$…$GeCl_2$ van der Waals dimer complex based on our CIS(D)/cc-pVTZ calculations. Three isomers

on the ground-state potential energy surface have been characterized. The most stable dimer has a dissociation energy of 0.74 eV and has a trans-$(GeCl_2)_2$ structure. There is also a related, less stable, cis-minimum. These isomers are not responsible for the diffuse spectra in $GeCl_2$ as they have zero Frank-Condon intensity to the first excited singlet electronic state. A third, C_i symmetry, isomer has a binding energy of 0.31 eV. It is found that this C_i isomer has substantial dipole transition strength to the first excited singlet state of the dimer with a vertical excitation energy of 3.33 eV. The transition energy (T_0) between this C_i isomer and the van der Waals complex on the singlet excited state is predicted to be 4.007 eV, or a 1104 cm^{-1} blue shift with respect to that of the $GeCl_2$ *A*–*X* transition. We therefore propose that dimer absorption and emission can explain the diffuse structure that has been observed in the ultraviolet LIF spectra of $GeCl_2$.

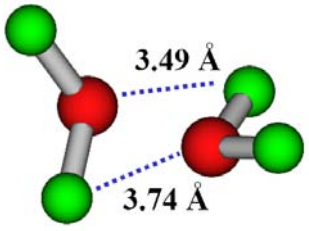

Geometry for the *X*…*A* dimer

Rigorous full-dimensional quantum dynamics study of the vibrational energies of $H_3O_2^-$

The vibrational energy levels of the $H_3O_2^-$ anion have been calculated using a rigorous quantum dynamics method based on an accurate *ab initio* potential energy surface. The eigenvalue problem is solved using the two-layer Lanczos iterative diagonalization algorithm in a mixed grid/nondirect product basis set , where the system Hamiltonian is expressed in a set of orthogonal polyspherical coordinates. The lowest 312 vibrational energy levels in each inversion symmetry, together with a comparison of fundamental frequencies with previous quantum dynamics calculations, are reported. Finally, a statistical ananlysis of nearest level spacing distribution is carried out, revealing a strongly chaotic nature.

Energetics and dynamics of the reaction of O_2 with HOCO

The important combustion reaction of O_2 with HOCO has been studied using an *ab initio* direct dynamics method based on the UB3PW91 density functional theory (DFT). This DFT method is selected by minimizing the errors of the relative energies of the stationary points on the ground-state electronic surface of $HOC(O)O_2$ with respect to the best *ab initio* values of Poggi and Francisco. Results show that the reaction can occur *via* two mechanisms: direct hydrogen abstraction and an addition reaction through a short-lived $HOC(O)O_2$ intermediate. The lifetime of the intermediate is predicted to be 660±30 fs. Although it is an activated reaction, the activation energy is only 0.71 kcal/mol. The thermal rate coefficients are calculated over the temperature range 200-1000 K. The values vary from 1.36×10^{-12} $cm^3molec^{-1}s^{-1}$ at 200K to 7.08×10^{-12} $cm^3molec^{-1}s^{-1}$ at 1000 K. At room temperature, the thermal rate coefficient obtained is 2.1×10^{-12} $cm^3molec^{-1}s^{-1}$, which is in

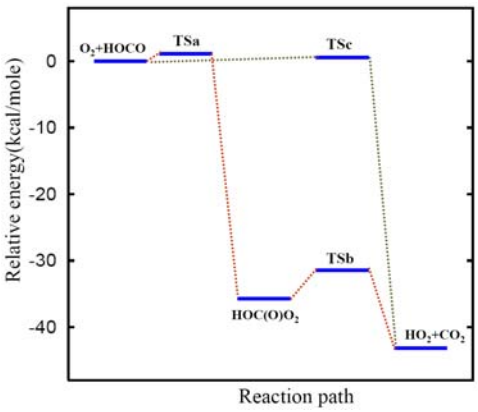

A B3PW91 energy diagram for the O_2 + OCO reaction

good agreement with the experimental results of 1.44×10^{-12}-1.90×10^{-12} $cm^3molec^{-1}s^{-1}$. Compared to the OH + HOCO reaction, this reaction is about an order of magnitude slower.

Future Plans

Kinetics and dynamics study of the reaction of HOCO with oxygen

We will apply our direct *ab initio* molecular dynamics program for studying some important combustion reactions. Of particular interest currently is the reactivity of the HOCO radical with the oxygen atom and molecule. For the O + HOCO reaction, in collaboration with J. Francisco (Purdue), we will address the energies, geometries, and vibrational frequencies of the stationary points on the ground-state doublet potential energy surface, and the reaction mechanism by using a SAC/UCCD method. Besides the kinetics and dynamics studies of the reaction, we also hope to predict the lifetime of the HOC(O)O intermediate produced through the reaction course. The temperature dependence of the thermal rate constants will be calculated .

Molecular dynamics simulation of photoinitialized reactions

The molecular dynamics program will be extended to study photoinitialized reactions through vibrational overtone excitations and photodetachment processes. The first example to be considered is the photodetachment reaction of cyclopentoxide since cyclopentoxy (cyc-C_5H_9O) radicals are important intermediates in combustion environments and atmospheric chemistry. The molecular dynamics simulation is carried out using the HCTH/6-31G(d) DFT method. Here, the ring-opening reaction of cyclopentoxy to the 5-oxo-pentan-1-yl radical is of special interest. This research hopes to predict the lifetime of cyclopentoxy as well as the photoelectron kinetic energy (eKE) spectrum.

Rovibrational spectroscopy of large amplitude molecule HO_3

HO_3 is an interesting molecule, which is an important intermediate in atmospheric chemistry. Its structure and stability has been the subject of longstanding debate. In 2005, a trans-HO_3 molecule was first observed by Endo et al. using Fourier-transform microwave (FTMW) spectroscopy. Surprisingly, they obtained a rather long central O-O bond length of 1.688 Å, which has not been predicted by most high level *ab initio* methods. The theoretical value is around 1.54 Å, which is substantially shorter than the experimental result. Recently, Lester and her co-workers measured a binding energy of 6.8 kcal/mol for this trans-HO_3 molecule with respect to the OH + O_2 limit. So it is a weakly bound molecule. We expect that this may explain the discrepancy in structure between theory and experiment. Theoretical results are the equilibrium values while the experimental ones are vibrationally averaged. A large amplitude motion of the floppy HO_3 molecule could give such a big difference. In order to verify our assumption, we are going to perform a full dimensionality quantum dynamics calculation using an accurate *ab initio* potential energy surface. The construction of the surface will be first priority in this work.

Publications since 2005

H.-G. Yu and J.T. Muckerman, *Ab initio and direct dynamics studies of the reaction of singlet methylene with acetylene, and the lifetime of the cyclopropene complex,* J. Phys. Chem. A **109**, 1890 (2005).

H.-G. Yu, J.T. Muckerman and J.S. Francisco, *Direct ab initio dynamics study of the OH + HOCO reaction*, J. Phys. Chem. A 109, 5230 (2005).

H.-G. Yu, *A coherent discrete variable representation method for multidimensional systems in physics*, J. Chem. Phys. 122, 164107 (2005).

H.-G. Yu, T.J. Sears and J.T. Muckerman, *Potential energy surfaces and vibrational energy levels of DCCl and HCCl in three low-lying states*, Mol. Phys. **104**, 47 (2006).

G. E. Hall, T. J. Sears and H.-G. Yu, *Rotationally Resolved Spectrum of the A(060) --- X(000) Band of HCBr*, J. Molec. Spectrosc. **235**, 125 (2006).

Z. Wang, R.G. Bird, H.-G. Yu and T.J. Sears, *Hot bands in jet-cooled and ambient temperature spectra of chloromethylene*, J. Chem. Phys. 124, 74314 (2006).

H.-G. Yu, *A rigorous full-dimensional quantum dynamics calculation of the vibrational energies of* $H_3O_2^-$, J. Chem. Phys., **125**, 204306 (2006).

H.-G. Yu and T.J. Sears, *A clue to the diffuse structure in ultraviolet spectra of the* $GeCl_2$ *X-A transition*, J. Chem. Phys., **125**, 114316 (2006).

H.-G. Yu, *Density functional theory study of ethylene partial oxidation on* Ag_7 *cluster,* Chem. Phys. Lett., **431**, 236 (2006).

H.-G. Yu and J. T. Muckerman, *Quantum molecular dynamics study of the* O_2 *plus HOCO reaction*, J. Phys. Chem. A, **111**, 5312 (2006).

H.-G. Yu, *Ab initio molecular dynamics simulation pf photodetachment reaction of cyclopentoxide*, Chem. Phys. Lett, (submitted, 2007).

Experimental Characterization of the Potential Energy Surfaces for Conformational Isomerization in Aromatic Fuels

Timothy S. Zwier
Department of Chemistry, Purdue University, West Lafayette, IN 47907-2084
zwier@purdue.edu

Program Definition and Scope

Gasoline and diesel fuels are complicated mixtures containing about 30% aromatics, including alkylbenzene, alkenylbenzene, and alkynylbenzenes of various chain lengths. The combustion of these molecules is influenced by their structural and conformational make-up, and by the rates of isomerization between them. The objective of this research program is to develop and utilize laser-based methods to characterize the spectroscopy and isomerization dynamics of conformational isomers of aromatic derivatives that play a role in soot formation. As a first step in all these studies, UV-UV hole-burning and resonant ion-dip infrared (RIDIR) spectroscopy are being used to determine the number and identity of the conformations present, based on their ultraviolet and infrared spectral signatures. These structural studies then serve as a foundation for studies of the dynamics of conformational isomerization using stimulated emission pumping-population transfer (SEP-PT) spectroscopy or infrared population transfer (IR-PT) spectroscopy (Figure 1). SEP is used to selectively excite a single conformation of the molecule of interest to a well-defined vibrational energy early in the supersonic expansion. If the excited molecules have sufficient energy, they can isomerize before being re-cooled in the expansion to allow isomer-specific detection via laser-induced fluorescence. By tuning the SEP dump laser in a 20-10-20 Hz laser configuration, it is possible to directly measure the energy thresholds separating individual A→B reactant-product isomer pairs, thereby mapping out key stationary points on the multi-dimensional potential energy surface for isomerization. We are using these methods to study conformational isomerization in substituted benzenes spanning a range of types and degrees of conformational flexibility. From near-threshold intensity measurements we hope to explore the rate of isomerization relative to collisional cooling as a function of energy above threshold. These results can provide new tests of RRKM descriptions of isomerization in large molecules.

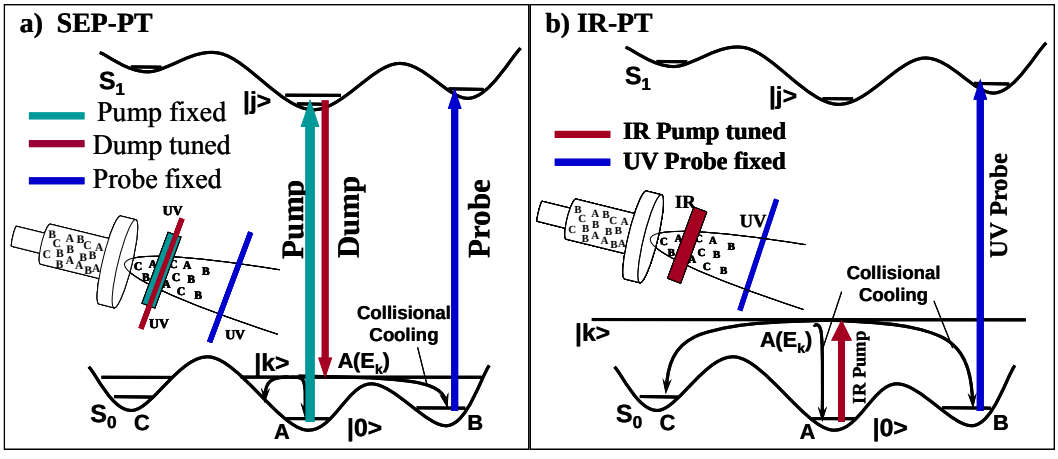

Figure 1: Schematic diagrams for SEP-PT and IR-PT spectroscopy.

Recent Progress

A. Spectroscopy and isomerization of *ortho-*, *meta-*, and *para*-divinylbenzene

Last year we reported the initial results of our spectroscopy and SEP-PT studies of *ortho-*, *meta-*, and *para*-divinylbenzene (*o-*, *m-*, *p*-DVB). Since then, we have engaged in a detailed analysis of the vinyl torsional structure in *m*-DVB, including fitting the torsional level data to a two-dimensional potential. The calculated 2D surface is shown in Figure 2. Despite considerable effort, the fitted form of the potential (not shown) has best-fit parameters that are strongly correlated with one another, leading to large uncertainties in the relative energies of the minima and in the derived isomerization barrier heights (with acceptable fits to 2D potentials with barriers ranging from 500 to 1400 cm^{-1}). This attempt to map out the 2D surface based on spectroscopy alone failed because the observed torsional levels in each well are far below the torsional barriers, and are unaffected by the presence of the other wells.

This spectroscopic study highlighted the need for an alternative method of measuring isomerization barrier heights, as provided by SEP-PT spectroscopy. We have used SEP-PT to place direct experimental bounds on the barriers to conformational isomerization between the three isomers of *m*DVB (*cis-cis*, *cis-trans,* and *trans-trans*). These studies used the new dispersed fluorescence chamber with its high-efficiency fluorescence collection optics and high throughput pumping capacity designed for hole-filling studies. We have proven that the isomerization pathway between *cis-cis* and *trans-trans* involves sequential isomerization of the two vinyl groups traversing over two barriers each of about 1200 cm^{-1} (15 kJ/mol) rather than concerted motion over one barrier of about twice that size. Using these measurements to constrain the 2D surface led to a fitted 2D potential for the torsional degrees of freedom of *m*DVB in excellent agreement with both torsional structure and the SEP-PT data.

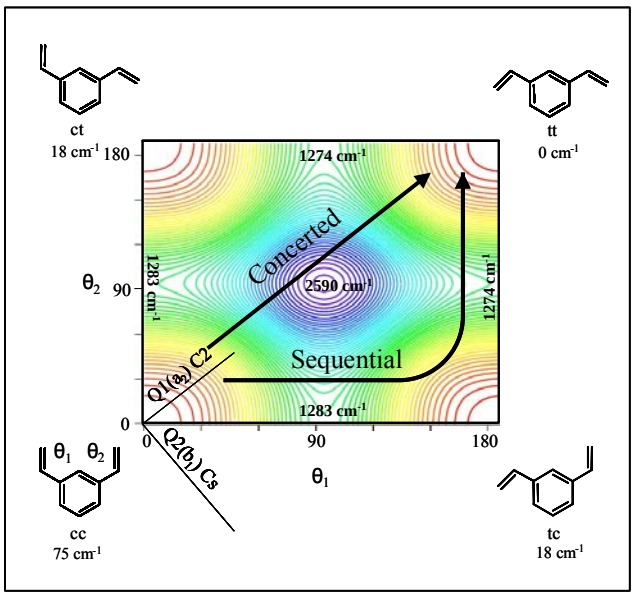

Figure 2: DFT B3LYP/6-31+G relaxed 2D potential energy surface for the phenyl torsional coordinates of mDVB.*

B. Diphenylmethane and 4-methyldiphenylmethane

Diphenylmethane (DPM) and 4-methyldiphenylmethane (4-mDPM) are two prototypical members of another series of molecules with a different type of conformational flexibility, with two torsional coordinates in DPM (specifying the torsional angles of the two phenyl rings) and three in 4-mDPM (two phenyl torsions plus a methyl internal rotor). In this series, our interest is fueled in part by the fact that the conformational flexibility occurs between two ultraviolet chromophores, which complicate and enrich the ultraviolet spectroscopy, and show promise for providing novel insight to the unique vibronic coupling that accompanies such a circumstance.

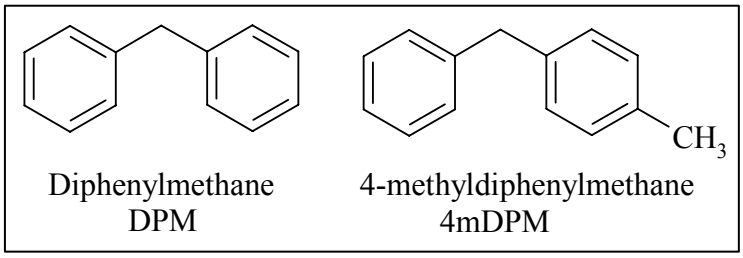

Last year's report described the complicated ultraviolet spectroscopy of these flexible bichromophores. Now, in collaboration with David Plusquellic at NIST, we have completed extensive calculations on the ground state and excited state surfaces that illustrate the challenge

these molecules present to spectroscopic and computational study. According to calculations, in the ground states of DPM and 4mDPM, the two phenyl rings are able to internally rotate with respect to one another with only modest barriers of about 200 cm^{-1} separating the C_2 minima, as shown in Figure 2. Analogous calculations on the S_1 and S_2 states at the MP2/6-311++G(d,p) level of theory show a complicated interweaving of the two surfaces, with varying degrees of electronic localization or delocalization depending on the relative orientations of the two rings. The crossing seams on the two-dimensional torsional surface are shown in Figure 3.

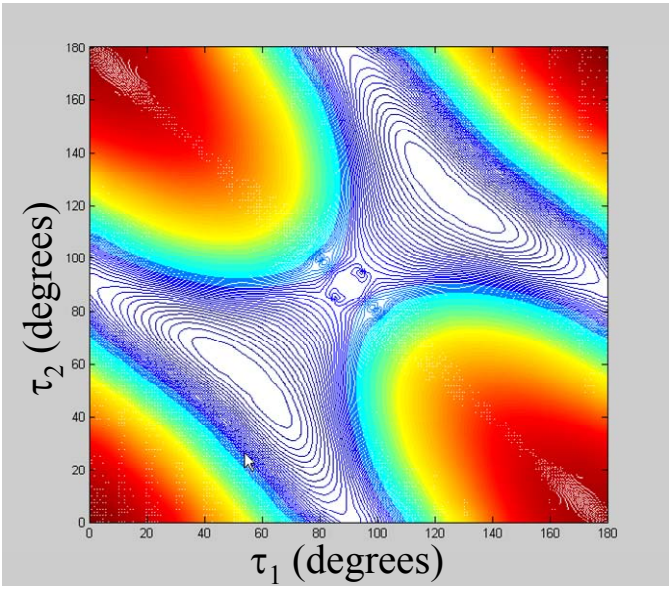

Figure 3: Ground state potential energy surface for the torsional coordinates of DPM, calculated at the MP2/6-311++G(d,p) level of theory.

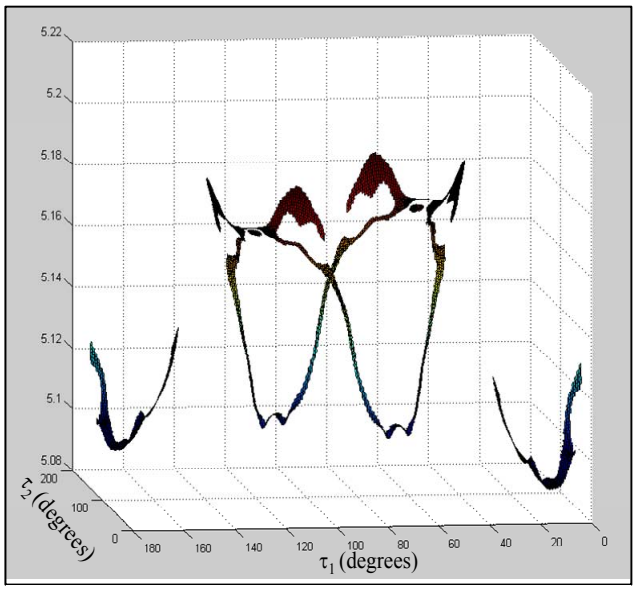

Figure 4: DPM S_1-S_2 surface crossing regions calculated at the TDDFT B3LYP 6-311++G(d,p) level of theory.

C. 2-hydroxy-diphenylmethane and bis-(2-hydroxyphenyl)methane

In bis-(2-hydroxyphenyl)methane, $(2\text{-OH})_2$DPM, the addition of two OH groups in the *ortho* positions on the two rings produces four flexible degrees of freedom: adding the two OH torsions to the two C-phenyl torsions. We have studied the ultraviolet and infrared spectroscopy of $(2\text{-OH})_2$DPM cooled in a supersonic expansion. UVHB spectroscopy revealed the presence of two conformational isomers. The fluorescence-dip infrared (FDIR) spectra of these two conformers in the OH stretch region were used to assign the two isomers, by comparison with calculation, to two unique H-bonded structures, one in which the two OH groups H-bond to one another, and the other in which the two OH groups each form π H-bonds with the other ring (see below). We have also recorded excited state FDIR spectra that highlight the effects of electronic excitation on the H-bonding. The S_1-state FDIR spectrum of the π H-bonded conformer shows strong combination bands involving the OH stretch and phenyl torsions.

In order to understand the vibronic level excitation spectrum and the coupling between the excited states of $(2\text{-OH})_2$DPM, we have again collaborated with David Plusquellic (NIST) to obtain high resolution spectra of the rotational structure of several of the vibronic transitions observed. The rotational constants obtained in the fits confirmed the assigned structures of the two conformers and provided transition dipole moment directions for the $S_1 \leftarrow S_0$ origin transitions of the two conformers. To complement this data, dispersed fluorescence scans of a large number of excited state vibronic levels have also been recorded. In the OH···O H-bonded conformer, the S_1 and S_2 states are found to be localized on the two rings, as one would expect

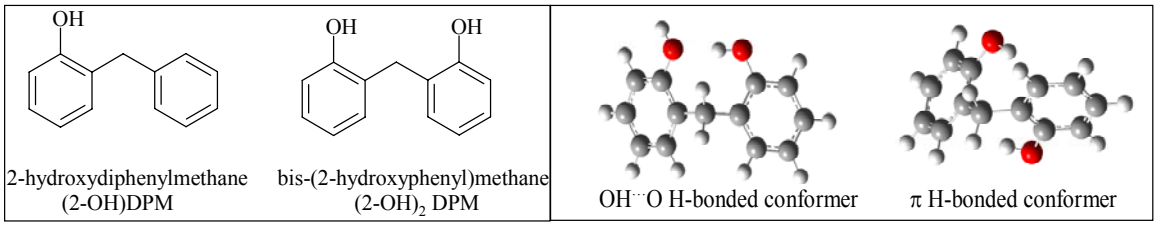

based on the distinct donor and acceptor roles played by the two rings. However, even in the π-bound conformer, the excited state infrared spectrum reflects at least a partial localization in the excited states of this conformer as well. We are presently writing up this work, which will serve as a basis for SEP-PT spectra on this model four-dimensional potential energy surface.

D. The singlet-triplet spectroscopy of cyclopentenone

In collaboration with Prof. Stephen Drucker (UW-Eau Claire) we have studied the singlet-triplet spectroscopy of expansion-cooled cyclopentenone (CP) using phosphorescence excitation spectroscopy. CP is a model cyclic enone, which Drucker and his group had studied in some detail at room temperature using cavity ring-down spectroscopy.(Pillsbury et al., JPCA 107, 10648 (2003)). Those spectra were complicated by hot bands from the singlet manifold, which interfered with detection of bands near the S_1 origin, and lent some uncertainty to the assignments. Our new fluorescence chamber has sensitive fluorescence collection optics that enabled the acquisition of a high-quality jet-cooled phosphorescence excitation spectrum for the $T_1(n\pi^*)\leftarrow S_0$ transition in CP. Etalon scans were used to resolve the rotational structure in the $T_1\leftarrow S_0$ origin transition, which has been fit in collaboration with Richard Judge (UW-Parkside).

E. SEP-PT spectroscopy of alkynylbenzenes

Based on earlier studies of the single-conformation spectroscopy of 4-phenyl-1-butyne, 5-phenyl-1-pentyne, 3-benzyl-1,5-hexadiyne, and 5-phenyl-1-pentene, we are now beginning a detailed study using SEP-PT spectroscopy to measure the energy barriers to isomerization between specific isomer pairs and the product isomerization yields as a function of energy.

Publications acknowledging DOE support, 2005-present

1. Talitha M. Selby, Jasper R. Clarkson, Diane Mitchell, James A.J. Fitzpatrick. H. Daniel Lee, David W. Pratt, and Timothy S. Zwier, "Conformation-specific Spectroscopy and Conformational Isomerization Energetics of *ortho*-, *meta*-, and *para*-Ethynylstyrenes", J. Phys. Chem. A **109**, 4484-96 (2005).
2. Talitha M. Selby and Timothy S. Zwier, "Conformation-specific spectroscopy of 4-phenyl-1-butyne and 5-phenyl-1-pentyne", J. Phys. Chem. A **109**, 8487-8496 (2005).
3. Talitha M. Selby, Aloke Das, T. Bekele, H. Daniel Lee, Timothy S. Zwier, "Conformation-specific Spectroscopy of 3-benzyl-1,5-hexadiyne", J. Phys. Chem. A **109**, 8497-8506 (2005).
4. Bruce C. Garrett, *et al.,* "The Role of Water on Electron-Initiated Processes and Radical Chemistry: Issues and Scientific Advances", Chemical Reviews **105**, 355-389 (2005).
5. Talitha M. Selby, W. Leo Meerts, and Timothy S. Zwier, "Isomer-specific ultraviolet spectroscopy of *meta*-, and *para*-divinylbenzene", J. Phys. Chem. A, Web Release Date: 16-Mar-2007; DOI:10.1021/jp068275+.
6. Talitha M. Selby and Timothy S. Zwier, "Flexing the muscles of divinylbenzene: Direct measurement of the barriers to conformational isomerization", J. Phys. Chem. A, Web Release Date: 16-Mar-2007; DOI:10.1021/jp0682762.
7. Nathan R. Pillsbury, Timothy S. Zwier, Richard H. Judge, and Stephen Drucker, "Jet-cooled phosphorescence excitation spectrum of the $T_1(n,\square^*)\leftarrow S_0$ transition of 2-cyclopenten-1-one", (submitted).

Author Index

Ahmed, M. 134
Allen, W.D. 237
Baer, T.....1
Barlow, R.S. 5
Belau, L. 134
Bowman, C. T 91
Bowman, J. M. 9
Brown, N.J. 13
Butler, L. J.....17
Chandler, D.W. 21
Chen, J.H. 25, 103
Continetti, R.E. 29
Cool, T.A. 33
Crim, F.F. 37
Davis, H.F. 41
Davis, M.J. 45
Dryer, F.L.....49
Ervin, K.M. 53
Field, R.W. 57
Flynn, G. 61
Frank, J.H. 65
Frenklach, M. 69
Goulay, F.....134
Gray, S.K. 73
Green, Jr., W.H. 76
Guo, H. 79
Hall, G.E. 83
Hansen, N. 87
Hanson, R.K. 91
Harding, L.B. 95
Hawkes, E.R.....25
Heaven, M.C. 149
Hershberger, J.F. 99
Howle, C. 134
Im, H.G. 103
Johnson, P.M. 107
Kaiser, R.I. 111
Kellman, M.E. 115
Kerstein, A.R. 119
Kiefer, J.H. 123
Klippenstein, S.J. 126
Krylov, A.I. 130
Leone, S.R. 134
Lester, M.I. 138
Lester, Jr., W.A. 142
Lignell, D 25
Lin, M.C. 145
Long, M.B. 253
Lucht, R.P. 149
Macdonald, R.G. 153
Mebel, A. 156
Michael, J.V. 160
Michelsen, H.A. 164
Miller, J.A. 168
Miller, T.A. 172
Miller, W.H. 176
Mountziaris, T.J. 285
Muckerman, J.T. 180
Mullin, A.S.....184
Najm, H.N. 188
Nesbitt, D. J.....192
Ng, C.Y. 197
Oefelein, J. 201
Osborn, D.L. 205
Perry, D.S. 209
Pitz, W.J. 213
Pope, S.B. 217
Pratt, S.T. 221
Reisler, H. 225
Ruedenberg, K. 229
Ruscic, B. 233
Rutland, C.J. 103
Sankaran, R. 25
Schaefer III, H.F. 237
Sears, T.J. 241
Settersten, T.B. 245
Shepard, R. 249
Smooke, M.D. 253
Smith, J. 134
Suits, A.G. 257
Taatjes, C.A. 261
Thompson, D.L. 265
Tranter, R.S. 269
Trouvé, A. 103
Truhlar, D.G. 273
Tsang, W. 277
Weber, P.M. 281
Westbrook, C.K. 213
Westmorelend, P.R. ...285
Wilson, K. 134
Wittig, C. 289
Yarkony, D.R. 293
Yoo, C.S. 25
Yu, H-G.....297
Zwier, T.S. 301

Participants

Tomas Baer
University of North Carolina
Chemistry Department
Chapel Hill, NC 27599
Phone: (919)962-1580
E-Mail: baer@unc.edu

Robert Barlow
Sandia National Laboratories
7011 East Avenue, MS9051
Livermore, CA 94550
Phone: (925)294-2688
E-Mail: barlow@sandia.gov

Joel Bowman
Emory University
1515 Dickey Drive
Atlanta, GA 30322
Phone: (404)727-6592
E-Mail: jmbowma@emory.edu

Bastiaan Braams
Emory University, Dept. Math/CS
400 Dowman Drive #W401
Atlanta, GA 30322
Phone: (404)727-1980
E-Mail: braams@mathcs.emory.edu

Nancy Brown
Lawrence Berkeley National Laboratory
One Cyclotron Road, MS: 90K
Berkeley, CA 94720
Phone: (510)486-4241
E-Mail: NJBrown@lbl.gov

Laurie Butler
The University of Chicago, James Franck Inst.
929 E 57th Street, CIS E 211
Chicago, IL 60637
Phone: (773)702-7206
E-Mail: l-butler@uchicago.edu

Michael Casassa
DOE Office of Basic Energy Sciences, SC22.1
19901 Germantown Road
Germantown, MD 20874
Phone: (301) 903-0448
E-Mail: michael.casassa@science.doe.gov

David Chandler
Sandia National Laboratories
PO Box 969
Livermore, CA 94550
Phone: (925)294-3132
E-Mail: chand@sandia.gov

Jacqueline Chen
Sandia National Laboratories
PO Box 969
Livermore, CA 94550
Phone: (925)294-2586
E-Mail: jhchen@sandia.gov

Robert Continetti
UC San Diego
Dept. of Chem and Biochem 0340, 9500
Gilman Drive
La Jolla, CA 92093
Phone: (858)534-5559
E-Mail: rcontinetti@ucsd.edu

Terrill Cool
Cornell University
228 Clark Hall
Ithaca, NY 14853
Phone: (607)255-4191
E-Mail: tac13@cornell.edu

Fleming Crim
University of Wisconsin-Madison
1101 University Ave.
Madison, WI 53706
Phone: (608)263-7364
E-Mail: fcrim@chem.wisc.edu

H. Floyd Davis
Cornell University
Dept. of Chem. & Chem. Bio., Baker Laboratory
Ithaca, NY 14853
Phone: (607)255-0014
E-Mail: hfd1@cornell.edu

Michael J. Davis
Argonne National Laboratory
Chemistry Division
Argonne, IL 60439
Phone: (630)252-4802
E-Mail: davis@tcg.anl.gov

Participants

Frederick Dryer
Princeton University
D329-D Engineering Quadrangle
Princeton, NJ 08544
Phone: (609)258-5206
E-Mail: fldryer@princeton.edu

James Eberhardt
US DOE Office of FreedomCAR and Vehicle Technologies
EE-2G, 1000 Independence Ave. SW
Washington, DC 20585
Phone: (202)586-9837
E-Mail: james.eberhardt@ee.doe.gov

Kent M. Ervin
University of Nevada, Reno
1664 N. Virginia St., MS 216
Reno, NV 89557
Phone: (775)784-6676
E-Mail: ervin@unr.edu

Robert Field
MIT
Room 6-219, Department of Chemistry
Cambridge, MA 02139
Phone: (617)253-1489
E-Mail: rwfield@mit.edu

George Flynn
Columbia University
MC 3109 Havemeyer, 3000 Broadway
New York, NY 10027
Phone: (212)854 4162
E-Mail: gwf1@columbia.edu

Jonathan Frank
Sandia National Laboratories
P.O. Box 969, MS9051
Livermore, CA 94550
Phone: (925)294-4645
E-Mail: jhfrank@sandia.gov

Michael Frenklach
University of California, Berkeley
Dept of Mech Eng
Berkeley, CA 94720
Phone: (510) 643-1676
E-Mail: myf@me.berkeley.edu

David Golden
Stanford University
Department of Mechanical Engineering
Stanford, CA 94305
Phone: (650)723-5009
E-Mail: david.golden@stanford.edu

Stephen Gray
Argonne National Laboratory
Chemistry Division
Argonne, IL 60439
Phone: (630)252-3594
E-Mail: gray@tcg.anl.gov

William Green
MIT, Department of Chemical Engineering
66-270, 77 Massachusetts Avenue
Cambridge, MA 2139
Phone: (617)253-4580
E-Mail: whgreen@mit.edu

Hua Guo
University of New Mexico
Department of Chemistry
Albuquerque, NM 87131
Phone: (505)277-1716
E-Mail: hguo@unm.edu

Gregory Hall
Brookhaven National Laboratory
Chemistry Department
Upton, NY 11973
Phone: (631)344-4376
E-Mail: gehall@bnl.gov

Nils Hansen
Sandia National Laboratories
PO Box 969 MS 9055
Livermore, CA 94551
Phone: (925)294-6272
E-Mail: nhansen@sandia.gov

Ronald Hanson
Stanford University
Mechanical Engineering, room 520-E
Stanford, CA 94305
Phone: 650-723-6850
E-Mail: rkhanson@stanford.edu

Participants

Lawrence Harding
Argonne National Laboratory
9700 South Cass Avenue
Argonne, IL 60439
Phone: (630)252-3591
E-Mail: harding@anl.gov

Alex Harris
Brookhaven National Laboratory
Chemistry Department, Building 555
Upton, NY 11973
Phone: (631)344-4301
E-Mail: alexh@bnl.gov

Michael Heaven
Emory University
1515 Dickey Drive
Atlanta, GA 30322
Phone: (404)727-6617
E-Mail: mheaven@emory.edu

John Hershberger
North Dakota State University
Department of Chemistry and Molecular Biology
Fargo, ND 58105
Phone: (701)-231-8225
E-Mail: john.hershberger@ndsu.edu

Richard Hilderbrandt
DOE Office of Basic Energy Sciences, SC22.1
19901 Germantown Road
Germantown, MD 20874
Phone: (301)903-0035
E-Mail: Richard.Hilderbrandt@science.doe.gov

Ahren Jasper
Sandia National Laboratories
1500 Ovaltine Ct APT 1531
Villa Park, IL 60181
Phone: (630)782-5030
E-Mail: ahrenjasper@gmail.com

Philip Johnson
Stony Brook University
Department of Chemistry
Stony Brook, NY 11794
Phone: 631-632-7912
E-Mail: philip.johnson@sunysb.edu

Ralf Kaiser
University of Hawaii
2545 The Mall
Honolulu, HI 96822
Phone: (808)956-5731
E-Mail: kaiser@gold.chem.hawaii.edu

Michael Kellman
University of Oregon
Department of Chemistry
Eugene, OR 97403
Phone: (541)346-4196
E-Mail: kellman@uoregon.edu

Alan Kerstein
Sandia National Laboratories
MS 9051
Livermore, CA 94526
Phone: 925-294-2390
E-Mail: arkerst@sandia.gov

John Kiefer
Univ. Illinois at Chicago
810 S. Clinton
Chicago, IL 60680
Phone: (312)996-5711
E-Mail: kiefer@uic.edu

William Kirchhoff
DOE (RET)
14511 Woodcrest Dr.
Rockville, MD 20853
Phone: (301)460-5580
E-Mail: william.kirchhoff@att.net

Stephen Klippenstein
Argonne National Laboratory
Chemistry Division, 9700 S. Cass Ave.
Argonne, IL 60439
Phone: (630)252-3596
E-Mail: sjk@anl.gov

Allan Laufer
DOE(RET)
5106 Russett Road
Rockville, Md 20853
Phone: (301)975-2062
E-Mail: allan.laufer@nist.gov

Participants

Stephen Leone
University of California, Berkeley
Department of Chemistry
Berkeley, CA 94720
Phone: (510)643-5467
E-Mail: srleone@berkeley.edu

William A. Lester Jr.
Lawrence Berkeley National Laboratory
Department of Chemistry, University of California
Berkeley, CA 94720
Phone: (510)643-9590
E-Mail: walester@lbl.gov

Robert Lucht
Purdue University
School of Mechanical Engineering, 585 Purdue Mall
West Lafayette, IN 47907
Phone: (765)494-5623
E-Mail: lucht@purdue.edu

Andrew McIlroy
Sandia National Laboratories
POB 969 MS 9054
Livermore, CA 94551
Phone: (925)294-3054
E-Mail: amcilr@sandia.gov

Joe Michael
Argonne National Laboratory
9700 S. Cass Avenue
Argonne, IL 60439
Phone: (630)252-3171
E-Mail: jmichael@anl.gov

James Miller
Sandia National Laboratories
MS 9055
Livermore, CA 94551
Phone: (925)294-2759
E-Mail: jamille@sandia.gov

William H. Miller
Lawrence Berkeley National Laboratory
Dept of Chemistry, University of California
Berkeley, CA 94720
Phone: (510)642-0653
E-Mail: millerwh@berkeley.edu

Marsha Lester
Department of Chemistry, University of Pennsylvania
231 South 34th Street
Philadelphia, PA 19104
Phone: (215)898-4640
E-Mail: milester@sas.upenn.edu

Mark Linne
Sandia National Laboratories
7011 East Ave, MS 9055
Livermore, CA 94550
Phone: (925)294-3704
E-Mail: mlinne@sandia.gov

Robert Macdonald
Argonne National Laboratory
9700 South Cass Ave
Argonne, IL 60439
Phone: (630)252-7742
E-Mail: rgmacdonald@anl.gov

Alexander Mebel
Department of Chemistry and Biochemistry, Florida International University
11200 SW 8th Street
Miami, FL 33193
Phone: (305)348-1945
E-Mail: mebela@fiu.edu

Hope Michelsen
Sandia National Laboratories
7011 East Ave MS 9055
Livermore, CA 94551
Phone: (925)294-2335
E-Mail: hamiche@sandia.gov

Terry Miller
Ohio State University
120 W. 18th
Columbus, OH 43210
Phone: (614)292-2569
E-Mail: tamiller@chemistry.ohio-stte.edu

James Muckerman
Brookhaven National Laboratory
Chemistry Department
Upton, NY 11973
Phone: 631-344-4368
E-Mail: 631-344-5815

Participants

Amy Mullin
University of Maryland
Department of Chemistry and Biochemistry
College Park, MD 20742
Phone: (301)405-6569
E-Mail: mullin@umd.edu

Habib Najm
Sandia National Laborties
7011 East Ave
Livermore, CA 94550
Phone: (925)294-2054
E-Mail: hnnajm@sandia.gov

David Nesbitt
JILA/NIST University of Colorado Boulder
UCB 440
Boulder, CO 80309
Phone: (303)492-8857
E-Mail: djn@jila.colorado.edu

Cheuk-Yiu Ng
University of california, Davis
Department of Chemistry, One Shields Ave
Davis, CA 95616
Phone: (530)754-9645
E-Mail: cyng@chem.ucdavis.edu

Joseph Oefelein
Sandia National Laboratories
7011 East Avenue, Building 905, Room 172
Livermore, CA 94550
Phone: (925)294-2648
E-Mail: oefelei@sandia.gov

David Osborn
Sandia National Laboratories
PO Box 969
Livermore, CA 94551
Phone: (925)294-4622
E-Mail: dlosbor@sandia.gov

Joon Park
Emory. University
1515 Dickey Dr
Atlanta, GA 30322
Phone: (404)727-2823
E-Mail: jpark05@emory.edu

Charles Parmenter
Indiana University
Department of Chemistry
Bloomington, IN 47405
Phone: (812)855-3522
E-Mail: parment@indiana.edu

David Perry
The University of Akron
Department of Chemistry
Akron, OH 44325
Phone: (330)972-6825
E-Mail: dperry@uakron.edu

William Pitz
Lawrence Livermore National Laboratory
P.O. Box 808, L-372
Livermore, CA 94588
Phone: (925)422-7730
E-Mail: pitz1@llnl.gov

Stephen Pope
Cornell University
254 Upson Hall
Ithaca, NY 14853
Phone: (607)255-4314
E-Mail: pope@mae.cornell.edu

Stephen Pratt
Argonne National Laboratory
Building 200
Argonne, IL 60439
Phone: (630)252-4199
E-Mail: stpratt@anl.gov

Hanna Reisler
University of Southern California
Chemistry Department
Los Angeles, CA 90089
Phone: (213)740-7071
E-Mail: reisler@usc.edu

Branko Ruscic
Argonne National Laboratory
9700 S Cass Ave - CHM 200
Argonne, IL 60439
Phone: (630)252-4079
E-Mail: ruscic@anl.gov

Participants

Trevor Sears
Brookhaven National Laboratory
Chemistry Department
Upton, NY 11973
Phone: (631)344-4374
E-Mail: sears@bnl.gov

Mitchell Smooke
Yale University
15 Prospect Street
New Haven, CT 06520
Phone: (203)432-4344
E-Mail: mitchell.smooke@yale.edu

Craig Taatjes
Sandia National Laboratories
7011 East Ave., MS 9055
Livermore, CA 94551
Phone: (925)294-2764
E-Mail: cataatj@sandia.gov

Donald Thompson
University of Missouri - Columbia
601 S. College Avenue, 125 Chemistry
Columbia, MO 65211
Phone: (573)489-7739
E-Mail: thompsondon@missouri.edu

Julian Tishkoff
AFOSR
875 North Randolph Street, Suite 325, Room 3112
Arlington, VA 22203
Phone: (703)696-8478
E-Mail: 703-696-8451

Robert Tranter
Argonne National Laboratory
9700 S Cass Ave
Argone, IL 60439
Phone: 630-252-6505
E-Mail: tranter@anl.gov

Donald Truhlar
University of Minnesota
5033 Thomas Avenue South
Minneapolis, MN 55410
Phone: (612)929-2833
E-Mail: truhlar@umn.edu

Wing Tsang
NIST
100 Bureau Drive, Stop 8830
Gaithersburg, MD 20899
Phone: (301) 975-2507
E-Mail: wing.tsang@nist.gov

Frank Tully
DOE Office of Basic Energy Sciences, SC22.1
19901 Germantown Road
Germantown, MD 20874
Phone: (301)903-5998
E-Mail: frank.tully@science.doe.gov

Albert Wagner
Chemistry Division, Argonne National Laboratory
9700 S. Cass Avenue, #200
Argonne, IL 60439
Phone: (630)252-3570
E-Mail: wagner@tcg.anl.gov

Peter Weber
Brown University
Box H, Department of Chemistry
Providence, RI 02912
Phone: (401)863-3767
E-Mail: Peter_Weber@brown.edu

Charles Westbrook
LLNL
P.O. Box 808
Livermore, CA 94550
Phone: (925)422-4108
E-Mail: westbrook1@llnl.gov

Phillip Westmoreland
National Science Foundation
4201 Wilson Blvd, Suite 525
Arlington, VA 22230
Phone: (703)292-8371
E-Mail: pwestmor@nsf.gov

Kevin Wilson
Lawrence Berkeley National Laboratory
One Cyclotron Road, Mail Stop 6R2100
Berkeley, CA 94720
Phone: (510)495-2474
E-Mail: KRWilson@lbl.gov

Participants

Curt Wittig
USC
Department of Chemistry
Los Angeles, CA 90089
Phone: (213)740-7368
E-Mail: wittig@usc.edu

David Yarkony
Johns Hopkins University
Department of Chemistry
3400 N Charles Street
Baltimore, MD 21218
Phone: (410)516-4663
E-Mail: yarkony@jhu.edu

Hua-Gen Yu
Brookhaven National Lab
Chemistry Bldg.555A
Upton, NY 11973
Phone: (631)344-4367
E-Mail: hgy@bnl.gov

Timothy Zwier
Purdue University
Dept. of Chemistry, 560 Oval Drive
West Lafayette, IN 47907
Phone: (765)494-5278
E-Mail: zwier@purdue.edu